



University of Fort Hare
Together in Excellence

BASIN ANALYSIS OF THE SOUTPANSBERG AND TULI COALFIELDS, LIMPOPO PROVINCE OF SOUTH AFRICA

By

Ntokozo Malaza

Thesis submitted in the fulfillment of the requirement for the degree of

DOCTOR OF PHILOSOPHY

In
GEOLOGY

FACULTY OF SCIENCE AND AGRICULTURE

UNIVERSITY OF FORT HARE

SUPERVISOR: PROFESSOR B. ZHAO
CO-SUPERVISORS: PROFESSOR K. LIU

MAY 2014

DECLARATION

I, Ntokozo Malaza, declare this dissertation to be my own unaided work. Where other sources of information have been used, they have been acknowledged and referenced. It is being submitted for the Degree of Doctor of Philosophy at the University of Fort Hare, Alice. It has not been submitted before for any degree or examination in any other university.

Ntokozo Malaza

May 2014

ABSTRACT

The Soutpansberg and Tuli Coalfields are both hosted in the Karoo Basin, Limpopo Province of South Africa. The Soutpansberg Coalfield is situated north of the Soutpansberg Mountain Range and has a strike length of about 200 km and width of about 80 km which is fault controlled and extends from Waterpoort in the west to the Kruger National Park in the east. The Tuli Coalfield occurs in a small intracratonic, east-west trending fault-controlled sedimentary basin with a preserved width of 80 km and length of 120 km. The east to west trend of the Tuli Coalfield parallels that of the Soutpansberg Coalfield further east, and the two coalfields link up with the north-south trending Lebombo Basin. The Tuli Coalfield occurs in the Tuli Basin, while the Soutpansberg Coalfield occurs in the Soutpansberg Basin. The two basins preserve a heterogeneous succession of the Upper Paleozoic to Lower Mesozoic sedimentary and volcanic rocks of the Karoo Supergroup. Because the area is largely covered by the Quaternary Kalahari Group sands, the stratigraphy of the succession is not as well understood as the Main Karoo Basin in South Africa. This study deals with the intra-basinal stratigraphic correlation, facies and depositional environments, petrography, geochemistry, provenance, geophysics, structural geology, diagenesis of sandstone, subsidence history and coal quality in the Soutpansberg and Tuli Coalfields.

Based on the field work and detailed sedimentological analyses of over 2000 borehole data, seven facies associations (FAs) comprising sixteen major lithofacies were identified. The facies associations are: Glacial diamictite and sandstone (FA 1), Clast supported conglomerate and sandstone (FA 2), Tabular cross-bedded sandstone (FA 3), Trough and planar cross-bedded sandstone (FA 4), Fine calcareous and micaceous siltstone and mudstone (FA 5), Sandy shale/mudstone (FA 6), Laminated or thin-bedded Carbonaceous shale/mudstone and coal (FA 7). The facies associations (FA 1 to FA 7) correspond to the lithostratigraphic sub-divisions of the Tshidzi, Madzaringwe and Mikambeni Formations. The Madzaringwe Formation in this study is informally sub-divided into the Lower, Middle and Upper Members while the Mikambeni Formation is informally sub-divided into the Lower and Upper Members.

Sedimentological characteristics of the identified facies associations indicate the following depositional environments: Fluvioglacial (braided streams) depositional environment (FA 1, Tshidzi Diamictite Formation); Floodplain ponds, lakes, marshes and backswamps (FA 6 and FA 7, Lower Member of the Madzaringwe Formation);

Meandering and braided channels, crevasse splays, levees and crevasse channels (FA 2, FA 3, FA 4 and FA 5, Middle Member of the Madzaringwe Formation); Floodplain ponds, lakes and backswamps (FA 6 and FA 7, Upper Member of the Madzaringwe Formation); Meandering and braided channels, crevasse splays, swamps and shallow lakes (FA 5, FA 6 and FA 7, Lower Member of the Mikambeni Formation) and lastly braided channels, meandering channels, levees and crevasse channels (FA 2, FA 3, FA 4 and FA 5, Upper Member of the Mikambeni Formation). Paleocurrent directions were measured using directional structures (cross-bedding and asymmetric ripple marks). The paleocurrent analysis shows that the direction of the channels was from south-west to north-east in both coalfields.

Based on the structural study and geophysical interpretations, the structural and tectonic settings of the two coalfields have been revealed, both coalfields are normal fault-bounded. The geological evolution of the Karoo strata, at least since the Upper Carboniferous, essentially follows the type model for passive continental margin terrain. Paleostress inversion techniques have been employed to interpret the stress regime of the two coalfields. The Soutpansberg Basin is characterised by W-E to ENE-WSW extension and N-S to NNW-SSE compression. The Tuli Basin is characterised by N-S to NNW-SSE compression and W-E to ENE-WSE extension. This stress field reflects the established structural trend of the two shear belts (the Tshipise and Siloam shear zones) bounding the Central Zone of the Limpopo Mobile Belt. The geophysical interpretations were focused on outlining structures, contacts and on the delineation of gravity, magnetic and radiometric signatures in areas defined as anomalous. The magnetic, gravity and radiometric data showed low amplitudes in the sedimentary strata compared to the surrounding and basement geological bodies. The E-N-E fault system has a notable signature, defining two magnetic domains on both southern and northern sides of the Soutpansberg Coalfield. The intrusive emplacements are mainly fault controlled and they trend in the same direction as the two fault systems. Jurassic volcanics (Letaba and Jozini Formations) follow a SW-NE trend, outcropping in the east (Soutpansberg Basin), producing a strong magnetic response in this area, and partly buried in the west, where magnetic intensity tends to be reduced.

Petrographic and geochemical analyses of the Soutpansberg sandstones revealed immature sub-litharenite, sub-arkose and minor arkosic arenites in nature, dominated by sub-angular to rounded detrital grains, sourced from recycled orogens, craton interior to transitional continental. The sandstones of the Tuli Coalfield are classified as sub-arkoses and minor sub-litharenites and sourced from the craton interior and recycled orogen

provenances. Both petrographic and geochemical results suggest a passive continental margin source. Petrographic and geochemical results of the samples of the Soutpansberg Coalfield suggest uplifted basement source areas dominated by sedimentary rocks with minor granite-gneiss rocks. The petrography and geochemistry of the Tuli sandstones suggest source areas dominantly composed of plutonic (granites) and metamorphic (gneisses and schists) rocks with a component from a sedimentary (quartz-arenites, quartzites, shales, arkoses and meta-arkoses) rocks.

Diagenetic features of Mikambeni and Madzaringwe sandstones are subdivided into early, middle and late stages. Time is relative with the earliest diagenetic event occurring shortly after deposition and the latest occurring up until present time. The main diagenetic processes that have affected the sandstones include mechanical compaction, cementation and the dissolution of framework grains and cements. Early diagenetic processes include mechanical compaction, silica and calcite cementation, clay minerals (pore lining and pore-filling kaolinite, illite and smectite), feldspar authigenesis and the formation of hematite cements and coatings. Late diagenesis includes quartz and feldspar overgrowths, seritisation, chlorite alteration, grain deformation, pressure-solution and fracturing and albitisation.

The subsidence of the basins is believed to be initiated and thermally controlled by tectonics (i.e. faults of basements blocks) rather than sedimentary burial. The subsidence within the basins supports the primary graben system which must have been centered within the present basins, and later became a region of major faulting. This gave way to the Late Carboniferous rapid subsidence, with areas of greater extension subsiding more rapidly. The Early Permian (last phase) is characterised by a slow subsidence representing the post-rift thermal subsidence. The rift flanks were gradually uplifted and, and then generally subsided as a results of thermal contraction after the extension terminated.

Based on the coal analysis, both coalfields are characterised by coking bituminous coal. The study has revealed that the eastern Soutpansberg Coalfield is likely to present better opportunities for identification of potentially exploitable coal deposits as compared to the Tuli Coalfield.

ACKNOWLEDGEMENTS

First, I wish to express my profound gratitude to my supervisor, Prof Baojin Zhao and co-supervisors Prof Ken Liu and Dr. Hongzhuen Ye for their valuable scientific guidance, persistence, positive criticism and motivation during my study. I would like to thank the Coaltech Research Association (Coaltech) for funding this study, specifically Mr. Johann Beukes, the executive director of Coaltech for his kind support and encouragement. I would also like to thank the staff members at Tshikondeni Coal Mine for providing accommodation during my fieldwork. Dr. Gunther Brandl, (Council for Geoscience, Polokwane) is acknowledged for his technical assistance. Siyanda Mbatyoti (Honours student, 2011) is acknowledged for assistance during the field data collection.

I express my appreciation to the Council for Geoscience for providing me with geophysical data in the form of regional magnetic, gravity and radiometric profiles and for borehole core data, and chemical and XRD analyses. I would like to thank Prof. Oswald Gwavava (Head of Department), staff members and fellow students from the Department of Geology, University of Fort Hare for their help and assistance. My heartfelt thanks going to my family, friends and all others whose names I did not mention here, who contributed in various ways towards the successful completion of the thesis.

TABLE OF CONTENTS

DECLARATION	i
ABSTRACT	ii
ACKNOWLEDGEMENTS	v
LIST OF FIGURES	xii
LIST OF TABLES	xxi
LIST OF APPENDICES	xxiii
LIST OF ABBREVIATIONS AND ACRONYMS	xxiv
CHAPTER 1: INTRODUCTION	1
1.1. Location of the Study Area	1
1.2. Rational	3
1.3. Aims and Objectives of the Study	3
1.4. Methodologies.....	3
1.4.1. Comprehensive literature review and data collection	4
1.4.2. Geological fieldwork and sampling	4
1.4.3. Stratigraphy.....	4
1.4.4. Sedimentary Facies	4
1.4.5. Structural Analysis.....	5
1.4.6. Petrographic Studies	5
1.4.7. Geochemical Analysis	5
1.4.8. Geophysical Techniques	6
1.4.9. Coal Analysis	6
1.4.10. Diagenesis of sandstone.....	6
1.4.11. Subsidence Analysis	7
1.5. Outline.....	7
CHAPTER 2: GEOLOGICAL SETTING	9
2.1. Regional Geology	9
2.1.1. The Soutpansberg Coalfield.....	9
2.1.2. The Tuli Coalfield.....	13
2.2. Previous work in the Soutpansberg and Tuli Coalfields.....	16
2.2.1. Summary of the work by Brandl and McCourt (1980) in the Soutpansberg Basin.....	17
2.2.1.1. Stratigraphic Units and Depositional Environments by Brandl and McCourt ...	17
2.2.1.2. Structural Geology and Basin Evolution of the Soutpansberg Basin proposed by Brandl and McCourt	19
2.2.1.3. Summary (Brandl and McCourt, 1980)	20
2.2.2. Summary of the work by Chidley (1985) in the Tuli Basin	21
2.2.2.1. Stratigraphic Units and Depositional Environments recognised by Chidley.....	21

2.2.2.2: Structural Geology and Basin Evolution of the Tuli Basin by Chidley.....	23
2.2.3. Summary of the work by Bordy (2000); Bordy and Catuneanu (2001); (2002)	23

CHAPTER 3: STRATIGRAPHY25

Abstract.....	25
3.1. Introduction.....	25
3.2. Methodology.....	27
3.3. Stratigraphic approach to coal-bearing strata	28
3.4. Discussions	77
3.5. Conclusions.....	80

CHAPTER 4: STRUCTURAL GEOLOGY AND EVOLUTION OF THE SOUTPANBERG AND TULI COALFIELDS.....108

Abstract.....	108
4.1. Introduction.....	109
4.2. Geological evolution.....	109
4.2.1. The Limpopo Mobile Belt	109
4.2.2. The Soutpansberg Group	83
4.2.3. The Soutpansberg and Tuli Basins	84
4.2.4. Faulting	85
4.3. Methodology.....	87
4.4. Results.....	88
4.4.1. The Soutpansberg Coalfields (Tshipise-Pafuri and Mopane).....	88
4.4.2. Tuli Coalfield.....	96
4.5. Discussions	127
4.5.1. The Formation of a rift basin	101
4.5.2. Proposed tectonic and structural model of the Soutpansberg and Tuli Basins	103
4.6. Conclusions.....	106

CHAPTER 5: FACIES ANALYSIS, DEPOSITIONAL ENVIRONMENTS AND PALEOCURRENT ANALYSIS.....135

Abstract.....	136
5.1. Introduction.....	136
5.2. Methodologies.....	137
5.3. Facies and facies associations	138
5.3.1. Glacial diamictite and sandstone facies association (FA 1).....	140
5.3.1.1. Description	140
5.3.1.2. Interpretation.....	142
5.3.2. Clast Conglomerate and sandstone facies association (FA 2)	143
5.3.2.1. Description.....	143
5.3.2.2. Interpretation.....	145
5.3.3. Tabular cross-bedded sandstone facies associations (FA 3).....	146

5.3.3.1. Description.....	146
5.3.3.2. Interpretation.....	152
5.3.4. Trough and planar cross-bedded sandstone facies association (FA 4).....	121
5.3.4.1. Description.....	121
5.3.4.2. Interpretation.....	121
5.3.5. Fine calcareous and micaceous siltstone and mudstone facies association (FA 5).....	122
5.3.5.1. Description.....	122
5.3.5.2. Interpretation.....	123
5.3.6. Laminated sandy shale/mudstone facies association (FA 6)	124
5.3.6.1. Description.....	124
5.3.6.2. Interpretation.....	124
5.3.7. Laminated or thin bedded carbonaceous shale and coal facies association (FA 7).....	125
5.3.7.1. Description.....	125
5.3.7.2. Interpretation.....	126
5.4. Depositional environments	159
5.4.1. Glacial depositional environments:.....	159
5.4.2. Alluvial and braided fluvial channel deposits.....	159
5.4.3. Meandering, braided and lacustrine depositional environments	160
5.4.4. Fluvial floodplains, ponds and lakes depositional environments	160
5.4.5. Paludal depositional environments (backswamps and oxbow lakes)	161
5.5. Depositional environments for the Soutpansberg and Tuli Coalfield.....	165
5.5.1. Diamictite Tshidzi Formation	165
5.5.2. Madzaringwe Formation	165
5.5.3. The Mikambeni Formation	165
5.6. Paleocurrent Directions.....	166
5.6.1. Cross-bedding	166
5.6.2. Asymmetric ripple marks	167
5.7. Discussions	170
5.7.1. Diamictite Tshidzi Formation	170
5.7.2. Madzaringwe Formation.....	170
5.7.3. Mikambeni Formation	171
5.7.4. Paleocurrent Directions.....	171
5.8. Conclusions.....	140
CHAPTER 6: PETROGRAPHY, GEOCHEMISTRY AND PROVENANCE	173
Abstract.....	174
6.1. Introduction.....	174
6.2. Methodology	176
6.3. Petrography.....	177
6.3.1. Texture	178
6.3.2. Clast composition.....	179
6.3.2.1. Quartz.....	179

6.3.2.2. Feldspar.....	179
6.3.2.3. Lithic fragments	180
6.3.2.4. Cement/Matrix	180
6.4. Tectonic setting	204
6.5. Geochemistry	207
6.5.1. Major elements.....	207
6.5.1.1. Source area weathering	216
6.5.2: Trace Elements	221
6.5.2.1. Large ion lithophile elements.....	221
6.5.2.2. High field strength elements	221
6.5.2.3. Transition trace elements	221
6.6. Discussions	229
6.7. Conclusions.....	188
CHAPTER 7: GEOPHYSISCS	190
Abstract.....	190
7.1. Introduction.....	190
7.2. Methodologies.....	191
7.2.1 Gravity survey.....	236
7.2.2. Magnetic survey.....	193
7.2.3. Radiometric survey	194
7.3. Results.....	196
7.4. Soutpansberg Basin.....	201
7.4.1. Gravity Data and Maps	201
7.4.2 Magnetic Data and Maps	202
7.4.2.1. Tshipise-Pafuri Coalfield	202
7.4.2.2. Mopane Coalfield.....	203
7.4.3. Radiometric Data and Maps.....	204
7.4.3.1. Mopane Basin	204
7.5. Tuli Basin.....	251
7.5.1. Magnetic Data and Maps	251
7.5.2. Radiometric Data and Maps.....	252
7.6. Discussion	256
7.6.1. Tectonic implications	256
7.6.2 Lithologic units identification.....	258
7.7. Conclusions.....	263
CHAPTER 8: COAL ANALYSIS.....	265
Abstract.....	265
8.1. Introduction.....	265
8.2. Methodologies.....	267
8.3. Results of Proximate Analysis	269

8.3.1. Tshipise-Pafuri Coal Analysis (Central and Eastern Soutpansberg)	270
8.3.2. Mopane Coal Analysis (Western Soutpansberg)	272
8.3.3. Tuli Coal Analysis	274
8.4. Coal Ash Analysis.....	277
8.4.1. Results.....	279
8.5. Discussions	282
8.6. Conclusions.....	239
CHAPTER 9: DIAGENESIS OF SANDSTONE.....	285
Abstract.....	285
9.1. Introduction.....	285
9.2. Methodology	286
9.3. Diagenesis Processes	286
9.3.1. Early Diagenetic processes	287
9.3.2. Late Diagenetic processes.....	288
9.4. Results of diagenetic features	288
9.4.1. Compaction.....	288
9.4.2. Pore lining and pore filling clays	295
9.4.3. Quartz Cementation	299
9.4.4. Chlorite cementation.....	305
9.4.5. Calcite cementation.....	305
9.4.6. Albitisation of feldspar	307
9.5. Discussions	310
9.6. Conclusions.....	267
CHAPTER 10: SUBSIDENCE ANALYSIS.....	317
Abstract.....	317
10.1. Introduction.....	317
10.2. Methodology	318
10.2.1. Age assessment	318
10.2.2. Decompaction	319
10.2.3. Backstripping	324
10.2.4. Palaeobathymetric and eustatic corrections	275
10.2.5. The 1D Airy Backstripping.....	275
10.2.6. Sources of error.....	276
10.3. Results and Interpretations.....	276
10.3.1. The 1D Airy subsidence model.....	279
10.3.2. The 1D PetroMod modelling	282
10.3.2.1. Source rock maturation and hydrocarbon generation	282
10.4. Discussions	288
10.5. Conclusions.....	292

CHAPTER 11: SUMMARY	293
REFERENCES.....	297

LIST OF FIGURES

Figure 1.1: Location of the study coalfields.	2
Figure 2.1: Geological map of the Tshipise-Pafuri Coalfield.....	11
Figure 2.2: Geological map of the Mopane Coalfield	12
Figure 2.3: Geological map of the Tuli Coalfield.....	14
Figure 2.4: Stratigraphy and correlation of the Karoo Basins	16
Figure 3.1: Topographic contour map and cross-section of the Tshipise-Pafuri Coalfield.	29
Figure 3.2: Thickness contour map of the Mikambeni Formation in the Tshipise-Pafuri Coalfield.....	30
Figure 3.3: 3d topographic map of the Mikambeni Formation in the Tshipise-Pafuri Coalfield.....	31
Figure 3.4: Thickness contour map of the Madzarinwe Formation in the Tshipise-Pafuri.	32
Figure 3.5: 3d topographic map of the Madzaringwe Formation in the Tshipise-Pafuri Coalfield.....	33
Figure 3.6: Thickness contour map of the Tshidzi Formation in the Tshipise-Pafuri Coalfield.....	34
Figure 3.7: 3d topographic map of the Tshidzi Formation in the Tshipise-Pafuri Coalfield	35
Figure 3.8: Cross-section 1 in the Tshipise-Pafuri Coalfield.....	36
Figure 3.9: Cross-section 2 in the Tshipise-Pafuri Coalfield.....	37
Figure 3.10: Cross-section 3 in the Tshipise-Pafuri Coalfield.....	38
Figure 3.11: Cross-section 4 in the Tshipise-Pafuri Coalfield.....	39
Figure 3.12: Cross-section 5 in the Tshipise-Pafuri Coalfield.....	40
Figure 3.13: Cross-section 6 in the Tshipise-Pafuri Coalfield.....	41
Figure 3.14: Cross-section 7 in the Tshipise-Pafuri Coalfield.....	42
Figure 3.15: Cross-section 8 in the Tshipise-Pafuri Coalfield.....	43
Figure 3.16: Cross-section 9 in the Tshipise-Pafuri Coalfield.....	44
Figure 3.17: Cross-section 10 in the Tshipise-Pafuri Coalfield.....	45
Figure 3.18: Cross-section 11 in the Tshipise-Pafuri Coalfield.....	46

Figure 3.19: Structure contour map and cross-section of the Mopane Coalfield.	47
Figure 3.20: Thickness contour map of the Mikambeni Formation in the Mopane Coalfield.....	48
Figure 3.21: 3d topographic map of the Mikambeni Formation in the Mopane Coalfield.	49
Figure 3.22: Thickness contour map of the Madzaringwe Formation in the Mopane Coalfield.....	59
Figure 3.23: 3d topographic map of the Madzaringwe Formation in the Mopane Coalfield	51
Figure 3.24: Thickness map of the Tshidzi Formation in the Mopane Coalfield	52
Figure 3.25: 3d topographic map of the Tshidzi Formation in the Mopane Coalfield	53
Figure 3.26: Cross-section 1 in the Mopane Coalfield.	64
Figure 3.27: Cross-section 2 in the Mopane Coalfield.	55
Figure 3.28: Cross-section 3 in the Mopane Coalfield	56
Figure 3.29: Cross-section 4 in the Mopane Coalfield.	57
Figure 3.30: Cross-section 5 in the Mopane Coalfield.	58
Figure 3.31: Cross-section 6 in the Mopane Coalfield.	59
Figure 3.32: Cross-section 7 in the Mopane Coalfield.	76
Figure 3.33: Cross-section 8 in the Mopane Coalfield.	61
Figure 3.34: : Cross-section 9 in the Mopane Coalfield.	62
Figure 3.35: Structure contour map and cross-section of the Tuli Coalfield.....	80
Figure 3.36: Thickness contour map of the Mikambeni Formation in the Tuli Coalfield.	804
Figure 3.37: 3d topographic map of the Mikambeni Formation in the Tuli Coalfield	65
Figure 3.38: Thickness contour map of the Madzaringwe Formation in the Tuli Coalfield	66
Figure 3.39: 3d topographic map of the Madzaringwe Formation in the Tuli Coalfield ..	67
Figure 3.40: Thickness contour map of the Tshidzi Formation in the Tuli Coalfield.....	68
Figure 3.41: 3d topographic map of the Tshidzi Formation in the Tuli Coalfield.	69
Figure 3.42: Cross-section 1 in the Tuli Coalfield.....	70
Figure 3.43: Cross-section 2 in the Tuli Coalfield.....	71
Figure 3.44: Cross-section 3 in the Tuli Coalfield.....	72
Figure 3.45: Cross-section 4 in the Tuli Coalfield.....	96

Figure 3.46: Cross-section 5 in the Tuli Coalfield.....	98
Figure 3.47: Cross-section 6 in the Tuli Coalfield.....	75
Figure 3.48: Cross-section 7 in the Tuli Coalfield.....	76
Figure 5.49: Generalised lithostratigraphic sub-division of the Soutpansberg Coalfield.	77
Figure 5.50: Generalised lithostratigraphic sub-division of the Tuli Coalfield.	78
Figure 4.1: Simplified map of the Limpopo Mobile Belt	83
Figure 4.2: Coalfields showing major shear zones and major faulting.....	86
Figure 4.3 (A): Progressive kinematic separation and stress tensor optimisation on fault slip data set measured along faults of the Tshipise-Pafuri Coalfield.....	89
Figure 4.3: (B): Progressive kinematic separation and stress tensor optimisation on fault slip data set measured along faults of the Tshipise-Pafuri Coalfield.....	117
Figure 4.3: (C): Progressive kinematic separation and stress tensor optimisation on fault slip data set measured along faults of the Tshipise-Pafuri Coalfield.....	118
Figure 4.3: (D): Progressive kinematic separation and stress tensor optimisation on fault slip data set measured along faults of the Tshipise-Pafuri Coalfield.....	119
Figure 4.4: (A): Progressive kinematic separation and stress tensor optimisation on fault slip data set measured along faults of the Mopane Basin.	93
Figure 4.4: (B): Progressive kinematic separation and stress tensor optimisation on fault slip data set measured along faults of the Mopane Basin.	94
Figure 4.4: (C): Progressive kinematic separation and stress tensor optimisation on fault slip data set measured along faults of the Mopane Basin.	95
Figure 4.5: (A): Progressive kinematic separation and stress tensor optimisation on fault slip data set measured along faults of the Tuli Coalfield.....	97
Figure 4.5: (B): Progressive kinematic separation and stress tensor optimisation on fault slip data set measured along faults of the Tuli Basin. The initial data base contains 21 fault-slip data, related to compression and extensional stages.	98
Figure 4.6: Distribution of the Karoo basins in Central and Southern Africa.	101
Figure 4.7: Geometry of a simple half graben	102
Figure 4.8: Fault-displacement geometry	103
Figure 4.9: Proposed tectonic and structural model of the Soutpansberg and Tuli Basins.	104
Figure 4.10: Summary of the tectonic setting during deposition of the Tuli and Soutpansberg Coalfields	104

Figure 4.11: Tectonic evolution of the Karoo Basin.....	105
Figure 5.1: The diamictite facies association.....	142
Figure 5.2: Conglomerate	144
Figure 5.3: Clast supported conglomerate	145
Figure 5.4: Formation of point bar sands by lateral accretion	147
Figure 5.5: Major tabular sandstones.....	149
Figure 5.6: Lenticular channels.....	149
Figure 5.7: Lenticular sandstone.....	150
Figure 5.8: Massive reddish brown, khaki to grey sandstone beds	152
Figure 5.9: Planar cross-bedding and trough cross-bedding in the coalfields	155
Figure 5.10: Siltstone	155
Figure 5.11: Shale overlain by sandstone in the Madzaringwe Formation at Mopane Coalfield.....	157
Figure 5.12: FA 7, alternating carbonaceous shale and coal seams in the Madzaringwe Formation at Mopane Coalfield overlain by siltstone layers (FA 4).	158
Figure 5.13: Braided river deposit	161
Figure 5.14: The sub environments of a meandering stream.....	162
Figure 5.15: Block diagram of a rift basin.....	162
Figure 5.16: Schematic block diagrams with sedimentary sequence showing the environments of deposition in the Soutpansberg and Tuli Coalfield.....	164
Figure 5.17: Tabular-planar cross-bedding and trough cross-bedding.	135
Figure 5.18: Constructed paleocurrent directions of the Tshipise-Pafuri	168
Figure 5.19: Constructed paleocurrent directions of the Mopane Coalfield.....	169
Figure 5.20: Constructed paleocurrent directions of the Tuli Coalfield	169
Figure 6.1: Photomicrographs of fine grained, well sorted and grain supported sandstone showing mosaic texture from Tshipise-Pafuri Coalfield	148
Figure 6.2: Photomicrographs of moderately sorted and grain supported sandstone from the Tuli Coalfield	149
Figure 6.3: Photomicrographs showing moderately sorted and grain supported sandstone from Tshipise-Pafuri Coalfield	149
Figure 6.4: Photomicrographs of monocrystalline angular grains with clay matrix in the Tshipise-Pafuri Coalfield	150

Figure 6.5: Photomicrographs of well-rounded and sub-angular quartz grains from the Tuli Coalfield	150
Figure 6.6: Photomicrographs of sub-rounded monocrystalline quartz grains and metasedimentary lithic fragment (Lsm) in the Tshipise-Pafuri Coalfield	151
Figure 6.7: Photomicrographs of silica cementing (arrow) quartz and feldspar.....	151
Figure 6.8: Photomicrographs of a plagioclase feldspar, Mopane Coalfield.....	152
Figure 6.9: Photomicrographs of Clay (illite/smectite) cement around feldspar and quartz grains in the Tshipise-Pafuri Coalfield	152
Figure 6.10: Photomicrographs of detrital muscovite compacted between quartz grains in the Tshipise-Pafuri Coalfield	153
Figure 6.11: Recrystallisation of clay matrix (sericite) shown by arrows around detrital grains and muscovite in the Tshipise-Pafuri Coalfield	154
Figure 6.12: Photomicrographs of hematite cement	155
Figure 6.13: Photomicrographs of hematite cement	156
Figure 6.14: Photomicrographs of inclusions of muscovite flakes in a monocrystalline quartz grain and quartz overgrowth	157
Figure 6.15: Photomicrographs of well rounded monocrystalline quartz grains with overgrowths in the Tuli Coalfield	158
Figure 6.16: Photomicrographs of lithic fragments from the Soutpansberg Coalfield....	159
Figure 6.17: Photomicrographs of lithic fragments from the Tuli Coalfield.....	160
Figure 6.18: Interpretation of the sandstone composition.	205
Figure 6.19: Interpretation of provenance from the petrography of the Tuli and Soutpansberg Coalfields sandstones.	205
Figure 6.20: Q-F-L tectonic provenance diagram.....	206
Figure 6.21: Major elements versus Al ₂ O ₃ graph (sandstone).....	209
Figure 6.22: Major elements versus Al ₂ O ₃ graph (shale).	210
Figure 6.23: Major element Discriminant Function diagram (sandstone) o.....	211
Figure 6.24: Major element Discriminant Function diagram (shale)	212
Figure 6.25: Tectonic-setting discrimination diagram for sandstone using SiO ₂ -log (K ₂ O/Na ₂ O).....	213
Figure 6.26: Tectonic-setting discrimination diagram for shale samples using SiO ₂ -K ₂ O/Na ₂ O.	214
Figure 6.27: Sandstone ternary Na ₂ O-CaO-K ₂ O plot.....	172
Figure 6.28: Shale ternary Na ₂ O-CaO-K ₂ O plot.....	216

Figure 6.29: A-CN-K ternary Al_2O_3 -($\text{CaO}+\text{Na}_2\text{O}$)- K_2O for sandstone.....	217
Figure 6.30: A-CN-K ternary Al_2O_3 -($\text{CaO}+\text{Na}_2\text{O}$)- K_2O for shale	218
Figure 6.31: Log ($\text{Na}_2\text{O}/\text{K}_2\text{O}$) versus Log ($\text{SiO}_2/\text{Al}_2\text{O}_3$) plot.....	219
Figure 6.32: Log ($\text{Fe}_2\text{O}_3/\text{K}_2\text{O}$) versus Log ($\text{SiO}_2/\text{Al}_2\text{O}_3$) plot	220
Figure 6.33: Spider plot of major and trace element compositions for the Soutpansberg and Tuli samples	222
Figure 6.34: TiO_2 versus Ni bivariate plot for the sandstones	223
Figure 6.35: Hf versus La/Th diagram A: shale, B: sandstone.....	224
Figure 6.36: V-Ni-Th*10 triangle diagram A: shale, B: sandstone.....	225
Figure 6.37: Ni-Cr bivariate plot A: shale, B: sandstone.....	226
Figure 6.38: The Th-Sc-Zr/10 tectonic discrimination diagram A: shale, B: sandstone.	227
Figure 6.39: La-Th-Sc tectonic discrimination diagram A: shale, B: sandstone.	228
Figure 7.1: Satellite image of the Tuli and Soutpansberg Coalfields	198
Figure 7.2: Magnetic map of the Tuli and Soutpansberg Coalfields	199
Figure 7.3: Gravity map of the Tuli and Soutpansberg Coalfields	200
Figure 7.4: Gravity map of the Soutpansberg Coalfield.	201
Figure 7.5: Magnetic anomaly map of the Tshipise-Pafuri Coalfield.	202
Figure 7.6: Magnetic anomaly map of the Mopane Coalfield	248
Figure 7.7: Thorium (Th) map of the Mopane Coalfield.....	249
Figure 7.8: Uranium (U) map of the Mopane Coalfield	250
Figure 7.9: Potassium (K) map of the Mopane Coalfield.....	250
Figure 7.10: Magnetic anomaly map of the Tuli Coalfield.	251
Figure 7.11: Thorium (Th) map of the Tuli Coalfield..	252
Figure 7.12: Uranium (U) map of the Tuli Coalfield.....	253
Figure 7.13: Potassium (K) map of the Tuli Coalfield.	254
Figure 7.14: Total counts (Tc) map of the Tuli Coalfield.....	255
Figure 7.15: Tectonic setting of the Tuli and Soutpansberg Coalfields	259
Figure 7.16: Cross-sections of the Tuli and Soutpansberg Coalfields.....	260
Figure 7.17: Idealized formation of some basic types of release faults.....	261
Figure 7.18: Model block diagram and cross-section showing the internal geometry of the Soutpansberg Basin.....	262
Figure 8.1: Proximate analysis of coal samples in the upper seams (Tshipise-Pafuri Coalfield).	270

Figure 8.2: Proximate analysis of coal samples in the middle seams (Tshipise-Pafuri Coalfield).	271
Figure 8.3: Proximate analysis of coal samples in the basal seams (Tshipise-Pafuri Coalfield).	271
Figure 8.4: Averages of all seams in the Tshipise-Pafuri Coalfield.	272
Figure 8.5: Proximate analysis of coal samples in the upper seams (Mopane Coalfield).	273
Figure 8.6: Proximate analysis of coal samples in the middle seams (Mopane Coalfield).	273
Figure 8.7: Proximate analysis of coal samples in the basal seams (Mopane Coalfield).	273
Figure 8.8: Averages of all seams in the Mopane Coalfield.	274
Figure 8.9: Proximate analysis of coal samples in the upper seams (Tuli Coalfield).	275
Figure 8.10: Proximate analysis of coal samples in the middle seams (Tuli Coalfield).	275
Figure 8.11: Proximate analysis of coal samples in the basal seams (Tuli Coalfield).	276
Figure 8.12: Averages of all seams in the Tuli Coalfield.	276
Figure 8.13: Average weight percentages of the ashes in the Soutpansberg and Tuli Coalfields.	280
Figure 8.14: Ternary oxide plots for classification of the coal ash analysis in the Soutpansberg and Tuli Coalfields.	281
Figure 9.1: Photomicrographs of straight contacts between neighbouring framework grains and concavo-convex in the Soutpansberg Coalfield.	245
Figure 9.2: Photomicrographs of plagioclase feldspar, quartz grains and grain-coating clay and pore-lining clays between neighbouring grains in the Soutpansberg Coalfield.	246
Figure 9.3: Pressure solution.	247
Figure 9.4: Fracturing of grains in the Mikambeni Formation of the Soutpansberg Coalfield.	248
Figure 9.5: A: Pore lining clays, B: Pore filling clays	249
Figure 9.6: A: Photomicrographs of Pore filling clays and Pore lining clays in the Mikambeni Formation of the Soutpansberg Coalfield.	250
Figure 9.7: SEM photomicrographs of clay cements in sandstones	251
Figure 9.8: Mechanically infiltrated illite/tsmectite.	252

Figure 9.9: SEM photomicrograph showing a grain being coated by illite/smectite (I/S) in the Madzaringwe Formation of the Tuli Coalfield	253
Figure 9.10: Sketch showing formation of quartz overgrowths.	300
Figure 9.11: EM photomicrographs of sandstone, showing quartz overgrowth cementing quartz grains in Mikambeni Formation in the Soutpansberg Coalfield.....	255
Figure 9.12: Photomicrographs of sandstone, showing quartz overgrowth cementing quartz grain	256
Figure 9.13: Photomicrographs of sandstone, showing quartz overgrowth cementing quartz grains in Mikambeni Formation of the Soutpansberg Coalfield.....	257
Figure 9.14: Calcite cementation in the Mikambeni Formation of the Soutpansberg Coalfield.....	259
Figure 9.15: Partially albitised plagioclase in the Soutpansberg Coalfield	261
Figure 9.16: Partially albitised plagioclase in the Tuli Coalfield	262
Figure 9.17: Paragenesis sequence of the Madzaringwe and Mikambeni Formations in the Soutpansberg Coalfield.....	313
Figure 9.18: Paragenesis sequence of the Madzaringwe and Mikambeni Formations in the Tuli Coalfield.....	315
Figure 10.1: Summary of porosity vs depth curves for different lithologies.....	321
Figure 10.2: Decompaction scheme.....	273
Figure 10.3: The thicknesses of compacted segments compared to decompact segments.....	278
Figure 10.4: The percentage decompaction compared to percentage compaction per formation in basins.....	278
Figure 10.5: Backstripping plots of the Tuli and Soutpansberg Basins.....	280
Figure 10.6: Tectonic subsidence curves of the Tuli and Soutpansberg Basins.....	281
Figure 10.7: Subsidence rates over time and corresponding	282
Figure 10.8: Burial history plots of the Soutpansberg and Tuli Basins.	283
Figure 10.9: Relationship between depth, temperature, and petroleum production	284
Figure 10.10: Burial History and temperature evolution of the Soutpansberg and Tuli Basins.....	285
Figure 10.11: Burial History and porosity of the Soutpansberg and Tuli Basins.....	286
Figure 10.12: Depth plots.	287
Figure 10.13: Flexural and surface profiles illustrating the evolution of the foreland system during stages of orogenic loading and unloading	289

Figure 10.14: Proposed basinal fill model of the Soutpansberg and Tuli Coalfields with major faulting.....291

LIST OF TABLES

Table 2.1: Chronostratigraphic Table of the Soutpansberg and Tuli Basins.	15
Table 2.2: Lithostratigraphic Correlation of the Karoo Supergroup in the Main Basin and study Sub-basins.	21
Table 2.3: The Tuli Basin in South Africa.	24
Table 3.1: A Tentative Correlation of the Lithostratigraphic Units of the Karoo Supergroup.	26
Table 3.2: Average thicknesses of the formations in the studied coalfields.	30
Table 4.1: Threshold values.	88
Table 4.2: Parameters used for estimating the quality of the results of progressive tensor optimisation and fault-slip separation in the Tshipise-Pafuri Coalfield.	119
Table 4.3: Value of the parameters used for estimating the quality of the results of progressive tensor optimisation and fault-slip separation in the Mopane Coalfield.	96
Table 4.4: Value of the parameters used for estimating the quality of the results of progressive tensor optimisation and fault-slip separation in the Tuli Basin.	99
Table 5.1: Lithofacies identified in the Soutpansberg and Tuli Coalfields.	138
Table 5.2: Facies associations identified in the Soutpansberg and Tuli Coalfields.	140
Table 6.1: Framework parameters of detrital modes.	176
Table 6.2: Average of point counting results in percentages of measured sections in the Tuli and Soutpansberg Coalfields.	178
Table 7.1: Densities of common rocks.	192
Table 7.2: Magnetic susceptibilities of common rocks and ores.	194
Table 7.3: Concentration and ratios of U, Th and K in some rocks and minerals.	195
Table 8.1: Standard Classification of Coals by Rank.	266
Table 8.2: Averages of proximate analysis of all seams in the Tuli Coalfield.	270
Table 8.3: Averages of proximate analysis of all seams in the Mopane Coalfield.	272
Table 8.4: Averages of proximate analysis of all seams in the Tuli Coalfield.	275
Table 8.5: Inorganic constituents in coal.	278
Table 8.6: XRF Analysis of coal ash in the Soutpansberg and Tuli Coalfields.	279

Table 9.1: Main differences in diagenesis between the two formations (Mikambeni and Madzaringwe) in the Soutpansberg and Tuli Coalfields.....	311
Table 10.1: The lithostratigraphic units deposited in the Tuli and Soutpansberg Basins.	270
Table 10.2: Compaction coefficients and parameters for main lithological types.	274
Table 10.3: Calculated results for porosity at specific depths, decompacted thickness, Percentage compaction and decompaction and thickness difference for lithostratigraphic units in the Tuli and Soutpansberg Basins.....	277
Table 10.4: Level of thermal maturity for oil.	283

LIST OF APPENDICES

Table A1: Facies classification of fluvial deposits	367
Table B1: Compiled data set for the Tshipise-Pafuri Basin	317
Table B2: Compiled data set for the Mopane Basin	318
Table B3: Compiled data set for the Tuli Basin	319
Table C1: Results of major elements (wt%)	320
Table C2: Results of major elements (wt%)	373
Table C3: Results of X-ray Diffraction (XRD).	374
Table C4: Results of trace elements (ppm)	375
Table C5: Results of trace elements (ppm)	377
Table D1: Data input table for the Backstripping and plotting of the subsidence curve on OSXBackstrip programme.....	379

LIST OF ABBREVIATIONS AND ACRONYMS

Al - Aluminium

Al₂O₃ - Alluminium Oxide

ASTM - American Society for Testing Materials

BSE - Back Scattered Electron

Ca - Calcium

CGS - Council for Geoscience

CIA - Chemical Index of Alteration

CLw - Slip sense confidence level for individual fault applied for the Tensor Program

Co - Cobalt

Cr - Chromium

CZ - Central Zone

DAFF - Department of Agriculture, Forestry and Fisheries

DTw - Fault slip data type

E - East

EDX - Energy Dispersive X-ray microanalyser

EDX - Energy Dispersive X-ray Microanalysis

FA - Facies Associations

Fe - Iron

Fe₂O₃ - Iron Oxide

Fm - Formation

G.P.S - Global Positioning System

Ga - Billion years

Ga - Billion years

Hf - Hafnium

HFSE - High Field Strength Elements

ICV - Index of Compositional Variability

ISO - International Organisation of Standardisation

K- K-felspar

K- Potassium
K₂O - Potassium Oxide
La - Lanthanum
LILE - Large Ion Lithophile Elements
LMB - Limpopo Mobile Belt
LOI - Loss on ignition
Ls - Sedimentary or metasedimentary lithic fragments
Lv - Volcanic or metavolcanic lithic fragments
Ma - Million years
Mg - Magnesium
Mn - Manganese
N - North
Na - Sodium
NaCl - Sodium Chlorite
Nb - Niobium
Ni - Nickel
NMZ - Northern Marginal Zone
P - Plagioclase
PAAS - Post-Archaean Australian Shale
PIA - Plagioclase Index of Alteration
Plen - Fault plain vector
QFL - Quartz Feldspar Lithic fragments
Qm - Monocrystalline quartz
Qp - Polycrystalline quartz
QRt - Tensor Quality Rank
QRwsm - World Stress Map Quality Rank
R - Principal stress difference
Ro - Vitrinite reflectance
S - South
SA - South African / South Africa
SABS - South African Bureau of Standards
SACS - South African Committee of Stratigraphy
SAMREC - South African Mineral Resource Committee
SAWS - South African Weather Service

Sc - Scandium
SEM - Scanning Electron Microscopy
Si - Silica
SiO₂ - Silica Oxide
Slen - Slip direction vector
SMZ - Southern Marginal Zone
Tc - Total counts
TDS - Total dissolved solids
Th - Thorium
Ti - Titanium
TTE - Transition Trace Elements
U - Uranium
UCC - Upper Continental Crust
V - Vanadium
W - West
WSM - World Stress Map
XRD - X-Ray Diffraction
XRF - X-Ray Fluorescence
Y - Yttrium
Zr - Zirconium

CHAPTER 1

INTRODUCTION

1.1. Location of the Study Area

The area investigated in this study is situated in the Limpopo Province of the Republic of South Africa (Figure 1.1). The study area includes the Soutpansberg and Tuli Coalfields hosted by the Soutpansberg and Tuli Basins respectively. The Soutpansberg Basin is situated north of the Soutpansberg Mountain Range and has a strike length of +/-200 km and extends from Waterpoort in the west to the Kruger National Park in the east (Brandl, 1981). The Soutpansberg Basin occupies an area of about 6000 km² and consists of clastic sedimentary rocks (diamictite, conglomerate, sandstone, siltstone, mudstone and coal) and igneous rocks (basalts) (Brandl, 1981). The Tuli Basin or sometimes called Limpopo Basin is situated north-west of Musina and has a strike length of +/- 80 km extending from Point Drift in the west to Beit Bridge in the east. The Tuli Basin occurs across the borders of South Africa, Zimbabwe and Botswana and is filled with sedimentary and igneous rocks of the Karoo Supergroup (Figure 1.1). In the South African part, the Tuli Basin occupies an area of about 1000 km² and consist of various terrigenous clastic and chemical deposits (parabreccias, conglomerate-breccias, conglomerates, sandstones, fine-grained sediments, calcretes and silcretes) (Bordy and Catuneanu, 2002). This area and the scope of the study were determined by the project sponsors.

The Soutpansberg Basin lies between latitudes 22° S and 23° S and longitudes 28° E and 32°E while the Tuli Basin lies between latitudes 21.80° S and 22.50° S and longitudes 29° E and 30° E in South Africa. The area is situated in a dry savannah region, characterised by open grasslands with scattered trees and bushes. Much of the study area is flat lying with elevation varying between 600 m and 900 m above sea level. Most of the rain falls in the summer months between October and March with an average annual rainfall between 300 mm and 600 mm. Winter, with little wind and clear skies, can also be quite hot (average maximum daily temperature of 27°C (SAWS, 2011). Due to the semiarid tropical climate, the area has savanna vegetation dominated by a fairly dense mopani (*Colophospermum mopane*) scrub. Other common tree species are the baobab (*Adansonia digitata*), marula (*Sclerocarya birrea*) and wild fig (*Ficus sycomorus*) (DAFF, 2012).

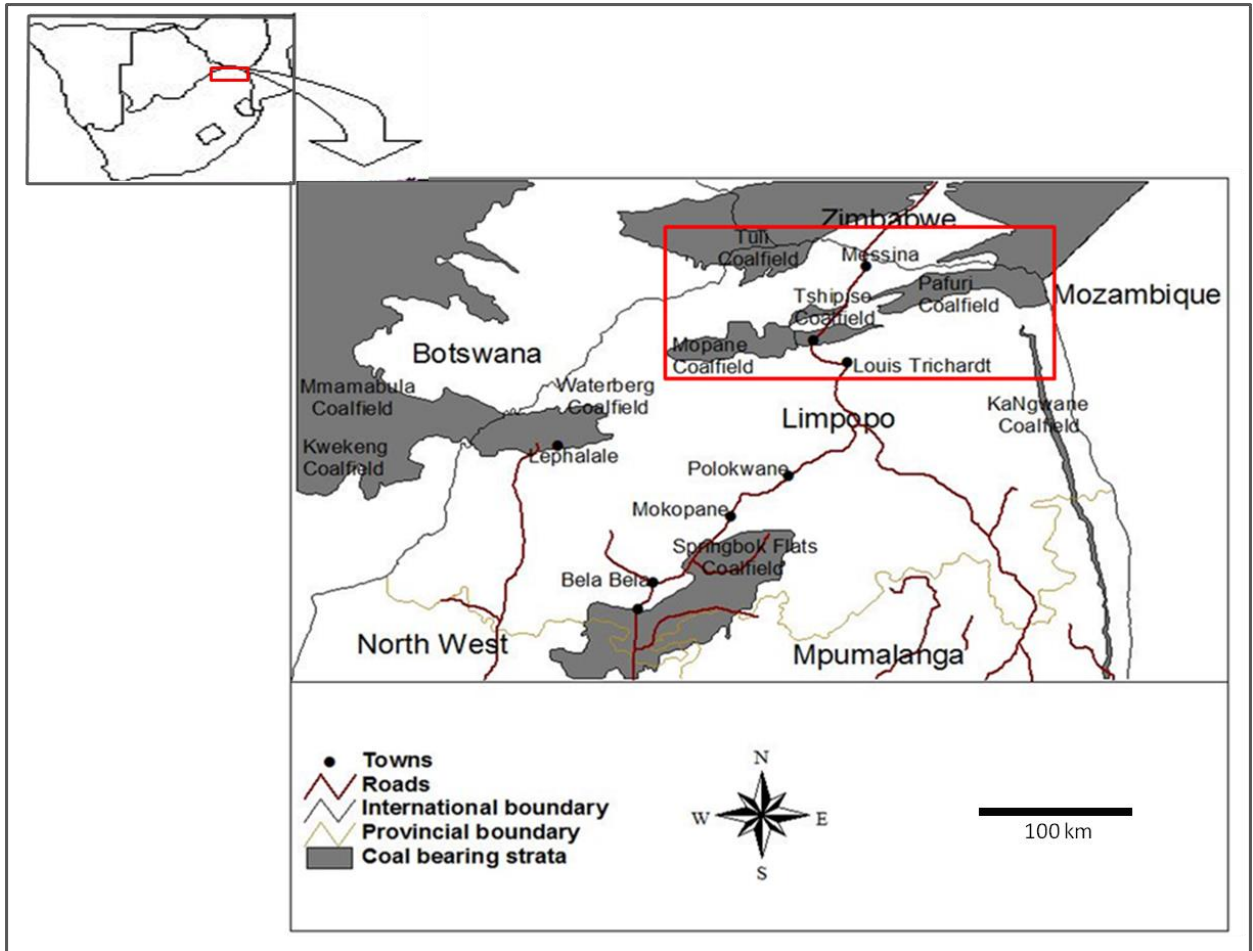


Figure 1.1: Location of the study coalfields (in red border) in relation to other Karoo basins in South Africa and other countries (modified from Snyman, 1998).

The study area is subdivided into several sparsely inhabited farms, with few settlements. Most of the farms function either as game hunting areas, farming areas or as game reserves. All farm names used in the present study are those which appear on the 1:250000 Geological Maps of the Alldays area (Brandl, 2002) and Messina area (Brandl, 1981).

The flat-lying portions of the study areas were accessible by gravel roads, access to the more mountainous areas can only be gained by foot. Flat relatively low-lying areas are generally covered by Quaternary sand and calcrete. Outcrop quality is considerably better along faults and road cuttings and consequently this areas form the main focus of the study.

1.2. Rational

Whilst the published data gives an overview of the geology of the coalfields, there is an absence of integrated analysis of sedimentary study, structure, evolution, mineralogical and geochemical analysis, diagenesis of sandstone, subsidence analysis, geophysics and coal analysis from the study areas. In addition, the collected geometrical data in this thesis compared to inferred depositional environmental in order to make a cohesive contribution to concepts of the evolutionary history of the coalfields. This study is a preliminary basin analysis rather than a definitive and final answer to a complex problem.

1.3. Aims and Objectives of the Study

The purpose of this work is to better define the depositional and evolution history of the Soutpansberg and Tuli Coalfields and quantify the factors controlling the evolution which led to the present geometry of the two coalfields. For this purpose, the project investigated:

- Sedimentary basin formation and classification;
- Depositional environments;
- Provenance, petrography and geochemistry;
- Basin structure and evolution;
- Stratigraphy;
- Tectono-sedimentary interactions and controls on basin fill in order to study the development and evolution of the basin;
- Coal analysis;
- Geophysics;
- Diagenesis and
- Basin analysis techniques like Basin Modelling to analyse the formation and evolution of sedimentary basins.

1.4. Methodologies

Fieldwork in the basins was limited due to the lack of outcrops within the region, and the difficulty to access private game reserves and farms, and this study thus relied mainly on borehole logs bought from the Council for Geoscience (CGS). The organisation kindly supplied over 2000 borehole logs located within the basins. Some boreholes were found to lack stratigraphic information and thus only a limited proportion of the boreholes could thus

be usefully applied to basin analysis study. The aims listed above were achieved by the following methods and procedures:

1.4.1. Comprehensive literature review and data collection

A literature review from scientific reports, exploration data, existing borehole logs, geophysical, geochemical and stratigraphic data has been the primary source of information for this study. This data has been analysed and incorporated into basinal and correlative models that explain the distribution of the various stratigraphic units and deposits within the Soutpansberg and Tuli Coalfields.

1.4.2. Geological fieldwork and sampling

Fieldwork was carried out between March to April 2011 and December 2012. The area shown in Figure 1.1 was mainly mapped on foot, and the use of geological data and field base maps. Navigation in the field was generally accomplished by the use of a G.P.S (Global Positioning System) receiver. Samples of conglomerates, sandstone, siltstone, mudstone and coal were collected for further petrographic studies and geochemical analysis.

1.4.3. Stratigraphy

A detailed review of the spatial stratigraphic variation of the sedimentary successions, including the analysis of facies changes based on widely distributed borehole records, field observations and paleocurrent measurements were performed with the use of Strater Software version. The subsurface data was processed and results were expressed in form of log plots and cross-sections for correlation purposes. Thickness maps of the geological formations (Tshidzi, Madzaringwe and Mikambeni) were constructed using Surfer 10 program.

1.4.4. Sedimentary Facies

The use of borehole data and data collected during the course of the field work was used for facies associations. Field data mostly comprised lithological features, sedimentary structures (primary and secondary structures). Primary sedimentological features were recorded for the identification of sedimentary facies in order to attempt and correlate strata in different parts of the study area and characterise the different depositional conditions. Detailed facies analysis was done using a modified version of Miall's (1988, 1990 and 2000) lithofacies classification scheme. The lithofacies were grouped into facies associations which represented different kinds of depositional environments of the Karoo Supergroup.

1.4.5. Structural Analysis

The fault-slip data were collected by measuring fault planes and slickenlines at different stations in the Soutpansberg and Tuli Coalfields. The measurements at each station included the fault plane, trend and plunge of slickenlines. The fault-slip data was collected from sub-horizontal strata of the Upper Palaeozoic to Lower Mesozoic sedimentary formations of the coalfields. Stress inversion of the fault-slip data was performed using an improved Right-Dihedral method, followed by the Rotational Optimization (WINTENSOR Program by Delvaux, 2012).

1.4.6. Petrographic Studies

Petrographic studies included thin section study by the use of a petrographic microscope, X-Ray Diffraction (XRD) analysis in order to determine the mineralogical composition of all samples. Detrital modes of sandstone suites reflect the different tectonic setting of provenance terranes, relief, depositional environment, diagenetic change, transport mechanism, and climate influence sandstone composition (Dickinson, 1985). The quantitative detrital modes of sandstones can be calculated from point counts of thin sections (Dickinson, 1985).

The Gazzi-Dickinson's point-count method was applied for quantitative compositional analysis. In the point count method, grains were grouped as Qm (Monocrystalline quartz), Qp (Polycrystalline quartz), P (Plagioclase), K (K-felspar), Lv (Volcanic or metavolcanic lithic fragments) and Ls (Sedimentary or metasedimentary lithic fragments). The detrital modes were then recalculated to 100%, excluding matrix, cement, micas, heavy minerals and carbonate grains (Dickinson, 1985). Values obtained are plotted on standard triangular diagrams (QFL) showing compositional fields associated with different provenances (i.e., continental block provenances, recycled orogen, magmatic arc provenances, arc orogen sources, collision suture and thrust belt sources and circum-pacific volcanoplutonic suites) (Dickinson, 1988). The obtained values were also plotted on QFL diagrams (Folk, 1980), which show different sandstone types. For modal analysis, 500 points were counted per thin section.

1.4.7. Geochemical Analysis

The major and trace element geochemistry of the rocks was determined by (XRF) at the Council for Geoscience laboratory, Pretoria. Major element geochemistry of sedimentary rocks is influenced by various factors such as source material, sedimentary processes within

the depositional basin, transportation, diagenesis, physical sorting and weathering (Bhatia, 1983; Bhatia and Crook, 1986;). Accordingly, the major and trace element geochemistry of sandstones can be used as a powerful tool to determine provenance and tectonic setting of sedimentary basins (Bhatia, 1983; Bhatia and Crook, 1986; Roser and Korsch, 1986). Several authors such as Pettijohn *et al.* (1987) and Herron (1988) have used the concentration ratios $\text{SiO}_2/\text{Al}_2\text{O}_3$ vs. $\text{Na}_2\text{O}/\text{K}_2\text{O}$, $\text{Fe}_2\text{O}_3/\text{K}_2\text{O}$ to classify sandstones and the concentration ratios $[\text{Fe}_2\text{O}_3 + \text{MgO}]$ vs. TiO_2 , $\text{Al}_2\text{O}_3/\text{SiO}_2$, $\text{K}_2\text{O}/\text{Na}_2\text{O}$ and $\text{Al}_2\text{O}_3/(\text{CaO} + \text{Na}_2\text{O})$, SiO_2 vs. $\text{K}_2\text{O}/\text{Na}_2\text{O}$] to discriminate tectonic settings of sandstones and sedimentary basins (Bhatia, 1983; Bhatia and Cook, 1986; Roser and Korsch, 1986). Some trace element concentration ratios (La-Th-Sc, Th-Co-Zr/10, Th-Sc-Zr/10, La/Sc vs. Ti/Zr, Sc/Cr vs. La/Y) are also used to discriminate the provenance and tectonic setting of sandstones (Bhatia and Crook, 1986).

1.4.8. Geophysical Techniques

Geophysical techniques (gravity, magnetic and radiometric) were used to outline the distribution of rocks and mineral types, geophysical gravity, magnetic and radiometric properties of the rocks, basement trends and hence give information on the overall structure and distribution of the coal-bearing sequence. The set of data used to process and draw maps came from the extensive geophysical exploration done by the CGS.

1.4.9. Coal Analysis

The borehole data supplied by the CGS also included proximate coal analysis. Proximate analysis determines the fixed carbon, volatile matter, moisture and ash percentages. The analysis was used to establish the rank of coal; to show the ratio of combustible to incombustible constituents; or to provide basis for exploration, buying and selling and otherwise evaluating coal for various purposes.

1.4.10. Diagenesis of sandstone

The description of primary and authigenic mineralogy of the sandstones is based on study of microscope thin sections, including point counting and Scanning Electron Microscopy (SEM). The SEM was useful in determining the rock textures, mineralogy and composition. Polished sections were coated with carbon using a Leica Emitech K950 Evaporator and gold using an Anatech Hummer VI Gold Coater. Scanning Electron Microscopy (SEM) was done by using Jeol JSM 6400, equipped with a link system Energy Dispersive X-ray microanalyser (EDX). The samples were examined in Secondary Electron

Image (SEI) and Back Scattered Electron (BSE) modes of imaging. Both SEM and petrographic microscopy were done at the University of Fort Hare and Rhodes University.

1.4.11. Subsidence Analysis

The subsidence history of the Tuli and Soutpansberg Coalfields was reconstructed by a tectonic subsidence analysis involving the Backstripping technique. The tectonic subsidence computation was done with the OSXBackstrip program which was developed by Cardozo (2012) (University of Stavanger, Norway). The program performs a “1D Airy Backstripping” based on the approach by Watts (2001) and Allen and Allen (2004). It is used for predicting the tectonic subsidence of sedimentary basins. Furthermore, PetroMod 1D Software by Schlumberger was used to construct burial, depth and time plots. The plots included burial history, temperature, porosity, pressure, vitrinite reflectance (R_o) and thermal conductivity of the basins. Finally a basinal fill model of the coalfields was constructed based on the data documented in all the different chapters.

1.5. Outline

This thesis consists of eleven chapters. Chapter 1 provides a brief introduction of the project and also defines the research area; the aims, objectives and statement of the major work undertaken; the methodologies and outline of the thesis. In Chapter 2, the geological background of the Soutpansberg and Tuli Coalfields and the status of research on the two coalfields are summarised, respectively. In Chapter 3, a stratigraphic analysis was carried out on the Late Permian deposits of the Karoo Supergroup in the Limpopo Province in order to understand the depositional processes and stratigraphic framework of the Soutpansberg and Tuli Coalfields. In Chapter 4, the first paleostress analysis results from fault-slip data on the sedimentary rocks of the Late Palaeozoic to Early Mesozoic Karoo Supergroup in the Soutpansberg and Tuli Coalfields is presented in order to understand the structural geology of the area. In Chapter 5, lithofacies analysis was performed with a view to deduce the nature of depositional environments of the deposits of the two coalfields. The petrography, geochemistry and provenance of the rocks in the Soutpansberg and Tuli Coalfields are documented in Chapters 6. Chapter 7 presents the geophysical investigations of the Soutpansberg and Tuli Coalfields which were undertaken in order to understand the surface lithology, structure and intrusive activity based on enhanced products of the recently acquired aeromagnetic, gravity and radiometric data, combined with the published geology and satellite imagery. In Chapter 8, coal analysis of the Soutpansberg and Tuli Coalfields, have

been investigated to establish the rank of coal and to provide basis for exploration. Chapter 9 provides a general account of the diagenesis of sandstones in the Mikambeni and Madzaringwe Formations of the Soutpansberg and Tuli Coalfields. Chapter 10 provides the basin subsidence analysis of the Tuli and Soutpansberg Coalfields. Finally, summary and conclusions of the data documented in the different chapters are presented in Chapter 11.

CHAPTER 2

GEOLOGICAL SETTING

2.1. Regional Geology

Within the study areas, outcrops can be assigned to three chronological units which make up the Karoo Supergroup in the Limpopo Province: the Permian Period which consists of the Tshidzi, Madzaringwe, Mikambeni and Fripp Formations; the Triassic Period which consists of the Solitude, Klopperfontein, Bosbokpoort and Clarens Formations and the Jurassic Period which consists of the Letaba and Jozini Formations (Table 2.1).

Before considering the detailed geology of the coalfields and their surrounding areas (Chapter 3 to 10), this section provides an outline of the general characteristics of the lithological units which are most important in this study. In this chapter the existing stratigraphic names and classifications approved by the South African Committee of Stratigraphy (SACS, 1980) will be used. The primary focus is on the Permian Geology which is a host of the coalfields in the northern part of the country.

2.1.1. The Soutpansberg Coalfield

The Soutpansberg Coalfield in the Soutpansberg Basin can be divided into three sub-coalfields namely the Pafuri (Eastern Soutpansberg), Tshipise (Central Soutpansberg) and Mopane (Western Soutpansberg) Sub-coalfields (Figure 1.1, 2.1 and 2.2). The location and shape of the Soutpansberg Coalfield were controlled by ENE-WSW faults that follow the trend of the Limpopo Belt (Johnson *et al.*, 2006).

The Pafuri Sub-coalfield extends eastwards into the Kruger National Park (Figure 2.1). The only area, where the Limpopo Province coals are being exploited is the Tshikondeni Colliery (Sullivan *et al.*, 1994) in the Pafuri Sub-coalfield. The area measures 109 km from east to west and 26 km from north to south at its widest. The surface geology within the area is dominated by Karoo Supergroup rocks, basalts and Quaternary sediments. The sequence is extensively faulted, with structures being pre-, syn- and post-depositional (Thabo and Sullivan, 2000). Dolerite intrusions are also common. Coals occur in the sandstone-rich Madzaringwe and overlying Mikambeni Formations (Brandl and McCourt, 1980). The Main seam is up to 3.5 m thick and is a composite seam made up of several coal bands interbedded with carbonaceous shale. At the base is the Tshidzi Formation which comprises diamictite interbedded with relatively coarse-grained sandstones.

The Tshipise Sub-coalfield has a similar stratigraphy to the easterly located Pafuri Sub-basin, except that the coal-bearing sequence is thinner and the coal seams are more intimately interlaminated with the mudrock/shale and siltstone (Van der Berg, 1980). In the middle of the basin are quartzite outcrops of the Soutpansberg Group and metasedimentary, amphibolites and granitoids of the Beit Bridge Complex (Figure 2.1). The coal seams are also composite, consisting of alternating bands of coal and mudstone.

The Mopane Sub-coalfield is located west of Tshipise, northwest of Waterpoort (Figure 2.2). The area is 140 km from east to west and is 26 km from north to south at its widest. Rocks of the Karoo Supergroup strike east-west and dip towards the north at angles of up to 12°. The area has been broken up into fault blocks into a number of strike faults. In the south of the area, the Karoo sediments are absent due to uplift and erosion, leaving exposed Beit Bridge Complex and Waterberg Group rocks. The arenaceous Madzaringwe Formation is scarce and sometimes not present here, either due to non-deposition or pinch-out of this unit, from east to west (De Jager, 1986). This deposit is also fault-bounded.

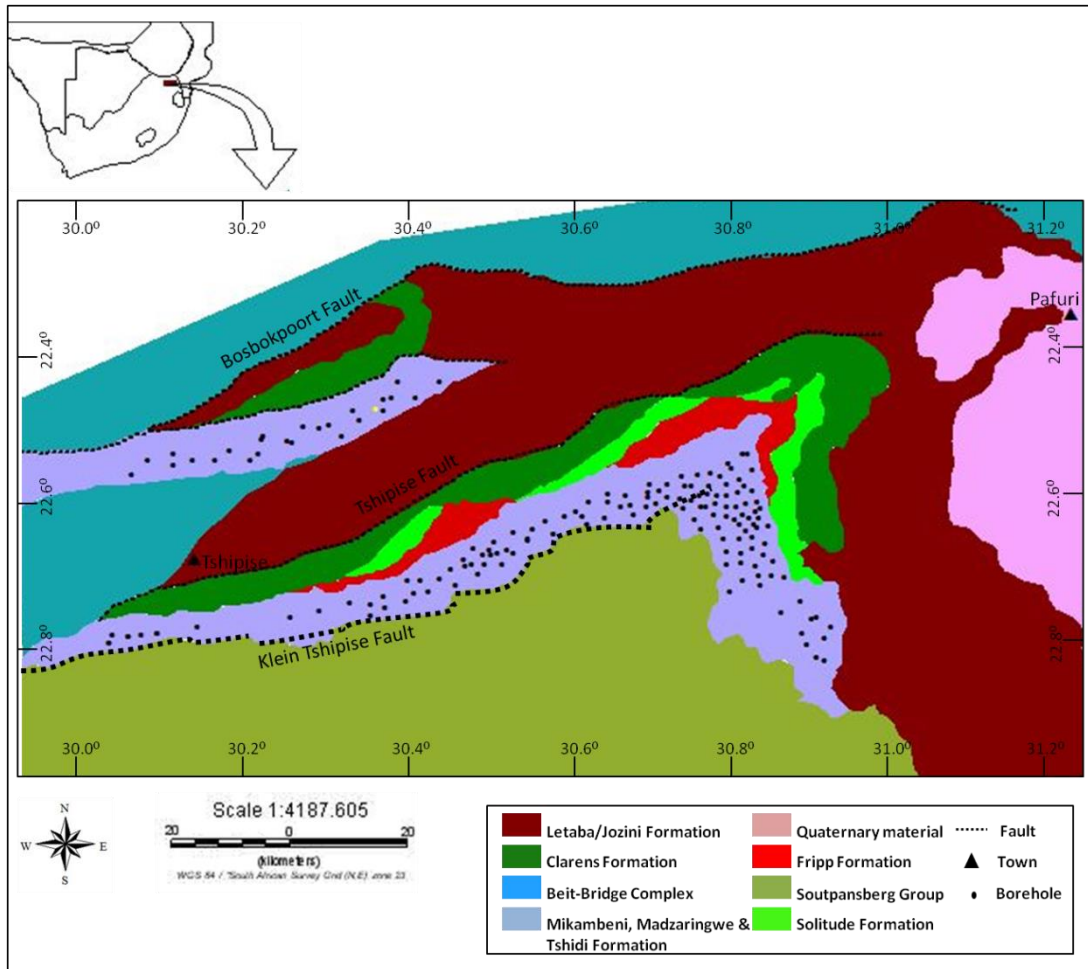


Figure 2.1: Geological map of the Tshipise-Pafuri Coalfield (Eastern and Central Soutpansberg). Modified and redrawn after Visser (1984).

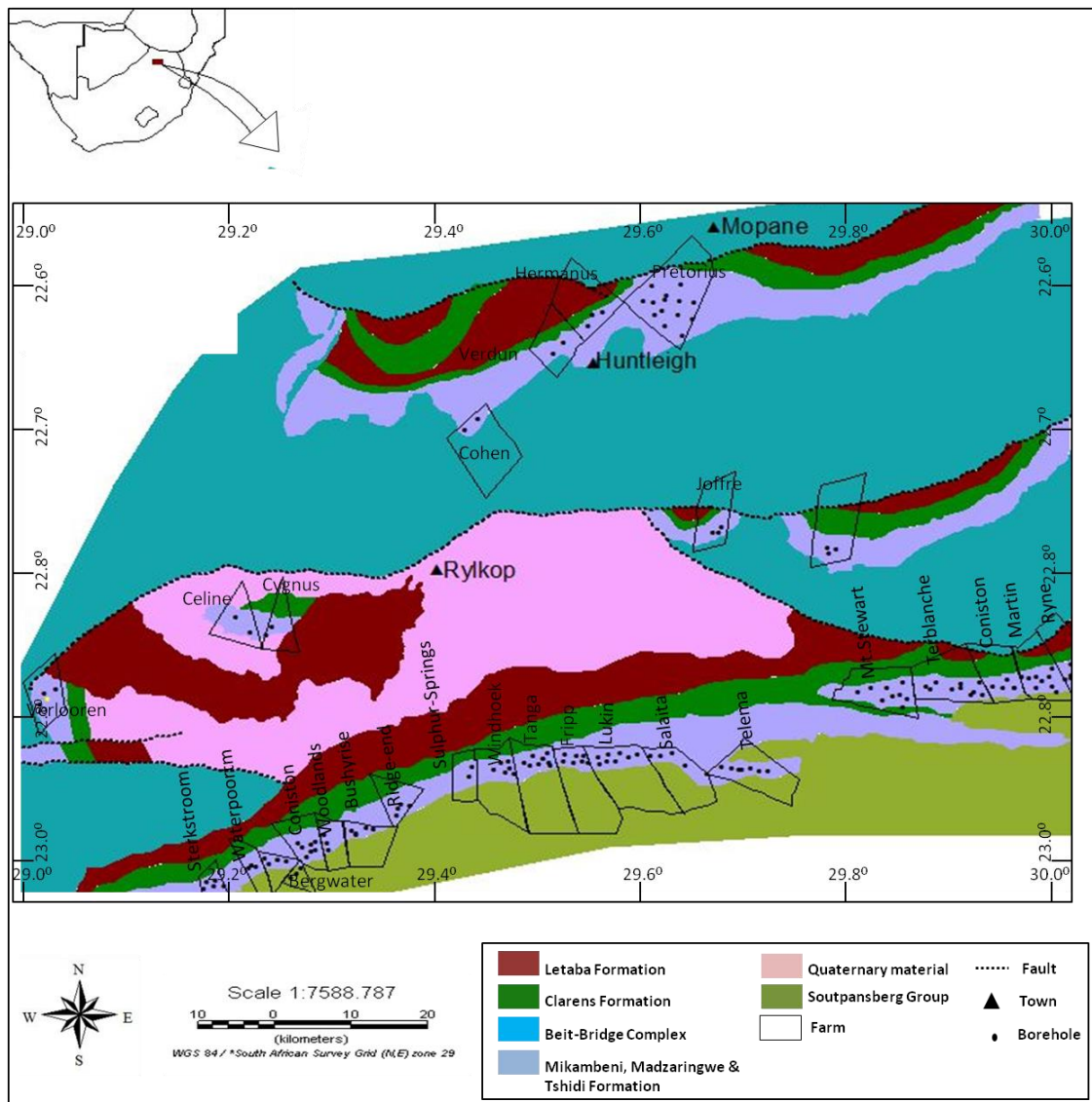


Figure 2.2: Geological map of the Mopane Coalfield (western Soutpansberg). Modified and redrawn from Visser (1984).

The Permian stratigraphy in the Soutpansberg Coalfield from the base consists of the Tshidzi Formation which generally comprises diamictite set in an argillaceous matrix, interbedded with relatively coarse-grained sandstones in places. Succeeding the Tshidzi is the Madzaringwe Formation which comprises up to 200 m of alternating feldspathic, often cross bedded sandstone, siltstone and shale containing coal seams (Brandl, 1981). Succeeding the Madzaringwe Formation is the Mikambeni Formation consists of alternating black shale, sandstone and coal (Johnson *et al.*, 2006).

The Triassic stratigraphy in the Soutpansberg Coalfield consists of the Solitude, Klopperfontein, Bosbokpoort and Clarens Formations (Johnson *et al.*, 2006). The Solitude Formation generally consists of purple to grey mudstones. In some areas, the bottom part of

the lower unit may consist of black shale with occasional bands of bright coal (Johnson *et al.*, 2006). Greenish or reddish, fine to coarse-grained sandstones, up to 5 m thick, occur in places. The Klopperfontein Formation comprises medium to coarse-grained feldspathic sandstone which reaches a maximum thickness of 20 m (Brandl, 2002). The Bosbokpoort Formation comprises of red mudstone to very fine-grained red sandstone. The Clarens Formation has been divided into the Red Sandstone Member and Tshipise Member. The Red Member comprises very fine and fine-grained, light-red, argillaceous sandstone with irregular patches or occasional layers of cream-coloured sandstone. The Tshipise Member consists of fine-grained, well sorted, white or cream-coloured sandstone (Brandl, 1981).

The Jurassic stratigraphy in the Soutpansberg Coalfield consists of the Letaba and Jozini Formations. The Letaba Formation is composed of basaltic lava with subordinate limburgite, andesite, rhyolite flows and turfs. The Jozini Formation is composed of pink to reddish rhyolite (Brandl, 1981).

Three major faults can be recognised in the Soutpansberg Coalfield. The faults trends east-north-east (E-N-E) parallel to the regional strike, and the delineate major host and graben structures (Figure 2.1). The faults are Bosbokpoort, Tshipise and Klein Tshipise Faults. All the faults which affect the basin appear to be normal and probably of post-Karoo age (Brandl, 1981). However, minor faulting also took place and can be recognisable in some areas. They are believed to be prior to the deposition of the Karoo rocks. It is believed that the dip of the Karoo strata in the Soutpansberg Basin is generally to the north and varies between 5° and 15° (Brandl, 1981).

2.1.2. The Tuli Coalfield

The Tuli Coalfield in the Tuli Basin extends into both Botswana and Zimbabwe (Figure 1.1). It is relatively small, east-west-trending, and fault-bounded in which sedimentation was fault-controlled from the onset. The coalfield is filled with the sedimentary and igneous rocks of the Karoo Supergroup (Figure 2.3), (Snyman, 1998). The sedimentary sequence is thinner (estimated maximum ~450-500 m) and less continuous than the correlative late Carboniferous-middle Jurassic sedimentary rocks of the Karoo Supergroup in the main Karoo Basin ~ 6000 m (Catuneanu *et al.*, 1998). In the South African part of the Tuli Basin, the Karoo sedimentary rocks occupy an area of about 1000 km² (Figure 2.3) and consist of various terrigenous clastic and chemical deposits (parabreccias, conglomerate-breccias, conglomerates, sandstones, finegrained sediments, calcretes and silcretes) (Bordy, 2000).

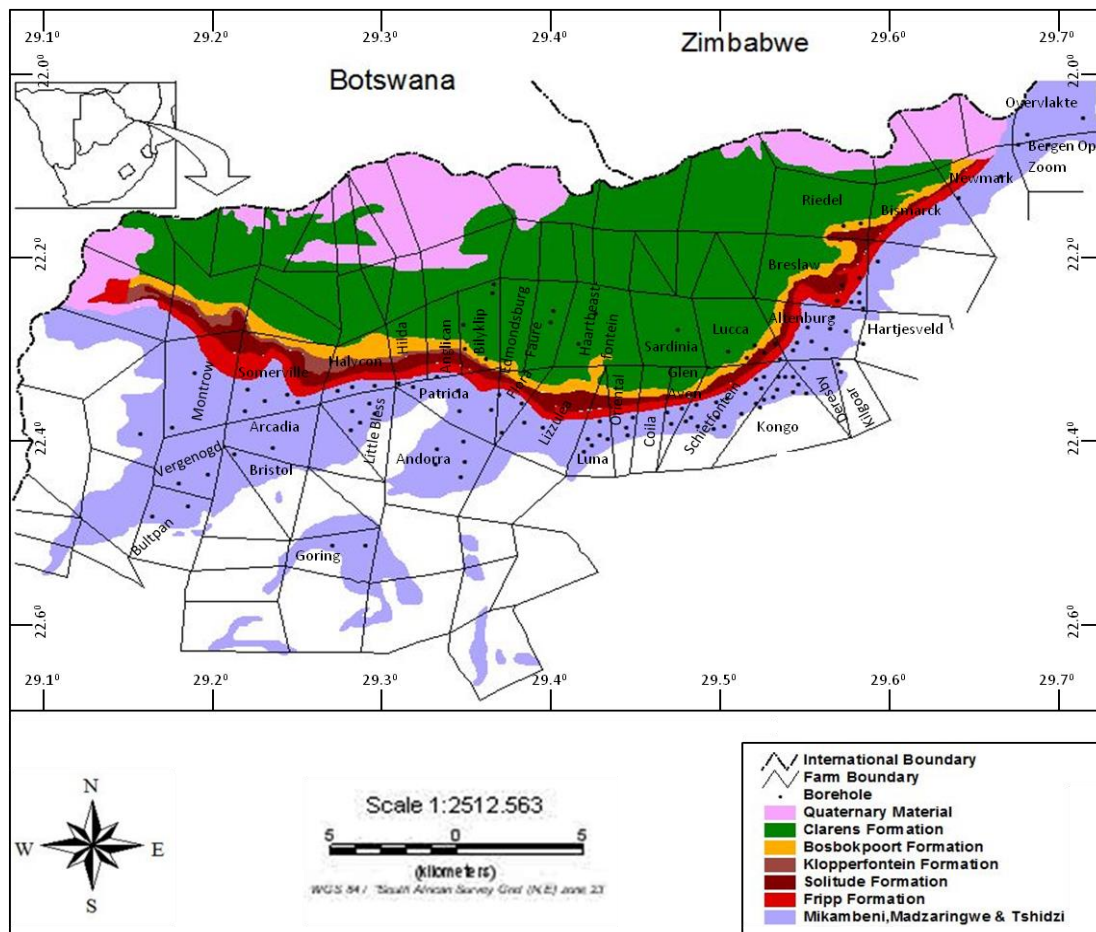


Figure 2.3: Geological map of the Tuli Coalfield. Modified and redrawn after Visser (1984) and Borden and Catuneanu (2002a, b and c).

The Permian stratigraphy in the Tuli Coalfield from the base consists of the Tshidzi Formation which generally comprises diamictite interbedded with relatively coarse-grained sandstones in places (Chidley, 1985). Succeeding the Tshidzi Formation is the Madzaringwe Formation which comprises up to 120 m of alternating feldspathic, often cross bedded sandstone, siltstone and shale containing thin coal seams. The Mikambeni Formation attains a thickness of about 80 m and consists of alternating black shale, sandstone and coal (Chidley, 1985). The Fripp Formation comprises 5-10 m of well-sorted, medium to coarse-grained, white, arkosic sandstone and conglomerates (Chidley, 1985).

The Triassic stratigraphy in the Tuli Coalfield consists of the Solitude, Klopperfontein, Bosbokpoort and Clarens Formations. The Solitude Formation consists of siltstones and very fine sandstones with grey mudstones. Its maximum thickness is about 25 m in the western part of the basin, but in some places is only 3.5 m thick (Chidley, 1985).

Shallow cross-lamination is common in the siltstones. The Klopperfontein Formation comprises coarse sandstone and subordinate conglomerate. It is only present in the central part of the basin and attains a maximum thickness of 10-12 m. The Bosbokpoort Formation consists of red to purple mudstones with subordinate white siltstone layers and some occasional conglomerates. It attains a thickness of up to 60 m (Chidley, 1985).

The Clarens Formation is subdivided into a lower Red Rocks Member and an upper Tshipise Member. The Red Rocks Member comprises of very fine to fine-grained, pinkish to red, argillaceous sandstones. It attains a maximum thickness of about 60 m. The Tshipise Member has a thickness which ranges from 5 to 140 m. It consists of fine to very-fine grained, khaki to yellowish sandstones.

The Jurassic stratigraphy in the Tuli Coalfield consists of the Letaba and Jozini Formations. The Letaba Formation is composed of basaltic lava. The Jozini Formation is composed of basalts. In the Tuli Coalfield there are no major faults although, minor faulting trends east-northeast. The faults are believed to be normal.

Table 2.1 and Figure 2.4 illustrate the stratigraphy and correlation of the Soutpansberg and Tuli Basins.

Table 2.1: Chronostratigraphic table of the Soutpansberg and Tuli/Limpopo Basins (Chidley, 1985).

<i>SOUTPANSBERG AND TULI BASINS</i>		
<i>PERIOD</i>	<i>FORMATION</i>	<i>LITHOLOGY</i>
JURASSIC	Jozini	basalts
	Letaba	basalts
TRIASSIC	Clarens	Sandstone
	Bosbokpoort	sandstone and shale
	Klopperfontein	sandstone and shale
	Solitude	sandstone and shale
PERMIAN	Fripp	sandstone, shale
	Mikambeni	sandstone, shale and coal
	Madzaringwe	sandstone, shale and coal
	Tshidzi	Diamictite

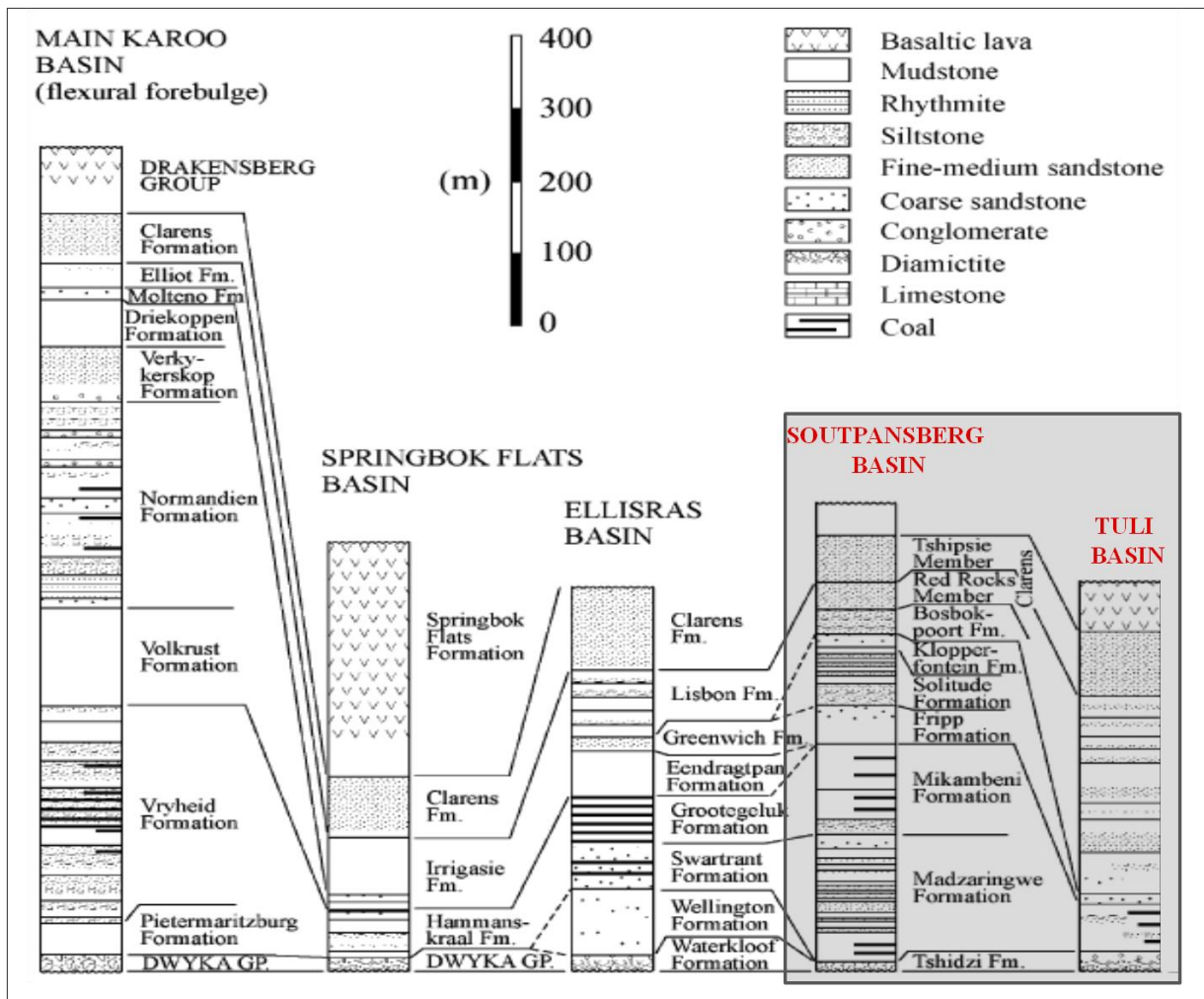


Figure 2.4: Stratigraphy and correlation of the Main Karoo Basin and the Northern sub-basins. The Soutpansberg and Tuli Basins are highlighted (modified after Johnson *et al.*, 1996).

2.2. Previous work in the Soutpansberg and Tuli Basins

Throughout this section, previous published work that has bearing on the present study will be examined, and many of the conclusions of earlier researchers will be highlighted. Although both coalfields in the Limpopo Province have not received much attention from researchers during the last century, more work has been done in surrounding areas, and on related lithologies that has bearing upon the strata within the coalfields.

The most detailed published work directly concerning the geology of the Soutpansberg Coalfield was done by Brandl and McCourt (1980); Brandl (1981); Van de Berg (1980) and the discussions of the area made by de Jager (1986); Sullivan (1995); Thabo and Sullivan (2000). In the Tuli Coalfield more work was done by Chidley (1985); Brandl (2002); Bordy (2000); Bordy and Catuneanu (2001) and (2002a, b and c). The following sections summarises the reasoning and conclusions of the work of Brandl and McCourt

(1980); Van de Berg (1980) in the Soutpansberg Basin, and Chidley (1985); Bordy (2000), Bordy and Catuneanu (2001) and (2002a, b and c); Brandl (2002) in the Tuli Basin.

2.2.1. Summary of the work by Brandl and McCourt (1980) in the Soutpansberg Basin

Brandl and McCourt (1980) recognised that the location and shape of the Soutpansberg Basin were controlled by ENE-WSW faults that follow the trend of the Limpopo Mobile Belt. The original basin was much larger than the extent of the present outcrops, which are preserved in fault blocks.

2.2.1.1. Stratigraphic Units and Depositional Environments recognised by Brandl and McCourt (1980)

Brandl and McCourt (1980) considered two stratigraphic periods namely the Permian and Triassic Periods. The Permian Period consists of four formations: the Tshidzi, Madzaringwe, Mikambeni and Fripp Formations, while the Triassic Period consists of four formations: the Solitude, Klopperfontein, Bosbokpoort and Clarens Formations. Their work was aimed at solving the geology of the formations and examining their depositional and structural patterns.

The Tshidzi Formation has a thickness of up to 20 m in diameter set in an argillaceous or sandy matrix. It is correlated to the Dwyka Group of the main basin. Coarse-grained sandstones are interbedded with the diamictite in places. The thickness of the formation ranges from 5 to 20 m. The diamictite and interbedded sandstone reflects glacial and fluvio-glacial depositional environments.

The Madzaringwe Formation has a thickness of up to 200 m of alternating sandstone, siltstone and shale, the latter containing thin coal seams. The sandstone is feldspathic, micaceous and commonly cross-bedded. The lithologies form fining-upward cycles. The basal 25 to 35 m of the formation comprises carbonaceous shale and thin coal seams. The main coal seam is developed between 85 and 100 m above the carbonaceous zone and is 2 to 3 m thick. A massive coarse-grained, micaceous, feldspathic sandstone, 10 to 15 m thick, caps the formation. The formation reflects a fluvial depositional system. It appears to have been laid down by meandering rivers flowing from the northwest. The sandstone probably represents point bar, levee and crevasse splay deposits. Plant material accumulated in flood basins under cool, reducing conditions, giving rise to coal seams.

The Mikambeni Formation has a thickness of up to 150 m of mudstones, shales and laminated sandstones. The formation consists of three recognisable units: a lower unit of

alternating black shale and grey, feldspathic sandstone 15 to 20 m thick; a 50 m thick middle unit of black carbonaceous shale with occasional bright coal seams and an upper unit comprising dark grey mudstone with plant fragments and occasional bright coal. The overall fine-grained character of the rocks points to deposition on the distal floodplains of meandering rivers.

Overlying the Mikambeni Formation is the Fripp Formation of the Beaufort Group of the Permian age. This unit is up to 110 m thick and comprises medium to coarse-grained feldspathic sandstones (grit) with thin pebble layers. The sandstone is interbedded with thin siltstone and mudstone and trough cross-bedding is present. The sandstones were probably deposited by braided river systems flowing towards the northwest and west. Overlying the Fripp formation is a sequence of units of Triassic and Jurassic age. The Triassic period is represented in the region by four clastic formations comprising interbedded siltstone, sandstone, feldspathic and coarse grained in part. These are followed upwards by mudstone, siltstone and sandstones of various colours. The clastic units are capped by the Clarens sandstone which is widely inundated by Jurassic age lavas which complete the succession in the area.

The lowest unit of the Triassic is the Solitude Formation. It is characterised by purple mudstones and grey shales with a maximum thickness of approximately 170 m. At the type locality on the farm Solitude, outside the area of this application, 30 m of grey shale is overlain by 80 m of alternating purple and grey mudstone with three intercalated siltstone units. In other parts of the basin, the lower unit of the formation may consist of black shale with occasional bands of bright coal and greenish or reddish fine to coarse-grained sandstone up to 5 m thick. The formation represents the overbank deposits of meandering rivers with extensive floodplains. The dark shale and associated coals accumulated in flood basins and marshes under reducing conditions.

Overlying the Solitude Formation is the Klopperfontein Formation. This formation comprises of medium to coarse-grained, cross-bedded, feldspathic sandstones and attains a maximum thickness of 20 m. Deposition was from braided river channels. This is followed by the Bosbokpoort Formation, which comprises up to 100 m of mainly red mudstones to very fine-grained sandstones. The red colours and abundance of concretions suggest deposition on the floodplains of meandering rivers under dry oxidising conditions.

The overlying Clarens Formation consists of the Red Rocks Member (up to 150 m thick unit of very fine to fine-grained light red sandstone with occasional thin cream-coloured

sandstone layers) and the Tshipise Member (approximately 150 m thick unit of fine-grained, white or cream coloured sandstone with calcareous concretions near the base and large scale cross-bedding). The Clarens Formation is considered to be aeolian, but water-lain deposits may be present in the lower part of the succession.

2.2.1.2. Structural Geology and Basin Evolution of the Soutpansberg Basin proposed by Brandl and McCourt (1980)

Brandl and McCourt (1980) noted that the Karoo Supergroup represents a variety of sedimentary environments which reflect the migration of the Gondwana continent from polar to lower latitudes over a period of 200 Ma. The final phase of sediment deposition was terminated by voluminous Jurassic outpouring of basaltic magma associated with the final break-up of the Gondwana continent. The rocks of the area reflect a complex deformation history. The Beit Bridge Complex underwent ductile deformation in the Archaean and possibly in the early Proterozoic, followed by brittle deformation of the Soutpansberg and Karoo strata during the Phanerozoic period.

The Beit Bridge Complex, Limpopo Orogeny and the Karoo strata

Roering *et al.* (1992) in Brandl (2002) proposed that the collision of the Zimbabwe and Kaapvaal Cratons (2.7 Ga), was accompanied by a major northward-verging thrust system. It is not known whether the Central Zone of the Limpopo Belt was at that time already attached to the Kaapvaal Craton, or was only caught up between the two cratons. The authors cited a number of circular and oval structures as evidence for deep-crustal northward-directed shearing. The foliation associated with these features defines cylindrical structures that plunge moderately to the south. As an accompanying mineral extension lineation plunges in the same direction, these structures are interpreted as large-scale sheath folds.

Fripp (1981); Watkeys *et al.* (1988); Watkeys (1984); Pienaar (1985); Pretorius (1992) came with a different view, maintaining that several temporally distinct deformational events have affected the Central Zone. The first structure generally recognised (D_1) is a prominent foliation, defined by mafic minerals, which is parallel to lithological layering. This was followed by isoclinal recumbent folding (D_2) about east trending horizontal axes. Subsequently the rocks were folded (D_3) about upright axial surfaces which trend mainly in a north-westerly direction, but locally as in the Mogalekwena River area, in a northerly

direction. In the last less severe event (D₄) all these structures were modified about northeast-trending axes and this gave rise to prominent dome and basin structures.

Movement along the Limpopo Mobile Belt (LMB) as tectonic re-activation due to continuous tension in the Karoo era, in the Soutpansberg and Limpopo fault zones occurred, controlled the formation of the Karoo sediments and finally acted as conduits for the extrusion of basalts which terminated the Karoo era (Barker, 1983). The Soutpansberg Basin is situated mainly in the South Marginal Zone and partly in the Central Zone of the Limpopo Orogenic Belt. The Tuli Basin is situated in the Central Zone (Figure 4.1).

2.2.1.3. Summary (Brandl and McCourt, 1980)

The Limpopo orogeny is generally believed to have occurred around 2.65 Ga, although it has never been dated directly. The Karoo strata of the Soutpansberg Basin are slightly tilted to the north-northwest at an angle of 10° to 20°. Intense block-faulting caused the development of a series of stepped half-grabens and these are now seen as repeatedly occurring narrow strips of Karoo rocks mostly around the Tshipise-Pafuri Basin.

Table 2.2: Lithostratigraphic Correlation of the Karoo Supergroup in the Main Karoo Basin and studied Sub-basins (SACS, 1980).

SUPERGROUP	GROUP	SUBGROUP	BASIN TYPE					
			Main Karoo Basin			Sub-basins		
Karoo			South Western Cape Province	Eastern Cape Province	KwaZulu Natal	Limpopo Province (Soutpansberg)	Limpopo Province (Tuli)	
	Lebombo			Drankensberg	Movene Jozini and Letaba	Letaba	Letaba	
	Stormberg			Clarens, Elliot Molteno	Clarens Nyoka Ntabeni	Clarens Bosbokpoort Kloperfontein Solitude	Clarens Bosbokpoort Kloperfontein Solitude	
	Beaufort	Tarkastad		Burgersdorp Katberg	Emakwezeni	Fripp	Fripp	
		Adelaide	Teekloof Abrahamskraal	Balfour Middleton Koonap				
	Ecca			Waterford	Waterford	Volkrust	Madzaringwe	Madzaringwe
				Fort Brown	Fort Brown			
				Laingsburg		Vryheid		
				Vischkuil	Ripon	Pietermaritzburg		
				Collingham	Collingham			
				White Hill	White Hill			
				Prince Albert	Prince Albert			
Dwyka					Tshidzi	Tshidzi		

2.2.2. Summary of the work by Chidley (1985) in the Tuli Basin

Chidley (1985) recognized that the Tuli Basin is a small intracratonic east-west trending fault controlled depository with a preserved basin width of 80 km. The East-west trend parallels the Soutpansberg Basin. The Karoo sedimentation was fault controlled from the onset.

2.2.2.1. Stratigraphic Units and Depositional Environments recognised by Chidley (1985)

Chidley (1985) adopted Brandl and McCourt's 1980 subdivision of the Tshipise and Kruger National Park area. The sub-division is the same as those used in the Soutpansberg Basin area. The lower most part of the Karoo succession, the Tshidzi Formation was deposited on a markedly uneven floor of the Beit-Bridge gneisses. The formation is represented by diamictite composed of angular blocks and fragments, derived from the angular strata. The clasts can measure up to 80 m in diameter and the rest is a matrix of coarse sand or grit. These diamictite occur irregularly and infrequently. They are considered

to be older than the Karoo Supergroup rocks. Where diamictite deposits are absent, grits rests directly on the Beit-Bridge gneisses.

The grits pass upwards into laminated shale of the Madzaringwe Formation, with intermittent lenses of red and yellowish grit in its lower part. The shales are generally grey and brown weathering, but occasional yellow and red horizons occur. A distinct coal zone of up to 20 m thick is developed higher up in this shale. The zones contain six independent continuous seams. The shales could be part of a flood-plain sequence, which could explain the various reddish and yellow discolourations.

The succeeding Mikambeni Formation comprises 15 m of grey (sometimes carbonaceous) or yellowish shales and siltstones with occasional coal seams. The mudrocks closely resemble those of the Madzaringwe Formation lying below the upper sandstone unit, and represent a return to shallow lacustrine conditions. The Fripp Formation comprises 5 to 10 m of clean, well sorted, and medium to coarse-grained, white arkosic sandstone, together with gritty layers and conglomerate lenses. The high feldspar content suggests rapid deposition from strongly uplifted granitic rocks, probably as point-bar and channel-lag deposits.

The Solitude Formation consists of siltstones and very fine sandstones with subordinate mudstones. It attains a maximum thickness of about 25 m in the western part of the basin, but in some places, it is only 3.5 m thick. The multi-coloured nature of the sediments, and the development of climbing ripples, is typical of fine-grained distal flood-plain overbank and crevasse-splay deposits associated with mature meandering streams.

The Klopperfontein Formation is only present in the central part of the basin and attains a maximum thickness of 10 to 12 m. It comprises coarse sandstone and subordinate conglomerate. The formation probably represents a proximal bedload dominated fluvial wedge associated with fast-flowing braided streams.

The Bosbokpoort Formation consists of up to 60 m of brick-red to purple mudstones with subordinate white siltstone layers and occasional conglomerate. The formation represents a long, relatively quiescent period of sub-aerial flood-plain deposits associated with mature meandering streams. The Clarens Formation is subdivided into two members namely, the Lower Red Rocks Member and an Upper Tshipise Member. Together the two attains a maximum thickness in the order of 200 m, the upper three-quarters of which represents the Tshipise Member.

The Red Rocks Member is up to 60 m thick and comprises very fine to fine-grained, pinkish to red, argillaceous sandstones. In the north-eastern part of the basin a wide-spread brick-red mudstone, up to 5 m thick, occurs 2 to 3 m below the top of the member. In the eastern part of the area a calcareous conglomerate about 3 m occurs. Trough cross-bedding developed in the conglomerate in places suggest a channel-fill origin. The Red Rocks argillaceous sandstone with climbing ripples suggest overbank deposition on a flood-plain associated with mature meandering streams.

The Tshipise Member sandstones cover much of the northern part of the basin and characteristically form flat-topped koppies. The thickness of the formation ranges from 5 to 140 m. The Tshipise sandstones were deposited by Aeolian processes under arid conditions, although waterlain sandstones were observed at several localities.

2.2.2.2: Structural Geology and Basin Evolution of the Tuli Basin proposed by Chidley (1985)

The two theories of the Beit-Bridge Complex, Limpopo Orogeny and the Karoo strata discussed in Section 2.2.1.2, apply to the Tuli Basin evolution. Chidley (1985) recognised that the Tuli Basin is a small intracratonic east-west-trending fault-controlled depository with a preserved basin width of 80 km. The east-west trend parallels the Soutpansberg Basin. The Karoo sedimentation was fault controlled from the onset.

2.2.3. Summary of the work by Bordy (2000); Bordy and Catuneanu (2001); (2002a, b and c)

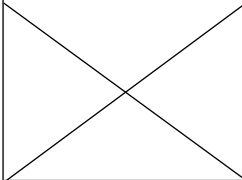
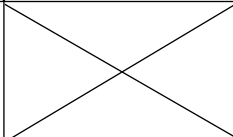
Bordy (2000); Bordy and Catuneanu (2001); (2002a, b and c) came up with a different naming of the lithology in the basin. The following four lithologically and genetically distinctive lithostratigraphic units are differentiated in their study; the informal Basal, the Middle and Upper Units, and the formal Clarens Formation (Bordy and Catuneanu, 2002a, b and c) (Table 2.3). In their paper they presented the findings of the sedimentological and paleontological investigation of the fluvial clastic deposits and aeolian strata of the basin.

According to a study by Bordy and Catuneanu (2002a, b and c), eighteen identified lithofacies types are grouped into three major facies associations: the gravelstone facies assemblage; the sandstone facies assemblage and the fine-grained facies assemblage.

The Basal Unit is composed of three sedimentary facies assemblages (Bordy and Catuneanu, 2002a and b).

- Gravelstones (breccias and conglomerate-breccias) with subordinate sandstones and siltstones.
- Sandstones with subordinate conglomerate and conglomerate-breccia intercalations.
- Fine-grained rocks.

Table 2.3: The Tuli Basin in South Africa.

Tuli (South Africa), (Bordy and Catuineanu, 2002a, b and c)		Tuli (South Africa), (Chidley, 1985 & Geological Map Alldays, 2002)	
Clarens Formation		Clarens Formation	Tshipise Member
Upper Limit			Red Rocks Member
		Bosbokpoort Formation	
		Klopperfontein Formation	
Middle Unit		Solitude Formation	
Basal Unit (Undifferentiated)		Fripp Formation	
		Basal Beds	Mikambeni Formation
			Madzaringwe Formation
			Tshidzi Formation

CHAPTER 3

STRATIGRAPHY OF THE SOUTPANSBERG AND TULI COALFIELDS

Abstract

A stratigraphic analysis was carried out on the Late Permian deposits of the Karoo Supergroup in the Soutpansberg and Tuli Coalfields of the Limpopo Province in order to understand the depositional processes and stratigraphic framework of the coalfields. In this study, focus is on the Permian stratigraphy in the Tuli and Soutpansberg Basins, which is a host of the coal seams. This portion in the Limpopo region includes the distinctive glacial tillite (diamictite) of the Tshidzi Formation in the bottom, the fluvial sedimentary rocks of the Madzaringwe Formation, containing most of the coal seams and the fluvial sedimentary rocks of the Mikambeni Formation with minor coal seams. Borehole log studies were used to understand lithostratigraphic correlations and establish comparisons with others parts of the Karoo Main Basin. Isopach maps and cross-sections were drawn to establish the basinal stratigraphic framework in order to understand the spatial and temporal distribution of the different genetic units in the coalfields. Different fluvial systems, including braided and meandering river systems, can be identified based on channel-sandstone geometrics, sedimentary structures and depositional facies associations. The frequent occurrence of coal seams indicates widespread development of forests and swamps on floodplains in a humid and warm climate. The Tshidzi Formation is developed at the base of the Karoo Sequence and consists of diamictite. The Madzaringwe Formation is divided into three members: the Basal Member, a laminated, grey and black carbonaceous shale and coal; the Middle Member, alternating beds of shale and fine-coarse grained sandstone to siltstone; Upper Member, a laminated, grey and black carbonaceous shale and coal. Succeeding the Madzaringwe Formation is the Mikambeni Formation. This formation can be subdivided into two members (Lower and Upper Members). The Lower Member is characterised by laminated, grey and black carbonaceous shale and coal and sandy shale/mudstone. The Middle Member is characterised by alternating beds of shale and fine-coarse grained siltstone. The quantification of the lithologies at different stages of basin evolution led to the reconstruction of generalised stratigraphic columns of the coalfields.

3.1. Introduction

As mentioned in Chapter 1, the Soutpansberg and Tuli Coalfields are assigned to the sedimentary portion of the Karoo Supergroup. This portion in the Limpopo Region includes

the distinctive glacial tillite (diamictite) of the Tshidzi Formation in the bottom, the fluvial sedimentary rocks of the Madzaringwe Formation, containing most of the coal seams, the sedimentary rocks of the Mikambeni Formation, which also hosts thin coal seams and the sedimentary rocks of the Fripp, Solitude, Klopperfontein, Bosbokpoort and the Clarens Formations. The volcanic Letaba Formation occurs on the top (Table 3.1).

Table 3.1: A Tentative Correlation of the Lithostratigraphic Units of the Karoo Supergroup in the far Northern Sub-basins with those of the Main Basin. The bolded columns show the studied coalfields (After SACS, 1980; De Jager, 1986; Roberts, 1992; Johnson *et al.* 1986).

Soutpansberg (SACS 1980)	Tuli/Limpopo (De Jager 1986)	Elisras (De Jager 1986; Johnson et al. 1996)	Springbok Flats (Roberts 1992)	Main Karoo basin (Johnson et al. 1996)
Letaba Formation ca. 300m, basalt & limburgite	Letaba Formation ca. 5 m, basalt, limburgite	Letaba Formation ca. 120 m basalt	Letaba Formation ca. 600 m basalt	Drakensburg Group
Clarens Formation ca. 300m, fine-grained sandstone	Clarens Formation ca. 90 m, fine-grained sandstone	Clarens Formation ca. 130 m fine-grained sandstone	Clarens Formation ca. 150 m fine-grained sandstone	Clarens Formation
Bosbokpoort Formation ca. 60m, reddish, mudstone, siltstone and sandstone				
Klopperfontein Formation ca. 20m course feldspathic sandstone	Elliot Formation ca. 130 m, reddish mudstone, siltstone and sandstone	Lisbon Formation ca. 100 m reddish mudstone, siltstone and sandstone	Worthing Formation ca. 80 m reddish sandstone, siltstone, mudstone	Elliot Formation
Solitude Formation ca. 110m greyish shale, purple and grey mudstone, sandstone and minor coal				
Fripp Formation ca. 120m gritty feldspathic sandstone, conglomerate	Molteno Formation ca. 20 m, fine sandstone	Greenwich Formation ca. 30 m fine sandstone	Codriron Formation ca. 30 m sandstone, conglomerate	Molteno Formation
		Eendragtpan Formation ca. 70 m mudrock	Lehun Formation ca. 30 m grey to reddish mudrock	Normandien Formation
Mikambeni Formation ca. 130 m, mudstone, shale, coal	Volkstrust Formation ca. 60 m, mudstone, main coal zone	Grootegeeluk Formation ca. 60 m mudstone, coal; Goedgedacht Formation	Wambard Formation ca. 12 m alternating coal and mudrock	Volkstrust Formation
Madzaringwe Formation ca. 220 m mudstone, sandstone, coal		Vryheid Formation ca. 50 m sandstone, siltstone, mudstone, coal	Turfpan Formation ca. 100 m sandstone, siltstone, mudstone, coal	Vryheid Formation
Tshidzi Formation ca. 30 m conglomerate, diamictite	Dwyka Group ca. 10 m conglomerate, diamictite	Dwyka Group ca. 10 m conglomerate, diamictite	Merinovlakte Formation ca. 20 m diamictite, varved mudrock	Dwyka Group

This chapter aims to investigate the stratigraphy and sedimentology of fluvial systems of the Soutpansberg and Tuli Coalfields. The sedimentary processes and sediment body architecture of the Late Permian deposits are examined. In this chapter stratigraphical procedures are applied, reviewed and discussed by making a distinction between different units.

3.2. Methodology

A detailed review of the spatial stratigraphic variation of the coal-bearing successions, including the analysis of facies changes based on over 2000 widely distributed borehole records, field observations and paleocurrent measurements were performed with the use of Strater Software version. The subsurface data was processed and results were expressed in form of log plots and cross-sections for correlation purposes.

The borehole data resulted from extensive coal exploration activities in the study area by different companies over the past 50 years. However some borehole logs lack stratigraphic information, and only a limited proportion of the boreholes data could be applied to stratigraphic and basin analysis studies. The borehole core log descriptions yielded little information on the structure and sedimentary characteristics of the rock sequences. To bridge this information gap, an extensive literature review on reports relevant to this study (e.g. from Brandl, 1981; Bordy and Catuneanu 2002a, b and c) was utilized. All borehole data used in this study was taken from the Council for Geoscience (CGS) archives.

Structure contour maps of the basins were constructed using the structural elevation of the upper surface of the basins. Contours were made with a modern digital contouring program (Surfer 10, a product of Golden Software Inc.). Thickness maps of the geological formations (Tshidzi, Madzaringwe and Mikambeni) were constructed using Surfer 10 program.

Since the borehole data were from different companies with different descriptive standards, it was necessary to convert the descriptions to a common format before the data could be used for lithostratigraphic subdivision correlation and lithofacies analysis. The contouring was digitally done using Surfer 10, a modern digital contouring. The contours were smoothed with the high smoothing option in order to remove the straight-line aspects of contours that are made without the smoothing option. Although smoothing results in contours more rounded and look more natural, this option can locally cause contour lines to cross over each other in areas where contour spacing is very close. One of the drawbacks to the kriging method in the gridding of data is that the method can extrapolate structural elevation values beyond the known range of values, thereby producing a map that in places may have unrealistically high or unrealistically low contours. However, kriging generally minimizes this effect compared to other gridding techniques and generally results in contours that more closely approximate a good hand-contoured map than other gridding techniques.

The stratigraphic subdivisions of the lower part of the Karoo Supergroup in the Limpopo region (Tshidzi, Madzaringwe and Mikambeni Formations) are adopted for the Soutpansberg and Tuli Coalfields and this part is a host of the region's coal. As mentioned earlier all the information presented in this study regarding the two coalfields is mainly derived from data collected during extensive coal exploration by various mining companies and the Council for Geoscience (CGS). Cross-sections were drawn to establish the basinal stratigraphic framework in order to understand the spatial and temporal distribution of the different genetic units of the coalfields. The structure contour maps of the Soutpansberg and Tuli Coalfields were constructed using the structural elevation of the upper surface of the basins in over 2000 borehole logs. These logs are shown in 29 cross sections of the coalfields (Figures 3.1 to 3.48). The names Tshidzi, Madzaringwe and Mikambeni Formations have been proposed by the South African Committee for Stratigraphy (SACS) for the lower Karoo Supergroup in the coalfields. These lithostratigraphic names are adhered to in this study.

3.3. Stratigraphic approach to coal-bearing strata

Stratigraphy is the study of sediments and sedimentary rocks in terms of repetitively arranged facies and associated stratal geometry (Van Wagoner *et al.*, 1988). It permits re-interpretation of well-known coal-bearing strata, solving some of the problems regarding coal seam formation, stratigraphic record and cyclicity (Holz *et al.*, 2002; Diessel, 2007). The investigation of coal formation and recognition of key surfaces within the stratigraphic framework of coal-bearing basins provide a clue for the formation of coal seams.

Petrographic parameters such as vitrinite content and type; vitrinite reflectance, etc., often show significant variation from seam base to top and can be related to the changes of water level and depositional regime (transgressive vs. regressive) under which the precursor peat accumulated (Diessel, 2007). With a good stratigraphic framework of a coal basin followed by a detailed petrographic, mineralogical, structural, geophysical and geochemical analysis of coal seams, coal quality may be predicted and guidelines to exploration could be provided.

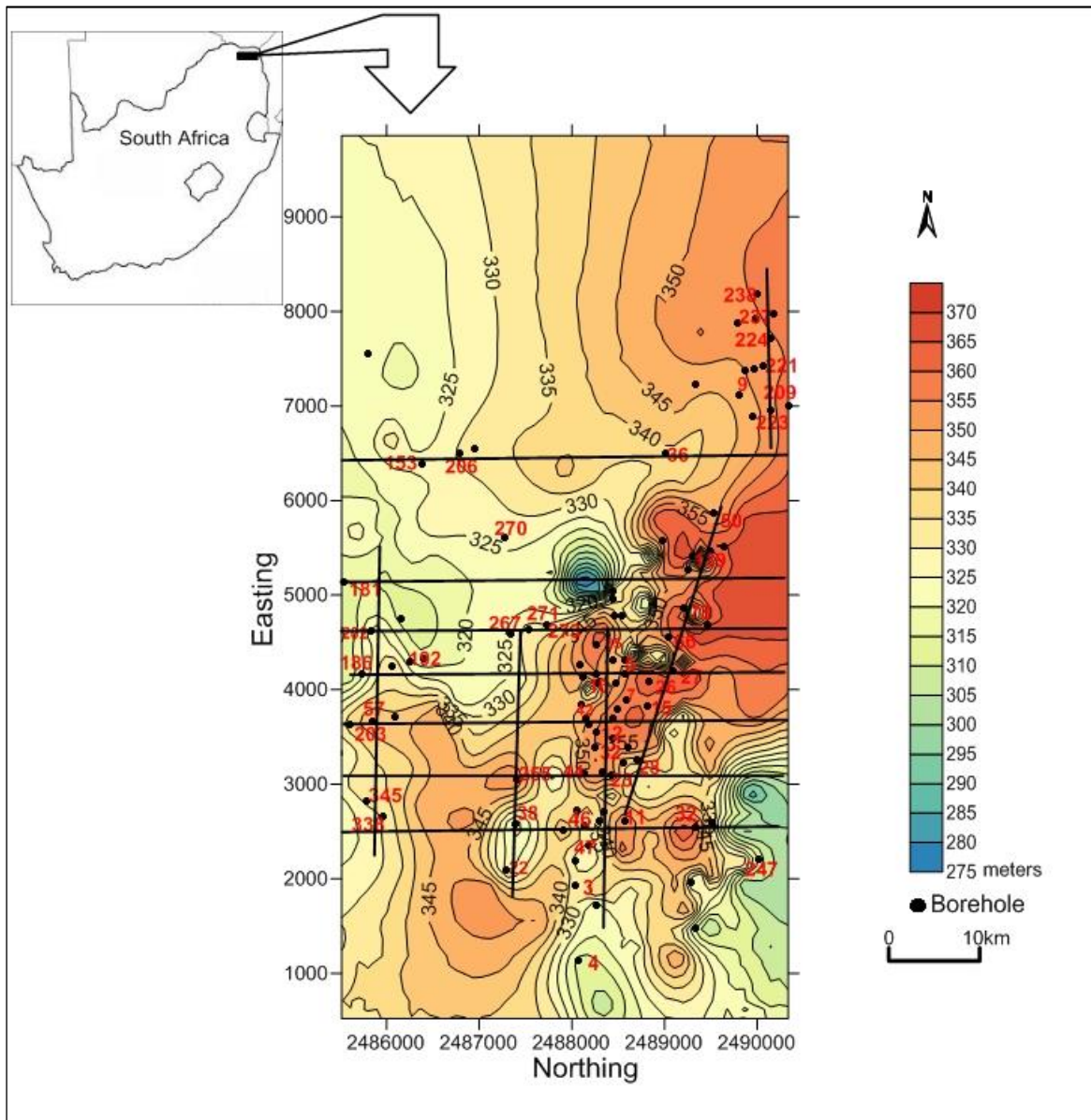


Figure 3.1: Topographic contour map and cross-section lines of the Tshipise-Pafuri Coalfield.

Because the Karoo Supergroup was affected by post-Karoo denudation events, the precise lateral thickness variation of the unit could not be determined from the outcrops. One hundred and twenty two (122) drill hole sections served to bridge this information gap. The processing of the borehole data produced the thickness map of the Tshidzi, Madzaringwe and Mikambeni Formations in the Tshipise-Pafuri, Mopane and Tuli Coalfields (Figures 3.2, 3.3, 3.4, 3.5, 3.6, 3.7, 3.20, 3.21, 3.22, 3.23, 3.24, 3.25, 3.36, 3.37, 3.38, 3.39, 3.40 and 3.41). The average thickness of the formations in the coalfields is shown in Table 3.2.

Table 3.2: Average thicknesses of the formations (Fm) in the studied coalfields.

Coalfield	Average thicknesses (m)		
	Mikambeni	Madzaringwe	Tshidzi
Tshipise-Pafuri	148	158	3.2
Mopane	160	118	2.8
Tuli	62	74	2.3

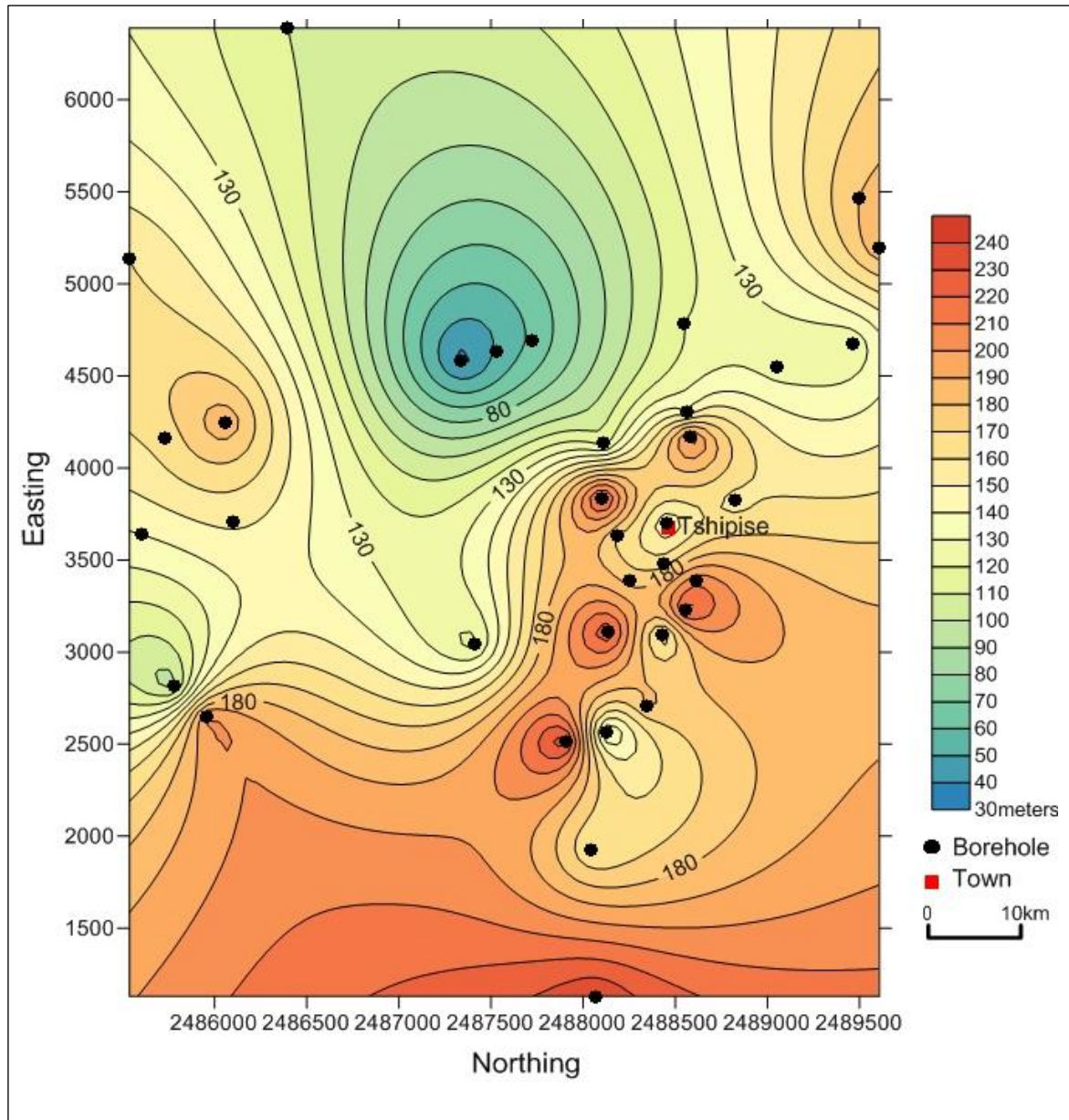


Figure 3.2: Thickness contour map of the Mikambeni Formation in the Tshipise-Pafuri Coalfield.

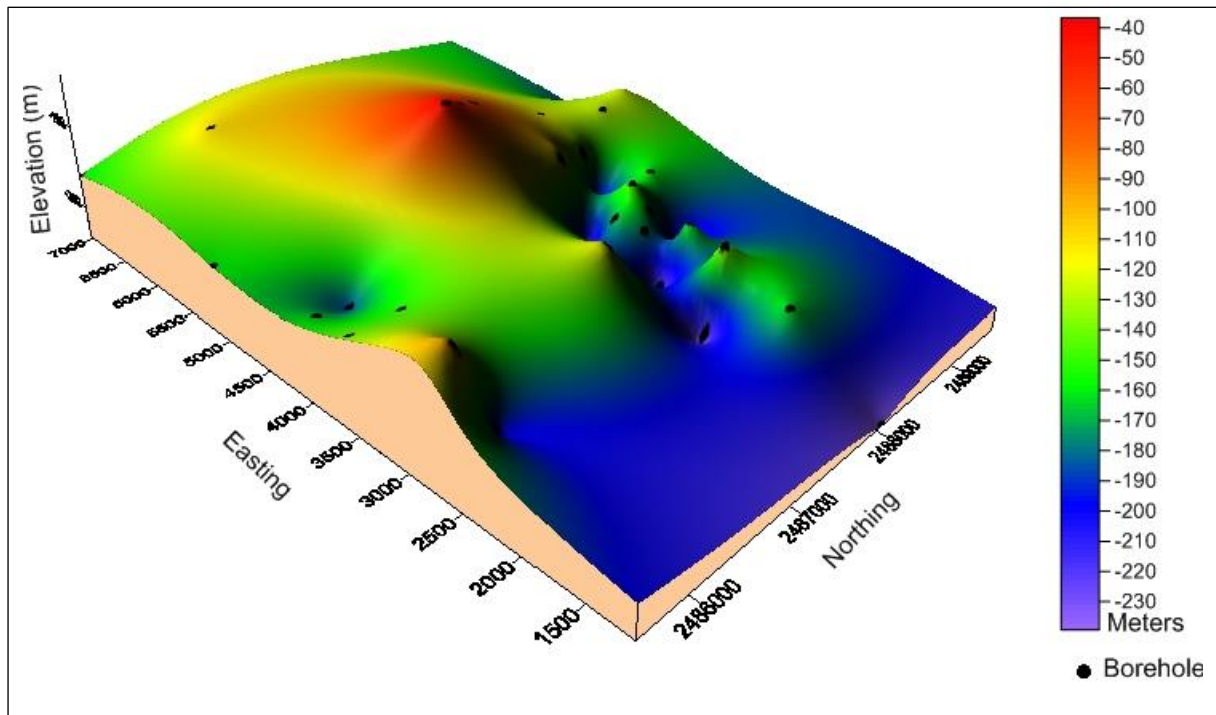


Figure 3.3: 3d topographic map of the Mikambeni Formation in the Tshipise-Pafuri Coalfield.

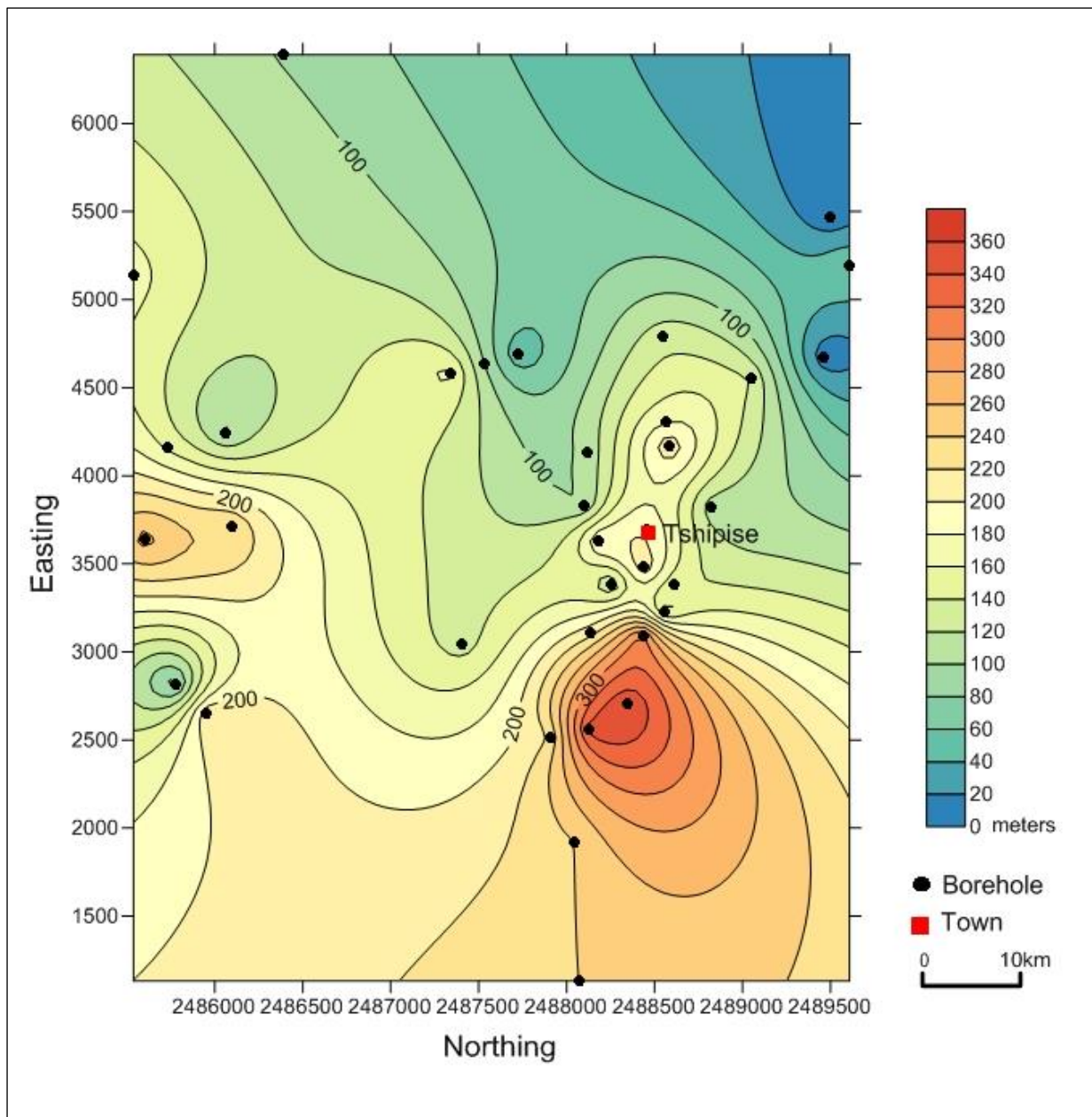


Figure 3.4: Thickness contour map of the Madzarinwe Formation in the Tshipise-Pafuri Coalfield.

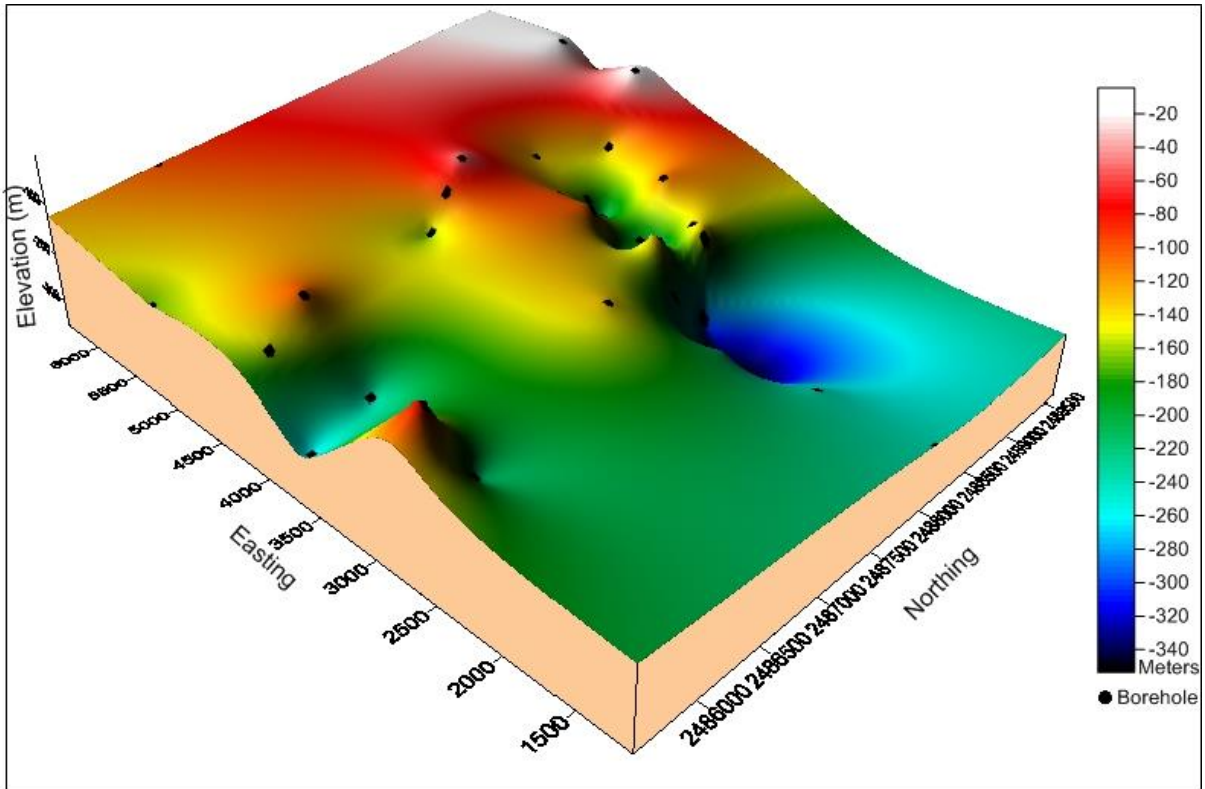


Figure 3.5: 3d topographic map of the Madzaringwe Formation in the Tshipise-Pafuri Coalfield.

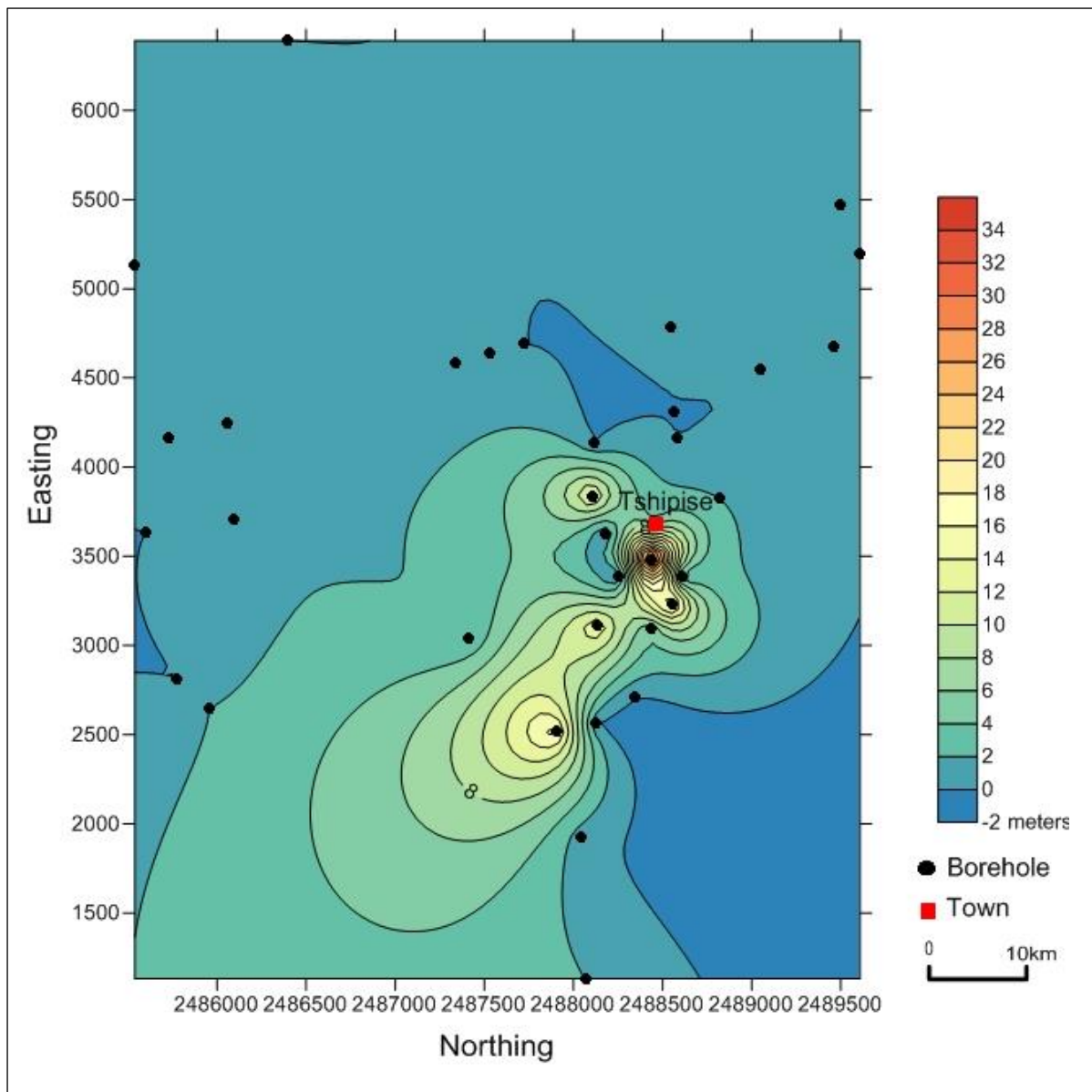


Figure 3.6: Thickness contour map of the Tshidzi Formation in the Tshipise-Pafuri Coalfield.

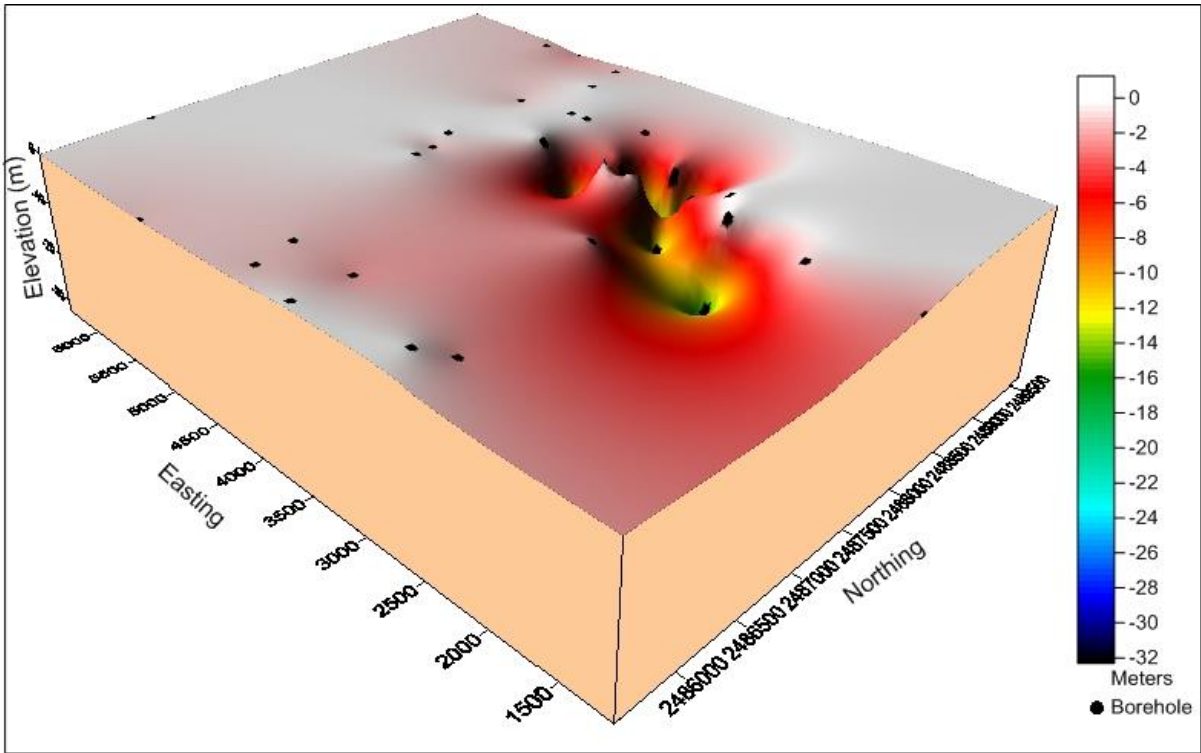


Figure 3.7: 3d topographic map of the Tshidzi Formation in the Tshipise-Pafuri Coalfield.

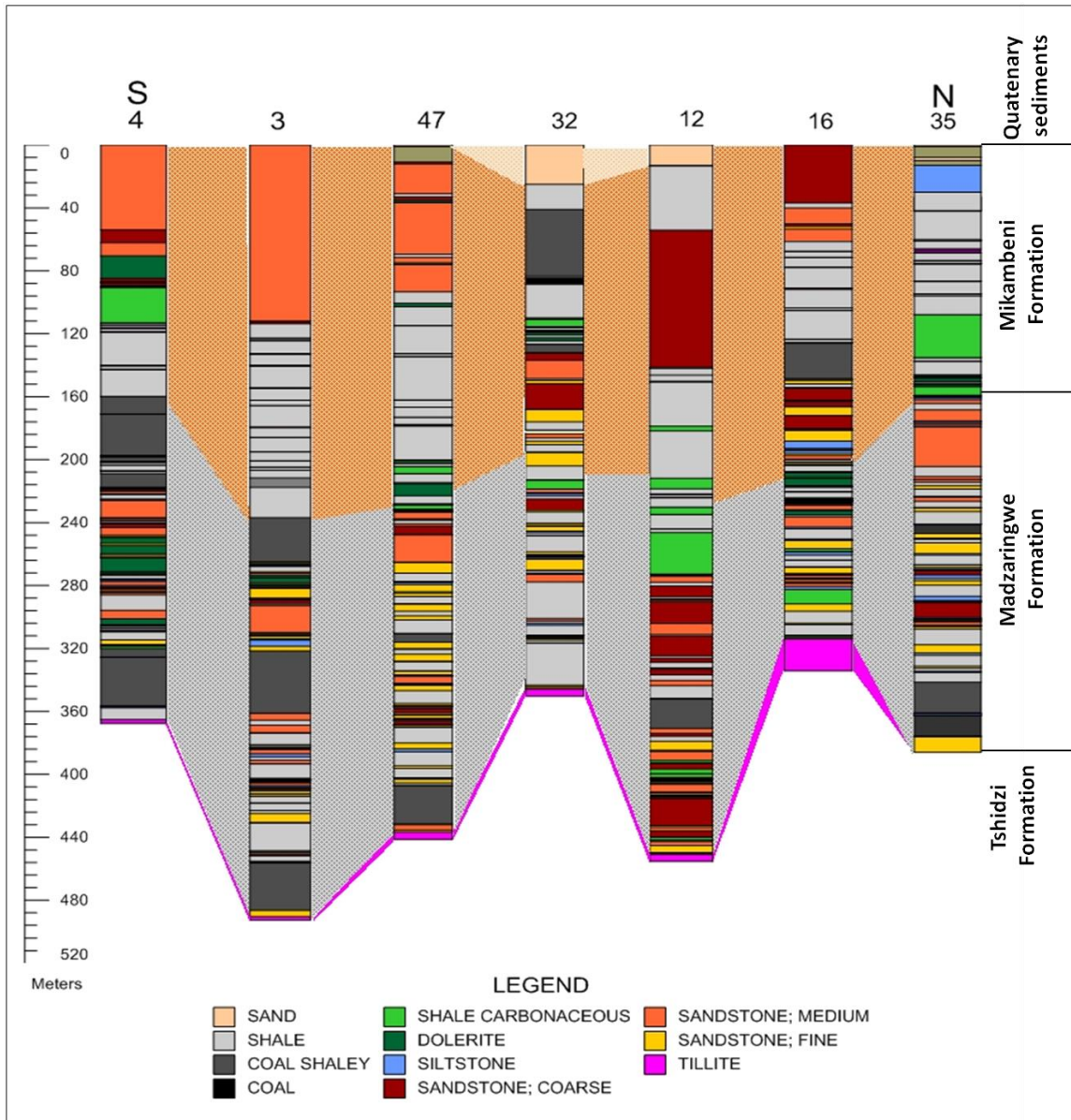


Figure 3.8: Stratigraphic column and correlation diagram (Cross-section 1) in the Tshipise-Pafuri Coalfield. The different colours between stratigraphic columns represent the correlation boundaries of the different stratigraphic units. The numbers above of the logs represents borehole core numbers in the CGS archives.

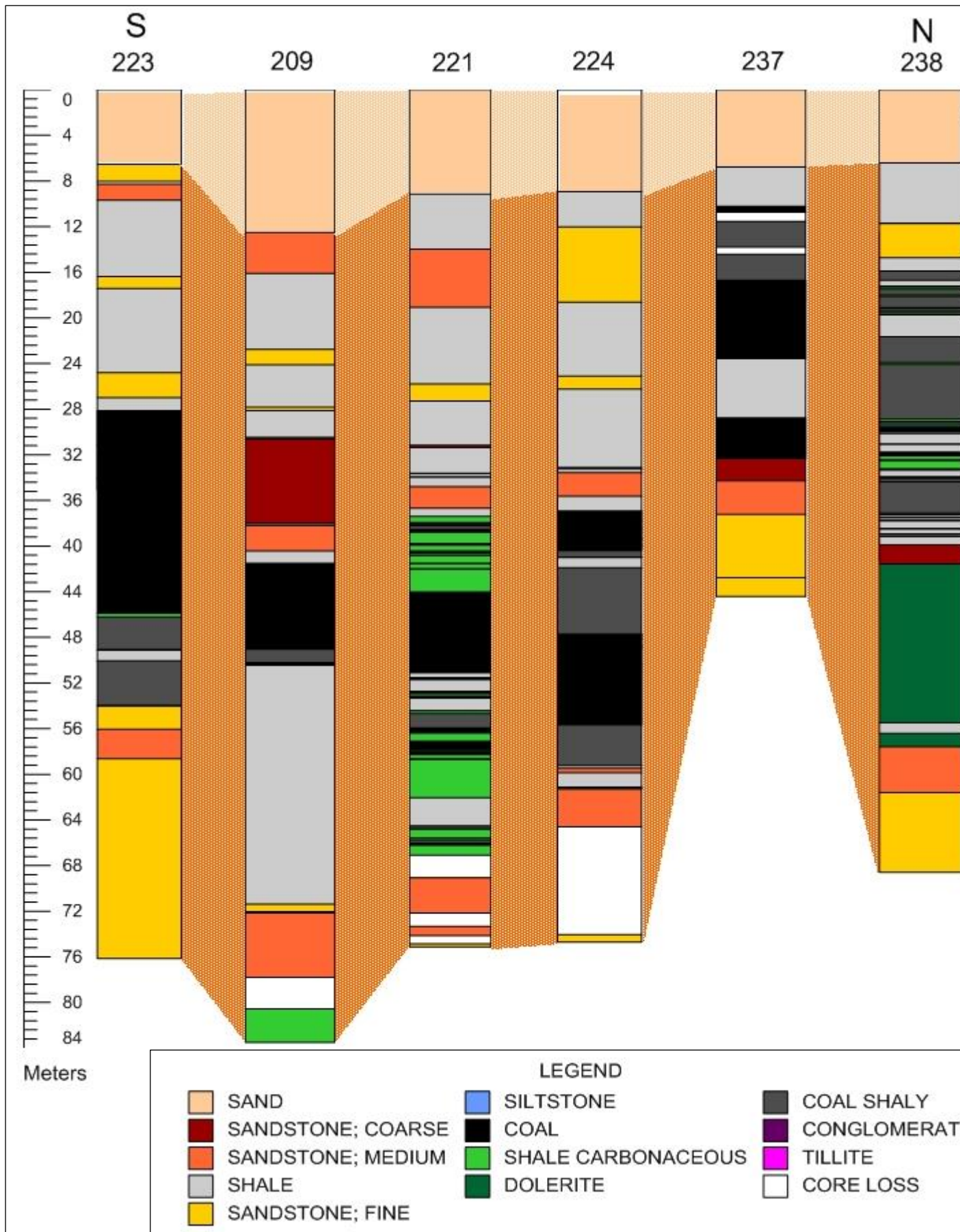


Figure 3.9: Stratigraphic column and correlation diagram (Cross-section 2) in the Tshipise-Pafuri Coalfield. The different colours between stratigraphic columns represent the correlation boundaries of the different stratigraphic units. The numbers above of the logs represents borehole core numbers in the CGS archives.

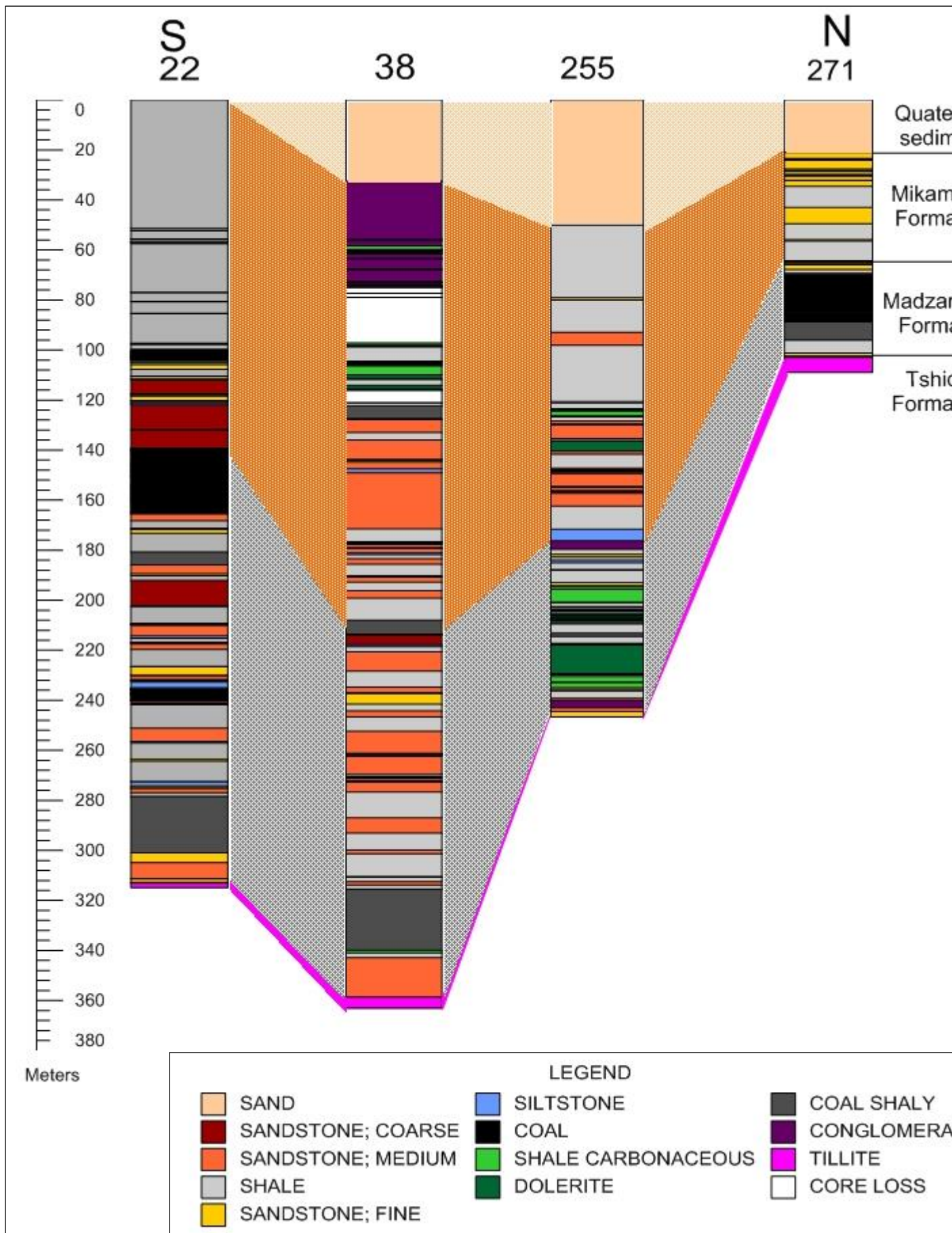


Figure 3.10: Stratigraphic column and correlation diagram (Cross-section 3) in the Tshipise-Pafuri Coalfield. The different colours between stratigraphic columns represent the correlation boundaries of the different stratigraphic units. The numbers above of the logs represents borehole core numbers in the CGS archives.

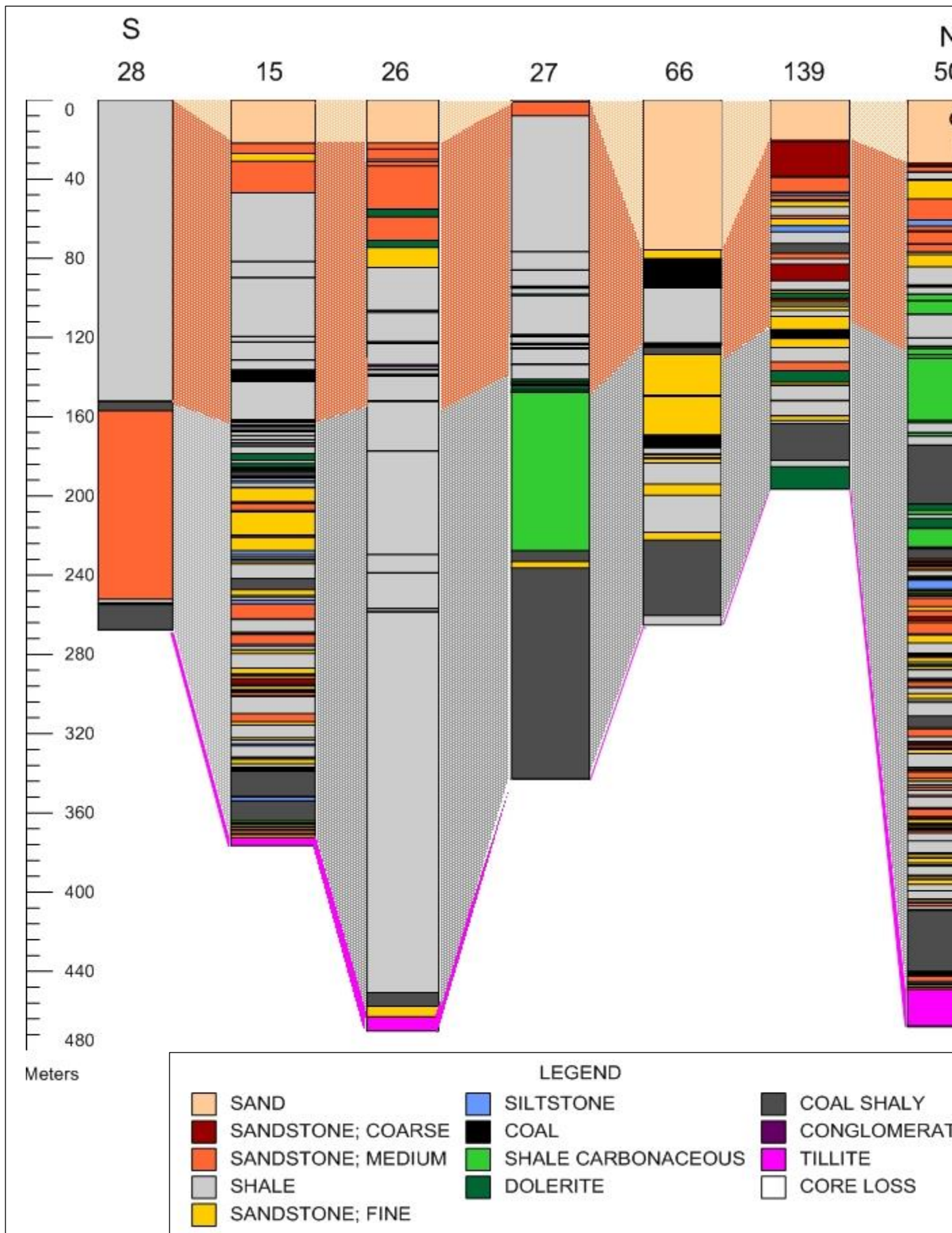


Figure 3.11: Stratigraphic column and correlation diagram (Cross-section 4) in the Tshipise-Pafuri Coalfield. The different colours between stratigraphic columns represent the correlation boundaries of the different stratigraphic units. The numbers above of the logs represents borehole core numbers in the CGS archives.

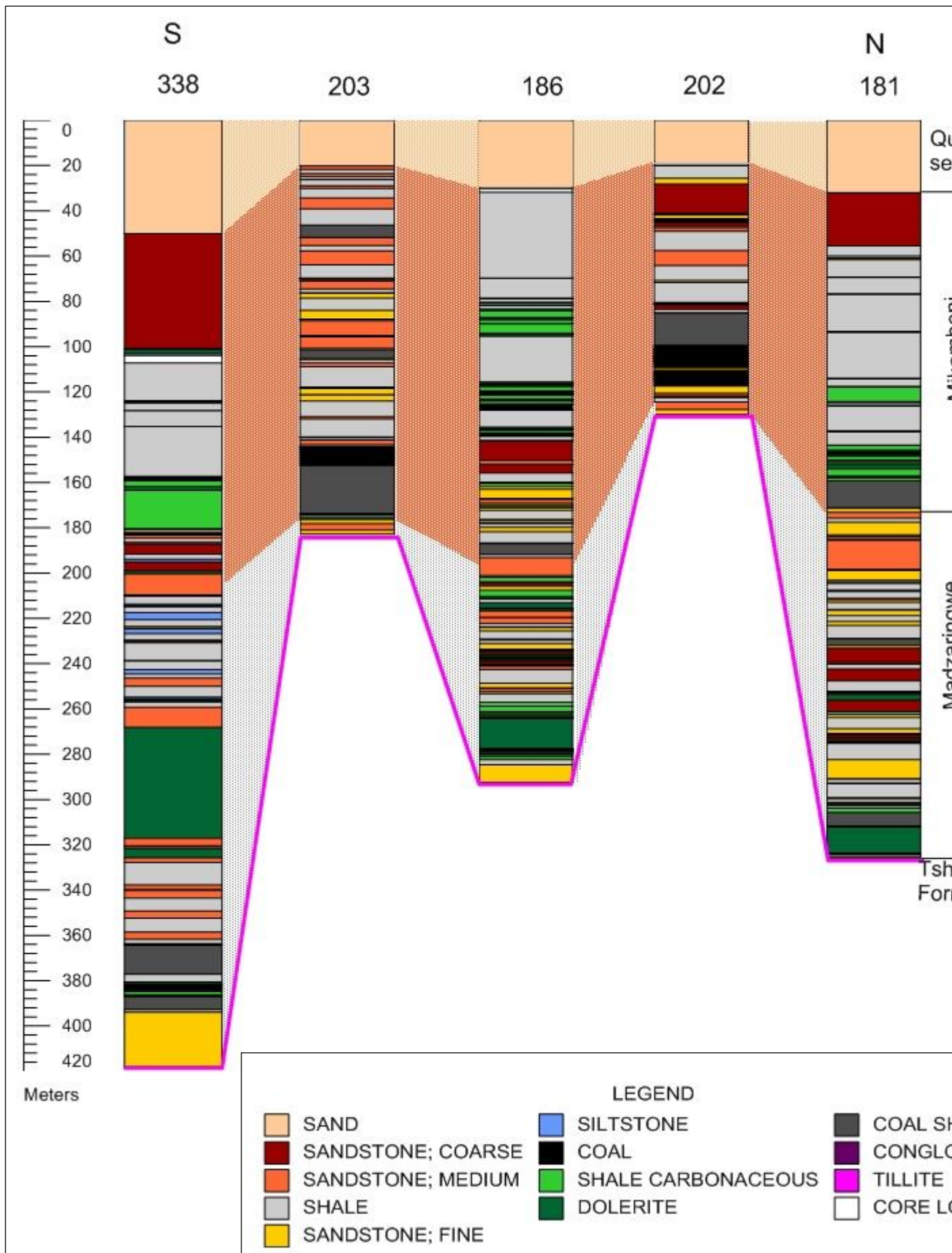


Figure 3.12: Stratigraphic column and correlation diagram (Cross-section 5) in the Tshipise-Pafuri Coalfield. The different colours between stratigraphic columns represent the correlation boundaries of the different stratigraphic units. The numbers above of the logs represents borehole core numbers in the CGS archives.

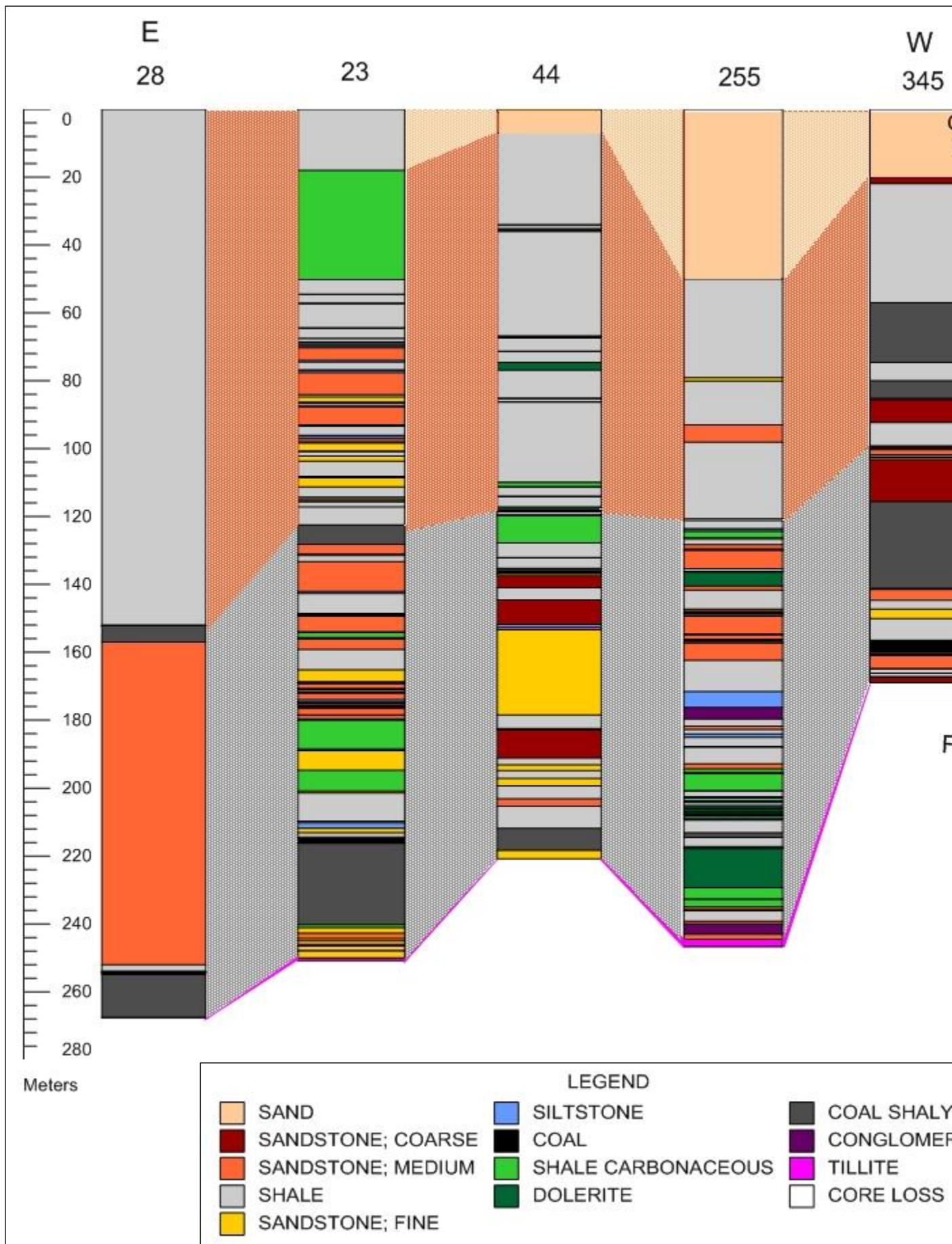


Figure 3.13: Stratigraphic column and correlation diagram (Cross-section 6) in the Tshipise-Pafuri Coalfield. The different colours between stratigraphic columns represent the correlation boundaries of the different stratigraphic units. The numbers above of the logs represents borehole core numbers in the CGS archives.

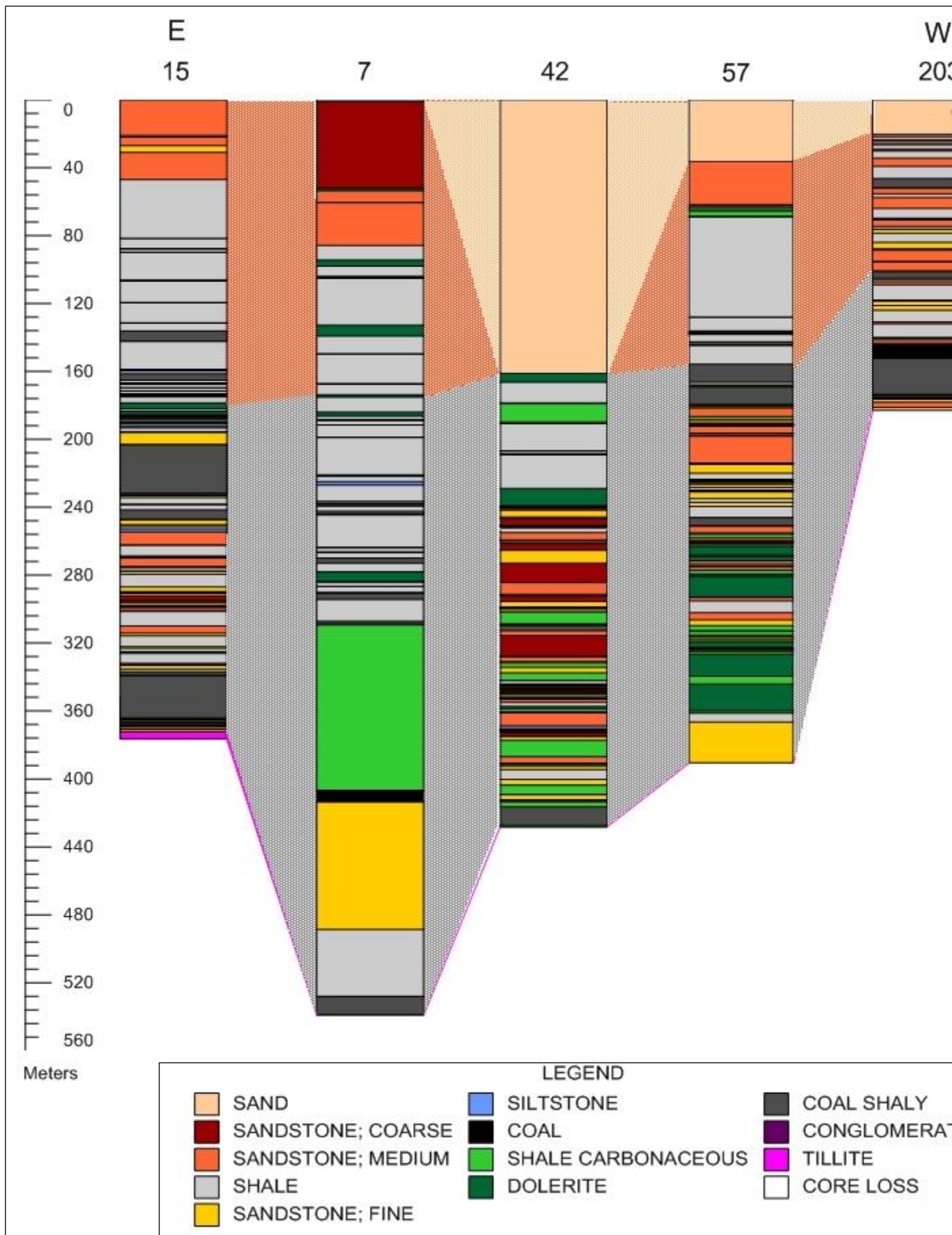


Figure 3.14: Stratigraphic column and correlation diagram (Cross-section 7) in the Tshipise-Pafuri Coalfield. The different colours between stratigraphic columns represent the correlation boundaries of the different stratigraphic units. The numbers above of the logs represents borehole core numbers in the CGS archives.

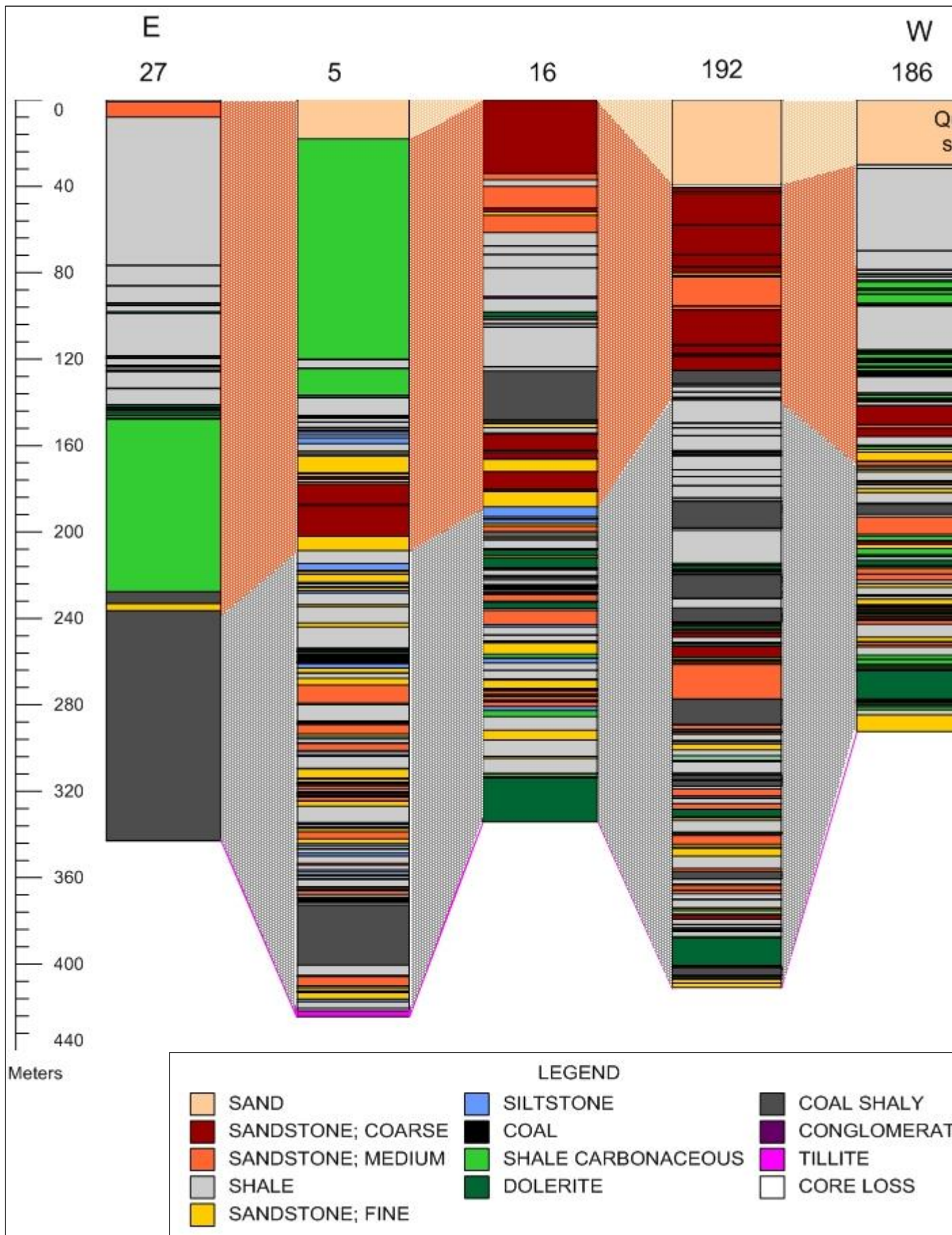


Figure 3.15: Stratigraphic column and correlation diagram (Cross-section 8) in the Tshipise-Pafuri Coalfield. The different colours between stratigraphic columns represent the correlation boundaries of the different stratigraphic units. The numbers above of the logs represents borehole core numbers in the CGS archives.

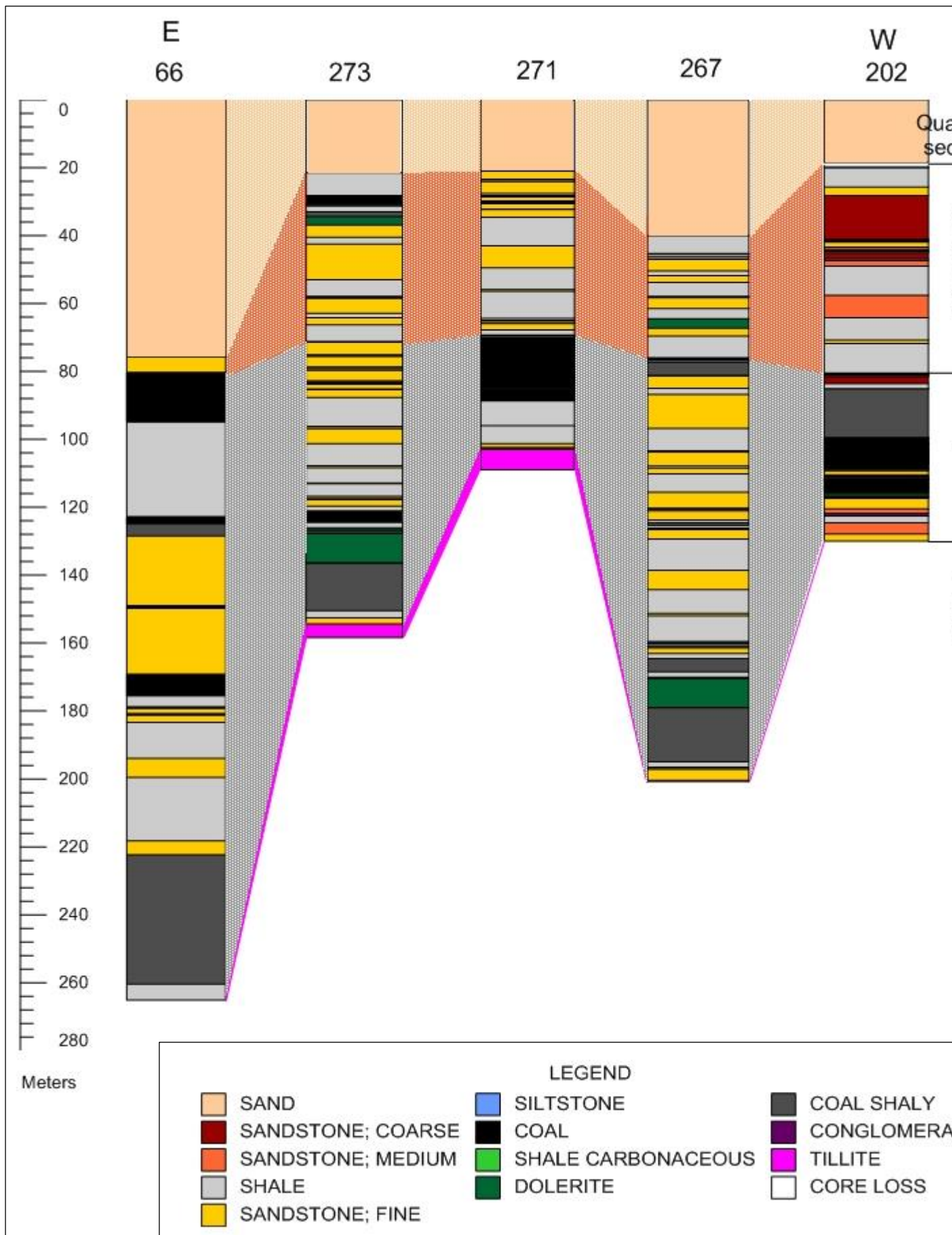


Figure 3.16: Stratigraphic column and correlation diagram (Cross-section 9) in the Tshipise-Pafuri Coalfield. The different colours between stratigraphic columns represent the correlation boundaries of the different stratigraphic units. The numbers above of the logs represents borehole core numbers in the CGS archives.

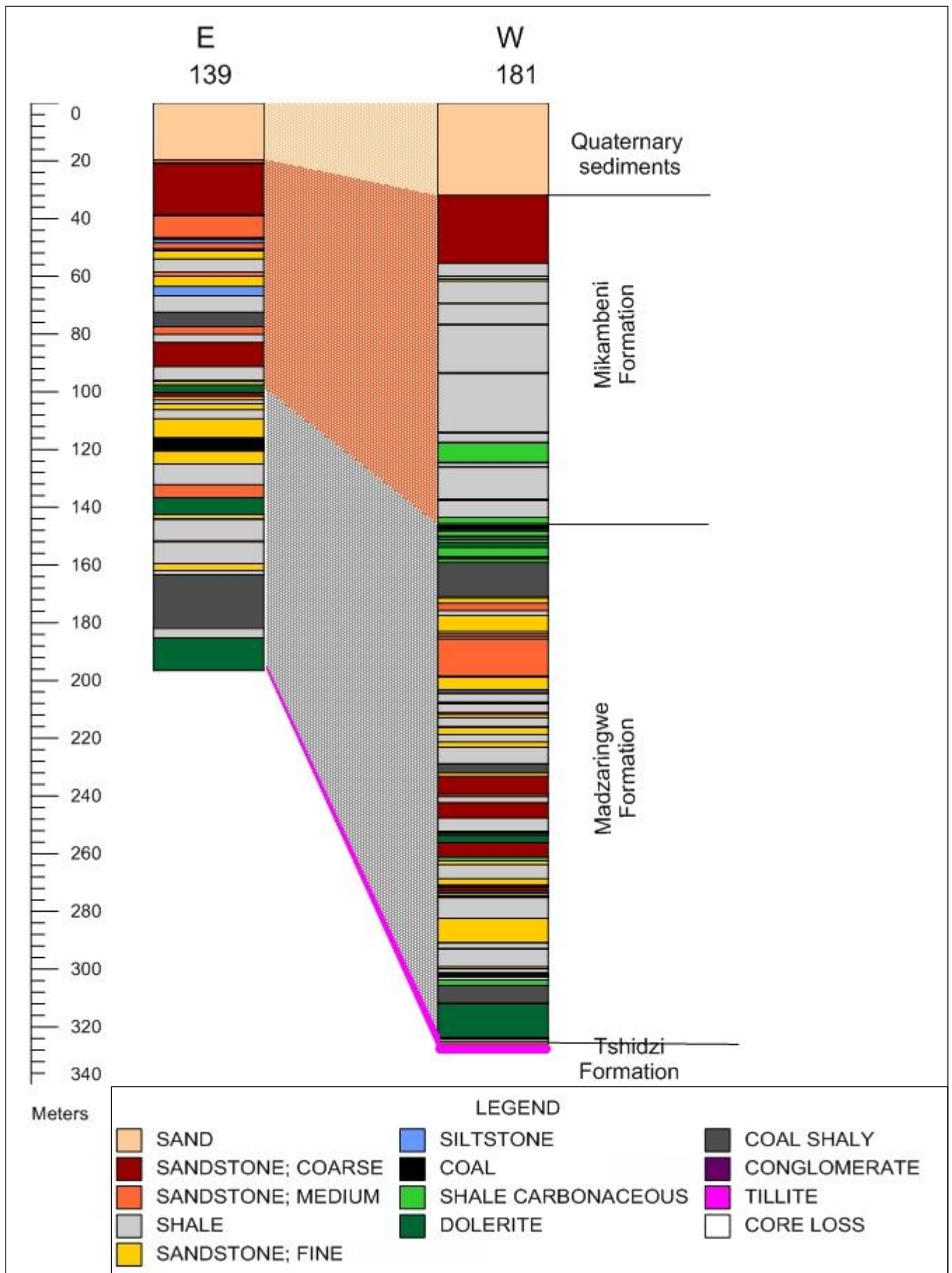


Figure 3.17: Stratigraphic column and correlation diagram (Cross-section 10) in the Tshipise-Pafuri Coalfield. The different colours between stratigraphic columns represent the correlation boundaries of the different stratigraphic units. The numbers above of the logs represents borehole core numbers in the CGS archives.

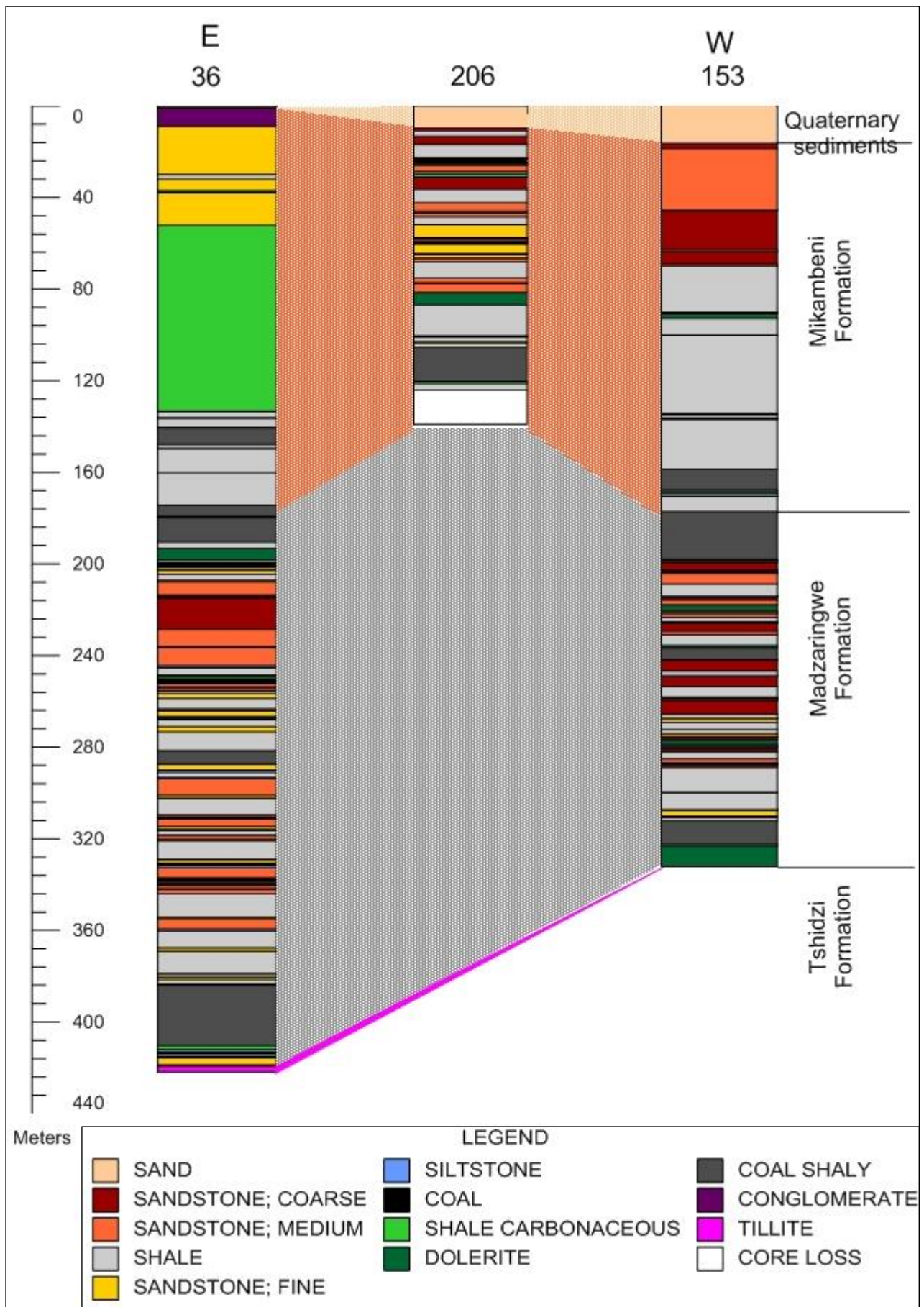


Figure 3.18: Stratigraphic column and correlation diagram (Cross-section 11) in the Tshipise-Pafuri Coalfield. The different colours between stratigraphic columns represent the correlation boundaries of the different stratigraphic units. The numbers above of the logs represents borehole core numbers in the CGS archives.

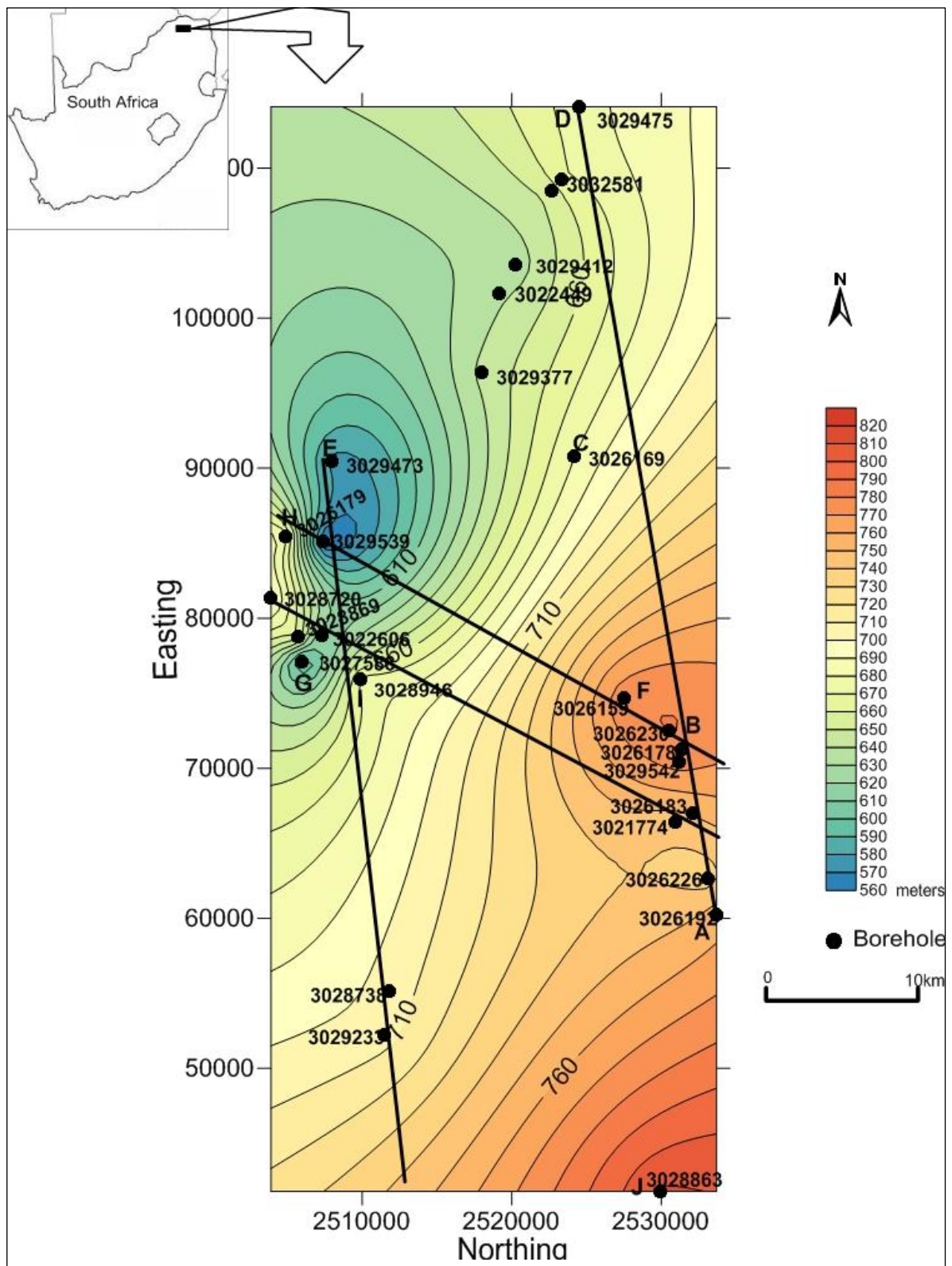


Figure 3.19: Structure contour map and cross-section lines of the Mopane Coalfield.

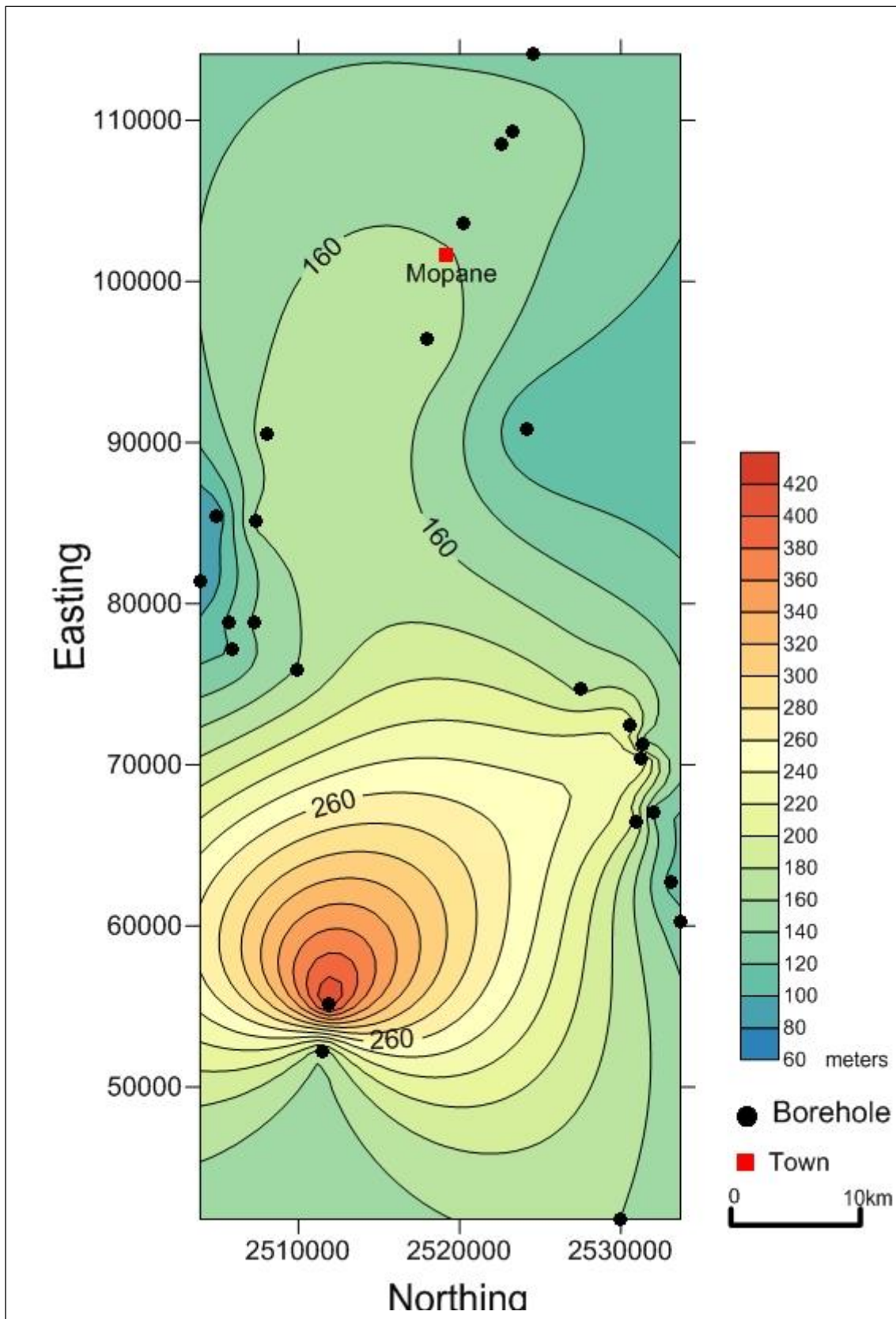


Figure 3.20: Thickness contour map of the Mikambeni Formation in the Mopane Coalfield.

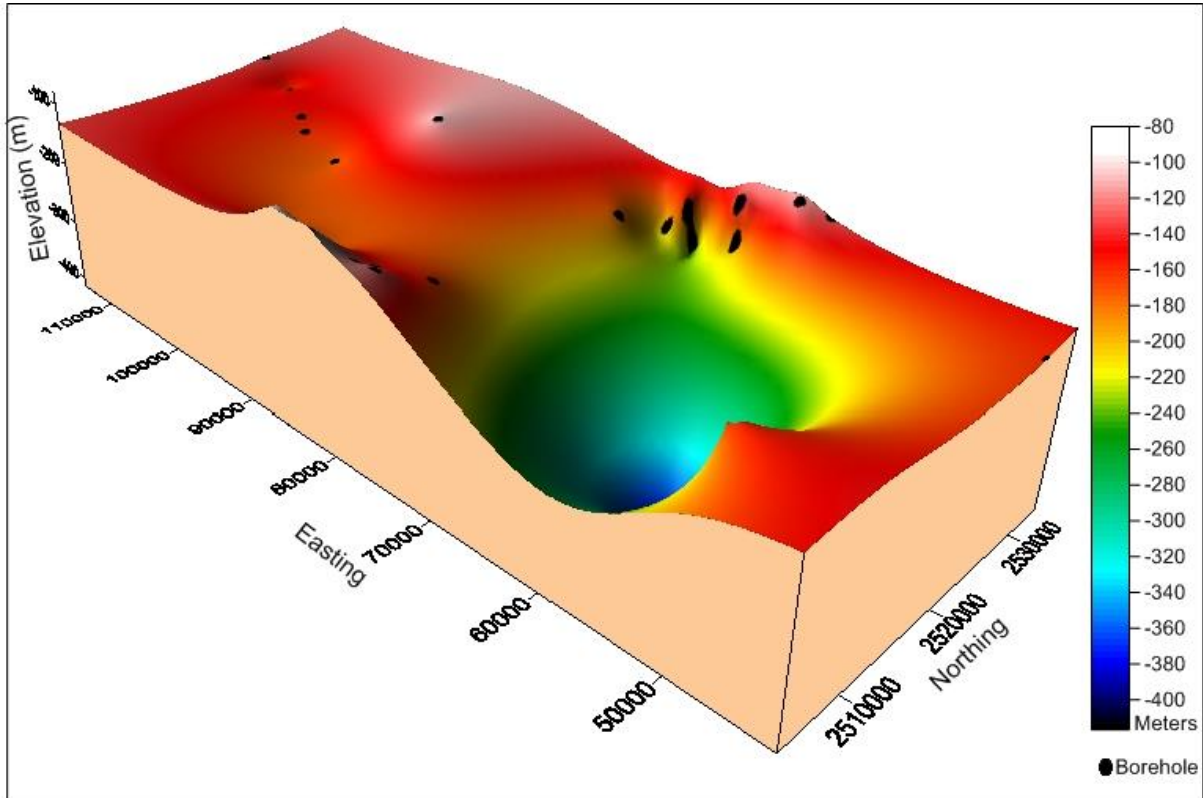


Figure 3.21: 3d topographic map of the Mikambeni Formation in the Mopane Coalfield.

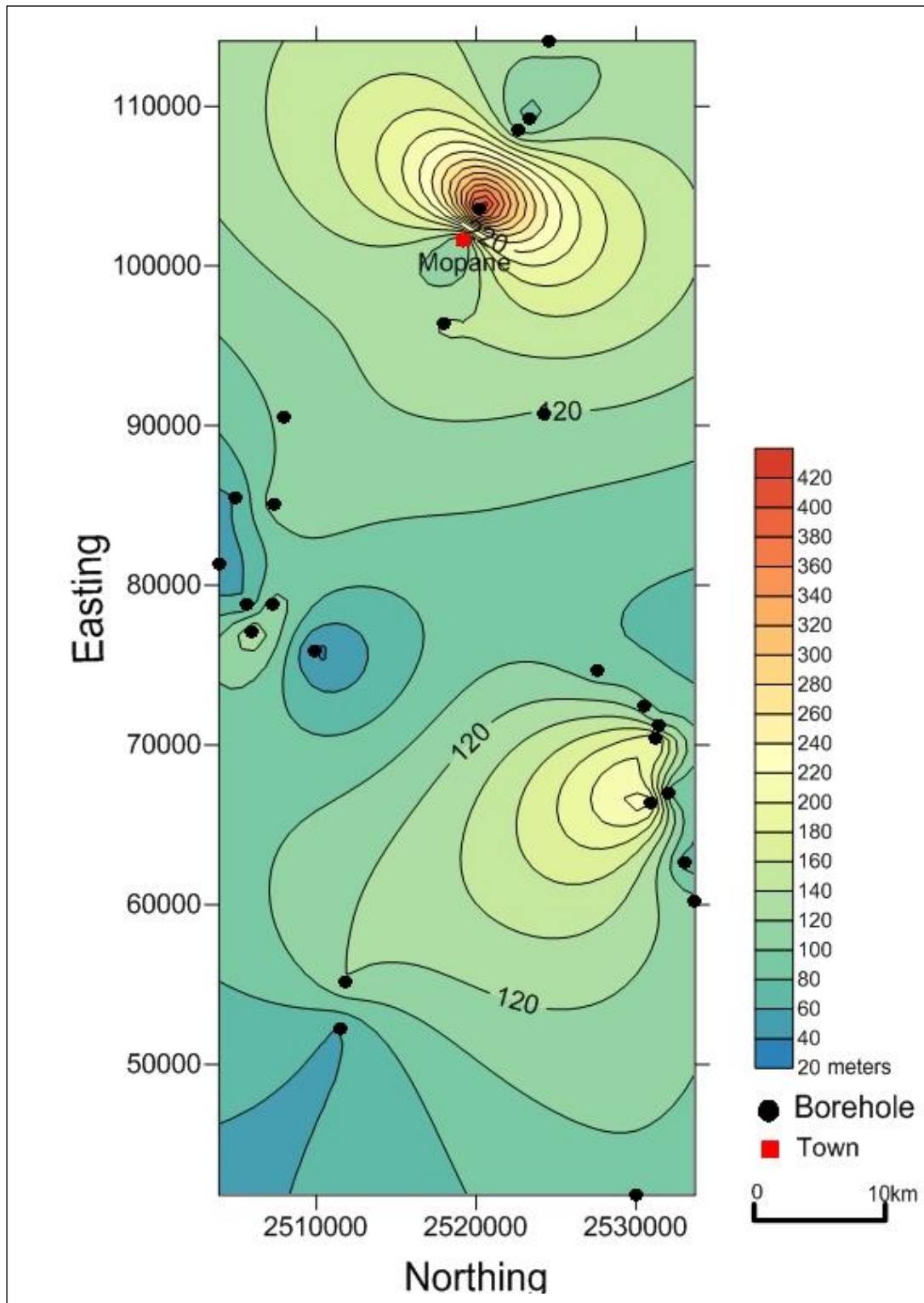


Figure 3.22: Thickness contour map of the Madzaringwe Formation in the Mopane Coalfield.

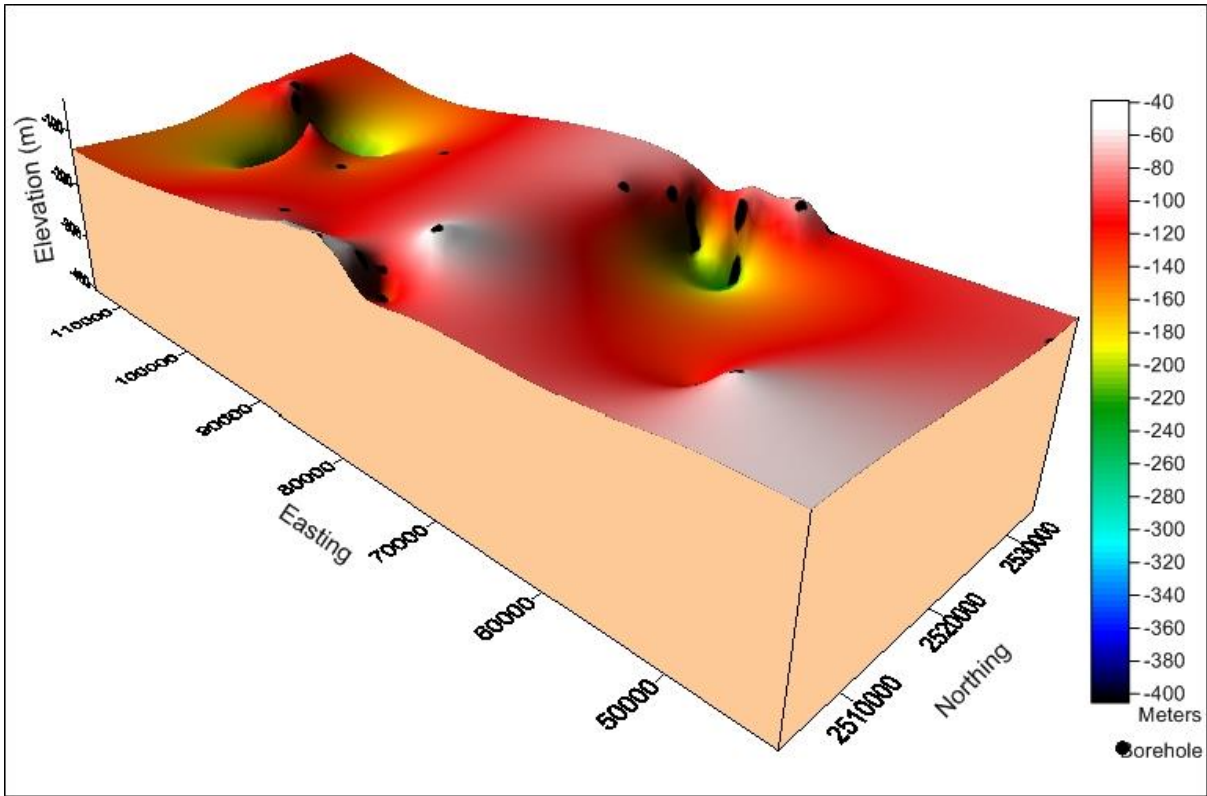


Figure 3.23: 3d topographic map of the Madzaringwe Formation in the Mopane Coalfield.

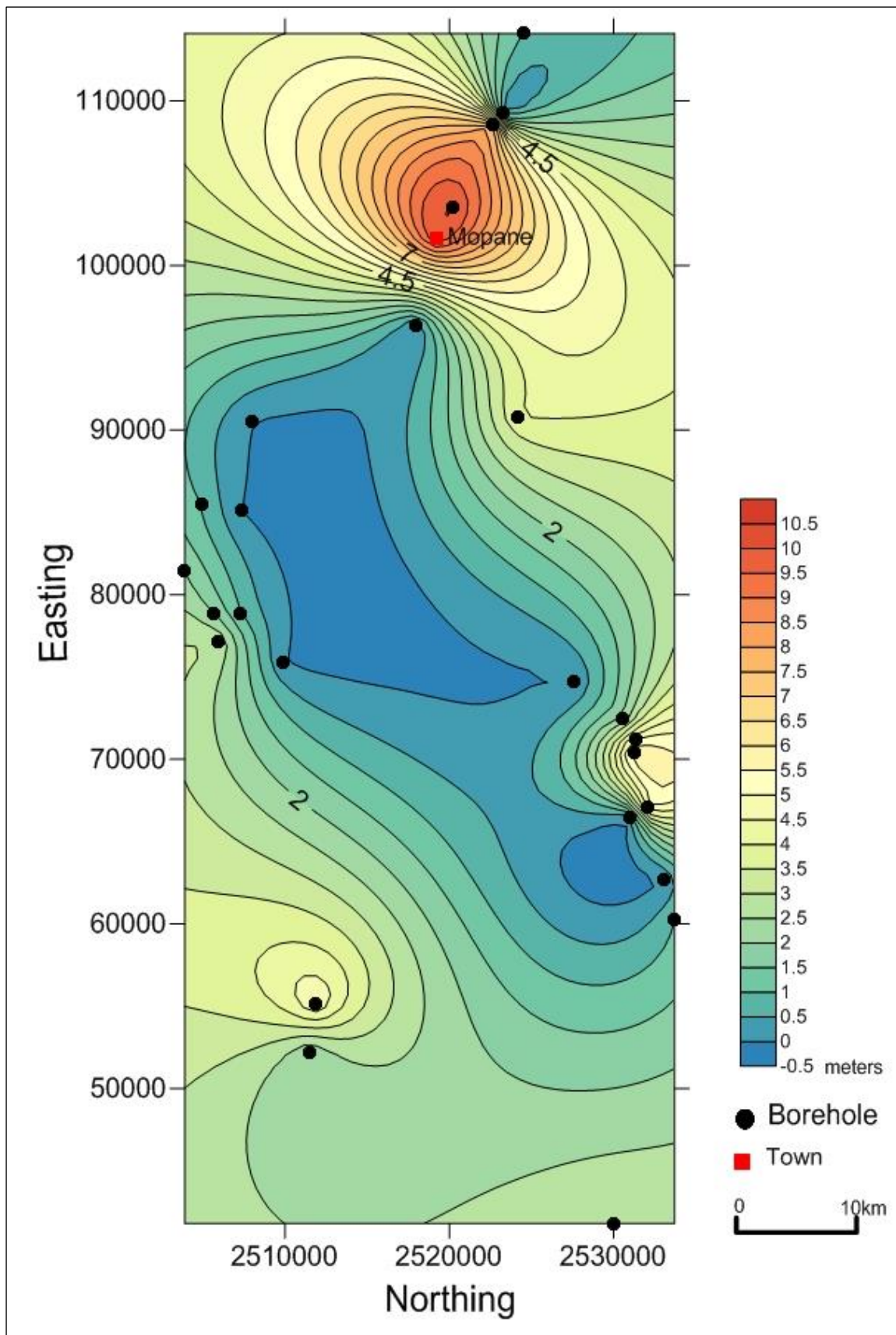


Figure 3.24: Thickness map of the Tshidzi Formation in the Mopane Coalfield.

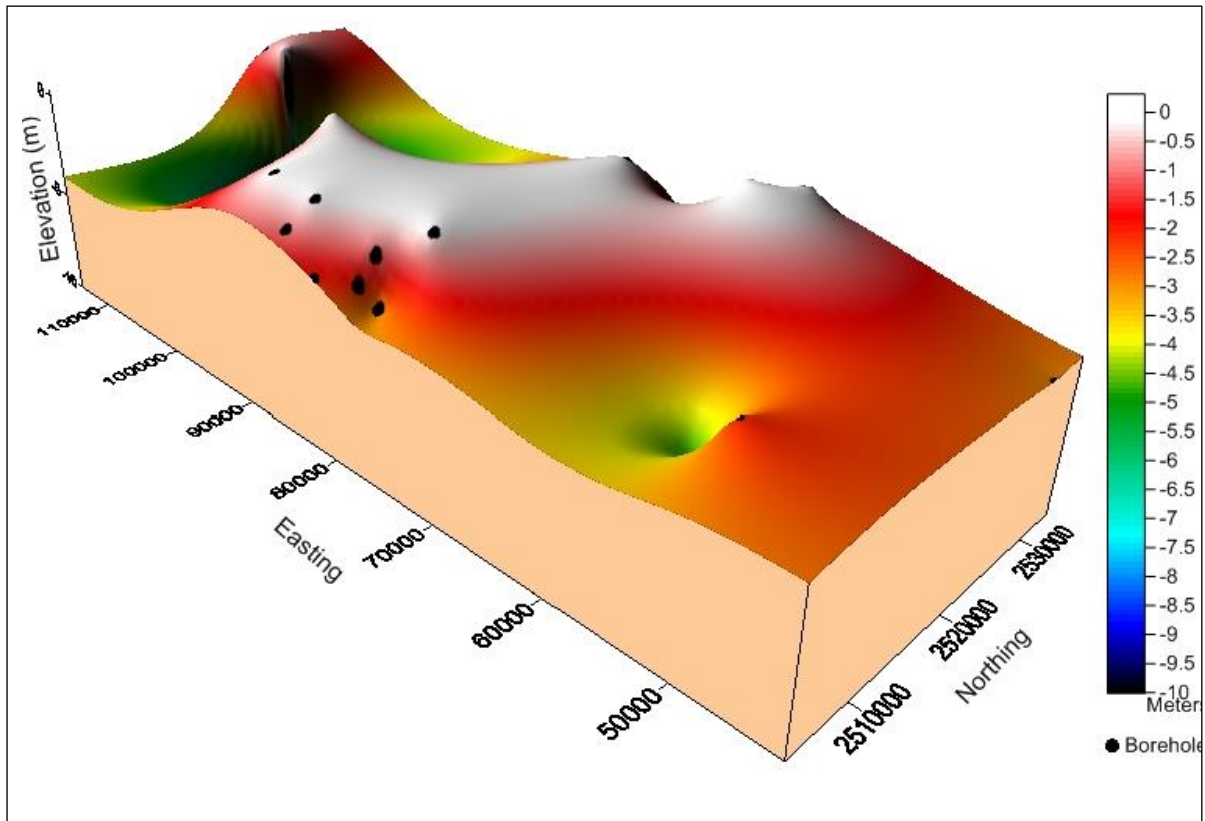


Figure 3.25: 3d topographic map of the Tshidzi Formation in the Mopane Coalfield.

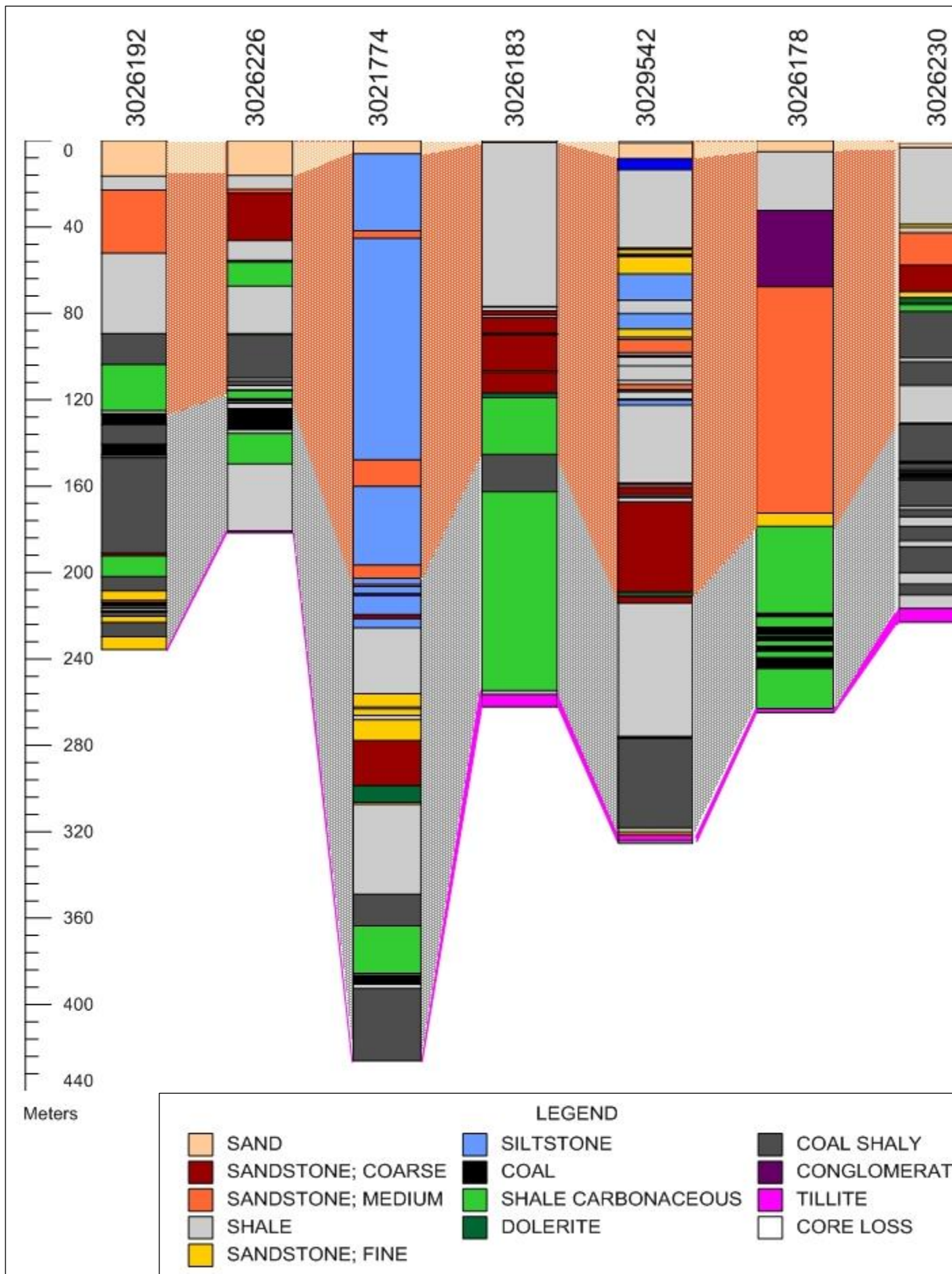


Figure 3.26: Stratigraphic column and correlation diagram (Cross-section 1) in the Mopane Coalfield. The different colours between stratigraphic columns represent the correlation boundaries of the different stratigraphic units. The numbers above of the logs represents borehole core numbers in the CGS archives.

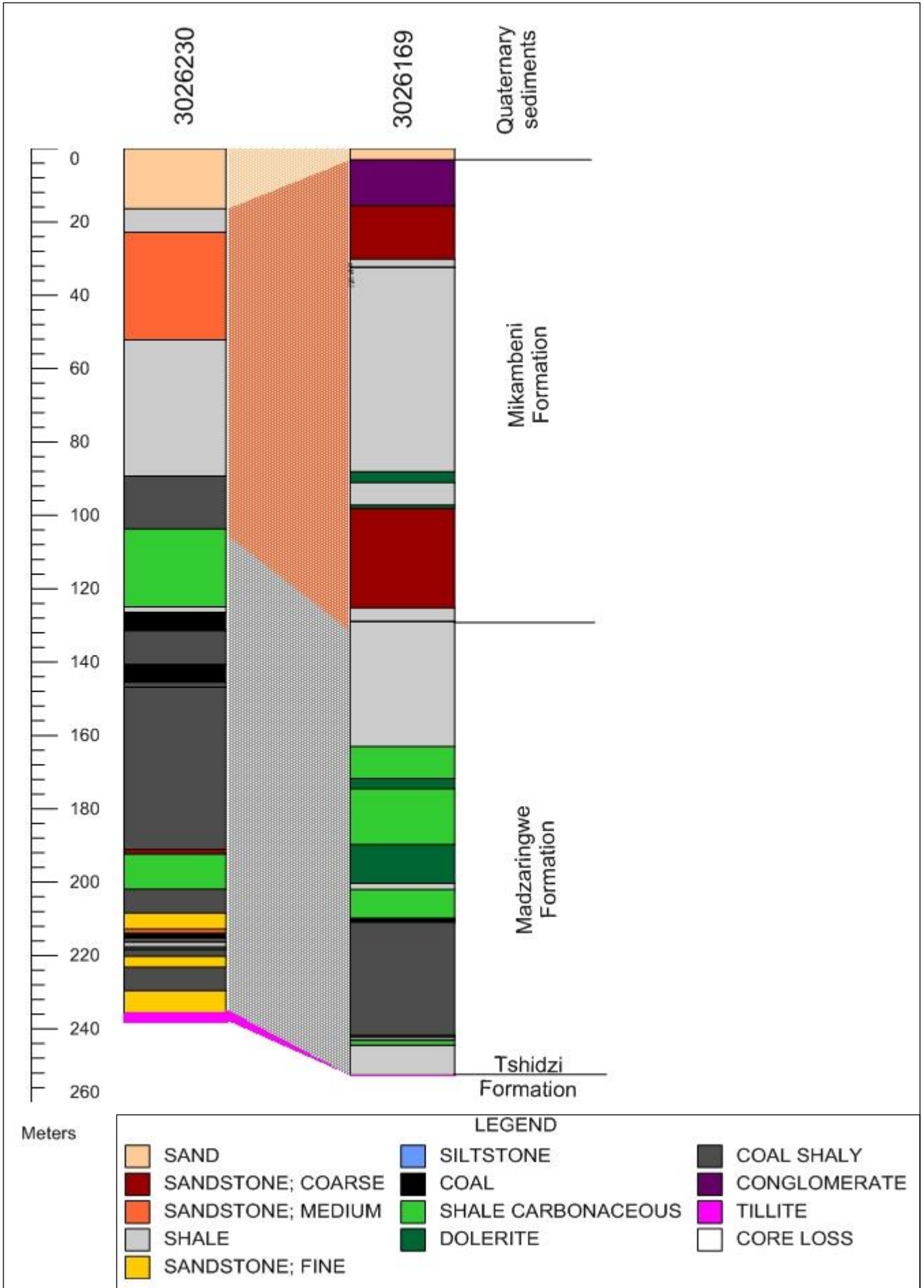


Figure 3.27: Stratigraphic column and correlation diagram (Cross-section 2) in the Mopane Coalfield. The different colours between stratigraphic columns represent the correlation boundaries of the different stratigraphic units. The numbers above of the logs represents borehole core numbers in the CGS archives.

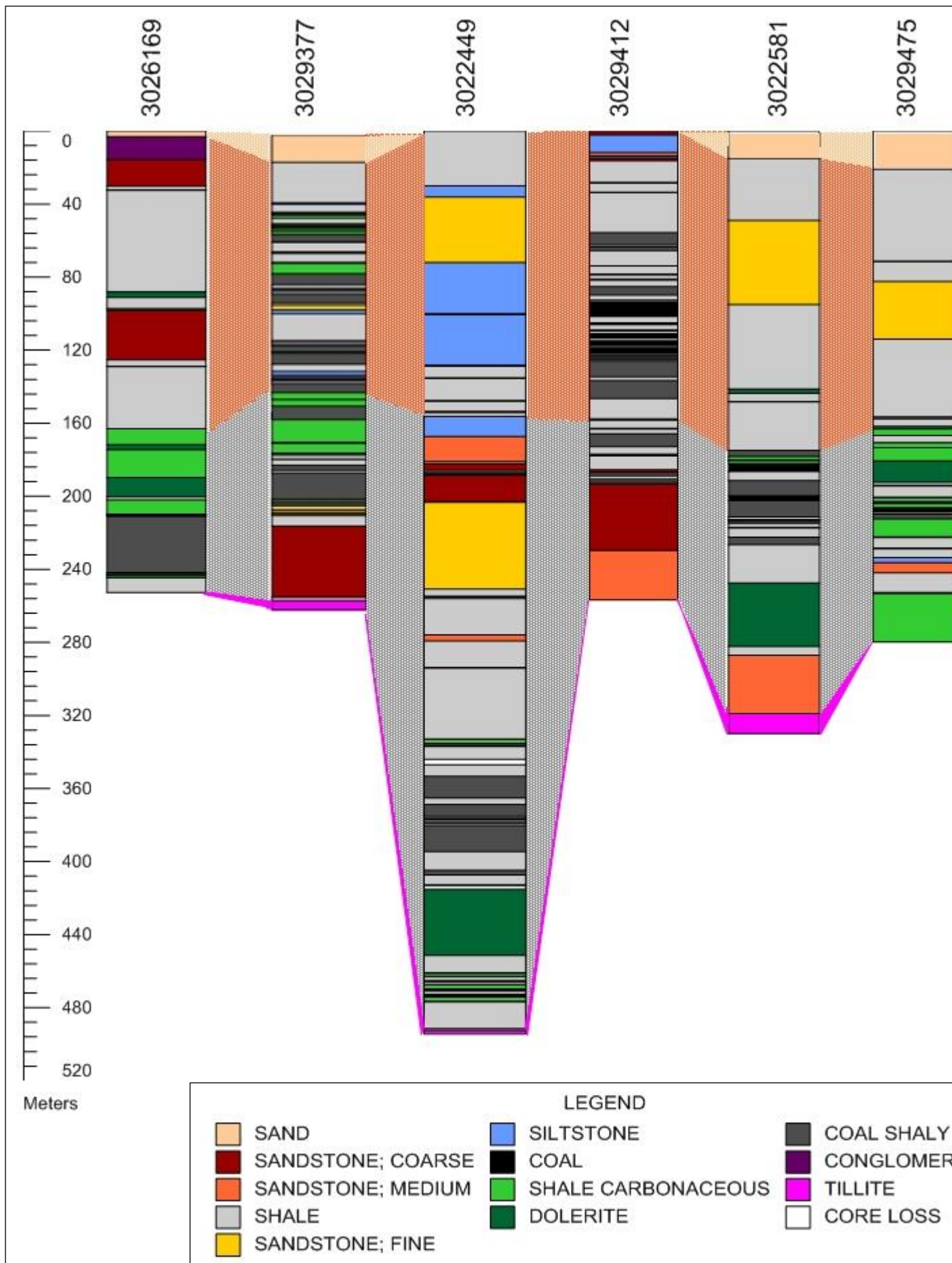


Figure 3.28: Stratigraphic column and correlation diagram (Cross-section 3) in the Mopane Coalfield. The different colours between stratigraphic columns represent the correlation boundaries of the different stratigraphic units. The numbers above of the logs represents borehole core numbers in the CGS archives.

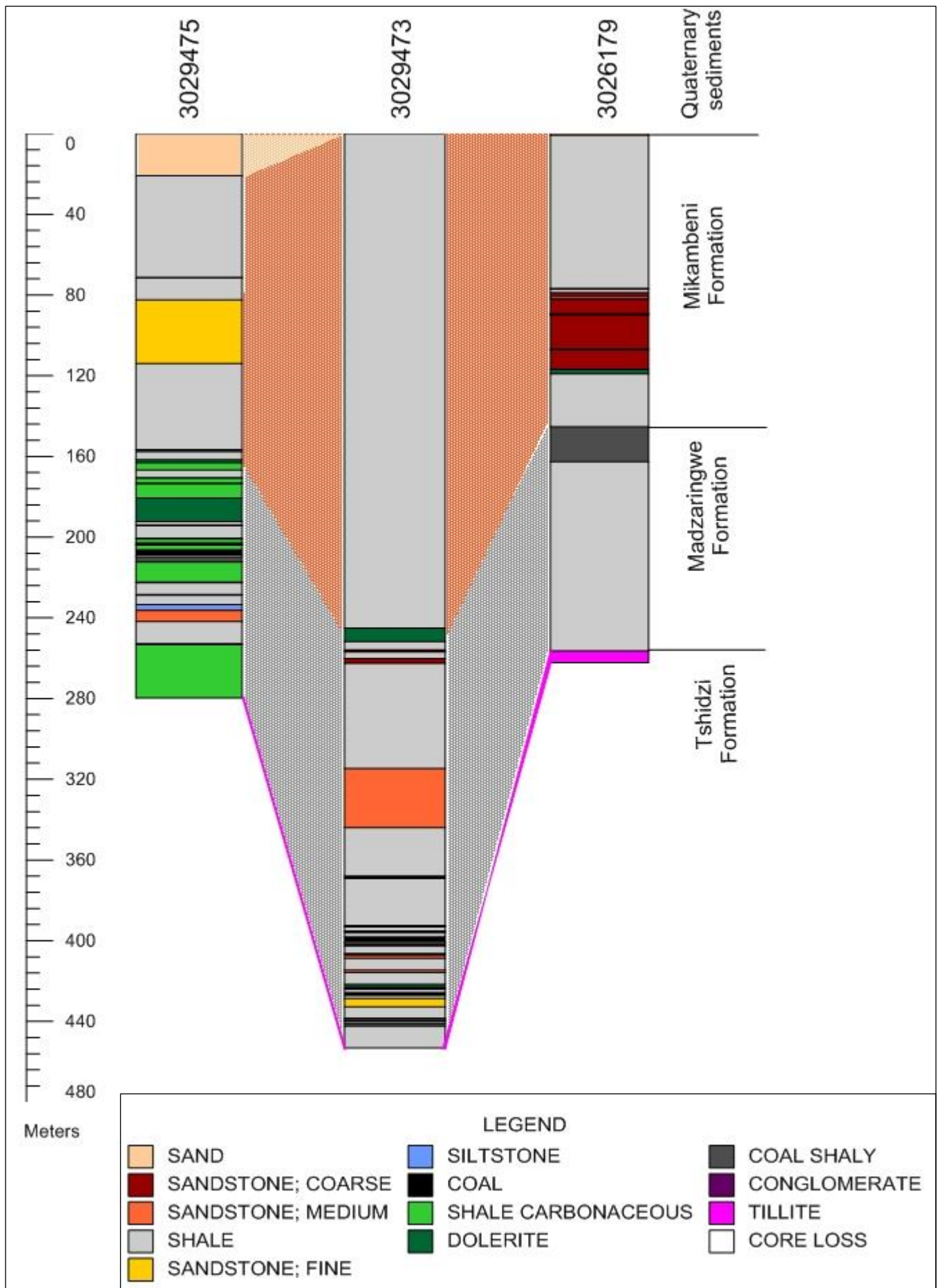


Figure 3.29: Stratigraphic column and correlation diagram (Cross-section 4) in the Mopane Coalfield. The different colours between stratigraphic columns represent the correlation boundaries of the different stratigraphic units. The numbers above of the logs represents borehole core numbers in the CGS archives.

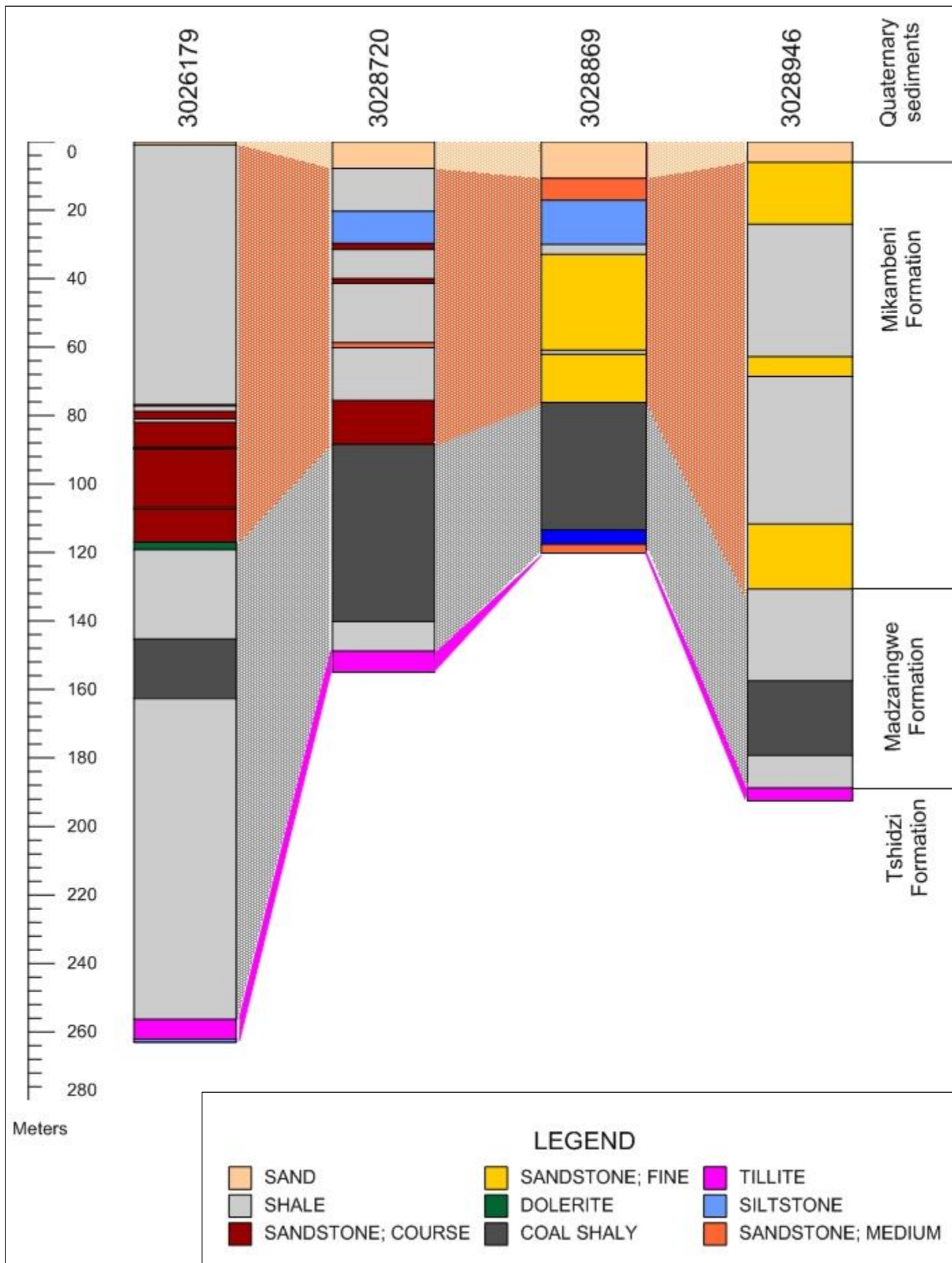


Figure 3.30: Stratigraphic column and correlation diagram (Cross-section 5) in the Mopane Coalfield. The different colours between stratigraphic columns represent the correlation boundaries of the different stratigraphic units. The numbers above of the logs represents borehole core numbers in the CGS archives.

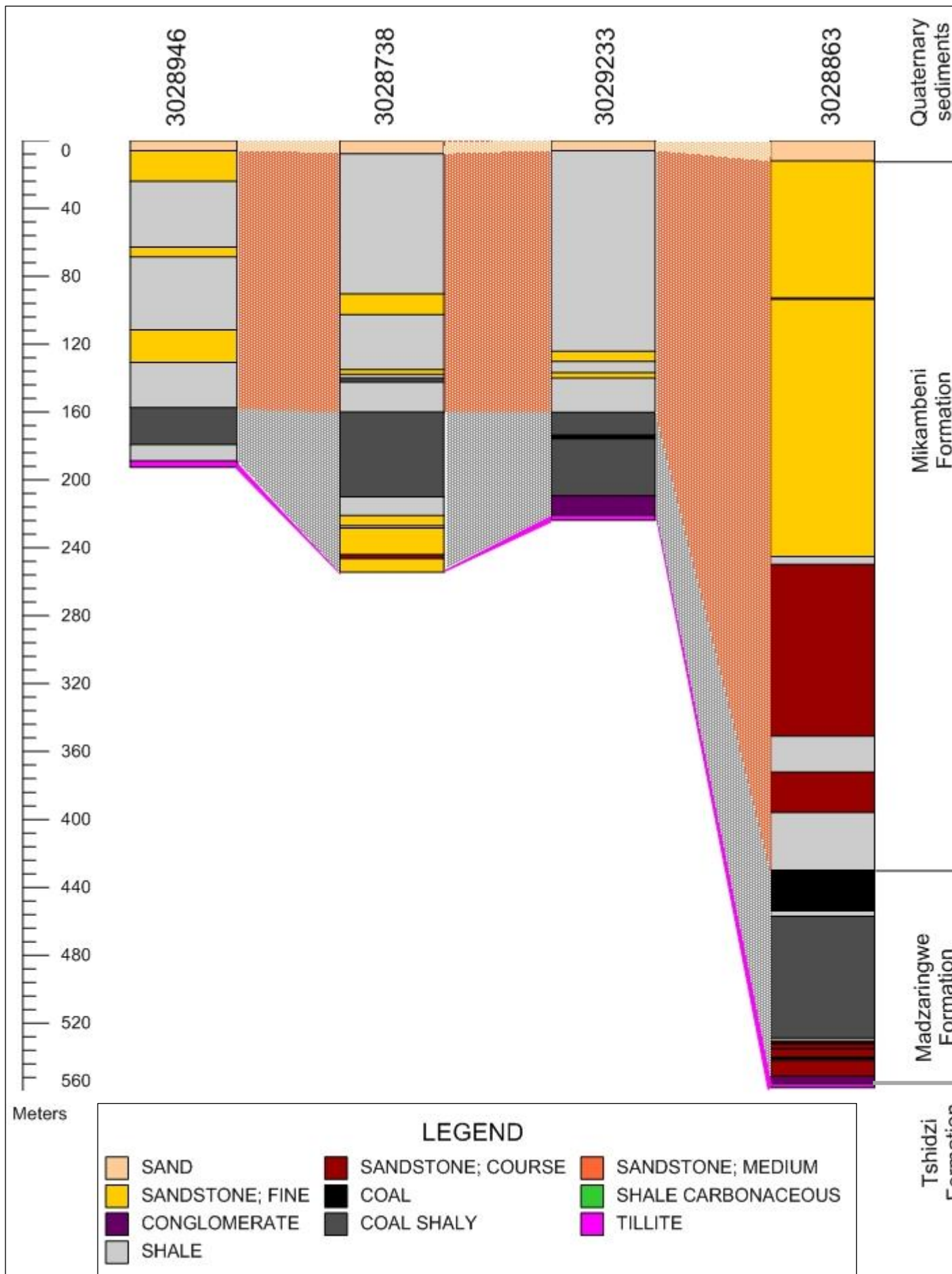


Figure 3.31: Stratigraphic column and correlation diagram (Cross-section 6) in the Mopane Coalfield. The different colours between stratigraphic columns represent the correlation boundaries of the different stratigraphic units. The numbers above of the logs represents borehole core numbers in the CGS archives.

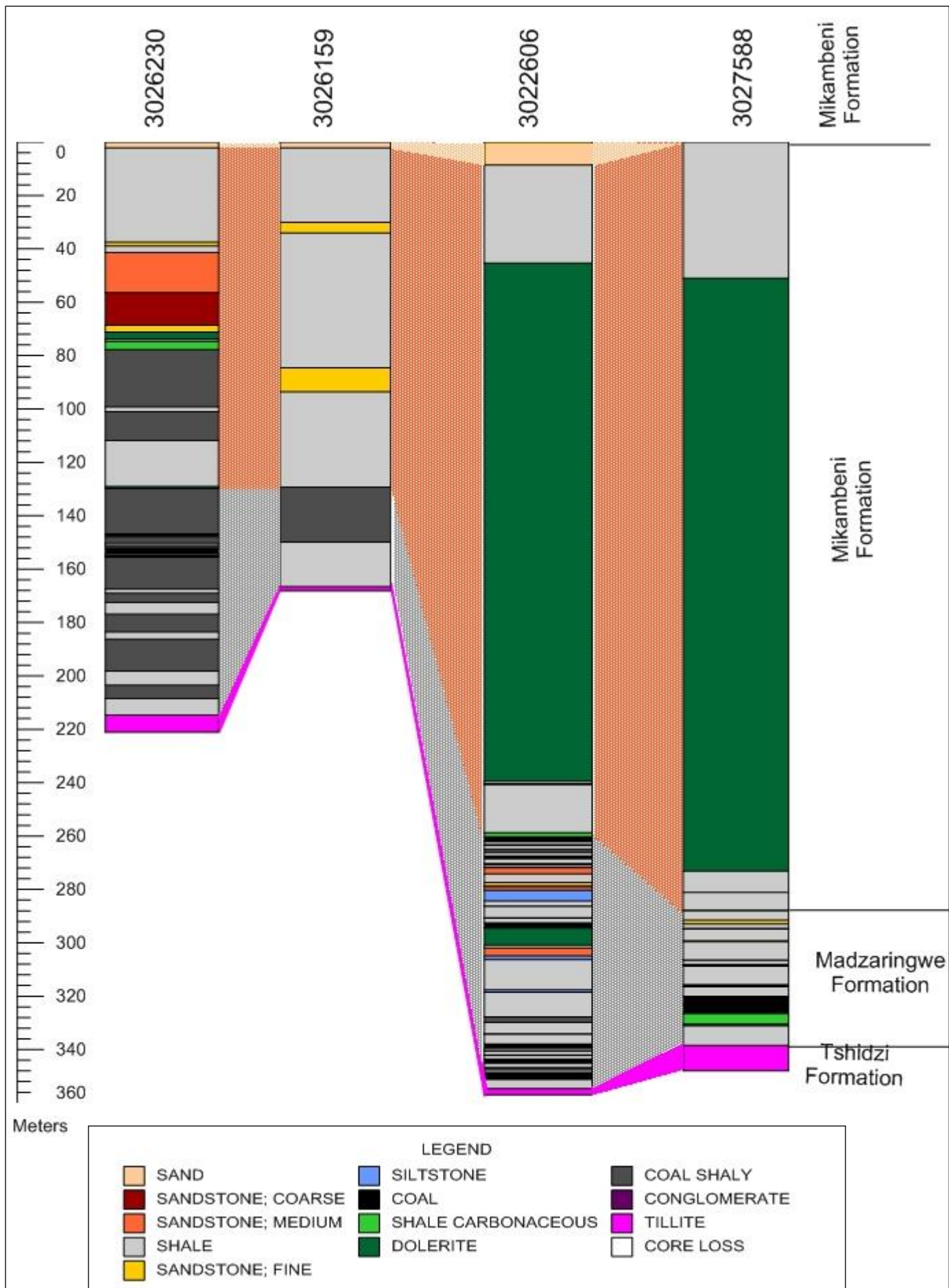


Figure 3.32: Stratigraphic column and correlation diagram (Cross-section 7) in the Mopane Coalfield. The different colours between stratigraphic columns represent the correlation boundaries of the different stratigraphic units. The numbers above of the logs represents borehole core numbers in the CGS archives.

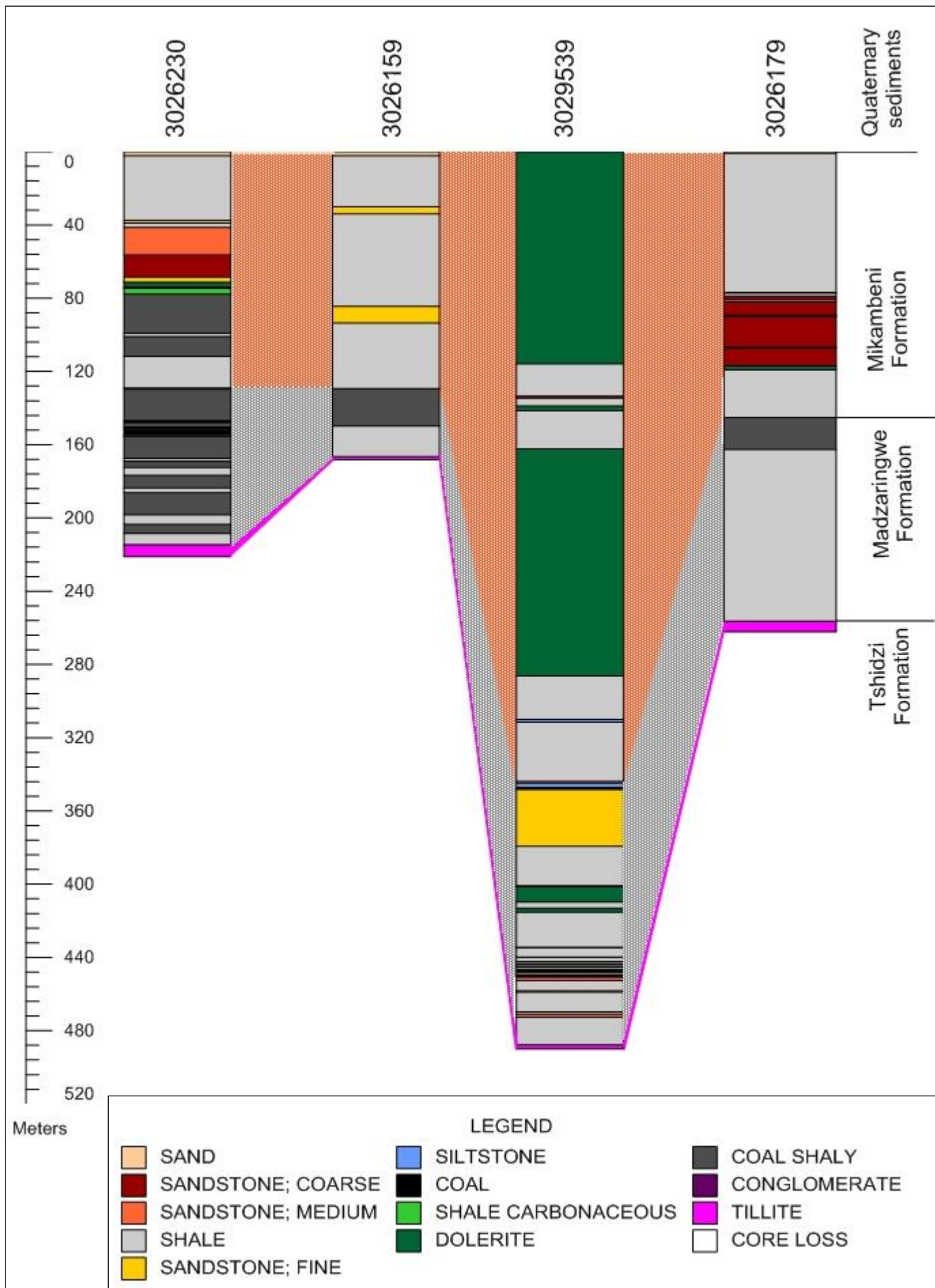


Figure 3.33: Stratigraphic column and correlation diagram (Cross-section 1) in the Mopane Coalfield. The different colours between stratigraphic columns represent the correlation boundaries of the different stratigraphic units. The numbers above of the logs represents borehole core numbers in the CGS archives.

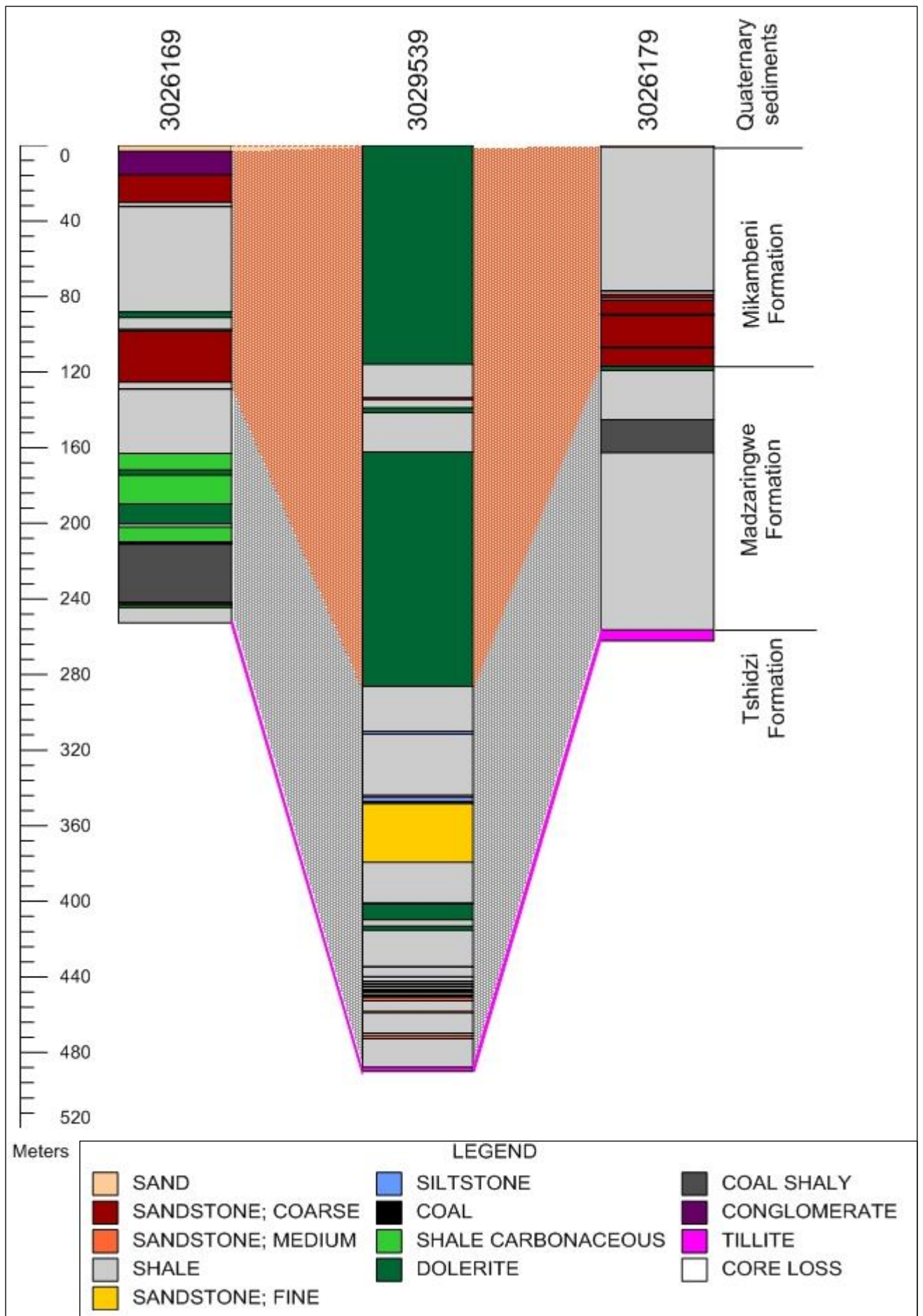


Figure 3.34: Stratigraphic column and correlation diagram (Cross-section 9) in the Mopane Coalfield. The different colours between stratigraphic columns represent the correlation boundaries of the different stratigraphic units. The numbers above of the logs represents borehole core numbers in the CGS archives.

In the Tuli Coalfield, the Tshidzi Formation generally comprises diamictite, interbedded with relatively coarse-grained sandstones in places. The Madzaringwe Formation comprises up to 120 m of alternating feldspathic, often cross bedded sandstone, siltstone and shale containing thin coal seams. The Mikambeni Formation attains a thickness of about 80 m and consists of alternating black shale, sandstone and coal.

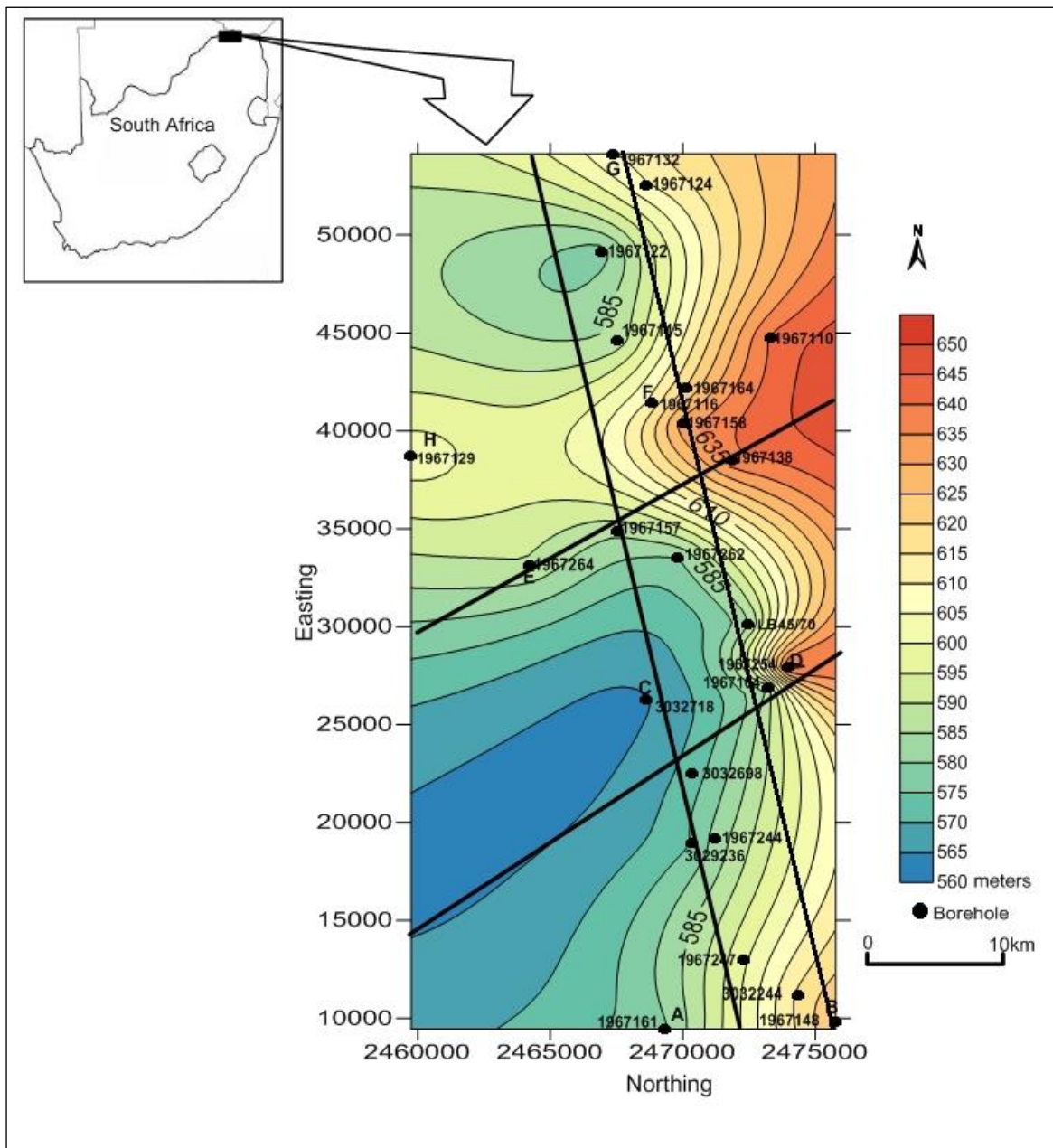


Figure 3.35: Structure contour map and cross-section of the Tuli Coalfield. Contour lines are in meters above sea level.

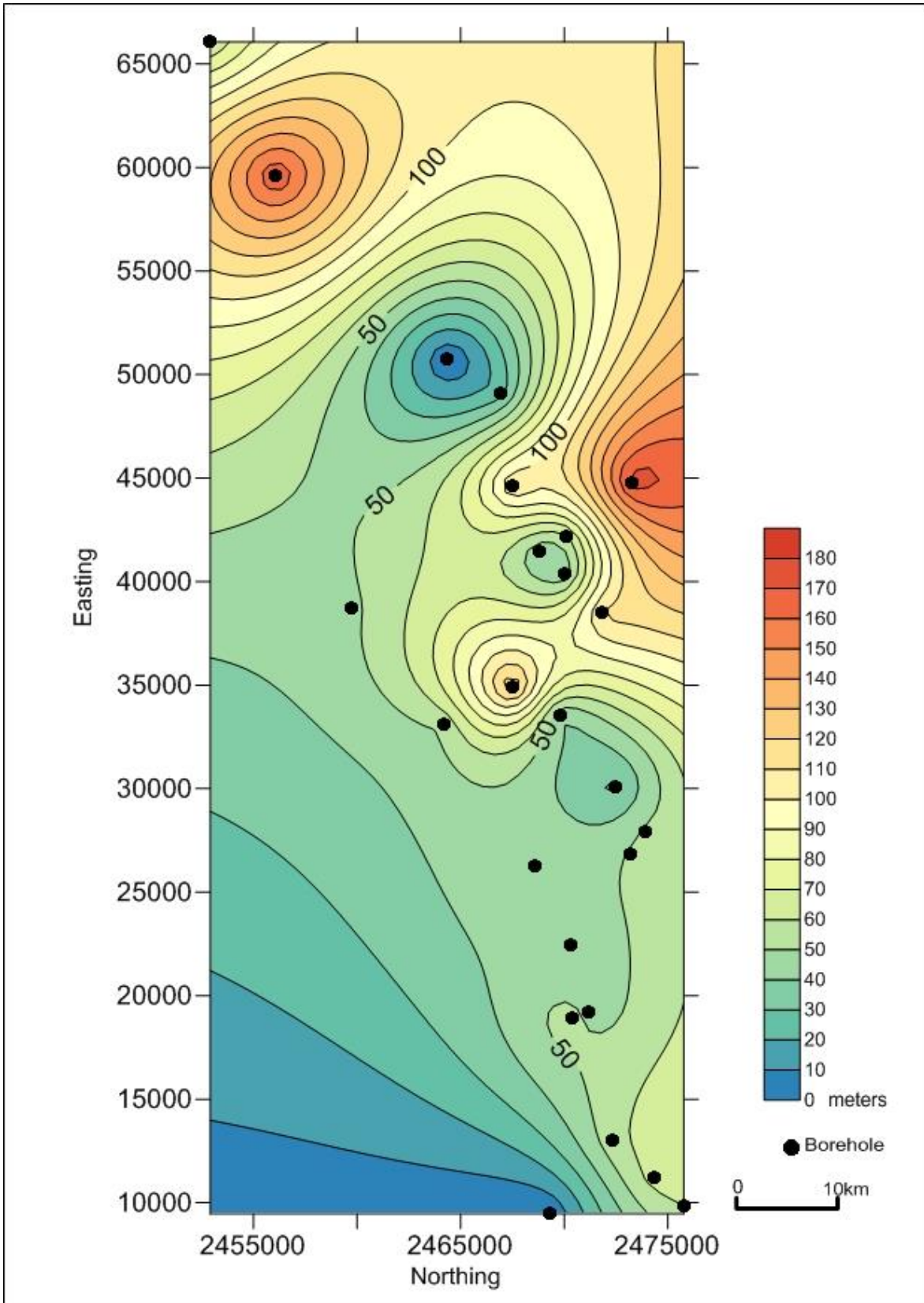


Figure 3.36: Thickness contour map of the Mikambeni Formation in the Tuli Coalfield.

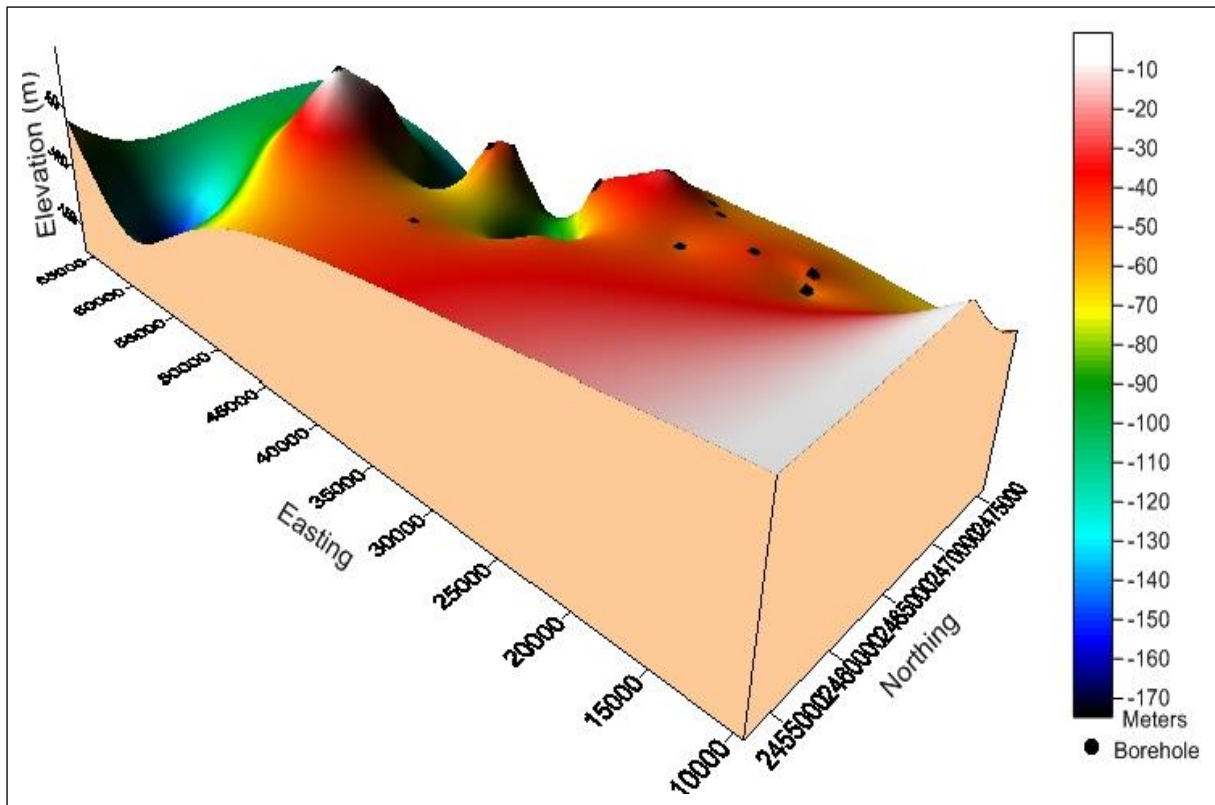


Figure 3.37: 3d topographic map of the Mikambeni Formation in the Tuli Coalfield.

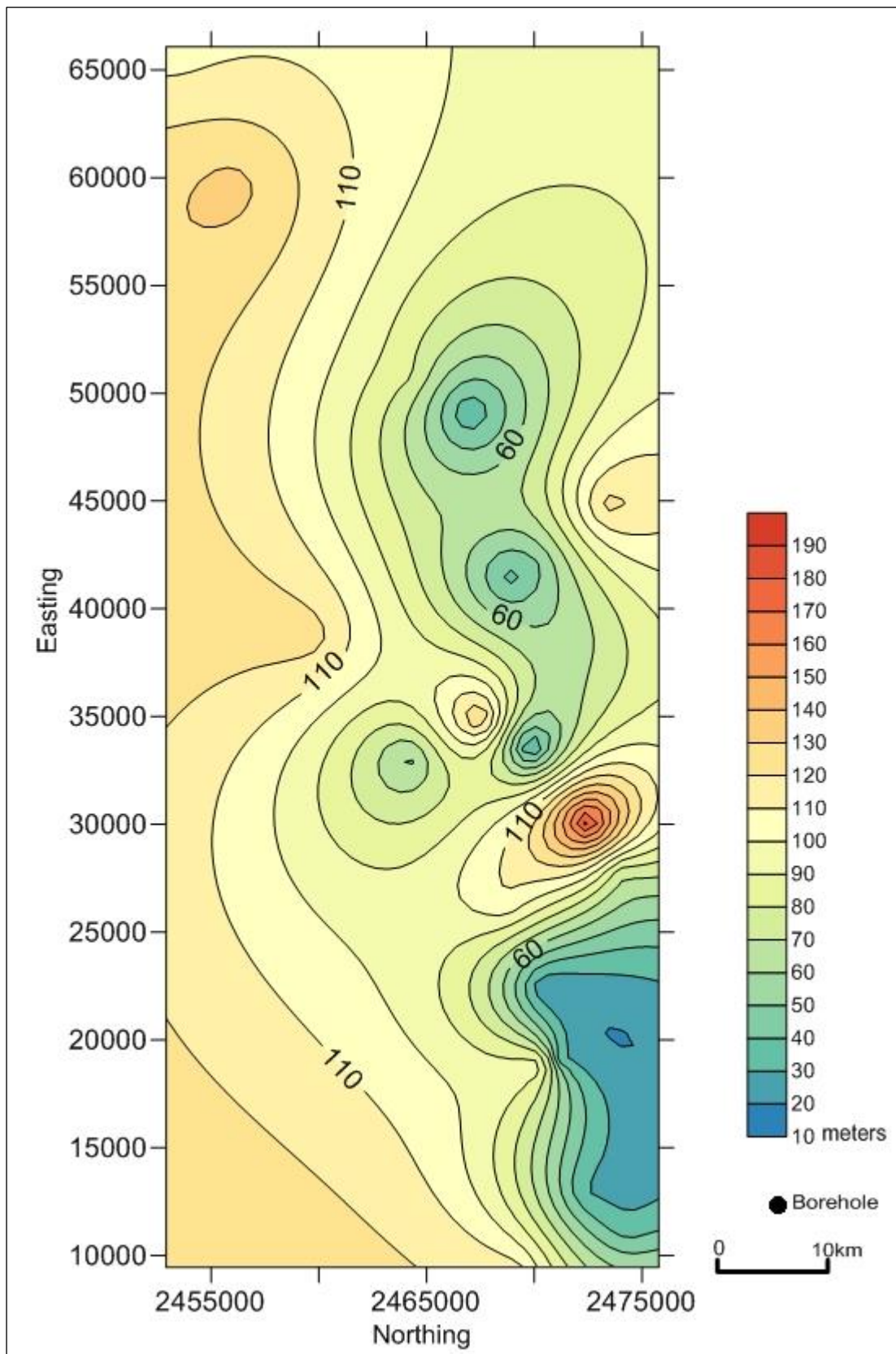


Figure 3.38: Thickness contour map of the Madzaringwe Formation in the Tuli Coalfield.

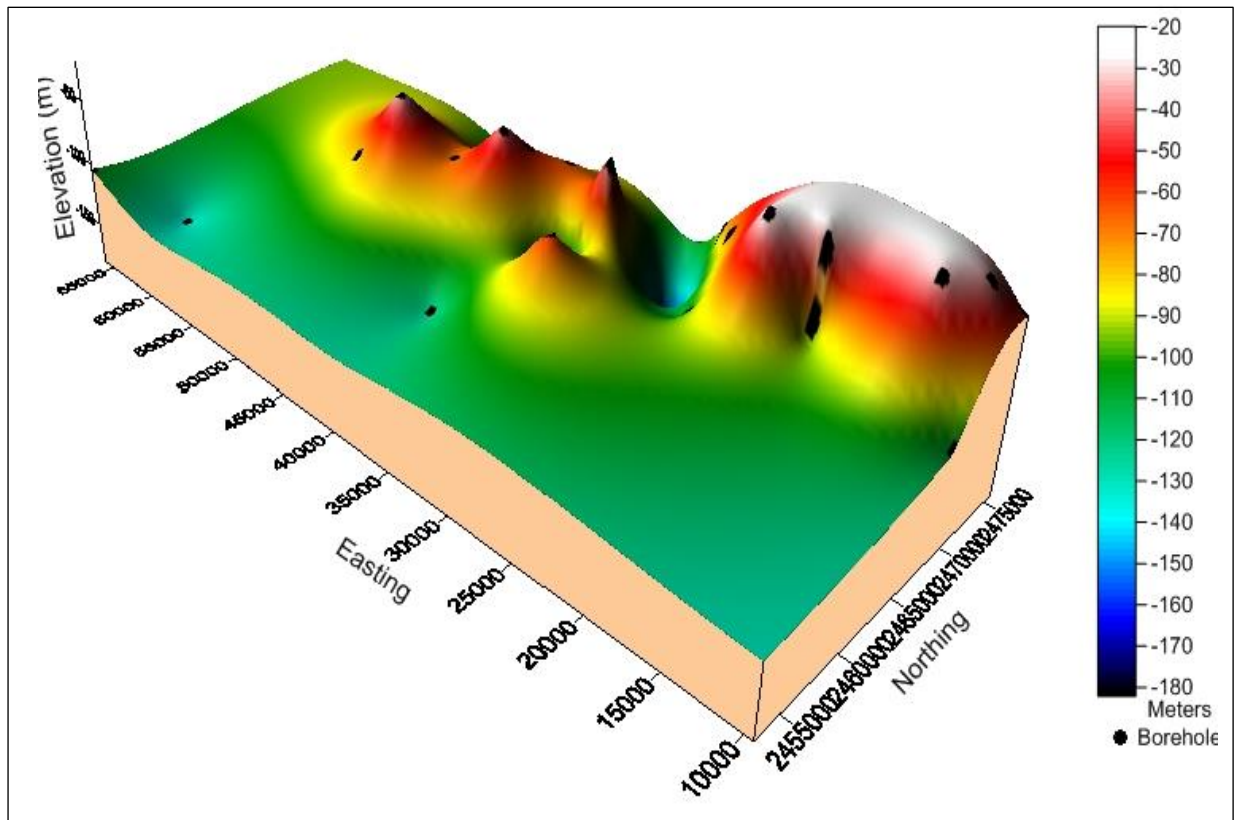


Figure 3.39: 3d topographic map of the Madzaringwe Formation in the Tuli Coalfield.

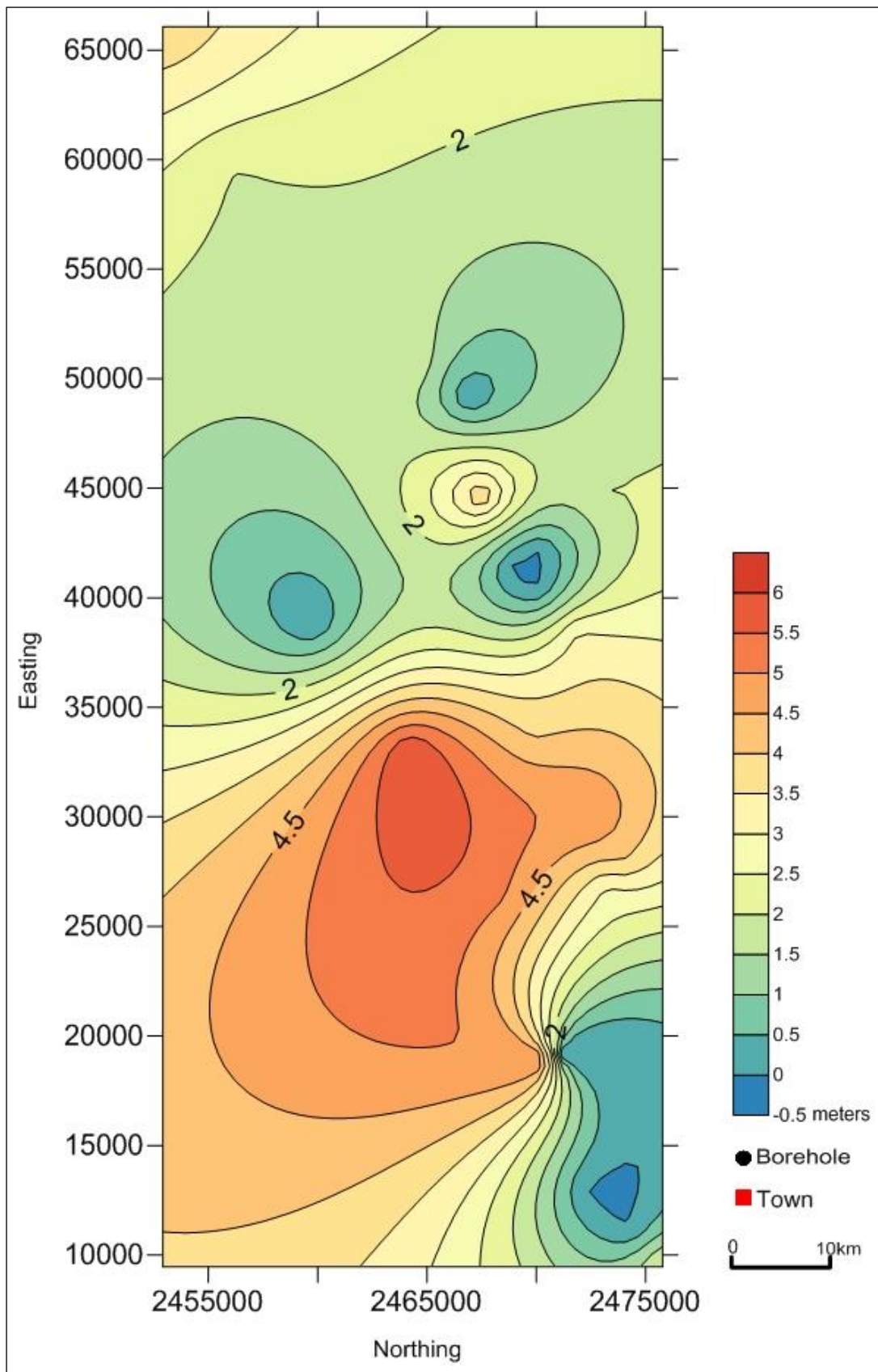


Figure 3.40: Thickness contour map of the Tshidzi Formation in the Tuli Coalfield.

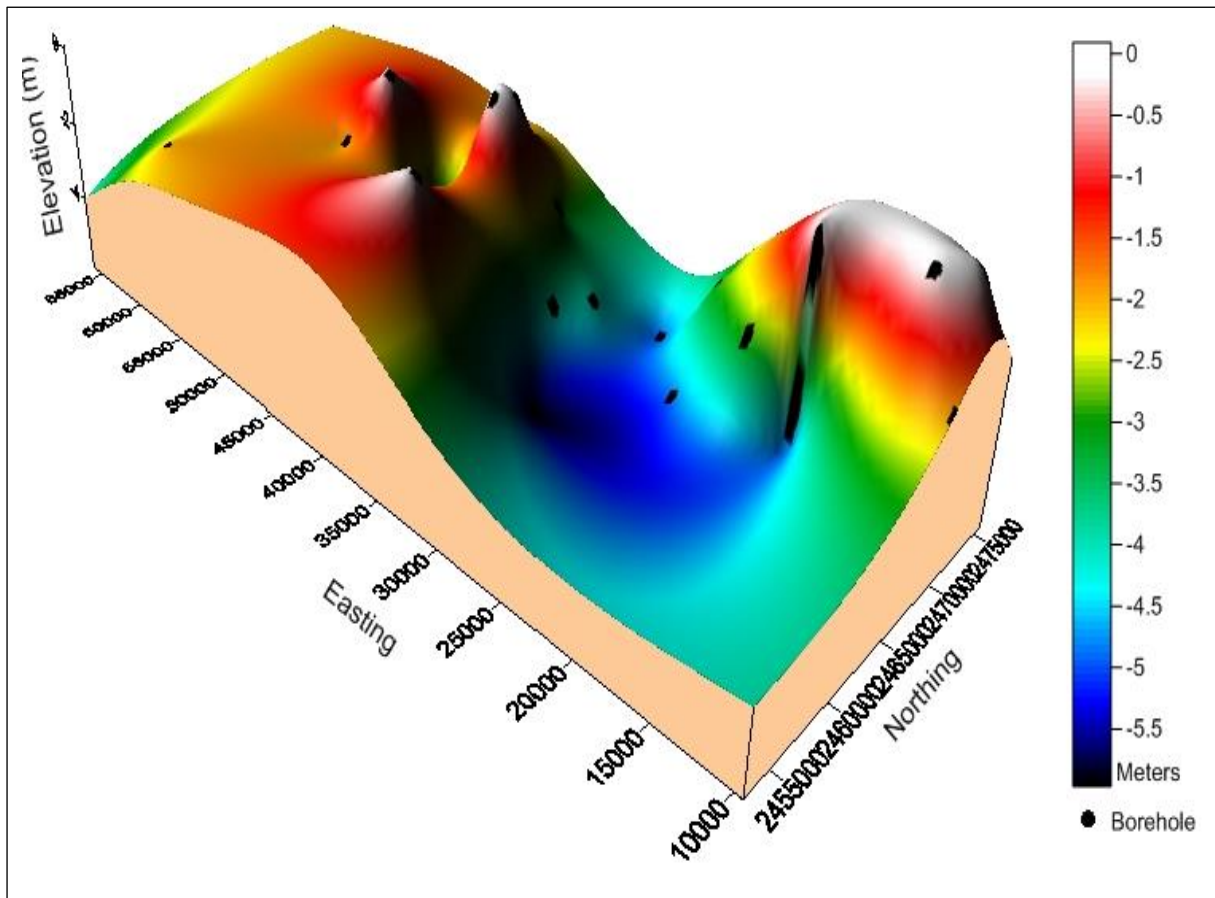


Figure 3.41: 3d topographic map of the Tshidzi Formation in the Tuli Coalfield.

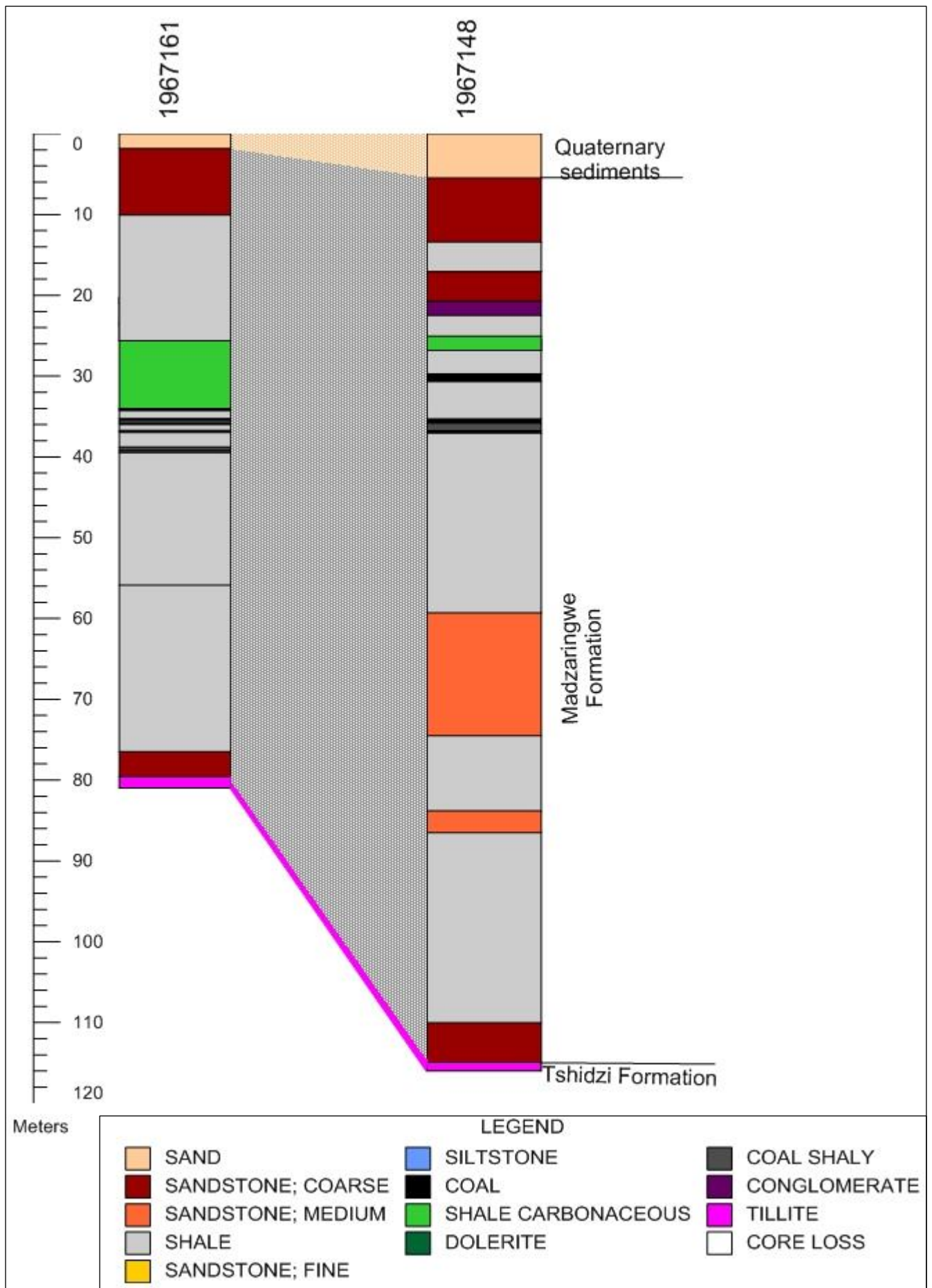


Figure 3.42: Stratigraphic column and correlation diagram (Cross-section 1) in the Tuli Coalfield. The different colours between stratigraphic columns represent the correlation boundaries of the different stratigraphic units. The numbers above of the logs represents borehole core numbers in the CGS archives.

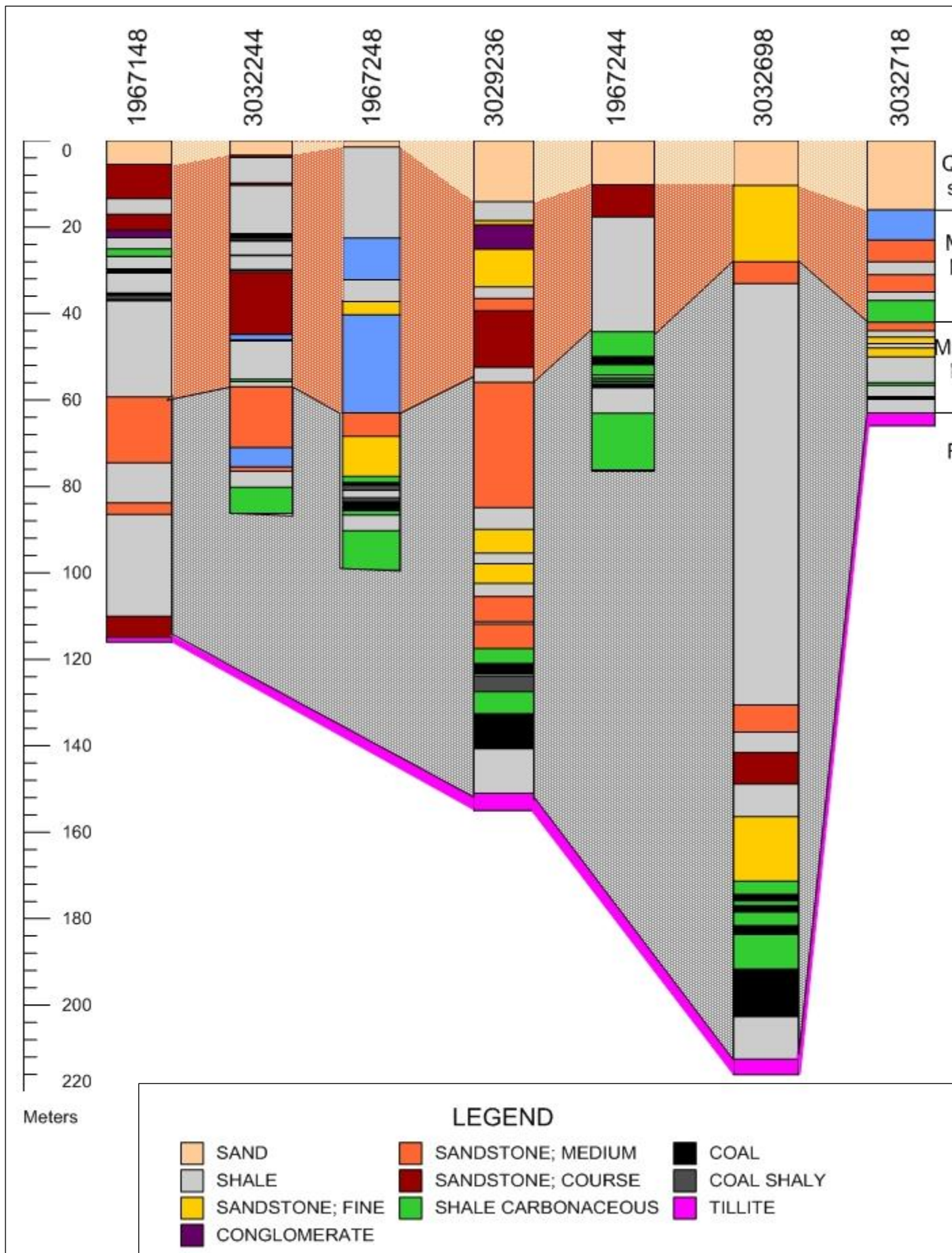


Figure 3.43: Stratigraphic column and correlation diagram (Cross-section 2) in the Tuli Coalfield. The different colours between stratigraphic columns represent the correlation boundaries of the different stratigraphic units. The numbers above of the logs represents borehole core numbers in the CGS archives.

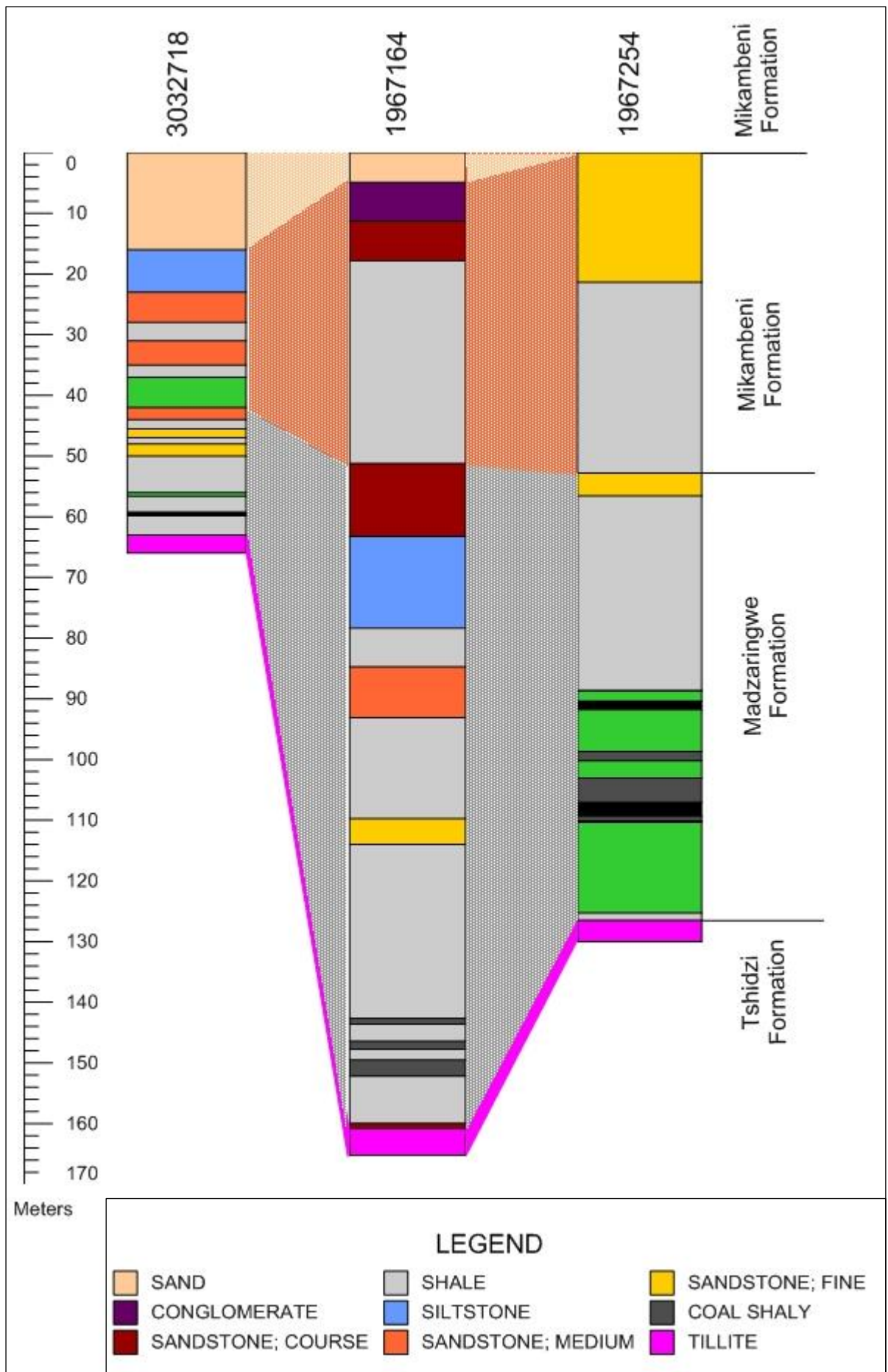


Figure 3.44: Stratigraphic column and correlation diagram (Cross-section 3) in the Tuli Coalfield. The different colours between stratigraphic columns represent the correlation boundaries of the different stratigraphic units. The numbers above of the logs represents borehole core numbers in the CGS archives.

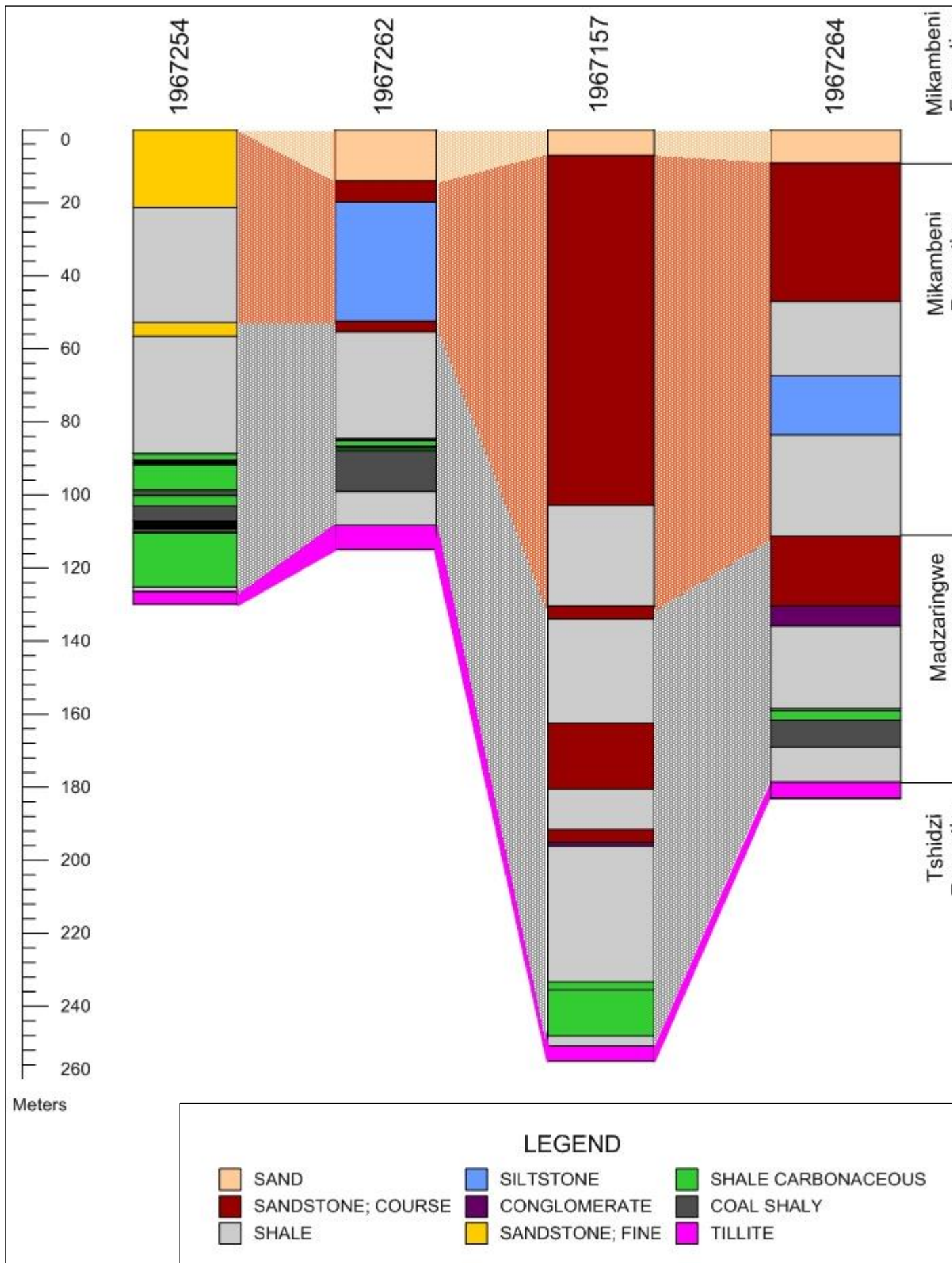


Figure 3.45: Stratigraphic column and correlation diagram (Cross-section 4) in the Tuli Coalfield. The different colours between stratigraphic columns represent the correlation boundaries of the different stratigraphic units. The numbers above of the logs represents borehole core numbers in the CGS archives.

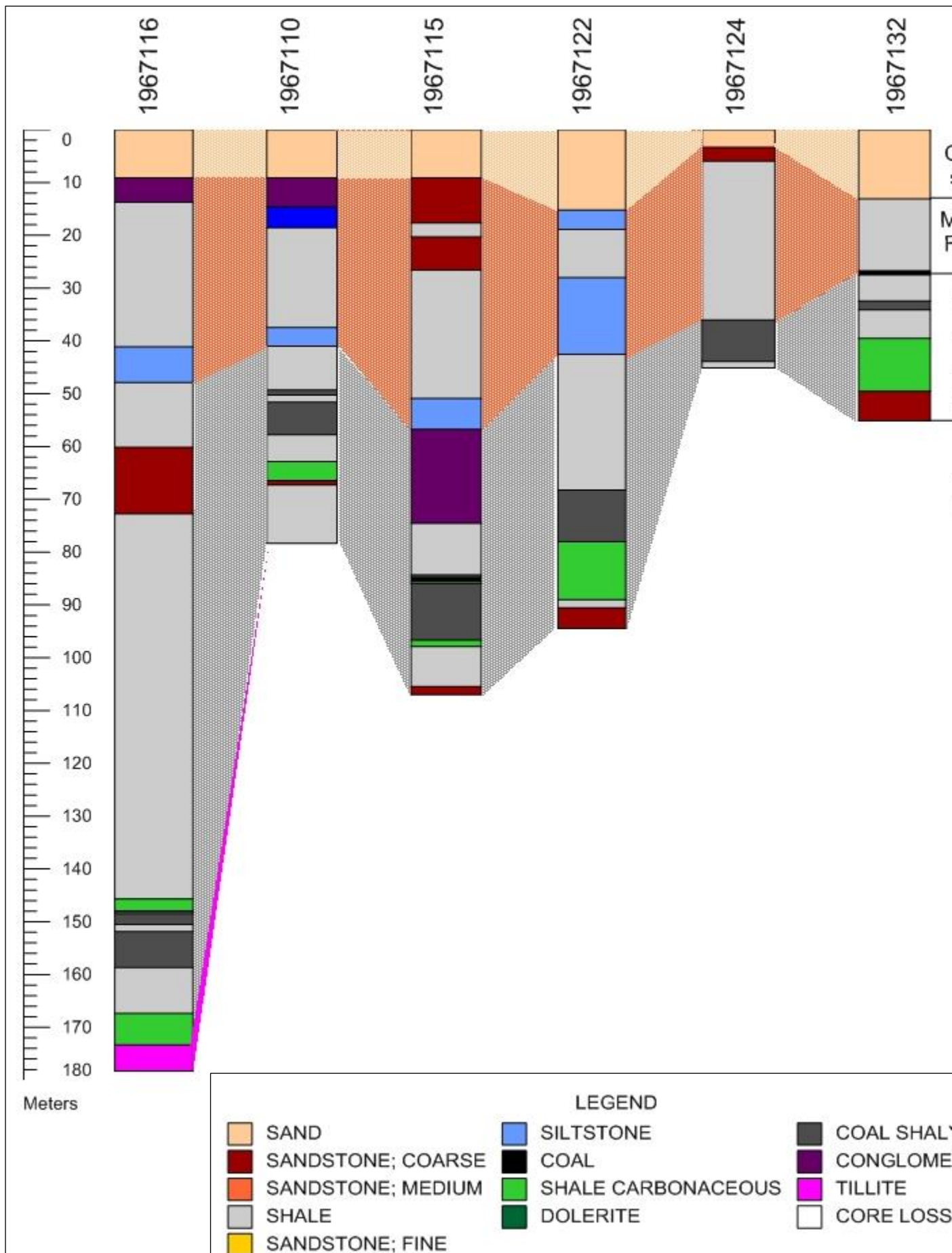


Figure 3.46: Stratigraphic column and correlation diagram (Cross-section 5) in the Tuli Coalfield. The different colours between stratigraphic columns represent the correlation boundaries of the different stratigraphic units. The numbers above of the logs represents borehole core numbers in the CGS archives.

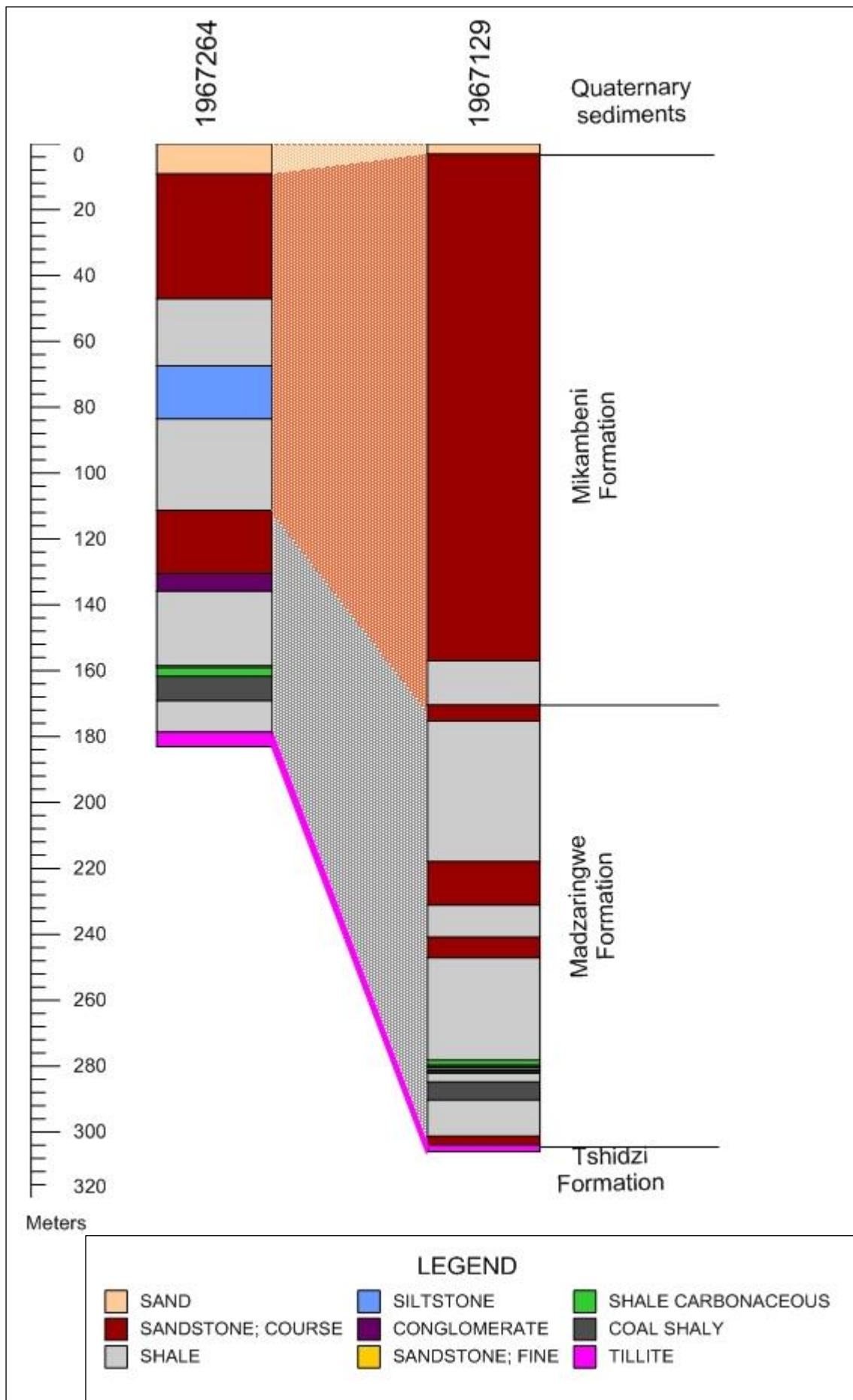


Figure 3.47: Stratigraphic column and correlation diagram (Cross-section 6) in the Tuli Coalfield. The different colours between stratigraphic columns represent the correlation boundaries of the different stratigraphic units. The numbers above of the logs represents borehole core numbers in the CGS archives.

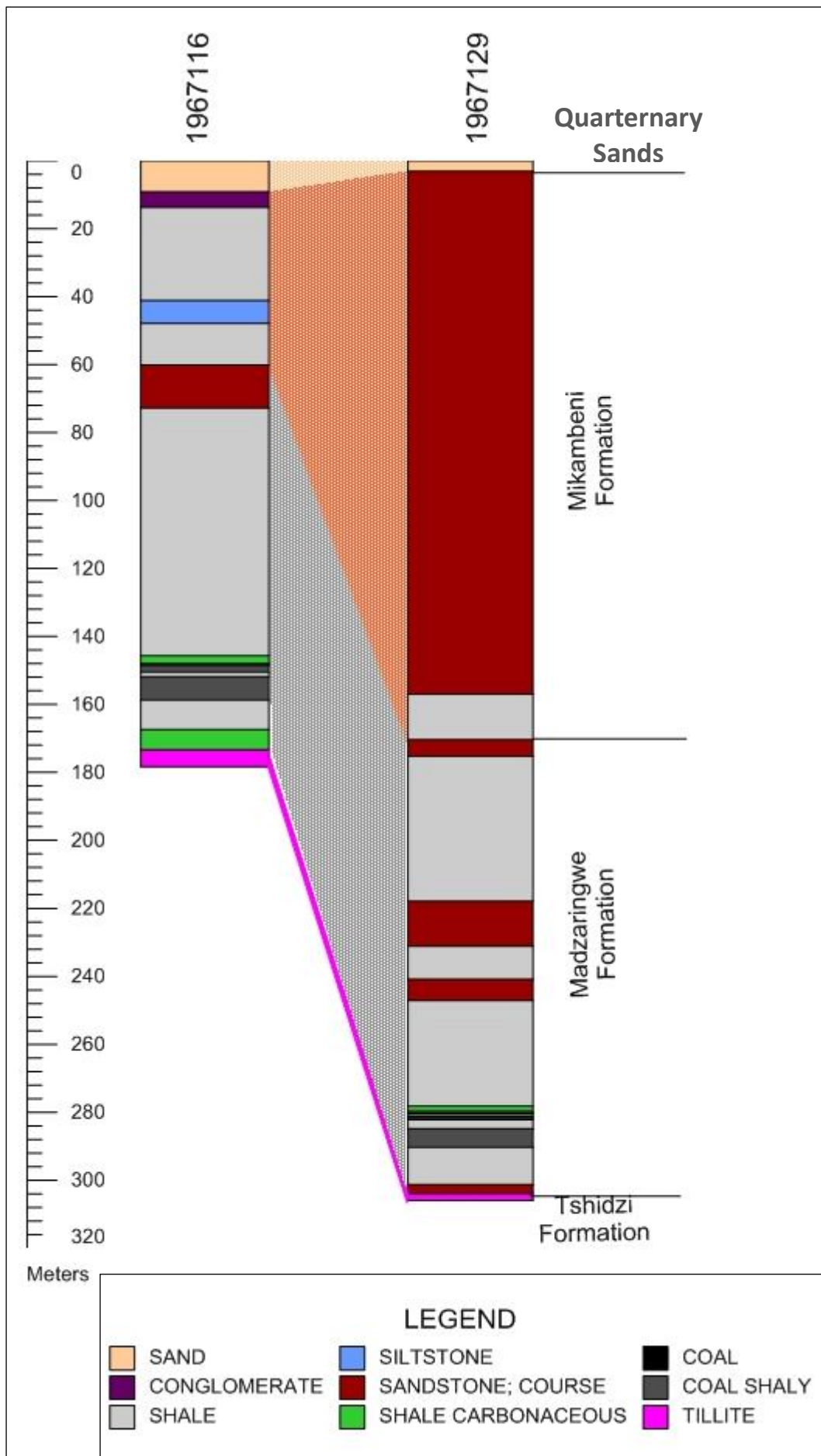


Figure 3.48: Stratigraphic column and correlation diagram (Cross-section 7) in the Tuli Coalfield. The different colours between stratigraphic columns represent the correlation boundaries of the different stratigraphic units. The numbers above of the logs represents borehole core numbers in the CGS archives.

3.4. Discussions

The present study was undertaken to define more clearly the stratigraphic correlation of the Soutpansberg and Tuli Coalfields. For this particular area a superposed sequence of three stratigraphic units is proposed to represent the lower Paleozoic sedimentary rocks which are exposed here. These units are consistent with the earlier descriptions of Brandl (1981), Brandl and McCourt (1980), and Bordy and Catuneanu (2002).

In the present study, the Tshidzi Formation is developed at the base of the Karoo Sequence and consists of diamictite resting with a disconformity contact on the upper formations of the Soutpansberg Group. The formation is confined to a few sporadic outcrops which probably developed in pre-Karoo depressions. The diamictite attains a maximum thickness of 20 m and is composed of angular and subrounded clasts. This formation may be correlated to the Dwyka Formation in the main Karoo Basin.

In this study the Madzaringwe Formation is divided into three superposed members: the Basal Member, a grey and black laminated carbonaceous shale and coal; Middle Member, alternating beds of shale, siltstone and fine-coarse grained sandstone; Upper Member, a grey and black laminated carbonaceous shale and coal again, similar to the Basal Member.

Succeeding the Madzaringwe Formation is the Mikambeni Formation, which can be informally subdivided into two members (Lower and Upper Members). The Lower Member is characterised by laminated, grey and black carbonaceous shale and coal and sandy shale/mudstone. The Middle Member is characterised by alternating beds of shale, siltstone and fine-coarse grained sandstone.

In the Tshipise-Pafuri Coalfield, the average thickness of the Tshidzi Formation is ~3.2 m, while the Madzaringwe Formation is ~158 m and the Mikambeni Formation is ~148 m. In the Mopane Coalfield the average thickness of the Tshidzi Formation is ~2.8 m, while the Madzaringwe Formation is ~ 18 and the Mikambeni Formation is ~160 m. In the Tuli Coalfield the average thickness of the Tshidzi Formation is 2.3 m, while the Madzaringwe Formation is 74 m and the Mikambeni Formation is 62 m.

Figure 3.49 and 3.50 illustrates the generalised lithostratigraphic sub-division of the Soutpansberg and Tuli Coalfields.

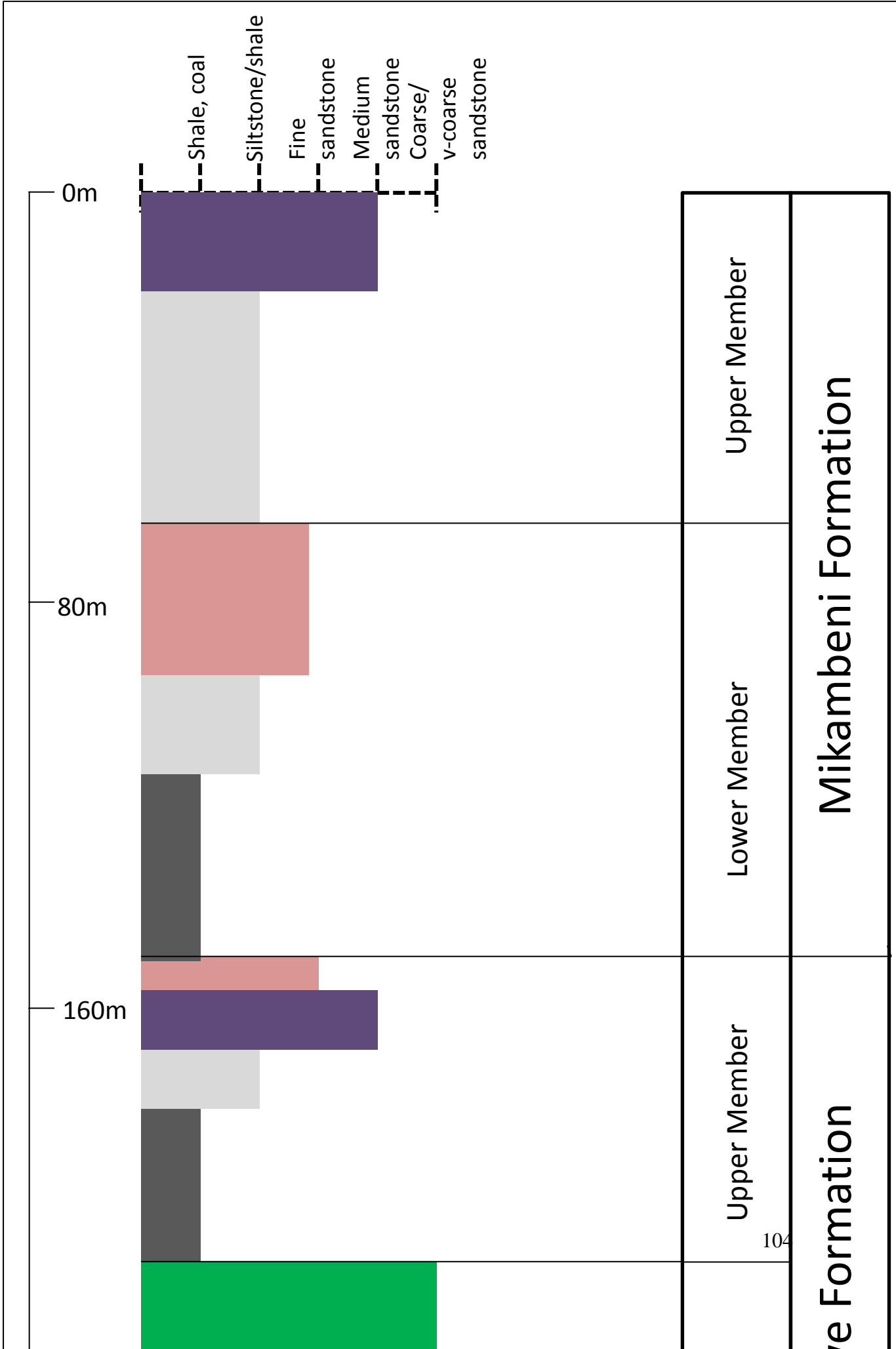


Figure 3.49: Generalised lithostratigraphic sub-division (informal) of the Soutpansberg Coalfield.

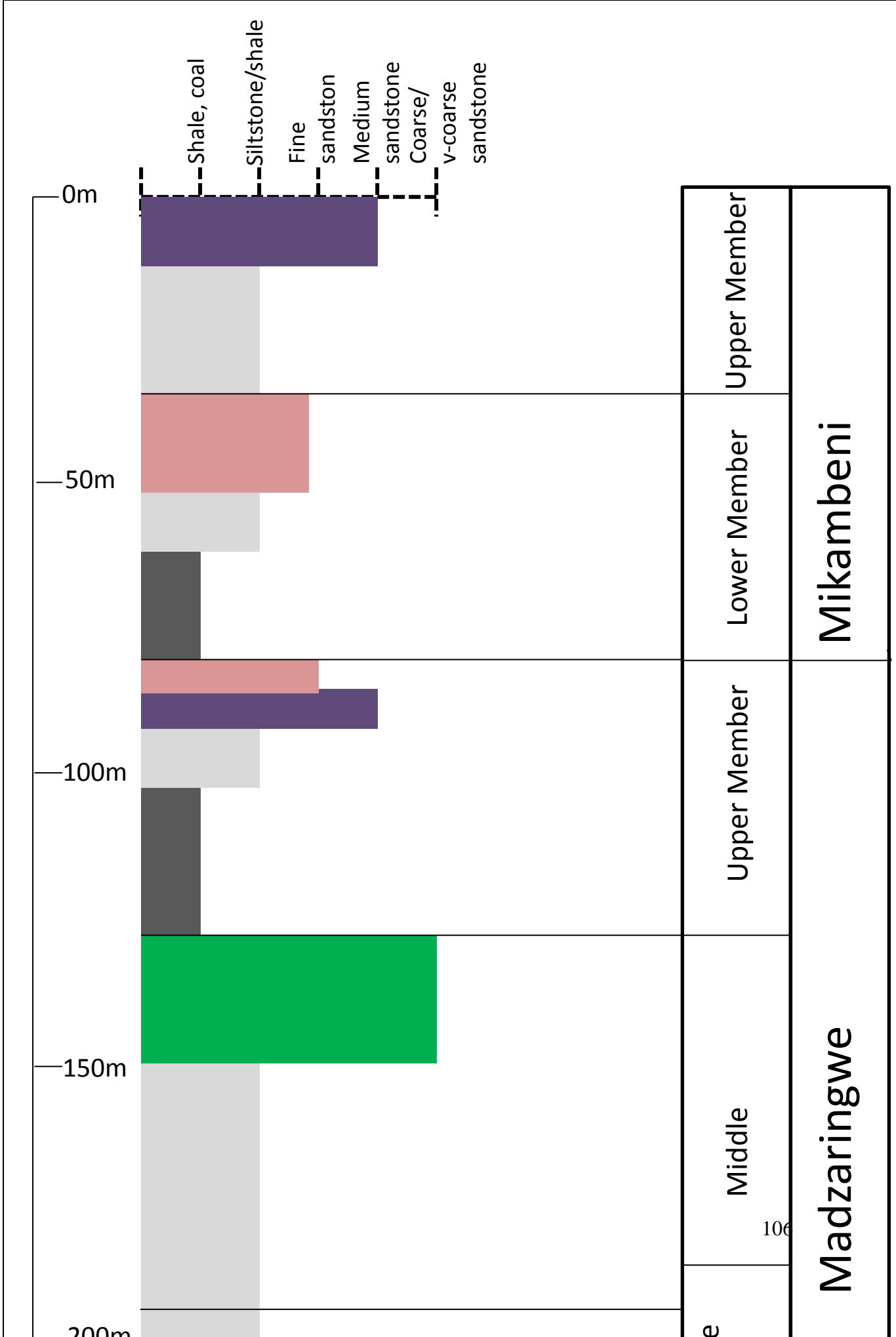


Figure 3.50: Generalised lithostratigraphic sub-division (informal) of the Tuli Coalfield.

3.5. Conclusions

The late Mesozoic to early Palaeozoic stratigraphy of the Soutpansberg and Tuli Basins has been substantially modified. The coalfields now essentially constitutes a sequence of late Carboniferous (Tshidzi, Madzaringwe, Mikambeni and Fripp Formations), Permian (Solitude, Klopperfontein, Bosbokpoort and Clarens Formation) and lastly the Lebombo and Letaba Formations of Jurassic basalts.

In summary, outcrops in the Soutpansberg and Tuli Basins can be assigned to three chronostratigraphic and lithological units which make up the Karoo Supergroup in the Limpopo Province in the periods of the:

- Permian which is consists of the Tshidzi Formation dominated by diamictite and minor sandstone and the Madzaringwe, Mikambeni and Fripp Formations dominated by sandstone, shale, conglomerates and coal.
- Triassic which consists of the Solitude, Klopperfontein, Bosbokpoort and Clarens Formations dominated by sandstone and shale.
- Jurassic which consists of the basaltic Letaba and Jozini Formations.

CHAPTER 4

STRUCTURAL GEOLOGY AND EVOLUTION OF THE SOUTPANSBERG AND TULI COALFIELDS

Abstract

This chapter presents the paleostress-analysis which resulted from interpretation of the fault-slip data collected on the sedimentary rocks of the Karoo Supergroup in the Soutpansberg and Tuli Coalfields. Stress inversion of 69 fault-slip data was performed using an improved Right-Dihedral method, followed by rotational optimization (WINTENSOR Program, Delvaux, 2012). Fault-slip data including fault planes, striations and sense of movements, were obtained from outcrops in the coalfields. The orientation of the principal stress axes (σ_1 , σ_2 and σ_3) and the ratio of the principal stress differences (R) show a paleostress field marking two main stress regimes. The main stress fields in the Soutpansberg Coalfield are characterised by W-E to ENE-WSW extension and N-S to NNW-SSE compression. It includes two paleostress regimes, one with dominantly dip-slip normal faulting (extensional regime) and a minor strike-slip faulting (strike-slip regime). The second paleostress field is characterised by a NE-SW to ENE-WSW extension and NW-SE to NNW-SSE compression. The main stress fields in the Tuli Coalfield is characterised by a N-S to NNW-SSE compression and W-E to ENE-WSW extension. The stress regimes are related to a spreading process along the Tethyan margin of Gondwana controlling the deposition of Karoo sediments in grabens and subsequent rift structures. Continuing extension along the East African Rift Valley defines the tectonic framework of the coalfields. The East-West trends of the stress fields in the coalfields follows the E-W elongated low lying Limpopo Mobile Belt.

4.1. Introduction

This chapter aims to investigate the structural settings of the two coalfields in the Soutpansberg and Tuli Basins. Topics such as the influence of the tectonic instability mainly within the northern Karoo Basins and its influence on the formation of the basins are addressed. In addition, more fundamental geological features such as the Limpopo Mobile Belt (LMB), the Soutpansberg Group together with other Karoo neighbouring basins (such as the Elisras Basin) are discussed with the aim of further understanding the formation of the two coalfields. Paleostress Analysis was performed in order to understand the stress regime of the basins. Both the coalfields are characterised by normal faults and minor strike slip faults trending north-northeast in the Soutpansberg Coalfield and east-northeast in the Tuli Coalfield.

4.2. Geological Evolution

4.2.1. The Limpopo Mobile Belt

The Limpopo Mobile Belt (LMB) in Southern Africa has been a major focus of research on Archaean tectonics and crustal evolution, and has been regarded as an area of typical Archaean high grade deformation, often referred to as a mobile belt (Van Reenen *et al.*, 1992). The belt is a zone of granulite facies rocks situated between the greenschist-amphibolite rocks of the Zimbabwe Craton to the north and the Kaapvaal Craton to the south. It is a near East-West elongated low lying belt straddling eastern Botswana, southern Zimbabwe and the northern part of the Limpopo Province in South Africa. The belt is subdivided into three zones on the basis of lithological and structural characters; the Northern Marginal Zone (NMZ), the Central Zone (CZ) and the Southern Marginal Zone (SMZ) as shown in Figure 4.1. A slightly larger proportion falls within the borders of Zimbabwe; for example the whole of the NMZ and a substantial amount of the CZ are exposed in Zimbabwe.

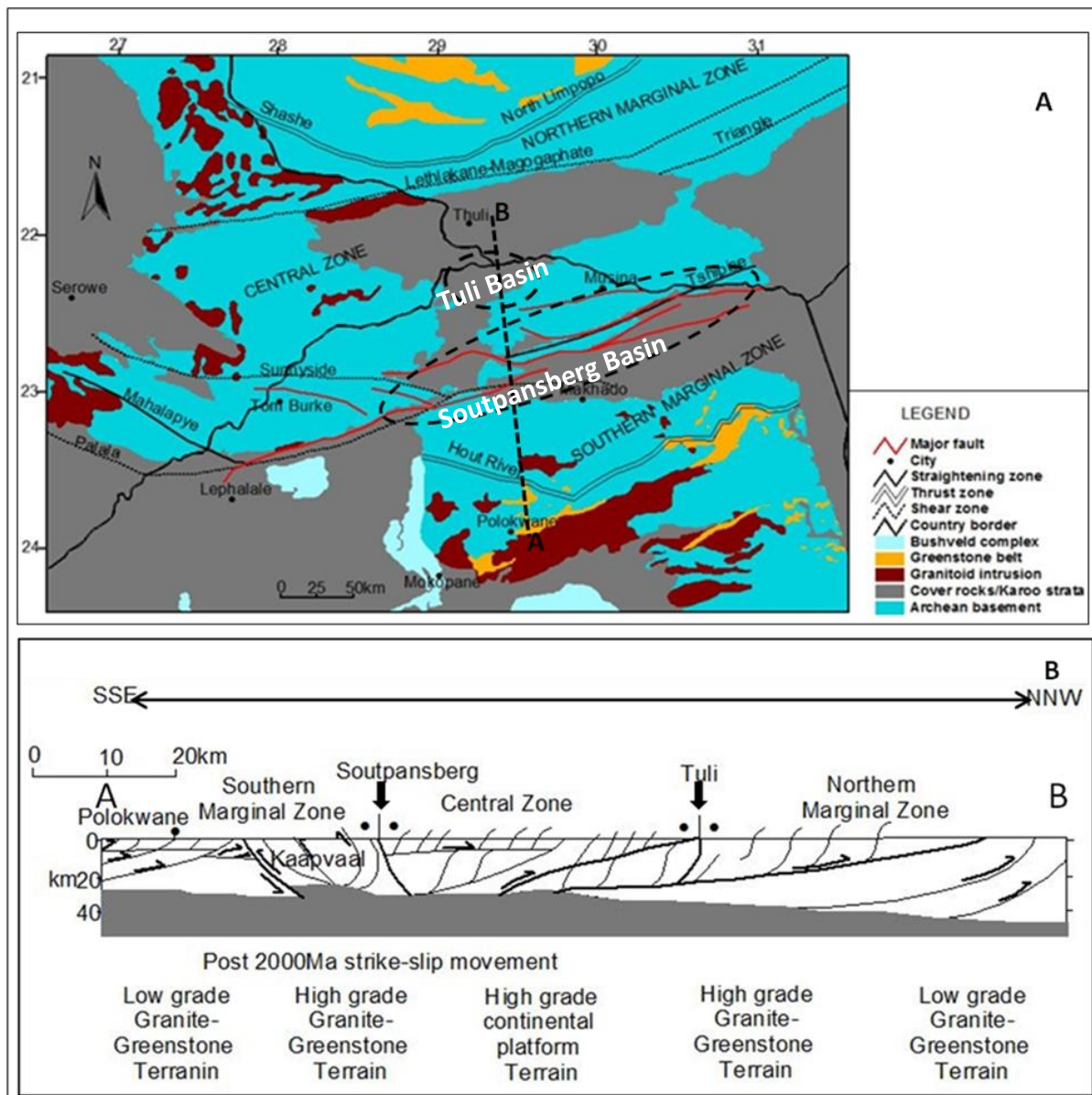


Figure 4.1: (A) Simplified map of the Limpopo Mobile Belt showing its subdivisions, major shear zones, adjacent cratons and the Tuli and Soutpansberg Basins. (B) Cross-section of the area. Modified and redrawn after McCourt and Verncombe (1992); Barton *et al.* (2003).

4.2.2. The Soutpansberg Group

The ~ 1850 Ma Soutpansberg Group has in the past been interpreted as a volcano-sedimentary sequence deposited either within an aulacogen/rift basin, or as a more extensive cover sequence preserved only within a post sedimentary graben (Brandl, 2002). Bumby *et al.* (2001) gave some evidence from the Blouberg area of Limpopo Province, South Africa, indicating that the Soutpansberg strata were laid down within a half-graben bound to the south by a northwards-dipping normal fault. Paleocurrent directions within the Wyllie's Poort

Formation of the Soutpansberg Group suggest that planar-bedded, ripple-marked sandstones were deposited by transverse-flowing rivers, whilst small- to large-scale trough and planar cross-bedded sandstones indicate transport in large, low sinuosity longitudinal trunk rivers, flowing approximately parallel to the axis of the half-graben. The N-S oriented Soutpansberg extensional regime may reflect orogenic collapse after the cessation of N-S orientated compression developed at ca. 2.0 Ga by collision or reactivation tectonics in the Limpopo Belt (Brandl, 2002).

4.2.3. The Soutpansberg and Tuli Basins

The geology of the two basins is developed over a region which is underlain by a craton suture (Bumby *et al.*, 2001). The suture was formed during the Kaapvaal Craton and the Central Zone of the Limpopo Mobile Belt (LMB) either 2650 Ma or 2000 Ma. The Soutpansberg sedimentary basin was developed on the Tshipise Straightening Zone and the Tuli Sedimentary Basin is developed on the Triangle Shear Zone (Figure 4.2).

The Palala Shear Zone (Figure 4.2) on the west generally has a sinistral sense of shear; though it has been reactivated locally in an opposite sense (McCourt and Vearncombe 1987, 1992). Schaller *et al.* (1999) argued that the Palala has a predominantly dextral sense of shear. Eastwards, the Palala becomes covered by younger Proterozoic sedimentary rocks of the Blouberg area. Still further eastwards, the Palala Shear Zone may be represented by the Tshipise Straightening Zone which runs parallel to, and north of the Proterozoic aged Soutpansberg Group (Bahnemann, 1972). At this point the Tshipise Straightening Zone is covered by Karoo strata of the Soutpansberg Sedimentary Basin (Figure 4.2). The contact between the Central Zone and the North Marginal Zone is marked by the Triangle Shear Zone on the East and Magothate Shear Zone on the west, though much of their length is covered by the Phanerozoic (Karoo) strata of the Tuli sedimentary basin (Bumby *et al.*, 2001).

In Southern Africa, the deposition of the Karoo sediments occurred in two broadly different tectonic settings (Rust, 1975; Cairncross, 2001). According to Catuneanu *et al.* (1998), the sedimentary rocks of the main Karoo Basin are retroarc foreland fills. North of the Main Karoo Basin, the sub-basins (Soutpansberg, Tuli and Elisras) are preserved in separate, fault-bounded depositories which are interpreted either as rift basins or intracratonic thermal sag basins (Watkeys and Sweeney, 1988; Groenewald *et al.*, 1991; Johnson *et al.*, 1996). Subsidence in the Tuli and Soutpansberg Basins of the Limpopo area was initially attributed to extension that accompanied the formation of the western arm of a failed rift in a

triple junction setting (Bordy and Catuneanu, 2002). Instead, it has been proposed that flexural subsidence in the back-bulge region of the Karoo foreland system was the primary control in the creation of accommodation for the deposition of Permo-Carboniferous units (at least Dwyka and Ecca equivalents) in the Limpopo area (Catuneanu *et al.*, 1998; Bordy and Catuneanu, 2001, 2002; Catuneanu, 2004).

4.2.4. Faulting

Movement along the LMB, as tectonic re-activation due to continuous tension in the Karoo era, fault zones occurred, controlled the formation of the Karoo sediments and finally acted as conduits for the extrusion of basalts which terminated the Karoo era (Barker, 1983). Intense block-faulting caused the development of a series of stepped half-grabens and these are now seen as repeatedly occurring narrow strips of Karoo rocks mostly around the Soutpansberg Basin.

In the Soutpansberg Basin, two intersecting fault systems can be recognised (Brandl, 1981). One system is composed of faults which trend East-North-East, parallel to the regional strike, and delineate major horst and graben structures. The throw is either to the north or south and the maximum vertical displacements probably do not exceed 500 m. The main faults of this type are named Bosbokpoort, Tshipise and Klein Tshipise (Figure 4.2). The second system is oblique to the regional strike and has faults trending West-North-West to North-West. The throw is generally to the south-west. The most prominent fault is the Siloam Fault. All faults affecting the Karoo strata appear to be normal and most are probably of post-Karoo age. However minor faulting probably took place prior to the deposition of the Karoo rocks in the Soutpansberg Basin. The dip of the strata in the basin is generally to the north and varies between 10° to 20° (Brandl, 1981).

Strata in the Tuli Basin gently dip about 5° to the north, and here they form the southern margin of the basin which extends north and northeast into Botswana and Zimbabwe. Chidley (1985) recognized that the Tuli Basin is a small intracratonic east-west-trending fault-controlled depository with a preserved basin width of 80 km. The East-west trend parallels the Soutpansberg basin. The Karoo sedimentation was fault controlled from the onset.

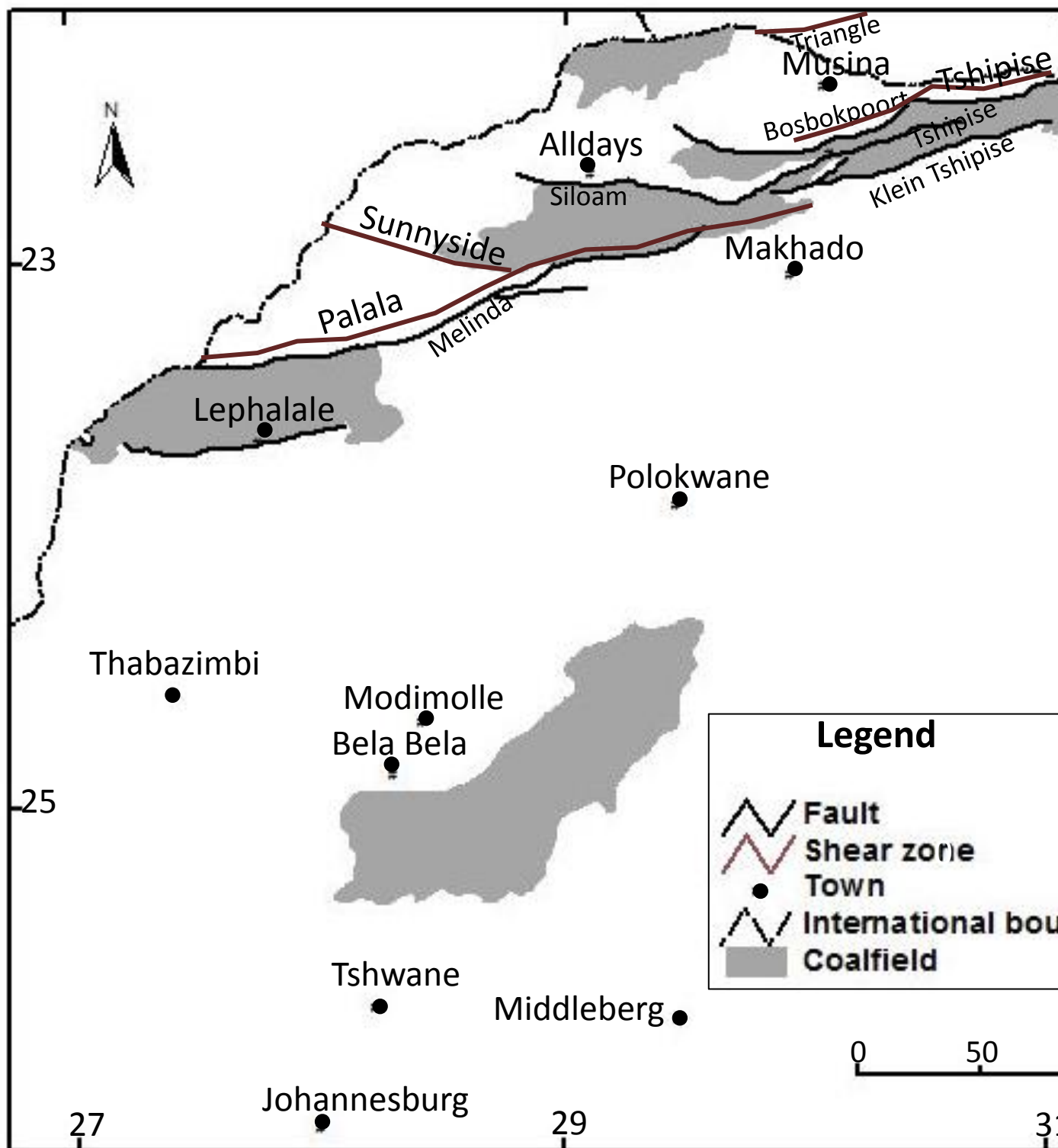


Figure 4.2: Coalfields in Northern South Africa showing major shear zones and major faulting. Modified and redrawn after McCourt and Verncombe (1992); Barton *et al.* (2003).

4.3. Methodology

The fault-slip data were collected by measuring fault planes and slickenlines at different locations in the Soutpansberg and Tuli Coalfields. The measurements at each location included the fault plane, trend and plunge of slickenlines. Sixty nine fault-slip data were collected from sub-horizontal strata of the Upper Palaeozoic to Lower Mesozoic sedimentary formations of the coalfields. The faults on which slickenlines were measured are generally of normal and minor thrust and strike-slip in nature.

Stress inversion of 69 fault-slip data was performed using an improved Right-Dihedral method, followed by the Rotational Optimization (WINTENSOR Program, Delvaux, 2012). Paleostress inversion techniques have been used by various researchers for more than 30 years. They are based upon the work of Wallace (1951); Bott (1959), who assumed that slip on a plane, occurs in the direction of the maximum resolved shear stress. The World Stress Map (WSM) by Sperner *et al.* (2003) and the Tensor Program by Delvaux (2012) was used for the rating of the quality and a better comparability of the results. In accordance with the ranking scheme for the WSM, the quality ranges from A (best) to E (worst) and is determined as threshold values of series of criteria (Table 4.1). The threshold values were chosen more or less arbitrarily and then tested with the field data and checked whether they gave a good range of quality of the results. A given quality was assigned if the threshold values corresponding to that particular rank were met for all the criteria.

Fault plane and slickenline orientations, including slip senses are used to compute the four parameters of paleostress tensors (σ_1 , σ_2 , σ_3 and R): the principal stress axis σ_1 (maximum compression), σ_2 (intermediate compression) and σ_3 (minimum compression) and the ratio of principal stress difference $R = (\sigma_2 - \sigma_3) / (\sigma_1 - \sigma_3)$. The stress regime is defined by the nature of the vertical stress axes:

1) Normal faulting when σ_2 is the maximum horizontal stress axes (σ_2 SHmax) and σ_1 is vertical, 2) strike- slip faulting when σ_1 is the maximum horizontal stress axes (σ_1 SHmax) and when σ_2 is vertical and 3) thrust/ reverse faulting when σ_1 is the maximum horizontal stress axes (σ_1 SHmax) and σ_3 is vertical (Delvaux *et al.*, 1997; Delvaux and Sperner, 2003).

Table 4.1: Threshold values as defined in Sperner *et al.* (2003) for the individual criterion used in the quality ranking scheme for the WSM (n-DTw) and the values of Plen and Slen are added for the Tensor Quality Rank (QRT).

WSM Quality Rank (QRwsm)	n	n/nt	CLw	α_w	DTw	Plen	Slen	Tensor Quality Rank
A	≥ 25	≥ 0.60	≥ 0.70	≤ 9	≥ 0.90	≤ 0.80	≤ 0.80	A
B	≥ 15	≥ 0.40	≥ 0.55	≤ 12	≥ 0.75	≤ 0.85	≤ 0.85	B
C	≥ 10	≥ 0.30	≥ 0.40	≤ 15	≥ 0.50	≤ 0.92	≤ 0.92	C
D	≥ 6	≥ 0.15	≥ 0.25	≤ 18	≥ 0.25	≤ 0.95	≤ 0.95	D
E	< 6	< 0.15	< 0.25	> 18	< 0.25	> 0.95	> 0.95	E

Where:

n-The initial data

n/nt- Ratio of the initial and total number of fault measured

CLw- Slip sense confidence level for individual fault applied for the Tensor Program

α_w - Deviation between observed and theoretical slip direction

DTw- Fault slip data type

Plen- Fault plain vector

Slen- Slip direction vector

QRwsm- World Stress Map Quality Rank

QRt- Tensor Quality Rank

4.4. Results

4.4.1. The Soutpansberg Coalfields (Tshipise-Pafuri and Mopane)

The main stress field in the Soutpansberg Coalfield is characterised by W-E to ENE-WSW extension and N-S to NNW-SSE compression, Figure 4.3 (A to D) and Figure 4.4 (A to C). This stress field is associated with the subsidence in the basin which was initially attributed to extension that accompanied the formation of the western arm of a failed rift in a triple junction setting. In the extreme eastern part of the Soutpansberg Basin the strike is north-north-west with an easterly dip of 50° . This has been explained by rifting along fracture zones trending north-north-west and subsequent subsidence of the area now forming the Mozambique Channel (Flores, 1970; Forster, 1975). The orientation of the principal stress axes (σ_1 , σ_2 , and σ_3) and the ratio of the principal stress differences (R) show that σ_1 and σ_3 are generally sub-vertical and σ_2 is sub-horizontal in most of the paleostress tensors, which are belonging to a major normal fault system with σ_1 swinging around NNE direction.

Tshipise-Pafuri Coalfield

The initial data base contains 28 fault-slip data, related to compression and extensional stages (Table B1). All stereograms have Schmidt Lower Hemisphere projections. The different parameters used for estimating the quality results are reported in Table 4.2 a and b. Figure 4.3A (1-2) Initial data base; Figure 4.3B (3-6) progressive fault separation using the Right Dihedron; Figure 4.3C (7-10) after successive optimisations and eliminations of incompatible data; Figure 4.3D (11-14) the final solution.

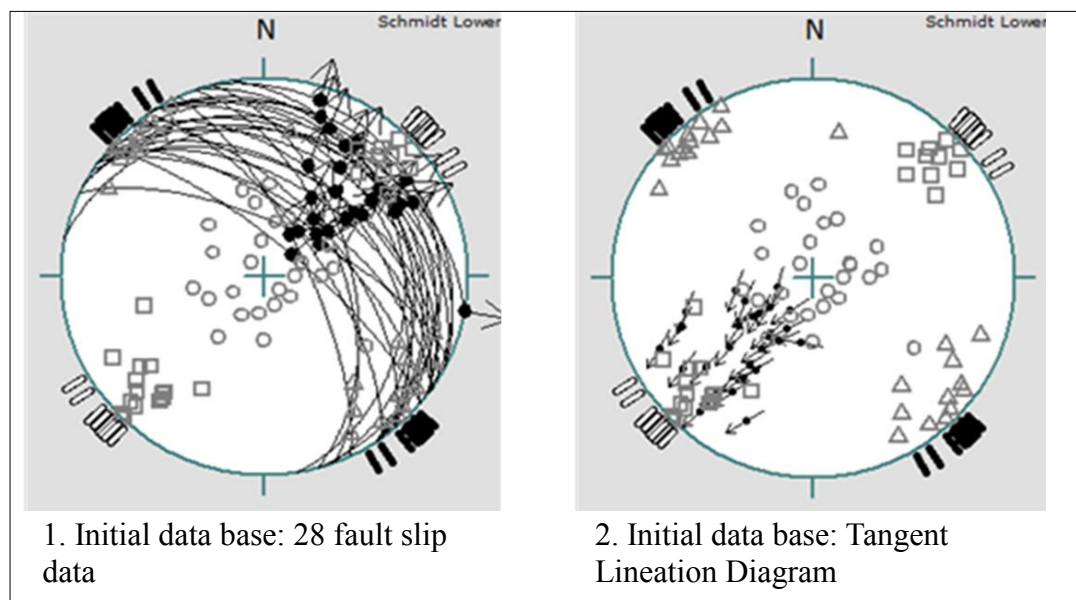


Figure 4.3 (A): Progressive kinematic separation and stress tensor optimisation on fault slip data set measured along faults of the Tshipise-Pafuri Coalfield.

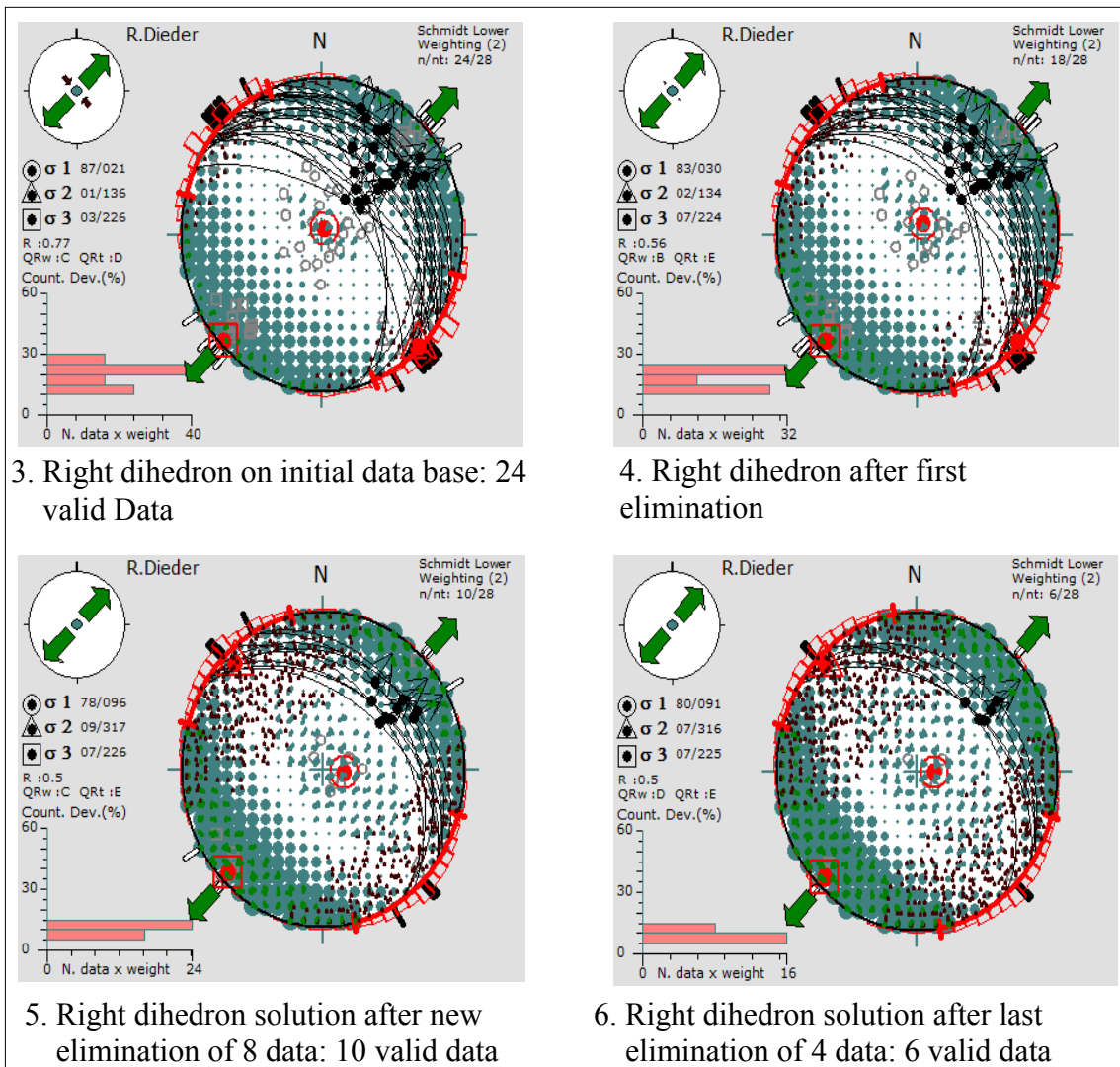


Figure 4.3 (B): Progressive kinematic separation and stress tensor optimisation on fault slip data set measured along faults of the Tshipise-Pafuri Coalfield.

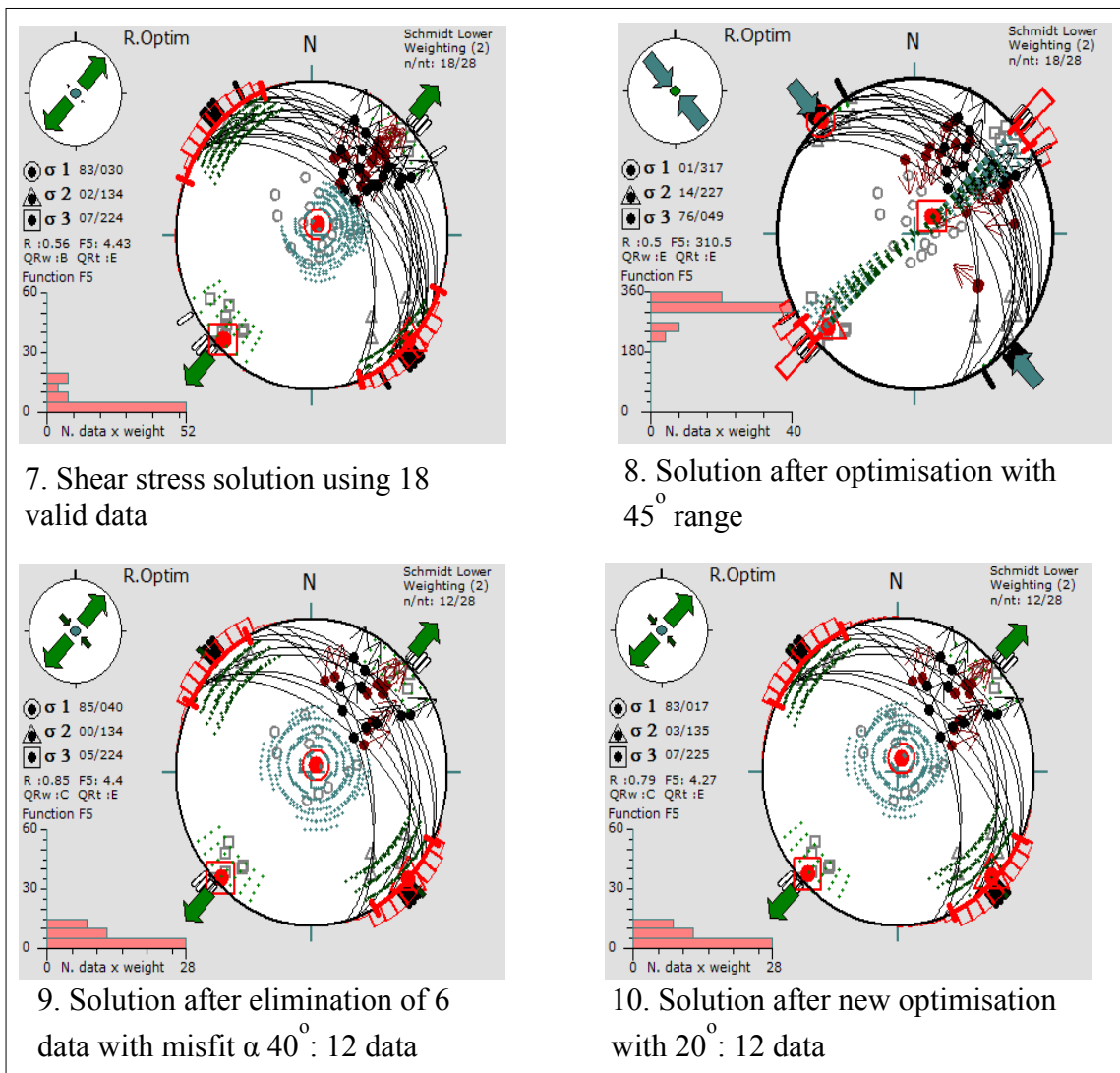


Figure 4.3 (C): Progressive kinematic separation and stress tensor optimisation on fault slip data set measured along faults of the Tshipise-Pafuri Coalfield.

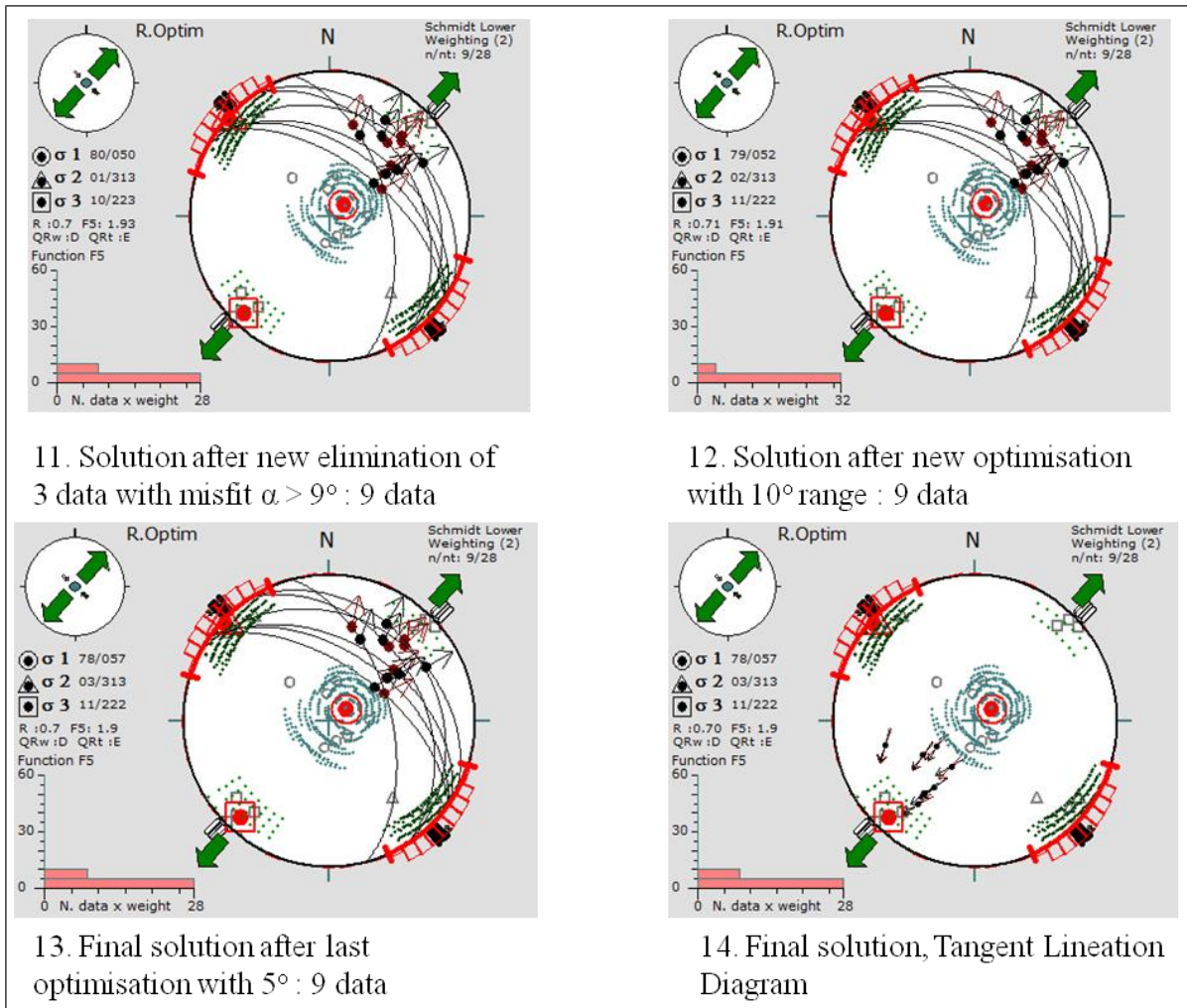


Figure 4.3 (D): Progressive kinematic separation and stress tensor optimisation on fault slip data set measured along faults of the Tshipise-Pafuri Coalfield.

Table 4.2: Parameters used for estimating the quality of the results of progressive tensor optimisation and fault-slip separation using successively the (a) Right Dihedron and (b) Rotational Optimisation in the Tshipise-Pafuri Basin.

(a) The Right Dihedron.

Step	Difference between extreme Counting values	Average counting deviation (% $\pm 1\sigma$)
3	20.3	85.7 ± 5
4	17	64.3 ± 4.3
5	10.9	35.7 ± 2.3
6	7.9	21.4 ± 2.3

(b) The Rotational Optimisation.

n	n/nt	CLw	DTw	QRwsm	Plen	Slen	QRt	SHmax
18	0.64	1	1	B	0.96	0.96	E	134
18	0.64	1	1	E	0.96	0.96	E	136
12	0.43	1	1	C	0.95	0.95	E	134
12	0.43	1	1	C	0.95	0.95	E	135
9	0.32	1	1	D	0.96	0.96	E	133
9	0.32	1	1	D	0.96	0.96	E	132
9	0.32	1	1	D	0.96	0.96	E	132

Mopane Coalfield

The initial data base contains 20 fault-slip data, related to compression and extensional stages (Table B2). All stereograms have Schmidt Lower Hemisphere projections. The different parameters used for estimating the quality results are reported in Table 4.3 a and b. Figure 4.4A (1 to 2) Initial data base; Figure 4.4B (3 to 6) progressive fault separation using the Right Dihedron; Figure 4.4C (7 to 10) after successive optimisations and eliminations of incompatible data; Figure 4.4C (10 to 12) the final solution.

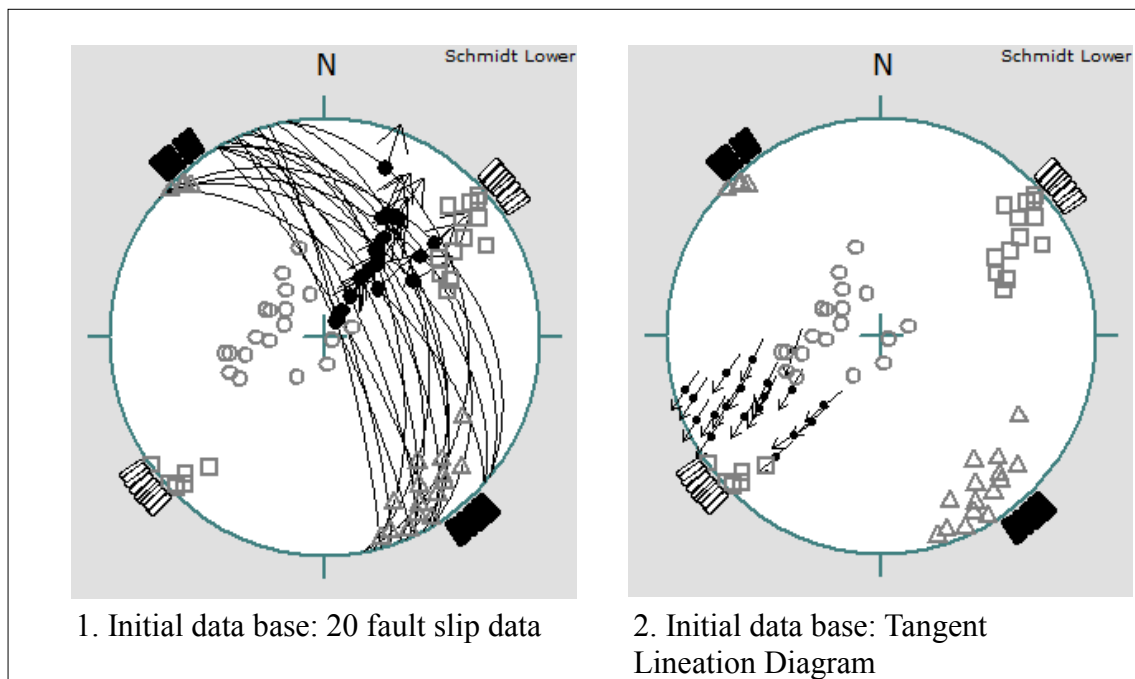


Figure 4.4 (A): Progressive kinematic separation and stress tensor optimisation on fault slip data set measured along faults of the Mopane Basin.

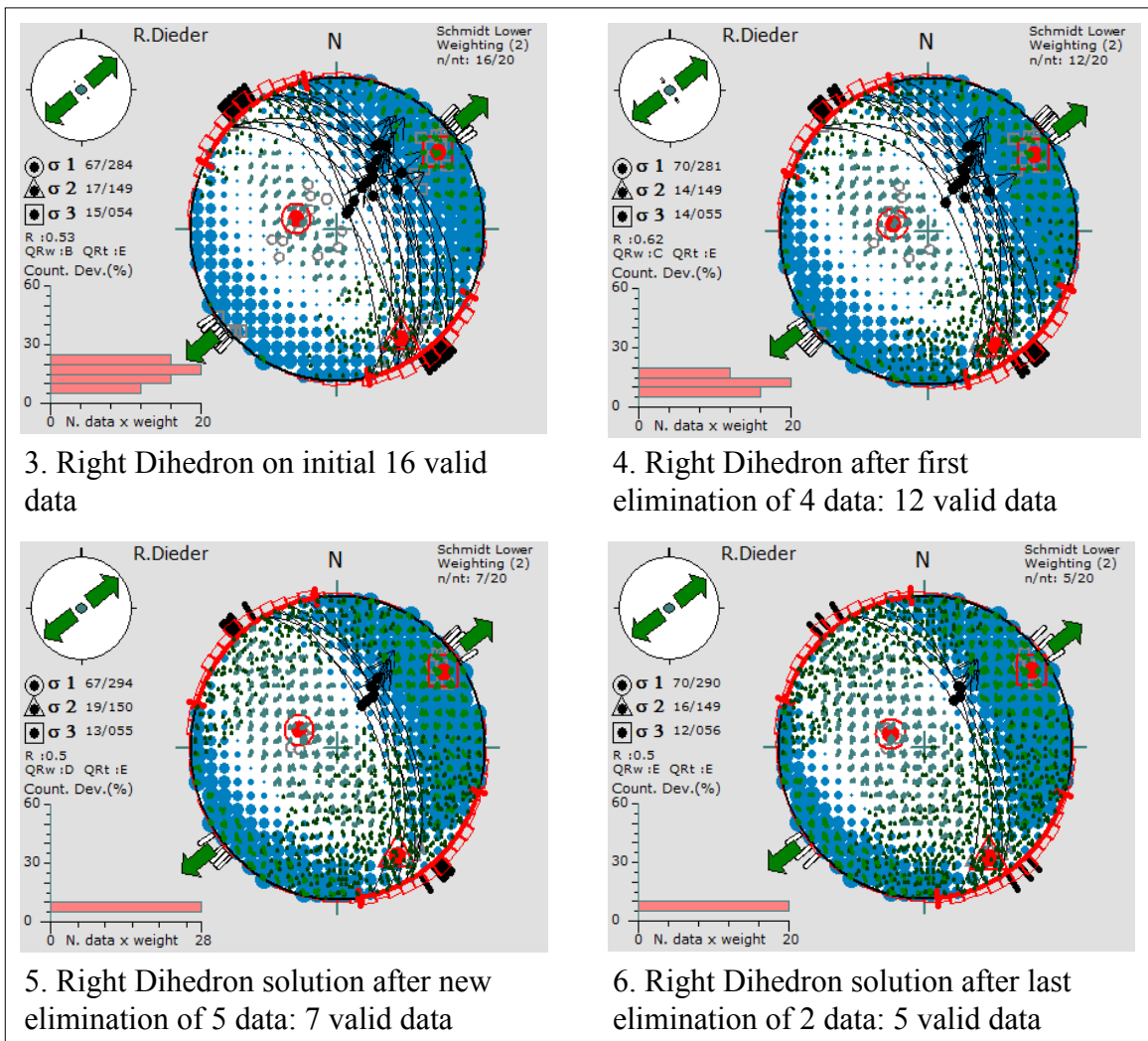


Figure 4.4: (B): Progressive kinematic separation and stress tensor optimisation on fault slip data set measured along faults of the Mopane Basin.

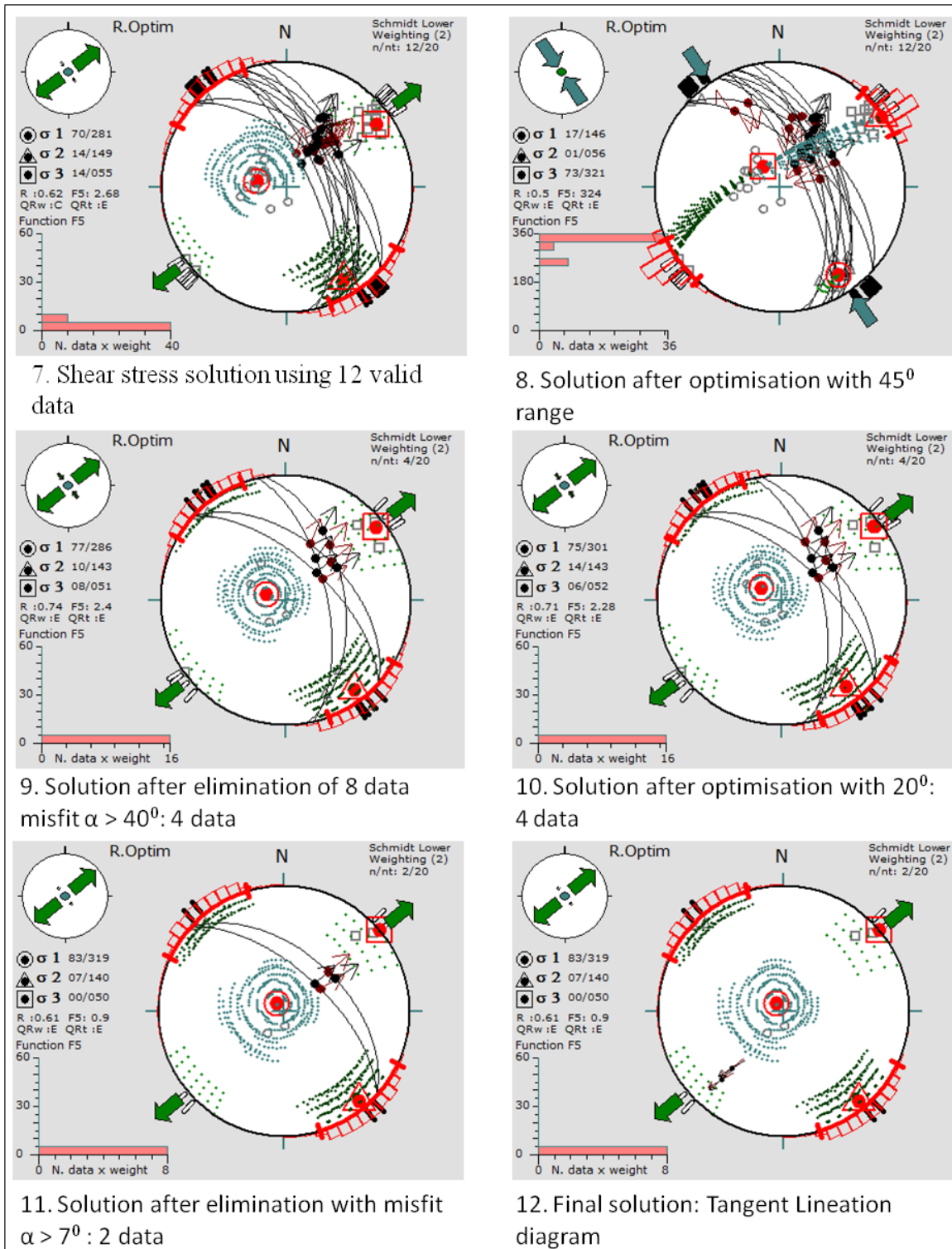


Figure 4.4: (C): Progressive kinematic separation and stress tensor optimisation on fault slip data set measured along faults of the Mopane Basin.

Table 4.3: Value of the parameters used for estimating the quality of the results of progressive tensor optimisation and fault-slip separation using successively (a) Right Dihedron and (b) Rotational Optimisation in the Mopane Basin.

(a) The Right Dihedron

Step	Difference between extreme Counting values	Average counting deviation (% $\pm 1\sigma$)
3	15.5	80 \pm 4.8
4	12.2	60 \pm 3.5
5	7.6	35 \pm 1.4
6	5.8	25 \pm 0.7

(b) The Rotational Optimisation

n	n/nt	CLw	DTw	QRwsm	Plen	Slen	QRT	SHmax
12	0.6	1	1	C	0.98	0.98	E	143
12	0.6	1	1	E	0.98	0.98	E	146
4	0.2	1	1	E	0.96	0.98	E	141
4	0.2	1	1	E	0.96	0.98	E	142
2	0.1	1	1	E	0.99	0.99	E	140
2	0.1	1	1	E	0.99	0.99	E	140

4.4.2. Tuli Coalfield

The initial data base contains 21 fault-slip data, related to compression and extensional stages (Table B3). The main stress field in the Tuli Coalfield is characterised by N-S to NNW-SSE compression and W-E to ENE-WSW extension (Figure 4.5 A-B). This stress field reflects the established structural trend of the two shear belts bounding the Central Zone of the Limpopo Mobile Belt. The coalfield is bounded by east-northeast-trending normal faults.

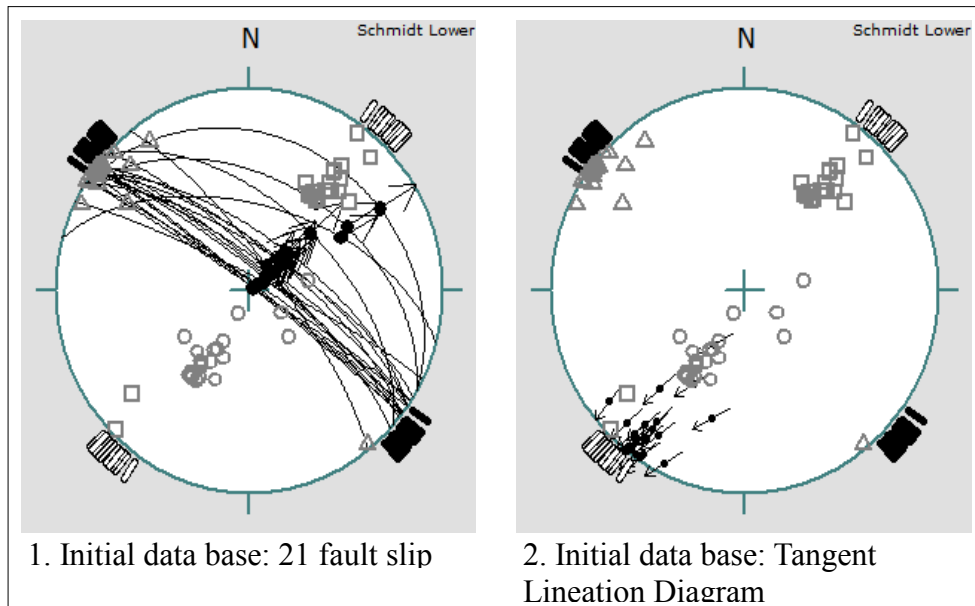


Figure 4.5: (A): Progressive kinematic separation and stress tensor optimisation on fault slip data set measured along faults of the Tuli Coalfield.

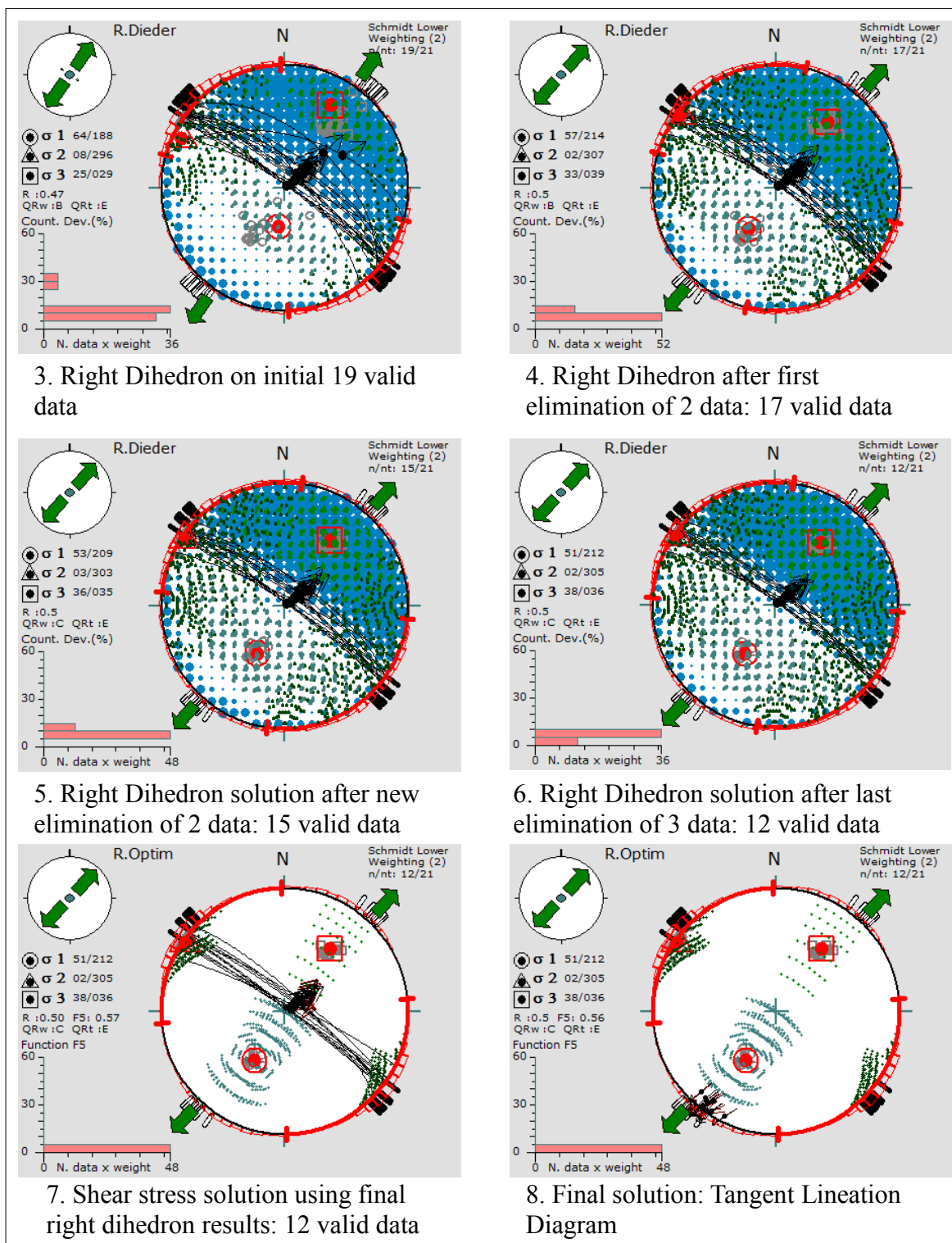


Figure 4.5: (B): Progressive kinematic separation and stress tensor optimisation on fault slip data set measured along faults of the Tuli Basin. The initial data base contains 21 fault-slip data, related to compression and extensional stages.

All stereograms have Schmidt Lower Hemisphere projections. The different parameters used for estimating the quality results are reported in Table 4.4 a and b. Figure 4.5A (1 to 2) Initial data base; Figure 4.5B (3 to 6) progressive fault separation using the Right Dihedron; Figure 4.5B (7 to 8) after successive optimisations and eliminations of incompatible data; Dispersion of planes was too small, $Plen = 1$, thus optimisation of different angles was impossible.

Table 4.4: Value of the parameters used for estimating the quality of the results of progressive tensor optimisation and fault-slip separation using successively (a) Right Dihedron and (b) Rotational Optimisation in the Tuli Coalfield.

(a) The Right Dihedron

Step	Difference between extreme Counting values	Average counting deviation (% $\pm 1\sigma$)
3	12.3	90.5 \pm 5.7
4	8.9	81 \pm 1.9
5	7.9	71.4 \pm 1.5
6	5.9	57.1 \pm 1.1

(b) The Rotational Optimisation

n	n/nt	CLw	DTw	QRwsm	Plen	Slen	QRt	SHmax
12	0.57	1	1	C	1	1	E	133

4.5. Discussions

Movement along the Limpopo Mobile Belt (LMB) as tectonic re-activation due to continuous tension in the Karoo era resulted to fault zones. This fault zones controlled the formation of the Karoo sediments and finally acted as conduits for the extrusion of basalts which terminated the Karoo era (Barker, 1983). Intense block-faulting caused the development of a series of stepped half-grabens. The Karoo sedimentation was fault controlled from the onset. The East African Rift Valley defines the tectonic framework for the basin. Due to the active divergent tectonic plates of the rift, there is continuous extension in the subordinate basins (Figure 4.6).

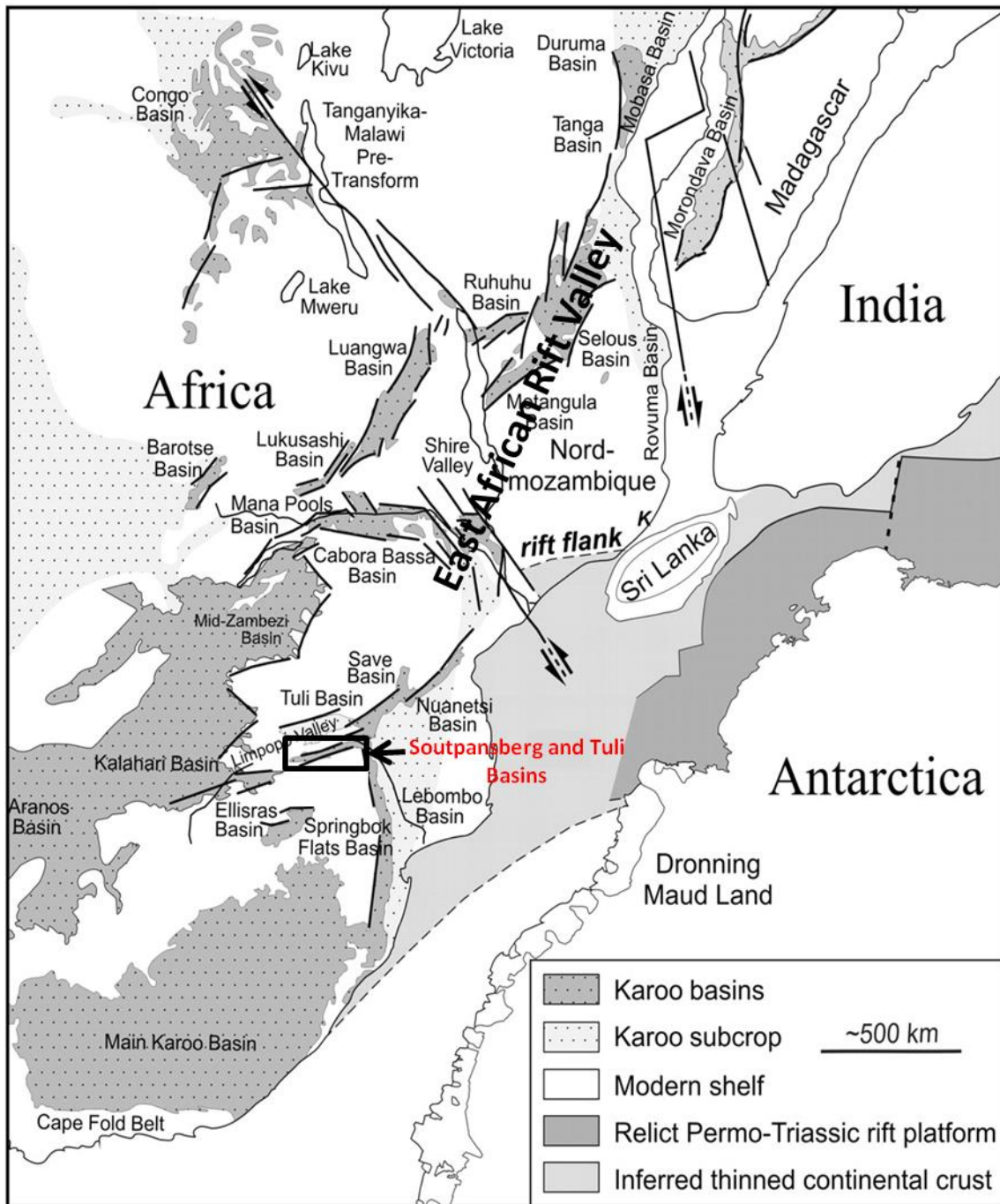


Figure 4.6: Distribution of the Karoo basins in Central and Southern Africa during Gondwana times in relation with the East African Rift Valley (after Daszinnies *et al.*, 2009).

4.5.1. The Formation of a rift basin

A typical rift basin is a fault-bounded feature known as a half graben (Figure 4.7a). In a cross section oriented perpendicular to the boundary fault (transverse section), the half graben has a triangular geometry (Figure 4.7b). The three sides of the triangle are the border fault, the rift-onset unconformity between prerift and synrift rocks, and the postrift

unconformity between synrift and postrift rocks (or, for modern rifts, the present-day depositional surface).

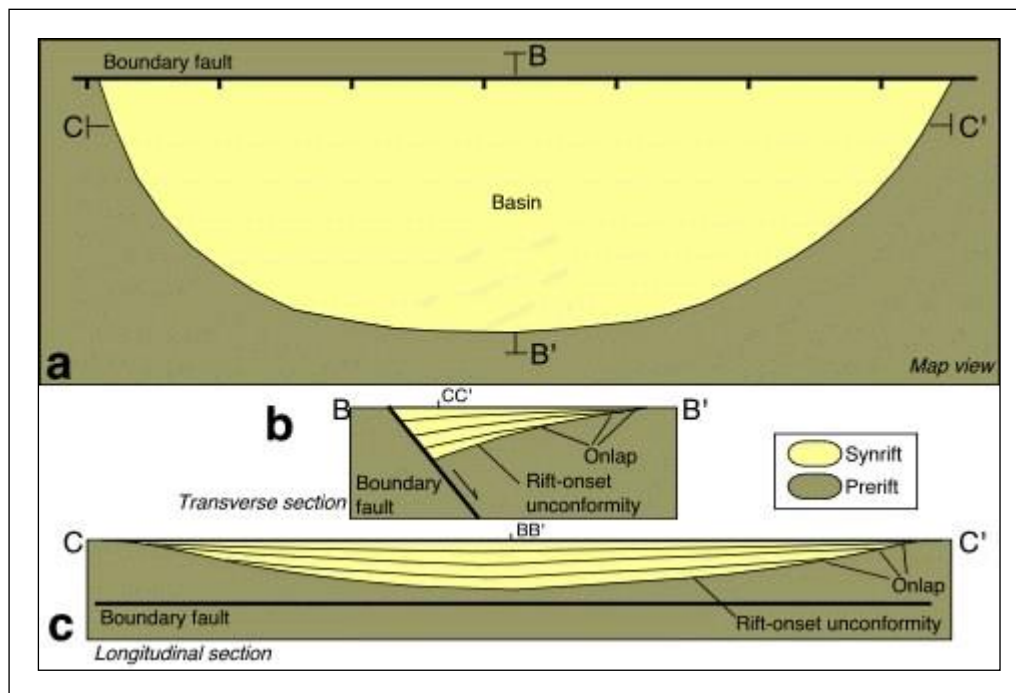


Figure 4.7: Geometry of a simple half graben. (a) Map-view geometry (b) Geometry along a cross section oriented perpendicular to the boundary fault, showing wedge-shaped basin in which synrift strata exhibit a fanning geometry, thicken toward the boundary fault, and onlap prerift rocks. (c) Geometry along a cross section oriented parallel to the boundary fault, showing syncline-shaped basin in which synrift strata thin away from the center of the basin and onlap prerift rocks, (Schlische, 1991).

The half-graben geometry described above is directly controlled by the deformation (displacement) field surrounding the boundary fault system (Schlische, 1991; Schlische and Anders, 1996). In a gross sense, displacement is greatest at the center of the fault and decreases to zero at the fault tips (Figure 4.8a); this produces the syncline-shaped basin in longitudinal section. In traverse section, the displacement of an initially horizontal surface that intersects the fault is greatest at the fault itself and decreases with distance away from the fault. This produces footwall uplift and hanging-wall subsidence, the latter of which creates the sedimentary basin (Figure 4.8b). However, this geometry is affected by fault propagation and forced folding (Schlische, 1991). As displacement accumulates on the boundary fault, the basin deepens through time. Because the width of the hanging-wall deflection increases with increasing fault displacement, the basin widens through time. As the length of the fault

increases with increasing displacement, the basin lengthens through time. The growth of the basin through time produces a progressive onlap of synrift strata on prerift rocks (Figure 4.8b).

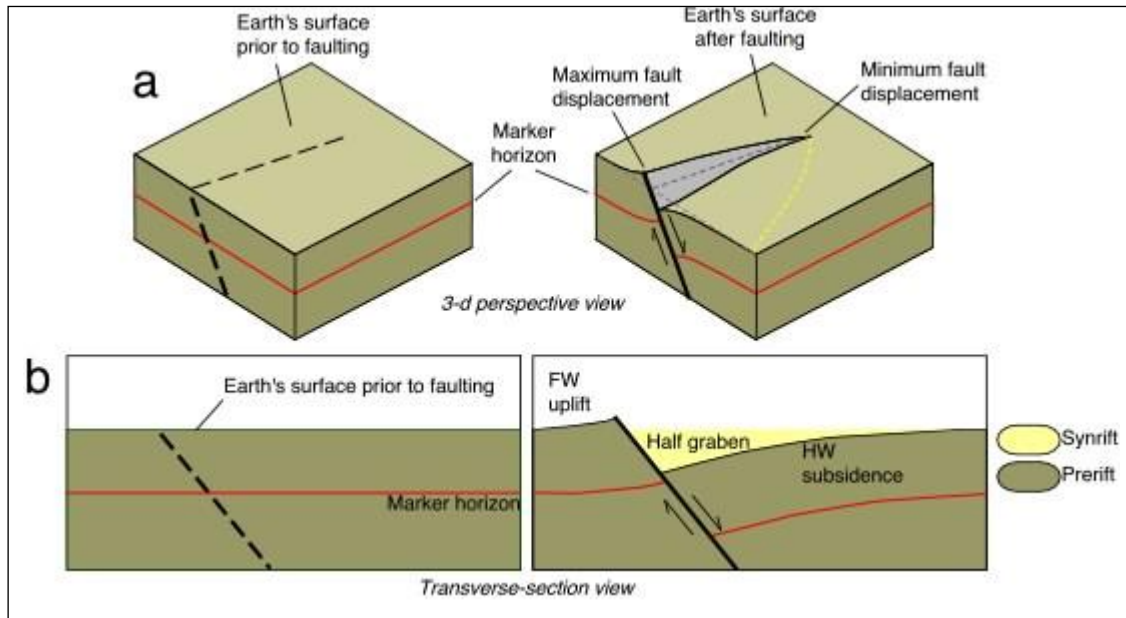


Figure 4.8: Fault-displacement geometry controls the first-order geometry of a half graben. (a) Before faulting (left) and (right) after faulting showing how normal faulting uplifts the footwall block and produces subsidence in the hanging-wall block. (b) Traverse section before faulting (left) and after faulting and sedimentation showing footwall uplift and hanging-wall subsidence. The latter produces a wedge-shaped basin (half graben). (Schlische, 1991).

4.5.2. Proposed tectonic and structural model of the Soutpansberg and Tuli Coalfield

During periods of relatively strong extension of the East African Rift Valley, the northern Karoo basins experienced normal, minor strike-slip and thrust movements. During periods of relatively weak compression the fault-zone experienced dip slip normal faulting (Figure 4.9).

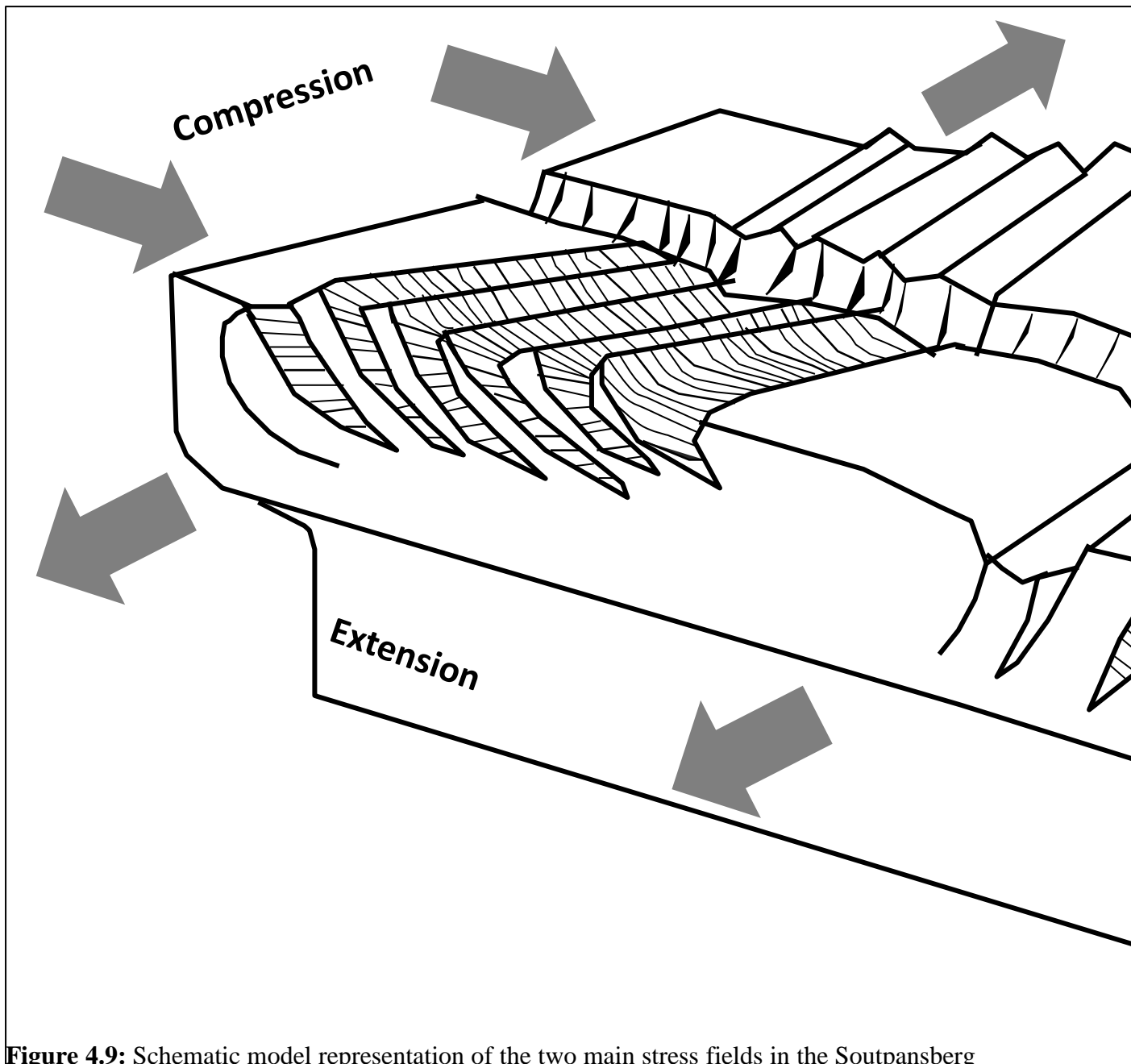


Figure 4.9: Schematic model representation of the two main stress fields in the Soutpansberg and Tuli Basins. The first W-E to ENE-WSW extensional period of the East African Rift Valley generated the main extensional structures including normal faulting, minor strike slip and thrust faulting. A minor second paleostress field is characterized by N-S to NNW-SSE compression. In addition, a second system of N-S dip-slip normal faulting was generated during this compressional regime.

Figures 4.10 and 4.11 illustrate the tectonic setting during deposition of the Tuli and Soutpansberg Basins.

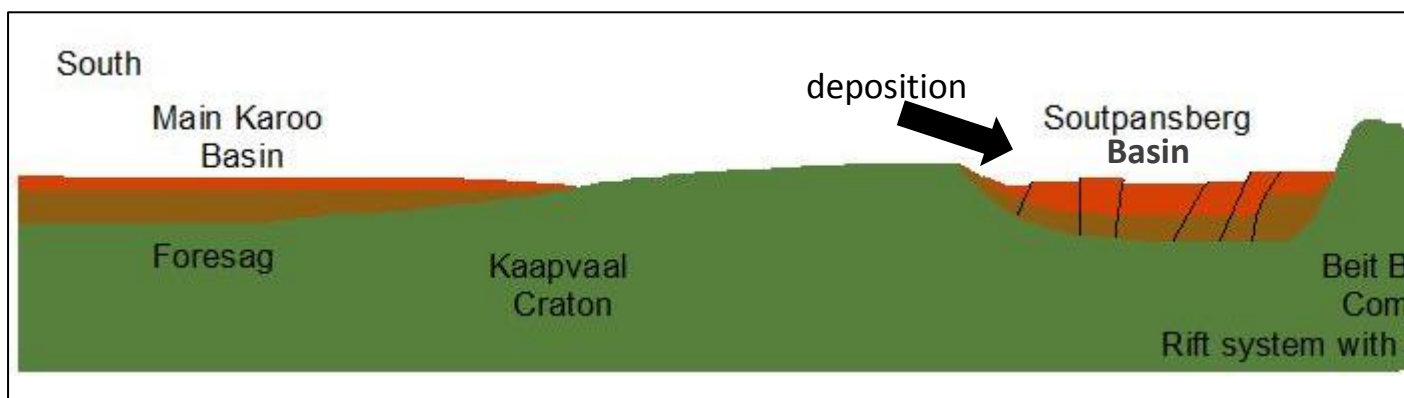


Figure 4.10: Summary of the tectonic setting during deposition of the Tuli and Soutpansberg Basins. Redrawn from Bordy and Catuneanu, 2002 (not to scale).

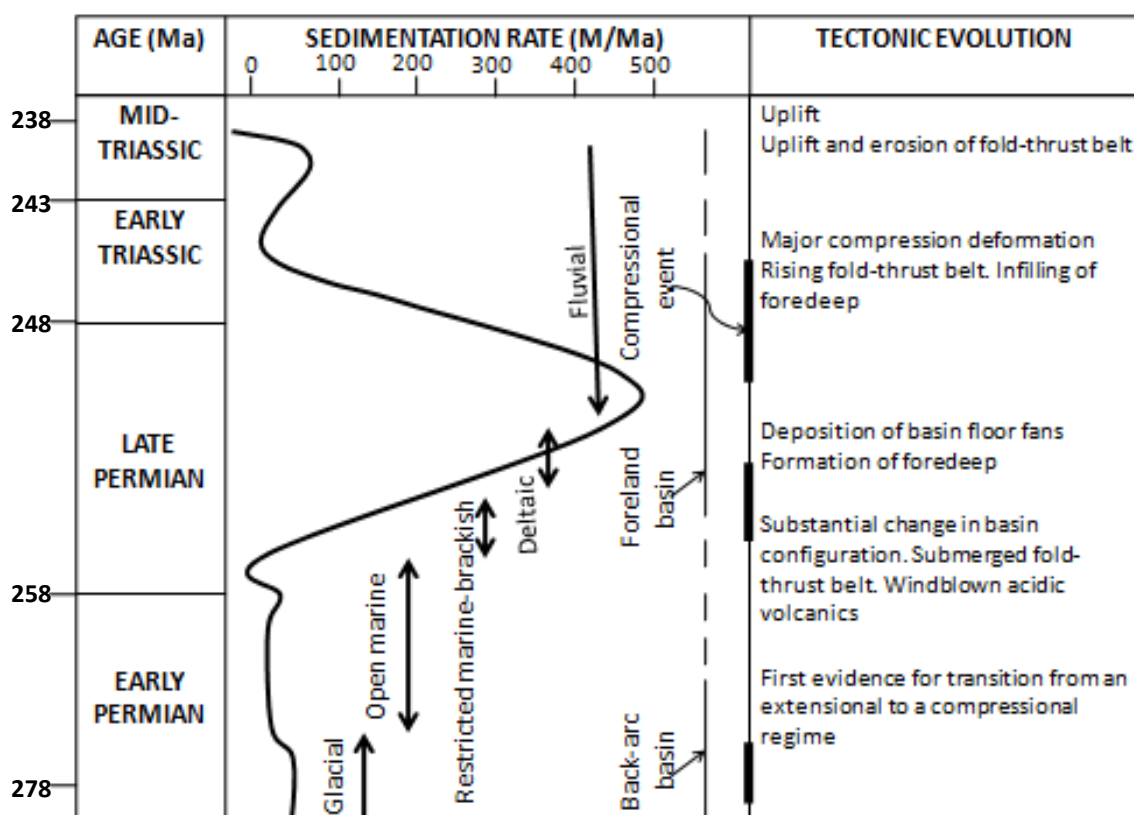


Figure 4.11: Tectonic evolution of the Karoo Basin from the Permian to the Mid-Triassic compressional events (after Halbich *et al.*, 1983).

4.6. Conclusions

All the W-E to ENE-WSW extension trends is compatible with the main faults of the basin (Bosbokpoort, Tshipise and Klein Tshipise Faults). They are parallel to the regional strike, and outcrops as major horst and graben structures. The second W-N-W to N-W trend system is oblique to the regional strike and is represented by the Siloam Fault.

The main stress fields in the coalfields are characterized by W-E to ENE-WSW extension and N-S to NNW-SSE compression which includes two paleostress regimes, one with predominantly dip-slip normal faulting (extensional regime) and a minor strike-slip faulting (strike-slip regime) and thrust faulting (reverse-slip regime). The second paleostress field is characterized by NE-SW to ENE-WSW extension and NW-SE to NNW-SSE compression. It is characterised by dip-slip normal faulting (compressional regime).

It is also noted that normal faulting of the paleostress field has the orientation of σ_1 vertical and σ_3 horizontal, whereas strike-slip faulting of the paleostress field has the orientation of σ_1 horizontal and σ_3 horizontal. The orientation of stress tensors in the different areas can be summarised in the following trends:

- A spreading process along the Tethyan margin of Gondwana propagated tensional stresses gradually to the south (Southern Africa), from the Tethyan margin controlling the Karoo sedimentation in grabens and subsequent rift structures.
- The dominant W-E to ENE-WSW extension and N-S to NNW-SSE compression in the basin follows the East-West elongated low lying Limpopo Mobile Belt which controlled the Karoo deposition. This fault zones which resulted in the movement of the LMB due to tectonic reactivation controlled the formation of the Karoo sediments and finally acted as conduits for the extrusion of basalts which terminated the Karoo era.
- From Late Palaeozoic onward, continuing extension along the East African Rift Valley defines the tectonic framework for the basins.
- These main E-W stress tensors may be responsible for the formation of the local E-W and ENE-WSW normal faults in the study area. The main faults of this type are named the Bosbokpoort, Tshipise and Klein Tshipise Faults.
- The orientation of the principal stress axes and the ratio of the principal stress differences show that σ_2 (SHmax) and σ_3 (SHmin) are generally sub-horizontal and σ_1 is sub-vertical in most of the paleostress tensors, which are belonging to a major normal fault system and a minor strike slip system.

CHAPTER 5

FACIES ANALYSIS, DEPOSITIONAL ENVIRONMENTS AND PALAEOCURRENT ANALYSIS OF THE SOUTPANSBERG AND TULI COALFIELDS

Abstract

Lithofacies analysis was performed with a view to deduce the nature of depositional environments of the deposits of the coalfields. Sedimentological and sequence stratigraphic evidence indicates that this unit represents a complex siliciclastic facies that was deposited in a fluvial environment. Sixteen major facies which were grouped into seven facies associations were recognised. The Tshidzi Formation is developed at the base of the Karoo Supergroup and consists of diamictite and sandstone resting on a disconformable contact on the upper formations of the Soutpansberg Group. The diamictite was probably fluvio-glacial in origin. Succeeding the Tshidzi Formation is the Madzaringwe Formation which can be further divided into three members. The Lower Member represents a sequence formed from meandering and braided channels. The coal deposits represent flood basin pond and swamp deposits in this member. The Member is characterised by shale, thick coal seams, siltstone and sandstone. The Middle Member is characterised by clast or matrix supported conglomerates, tubular and trough cross-bedded sandstones and fine calcareous, micaceous siltstone. The deposition represents a sequence formed from fluvial (meandering and braided) channels. The crudely stratified, coarse to pebbly sandstone indicates braided channel deposits within a heavy loaded fluvial system. The fine-grained sandstone represents deposition by vertical accretion on the top of channel sand bars during waning flow conditions. The Upper Member is characterised by facies associations similar to the Lower Member. The Mikambeni Formation is divided into the Lower and Upper Members. The Lower Member is characterised by laminated, grey and black carbonaceous shale, coal and sandy shale/mudstone. The thin coal seams and carbonaceous shale were probably deposited in well drained swamps whereas peat in poorly drained swamps. The Middle Member is characterised by alternating beds of shale and fine-coarse grained sandstone to siltstone. The depositional environments were probably associated with shallow lakes and water ponds. Paleocurrent directions were measured using directional structures (cross-bedding and asymmetric ripple marks). Both the Soutpansberg and Tuli Coalfields displayed a north-east trend and a south-west source.

5.1. Introduction

Sedimentary facies is a body of sedimentary rocks with specific characteristics that may be defined on the basis of geometry, colour, bedding, lithology, composition, texture,

fossil content, sedimentary structures and paleocurrent patterns. Two major groups of sedimentary facies can be classified, i.e. lithofacies and biofacies. Lithofacies refers to the observable petrological features of sedimentary rocks, whereas biofacies attributes to the biological features, such as different types of fossil contents. A generalized lithofacies scheme (Table A1) for description of the deposits of fluvial sediments was erected by Miall (1978). This scheme was modified and is further applied to a wide variety of alluvial deposits, including deltaic successions (Miall, 1990; Miall, 2000). The concept of sedimentary lithofacies associations has been widely used mainly to determine the origin and the depositional environments of the sedimentary units. This lithofacies scheme uses codes with two parts, a capital letter for modal grain size (G, gravel; S, sand; F, fine) and lowercase letter for a distinctive texture or structure of each lithofacies. Sedimentary facies in this study were described based on the lithological characteristics, bed thickness, grain-size, colour, and internal sedimentary structures.

Sixteen lithofacies were identified in the two coalfields (Table 5.1). Internal and external geometry strata in the coalfields have been subdivided into seven distinct facies associations (FA) which are interpreted in Table 5.2. The identified facies associations indicate the following depositional environments: fluvio-glacial depositional environment (FA1, Tshidzi Formation); meandering and braided fluvial channels (FA 6 and FA 7, Madzaringwe Lower Member); fluvial channels, crevasse splays, levees and crevasse channels (FA 2, FA 3, FA 4 and FA 5, Madzaringwe, Middle Member); fluvial channels, crevasse splays (FA 6 and FA 7, Madzaringwe Upper Member); meandering and braided fluvial channels, crevasse splays (FA 6, Mikambeni, Lower Member) and lastly meandering fluvial channels and crevasse splays (FA 2, FA 3, FA 4 and FA 5, Mikambeni, Upper Member).

5.2. Methodologies

Facies analysis was undertaken at the study sites, Soutpansberg and Tuli Coalfields. Field descriptions containing information regarding sedimentary structures, grain size, colour, mineral composition, lithology and paleocurrent patterns were made for the individual units. This information was used for the interpretation of the separate facies in terms of process and depositional sub-environments.

To evaluate the palaeoflow directions a compass clinometer was used to measure dip directions of bedding planes of the planar horizontally laminated sandstones and dip directions of parting lineations on the same facies respectively.

Detailed review of the spatial stratigraphic variations, including the analysis of facies changes based on over widely distributed borehole records, field observations and paleocurrent measurements were performed. The set of borehole data resulted from the extensive coal exploration activities in the study area by different companies over the past 50 years. Many units were walked out in order to characterise their regional extent and architecture. Detailed facies and architectural analyses were performed, with particular attention devoted to channel morphology, and vertical stacking patterns of sedimentary facies. Characterisation of bedding surface hierarchy was carried-out using the classification scheme of Miall (1988). Palaeocurrents were derived from asymmetric ripple marks, planar and trough cross-beddings.

5.3. Facies and facies associations

Facies analysis of the coalfields was carried out using a modified version of Miall's (1978, 1988, 1996) lithofacies classification scheme. Based on the identification of 16 lithofacies (Table 5.1), internal and external geometry in the formations have been subdivided into seven distinct facies associations (FA) and interpreted in Table 5.2.

Table 5.1: Lithofacies identified in the Soutpansberg and Tuli Coalfields. See Table A1 for explanation and interpretation of lithofacies.

Coarse grained lithofacies	Description	Fine grained lithofacies	Description
Gm	Matrix-supported tillite. Colour: grey to dark grey. Matrix: fine clay to fine sand; occasionally laminated. Clasts: typically granule to pebble-sized; up to boulder-size; sub-angular to subrounded and poorly sorted.	Sf	Massive to slightly laminated muddy sandstones. Colour: light grey, grey to khaki. Grain size: very fine to fine-grained sand, poorly sorted.
Gcm	Clast-supported conglomerate. Colour: light brownish to red. Matrix: mostly absent; fine-medium sand if present. Clasts: typically granule to pebbly-sized, up to boulder-size; Grains are sub-angular to rounded, and poorly sorted.	Fl	Laminated siltstone, with very small ripples. Colour: Khaki grey to khaki.
Gmm	Matrix-supported conglomerate. Colour: light brownish grey, reddish grey. Matrix: clay to sand; typically massive, occasionally laminated, bedded. Clasts: typically granule to pebbly-sized; up to boulder-size; poorly sorted; sub-angular to sub-rounded.	Fsm	Massive silt and mudstone. Colour: black. Occurring in backswamps.
Se	Crudely stratified to massive sandstone. Color: light gray. Grain size: Coarse- to very-coarse sand. Structure: erosional surfaces and scour fills.	Fm	Massive mudstone and siltone. Colour: black. Occuring in overbank, or as drape deposits.
St	Trough cross-bedded sandstone. Colour: reddish brown, khaki to grey. Grain size: medium to coarse grained sand. Bedding thickness is 0.5-2.0 m.	Fc	Laminated carbonaceous mudstone/shale. Abundant to rare carbonized plant matter. Colour: grey to dark grey.
Sh	Horizontally stratified sandstone. Colour: light Grey, khaki to reddish brown. Grain size: very fine to medium-grained sand.	C	Coal stringers, 1-7 cm thick; < 2-3 m long. Colour: dark-black. Occurring within carbonaceous mudstone, or black shale.
Sp	Sand. Colour: reddish brown, khaki to grey. Grain size: very fine to medium-grained sand. Tabular-planar cross-bedded.		
Sr	Sand with ripples. Cross-laminated. Colour: reddish brown, khaki to grey. Grain size: fine to medium-grained sand.		

Sm	Sand with massive bedding or faint lamination. Colour: reddish brown, khaki to grey. Grain size: very fine to medium grained sand.		
Sl	Laminated sand. Colour: light grey, grey to khaki. Grain size: medium to very-coarse sand and may be pebbly.		

Table 5.2: Facies associations identified in the Soutpansberg and Tuli Coalfields.

Facies associations		Facies	Interpretation of depositional environments
Glacial diamictite and sandstone	FA1	Gm, Sl	Glacial diamictite with lenticular laminated sandstone
Clast-supported conglomerate and sandstone	FA2	Gcm, Gmm, Se, St	Dominantly alluvial and braided channel sediments, with trough cross-bedding.
Tabular cross-bedded sandstone	FA3	Sm, Sp, Sh, Sl, Sr	Fluvial sediments. Mainly meandering channel deposits.
Trough and planar cross-bedded sandstone	FA4	St, Sr, Sh, Sp, Sm, Sl	Fluvial sediments. Mainly braided channel deposits.
Fine calcareous and micaceous siltstone and mudstone	FA5	Fl, Fsm, Fm, Sr, St	Fluvial sediments, mainly floodplain deposits.
Laminated sandy shale/mudstone	FA6	Fl, Sh, St, C	Fluvial sediments. Floodplain ponds, lakes and weakly developed palaeosols.
Laminated or thin-bedded Carbonaceous shale/mudstone and coal	FA7	Fc, C	Backswamps and oxbow lakes.

5.3.1. Glacial diamictite and sandstone facies association (FA 1)

5.3.1.1. Description

FA1 is characterised by diamictite (Gm) with subordinate medium to coarse sandstone (St). In this study the diamictite and diamictite sandstone occur in all geographic subdivisions

across the study area. In some areas where the pre-Karoo basement is elevated, the Madzaringwe Formation sedimentary strata rest directly on the pre-Karoo basement with no intermediate Tshidzi Formation. It reaches up to a maximum thickness of 0.1 m to 20 m and composed of angular and sub-rounded clasts imbedded in a khaki sandy or bluish grey muddy matrix. The clasts can measure up to 80 cm in diameter, and rest in a matrix of coarse sand or grit. Clasts within diamictite are most commonly quartz.

The facies includes sub-rounded to angular clasts consisting of pre-Karoo material that is poorly sorted in a massive (Figure 5.1B), or interbedded, matrix of medium to coarse grained sand (Figure 5.1A). In some areas the diamictite shows characteristics of reworking (diamictite material that has been eroded and resedimented with a higher degree of sorting). This association commonly occurs at above the pre-Karoo sediments and below the Madzaringwe Formation.



Figure 5.1: The diamictite facies association. A: Sandstone interbedded with diamictite near the Tshidzini Village in the Tshipise-Pafuri Coalfield. B: Close up view of the clast-rich diamictite.

5.3.1.2. Interpretation

The diamictites and the interbedded sandstone represent glacial till-flow deposits which must have been deposited in a subaerial environment, probably on the flanks of the Beit-Bridge Complex, the Zimbabwe and the Kaapvaal Cratons. As the characteristics of most of the clasts indicate that they must have been transported (probably by moving ice) over an irregular surface before they became embedded in the glacial flow. The black colour, fine-grained composition and pyritic nature of this facies indicate deposition by ice into

backswamps and oxbow lakes. The interbedding noted in the reworked diamictite indicates the reworking of glacial meltwater.

The high roundness and sphericity of clasts indicate that they have endured extensive weathering, which is common in glacial environments and likely are the result of multiple cycles of transport within glacial and glacially influenced systems. Sandstone clasts were eroded from the Lower Palaeozoic sedimentary rocks and the quartz and granite clasts were derived from mid to Late Carboniferous granitic intrusions.

5.3.2. Clast supported conglomerate and sandstone facies association (FA 2)

5.3.2.1. Description

The conglomerates (Gcm, and minor Gmm) are characterised with a thicknesses from <0.1 to 3 m, and subordinate sandstone lithofacies Se and St, (Tables 5.1, 5.2 and Figures 5.2 and 5.3). The conglomerates are abundant in the Mikambeni Formation. They are reddish-grayish in colour. The clasts are almost exclusively composed of red to brownish grey, subangular to subrounded sandstone and siltstone clasts; white, brownish to reddish, subangular to subrounded mudstone and claystone (very fine shale which does not split) and reddish to whittish, subrounded to rounded quartz pebbles. The rounded cobbles and pebbles can measure from 1 to 30 cm in diameter (Figure 5.2b). The matrix is red to grayish brown siltstone, occasionally with coarse, rounded reddish quartz grains. FA 2 commonly occurs at or near the bases of tabular cross-bedded sandstones (FA 3) and trough and planar cross-bedded sandstone (FA 4). The conglomerates are invariably topped by, or interbedded with, sandstone units (Se and St) (Figure 5.2a). Some conglomerates show slight horizontal layering (Gh) or cross-bedding (Gp, Gt). Using the field observations and borehole data, the thickness of this association can be estimated to be >100 m in some places.



Figure 5.2: Conglomerate located at S22°.84'849°, E029°.88'450° (Mikambeni Formation in the Tshipise-Pafuri Coalfield). (a) Clast supported conglomerate with very coarse sandstone. (b) Rounded cobbles and pebbles measuring from 1 cm to 30 cm in diameter. (c) Matrix supported conglomerate (angular to sub-angular pebbles measuring 1cm to 10cm in diameter).



Figure 5.3: Clast supported conglomerate located at S22°.68'583°, E029°.80'658° (Mikambeni Formation in the Mopane Coalfield).

5.3.2.2. Interpretation

The conglomerates are polymictic, texturally immature and crudely stratified or massive (Figure 5.2). The clast-supported massive conglomerate units were deposited most probably as small bodies of channel lag or longitudinal braided bars of low sinuous streams. The occasionally matrix-supported and poorly sorted conglomerate unit might have been deposited as debris flow deposits. These conglomerates might have resulted from fan accumulation in response to uplift along faulted margin (Miall, 1981).

5.3.3. Tabular cross-bedded sandstone facies association (FA 3)

5.3.3.1. Description

The tabular cross-bedded sandstones are more common FAs in the Mikambeni and Madzaringwe Formations. They are composed of the following lithofacies, in descending order of abundance: Sm, Sp, Sh, Sl, and Sr (Tables 5.1, 5.2 and Figures 5.4, 5.5, 5.6, 5.7 and 5.8). FA 3 occurs as single and multi-storey units, which commonly exceed hundreds of meters in lateral extent. FA 3 beds exhibit the following internal bedding features:

- massive reddish brown, khaki to grey sandstone beds (Sm), the grain size is very fine to coarse with massive or faint lamination.
- horizontal light grey, khaki to reddish brown laminated sandstone (Sh), the grains ranges from very fine to medium sized.
- laminated sand, fine to coarse and may be pebbly with a light grey, grey to khaki colour (Sl).
- reddish brown, khaki to grey planar cross-bedded sandstone with very fine to medium grained sand (Sp).
- reddish brown to khaki grey ripple cross-laminated sandstone (Sr), the grain size is very fine to medium-grained.

Most sandstone grains in FA 3 are sub-angular to sub-rounded, moderately to poorly sorted, composed of quartz, feldspar, mica and rock fragments. The matrix/cementing materials are argillaceous, carbonaceous and at places, ferruginous. Coarse to pebbly sandstone is poorly developed sub-lithofacies that generally overlies the conglomerate and grades vertically into coarse to medium-grained sandstones. This sub-lithofacies commonly occur as multistoried channel-like sandstone bodies. Thin strata of mudstone and siltstone separate the successive bodies (Figure 5.5). Coarse-grained sandstone occurs as 2 to 5 m thick individual channels to sheet-like sandstone bodies that are massive and planar cross-stratified (Figure 5.8b). The medium-grained sandstone form 2 to 3.5 m in thickness (Figure 5.6). This sub-lithofacies occurs as sandstone bodies with erosional or transitional base and a flat top. It constitutes multistoried sandstone bodies having abundant successive sets of large-scale planar and parallel or ripple stratifications. Fine-grained sandstone sub-lithofacies comprises interbedded siltstone and mudstone (Figure 5.7). Individual bodies vary from 1 to 4 m in thickness.

The outcrops of major tubular sandstone facies assemblage have lateral extents of less than a few meters to more than one hundred meters. Sedimentary structures include thin (3-

10 cm) to medium (10-30 cm) beds of tabular-planar cross-bedded and cross-laminated sandstone.

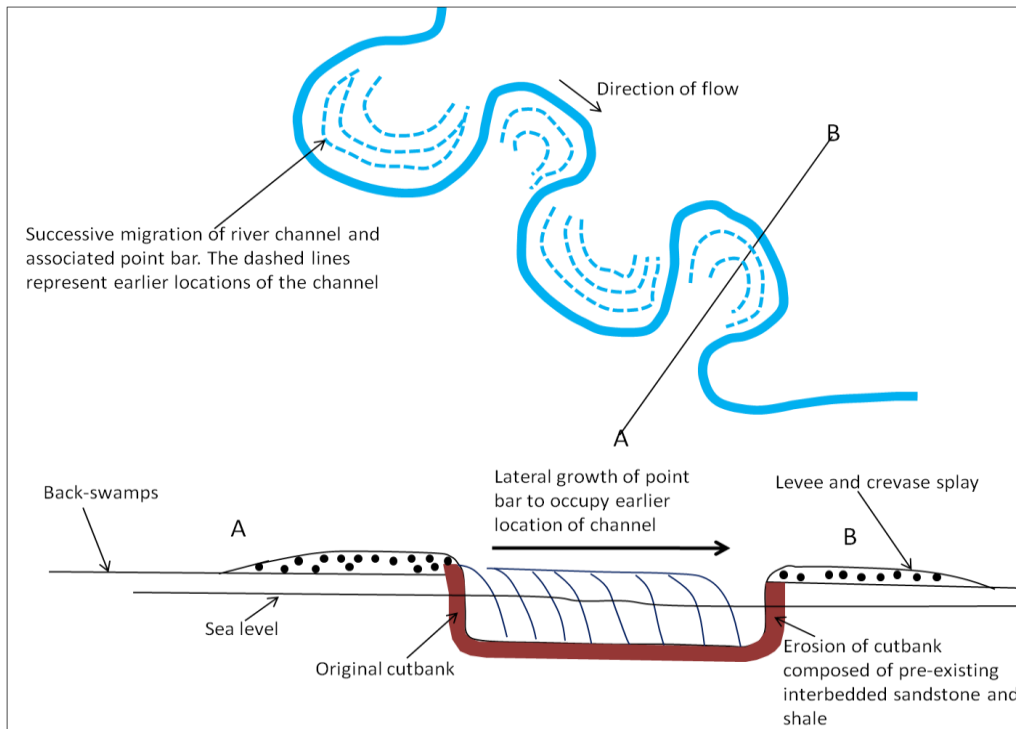


Figure 5.4: Formation of point bar sandstone by lateral accretion (after Edie and Andrichuck, 2005).

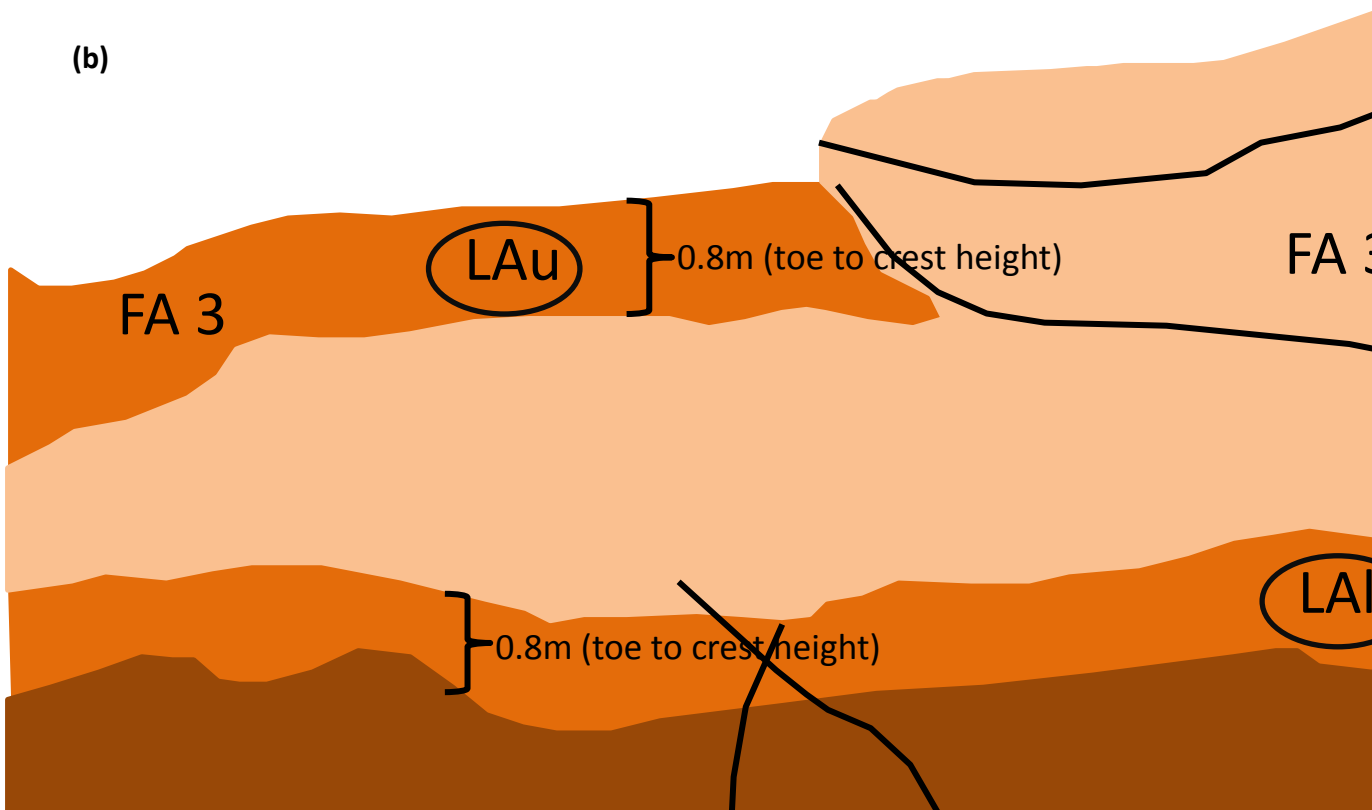


Figure 5.5: Tabular cross-bedded sandstones (FA 3) exhibiting fine-grained, point-bar lateral accretion sets (LA), which are used to estimate paleochannel dimensions; (a) Photomosaic of FA 3 from Mikambeni Formation in Mopane Coalfield (S22° 68'583°, E029° 80'658°); (b) Interpretation of photomosaic in (a). LAI: Lower lateral accretions, LAu: Upper lateral accretions.



Figure 5.6: Exposed section through the middle unit of the Mikambeni Formation in the Tuli Coalfield. The section is typical of the middle unit of the formation dominated by lenticular channels and tabular channels.

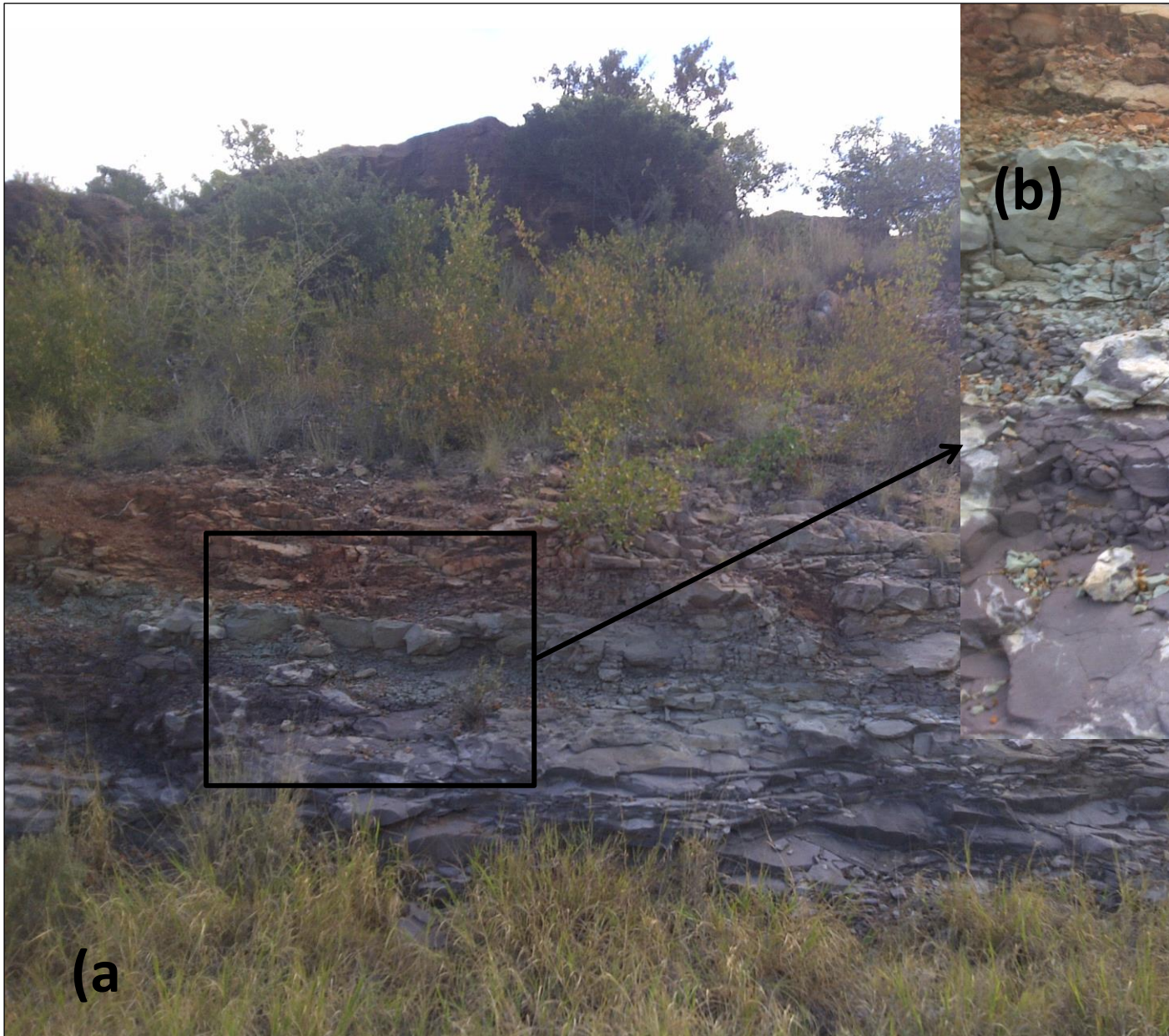


Figure 5.7 (a) Lenticular sandstone in the Tuli Coalfield ($S22^{\circ}.30'176''$, $E029^{\circ}20'258''$). (b) Close up view of (a).



Figure 5.8: Massive reddish brown, khaki to grey sandstone beds (Sm). A and B: Pafuri Coalfield located at 22°51'712°, 030.92'835°, C: Tuli Coalfield located at S22.80'398°, E029.88'952° and D: Mopane Coalfield located near Waterpoort River at S22.91'121°, E029.61'170°.

5.3.3.2. Interpretation

The tabular cross-bedded sandstones are interpreted as meandering fluvial channel deposits based upon their dimensions, facies distribution and sedimentary structures. The crudely stratified, coarse to pebbly sandstone indicates channel lag deposits within a heavy loaded fluvial system. The coarse to medium and locally, fine-grained sandstone bodies with erosional bases and flat top form channel-like deposits. Fine-grained sandstone represents deposition by vertical accretion on the top of channel sand bars during lower flow conditions (Rust, 1972). In the Soutpansberg area point-bar lateral accretions beds (LA) are common (Figures 5.4 and 5.5). The fine grain size (generally fine sandstone) and pointbar LA elements are consistent with meandering-style rivers (Miall, 1990).

5.3.4. Trough and planar cross-bedded sandstone facies association (FA 4)

5.3.4.1. Description

This facies assemblage consists of primarily trough and minor planar cross-bedded sandstone. They are composed of the following lithofacies, in descending order of abundance: St, Sm, Sh, Sp, Sl, and Sr (Tables 5.1, 5.2 and Figure 5.9). Lithofacies FA 4 consists of larger-scale (up to 1 m thick) sets of trough and planar cross-bedded, medium to very coarse-grained sandstone and occurs interbedded with FA 2 and FA 3. The sandstones are grey to dark grey, dirty white, and yellowish brown in colour, sub-angular to subrounded, moderately to poorly sorted, composed of quartz, feldspar, mica, dark minerals and rock fragments. The matrix/cementing materials are argillaceous, carbonaceous and at places, ferruginous. The facies association occurs as 1 to 3.5 m thick sheet-like sandstone bodies that are massive or trough and planar cross-stratified (Figure 5.9). Thin bedded (5-15 cm) mudstone is generally present between two sandstone bodies.

5.3.4.2. Interpretation

The presence of bar deposits, the dominance of bedload strata accumulated within shallow channels, and the lack of flood-plains facies, altogether suggest that this facies

association represents a braided river system. The coarse sandstone occurs as channel-like bodies which may correspond to deposition by longitudinal channel bars of low sinuous braided streams (Miall, 1977). Abundant large-scale trough and planar cross-stratified co-sets in multistoried sandstone sequence may be attributed to down-current migration of sand dunes, sand waves and transverse bars in shallow water stream channels (Miall, 1982).



Figure 5.9: A, Surface view of trough cross-bedding (arrow); B, Tabular planar cross-bedding (arrow); C, Cross laminated bedding. All photos are from the Soutpansberg Coalfield. Scale bar for A and B is 20 cm.

5.3.5. Fine calcareous and micaceous siltstone and mudstone facies association (FA 5)

5.3.5.1. Description

FA 5 is composed of bimodal, well-sorted, and fine to medium grained light gray siltstone and grey to light grey mudstone (Figure 5.10). It generally occurs as either individual strata or alternated with very fine-grained sandstones and shales in the upper part of the individual depositional units. Individual siltstone stratum is about 0.3 to 3 m and even less than a centimeter thick having either sharp or gradational contacts. The siltstones are dirty white, grey to black in colour with an argillaceous or carbonaceous matrix and show parallel and cross-lamination. The lithofacies tends to coarsen upward and the thicknesses ranges from 0.3 to 3 m. Based on core observations, the facies is regionally correlative in the Mikambeni Formation in all the coalfields. Common diagenetic features are calcite concretions (Figure 5.10c). FA 5 is interpreted to reflect deposition by shallow lakes and ponds.



Figure 5.10: (a) Massive siltstone with broken up top probably due to drastic change of weather. (b) Thinly laminated siltstone and (c) Calcite concretions in siltstone (Mikambeni Formation in the Tuli Coalfield at S22° 30' 176°, E029° 20' 258°).

5.3.5.2. Interpretation

The fine grained parallel and cross-laminated siltstones suggest deposition on top of the bars in abandoned channel and floodplain conditions during the periods of reduced discharge by vertical accretion or shallow water flow conditions (Walker and Cant, 1984). Thin and lenticular siltstone at bar top sequence suggests its deposition from suspension load during falling stage of flow due to rapid shifting of channel bars. Thick and persistent siltstone in association with floodplain sequence is attributed to deposition through extensive and long persistent overflow of stream channel. Siltstones with carbonaceous materials indicate that the channel was flanked by a vegetated overbank. The presence of load cast and other soft sediment deformation structures indicate rapid deposition and poor packing under water-saturated conditions (Walker and Cant, 1984).

5.3.6. Laminated Sandy shale/mudstone facies association (FA 6)

5.3.6.1. Description

It is the most dominant FA in the Madzaringwe Formation. FA 6 is characterised by lithofacies Fm, Fl, with minor St, Sh, and C (Tables 5.1, 5.2 and Figure 5.11). The lithofacies is commonly present in association with coal, carbonaceous siltstone and fine-grained sandstone (Figure 5.11). Individual bed ranges between 0.3 to 10 m thick persist laterally for 10 to 100s of meters. FA 6 mainly consists of massive to parallel laminated sandy shale (Fm, Fl) and contains interbedded dark grey carbonaceous mudstones and light grey, silty sandstone. Shale facies can be described as having three variations: ferruginous shale, pyritic shale, and micaceous shale. The top and bottom contacts of the lithofacies are sharp or gradational. It mainly overlies the sandstone and siltstone lithofacies. These variations are equivalent to Bordy and Catuneanu's (2002c) "Sedimentological study of the Fluvial Tuli Basin" facies in the Tuli Coalfield and Brandl's (2002) "Geology of the Alldays Area" in the Soutpansberg Coalfield.

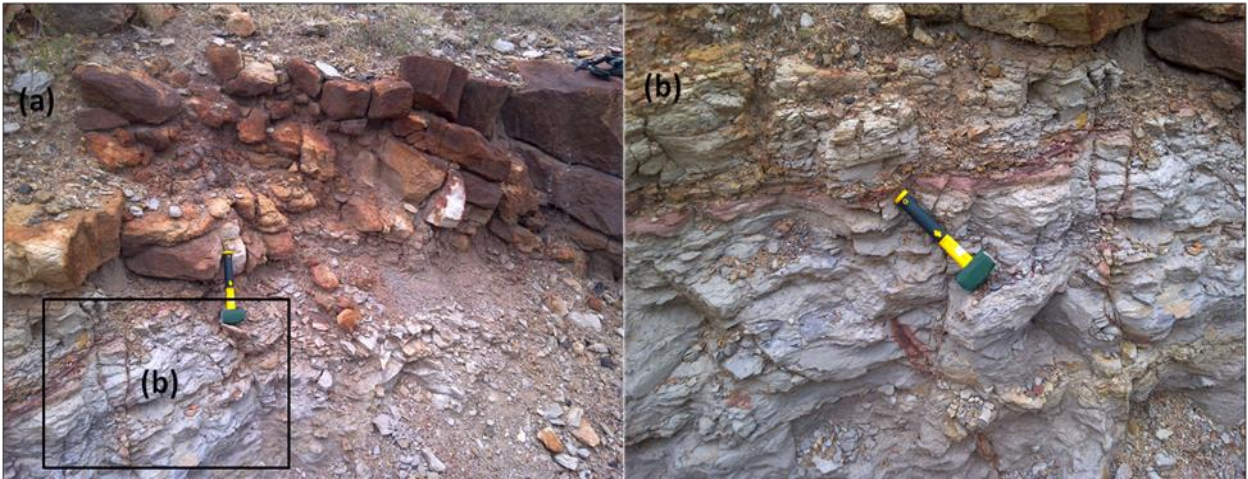


Figure 5.11: (a) and (b) FA 6 Shale overlain by sandstone (FA 5) in the Madzaringwe Formation at Mopane Coalfield.

5.3.6.2. Interpretation

Parallel laminated shale suggests that the sediments were deposited in floodplain environments with frequent variation of hydrodynamic energy. Thin mudstone at the top of the channel sandstones indicates deposition from suspension load during channel abandonment. The thick dark mudstone associated with coal suggests deposition by vertical accretion in backswamp or flood basin environments (Flores, 1981 and Walker and Cant, 1984). Bands of sandstone and siltstone within the facies association were introduced during periodic floods. The presence of carbonaceous mudstone indicates a moderate growth of vegetation in and around the basin.

5.3.7. Laminated or thin bedded carbonaceous shale and coal facies association (FA 7)

5.3.7.1. Description

Three coal zones are identified within the borehole profile in the coalfields (named the basal, middle and upper coal zones). FA 7 is characterised by lithofacies Fc and C (Tables 5.1, 5.2 and Figure 5.12). Lithofacies Fc is commonly interlayered with lithofacies C. It is overlain by FA 4, and consists of true coal (high volatile C to A bituminous), shaly coal, carbonaceous shale to carbonaceous siltstone. The thicknesses range from a few centimeters to a couple of meters, (3 m in common). In this study shaly coal is referred to as coal interlayered with thin bands of carbonaceous shale and shale. The lithofacies commonly overlies the alternated sequences of sandstone, siltstone and mudstone. The coal is dull black to shiny black in colour and vitreous to sub-vitreous in lustre. The coal is classified as sub-

bituminous to bituminous. At places, the coal grades into shaly coal to carbonaceous shale. Inter-seam partings of sandstone and mudstone are also commonly present.

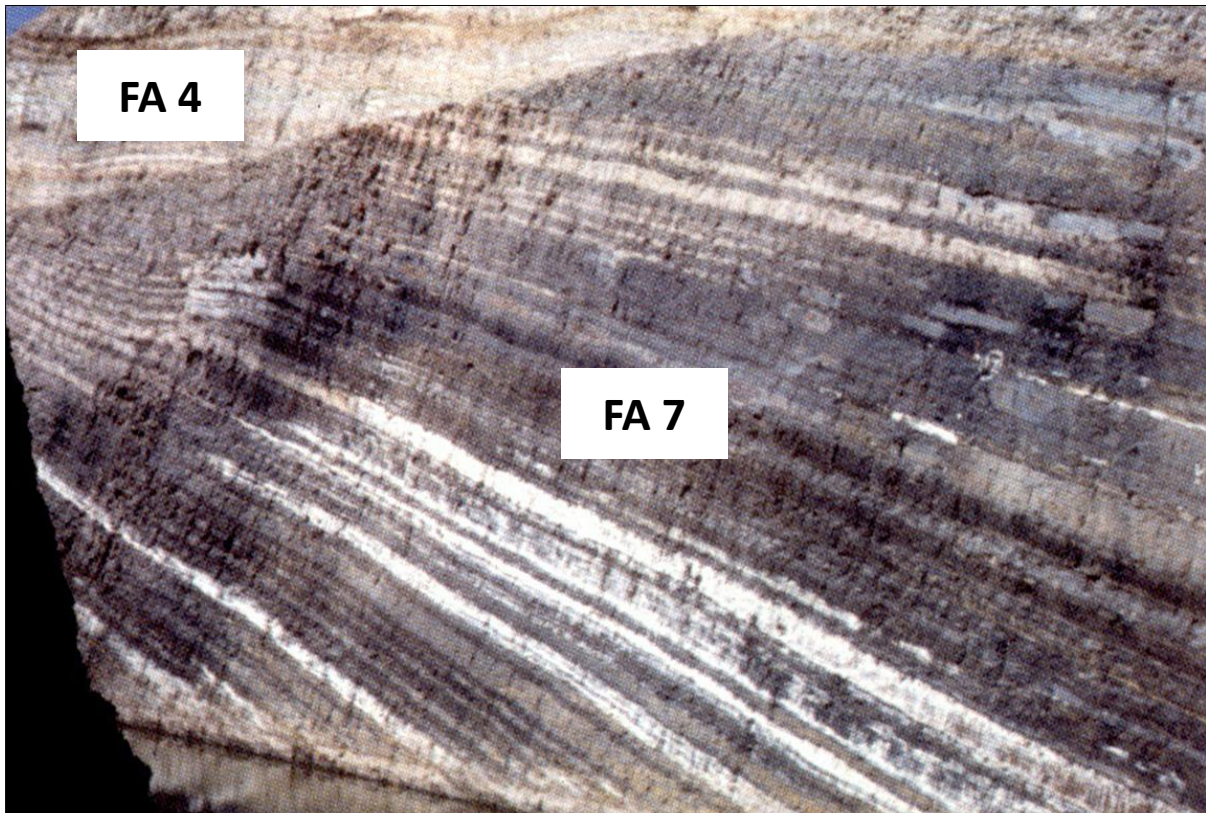


Figure 5.12: FA 7, alternating carbonaceous shale and coal seams in the Madzaringwe Formation at Mopane Coalfield overlain by siltstone layers (FA 4).

5.3.7.2. Interpretation

FA 7 is interpreted to represent flood basin pond and swamp deposits, based on the abundance of preserved organic matter. Carbonaceous shale is commonly observed as part of a facies progressively capping many floodplain pond successions. Due to their high carbon content, it shows common drab and dark gray colours and aquatic faunas, carbonaceous shales are interpreted to have been occurred within a well-vegetated, wet palaeoenvironment.

The thick coal seam indicates a long persistent, slowly subsiding, moderately drained and densely vegetated backswamp or flood plain (Diessel, 1992). The thin coal seams contains a lot of splits of carbonaceous mudstone that attesting to a short-lived flooding events during that period. The thick coal seams are thought to have been resulted from the combined interaction of various factors, such as localised aggradation of channels, slow and steady subsidence of the basin area, abundant rainfall to grow luxuriant vegetation, abundant

supply of paleoflora, comparatively higher water table and long period of time of water merge (Flores, 1981).

5.4. Depositional environments

Detailed analysis of lithofacies types and facies assemblages in the Soutpansberg and Tuli Coalfields suggests a fluvio-glacial to fluvial palaeo-channel depositional environments (Figures 5.13, 5.14, 5.15, and 5.16). Like the other Karoo basins in South Africa, the deposition in the basins was originally initiated by the onset of glacial and fluvio-glacial sedimentation of the lower succession. This was later followed by fluvial deposition of clastic sediments. In some cases little streams branch out from the mouth of rivers into the shore of lakes forming small deltas (Figure 5.15).

The depositional environments recognised in the Soutpansberg and Tuli Coalfields are discussed below:

5.4.1. Glacial depositional environments

Glacial environments are defined as those where ice is a major transport process. Because the flow is laminar, when the ice melts, it dumps all grain sizes into one deposit, forming a diamictite. Typical Tshidzi diamictite and sandstone (FA 1) rocks comprise angular to subrounded, mineral and lithic clasts in a fine-grained, clastic matrix rich in phyllosilicate minerals. The matrix also contains a large component of extremely fine-grained mineral fragments, mostly of quartz and some feldspar.

5.4.2. Alluvial and braided fluvial channel deposits

Alluvial deposits are defined as clay, silt or gravel carried by fast flowing streams and deposited where the stream slows down. The conglomerates of the coalfields are a characteristic of the deposition of transported materials in high energy environments. They were deposited in fluvial environments such as flood plains. The deposits form at the base of mountains where fast-flowing streams meet flat surfaces of basin floors or broad valleys. At this juncture, the gradients of streams decrease and gravel, sand, and other sediments are deposited.

Braided fluvial channel deposits tend to be relatively coarse-grained and consist of gravel and sand, with little or no mud. These channels form when fast moving water dramatically slows and the larger particles (such as gravels) are deposited within the channel and block the flow of water (Figure 5.13). Because braided stream systems are high energy,

smaller clast sizes such as silts and clays, are not deposited instead they are washed further down stream. As a result braided stream systems can be identified by their shallow channels of crossbedded-sands, gravel deposits, and the lack of mud or clays. Coarse grained sediments are transported and deposited as bars, locally dividing the channel into two or more channels (making “braids”). This type of depositional environments is associated with FA 2. Most of these depositional environments are found in the Middle Member of the Madzaringwe Formation.

5.4.3. Meandering, braided and lacustrine depositional environments

Meanders often begin as a result of existing topographic control, but as the stream velocity and the position of maximum turbulence change, the banks of the stream undergo differential erosion which leads to meandering. The maximum flow and erosion occurs on the outside of the meander while minimum erosion and deposition occur on the inside of the meander where point bars form (Figure 5.14). Braided Rivers exhibit numerous channels that split off and rejoin each other to give a braided appearance. They typically carry fairly coarse-grained sediment down a fairly steep gradient (Figure 5.13). Lacustrine deposits are defined as material deposited in fresh water areas (e.g. lakes) and exposed when the water level is lowered or the elevation of the land is raised. The deposits are associated with FA 3 and FA 4. The Middle Member of the Madzaringwe Formation and the Upper Member of the Mikambeni Formation are results of this type of depositional environments.

5.4.4. Fluvial floodplains and ponds depositional environments

A floodplain is defined as the portion of a river system, usually located at the lower reaches near the coast with relatively flat topography relief, which is built of sediments during previous flood stages (Figure 5.14). Floodplains develop when streams over-top their levees spreading discharge and suspended sediments over the land surface during floods. In this type of deposits, meandering rivers dominate with minor or no braided rivers. Meandering-river deposits tend to be finer-grained, more lenticular, and partially or completely covered in floodplain shales. The deposits are associated with FA 5 and FA 6. The Middle and Upper Members of the Madzaringwe Formation and the Lower Member of the Mikambeni Formation are results of this type of depositional environments.

5.4.5. Paludal depositional environments (backswamps and oxbow lakes)

Paludal environments are defined as swampy and marshy environments. Coal, shaly coal and carbonaceous shale were formed in these environments. The coal was formed when peat was altered physically and chemically after being buried. Peat deposits typically form in a waterlogged environment where plant debris accumulated; peat bogs and peat swamps are examples. The deposits are associated with FA 7. The Lower and Middle Members of the Madzaringwe Formation and the Lower Member of the Mikambeni Formation are results of this type of depositional environments.

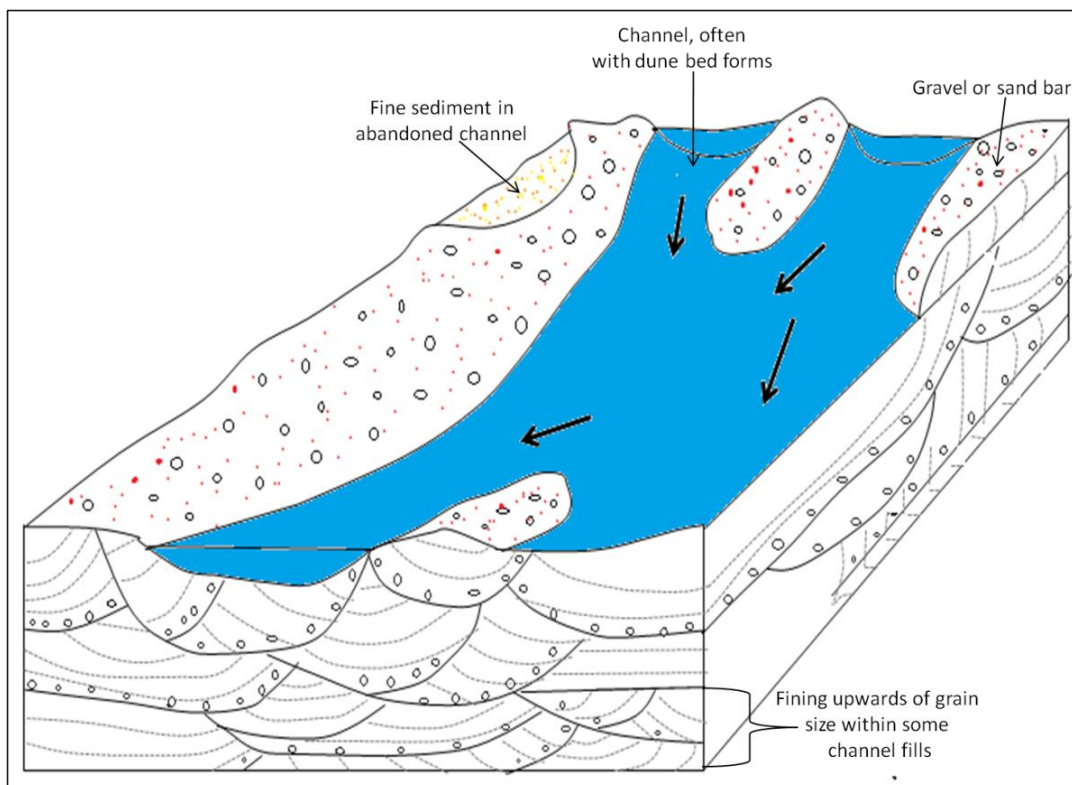


Figure 5.13: Sketch showing part of a braided river deposit. Modified and redrawn from Reading (1996).

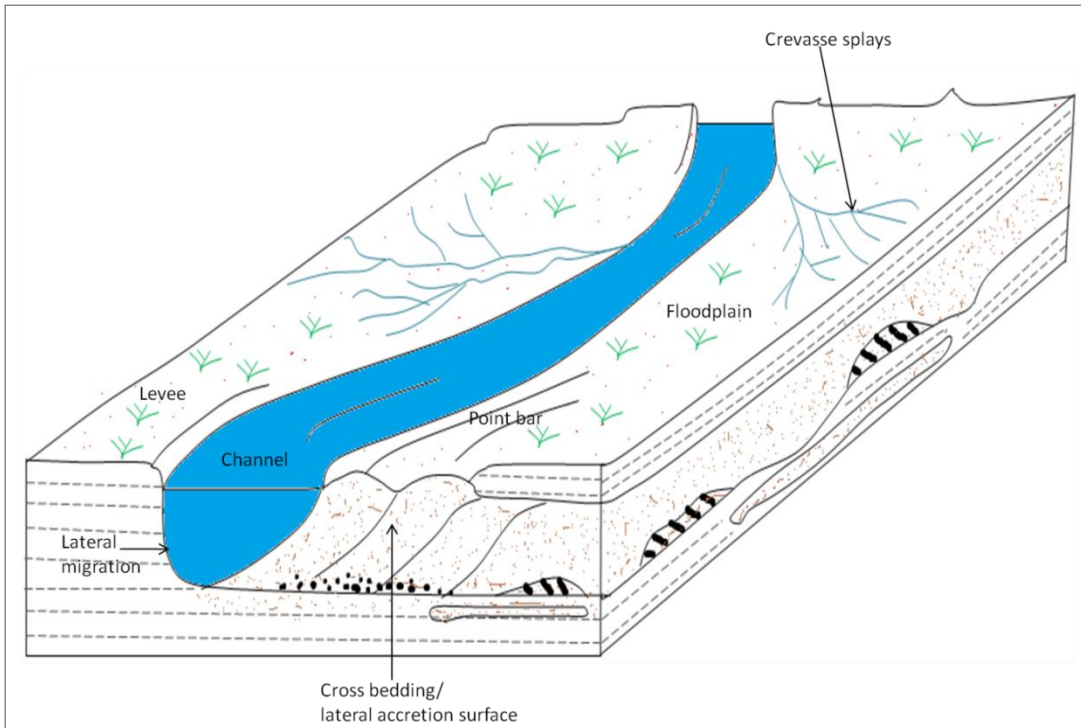


Figure 5.14: The sub environments of a meandering stream. Redrawn from Reading (1996).

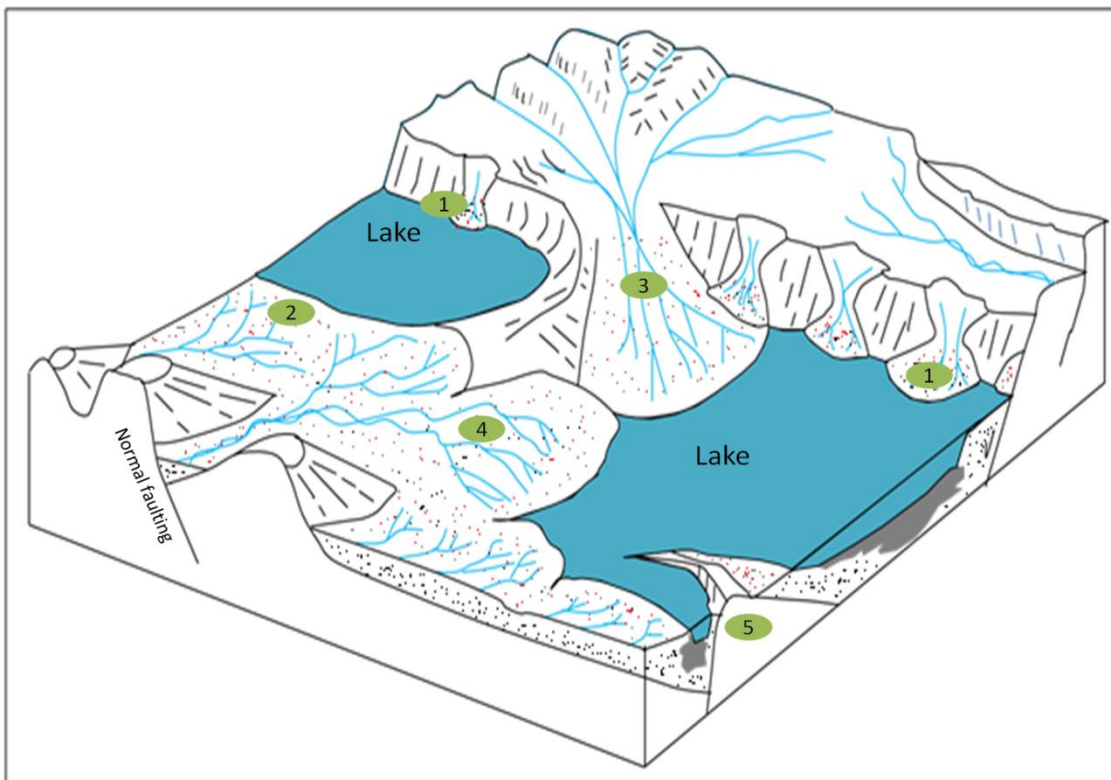


Figure 5.15: Block diagram of a rift basin illustrating (1) footwall-derived coarse grained and Gilbert-type deltas sourced from drainage basins developed along the dominant border fault zone; (2) Hanging-wall-derived sand rich deltas; (3) Delta sourced from a flexural transfer zone

separating two border fault segments; (4) Delta (5) Coarse grained deltas derived from an intra-basin fault block. Redrawn and modified from Gawthorpe and Colella (1990).

In the present study, a conceptual model was constructed to provide an idea of the paleogeography and environments of the deposition of the Soutpansberg and Tuli Coalfields (Figure 5.16). Internal sedimentary structures, boundary conditions lithofacies, their interrelationship, sequence and facies associations are taken into consideration for the interpretation of depositional environments. Likewise in the studied portions of the north Karoo deposits (Soutpansberg and Tuli Coalfields), the sedimentation commenced with the deposition of diamictite and coarser sandstones in a fluvio-glacial regime. This sequence is overlain by a thick conglomerate and alternated sequence of conglomerates and trough to planar cross-stratified sandstones and siltstones, alternating shale, shaly coal and carbonaceous shale.

All these suggest deposition under channelized conditions, in a braided alluvial fan-fluvial stream setting (Figure 5.16A). Consequently, the gradient of the stream reduced to form comparatively fine-grained and small-scale sequences of meandering streams with several horizons of thin coal seams. The peat-forming swamps existed for a short time and most probably were moderate to well drained, this is indicated by the presence of repeated sequence of coarse to fine clastics with intervening thin coal seams. Gradually, this situation changed to more peneplain condition where thick coal seams were deposited in a long moderately drained to poorly drained and densely vegetated peat-forming backswamps along sinuous streams. The mudstone/shale and siltstone were deposited in natural levee or flood basin. But the occurrence of carbonaceous mudstone indicates more stagnant condition in backswamp and abandoned channel conditions with sparse vegetation (Figure 5.16B).

The sedimentary facies, stratigraphic sequence and their vertical changes in facies association indicate a progressive decrease in coarse clastics and an increase in fine clastics and coal. The evidence for this comes from the fining-upward channel-fill sequences which were built up by numerous flooding events as indicated by the desiccated mud drapes and internal erosion surfaces (Bordy and Catuneanu, 2001). This in turn suggests a progressive decline of stream gradient and current competency from bottom to top of the sequence. The lithofacies of the succession of this basins form several repeated fining upward sequences and minor coarsening upward sequences. The fining upward sequences might have been deposited in several sub-environments of the fluvial regime (Figure 5.16).

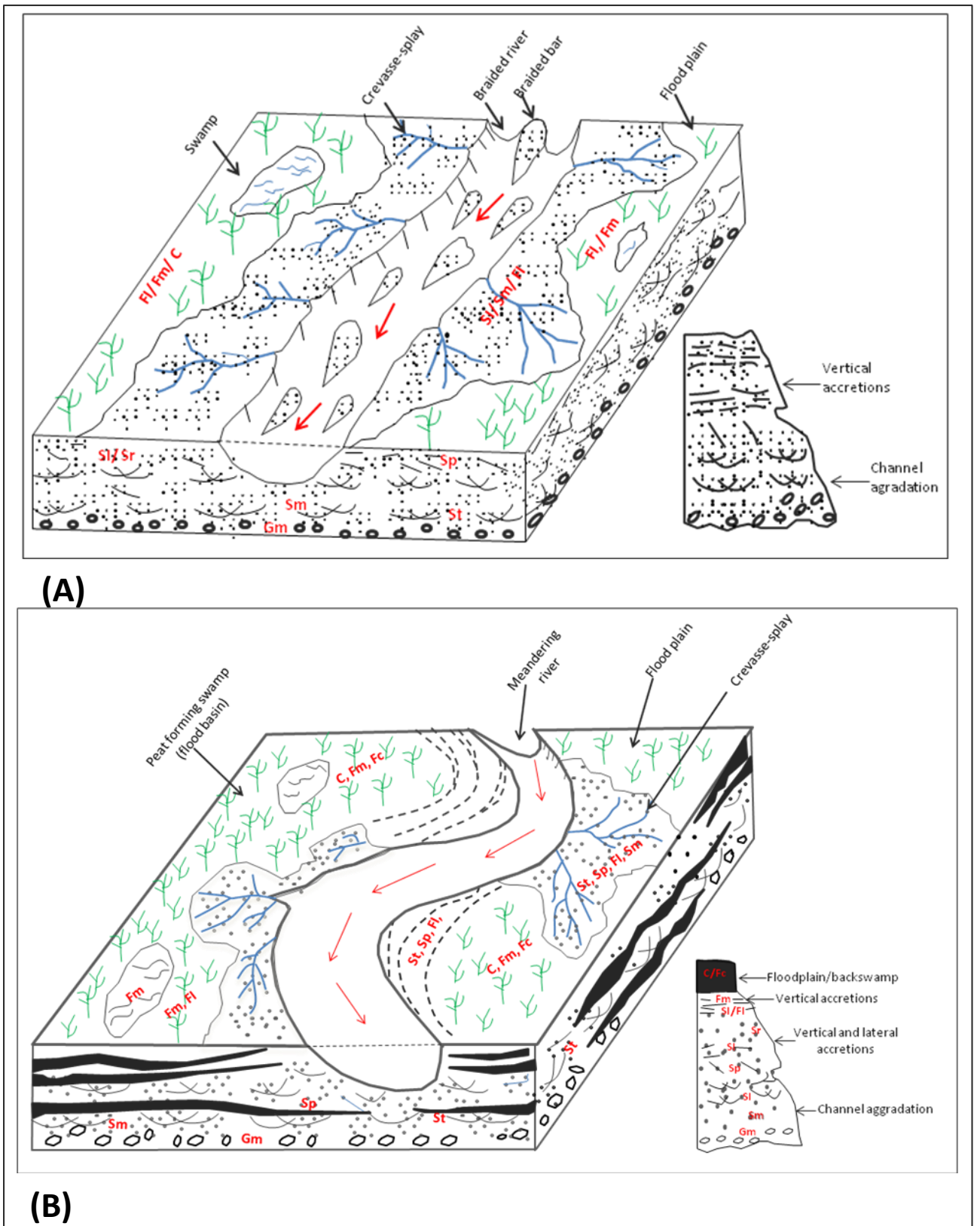


Figure 5.16: Schematic block diagrams with sedimentary sequence showing the environments of deposition in the Soutpansberg and Tuli Coalfields.

5.5. Depositional environments for the different formations

The facies associations identified in the coalfields resemble those of a fluvio-glacial to fluvial depositional environments dominated by braided and meandering streams, lakes, swamps and ponds as described below:

5.5.1. Diamictite Tshidzi Formation

The formation resembles characteristics of the facies association (**Gm and minor St**) in a fluvio-glacial depositional environment. This is evidenced by diamictite developing at the base of the Karoo Supergroup consisting of poorly sorted sediments characteristically carrying coarse-grained clasts in a fine-grained matrix (Heinz *et al.*, 2001).

5.5.2. Madzaringwe Formation

Three identified informal members (Lower, Middle and Upper) of the Madzaringwe Formation resemble characteristics of the Facies Associations (FAs) 2, 3, 4, 5, 6 and 7 in a prograding fluvial depositional environment. The laminated, grey and black carbonaceous shale and coal of FA 7 (**Fc and C**) and sandy shale/mudstone of FA 6 (**FI, Sh, St, and C**) forms the Lower Member. The Middle Member is characterised by alternating beds of shale and fine-medium grained sandstone, FA 2 (**Se and St**), FA 3 (**Sp, Sr and Sh**), FA 4 (**St, Sm and Sp**) and FA 5 (**FI, Sr and St**). Succeeding the Middle Member is the Upper Member which has almost the same depositional environments as that of the Lower Member.

5.5.3. The Mikambeni Formation

This formation can be informally subdivided into two members (Lower and Upper Members) in a fluvial depositional environment. The Lower Member is characterised by laminated, grey and black carbonaceous shale and coal of FA 7 (**Fc and C**) and sandy shale/mudstone of FA 6 (**FI, Sh, St, and C**). Succeeding the Lower Member is the Upper Member which is characterised by alternating beds of shale and fine to coarse grained sandstone, FA 2 (**Se and St**), FA 3 (**St, Sr and Sh**), FA 4 (**St, Sm and Sp**) and FA 5 (**FI, Sr and St**).

5.6. Paleocurrent Directions

A paleocurrent or paleocurrent indicator is a geological feature (typically a sedimentary structure) that helps a researcher to determine the direction of flowing water in the geologic past. Paleocurrent directions are measured by sporadic exposures which greatly limit the recording of the paleocurrent data and their interpretations. All structures discussed in this study were measured and studied while the writer was in the field. A pocketknife and brush were used to obtain cleaner and fresher exposures of sedimentary structures. A geological compass was then used to measure the directional orientation of these structures. Each structure is discussed in regard to definition, description, type and origin.

5.6.1. Cross-bedding

Cross-bedding is a layering within one or more beds in a series of rock strata that does not run parallel to the plane of stratification. This structure was found to be the most useful directional structure studied in the field. It is probably the most widely recognised and described of all sedimentary structures and has been proven by many to be an excellent paleocurrent direction indicator. Two types of cross-beddings were used in collecting data for this thesis namely, tabular-planar cross-bedding and trough cross-bedding.

Tabular-planar cross-bedding consist of cross-bedded units that have large horizontal extent relative to set thickness and that have essentially planar bounding surfaces (Figures 5.9b and 5.17a). It is formed mainly by migration of large scale, straight crested ripples and dunes. It forms during lower flow regime conditions and its individual beds range in thickness from a few tens of centimeters to a meter or more, but bed thickness down to 10 centimeters has been observed. Where the set height is less than 6 centimeters and the cross-stratification layers are only a few millimeters thick, the term cross-lamination is used (Figure 5.9c). In tabular-planar cross-bedding, the down-dip direction of a tabular cross-bed point to the direction of paleo flow.

Trough cross-bedding are layers of sediment that are inclined relative to the base and top of the bed they are associated with (Figures 5.9a and 5.17b). They are deposited at an angle rather than deposited horizontally and deformed later on. Trough cross-beds have lower surfaces which are curved or scoop shaped and replaces the underlying beds. In trough cross-bedding the axis of a trough cross-bed point to the direction of paleo flow.

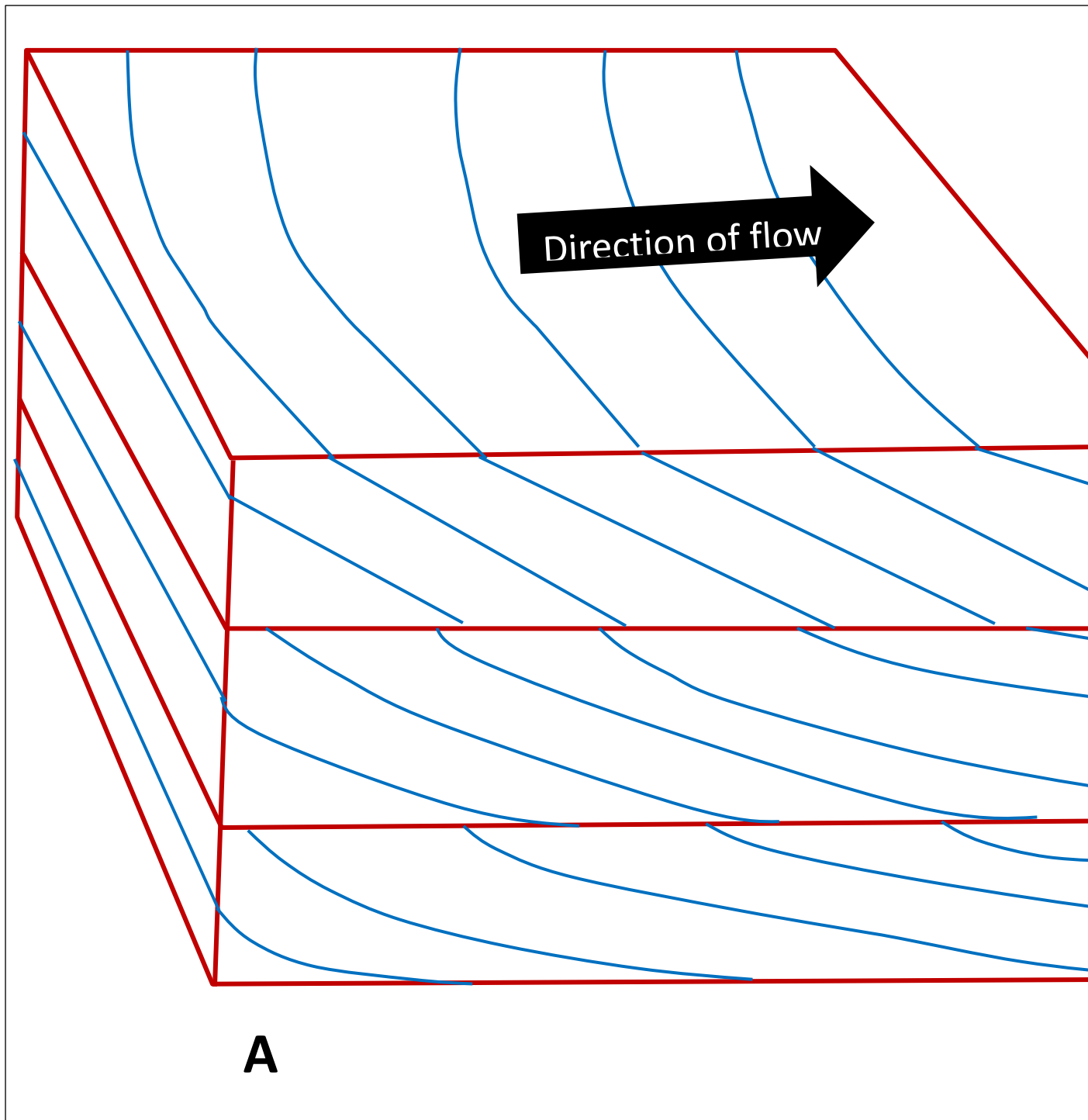


Figure 5.17: A: Tabular-planar cross-bedding showing palaeocurrent direction. B: Trough cross-bedding showing palaeocurrent direction.

5.6.2. Asymmetric ripple marks

Current ripple marks are one of the second most common sedimentary structures in the study area. They are usually found at the tops of cross-bedded sandstone and are associated with thinly laminated beds. According to Potter and Pettijohn (1963), ripple marks

refer to rhythmic or periodic undulations that occur on bedding planes and are formed in granular materials at the sedimentary interface in response to a moving fluid. The ripple marks observed in the study area have wave lengths ranging from 10 to 30 cm and amplitudes from 1 to 4 cm. Both the crests and troughs of the ripples are smooth and rounded in shape.

Paleocurrent directions of oriented primary structures are presented on rose diagrams (Figures 5.18, 5.19 and 5.20). They were mainly derived from planer and trough cross-beddings and asymmetric ripple cross-lamination in the Mikambeni and Madzaringwe Formations. The Tshipise-Pafuri and the Mopane Coalfields displays a South-West to North-East trend. In the Tuli Coalfield, a South-West to North-East paleocurrent trend can be observed. Studies by Brandl (1981, 2002) revealed that the depositional flow in the Soutpansberg and Tuli Coalfields was south-west to north-east.

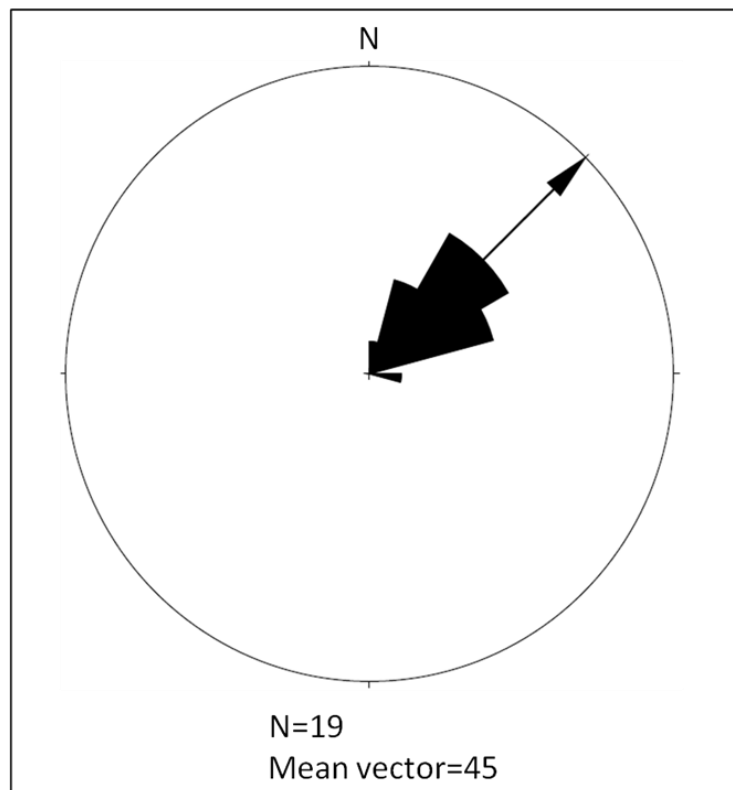


Figure 5.18: Constructed paleocurrent directions of the Tshipise-Pafuri Coalfield, Mikambeni Formation.

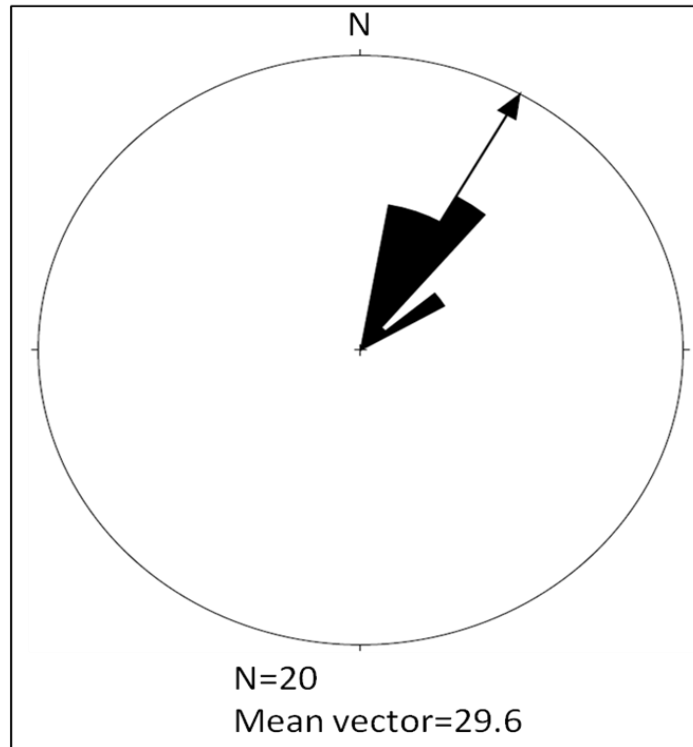


Figure 5.19: Constructed paleocurrent directions of the Mopane Coalfield, Mikambeni Formation.

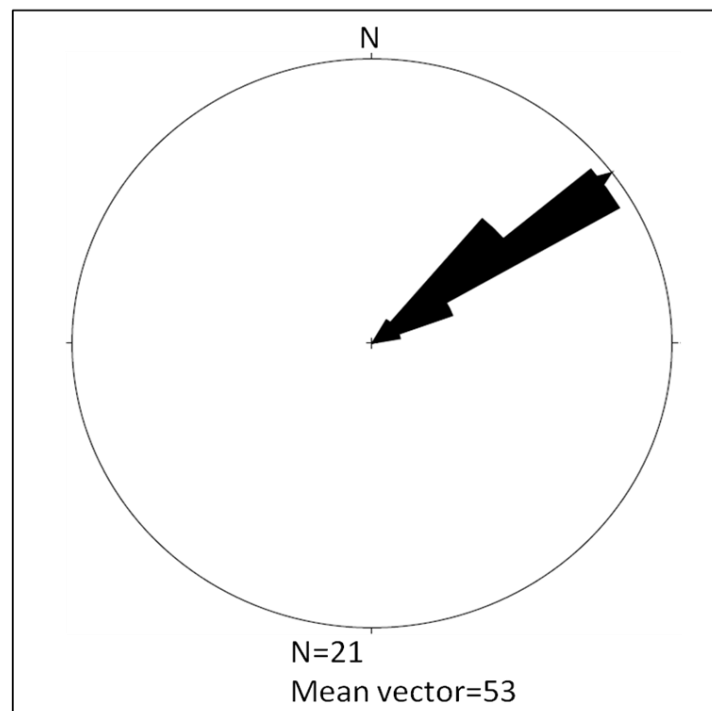


Figure 5.20: Constructed paleocurrent directions of the Tuli Coalfield, Mikambeni Formation.

5.7. Discussions

Seven recurrent FAs were identified and interpreted. The lithofacies types and facies assemblages in the Soutpansberg and Tuli Coalfields suggest a glacio-fluvial to fluvial depositional environment. The facies analysis is discussed below:

5.7.1. Diamictite Tshidzi Formation

The formation is of glacio-fluvial depositional environments. It was developed at the base of the Karoo Supergroup consisting of poorly sorted sediments characteristically carrying coarse-grained clasts in a fine-grained matrix. The formation resembles characteristics of the facies association (Gm and minor St) and is characterised by diamictite and minor sandstone.

5.7.2. Madzaringwe Formation

The formation resembles characteristics of fluvial depositional environment. Three identified informal members (Lower, Middle and Upper) of the Madzaringwe Formation are recognised.

The Lower Member rests on pre-Karoo rocks or Tshidzi Formation. It is characterised by laminated, grey and black carbonaceous shale and coal of FA 7 (Fc and C) and sandy fluvial shale/mudstone of FA 6 (Fl, Sh, St and C). Coal and carbonaceous shale were

probably deposited in well drained ponds and swamps whereas peat in poorly drained swamps.

The Middle Member is characterised by alternating beds of shale and fine-medium grained sandstone to siltstone (FA 2, FA 3, FA 4 and FA 5).

Succeeding the Middle Member is the Upper Member which has almost the same depositional environments as that of the Lower Member.

5.7.3. Mikambeni Formation

This formation is informally subdivided into two members (Lower and Upper Members). The Lower Member is characterised by laminated, grey and black carbonaceous shale and coal of FA 7 (Fc, C) and sandy fluvial shale/mudstone of FA 6 (Fl, Sh, St and C). The Upper Member is characterised by alternating beds of shale and fine-coarse grained sandstone to siltstone (FA 2, FA 3, FA 4 and FA 5).

5.7.4. Paleocurrent Directions

The Tshipise-Pafuri Coalfield displayed a south-west to north-east trend of average 45° while the Mopane Coalfield displayed a north-east trend of 29.6° . In the Tuli Coalfield, a north-east palaeo-current trend of average 53° was observed.

5.8. Conclusions

Detailed sedimentological facies analysis of borehole cores from across the Tuli and Soutpansberg Coalfields revealed a variety of depositional environments which existed during the Karoo Supergroup era. The inferred depositional environments are in agreement with the previous documented depositional environments by Brandl (1981 and 2002), SACS (1980), and Bordy and Catuneanu (2002a, b and c). The results obtained from this

investigation demonstrate detailed facies associations and different depositional environments present within the Karoo Supergroup in the Soutpansberg and Tuli Coalfields of South Africa.

A total of sixteen lithofacies were identified in the coalfields. Internal and external geometry of the strata in the coalfields have been subdivided into seven distinct facies associations (FA) which are: Glacial diamictite and sandstone (FA 1), Clast supported conglomerate and sandstone (FA 2), Tabular cross-bedded sandstone (FA 3), Trough and planar cross-bedded sandstone (FA 4), Fine calcareous and micaceous siltstone and mudstone (FA 5), Sandy shale/mudstone (FA 6), Laminated or thin-bedded Carbonaceous shale/mudstone (FA 7).

Detailed analysis of lithofacies types and facies assemblages in the Soutpansberg and Tuli Coalfields suggests a glacio-fluvial to fluvial depositional environment. The deposition in the coalfields was probably started with the onset of glacial and fluvio-glacial sedimentation on the basement. This was later followed by braided, meandering stream deposition, and lacustrine or swamp deposits within the fluvial sediments.

CHAPTER 6

PETROGRAPHY, GEOCHEMISTRY AND PROVENANCE OF THE SOUTPANSBERG AND TULI COALFIELDS

Abstract

Petrography and geochemistry (major, trace and rare earth elements) of clastic rocks from the late Palaeozoic Madzaringwe and Mikambeni Formation, in the Soutpansberg and Tuli Coalfields, have been investigated to understand their source, provenance, paleoweathering and tectonic setting. Sandstone petrography and detrital modes indicates that the Permian succession was derived from craton interior and recycled orogen provenance. Sandstones in the northern Karoo depositional system are sub-arkose, lithic arkose. The sediments may represent a recycled to craton interior provenance. The geochemical data of major elements show that sandstone and shales have the same source. The study of paleoweathering conditions based on modal composition, chemical index of alteration (CIA), Plagioclase Index of Alteration (PIA) and A-CN-K ($Al_2O_3-CaO + Na_2O-K_2O$) relationships indicate that probably chemical weathering in the source area and recycling processes have been more important in shale and sandstone rocks. The relatively high CIA values (70 to 90%) indicates moderate to high weathering conditions of the samples and the palaeoclimate of the source area was probably warm. K_2O/Na_2O versus SiO_2 and $Na_2O-CaO-K_2O$ tectonic setting discrimination plots, suggest a passive continental margin. In the study of trace elements, the ternary plots of Th-Sc-Zr/10 and La-Th-Sc both suggest a passive margin setting of the provenance. Petrographic and geochemical results of the samples of the coalfields suggest uplifted basement source areas dominated by sedimentary rocks and/or granite-gneiss rocks. The source rocks might have been the recycled pre-Soutpansberg Karoo Supergroup rocks and the metasedimentary rocks of the Soutpansberg Group. Other source rocks may have been the pre-Beit-Bridge Complex basement rocks (granites and gneisses).

6.1. Introduction

The composition of the source rocks has a great influence on the ultimate composition of sandstone and shales. Therefore provenance studies are mainly based on modal analysis of clasts grains (Dickinson and Suczek, 1979; Dickinson *et al.*, 1983) and bulk rock geochemistry (Bhatia; 1983; 1985; Bhatia and Crook, 1986; Roser and Korsch, 1986). Detrital modes of sandstone also provide information about the tectonic settings of depositional basins (Dickinson *et al.*, 1983). The relationship between sandstone petrography and tectonic setting has been studied by many workers (Dickinson *et al.*, 1983; Dickinson and Suczek, 1979; Ingersoll and Suczek, 1979). Both mineralogical & geochemical compositions of fine grained sedimentary rocks such as mudstone and shale are generally used as the sensitive indicators of provenance, weathering conditions and tectonic settings (Nesbitt and

Young, 1996; Nesbitt *et al.*, 1997; Taylor and McLennan, 1985; McLennan and Taylor, 1991).

The geochemistry of shale and sandstone is useful in understanding provenance characterization, palaeoclimatic conditions and intensity of chemical weathering (Baulaz *et al.*, 2000; 2005; Maslov *et al.*, 2003; 2010). In this regard major elements of sediments are helpful for the determination of their original detrital mineralogy. Bhatia (1983) and Roser and Korsch (1986) proposed tectonic setting discrimination fields for sedimentary rocks to identify the tectonic setting of unknown basins. These tectonic setting discrimination diagrams are still extensively used by many researchers to infer the tectonic setting of ancient basins (Maslov *et al.*, 2010; Wani and Mondal, 2010). The functionality of the major element tectonic setting discrimination diagrams proposed by Bhatia (1983) and Roser and Korsch (1986) are evaluated in many cases while researchers have observed that the tectonic setting discrimination diagram proposed by Roser and Korsch (1986) works better than Bhatia's (1983) diagram.

The K_2O/Al_2O_3 ratio, Index of Compositional Variability (ICV), Chemical Index of Alteration (CIA), $SiO_2-Al_2O_3+K_2O+Na_2O$ diagram and $Al_2O_3-CaO+Na_2O-K_2O$ (A-CN-K) plot are useful geochemical parameters for the study of provenance and maturity of the rocks (Weaver, 1989; Nesbitt and Young, 1984).

In the past, alkali metal oxides were used by several authors to reveal information about the provenance of clastic sediments (e.g. Crook, 1974; Roser and Korsch, 1986; McCann, 1991). The K_2O/Na_2O versus SiO_2 tectonic setting discrimination diagram was proposed by Roser and Korsch (1986). Analogue, but more detailed results can be obtained by the calc-alkaline oxide ternary diagram ($CaO-Na_2O-K_2O$) of Bhatia (1983) modified by Toulkeridis *et al.* (1999).

Sandstone petrology and geochemistry of shales and sandstones of the Tuli and Soutpansberg Coalfields have not been studied previously in detail to determine their provenance and geochemical parameters. This chapter therefore was aimed to deal with petrology of sandstone, geochemistry of sandstone and shale in order to understand provenance and chemical weathering degree due to paleoclimatic conditions in the source area. Furthermore, relationship of paleoclimate conditions with intensity of chemical weathering in source area was interpreted by using geochemical models of shale and sandstone. Lastly the provenance of source materials is further related to coal formation and tectonic settings of the coalfields.

6.2. Methodology

Mineralogical identification of sandstone and shale from the Tuli and Soutpansberg Coalfields was undertaken using microscopic study of petrography and X-ray diffraction (XRD). Thin sections of sandstone were prepared and studied under the Olympus BH-2 Modal research microscope at the Ore Microscopy Laboratory, Rhodes University. Thin sections of different types of sandstone were selected to cover textural variations. In textural variation the physical appearance or character of a rock, such as grain size, shape and arrangement were considered. Five hundred (500) points at stage interval 1 for finer grains and stage interval 2 for coarser grains were counted in each thin section using the Gazzi Dickinson method, which manages to minimize the effect of grain size (Ingersoll *et al.*, 1984; Ingersoll, 1988; Zuffa, 1985). Constituent minerals of the sandstone were classified into monocrystalline quartz, polycrystalline quartz, K-feldspar, plagioclase, volcanic lithic fragments and sedimentary lithic fragments. Compositional fields are shown in ternary plots of Q-F-L (quartz-feldspar-lithic fragments), Qm-F-Lt (monocrystalline quartz-feldspar-total lithic fragments) and Qt-F-L (total quartz-feldspar-lithic fragments). Framework parameters of detrital modes in sandstone by Ingersoll and Suczek, 1979 and Tucker, 2001 were used.

XRD analyses were performed at the Council for Geoscience, Pretoria, South Africa. The Bruker D8 Advance diffractometer was used to make the X-ray diffraction scans at $2^\circ\theta/\text{min}$ on air-dried and heated samples. X-Ray Fluorescence (XRF) analysis of the major and trace elements geochemistry of the samples was performed using MagiX Fast, XRF spectrometer. The XRF analysis was also carried out at the Council for Geoscience, Pretoria, South Africa. Graphs and ternary diagrams were drawn and interpreted for compositional analysis of samples (sandstone and shale).

Table 6.1: Framework parameters of detrital modes (Ingersoll and Suczek, 1979; Tucker, 2001).

<i>Parameter</i>	<i>Explanation</i>
------------------	--------------------

Q	Quartz (Qm + Qp)
Qp	Polycrystalline quartz
Qm	Monocrystalline quartz
Qt	Total quartzose grains (Qm + Qp)
P	Plagioclase feldspar
K	Potassium feldspar
F	Total feldspar grains (P + K)
Lv	Volcanic–metavolcanic rock fragments
Ls	Sedimentary rock fragments
Lm	Metamorphic lithic fragments
Lsm	Metasedimentary lithic fragments
L	Unstable (Siliciclastic) lithic fragments (Lv + Ls + Lsm)
Lt	Total siliciclastic lithic fragments (L + Qp)

6.3. Petrography

The major clast components of the sandstones, especially quartz, feldspar and rock fragments have been recalculated as 100% (Table 6.2) for QFL diagrams, allowing these to occupy one of the three poles in the ternary plot diagrams. Plots in the QFL diagrams

proposed by Pettijohn (1975) and Folk (1980) show that the sandstone ranges from sub-arkosic to sub-litharenite (Figure 6.18). Interpretation of provenance from the petrography of the Soutpansberg and Tuli Coalfields sandstones proposed by Dickinson *et al.* (1983) is indicated in Figure 6.19. Q-F-L tectonic provenance diagram for the sandstones after Yerino and Maynard (1984) is indicated in Figure 6.20.

Table 6.2: Average of point counting results in percentages of measured sections in the Soutpansberg and Tuli Coalfields.

Samples	Q	F	L	Qm	Qp	Lt
Tuli 1	62.8	19.8	17.2	60.6	2.2	19.4
Tuli 2	79.8	9.6	10.6	78.2	1.6	12.2
Tuli 3	75.8	14.2	10	73.2	2.6	12.6
Tuli 4	85.8	9.2	5	78.4	7.4	12.4
Tuli 5	88.6	6.6	4.8	83.2	5.4	10.2
Tuli 6	61.2	22.4	16	60.2	1	17
Tuli 7	79.6	8.4	12	75.4	4.2	16.2
Mopane 1	70.2	15.8	14	69.2	1	15
Mopane 2	78.4	9.6	12	75.6	2.8	14.8
Mopane 3	85.2	7.4	7.4	81	4.2	11.6
Mopane 4	69.6	25.6	4.6	66.6	3	7.6
Mopane 5	85.6	5.2	9.2	78.4	7.2	16.4
Tshipise-Pafuri 1	65	15.6	19.4	60.8	4.2	23.6
Tshipise-Pafuri 2	71	15	13.8	67.2	3.8	15.6
Tshipise-Pafuri 3	61.4	22.6	16	60.2	1.2	17.2
Tshipise-Pafuri 4	80.2	14	5.8	77	3.2	9
Tshipise-Pafuri 5	90.2	4	5.8	82.4	7.8	13.6
Average	75.91	13.24	10.8	72.21	3.69	14.38
Standard Deviation	9.72	6.51	4.77	8.21	2.19	3.93

6.3.1. Texture

Thin sections were prepared from fine to coarse grained sandstone samples. Some samples are coarse (Figure. 6.4 and Figures 6.11), whereas, others are fine to very fine grained (Figure 6.1, 6.2 and 6.3). Sorting of samples ranges from moderate to well sorted

(Figure 6.1); poor to moderately sorted (Figures 6.2 and 6.3). Grain morphology ranges from very angular to angular (Figure 6.4 and 6.7 and 6.10); sub-angular to sub-rounded (Figure 6.1 and 6.16B) and rounded to well rounded (Figure 6.11 and 6.12) based on the different stratigraphic positions. Most sandstone samples are cemented with mud matrix (Figure 6.4 and 6.7), whereas, some are grain supported (Figures 6.1, 6.2 and 6.5).

6.3.2. Clast composition

6.3.2.1. Quartz

Quartz is the most dominant mineral within all sandstone samples, and it ranges from 61.4 to 90.2% of the overall composition. Grain sizes range from 0.01 mm to 0.84 mm, grain shape is mostly sub-angular to sub-rounded and sorting is poor to moderate. Both monocrystalline (Qm) and polycrystalline (Qp) quartz grains are present (Figures 6.1 to 6.17), with monocrystalline quartz grains comprising 72.21% of the total grains in the samples. Inclusions of muscovite were observed in some thin sections (Figure 6.2 and 6.14 A). The presence of monocrystalline and polycrystalline quartz grains indicates possible derivation from variable sources (igneous, metamorphic and pre-existing sediments). Monocrystalline grains are characterised mostly by non-undulatory (unstrained) and more rarely by slightly undulatory (strained) extinction types, suggesting a plutonic igneous or metamorphic origin. Monocrystalline quartz (Qm) is usually in the form of sub-angular to sub-rounded and occasionally well-rounded grains indicating the reworked sedimentary origin or strong hydrodynamic movement (Figures 6.2 and 6.3). Polycrystalline quartz (Qp) grains consisting of two or more crystals comprise 3.69% of the total grains. The dominance of monocrystalline quartz grains indicates that the sediments were derived from a granitic or a metamorphic rock source, probably related to the Kaapvaal Craton and Limpopo Mobile Belt. It also suggests that such grains may be the result of the disaggregation of original polycrystalline quartz during high energy or long distance transportation from the source areas. Recycled monocrystalline quartz grains can also be recognised by the abrasion of overgrowths that were precipitated around the grain boundary in the original sandstone. The low percentage of feldspar and rock fragments in many samples indicates higher mineral maturity and favours a cratonic source. The sparse sedimentary rock fragments (Figure 6.6) and overgrowth on quartz grains Figure (6.5 and 6.15) indicate several phases of recycling from older sedimentary sources.

6.3.2.2. Feldspar

Feldspar is the second most abundant detrital constituent of the samples with different grain sizes and types. Both alkali feldspar (orthoclase and microcline) and plagioclase feldspar constitutes an average of 13.24% of the total grains in the samples. Rarely, feldspar grains show perthitic intergrowth. Both K-feldspar and plagioclase grains are sub-rounded to rounded (Figures 6.8 and 6.9). About sixty percent of the feldspar grains are partially altered, and appear cloudy in thin section. Commonly, altered feldspar is partially or totally (preserving only its shape) replaced by sericite or kaolinite (Figures 6.11A and 6.11B), which in many cases has itself altered to illite. Plagioclase shows distinctive parallel twinning, while orthoclase is untwinned (Figure 6.8 and 6.9). Plagioclase feldspar occurs in both twinned and untwinned forms.

6.3.2.3. Lithic fragments

Rock fragments formed from clusters of multiple mineral grains comprise an average of 10.8% of the total grains in the samples (Figures 6.16 and 6.17) and are mostly medium or coarse-grained, sub-rounded, rounded or rarely angular. The fragments are of igneous, metamorphic and sedimentary origin. Igneous and metamorphic clasts constitute a lesser percentage than sedimentary clasts. Clast from igneous origin includes granitic and granodioritic rock types with angular to sub-rounded grain shapes. Igneous rock fragments, are sub-rounded in shape (Figure 6.17B). Sedimentary rock fragments of sandstone, siltstone and shale constituting a larger percentage of the total lithic volume, are fine to medium-grained, and are sub-rounded in shape (Figures 6.16A, 6.16B and 6.17C).

6.3.2.4. Cement/Matrix

The framework grains are bounded by both cement and matrix. The most common cement is clay, quartz, iron oxide, quartz and feldspar overgrowth. Clay matrix (Figures 6.4 and 6.7, 6.9 and 6.10) is the most common matrix. Some rocks contain iron oxide cement (Figures 6.12 and 6.13).

Quartz overgrowths are best developed in rocks from both coalfields. Quartz cement in the form of quartz overgrowth is present in most of the samples. In thin sections quartz overgrowth can only be distinguished from the detrital grains by rims of quartz cements around detrital grains. Clay minerals include kaolinite, chlorite and illite, which were identified with the help of optical microscope, X-Ray Diffraction method (XRD) and Scanning Electron Microscopy (SEM). Kaolinite and illite (Figures 6.4 and 6.7) is the most

abundant clay mineral followed by chlorite, hematite, calcite and smectite present in comparatively low amount.

Minor accessory minerals, including mica, heavy minerals and organic matter, are present in all samples in minor or trace amounts. Both muscovite and biotite micas form a minor detrital grain component (Figure 6.10).

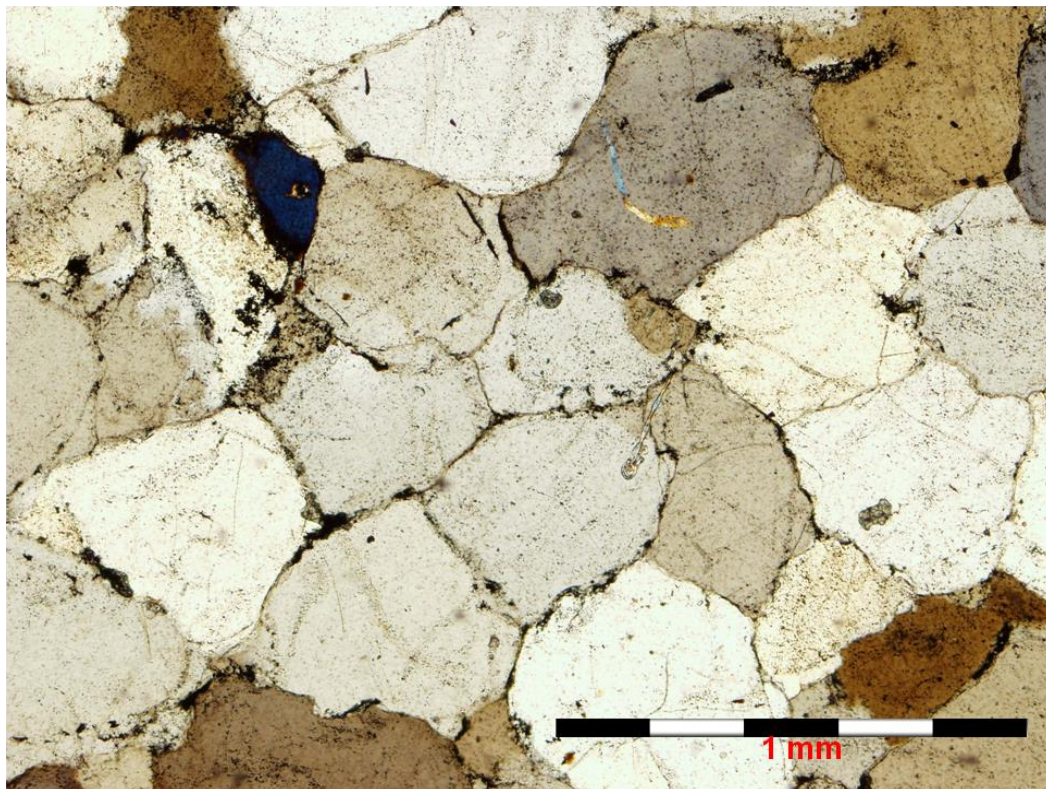


Figure 6.1: Photomicrographs of fine grained, well sorted and grain supported sandstone showing mosaic texture from Tshipise-Pafuri Coalfield. The whole scale bar is 1mm long and applies to all photographs in the thesis.

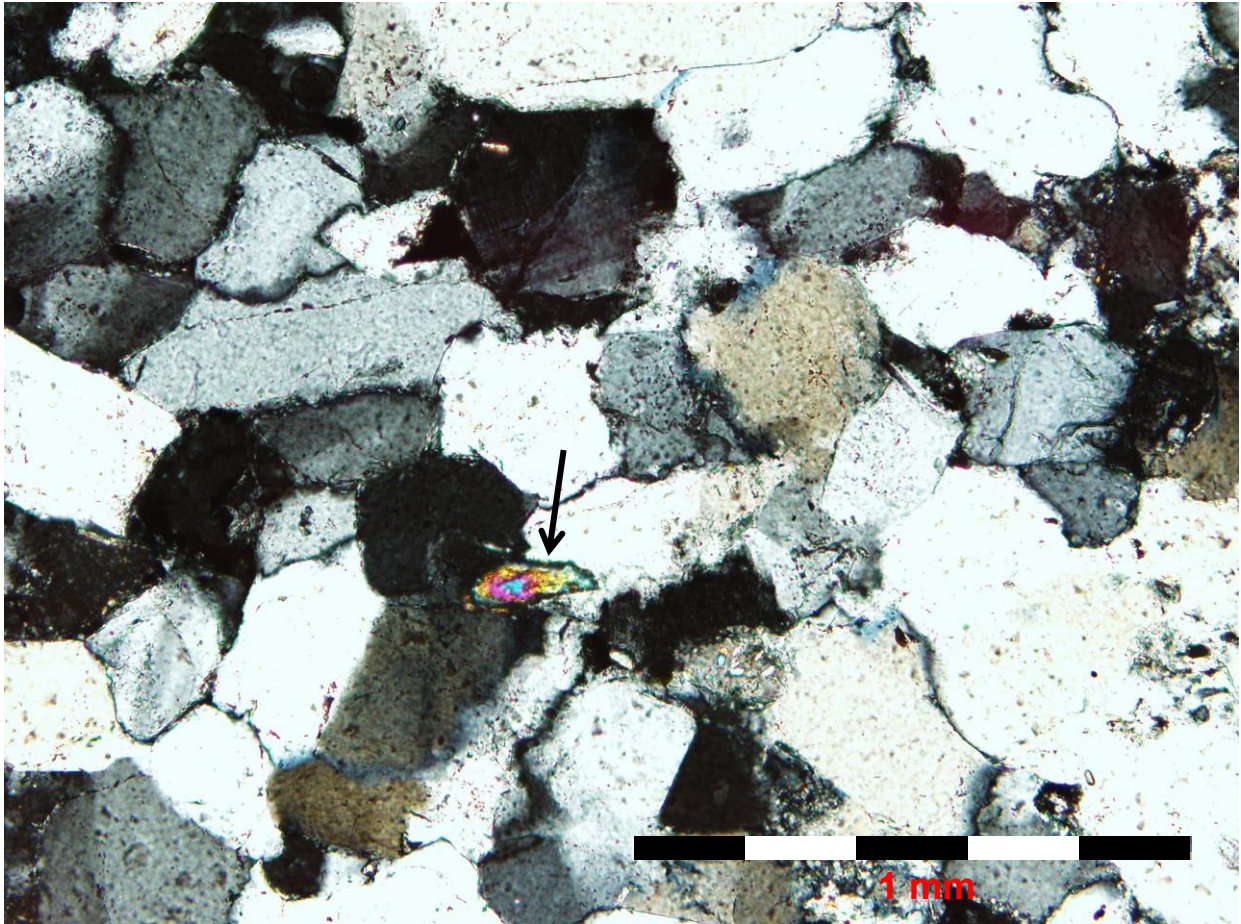


Figure 6.2: Photomicrographs of moderately sorted and grain supported sandstone from the Tuli Coalfield. The arrow shows muscovite inclusion.

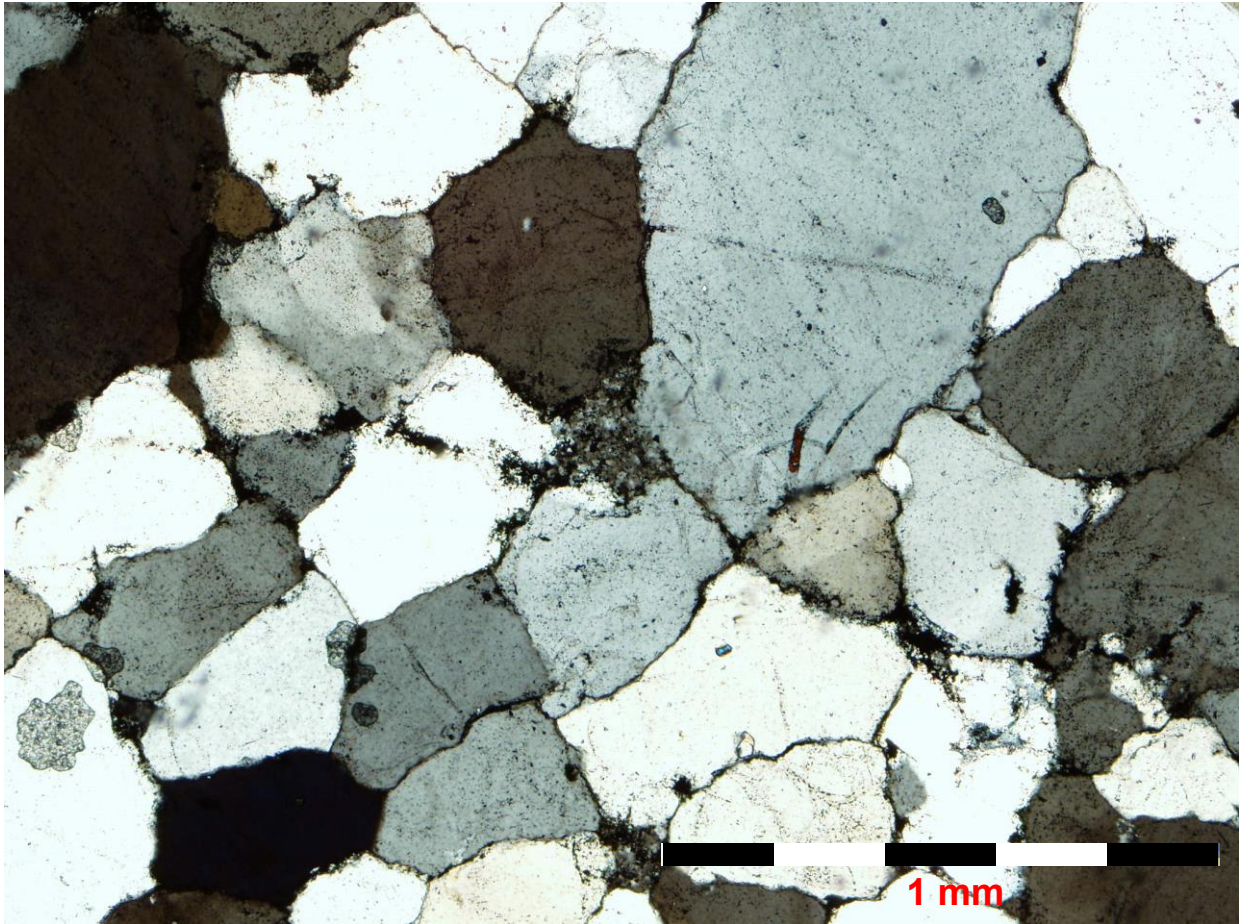


Figure 6.3: Photomicrographs showing moderately sorted and grain supported sandstone from Tshipise-Pafuri Coalfield.

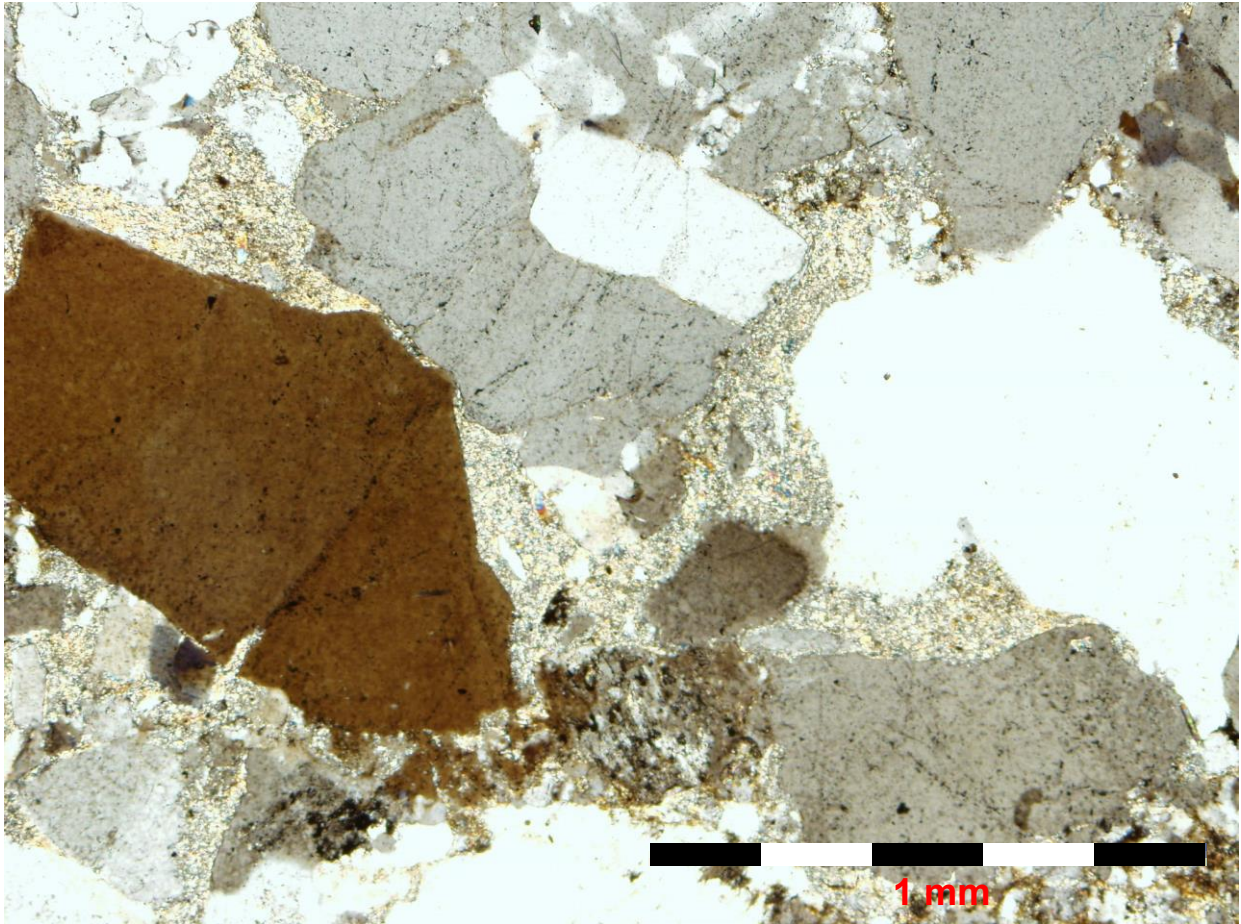


Figure 6.4: Photomicrographs of monocrystalline angular grains with clay matrix in the Tshipise-Pafuri Coalfield.

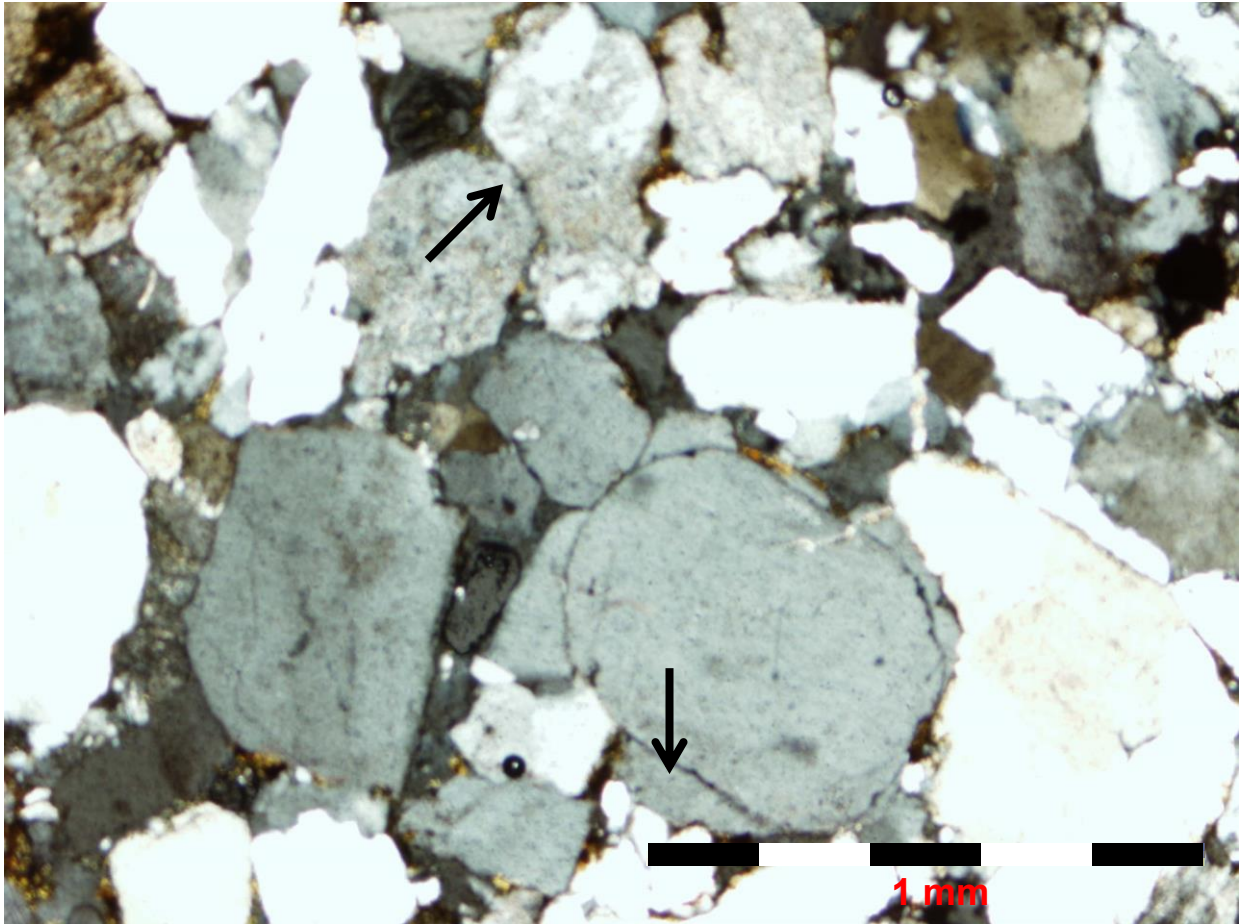


Figure 6.5: Photomicrographs of well-rounded and sub-angular quartz grains from the Tuli Coalfield. Arrow shows quartz overgrowths.

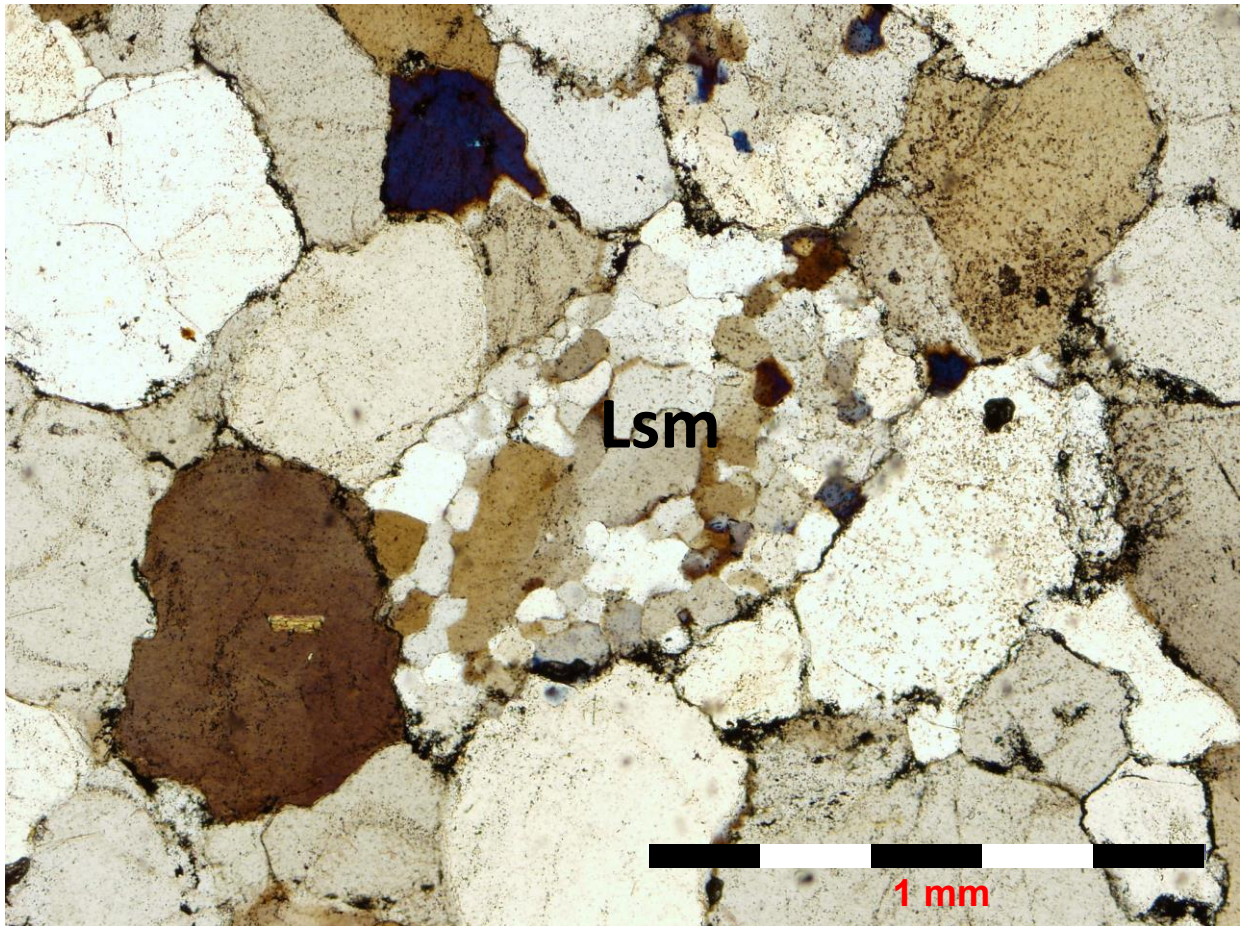


Figure 6.6: Photomicrographs of sub-rounded monocrystalline quartz grains and metasedimentary lithic fragment (Lsm) in the Tshipise-Pafuri Coalfield.

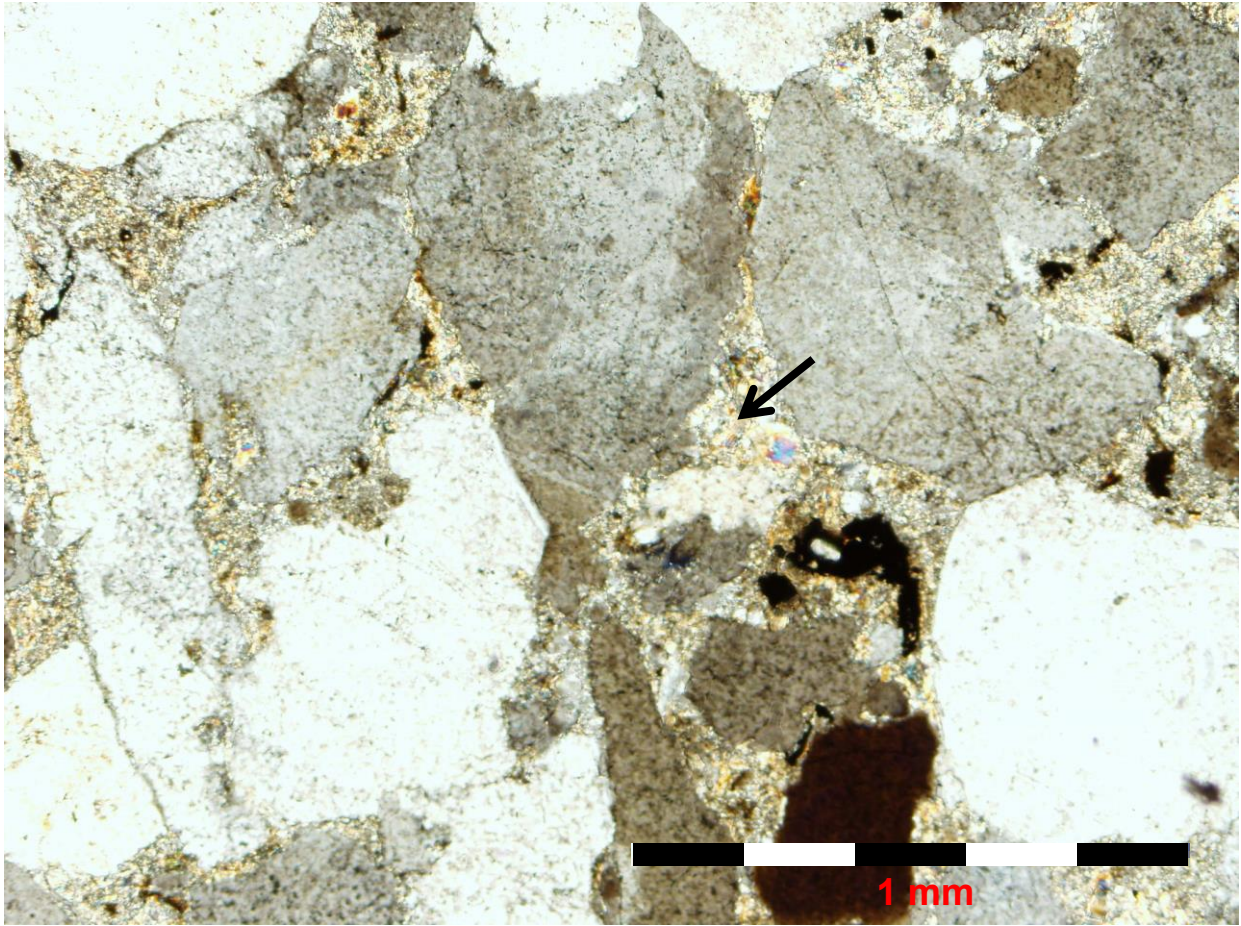


Figure 6.7: Photomicrographs of silica cementing (arrow) quartz and feldspar grains.

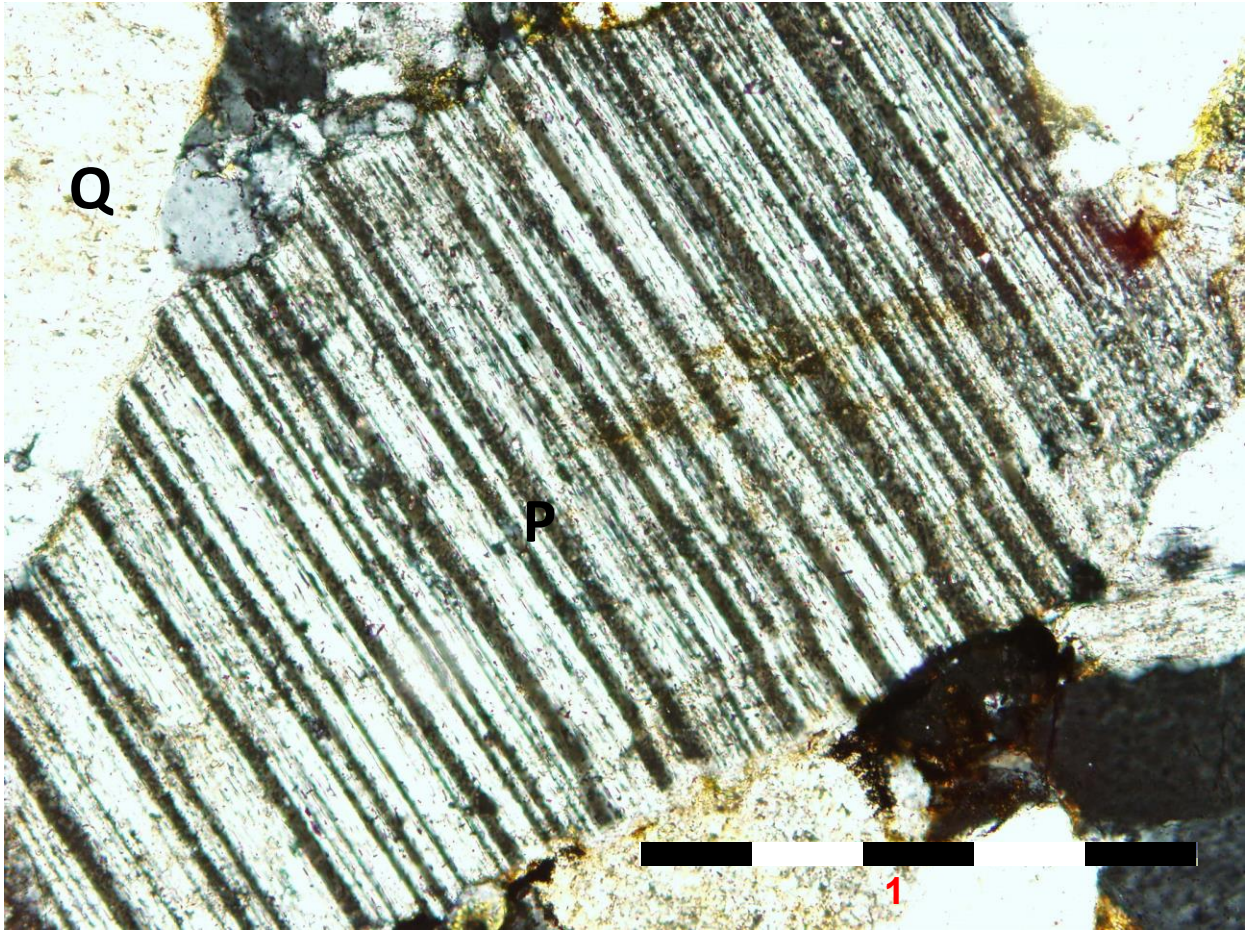


Figure 6.8: Photomicrographs of a plagioclase feldspar (P) showing albite type twinning Mopane Coalfield.

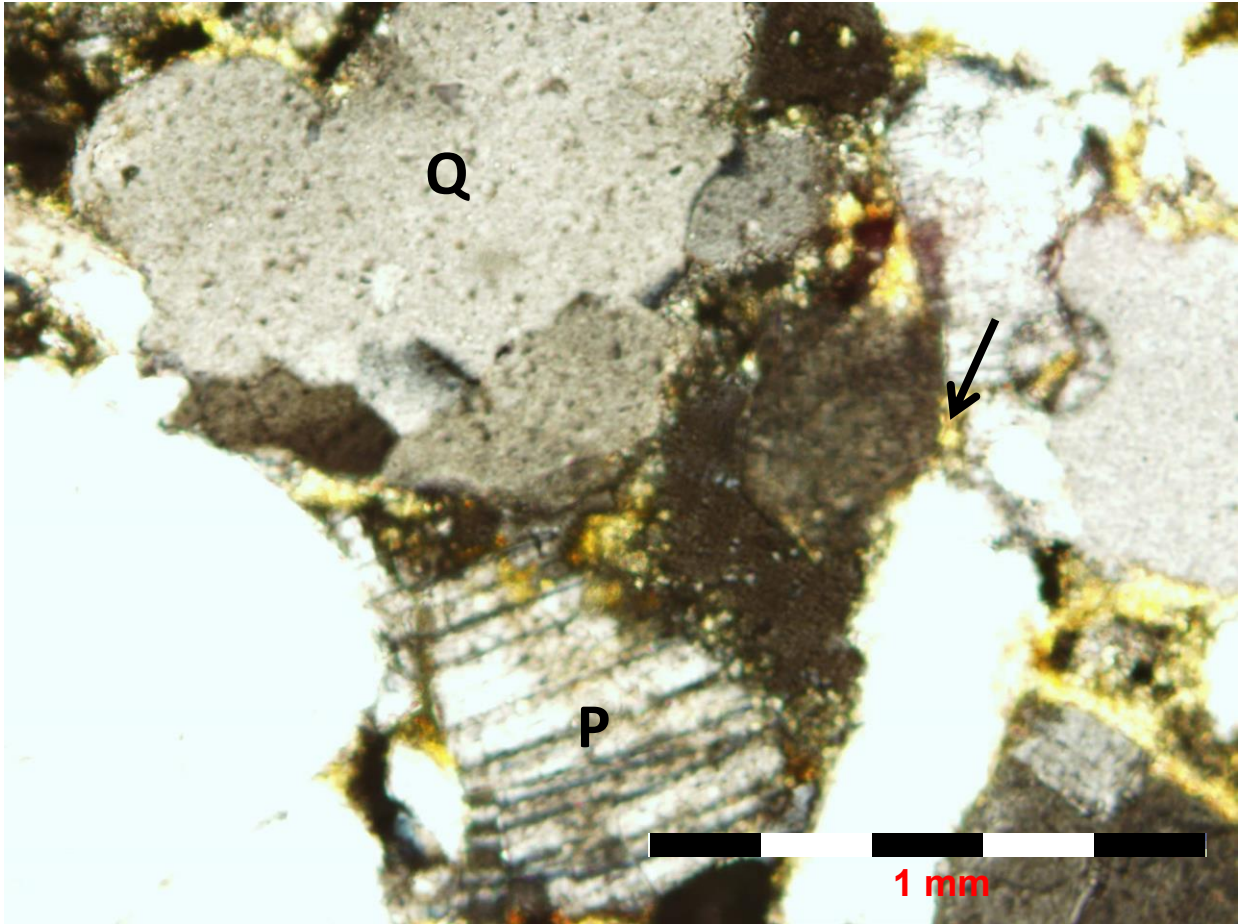


Figure 6.9: Photomicrographs of Clay (smectite) cement (arrows) around feldspar (P) and quartz (Q) grains in the Tshipise-Pafuri Coalfield.

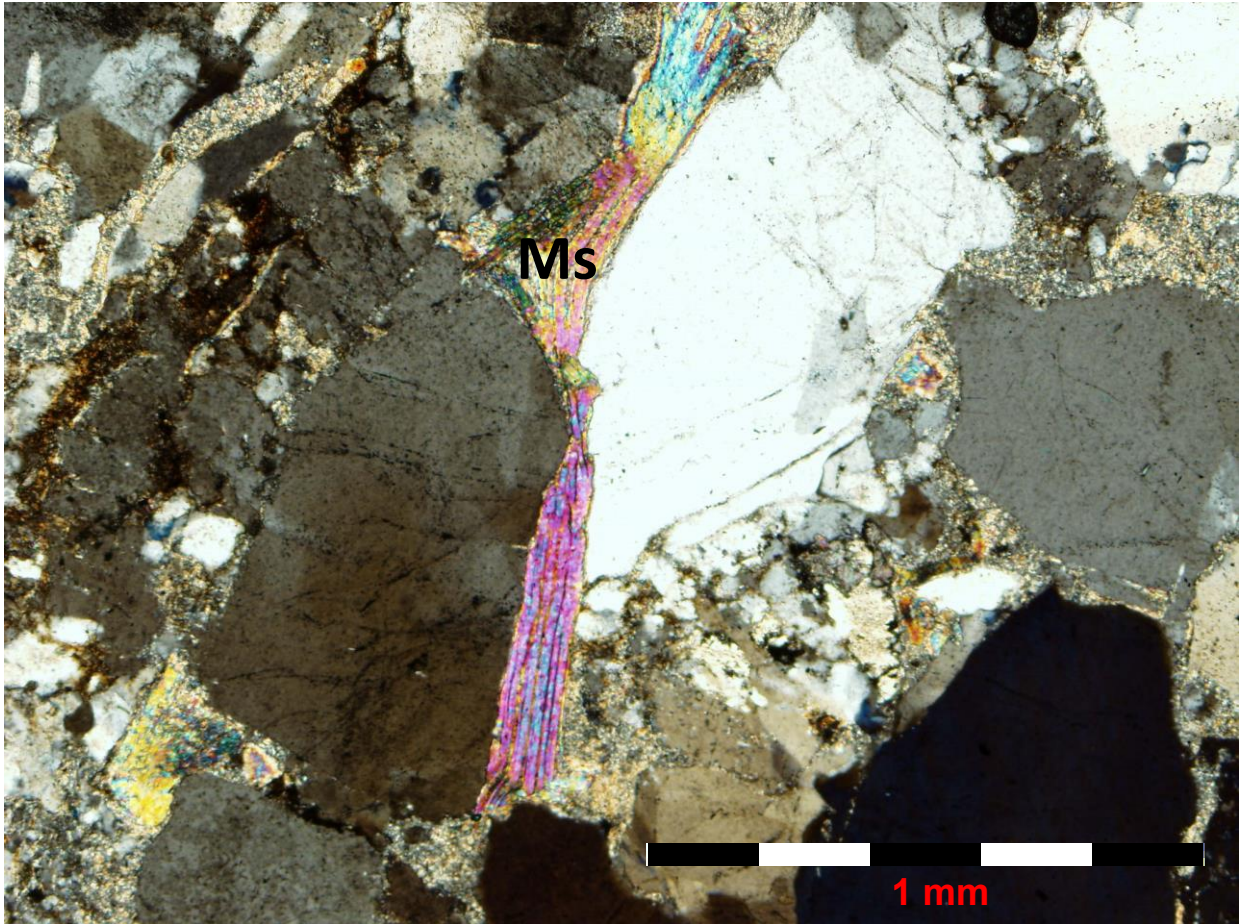


Figure 6.10: Photomicrographs of detrital muscovite compacted between quartz grains in the Tshipise-Pafuri Coalfield.

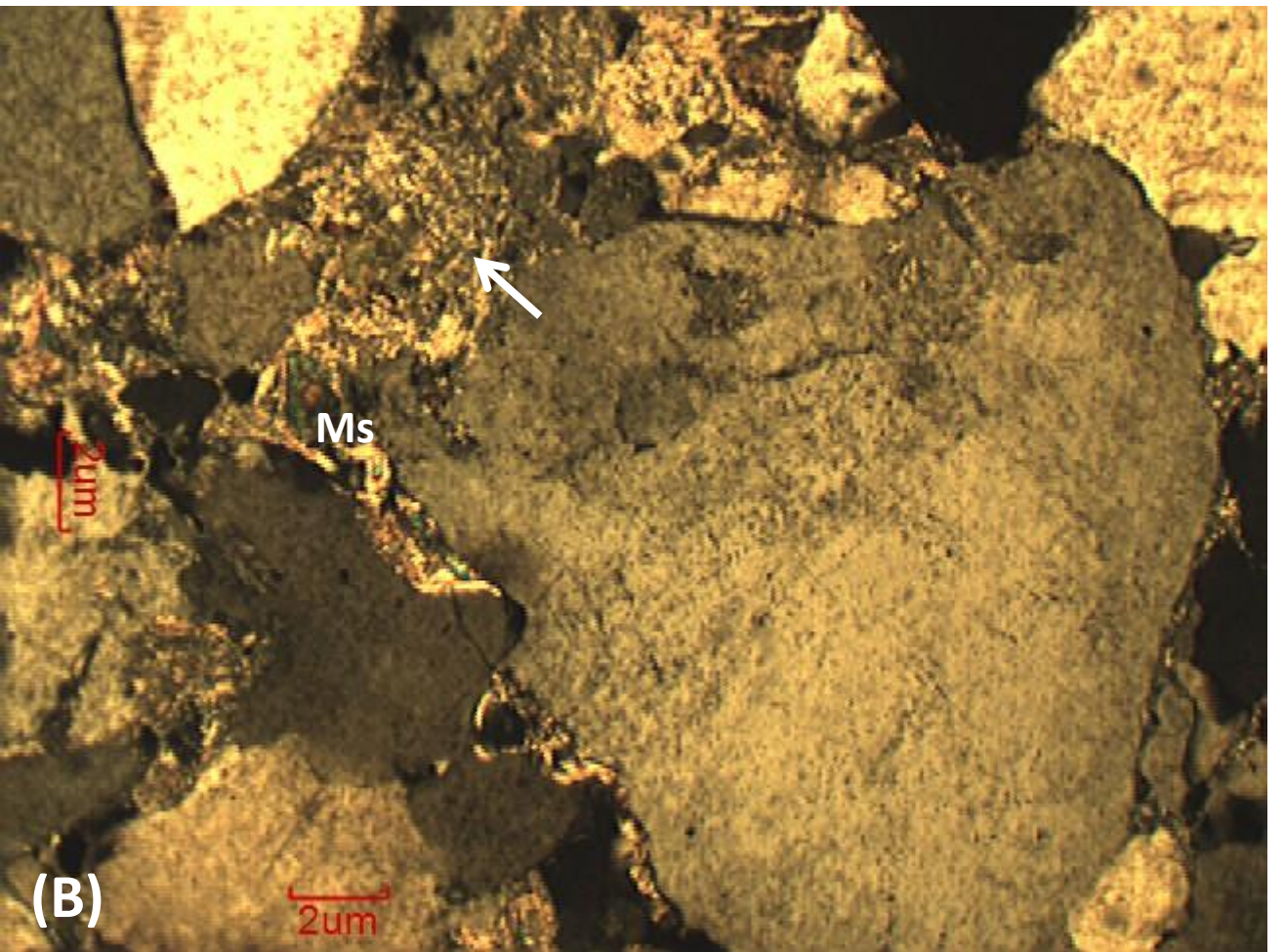
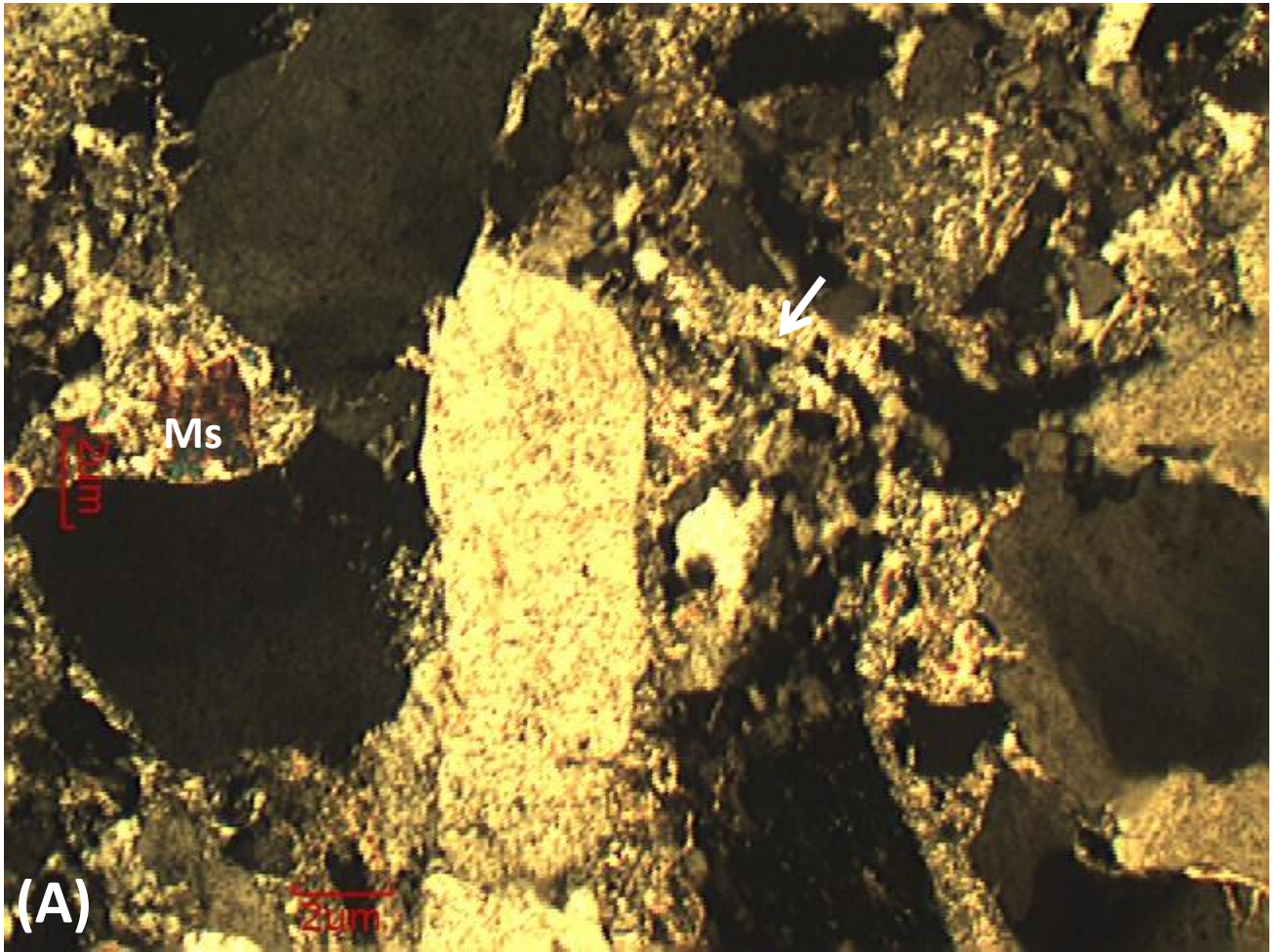


Figure 6.11: (A) Recrystallisation of clay matrix (smectite to illite and sericite shown by arrows between detrital grains; also showing sericite around detrital muscovite (Ms) at far left of the photo from the Tshipise-Pafuri Coalfield; (B) Recrystallisation of clay matrix to sericite shown by arrow around detrital grains. Ms indicates muscovite. Sample comes from the the Tuli Coalfield.

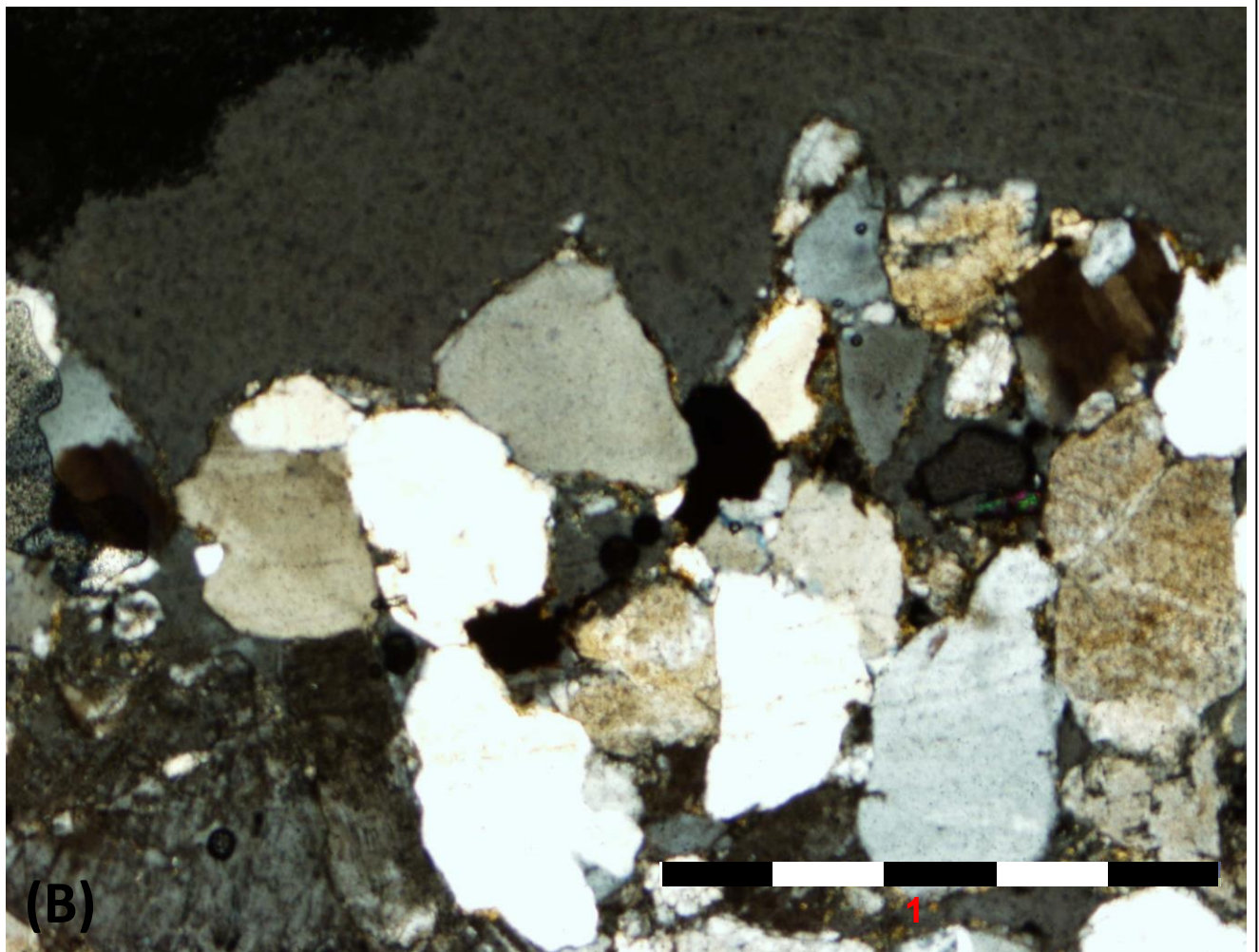
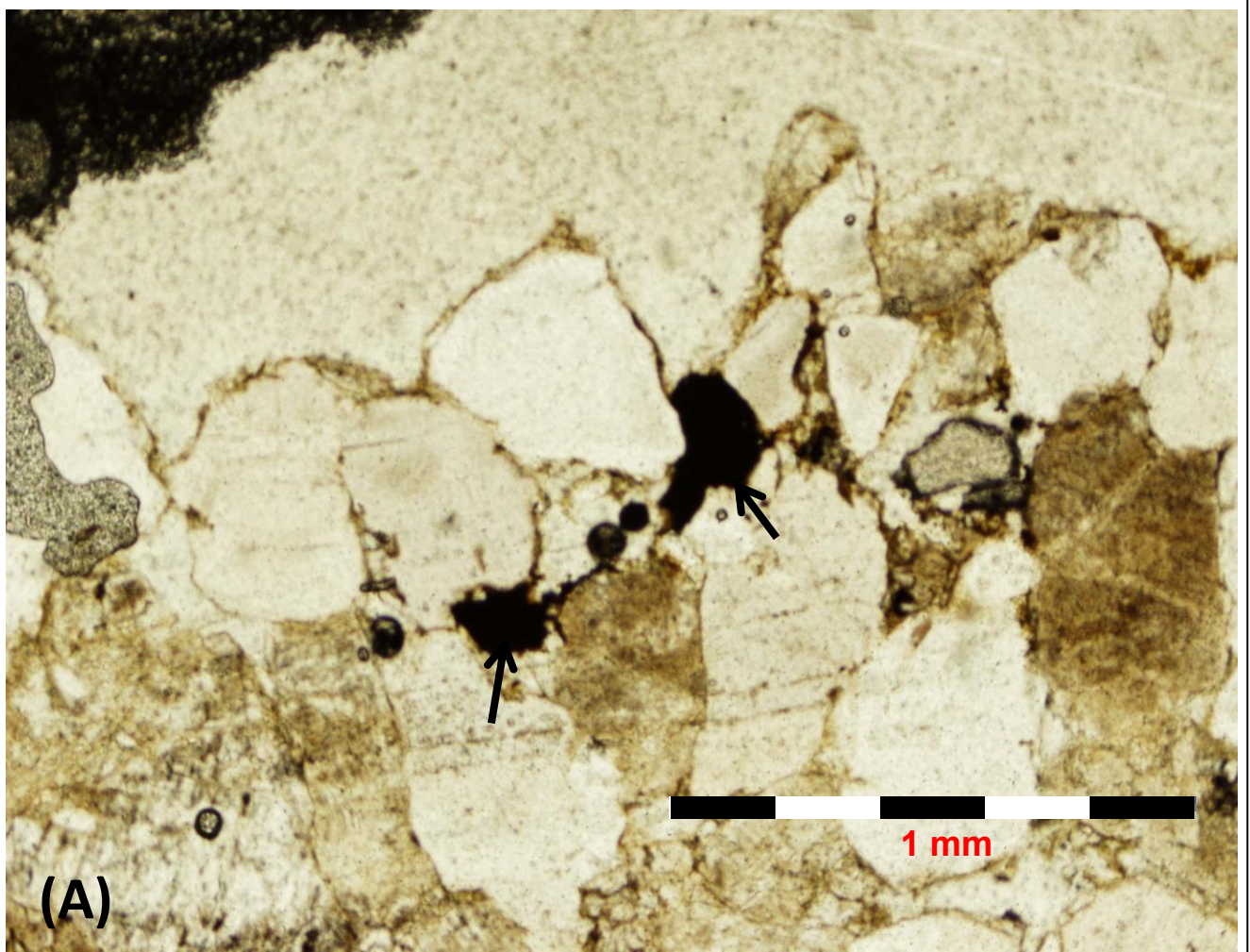


Figure 6.12: (A) Photomicrographs of hematite cement (arrows) around detrital grains (plane polarized) in the Mopane Coalfield; (B) Cross polarized image of A.

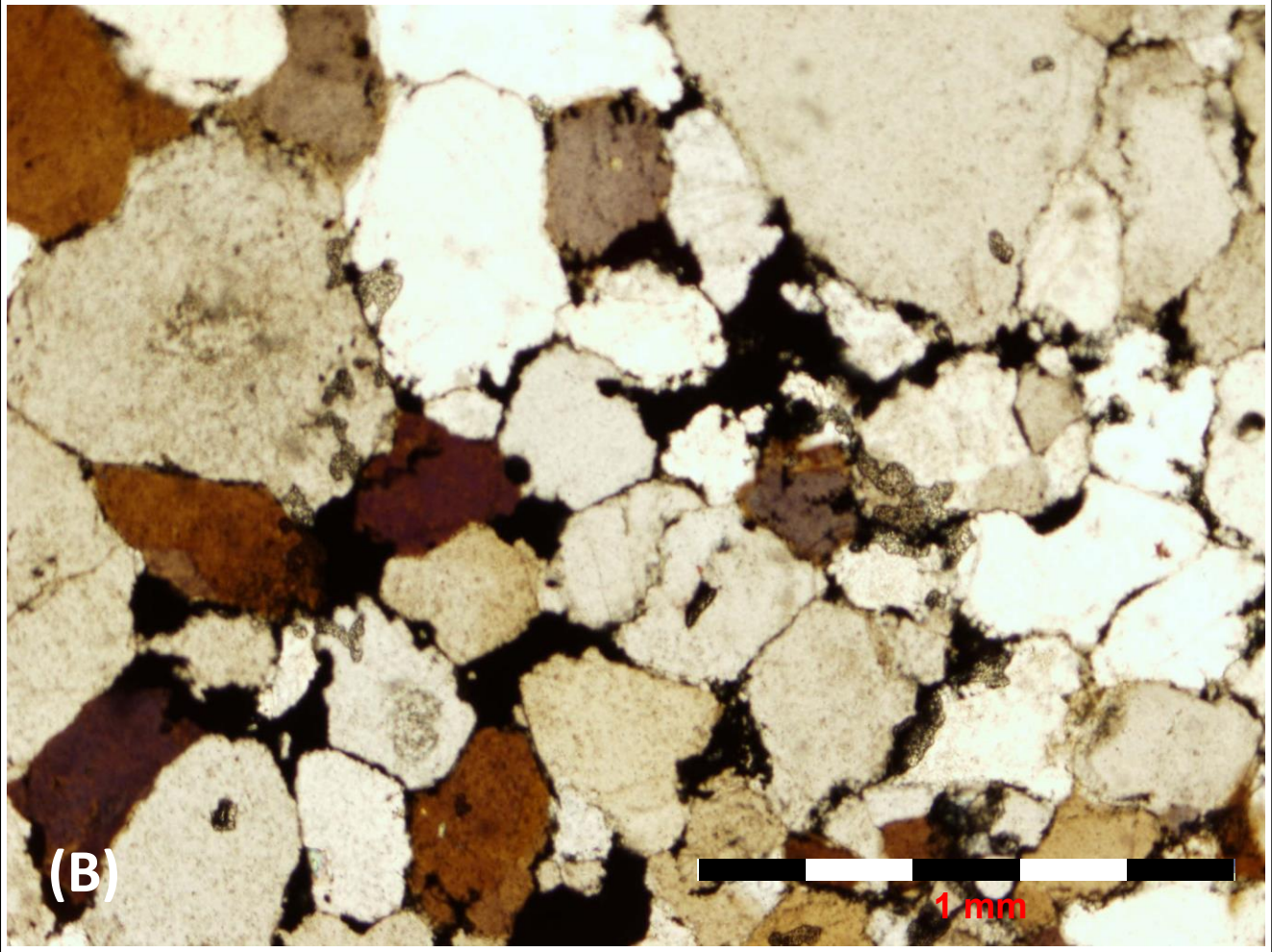
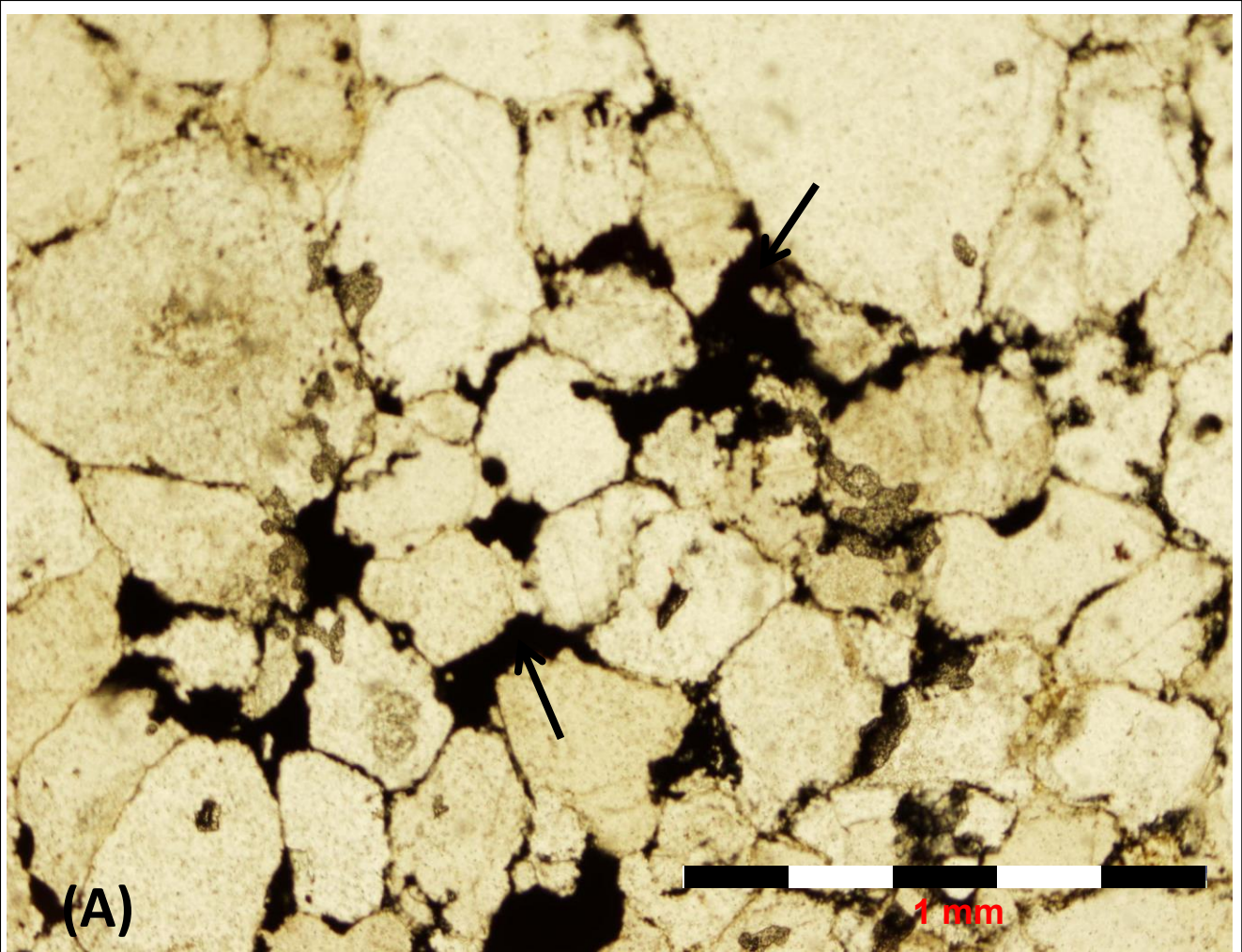


Figure 6.13: (A) Photomicrographs of hematite cement (arrows) around detrital grains (plane polarized) in the Tshipise-Pafuri Coalfield; (B) Cross polarized image of A.

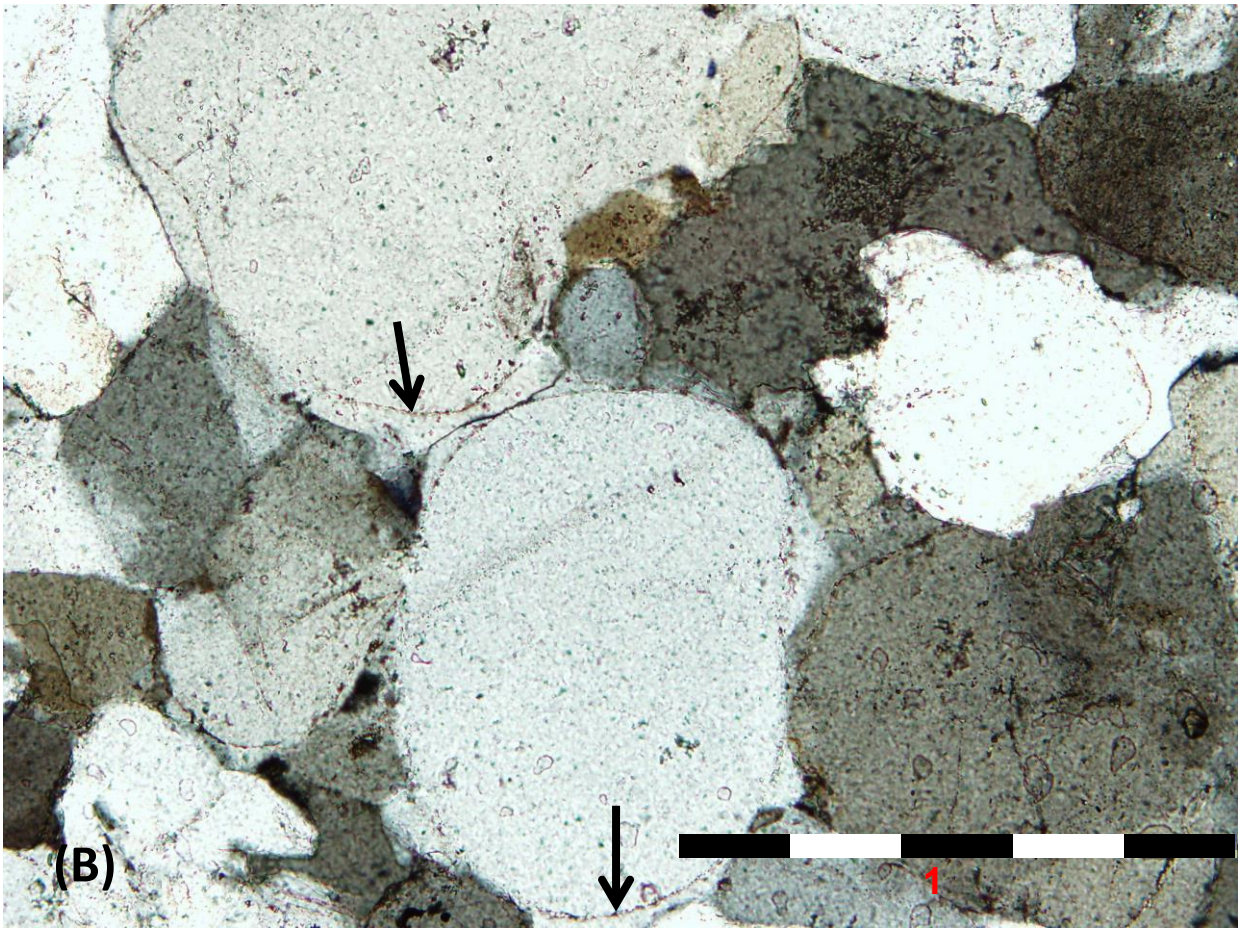
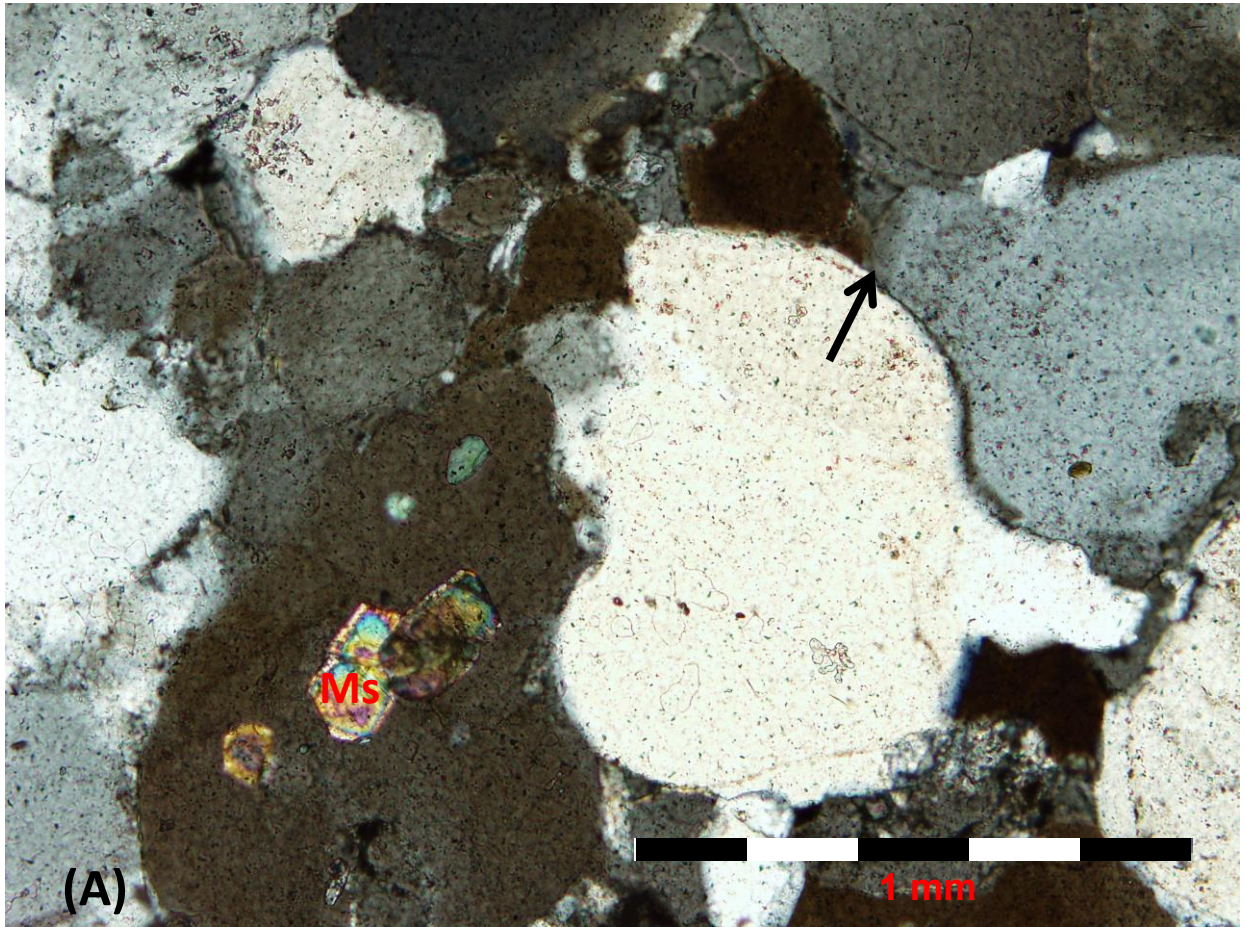


Figure 6.14: Photomicrographs of (A) Inclusions of muscovite flakes (arrows) in a monocrystalline quartz grain and quartz overgrowth (arrow) in another grain. (B) Rounded to well-rounded quartz grains and quartz overgrowths (arrow) in the Tshipise-Pafuri Coalfield.

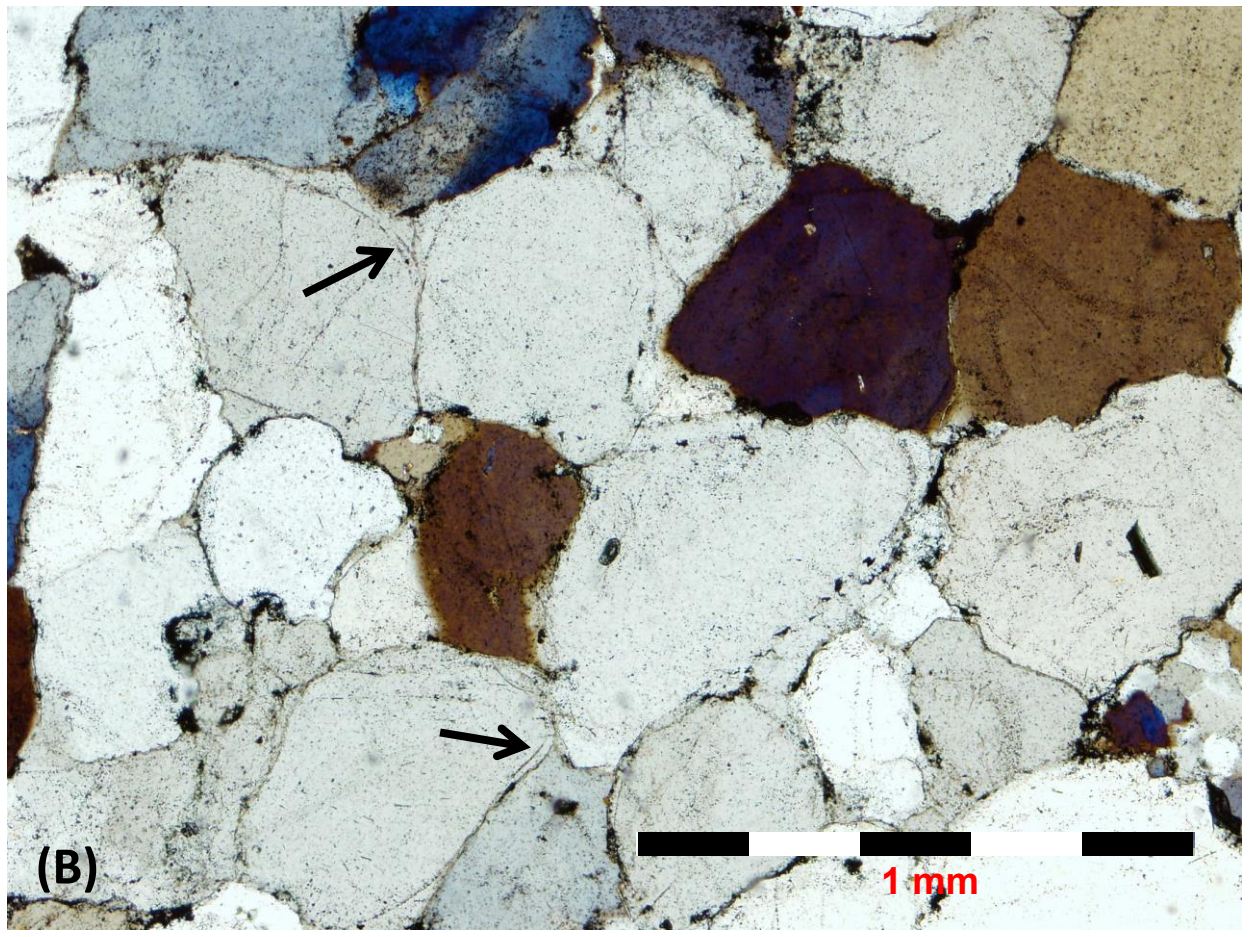
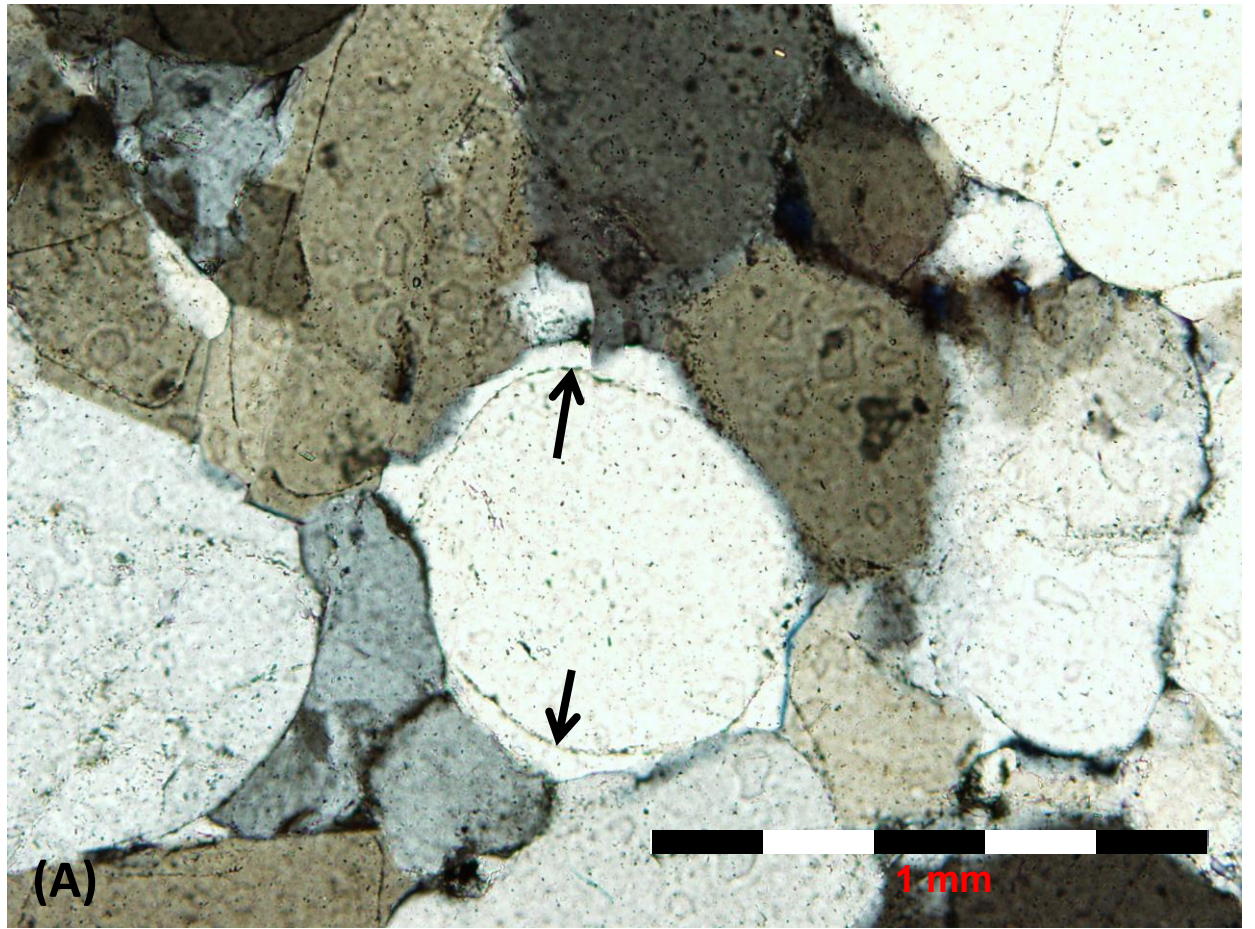


Figure 6.15: A and B: Photomicrographs of well rounded monocrystalline quartz grains with overgrowths (arrows) in the Tuli Coalfield.

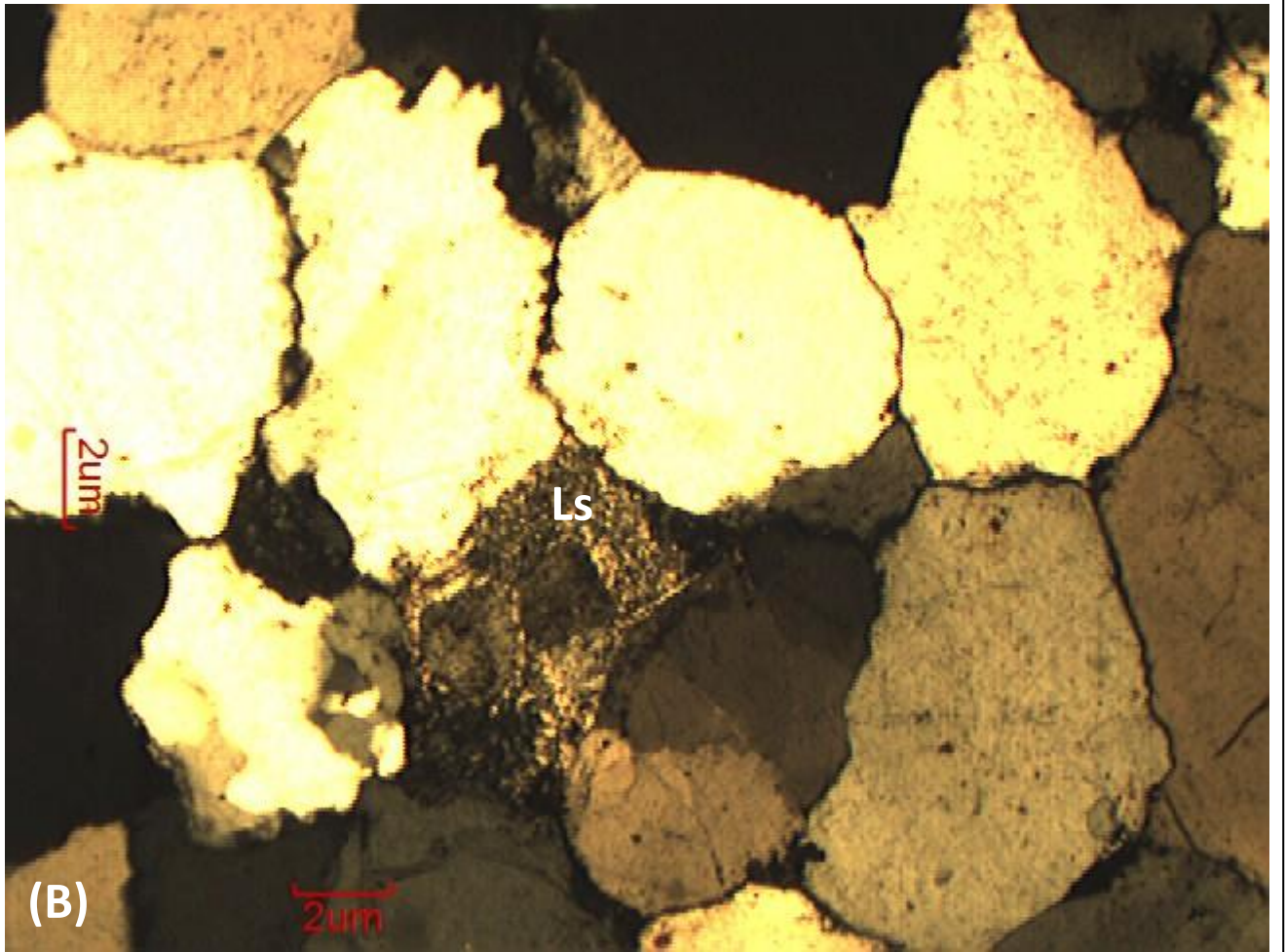
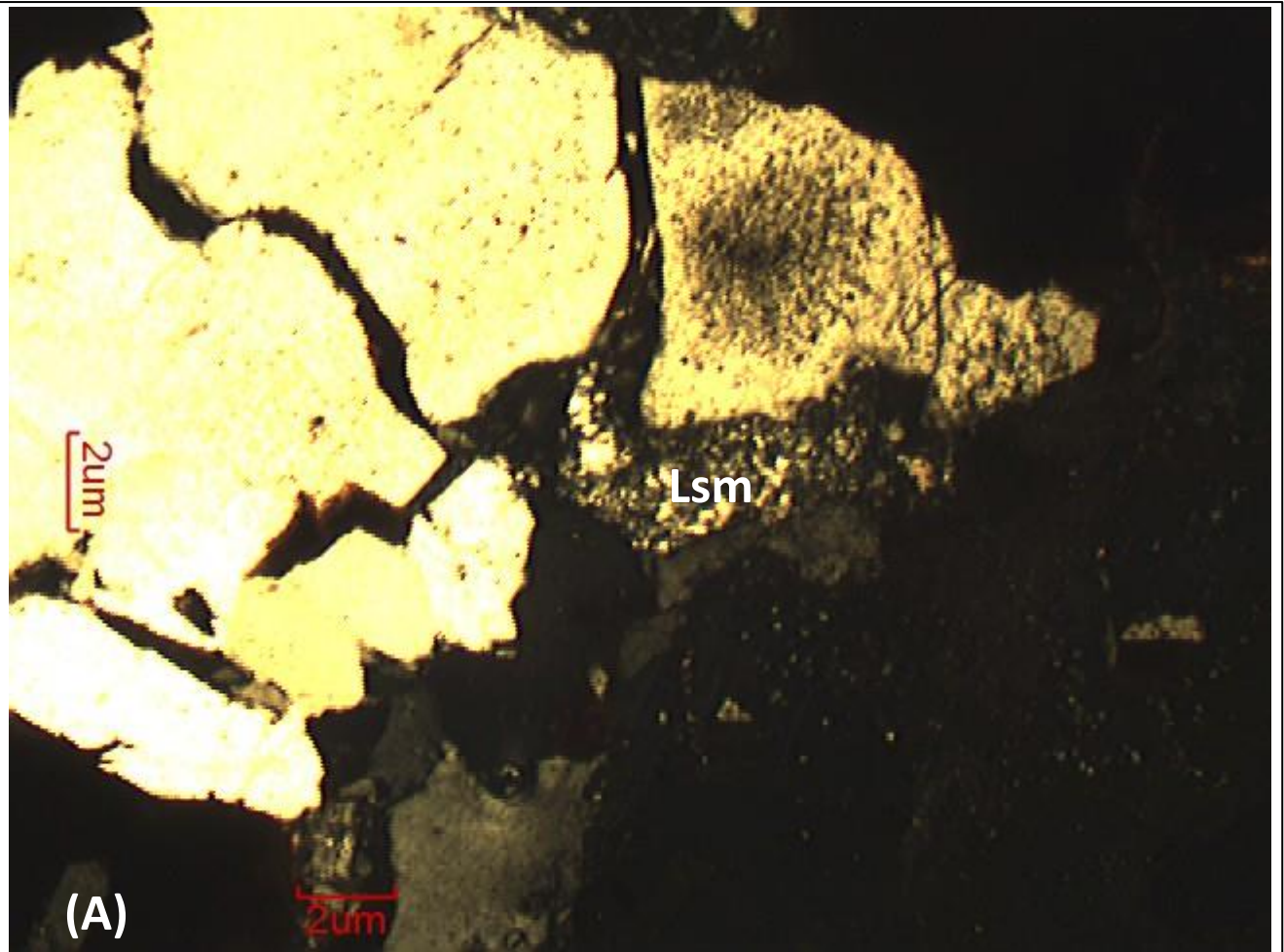


Figure 6.16: Photomicrographs of lithic fragments from the Soutpansberg Coalfield. (A) Metasedimentary lithic fragment (Lsm) from the Mopane Coalfield. (B) Sedimentary lithic fragments (Ls) in the Tshipise-Pafuri Coalfield.

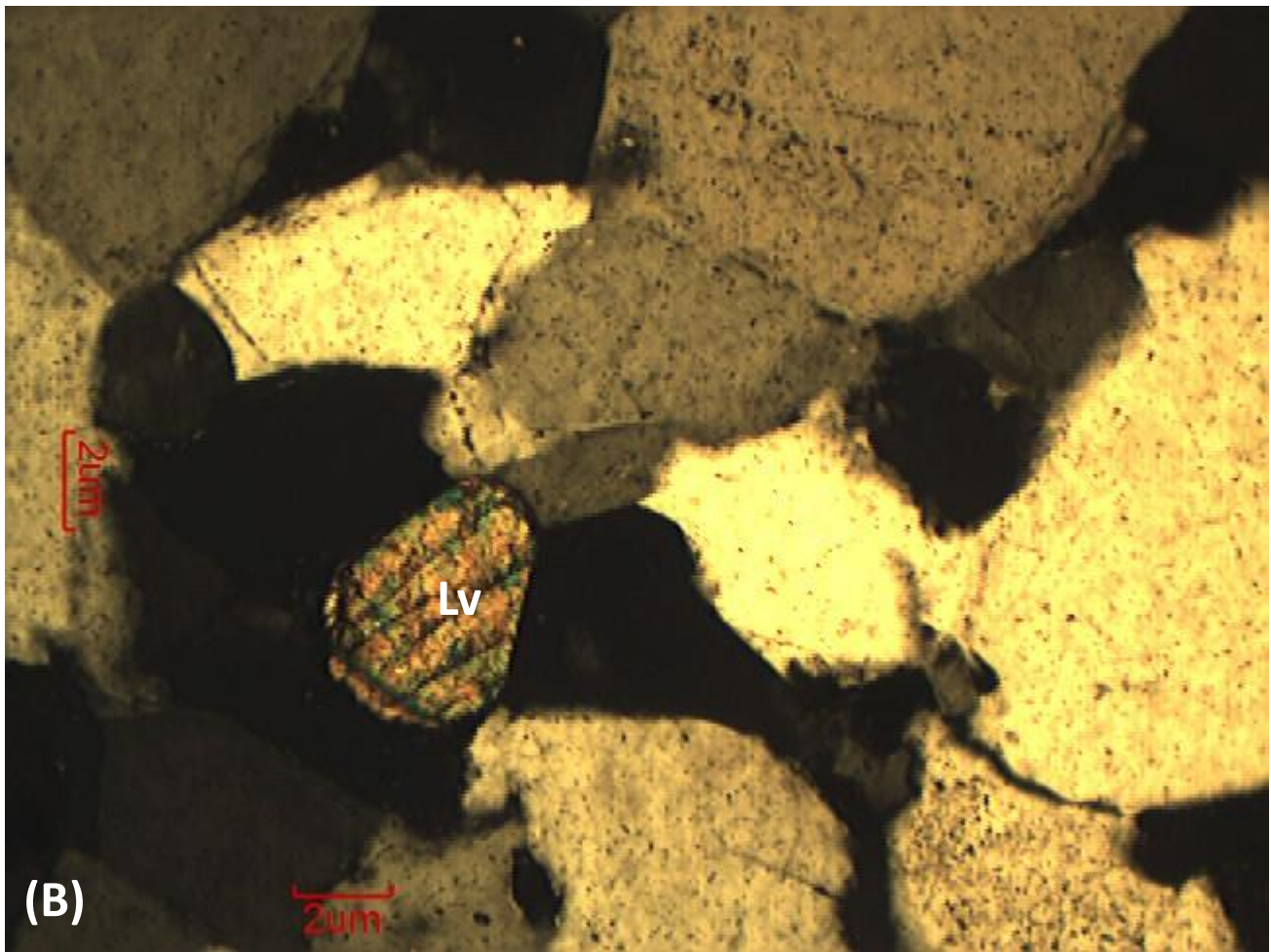
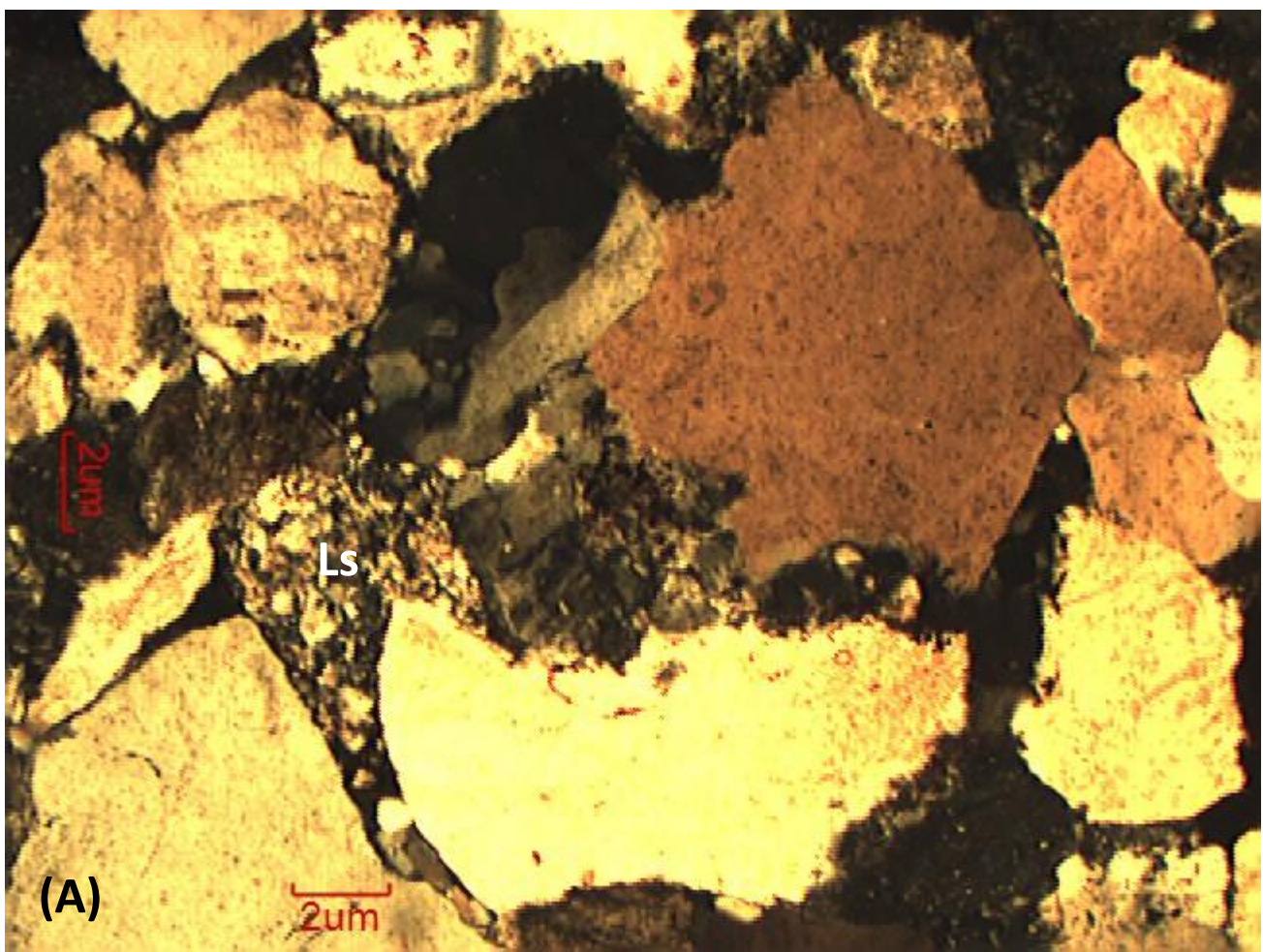


Figure 6.17: Photomicrographs of lithic fragments from the Tuli Coalfield. (A) Sedimentary lithic fragments (Ls). (B) Igneous lithic fragments (Lv) and quartz overgrowth (upper left).

6.4. Tectonic setting

The provenance of detrital sandstone compositions can be classified into different types, such as stable cratons, basement uplifts, magmatic arcs and recycled orogens. To interpret the tectonic discrimination source fields, the Tuli and Soutpansberg sandstones were plotted on Qt-F-L and Qm-F-Lt ternary diagrams of Dickinson *et al.* (1983). In the Qt-F-L plot both the Tuli and Soutpansberg sandstones fall in the recycled orogeny provenance. In the Qm-F-Lt plot, both the Tuli and Soutpansberg sandstone represents recycled to craton interior provenance (Figures 6.19A and B). The interpretation of the sandstone composition from the petrography of the Tuli and Soutpansberg Coalfields based on the schemes proposed by Pettijohn (1975) and Folk (1980) suggest a sub-arkose to sub-litharenite composition (Figures 6.18A and B).

Figures 6.19A and B shows that the sandstones are mature and derived from relatively low lying granitoid and gneissose sources, supplemented by recycled sands from associated platforms or passive margin basins. The Tuli and Soutpansberg sandstones are derived from craton interior, quartz recycled to transitional continental setting. The low percentage of unstable grains (feldspar and other rock fragments), dominance of monocrystalline quartz, and alteration of feldspar grains, indicate that these sandstones were transported from far along the rift. The weight percentages of major elements were used to discriminate the tectonic setting of sandstones. The discriminate function diagrams were used to understand the provenance for the Tuli and Soutpansberg sandstones. The discriminate function diagram of Roser and Korsch (1988) suggests that both the Soutpansberg and Tuli sandstones may be derived from quartzose sedimentary provenance (Figures 6.23 and 6.24). Tectonic discrimination diagrams of Roser and Korsch (1986) suggests that both Tuli and Soutpansberg sandstone falls into the field of passive continental margin and active continental margin (Figures 6.25 and 6.26). Recycled orogens contains sedimentary strata and subordinate igneous rocks and their metamorphic derivations which are exposed to erosion by orogenic uplift of fold belts and thrust sheets.

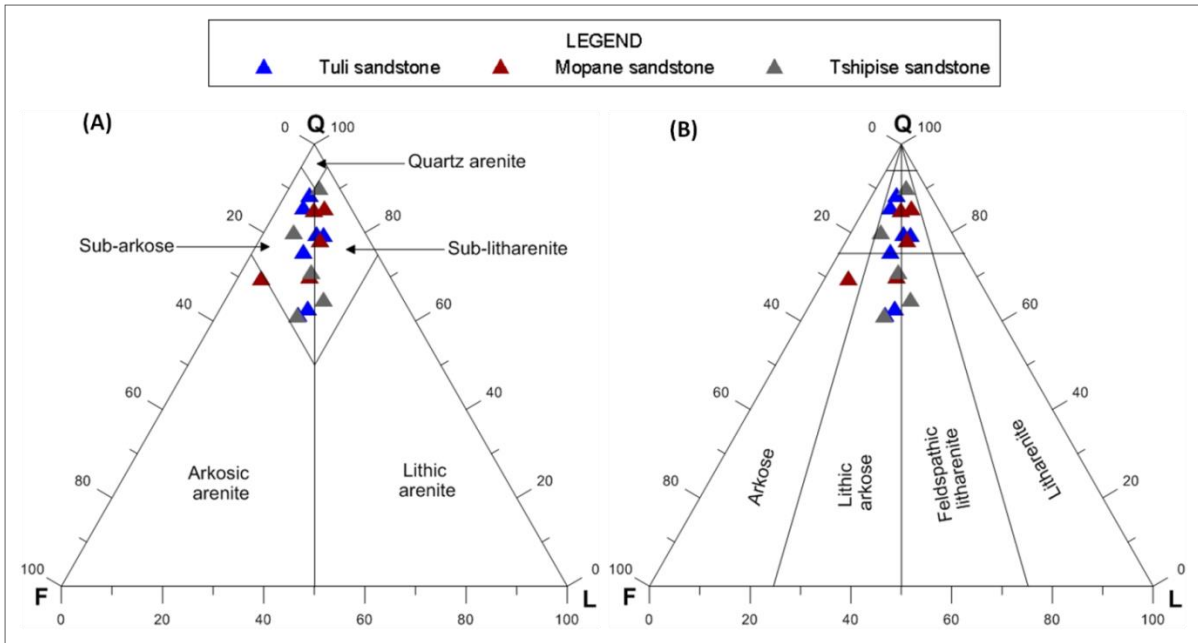


Figure 6.18: Interpretation of the sandstone composition from the petrography of the Tuli and Soutpansberg Coalfields based on the schemes proposed by (A) Pettijohn (1975) and (B) Folk (1980). Standard plots: Quartz, Feldspar, Lithic grains (Q, F, L), (A) sub-arkose to sub-litharenite, (B) arkose to litharenite.

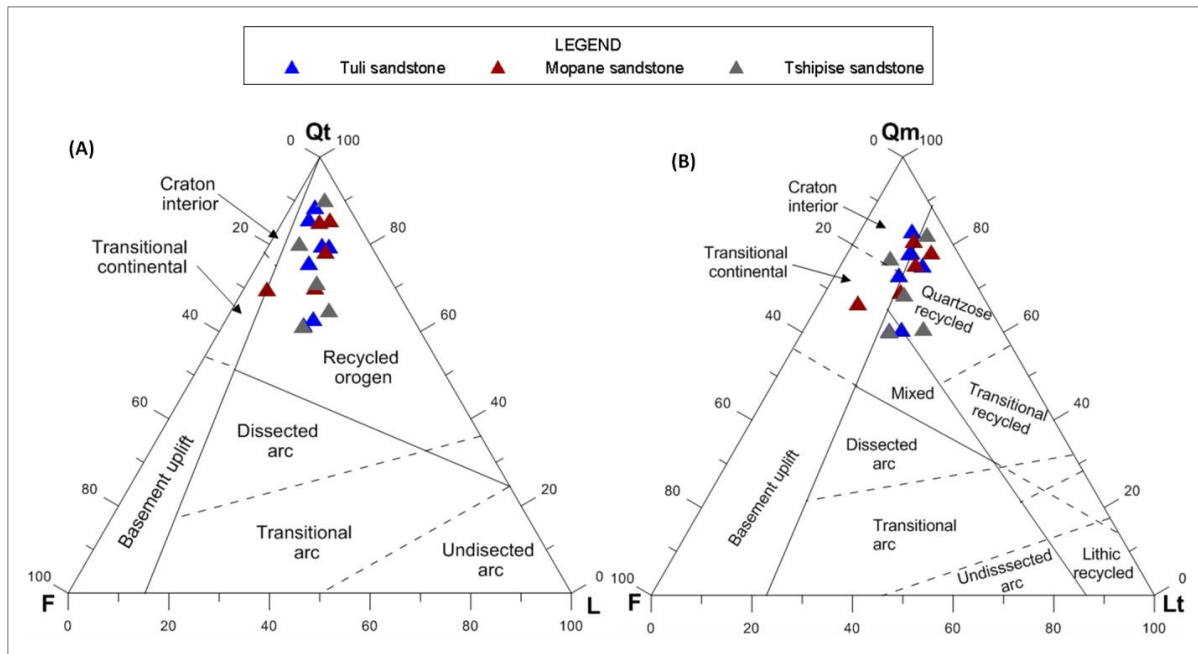


Figure 6.19: Interpretation of provenance from the petrography of the Tuli and Soutpansberg Coalfields sandstones (after Dickinson *et al.*, 1983). (A) Total quartz, feldspar, lithic fragments (Q, F, L). (B) Monocrystalline quartz, feldspar, total lithic grains (Qm, F, Lt).

The detrital modal compositions of both the Tuli and Soutpansberg sandstones are plotted in the Q-F-L diagram (Figure 6.20), which indicates that these sandstones are related to trailing-edge margin (TE), also called passive margin. The K_2O/Na_2O versus SiO_2 tectonic setting discrimination diagram (Figures 6.25 and 6.26) and ternary $Na_2O-CaO-K_2O$ plot (Figures 6.27 and 6.28) shows that most of the sandstone samples fall in the passive margin field as like the Q-F-L tectonic provenance diagram in Figure 6.20 below.

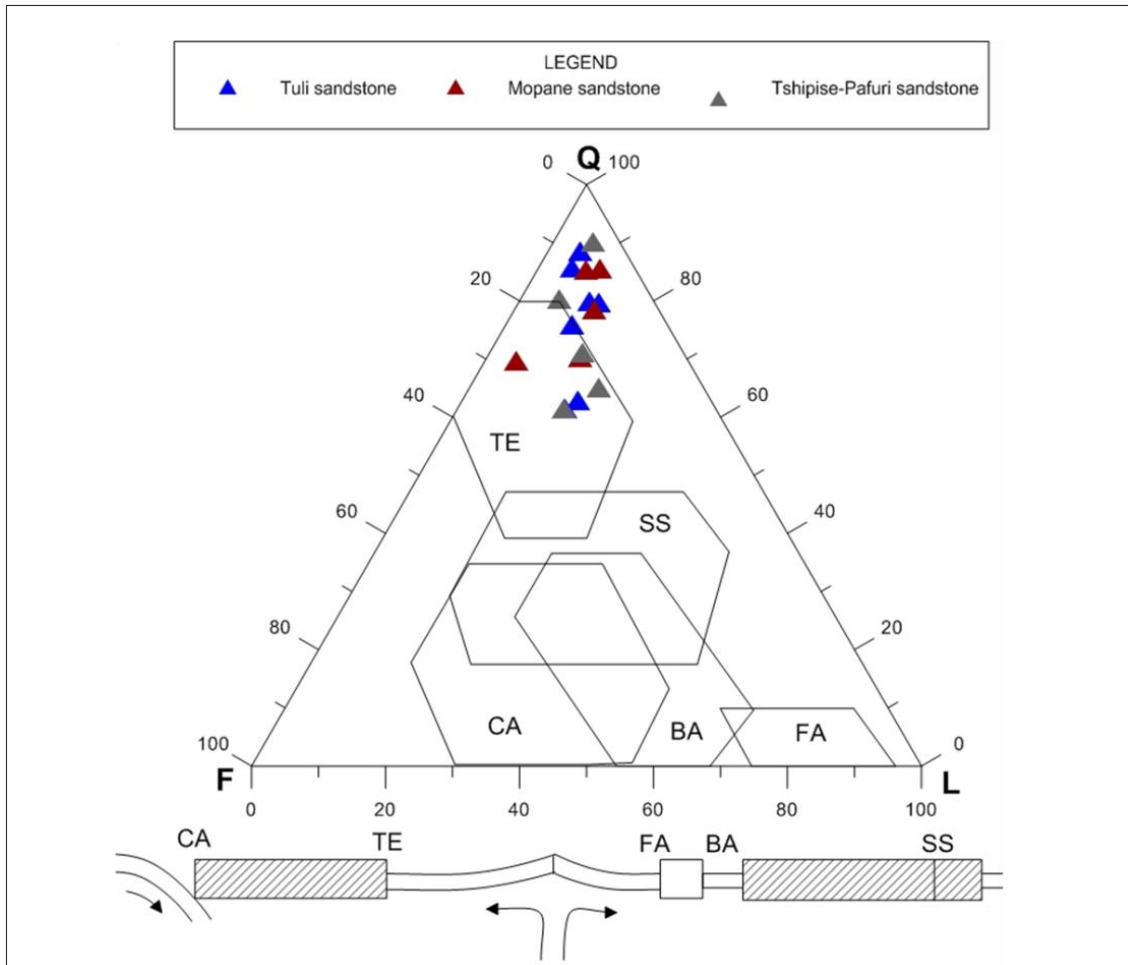


Figure 6.20: Q-F-L tectonic provenance diagram for the Tuli and Soutpansberg sandstones, after Yerino and Maynard (1984). The sandstones plot inside and near the TE field. TE: trailing edge (also called passive margin); SS: strike-slip; CA: continental-margin arc; BA: backarc to island arc; FA: forearc to island arc.

In summary, the petrographic attributes of the sedimentary cycles in the Tuli and Soutpansberg Coalfields suggest that sedimentation in the Carboniferous and Permian successions was influenced by tectonic uplift in the basement of the Kaapvaal Craton and the Limpopo Mobile Belt mainly from granitic sources within a continental tectonic setting.

6.5. Geochemistry

6.5.1. Major elements

The Major element distributions reflect the mineralogy of the studied samples. Sandstones are higher in SiO₂ content than shales (Figures 6.21 and 6.22). Similarly, shales are higher in K₂O, Fe₂O₃ and TiO₂ contents than sandstones, which reflect their association with clay-sized phases (Madhavaraju and Lee, 2010). Al₂O₃ abundances were used as a normalization factor to make comparisons among the different lithologies, because of its immobile nature during weathering, diagenesis, and metamorphism. In Figures 6.21 and 6.22, major oxides of sandstone and shale are plotted against Al₂O₃. Average UCC (Upper Continental Crust) and PAAS (Post-Archaean Australian Shale) values are also included for comparison purposes. In sandstone samples (Figure 6.21) major elements, Fe₂O₃, MgO, K₂O, CaO and P₂O₅ are consequently showing strong positive correlations with Al₂O₃, whereas, TiO₂, Na₂O and MnO exhibits a weak positive correlation (Figure 6.21). In shale samples major elements, TiO₂ shows positive correlations with Al₂O₃. The strong positive correlations of the major oxides with Al₂O₃ indicate that they are associated with micaceous/clay minerals.

Relative to UCC the concentrations of most major elements in the sandstones were generally similar, except for Na₂O, which consistently yields much lower average relative concentration values. The depletion of Na₂O (<1%) in sandstones can be attributed to a relatively smaller amount of Na-rich plagioclase in them, which is consistent with the petrographic results. K₂O and Na₂O contents and their ratios (K₂O/Na₂O > 1) are also consistent with the petrographic observations, according to which K-feldspar dominates over plagioclase (albite) feldspar.

In comparison with UCC, the shales are low in MgO, CaO, Na₂O, MnO and high in Al₂O₃. Al is easily absorbed by clays and concentrates in the finer, more weathered materials. In addition, XRD analysis of the shales reveals that they are dominated with the mineral kaolinite (Al₂Si₂O₅(OH)₄) (Table C3). On average, the shales have lower SiO₂ abundances relative to UCC.

LEGEND

- Tuli Coalfield
- Mopane Coalfield
- Tshipise-Pafuri Coalfield

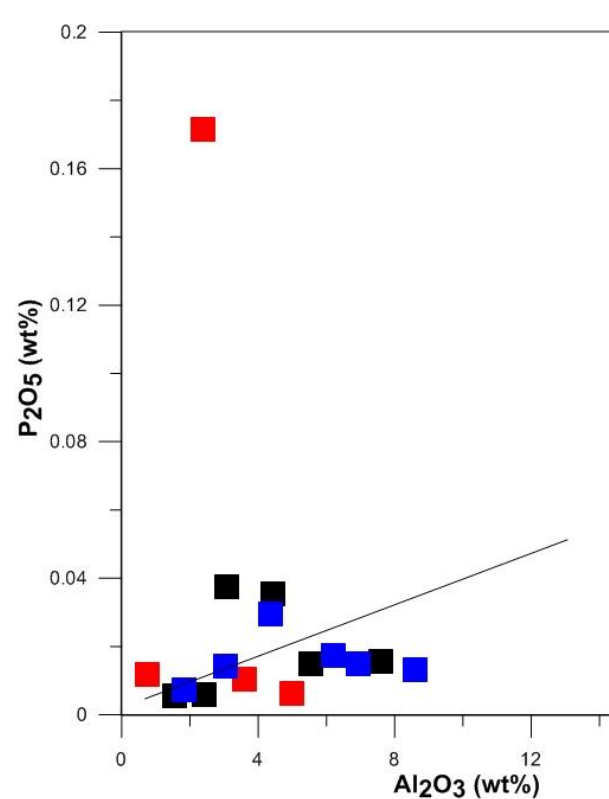
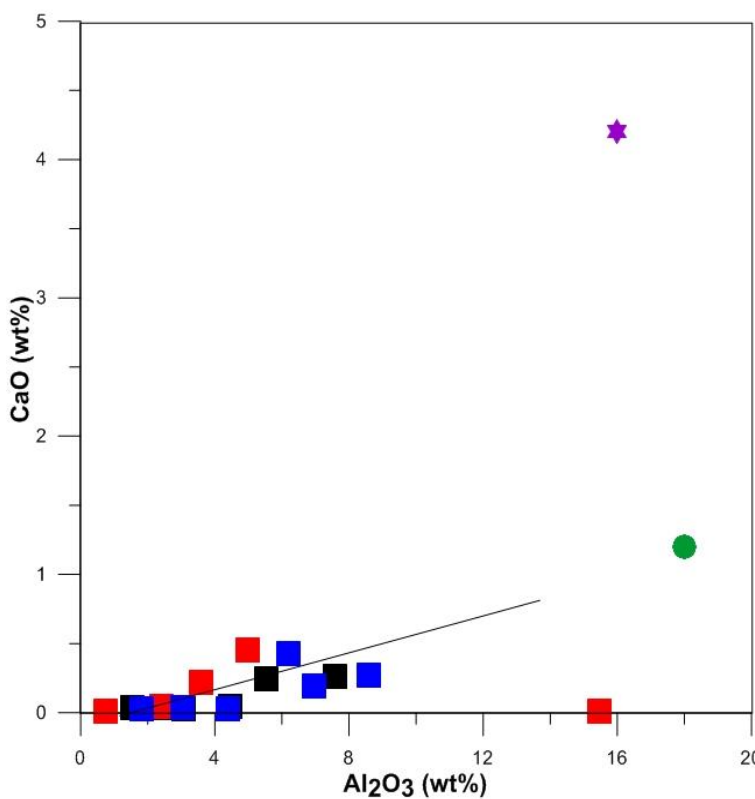
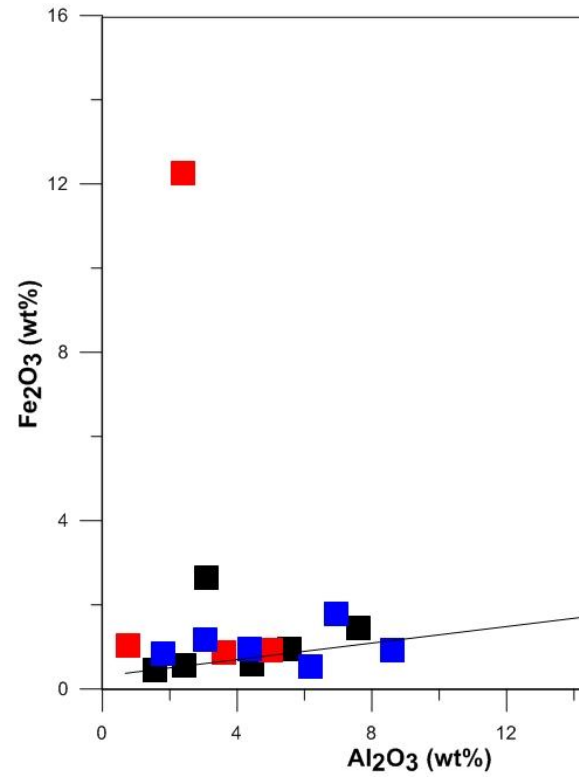
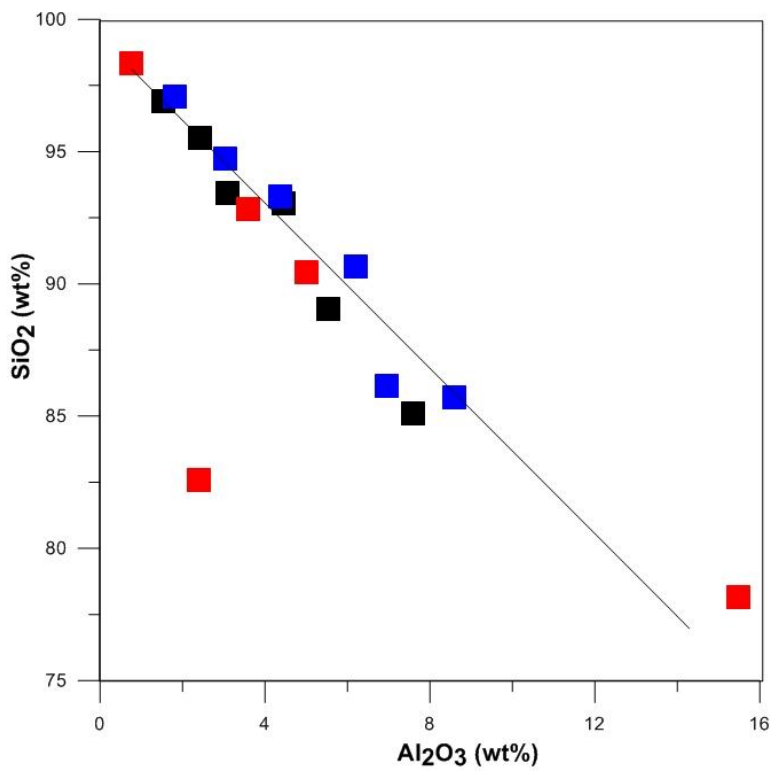


Figure 6.21: Major elements versus Al_2O_3 graph showing the distribution of sandstone samples from the Tuli and Soutpansberg Coalfields. Average data of UCC and PAAS from Taylor and McLennan (1985) are also plotted for comparison. (UCC: purple star, PAAS: green circle).

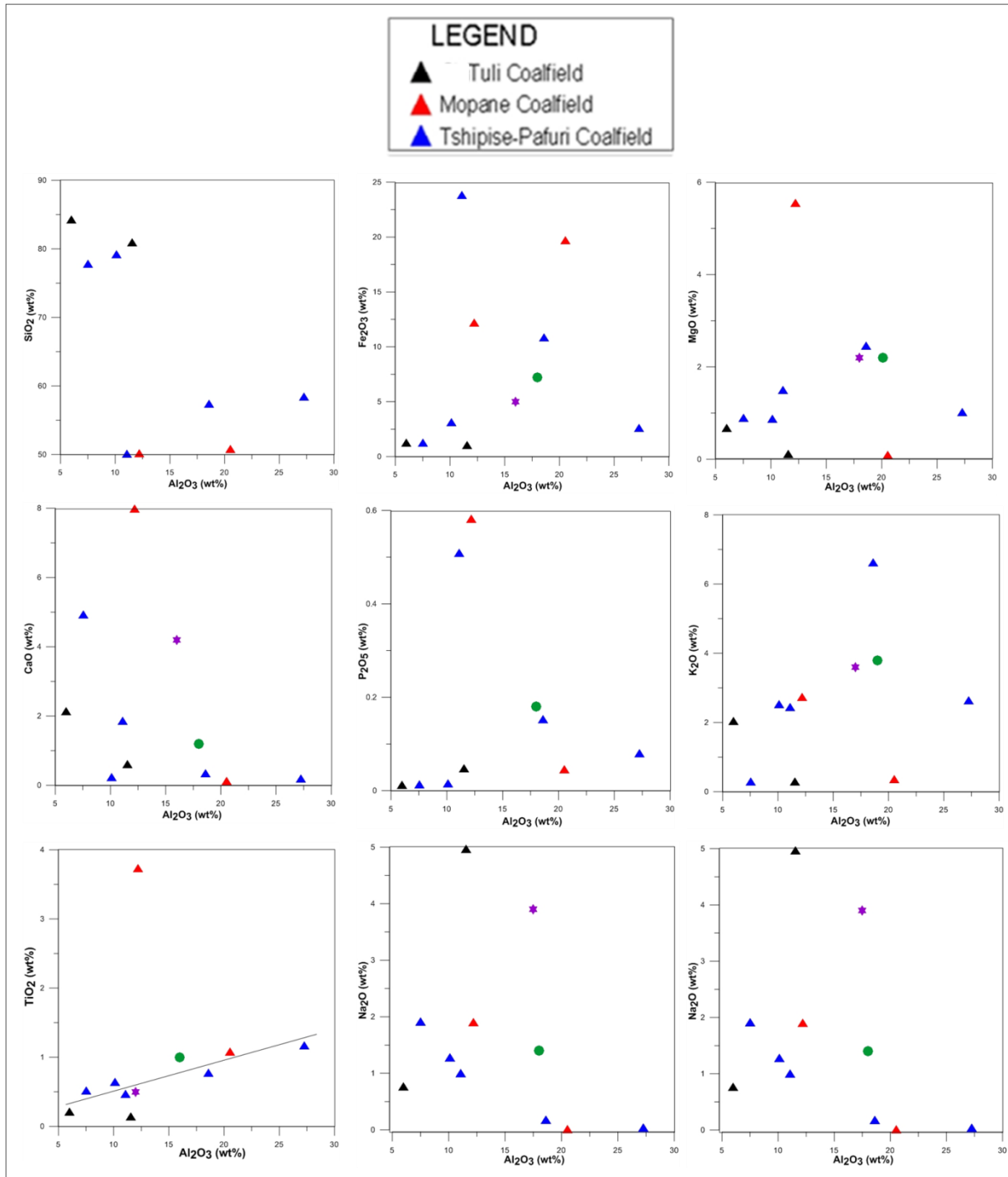


Figure 6.22: Major elements versus Al_2O_3 graph showing the distribution of shale samples from the Tuli and Soutpansberg Coalfields. Average data of UCC and PAAS from Taylor and McLennan (1985) are also plotted for comparison. (UCC: purple star, PAAS: green circle).

Using major oxides as variables, Roser and Korsch (1988) established major element discriminant functions to discriminate four major provenance fields, namely mafic, intermediate, felsic and quartzose recycled. In Figure 6.23, most of the sandstone samples from the coalfields plot in the quartzose sedimentary provenance field, suggesting that they were derived from a cratonic interior or recycled orogen. In Figure 6.24 most of the shale samples plot in the quartzose sedimentary provenance field. Some shale samples from Mopane and Tshipise-Pafuri Coalfields fall into the mafic igneous provenance. The recycled rocks are igneous rocks which have low silica 45 to 63% and typically high iron to magnesium content. The SiO_2 content in these shales is between 50.08 and 58.42 wt% and the Fe_2O_3 content is between 2.62 to 3.84 wt%.

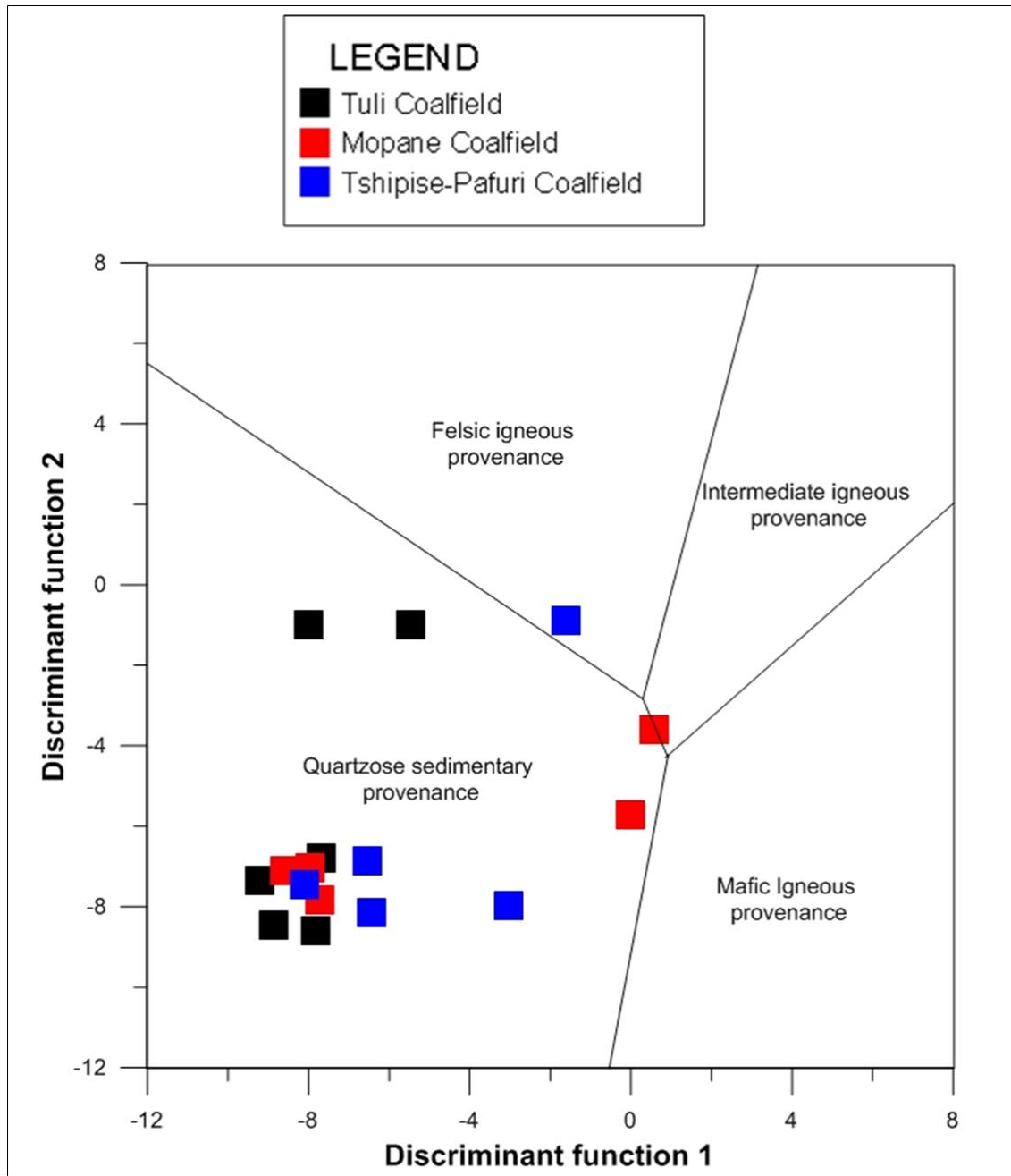


Figure 6.23: Major element Discriminant Function diagram for sedimentary provenance (sandstone) of Roser and Korsch (1988). The discriminant functions are: Discriminant Function 1 = $(-1.773 \text{ TiO}_2) + (0.607 \text{ Al}_2\text{O}_3) + (0.760 \text{ Fe}_2\text{O}_3) + (-1.500 \text{ MgO}) + (0.616 \text{ CaO}) + (0.509 \text{ Na}_2\text{O}) + (-1.224 \text{ K}_2\text{O}) + (-9.090)$; Discriminant Function 2 = $(0.445 \text{ TiO}_2) + (0.070 \text{ Al}_2\text{O}_3) + (-0.250 \text{ Fe}_2\text{O}_3) + (-1.142 \text{ MgO}) + (0.438 \text{ CaO}) + (1.475 \text{ Na}_2\text{O}) + (-1.426 \text{ K}_2\text{O}) + (-6.861)$.

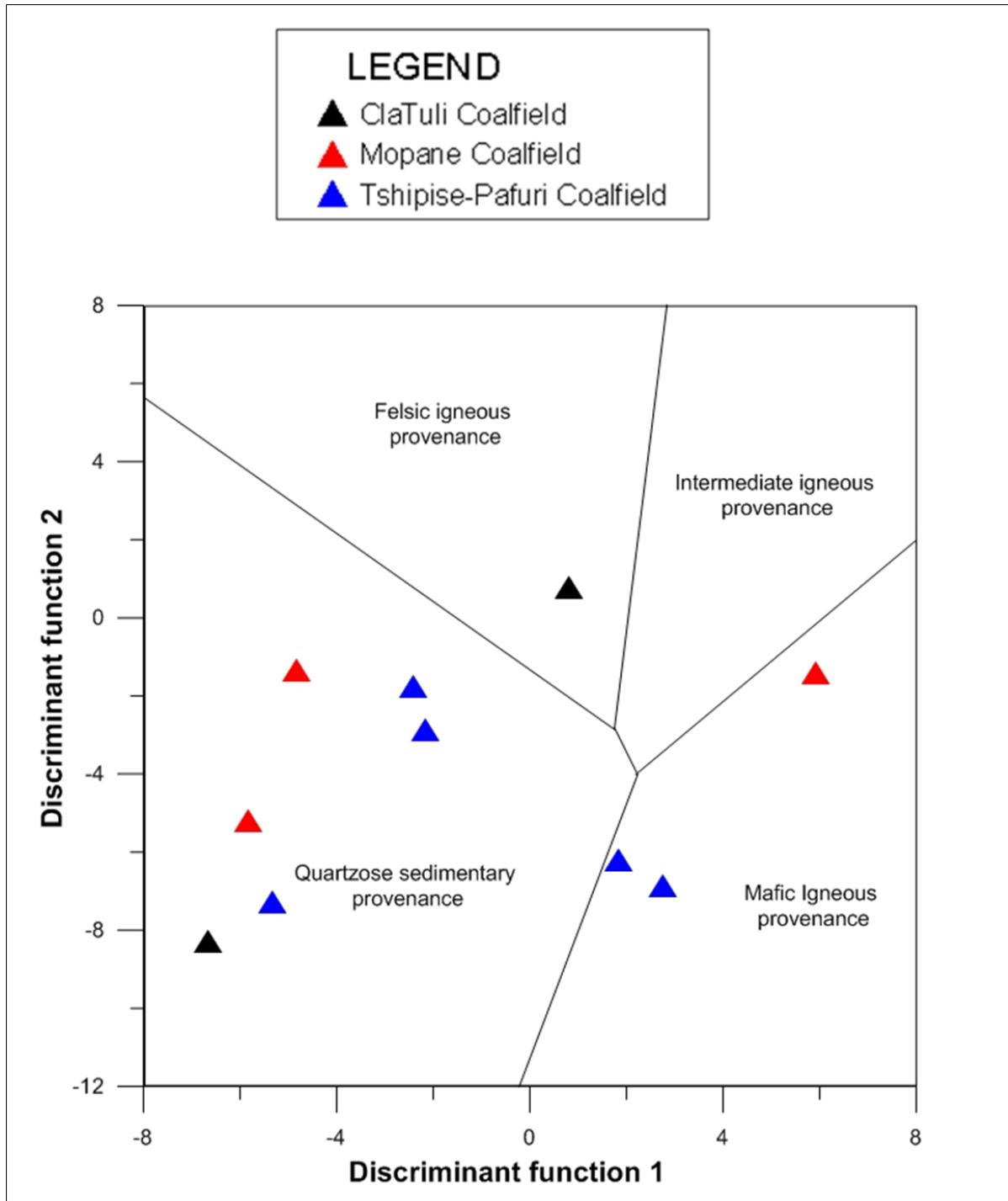


Figure 6.24: Major element Discriminant Function diagram for sedimentary provenance (shale) of Roser and Korsch (1988). The discriminant functions are: Discriminant Function 1 = $(-1.773 \text{ TiO}_2) + (0.607 \text{ Al}_2\text{O}_3) + (0.760 \text{ Fe}_2\text{O}_3) + (-1.500 \text{ MgO}) + (0.616 \text{ CaO}) + (0.509 \text{ Na}_2\text{O}) + (-1.224 \text{ K}_2\text{O}) + (-9.090)$; Discriminant Function 2 = $(0.445 \text{ TiO}_2) + (0.070 \text{ Al}_2\text{O}_3) + (-0.250 \text{ Fe}_2\text{O}_3) + (-1.142 \text{ MgO}) + (0.438 \text{ CaO}) + (1.475 \text{ Na}_2\text{O}) + (-1.426 \text{ K}_2\text{O}) + (-6.861)$.

In Figure 6.25, almost all the sandstone samples of the coalfields represent the passive continental margin and very few samples fall in the active continental margin field. Shale samples in Figure 6.26 represent the active continental margin with only one sample in the island arc field. The passive continental margins are basins on continental crust and basins associated with ocean floor spreading, failed rifts and Atlantic-type continental margins. The active continental margins are subduction related basins, continental basins and pull-apart basins associated with strike-slip fault zones.

Analogue, but more detailed results can be obtained by the calc-alkaline ternary diagram (CaO-Na₂O-K₂O). Here, most sandstone samples (Figure 6.27) can be related to a passive continental margin. Shale samples (Figure 6.28) are also represented in the passive continental margin, only a few shales can be attributed to an active continental margin source. The results correspond well with those of the logK₂O/Na₂O versus SiO₂ tectonic setting discrimination diagrams in Figures 6.25 and 6.26.

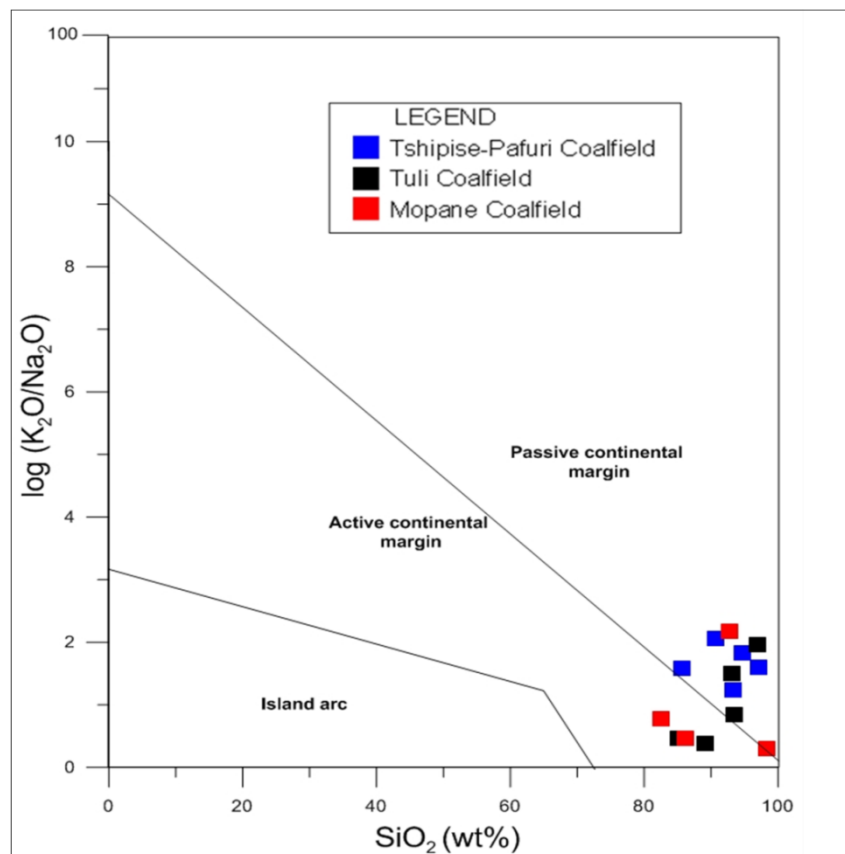


Figure 6.25: Tectonic-setting discrimination diagram for sandstone samples after Roser and Korsch (1986) using SiO₂-log (K₂O/Na₂O).

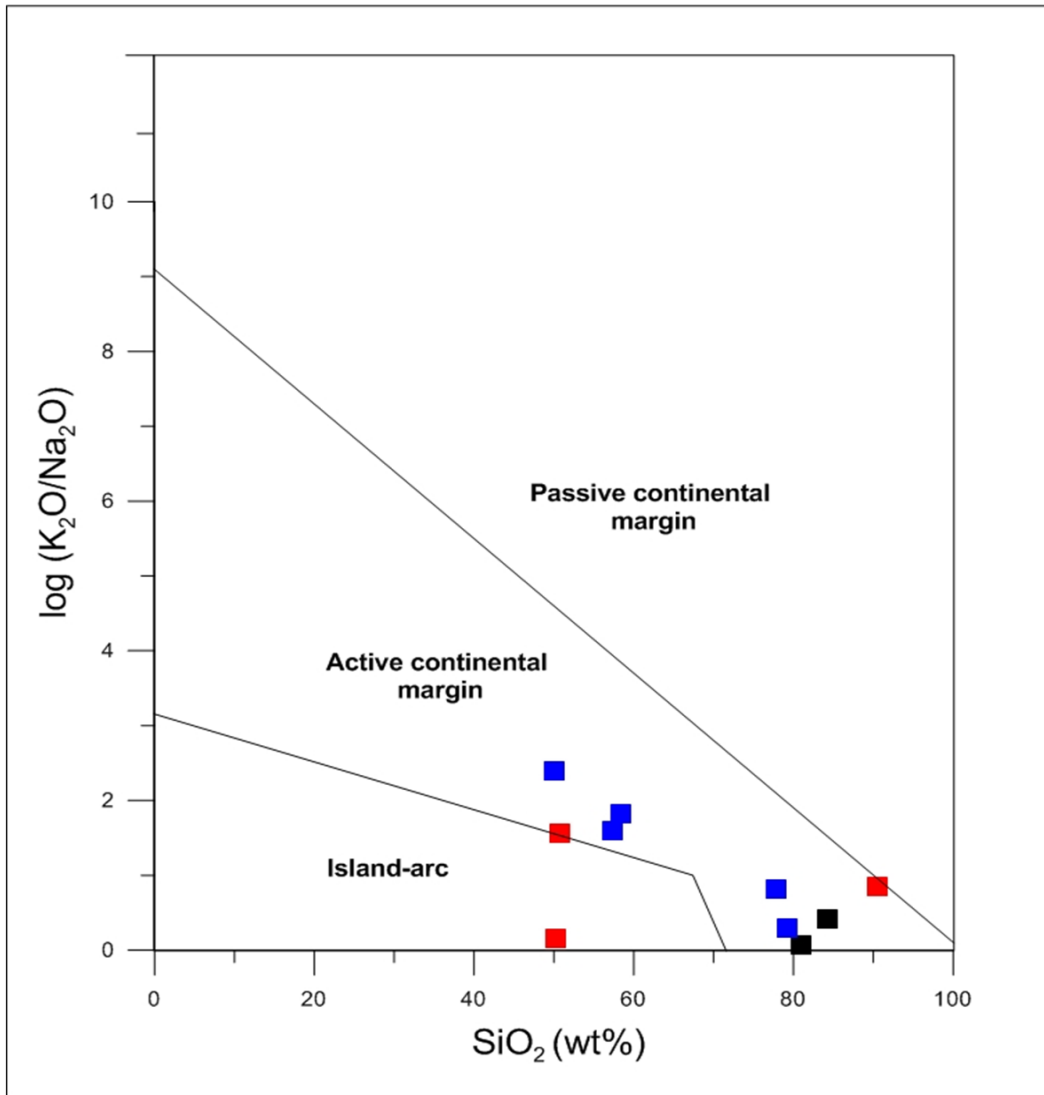


Figure 6.26: Tectonic-setting discrimination diagram for shale samples after Roser and Korsch (1986) using SiO_2 - K_2O/Na_2O .

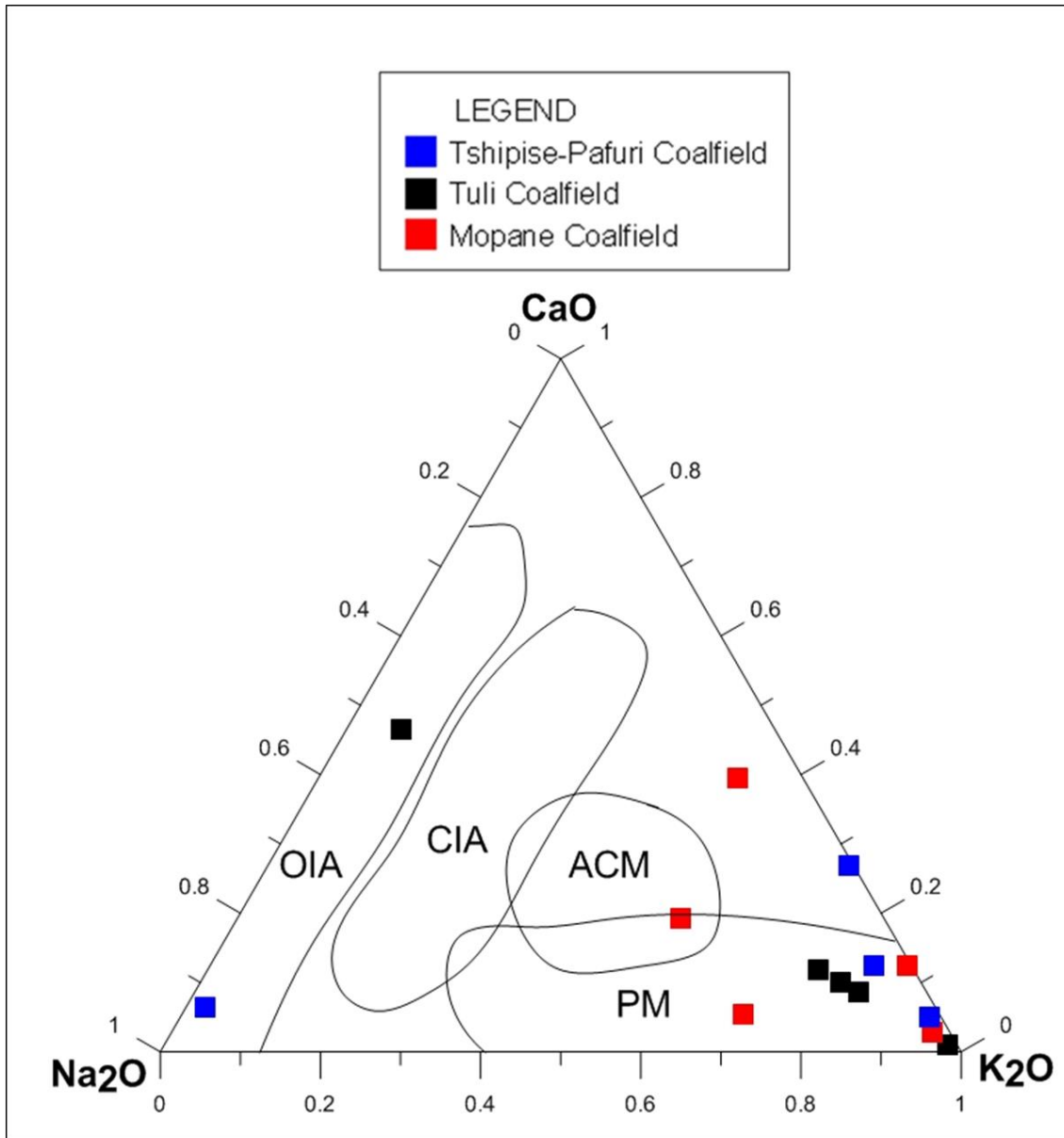


Figure 6.27: Sandstone samples from the coalfields in the ternary Na₂O-CaO-K₂O plot after Toulkeridis *et al.* (1999). OIA = oceanic island arc, CIA = continental island arc, ACM = active continental margin, PM = passive continental margin.

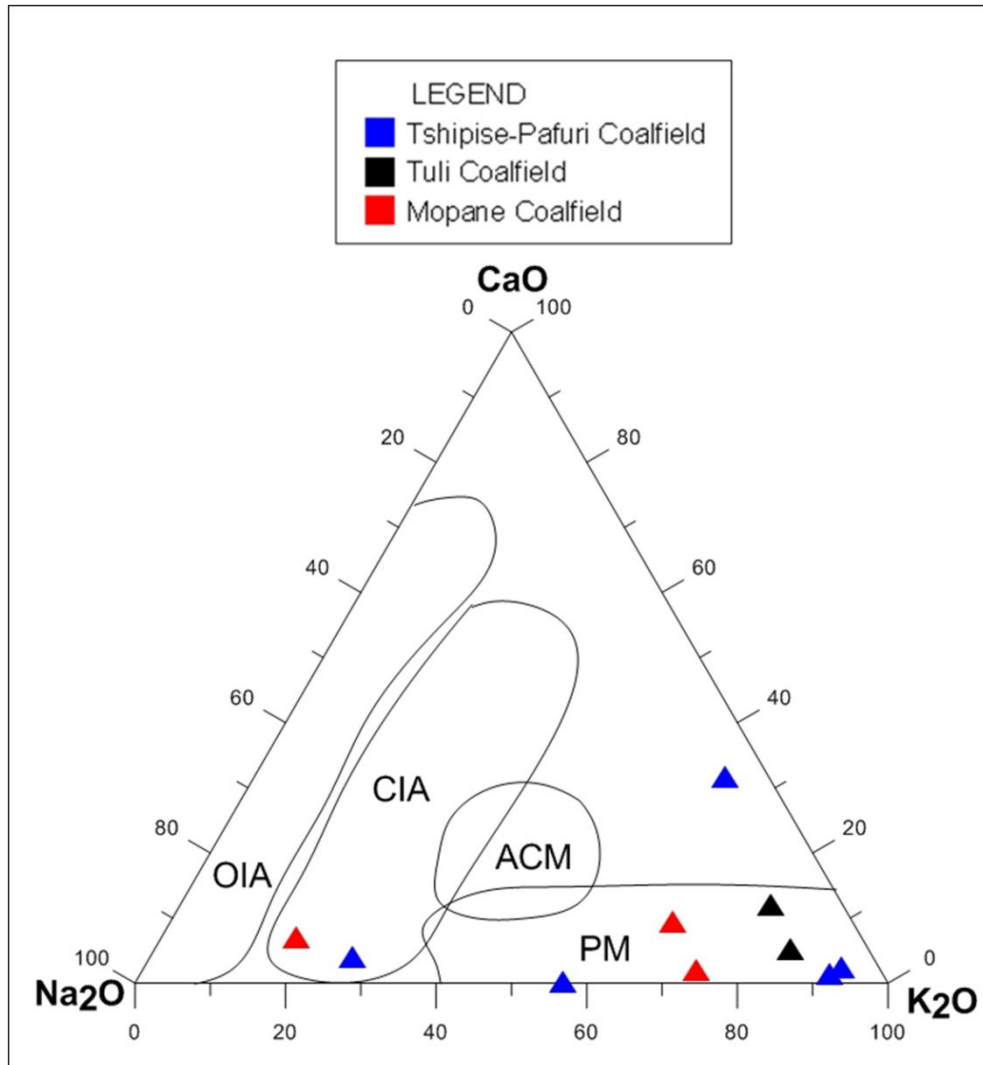


Figure 6.28: Shale samples from the coalfields in the ternary Na₂O-CaO-K₂O plot after Toulkeridis *et al.* (1999). OIA = oceanic island arc, CIA = continental island arc, ACM = active continental margin, PM = passive continental margin.

6.5.1.1. Source area weathering

Another approach to assess the composition of the original source rock is to plot the A-CN-K diagram proposed by Toulkeridis *et al.* (1999). A-CN-K represents Al₂O₃-(CaO + Na₂O)-K₂O respectively. Such a plot is useful for identifying compositional changes of shales and sandstones that are related to chemical weathering, diagenesis, and source rock composition. The average source rock composition of shales and sandstones can be deduced from the A-CN-K diagram. Data of samples from the coalfields were plotted in an A-CN-K diagram (Figures 6.29 and 6.30). Nesbitt and Young (1982) defined the Chemical Index of Alteration (CIA) formula to evaluate the degree of chemical weathering: $CIA = [Al_2O_3 / (Al_2O_3 + CaO + Na_2O + K_2O)] * 100$.

The CIA values of sandstone samples range from 70 to 99.8% (average = 84.9%), (Figure 6.29). For shale samples the CIA values of ranges from 52 to 99% (average = 75.5%), (Figure 6.30). The relatively high CIA values (70 to 90%) indicates moderate to high weathering conditions of the samples. The samples which plots near the A end member, suggest intense chemical weathering and transportation of the samples. The high CIA values in the sediments probably reflect the presence of clay minerals and absence of detrital feldspars. The low CIA values in the shales and some Tuli sandstones (50 to 60%) indicate low weathering conditions in the source area and may reflect cool and/or arid climate conditions. The A-CN-K ternary diagram $Al_2O_3-(CaO + Na_2O)-K_2O$ can also be used to constrain initial compositions of source rocks. The arrows 1 to 5 represent the weathering trends of different rock types (explained in Figures 6.29 and 6.30 captions).

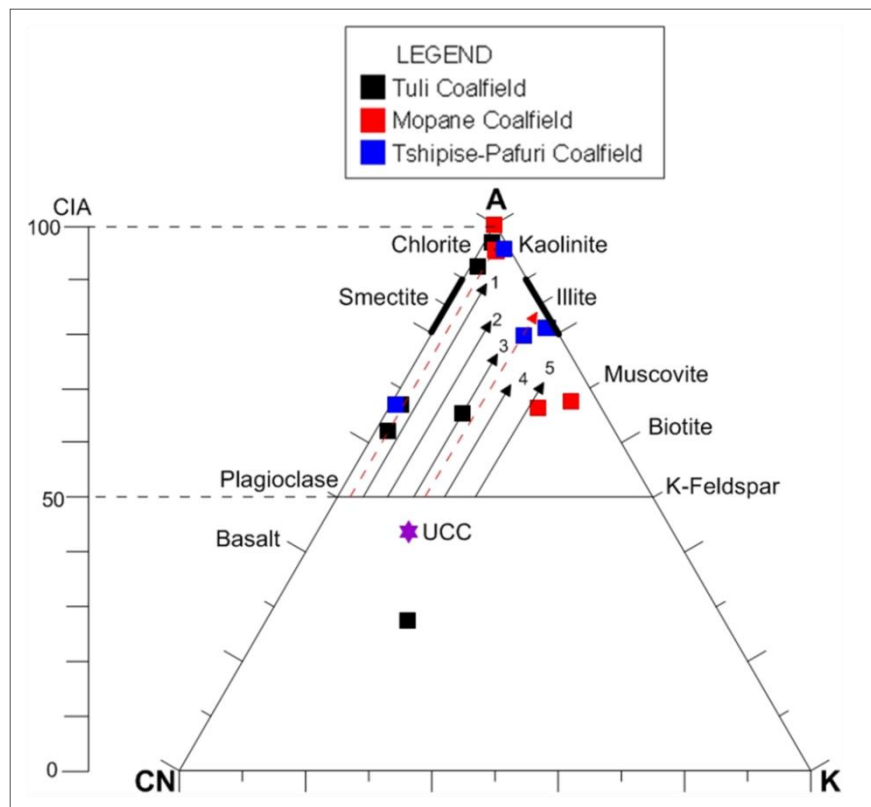


Figure 6.29: A-CN-K ternary diagram of molecular proportions of $Al_2O_3-(CaO+Na_2O)-K_2O$ for sandstone samples from the Soutpansberg and Tuli Coalfields (after Nesbitt and Young, 1984). The CIA scale shown at the left side of the figure for comparison. The arrows 1-5 represent the weathering trends of gabbro, tonalite, granodiorite, adamellite and granite, respectively, from (Fedo *et al.*, 1997). The dotted arrows show the actual weathering trend for the samples.

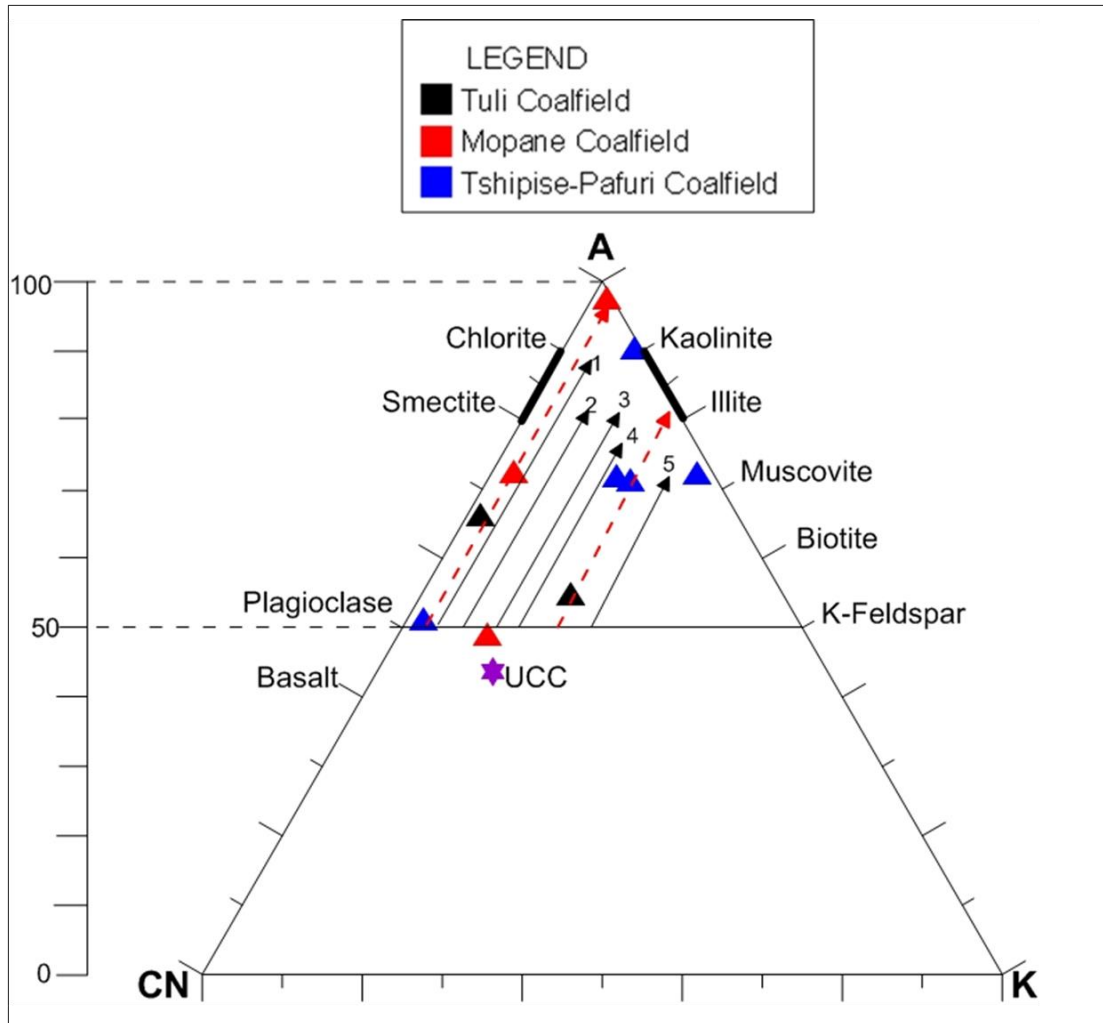


Figure 6.30: A-CN-K ternary diagram of molecular proportions of Al_2O_3 -($\text{CaO}+\text{Na}_2\text{O}$)- K_2O for shale samples from the Soutpansberg and Tuli Coalfields (after Nesbitt and Young, 1984). The CIA scale shown at the left side of the figure for comparison. The arrows 1-5 represent the weathering trends of gabbro, tonalite, granodiorite, adamellite and granite, respectively, from (Fedo *et al.*, 1997). The dotted arrows show the actual weathering trend for the samples.

In the geochemical classification diagram in Figure 6.31, the majority of sandstone occupies fields of quartz arenite and sub-lithic arenite. Figure 6.32 indicates that; sandstone falls in the lithic arenite, sub-arkose, sub-litharenite, and quartz arenite fields; Shale samples occupy fields of Fe shale, shale, wacke, Fe sand, and sub-arkose fields.

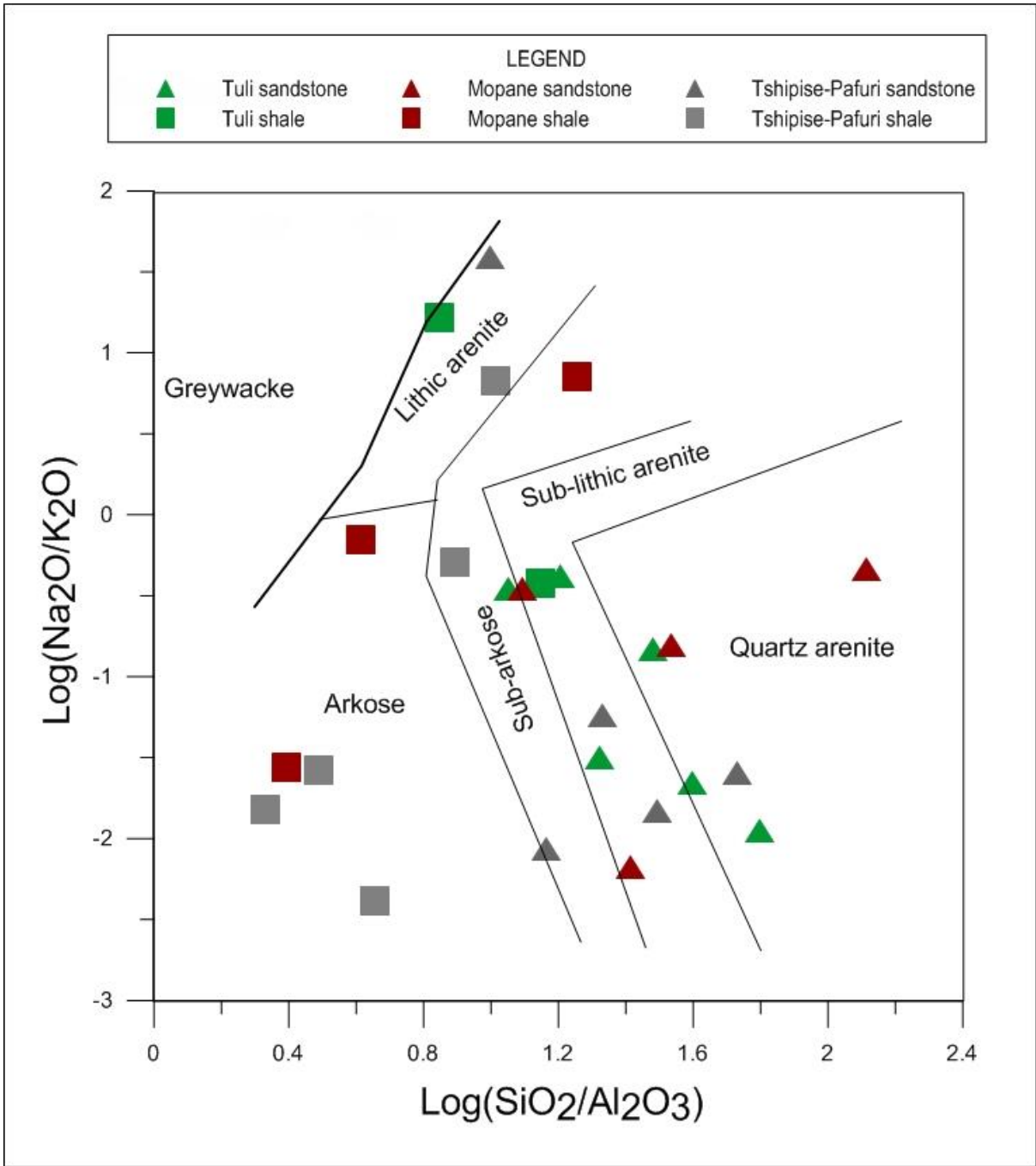


Figure 6.31: $\text{Log}(\text{Na}_2\text{O}/\text{K}_2\text{O})$ versus $\text{Log}(\text{SiO}_2/\text{Al}_2\text{O}_3)$ plot (after Pettijohn *et al.*, 1987) plot for geochemical classification of the Tuli and Soutpansberg rocks.

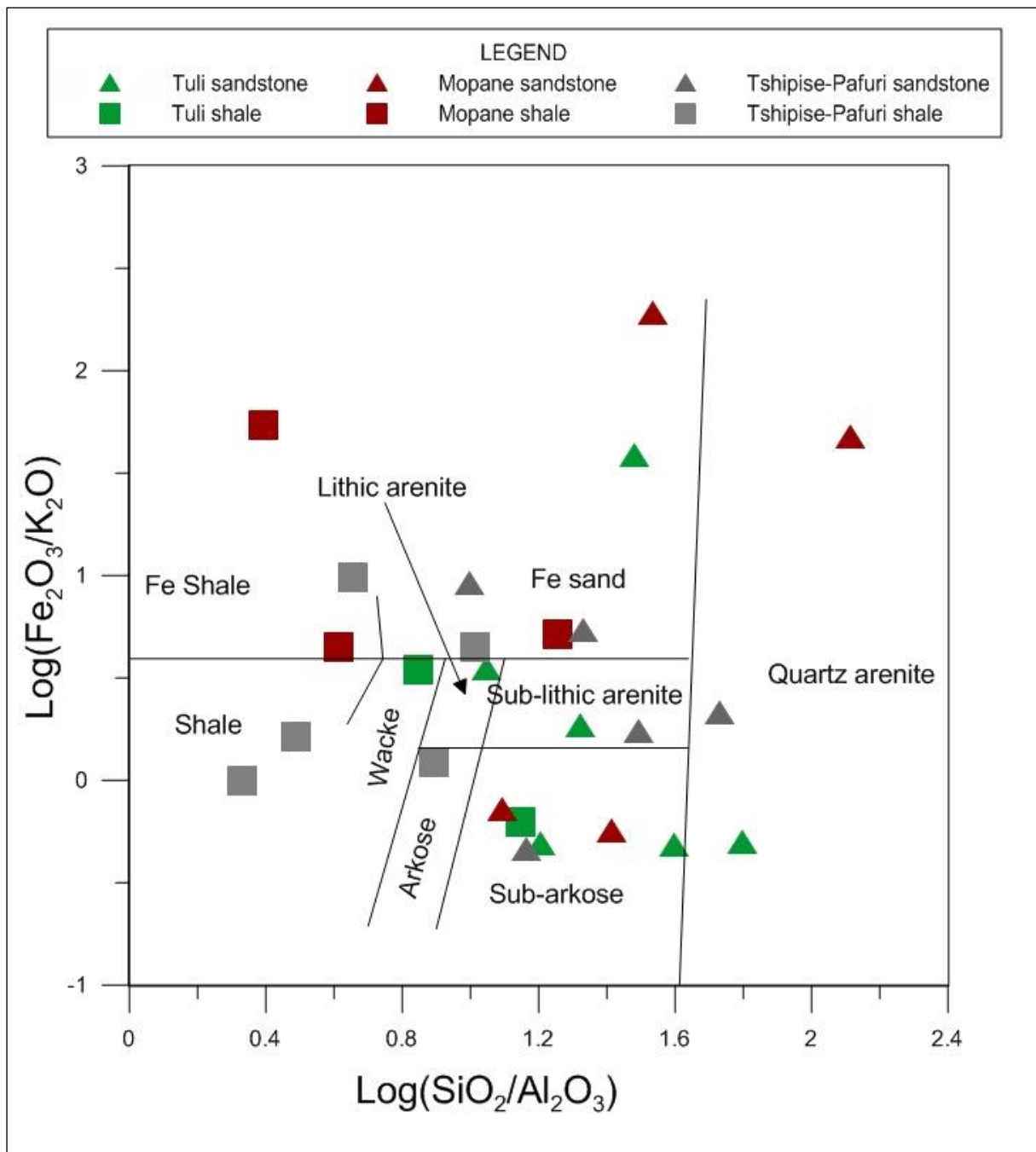


Figure 6.32: Log ($\text{Fe}_2\text{O}_3/\text{K}_2\text{O}$) versus Log ($\text{SiO}_2/\text{Al}_2\text{O}_3$) plot (after Herron, 1988) plot for geochemical classification of the Tuli and Soutpansberg samples.

6.5.2: Trace Elements

6.5.2.1. Large Ion Lithophile Elements (LILE): Rb, Ba, Sr, Th and U

On average, with the exception of Ba, all the sandstones exhibit similar LILE abundances relative to UCC in the Soutpansberg Coalfield (Figures 6.33A and B). In contrast, the shales exhibit similar Ba contents relative to UCC but are depleted in Rb, Sr, Th, and U in the Soutpansberg Coalfield. Th has very strong positive correlations with Nb in the Soutpansberg Coalfield (implying that it may be controlled by clays and/or other phases (e.g., Ti- and Nb-bearing phases) associated with clay minerals. Rb and Ba are positively correlated in the Tshipise-Pafuri sandstone and for all coalfields in shale indicating a similar geochemical behaviour. These correlations suggest that their distributions are mainly controlled by illites and other minor clays.

6.5.2.2. High Field Strength Elements (HFSE): Y, Zr, Nb and Hf

HFSE elements are enriched in felsic rather than mafic rocks (Bauluz *et al.*, 2000 and Bauluz *et al.*, 2005). The concentrations of Zr in the Soutpansberg sandstones are relatively similar to UCC contents (Figure 6.33) and Y, Nb and Hf are depleted. The shales from both coalfields show lower concentrations of these elements. Zr has high positive correlations suggesting that these elements are controlled by zircon (Murali *et al.*, 1983). Mean Zr contents for shales are lower than the associated sandstones, which indicate that the mineral zircon tends to be preferentially concentrated in coarse-grained sands.

6.5.2.3. Transition Trace Elements (TTE): V, Co, Cu, Ni and Sc

V in the Soutpansberg shales is quite similar to UCC, whereas it is depleted in the sandstone (Figure 6.33). The TTE in the Soutpansberg and Tuli sandstones do not behave uniformly. Among TTE, Sc is correlated positively with Ni which indicates that it is mainly concentrated in the phyllosilicates.

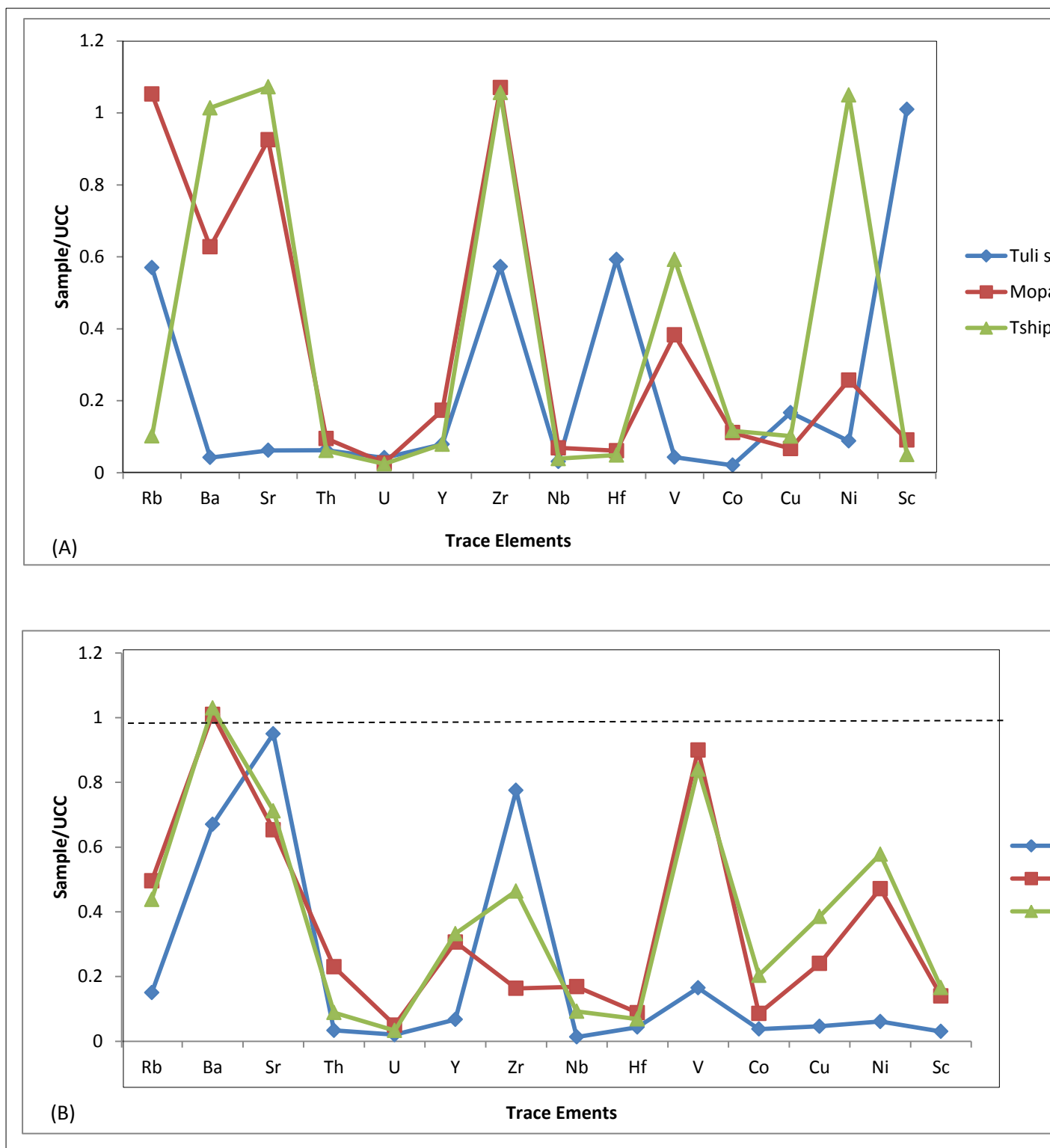


Figure 6.33: Spider plot of major and trace element compositions for the Soutpansberg and Tuli samples normalized against UCC values. The UCC values are from Taylor and McLennan (1985). The trace elements are ordered with the large ion-lithophile elements (LILE) on the left (Rb-U), followed by high field strength elements (HFSE) on the right (Y-Hf) and the transition metals (V-Sc). A: sandstone, B: shale.

According to the TiO₂-Ni diagram of Floyd *et al.* (1989), the source area for most samples from both coalfields was of a predominantly acidic magmatic nature (Figure 6.34), even though few samples plot outside the field assigned for felsic source. A sandstone sample from the western Soutpansberg (Mopane) shows a provenance from mature sedimentary rocks (Figure 6.34).

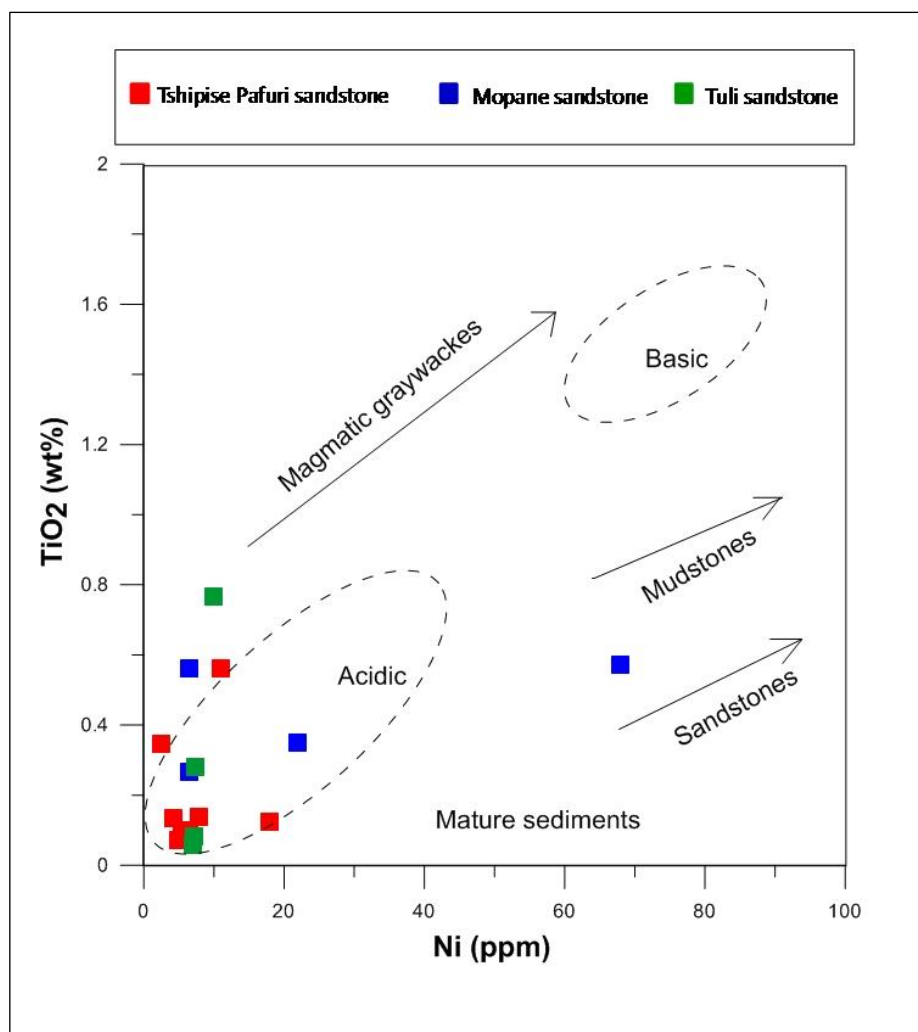


Figure 6.34: TiO₂ versus Ni bivariate plot for the sandstones from the Tuli and Soutpansberg Coalfields (fields after Floyd *et al.*, 1989). The majority of the samples plot near the acidic source field.

Furthermore, the La/Th versus Hf bivariate (Figure 6.35; after Floyd and Leveridge, 1987) and V-Ni-Th*10 (Figure 6.36; after Bracciali *et al.*, 2007) ternary diagrams also suggest that the Soutpansberg and Tuli sandstones were derived from felsic source rocks. The spread in these diagrams between the shales and sandstones suggests a difference in source rocks for the shales and sandstones.

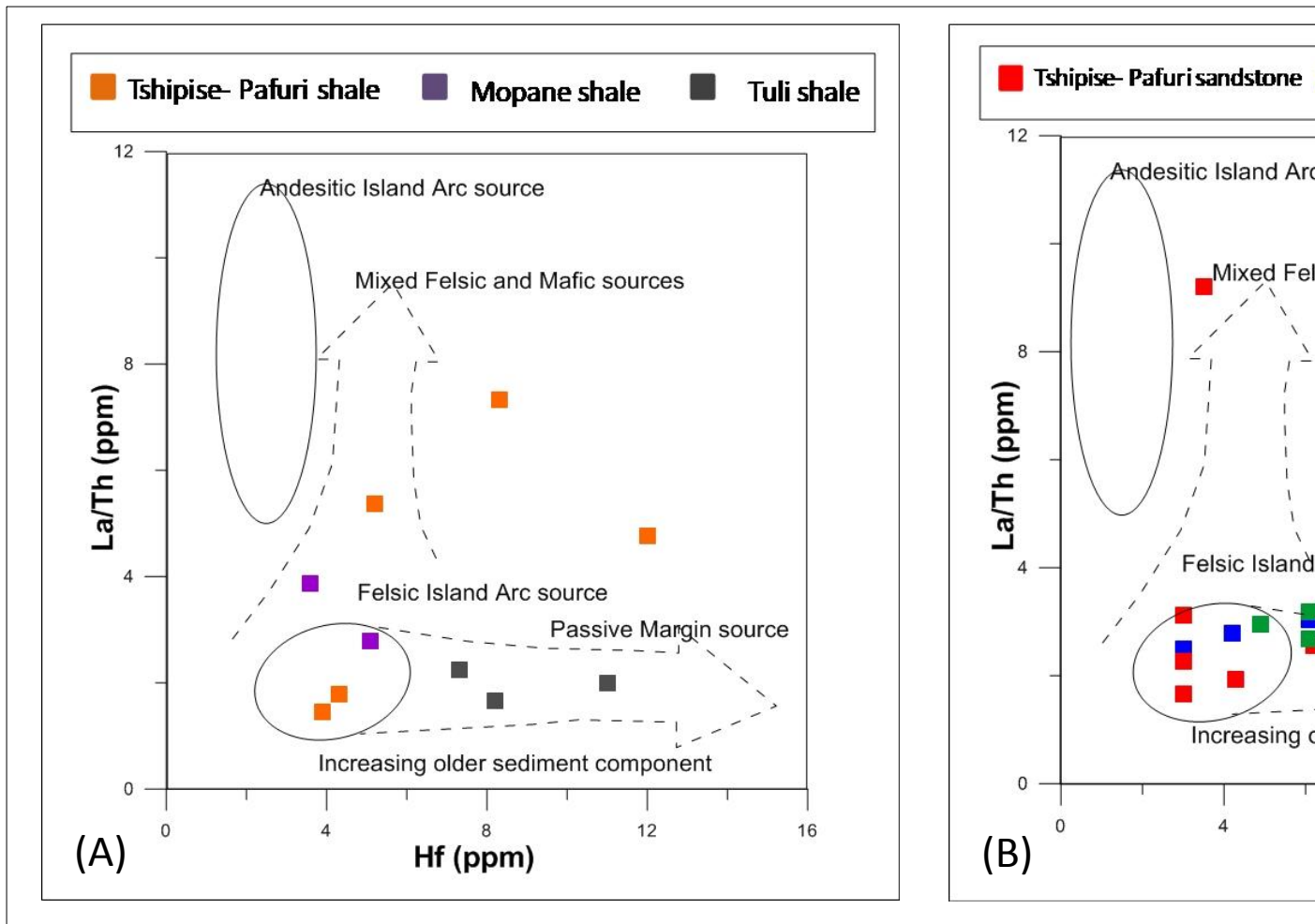


Figure 6.35: Hf versus La/Th diagram (after Floyd and Leveridge, 1987). A: shale, B: sandstone.

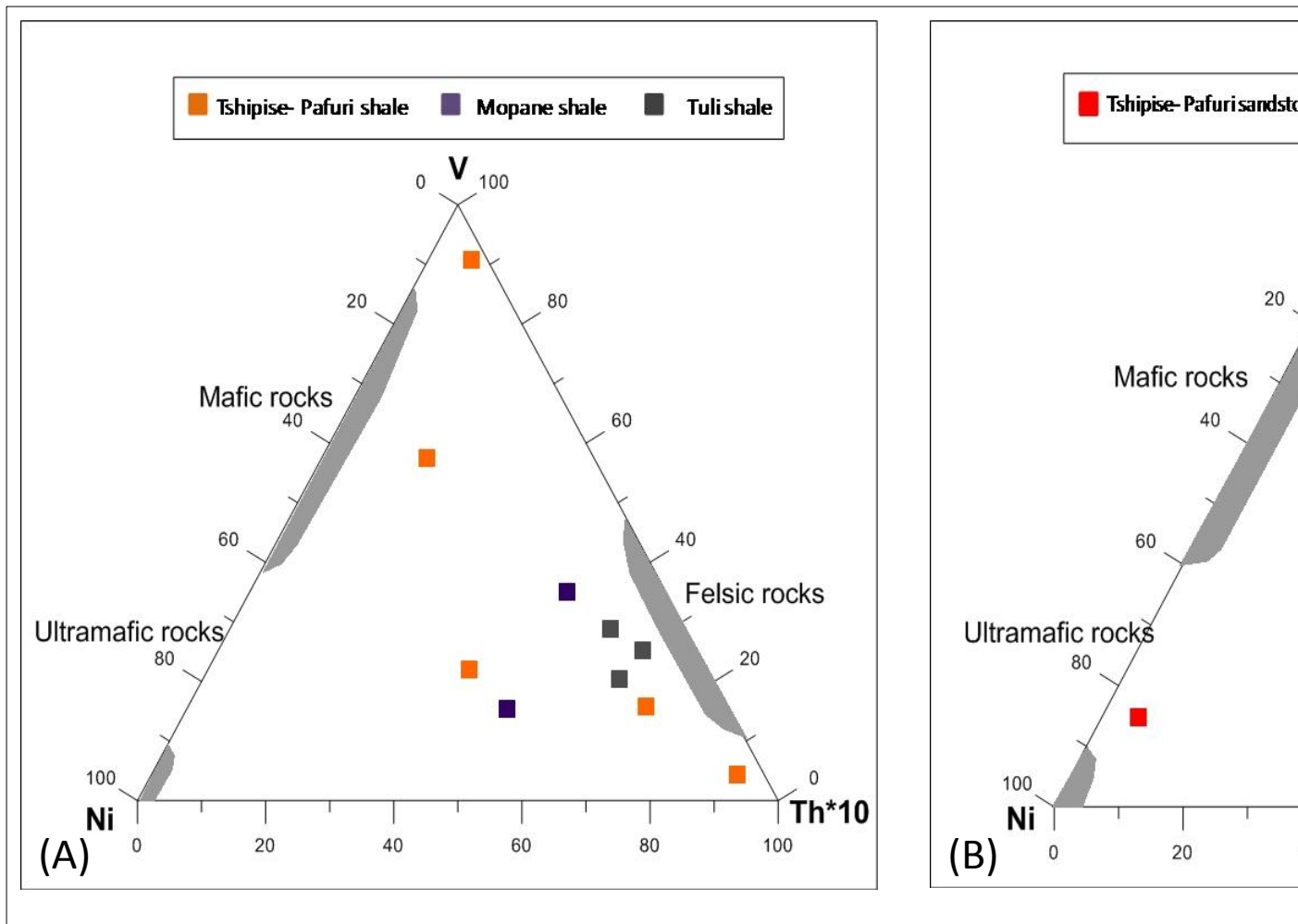


Figure 6.36: V-Ni-Th*10 triangle diagram (after Bracciali *et al.*, 2007). Shaded area represents composition of the felsic, mafic, and ultramafic rocks. The sandstones and shale plot near felsic source rocks. A sandstone sample with high Ni content (82.5 ppm) is shifting towards the Ni corner. A: shale, B: sandstone.

The post-Archaean pelites have low concentrations of mafic elements, particularly Ni and Cr, when compared to Archaean pelites (McLennan *et al.*, 1993). The reason for the high concentrations of Ni and Cr in the Archaean pelites is due to the deficiency of ultramafic rocks in the post-Archaean Period (Taylor and McLennan, 1985). The Soutpansberg and Tuli sandstones and shales plot in the post-Archaean field (Figure 6.37) and this suggests that the felsic component was dominant in the source area of both the coalfields.

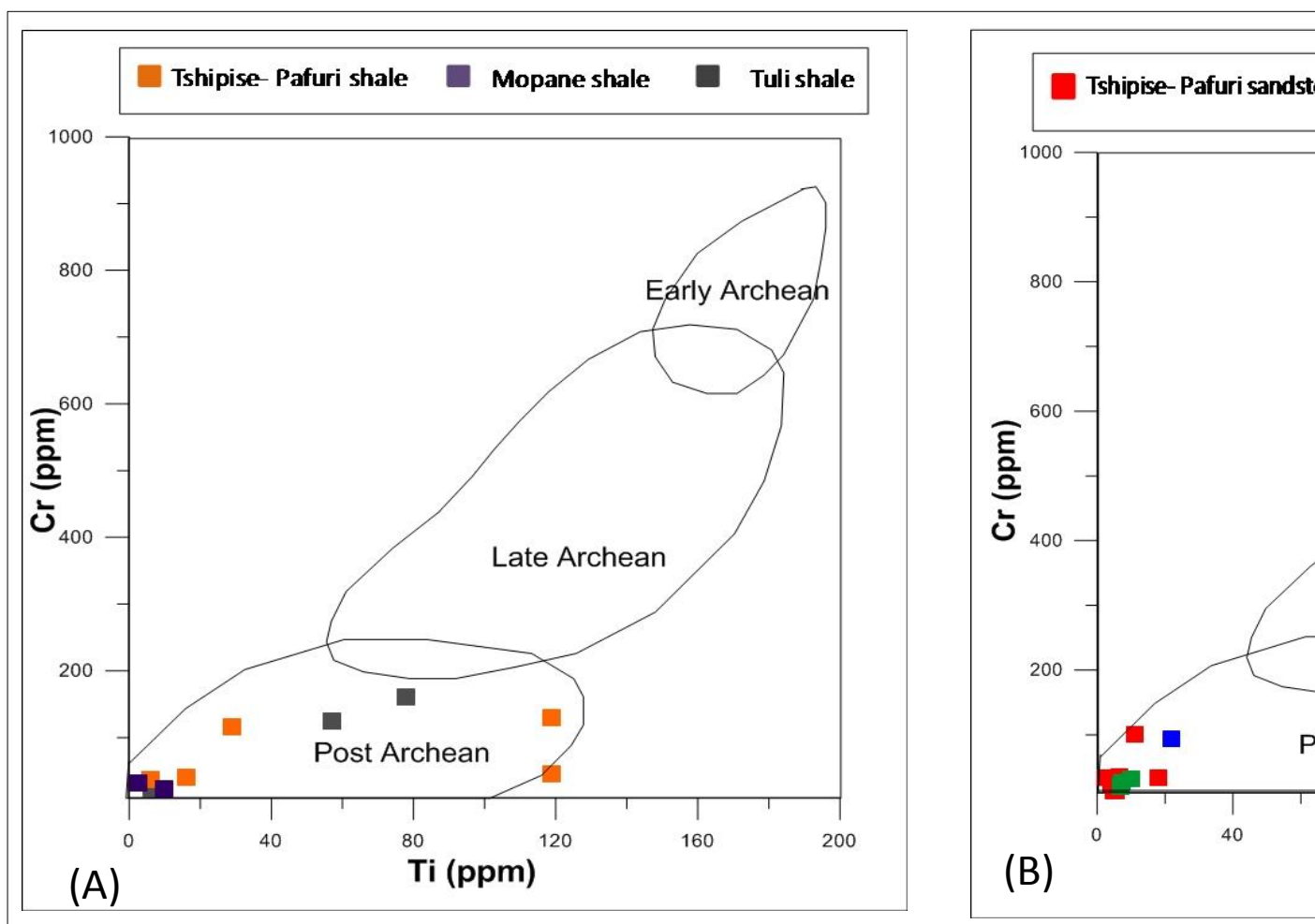


Figure 6.37: Ni-Cr bivariate plot for the samples from the Soutpansberg and Tuli Coalfields (McLennan *et al.*, 1993). A: shale, B: sandstone.

According to the Th-Sc-Zr/10 tectonic discrimination diagram of Bhatia and Crook (1986), the source area for most samples from both coalfields was of a predominantly passive margin nature (Figure 6.38). Only a few shale samples plot in the continental island arc. Two sandstone samples from the Soutpansberg plot outside the fields (Figure 6.38).

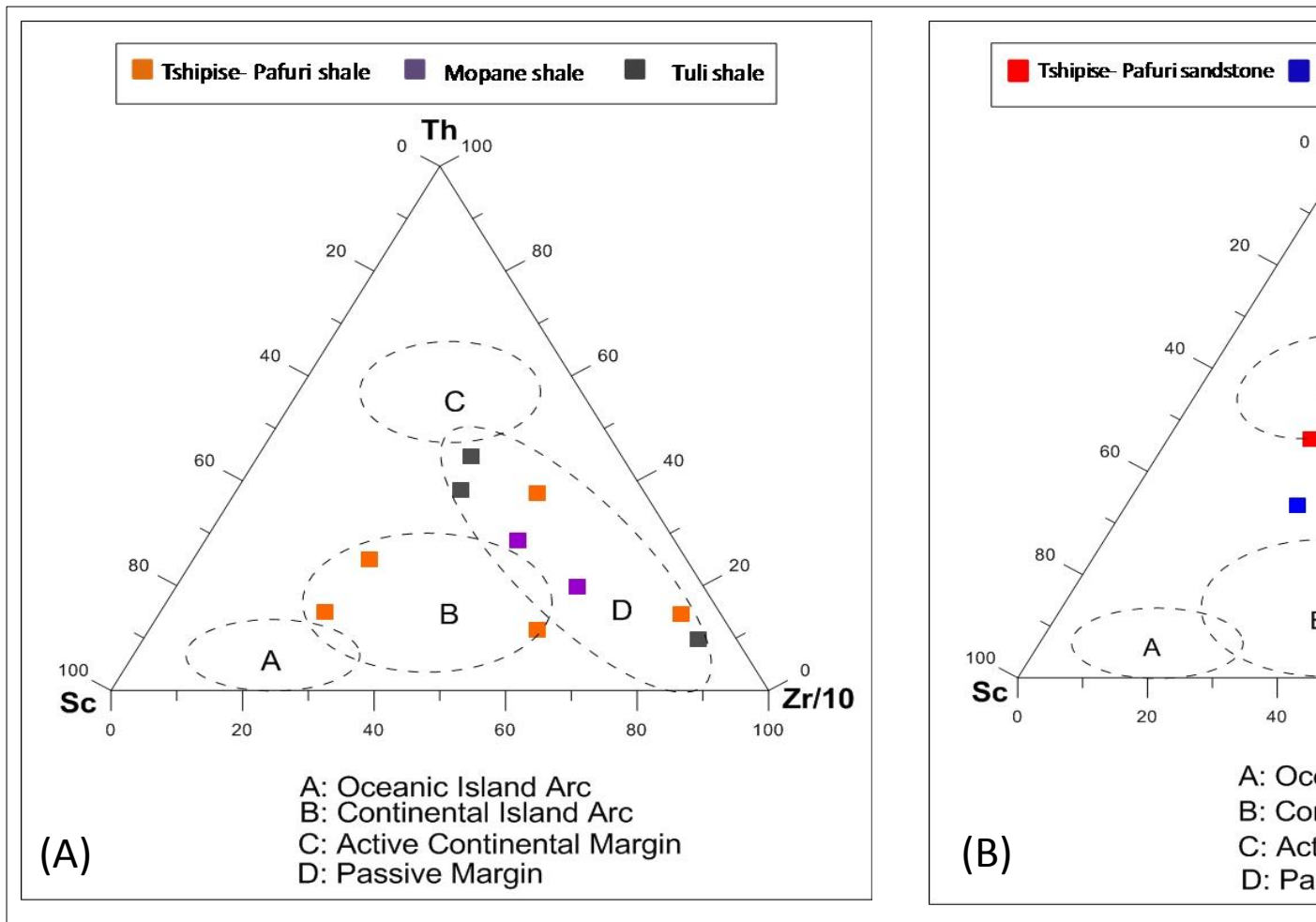


Figure 6.38: The Soutpansberg and Tuli shale and sandstone samples based on Th-Sc-Zr/10 tectonic discrimination diagram of Bhatia and Crook (1986). A: shale, B: sandstone.

Immobile elements like La, Zr, Hf, etc. are enriched in the passive margin setting (e.g. Bhatia, 1983). Figure 6.39 demonstrates the passive margin setting of the depositional basin for the Soutpansberg and Tuli sandstones (La-Th-Sc of Bhatia and Crook, 1986). The similarity of the Hf versus La/Th diagram (Figure 6.35) is a clear indication of a passive margin depositional basin. The data from these immobile trace elements correlates well with Figures 6.25 and 6.26 (SiO vs K_2O/Na_2O) of the discrimination diagram of Roser and Korsch (1986); Figures 6.27 and 6.28 ($Na_2O-CaO-K_2O$) with the ternary plot of Toulkeridis *et al.* (1999).

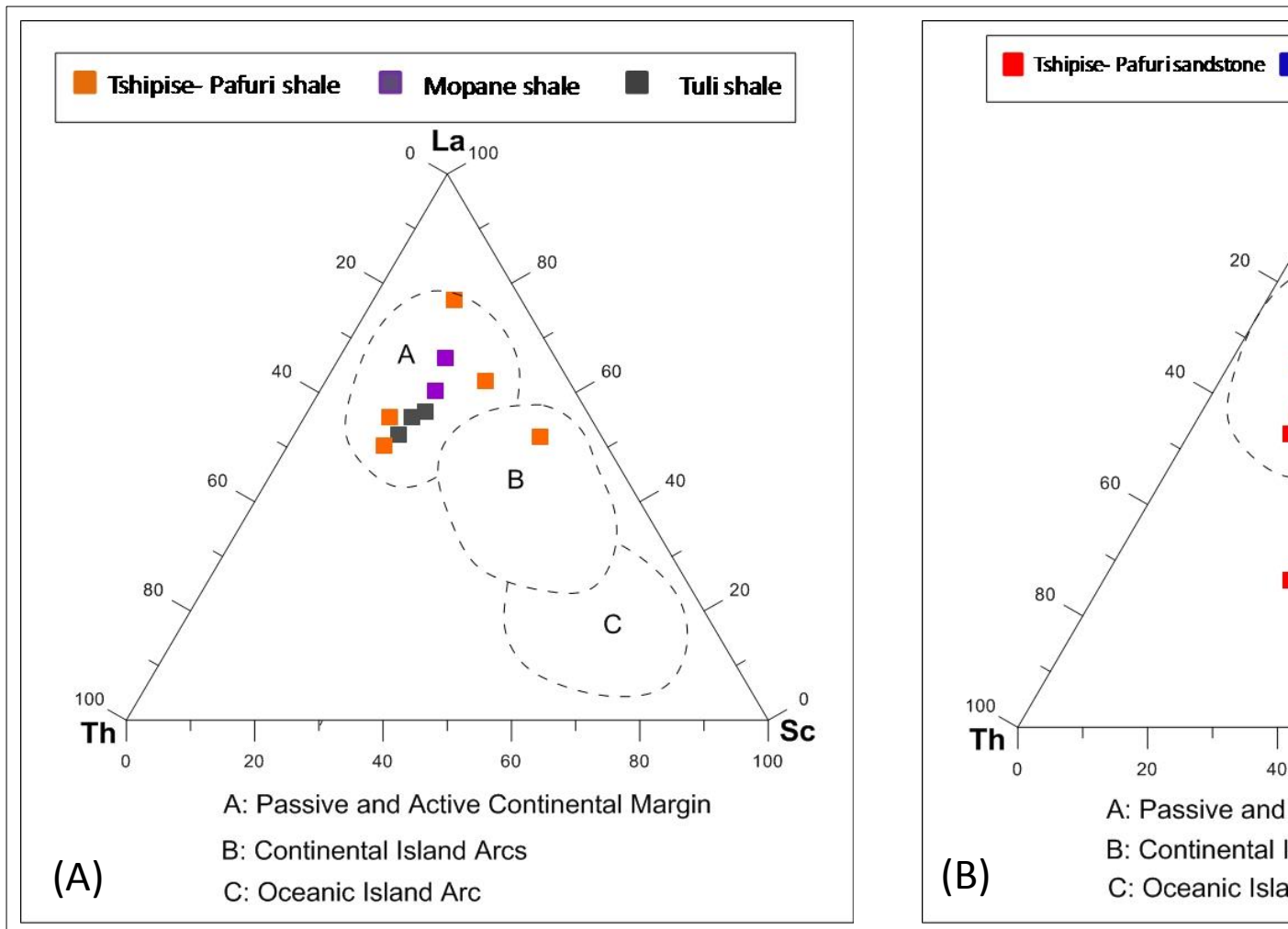


Figure 6.39: La-Th-Sc tectonic discrimination diagram for the Soutpansberg and Tuli sandstones. From Bhatia and Crook (1986). A: shale, B: sandstone.

6.6. Discussions

The combination of sandstone petrography and geochemistry studies has been used to identify provenance and ancient tectonic environment characteristics of the sedimentary basins, although relief, climate, transport mechanism, depositional environment and diagenetic change may all be important factors affecting the original composition of the sediment (Bhatia, 1983; Dickinson, 1985 and Bhatia and Crook, 1986).

Sandstone petrography and detrital modes on discrimination diagrams indicate that the source areas of the late Carboniferous and early Permian succession were derived from craton interior and recycled orogen provenance. Sandstones of the Tuli depositional system are classified as sub-quartzose and sub-litharenite (Pettijohn, 1975) in Figure 6.18A or lithic arkose and feldspathic litharenite (Folk, 1980) in Figure 6.18B. They were probably derived from the Archaean basement rocks of the Limpopo Mobile Belt (Northern and Central Marginal Zones).

Sandstones in the Soutpansberg Depositional System are sub-arkose and sub-litharenite (Pettijohn, 1975) in Figure 6.18A or arkose, lithic arkose and feldspathic litharenite (Folk, 1980) in Figure 6.18B. Overall, the sediments from both coalfields may represent a

recycled to craton interior provenance (Dickinson *et al.*, 1983) (refer to Figures 6.19A and B). High proportions of monocrystalline quartz (Qm) than polycrystalline quartz (Qp) and low percentages of lithic fragments and feldspars within the sandstones indicate long distance of transportation and acidic plutonic rocks or recycled sedimentary rocks as the source (Dickinson, 1988). All studied sandstones contain a few sedimentary and metamorphic rock fragments; this suggests that their source area is of sedimentary and metamorphic origin. Dickinson and Suczek (1979) classified all provenances of sandstone detritus suites into (1) continental block, which includes stable cratons and basement uplifts; (2) magmatic arc, which includes dissected and undissected arcs; and (3) recycled orogen. Continental block provenances are located within continental masses, which may be bounded on one side by a passive margin and on the other side by an orogenic belt. Recycled orogen provenances forms where there is a collision of major plates, which creates an uplifted source area next to the collision suture belt and the source rocks tend to be sedimentary and metamorphic rocks (Boggs, 2001).

Sources from recycled orogens include sedimentary strata (metasedimentary or sedimentary rocks) and subordinate volcanic rocks, partly metamorphosed and exposed to erosion by orogenic uplifted fold belts (Dickinson *et al.*, 1983). The sources may have been from the metasedimentary Soutpansberg Group and the volcanic rocks of the Beit-Bridge Complex. Some of the samples of the study area have revealed source areas representing a transitional continental setting, with minor contributions from a craton interior and recycled orogen (Figure 6.19). Most of these sandstones are arkosic and subarkosic in composition (Figure 6.18) and are likely to have been derived from the uplifted granite-gneiss or gneiss and schist basement and uplifted metasedimentary basement (Dickinson *et al.*, 1983). Some sandstone samples from the Soutpansberg Coalfield falls within the craton interior provenance (Fig. 6.19). This might indicate that it has been derived from uplifted basement rocks (granite-gneiss or metasedimentary rocks) (Dickinson *et al.*, 1983).

The geochemical data of major elements show that sandstone and shales have the same source. High content of Quartz (Figures 6.21 and 6.22), low primary clay, medium to high degree of sorting and roundness of framework grains in sandstone show medium to high maturity of sediments of the Permian succession. The relatively high CIA values (70 to 90%) indicates moderate to high weathering degree of the rocks. The rock samples which plots near the A end member, suggests intense chemical weathering and transportation of the samples (Nesbitt & Young, 1984). The high CIA values in the sediments probably reflect the

presence of clay minerals and absence of detrital feldspars. The low CIA values in the shales and few Tuli sandstones (50 to 60%) indicate low weathering condition in the source area and may reflect cool conditions. The Al_2O_3 -($\text{CaO}+\text{Na}_2\text{O}$)- K_2O (Nesbitt & Young, 1984) diagram of the sandstone and shale show that paleoclimate of the source area was warm, which caused chemical weathering of source rocks reducing some initial feldspar in source rocks. Long distance of transport, (i.e., perhaps hundreds of kilometers) is also an important process responsible for further reduction of feldspars. Diagenetic alteration of feldspar was the most important factor reducing feldspar in the sandstone. The A-CN-K ternary diagram (Figures 6.29 and 6.30); Al_2O_3 -($\text{CaO} + \text{Na}_2\text{O}$)- K_2O (Nesbitt and Young, 1984) can also be used to constrain initial compositions of source rocks. The arrows 1 to 5 represent the weathering trends of different rock types. Data from the coalfields in the ternary Na_2O - CaO - K_2O plot after Toulkeridis *et al.*, (1999), suggest a passive continental margin and only a shale samples can be attributed to active continental margin provenance (Figures 6.28 and 6.29). The results are almost the same as those of the $\text{K}_2\text{O}/\text{Na}_2\text{O}$ versus SiO_2 tectonic setting discrimination diagrams in Figures 6.25 and 6.26.

Selected trace elements, such as La, Ce, Nd, Y, Th, Zr, Hf, Nb, Sc, Co and Ti are useful in discriminating provenance and tectonic setting of sedimentary basins because of their relative immobility during sedimentary processes (Bhatia and Crook, 1986; Rollinson, 1993). These elements are present in very low concentrations in sea and river water, are chiefly transported as particulate matter, and reflect the signature of the parent material (Bhatia, 1983; Bhatia and Crook, 1986; Rollinson, 1993).

Triangular Th-Sc-Zr/10 plots by Bhatia and Crook (1986) suggest a passive margin with a minor contribution from a continental arc source for the shales of the Soutpansberg and Tuli Coalfield (Figure 6.38). A majority of sandstones from both coalfields suggests a passive margin with minor active continental margin source (Figure 6.26). Triangular plot of La-Th-Sc, of Bhatia (1983) also suggest a passive margin setting of the depositional basin for the Soutpansberg and Tuli Coalfields (Figure 6.39).

The TiO_2 -Ni diagram of Floyd *et al.* (1989) suggests that the source area for most samples from both coalfields was of an acidic magmatic nature (Figure 5.34). Furthermore, the La/Th versus Hf bivariate (Figure 6.35; Floyd and Leveridge, 1987) and V-Ni-Th*10 (Figure 6.36; Bracciali *et al.*, 2007) ternary diagrams also suggests that the Soutpansberg and Tuli sandstones were derived from felsic source rocks. The result of the trace elements correlates very well with that of the major elements.

6.7. Conclusions

Petrographic and geochemical results of the samples of the Soutpansberg Coalfield suggest uplifted basement source areas dominated by sedimentary rocks and/or granite-gneiss rocks. The source rocks in the eastern Soutpansberg Coalfield might have been the recycled pre-Soutpansberg Karoo Supergroup rocks and the metasedimentary rocks of the Soutpansberg Group. In the western part of the coalfield, the source rocks might have been the Waterberg and Blouberg Groups located at the south of the coalfield. Other source rocks may have been the pre-Beit-Bridge basement rocks (granites and gneisses) located further to the north of the coalfield.

The petrography and geochemistry of the Tuli sandstones in the western, northern and eastern parts of the study area suggest nearby source areas dominantly composed of plutonic (granites) and metamorphic (gneisses and schists) rocks with a component from a sedimentary (quartzarenite, shales, arkoses and metarkoses) rocks. These source areas might have been from adjacent areas which include the Limpopo Belt (metamorphic, plutonic and sedimentary rocks), the recycled pre-Karoo rocks as well as the basement uplifted rocks of the Beit-Bridge Complex (consisting of the granitic-gneisses and schists) at the south and north-east of the coalfield.

Sandstones in the northern Karoo depositional system are sub-arkose to lithic arkose. The study of paleoweathering conditions based on modal composition, chemical index of alteration (CIA), Plagioclase Index of Alteration (PIA) and A-CN-K (Al_2O_3 -CaO + Na₂O-K₂O) relationships indicate that probably chemical weathering in the source area and recycling processes have been more important in shale and sandstone rocks. The relatively high CIA values (70 to 90%) indicates moderate to high weathering conditions of the samples and the palaeoclimate of the source area was probably warm. K₂O/Na₂O versus SiO₂ and Na₂O-CaO-K₂O tectonic setting discrimination plots, suggest a passive continental margin. In the study of trace elements, the ternary plots of Th-Sc-Zr/10 and La-Th-Sc both suggest a passive margin setting of the provenance.

Based on analysis of composition and textural maturity, the Soutpansberg and Tuli sandstone is composed predominately of detritus that was derived from coarse grained, crystalline parent rocks and transported relatively long distances before accumulating in a fluvial depositional setting. The presence of kaolinite in almost all the samples is indicative of intense chemical weathering of the source rock under the influence of probably warm climate. A granitic or gneissic terrane ultimately contributed much of the straight extinction quartz and the K-feldspar grains and such rocks were probably the main sources

CHAPTER 7

GEOPHYSICS OF THE SOUTPANSBERG AND TULI COALFIELDS

Abstract

Geophysical investigations of the Soutpansberg and Tuli Coalfields was undertaken in order to understand the surface lithology, structure and intrusive activity based on enhanced products of the acquired aeromagnetic, gravity and radiometric data, combined with the published geology and satellite imagery. The airborne geophysics which covers the study area comprises three data sets: aeromagnetic, gravity and radiometric data. The magnetic, gravity and radiometric data all correlated well and showed low amplitudes in the sedimentary strata compared to the surrounding and basement geological bodies. The E-N-E fault system has a notable signature, defining two magnetic domains on both southern and northern sides of the Soutpansberg Basin. The W-N-W fault system is also outlined, with its recognizable control on the contact between the Mopane Coalfield and the Beitbridge Complex. The intrusive emplacements are mainly fault-controlled and trend in the same direction as the two fault systems. Jurassic volcanics (Letaba and Jozini Formations) follow a Southwest-Northeast trend, outcropping in the east (Soutpansberg Basin) and producing a strong magnetic response in this area, and partly buried in the west, where magnetic intensity tends to be reduced. Sedimentary units were outlined according to weak, amorphous magnetic signatures and low gravity densities. The units are composed of conglomerate,

sandstone, siltstone, shale and coal which are late Carboniferous to early Permian in age. It is concluded that the shapes and trends of the basins with respect to the faults clearly indicate that the origin of the basins is a result of overstepped divergent directional faults. The fault traces step left, forming areas of tension, where the coalfields were nucleated following the major E-W trending crustal discontinuity. The whole Tuli and Soutpansberg area consists of two easterly tilted sub-basins with half-graben geometry separated by uplifted Archaean (Beit-Bridge Complex) and Proterozoic (Soutpansberg Group) blocks.

7.1. Introduction

Gravity, magnetic and radiometric surveys of various scales can be used to outline the distribution of rock and mineral types, basement trends and hence give information on the overall structure and distribution of the coal-bearing sequence (Ward, 1984).

The main geophysical methods (magnetic, gravity and radiometric methods) based on geological data of the sub-surface were used. The set of data used to process and draw maps came from the extensive geophysical exploration done by the Council for Geoscience (CGS). All the data used in this study is kept in the CGS archives. Based on the geological information and the geological knowledge, including current conceptual geological models and metallogenic models in the study area, the gravitational, magnetic and radiometric data are all used to provide a better understanding of the sub-surface geology of the study sites.

The main aim of the study was to prepare a geological interpretation map of the area outlining lithology, structure and intrusive activity based on enhanced products of the recently acquired aeromagnetic, gravity and radiometric data, combined with the published geology and satellite imagery. The geological interpretation, signatures of the known mineral deposits (coal), in the area were recognised and the areas with similar signatures were compared and defined. From the radiometric data, structures were defined and correlate with those defined by magnetic data. Alteration areas identified based on radiometric anomalies and the corresponding structural and lithological interpretations.

7.2 Methodologies

The gravity, radiometric and magnetic data used in this project were provided by the CGS. The supplied data were in the following formats: ER Mapper Files, ERS Files, Grid Files and line data in XYZ files. Geosoft Oasis Montaj Educational software version 7.2.1 and Arc-View 3.2a was used to process and draw maps. The maps are presented as colour

maps or as hill-shaded versions that better show local variations and lineations by emphasizing the gradients of the anomalies. Some visually observed features are also emphasized on the maps.

7.2.1 Gravity survey

Gravity surveys, measures variations in the Earth’s gravitational field caused by differences in the density of sub-surface rocks. Gravity methods have been used most extensively in the search for heavy metals, oil and gas, particularly during the twentieth century. While such methods are still employed very widely in hydrocarbon exploration, many other applications have been found, some examples of which are: regional geological studies; isostatic compensation determination; exploration for, and mass estimation of mineral deposits; location of buried rock-valleys; shape of the earth (geodesy); and monitoring volcanoes (Reynolds, 1997). Measurements of gravity provide information about densities of rocks underground. The primary goal of studying detailed gravity data is to provide a better understanding of the subsurface rock distribution and geology. There is a wide range in density among rock types, and therefore this makes inferences about the distribution of strata, especially in the mapping of sub-surface lithologies and structures, such as faults (Riva *et al.*, 2009).

Rock gravity densities were used to interpret the maps. The SI unit of density is the kg m⁻³ but the Mg m⁻³ is widely used since the values are, numerically the same. Most crustal rocks have densities of between 2.0 and 2.9 Mg m⁻³. Density ranges for some common rocks are shown in Table 7.1.

Table 7.1: Densities of common rocks (Milsom, 2003).

<i>Material</i>	<i>Density (Mg m⁻³)</i>
Andesite	2.5 - 2.8
Basalt	2.8 - 3.0
Coal	1.1 - 1.4
Diabase	2.6 - 3.0
Diorite	2.8 - 3.0
Dolomite	2.8 - 2.9
Gabbro	2.7 - 3.3

Gneiss	2.6 - 2.9
Granite	2.6 - 2.7
Gypsum	2.3 - 2.8
Limestone	2.3 - 2.7
Marble	2.4 - 2.7
Mica schist	2.5 - 2.9
Peridotite	3.1 - 3.4
Quartzite	2.6 - 2.8
Rhyolite	2.4 - 2.6
Rock salt	2.5 - 2.6
Sandstone	2.2 - 2.8
Shale	2.4 - 2.8
Slate	2.7 - 2.8

7.2.2 Magnetic survey

Magnetic surveys may be useful in delineating igneous bodies containing magnetic signature on surface, such as dykes lava flows and intrusives. They are also used in search of magnetised material and subsurface structures. When a ferrous material is placed within the Earth's magnetic field, it develops an induced magnetic field. The induced field is superimposed on the Earth's field at that location creating a magnetic anomaly. Detection depends on the amount of magnetic material present and its distance from the sensor. The anomalies are typically presented on colour contour maps (Riva *et al.*, 2009). Where the rocks have high magnetic susceptibility the local magnetic field will be strong; where they have low magnetic susceptibility it will be weaker in magnetism. Deposits with magnetic minerals, for example iron, pyrrhotite bearing nickel, and skarn metal ores can be detected

directly. Magnetic surveying can be used as an aid to geological mapping; units with higher susceptibility will show up as areas of high magnetic strength field and vice versa.

Magnetic susceptibility

The susceptibility of a rock usually depends on its magnetite content. Sediments and felsic igneous rocks have weaker susceptibilities whereas mafic igneous rocks, such as basalt, dolerite, gabbro and metamorphic serpentinite are usually strongly magnetic (Milsom, 2003). Weathering generally reduces susceptibility because magnetite is oxidized to hematite, but some laterites are magnetic because of the presence of magnetite and magnetized hematite. A body placed in a magnetic field acquires a magnetization which, if small, is proportional to the field (Milsom, 2003):

$$M = kH$$

Where: **M** is the magnetic dipole moment per unit volume; **H** is the magnetic field, and **k** is the magnetic susceptibility in SI units.

The *susceptibility*, *k*, is very small for most natural materials, and may be either negative (diamagnetism) or positive (paramagnetism). The susceptibilities, in rationalized SI units, of some common rocks and minerals are given in Table 7.2 (Milsom, 2003).

Table 7.2: Magnetic susceptibilities of common rocks and ores (Milsom, 2003).

<i>Material</i>	<i>Susc. x 10³</i> <i>(SI)</i> *
Air	~0
Quartz	-0.01
Rock Salt	-0.01
Sphalerite	0.4
Pyrite	0.05 - 5

Hematite	0.5 - 35
Ilmenite	300 - 3500
Magnetite	1200 - 19,200
Limestone	0 - 3
Sandstones	0 - 20
Shales	0.01 - 15
Schist	0.3 - 3
Gneiss	0.1 - 25
Slate	0 - 35
Granite	0 - 50
Gabbro	1 - 90
Basalt	0.2 - 175
Peridotite	90 - 200

7.2.3 Radiometric survey

Radiometric surveys are often used for geological mapping because the radioactive elements occur in greater abundance in felsic igneous rocks, such as granite. The presence of radioactive elements can be determined by the Geiger counter. The instrument measures the energy released during the process of radioactive decay. As a uranium molecule decays, for instance, three kinds of rays are given off: alpha, beta and gamma rays. Of these, the alpha and beta rays can only travel short distance, while gamma ray is the most penetrating and is therefore the most likely to be detected by the Geiger counter. Gamma rays can distinguish between radiation from the three main radioactive elements that occur in nature - uranium,

potassium, and thorium by measuring the energy of the radiation (Reynolds, 1997). The primary goal of studying the gravity, magnetic and radiometric surveys is to provide a better understanding of the subsurface geology.

Radiometrics

The radiometric interpretation was focused on outlining structures and contacts and on the delineation of radiometric signatures in areas defined as anomalous. The images were designed to show intensities distribution of the elements Uranium (U), Thorium (Th) and Potassium (K) %. Table 7.3 shows concentrations of the elements in different rocks and minerals.

Table 7.3: Concentration and ratios of U, Th and K in some rocks and minerals (Musset and Khan, 2000).

<i>Rock or mineral</i>	<i>Concentration of element, ppm (parts per million)</i>			
	<i>Uranium (U)</i>	<i>Thorium (Th)</i>	<i>Potassium (K)</i>	<i>Ratio of U/Th</i>
Sedimentary				
limestone	2	2	3000	1.6
Sandstone	2	11	27000	0.35
Shale	4	12	25000	0.27
Igneous and metamorphic				
Andesite	2	6	25000	0.3
Basalt	1	3	10000	0.28
Gabbro	0.05	0.15	800	0.33
Granite	4	25	40000	0.25
Pegmatite	10-100			
Schist	3	11	27000	0.35
Ultramafic	0.001	0.004	30	0.26

7.3. Results

Geological models based on gravitational and magnetic data inversion are constructed to better understand geological structures and are used for mineral exploration. The maps are

presented as colour maps or as hill-shaded versions that better show local variations and lineations by emphasizing the gradients of the anomalies.

The major shear zones and faults are shown in Chapter 4 (Figure 4.2) and this chapter (Figure 7.1). The magnetic anomaly map (Figure 7.2) reveals a complex structural framework in the Soutpansberg and Tuli area. The magnetic pattern of the two basins comprises a zone of NE-SW trending. The red to purple colours denotes areas of high magnetic susceptibilities whereas the green to yellow colours denotes moderate magnetic susceptibilities. The blue colour denotes areas of low magnetic susceptibility (Figure 7.2). Anomalies (A and B) with high magnetic susceptibility are present at the southern boundary of the Soutpansberg Coalfield and represent a long linear anomaly zone. The lineaments (indicated with arrows in Figure 7.2) probably represent hill ranges and ridges. They trend SW-NE and separated by faults (Klein Tshipise Fault) with the Karoo sedimentary basin (Figures 4.2, 7.1 and 7.2). This lineament represents the Mabiligwe and Nzhelele Formations of the Soutpansberg Group and composed of quartzites, basalts and sandstone. These lineaments parallel the Palala Shear Zone.

The Karoo sedimentary deposits are depicted by the blue to green colour (low magnetic susceptibilities). Inside the Karoo deposits (black borders), anomalies 1, 2, 3 and 4 represent the Karoo volcanics which are highly magnetised and composed of rhyolites and basalts (Figure 7.2). North of the Soutpansberg Basin is the highly magnetised Beit-Bridge Complex composed of calc-silicate rocks, gneiss, magnetites, metapelites and metaquartzites. The complex and the Soutpansberg sedimentary deposits is separated by the Bosbokpoort Fault which trends SW-NE (Figures 4.2, 7.1 and 7.2).

The gravity pattern of the two coalfields also corresponds well with the magnetic data forming NE-SW-trending basins (Figure 7.3). The sediment fill of the coalfields has low densities and is depicted by the green to yellow colours whereas the Soutpansberg and Waterberg Groups have high densities and are represented by yellow to red colours (Figure 7.3). In general, the grid density of magnetic data is higher, than that of gravity data and they are more sensitive to shallow sources, thus being more useful for local-scale mapping compared to gravity data.

In general, the radiometric data are noisy and strongly dampened by overburden, especially in wetland areas; over lakes, radiometric anomalies cannot be detected at all. However, apparently due to the relatively dry overburden in the Limpopo Province, the data appear to be of high quality and useful for regional-scale interpretation and lithological

classification. The radiometric data measured in the area consist of 3+1 components: Potassium (K), Thorium (Th), Uranium (U) and Total counts (Tc).



Figure 7.1: Satellite image of the Tuli and Soutpansberg Basins (Google Earth).

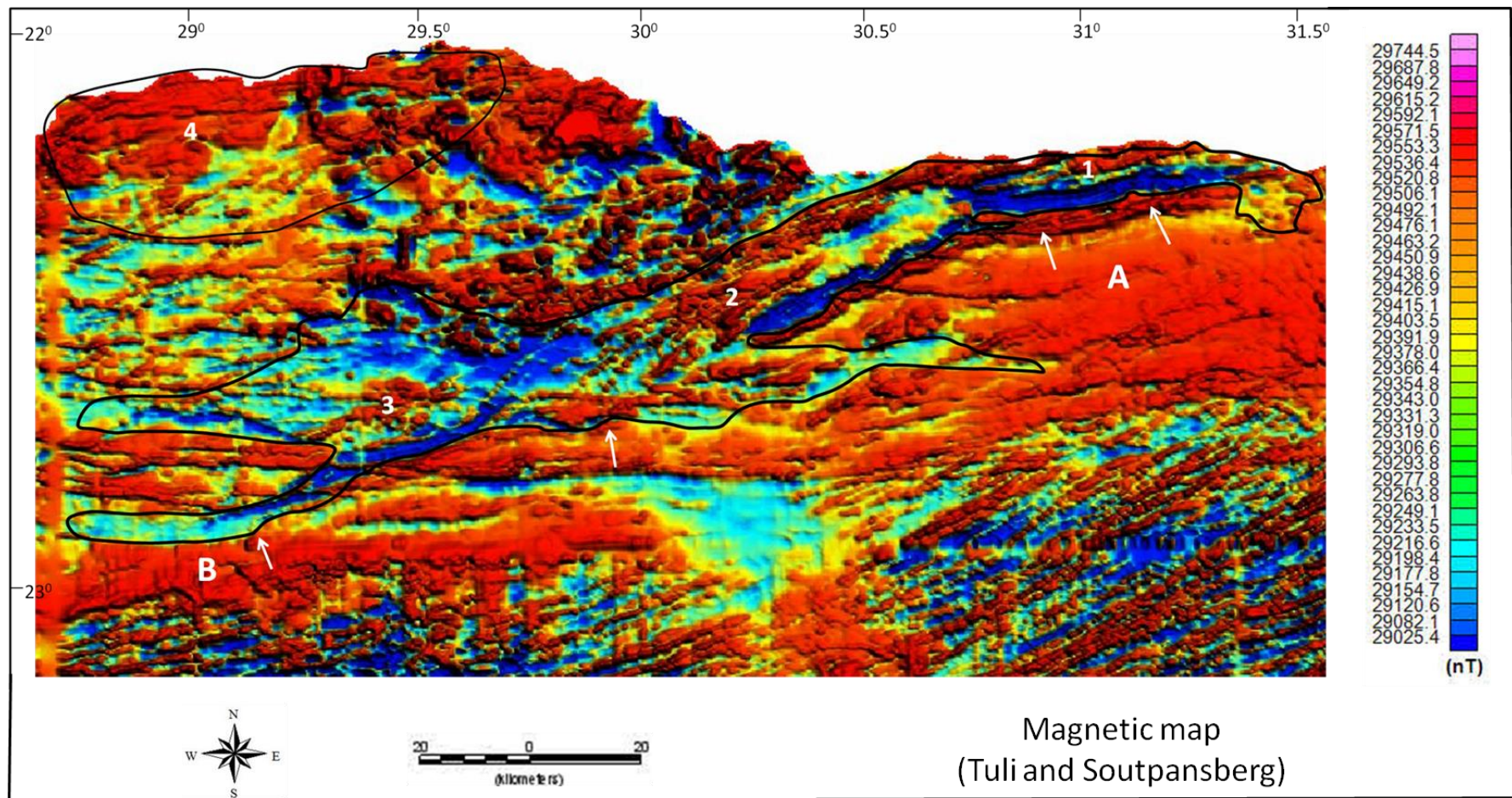


Figure 7.2: Magnetic map of the Tuli and Soutpansberg Basins. Anomalies: A; Soutpansberg Group, B; Waterberg and Blouberg Mountain Groups, 1, 2, 3 and 4; Karoo volcanics (Jozini and Letaba Formations).

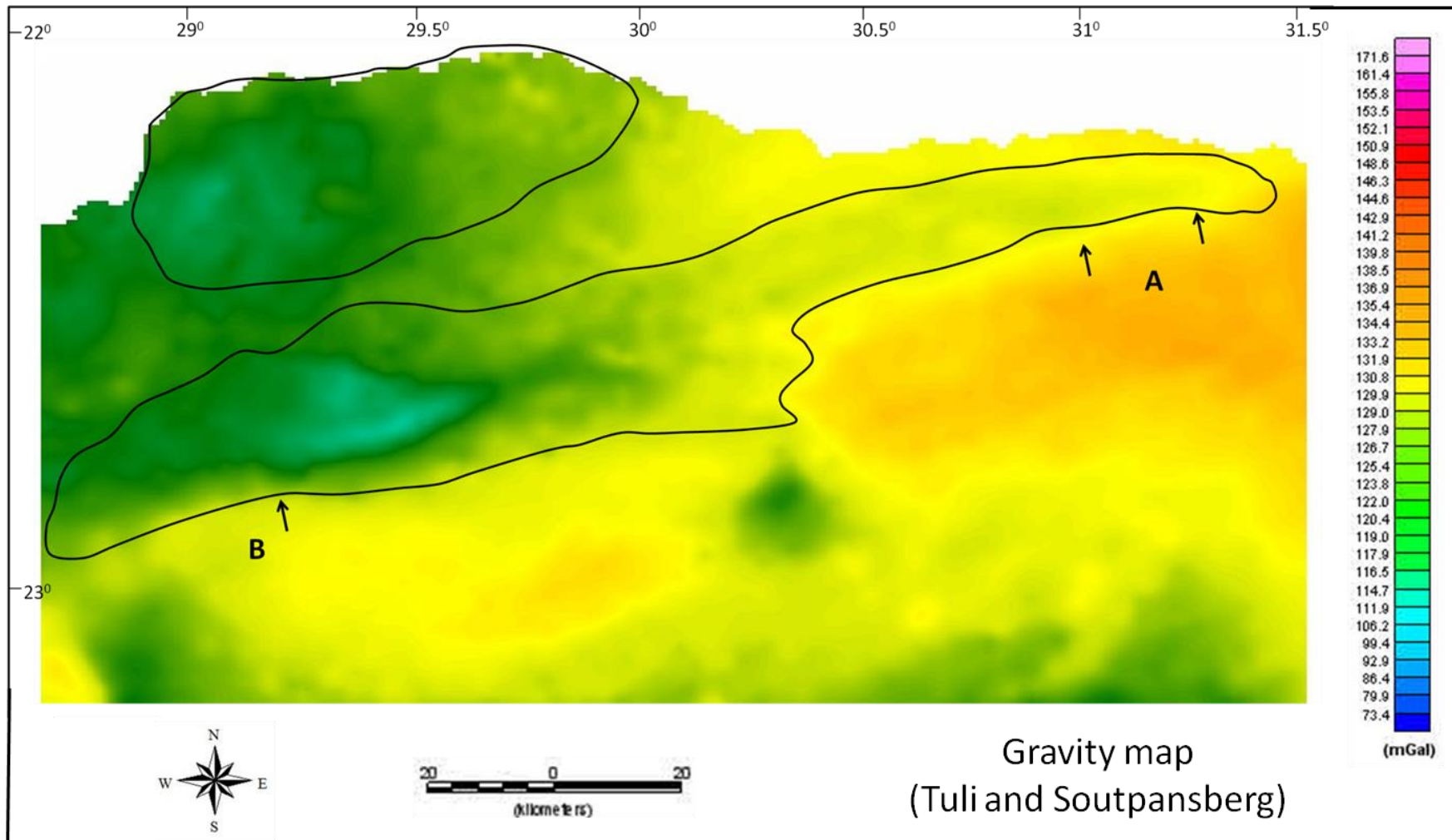


Figure 7.3: Gravity map of the Tuli and Soutpansberg Basins. Anomalies (A and B) are discussed in more detail in the text.

7.4. Soutpansberg Basin

7.4.1. Gravity Data and Maps

The gravity map is given in Figure 7.4. From the map it can be seen that the mafic Soutpansberg Group rocks (B) and the Beit-Bridge Complex rocks (C) are correlated with gravity highs. The gentle flanks of the anomalies also suggest that these rocks are dipping below the lighter sedimentary cover (A, Soutpansberg Sedimentary Basin). The gravity highs south of (B) in purple colour probably represents the mafic igneous rock (such as basalts) of the Lebombo Group.

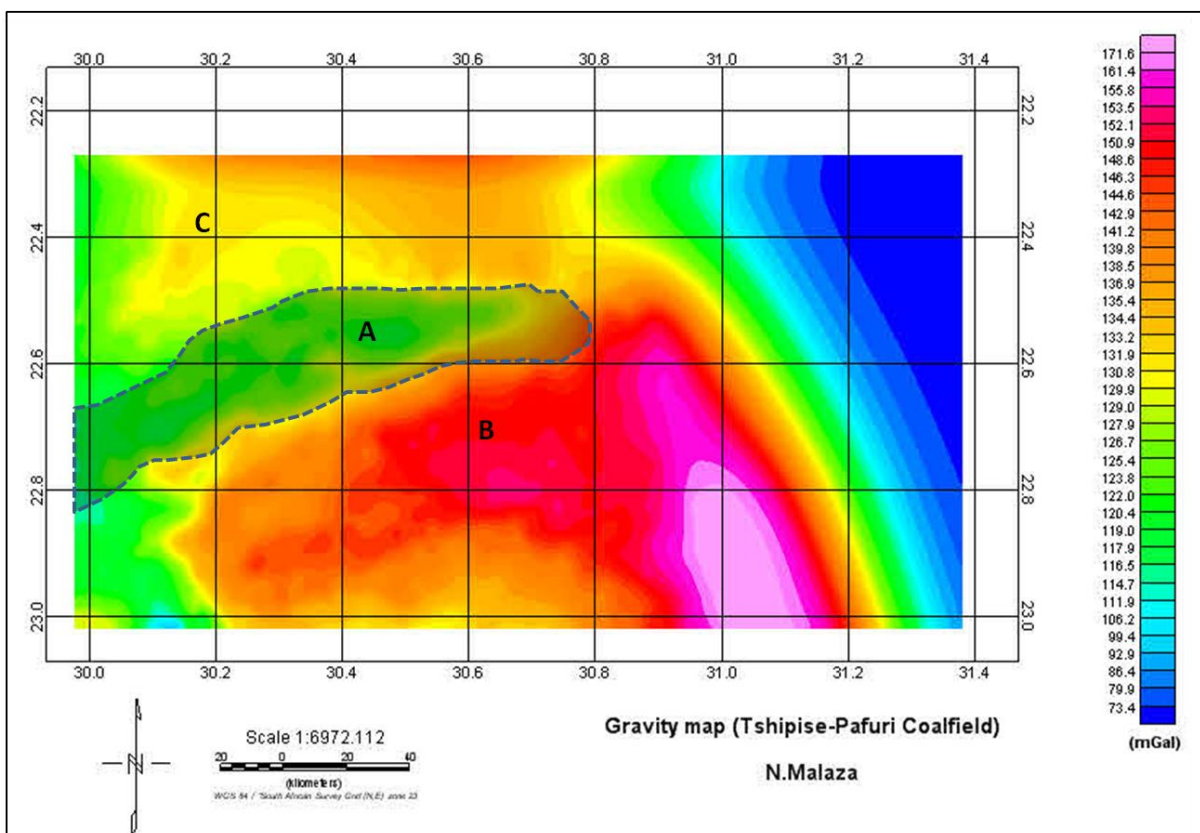


Figure 7.4: Gravity map of the Soutpansberg Basin (A).

7.4.2 Magnetic Data and Maps

7.4.2.1. Tshipise-Pafuri Basin (Eastern Soutpansberg)

A NE-SW trending, magnetic lineament pattern occurs from west to east on the map (Figure 7.5). Two long linear anomaly zones are observed. The Bosbokpoort Fault (1) in the north separates the basin from the Beit-Bridge Complex and the Klein Tshipise Fault (2) in the south separates the basin from the Soutpansberg Group. The Karoo sub-basin is characterised by low magnetic susceptibilities (green to blue colours) compared to the bordering anomalies. This map clearly demonstrates that the strongly folded, more magnetic anomalies (1) and (2) are distinct borders separating the low-anomaly sedimentary basin in (A).

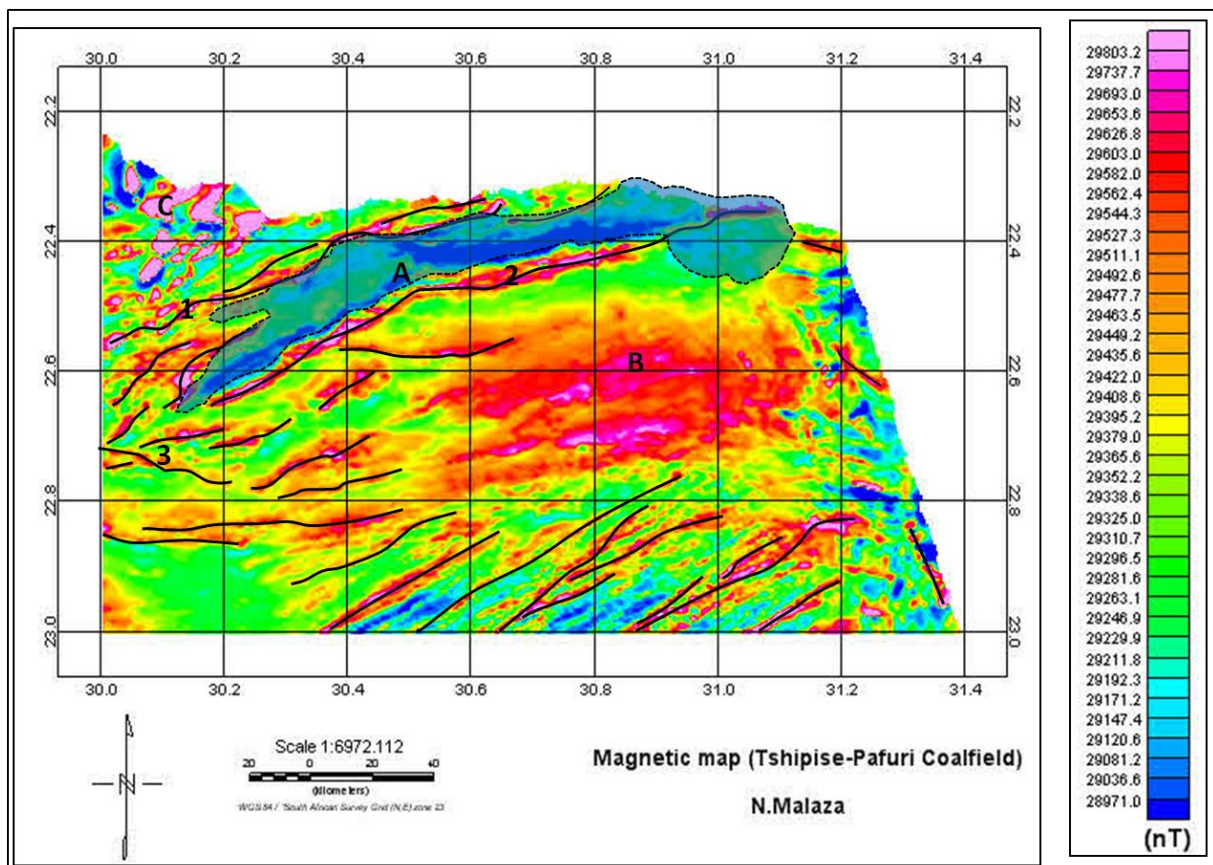


Figure 7.5: Magnetic anomaly map of the Tshipise-Pafuri Basin (A) with major magnetic lineaments (1, Bosbokpoort Fault, 2, Klein Tshipise; 3, Siloam). (B) Soutpansberg Group, (C) Beit-Bridge Complex.

7.4.2.2. Mopane Basin (Werstern Soutpansberg)

The magnetic map is given in Figure 7.6. From the maps it can be seen that the mafic Beit-Bridge Complex rocks (B) and the Waterberg Group rocks (C) are correlated with high magnetic susceptibilities. The Karoo basin fill is depicted by low magnetic susceptibilities (blue to green colour). The magnetic map indicates that there are short linear anomalies (yellow to red in colour) inside the basin (A) which may be due to dolerite intrusives and Karoo volcanics (basalts).

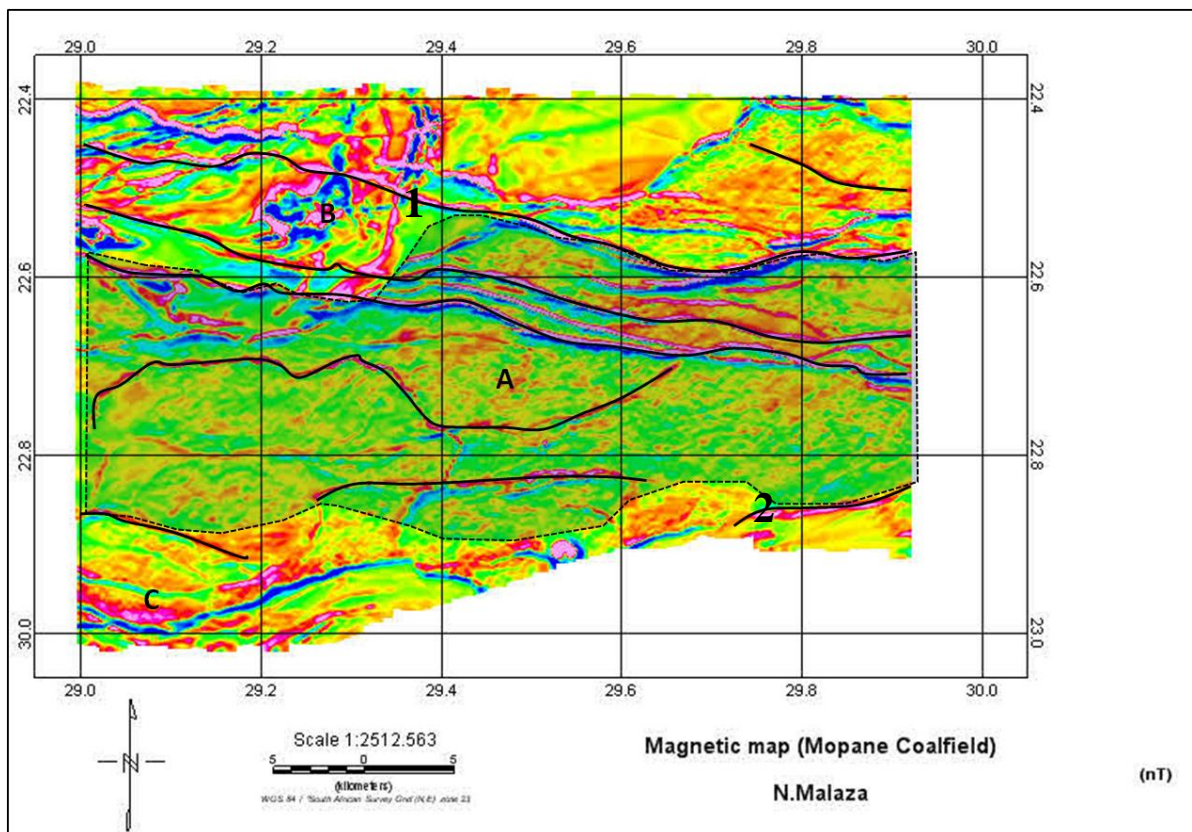


Figure 7.6: Magnetic anomaly map of the Mopane Basin (A) with major magnetic lineaments (1, Siloam Fault, 2, Melinda Fault). (B) Beit-Bridge Complex (C) Waterberg Group.

7.4.3. Radiometric Data and Maps

7.4.3.1. Mopane Basin (Werstern Soutpansberg)

In Figures 7.7, 7.8 and 7.9, the radiometric maps of Thorium (Th), Uranium (U) and Potassium (K) are presented. It can be seen that the Archaean rocks of the Beit-Bridge Complex (A) in the north-west corner of the maps are very anomalous (Figures 7.7 and 7.8). The Waterberg Group (B) in the south-west is also characterised by high Th, U and K levels. In the Karoo rocks both the Th and U counts are low (Figures 7.7 and 7.8). The potassium radiation is especially highly increased in the Karoo rocks (Figure 7.9). This may be due to the abundance of K-Feldspar in sandstone. The basin (Karoo strata) is characterised by low U and Th counts, whereas K is highly enriched in the east of the basin (Figure 7.9).

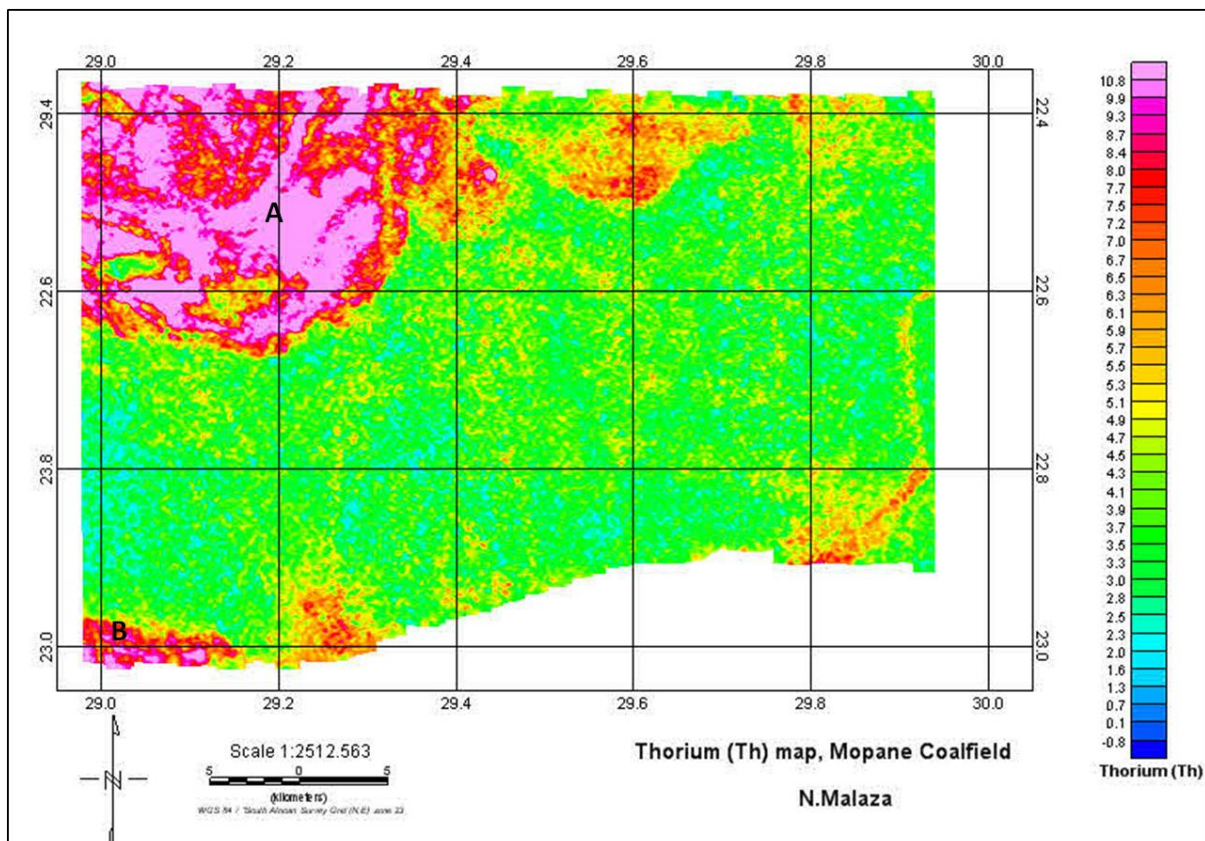


Figure 7.7: Thorium (Th) map of the Mopane Basin. Red: high radiation level; green- blue: low radiation level.

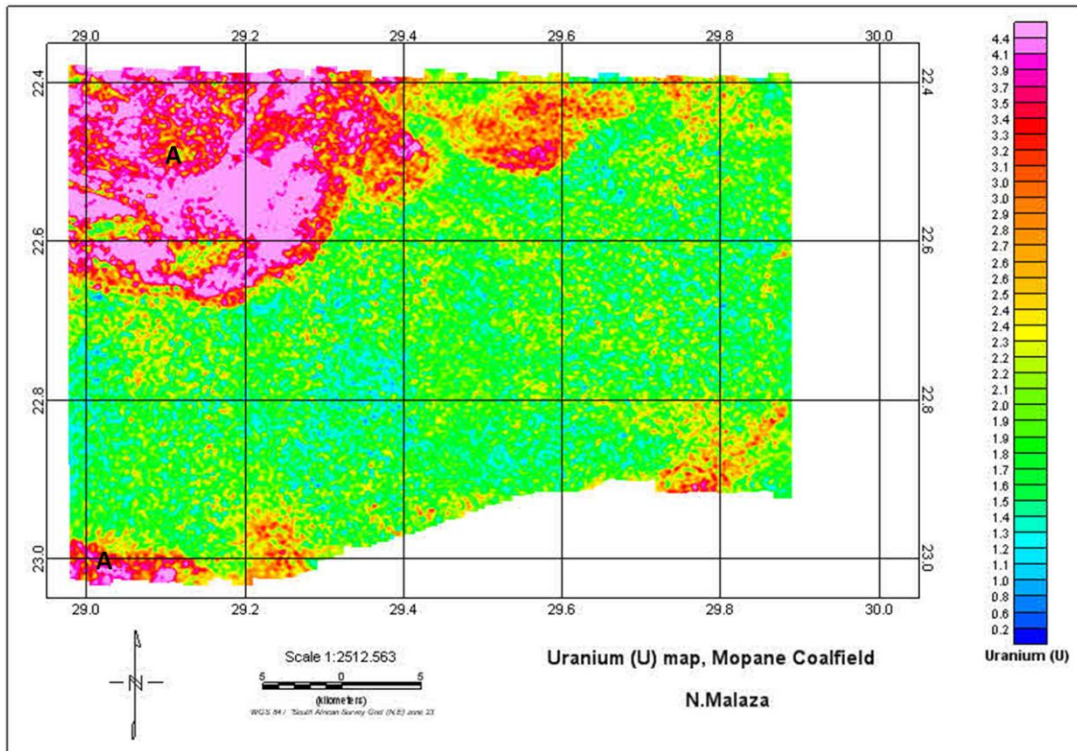


Figure 7.8: Uranium (U) map of the Mopane Basin. Red: high radiation level; green-blue: low radiation level.

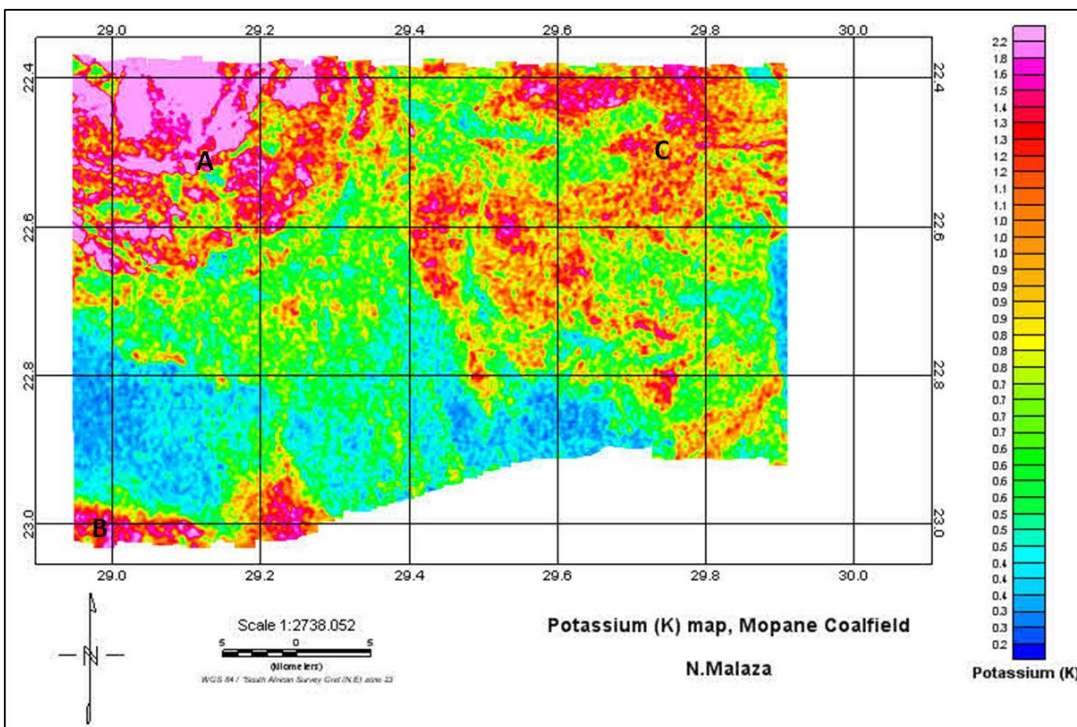


Figure 7.9: Potassium (K) map of the Mopane Basin. Red: high radiation level; green-blue: low radiation level.

7.5. Tuli Basin

7.5.1. Magnetic Data and Maps

The magnetic map of the Tuli Basin is given in Figure 7.10. From the maps it can be seen that the mafic Beit-Bridge Complex rocks (C) is characterised by high magnetic susceptibilities. The mafic Karoo rocks of the Clarens Formation (Tshipise and the Red Rock Members) (B) are also depicted by high magnetic susceptibilities. This may be due to the presence of magnetised hematite present in the sandstone. The Red Rocks Member is characterised by red sandstone. The map also indicates that there are small circular anomalies inside the basin which may be due to dolerite intrusives and Karoo volcanics (basalts).

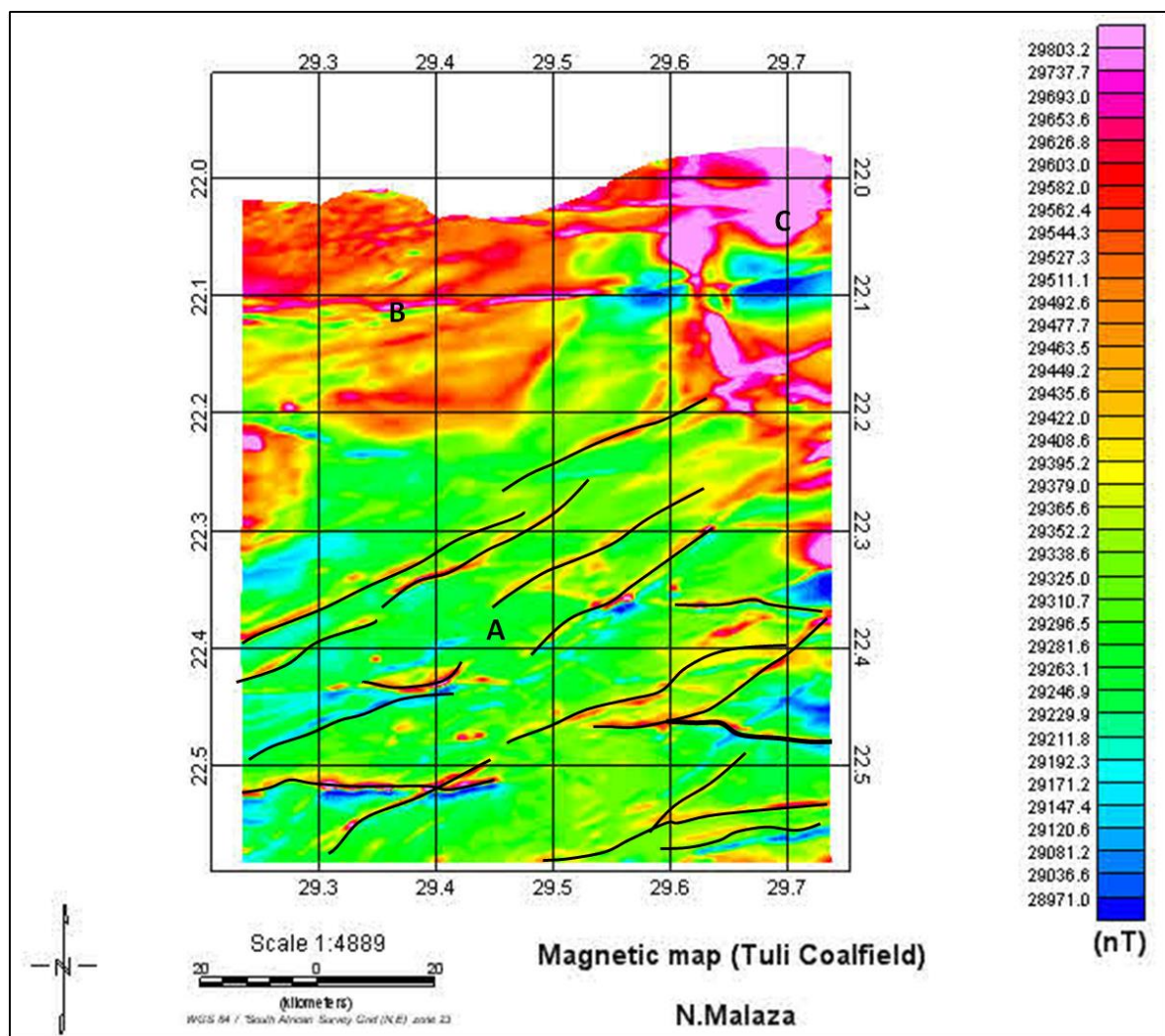


Figure 7.10: Magnetic anomaly map of the Tuli Basin (A) with major magnetic lineaments. (B) Mafic Karoo rocks of the Clarens Formation and (C) Beit-Bridge Complex.

7.5.2. Radiometric Data and Maps

The radiometric data measured in the area consist of 3+1 components: Potassium (K), Thorium (Th), Uranium (U) and Total radiation counts (Tc). In Figures 7.11, 7.12, 7.13 and 7.14 the radiometric maps of Th, U, K and Tc are presented. It can be seen that particularly the Archaean Beit-Bridge Complex in the south of the maps is highly anomalous. Moreover, the rocks of the Karoo strata are connected with low radiometric anomalies (blue to green colour). It is interesting to note that the radiation of the maps is especially highly increased in the Limpopo River beds (arrows). This may be due to mica containing clay-rich rocks.

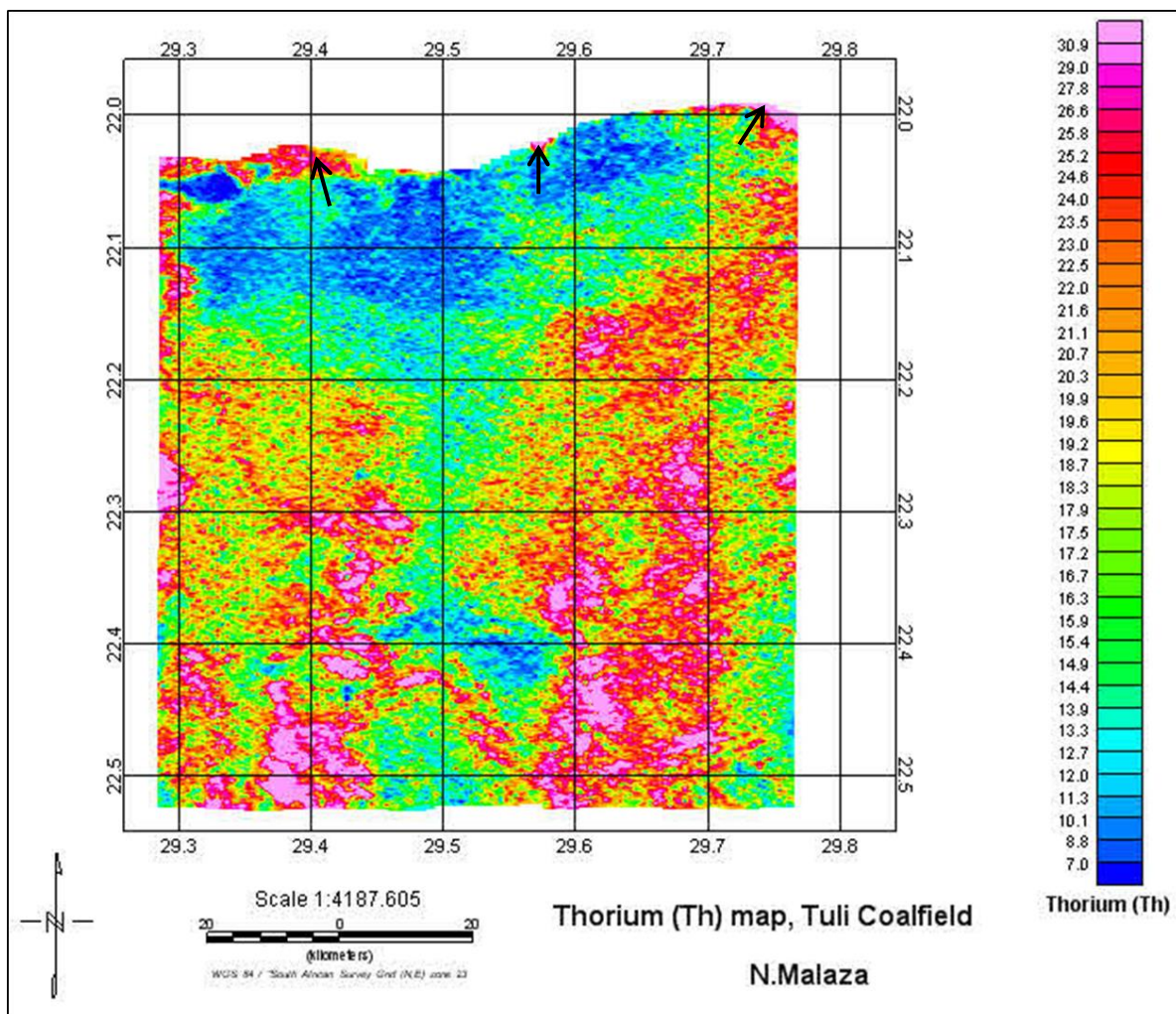


Figure 7.11: Thorium (Th) map of the Tuli Coalfield. Red: high radiation level; blue-green: low radiation level. The arrows indicate high radiation along the Limpopo River beds; this may be due to mica containing clay-rich rocks.

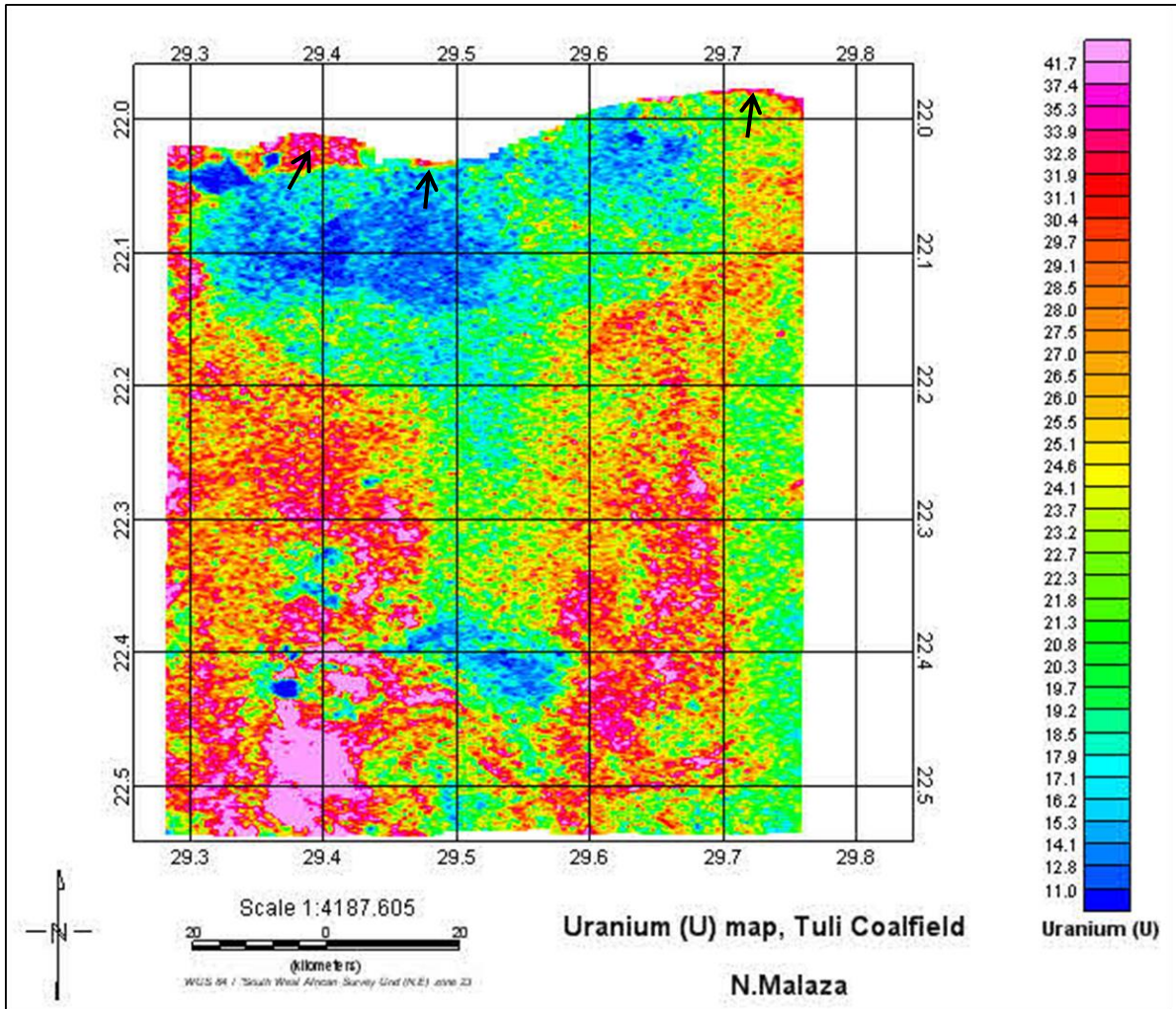


Figure 7.12: Uranium (U) map of the Tuli Coalfield. Red: high radiation level; blue-green: low radiation level. The arrows indicate high radiation along the Limpopo River beds; this may be due to mica containing clay-rich rocks.

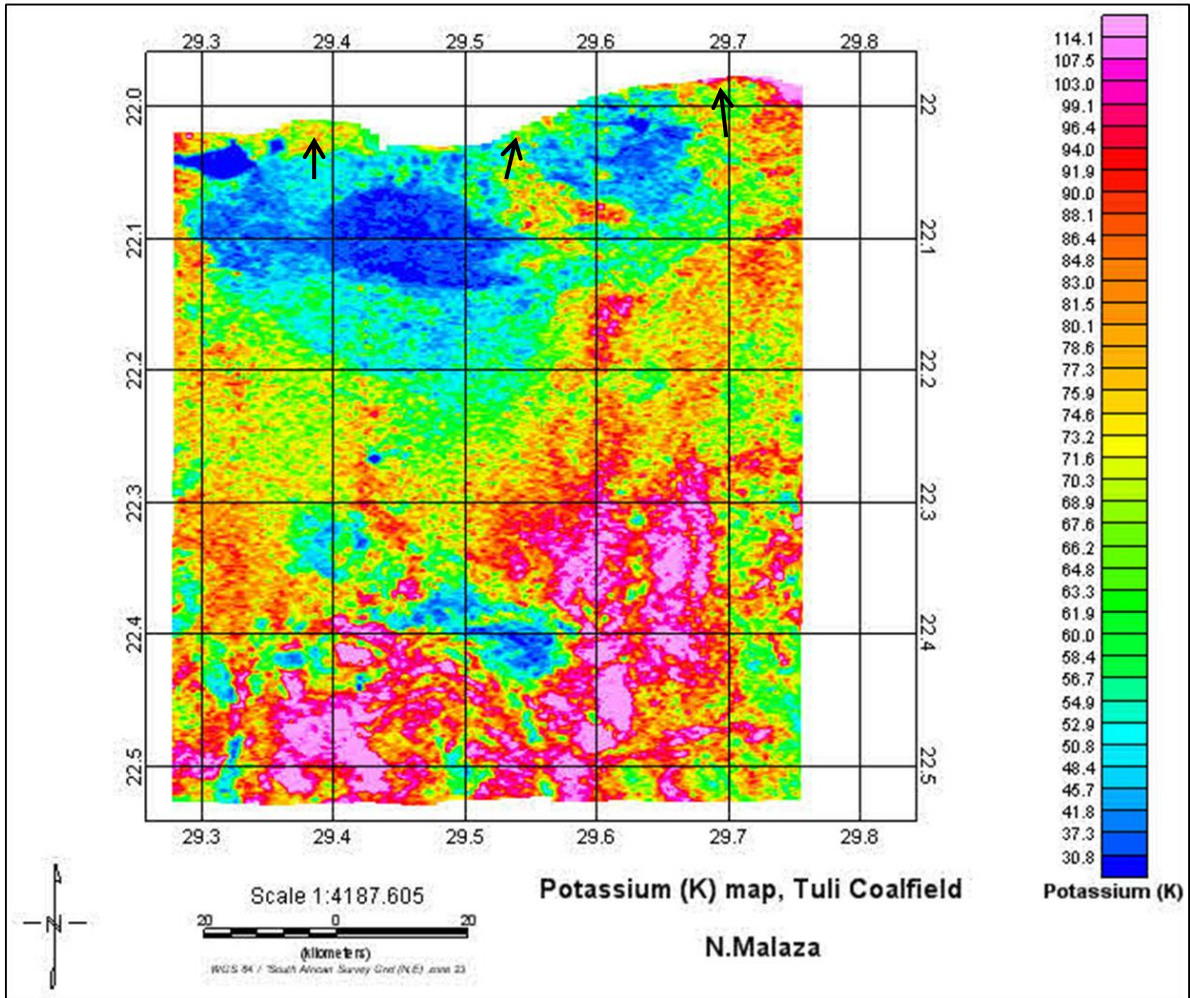


Figure 7.13: Potassium (K) map of the Tuli Coalfield. Red: high radiation level; blue-green: low radiation level. The arrows indicate high radiation along the Limpopo River beds; this may be due to mica containing clay-rich rocks.

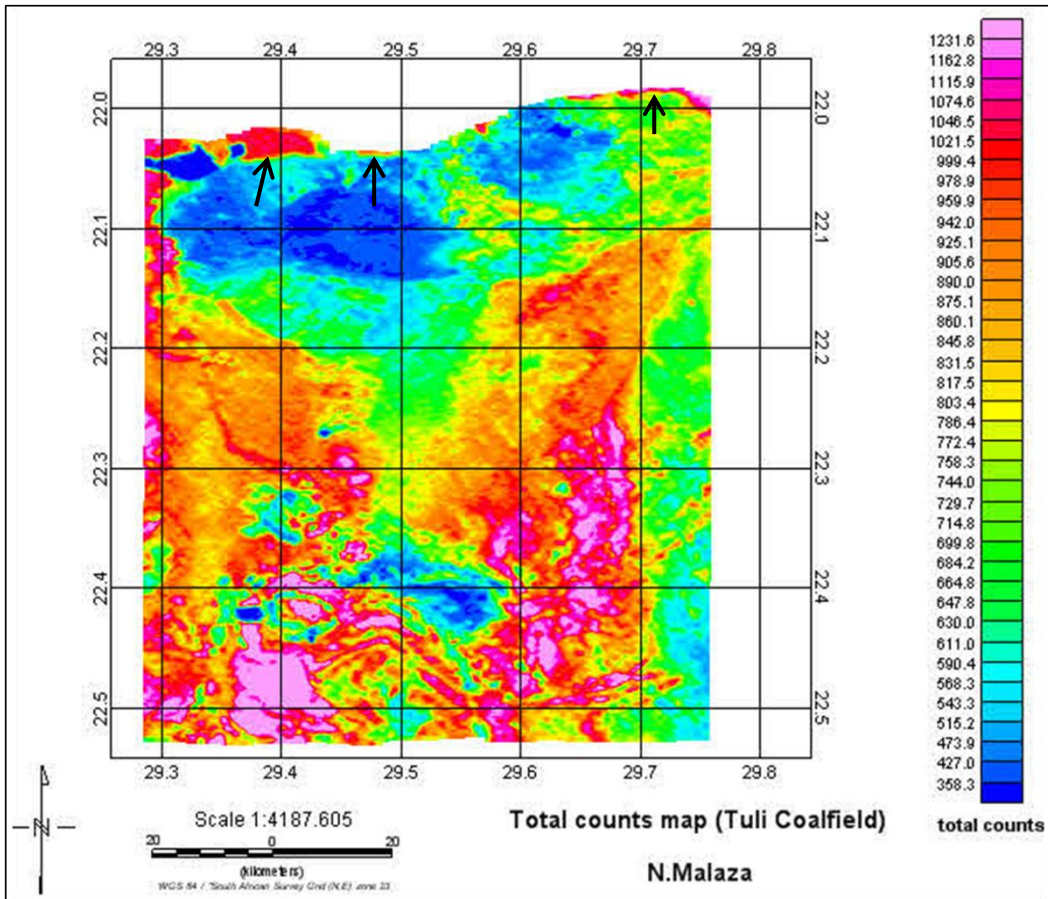


Figure 7.14: Total counts (Tc) map of the Tuli Coalfield. Red: high radiation level; blue-green: low radiation level. The arrows indicate high radiation along the Limpopo River beds; this may be due to mica containing clay-rich rocks.

7.6 Discussions

The study of geophysical techniques has revealed the structural and tectonic settings of the two basins. The geological evolution of the Karoo strata in the Tuli and Soutpansberg Basins, since the Upper Carboniferous, follows the type model for passive continental margin terrain. Both the basins are characterised by normal faults trending north-northeast in the Soutpansberg and east-northeast in the Tuli Basin. The basins are characterised by half-graben geometry and is directly controlled by the deformation (displacement) field surrounding the boundary fault system.

7.6.1. Tectonic implications

The comparison of local and regional basement elements with tectonostratigraphic aspects of the Tuli and Soutpansberg Basins, using aeromagnetic, gravity, and radiometric data, as well as structural features of the basement, suggests a complex geodynamic scenario. Both deep and shallow structural effects in the adjoining basin area are recorded. Initial analysis has determined the gamma ray and geopotential field signatures of key features, such as compositional variations in crustal blocks and regional fault patterns. Next, the role of regional deep shear zones, such as the Palala and Tshipise shear zones were investigated to access insights into the whole basin geodynamic evolution.

In the surrounding basement, the consistent geographic association of gravity and magnetic anomalies are best explained by a crustal source. The Mokolian terrains adjoining the Soutpansberg Basin in the south consist of metasedimentary rocks and intensively intruded by diabase (Figure 7.4). To the north, the basin is adjoined by the Archaean granite and gneiss of the Beit-Bridge Complex. Both gravity and magnetic maps (Figures 7.4 and 7.5) have high amplitude of positive anomalies in this area, reflecting the wide variation in rock physical properties. The Tuli Basin is adjoined by the Beit-Bridge Complex in the south. All geophysical data have strong NE-SW to E-W trending, which mimics the orientation of the major tectonic features of the rift border (i.e. the Limpopo Mobile Belt).

The shapes and trends of the basins with respect to the faults (Figure 7.15) clearly indicate that the origin of the basins is a result of overstepped divergent directional faults. The fault traces step left, forming areas of tension, where the coalfields were nucleated following the major E-W trending crustal discontinuity (Figure 7.15). The whole Tuli and Soutpansberg area consists of two easterly tilted sub-basins with half-graben geometry separated by uplifted Archaean (Beit-Bridge Complex) and Proterozoic (Soutpansberg Group) blocks.

The upper levels of the basement are considered to have a structure based on crustal blocks bounded by faults with varying depths of penetration, as is reflected both on gravity and magnetic anomaly maps (Figures 7.4 and 7.5). Some of these faults are confined to the upper levels of the crust, whereas others reach the mantle. Anomalies representing this NE-SW oriented directions change gradually to an E-W direction, with the amplitude of transcurrent displacements ranging from slight dislocations to dozens of kilometers (Figures 7.15 and 7.16).

Crustal extension during the period of rift climax resulted in progressive uplift of the central block, separating the whole Soutpansberg Basin into half-grabens and generating subsidiary internal NW-SE trending faults inside the eastern sub-basin and NNW-SSE oriented faults in the western area, both of which acted as release faults governed by the reactivation of the underlying basement fabric. Major release faults were formed over marginal strike ramps, which controlled the Soutpansberg Basin (Figures 7.17 and 7.18). Release faults form where cross faults associated with individual normal faults die out within the hanging wall before connecting to other normal faults, and have predominantly vertical displacements (Figure 7.18). The major fault bordering Soutpansberg Basin to the north coincides with a releasing bend of the Tshipise shear zone, enabling graben formation.

In general, the radiometric data are noisy and strongly dampened by overburden. It can be seen that particularly the Archaean-Proterozoic rocks of the Beit-Bridge Complex south of the Tuli and north of the Soutpansberg Basins are very anomalous. Moreover, the rocks of the Karoo group are less anomalous. It is interesting to note that the radiometric data radiation is especially highly increased in the banks of the Limpopo River (this may be due to mica containing clays).

The magnetic pattern of the two coalfields (Figure 7.2) comprises a zone of NE-SW trending. The Karoo depositional system is denoted by medium to low magnetic susceptibilities. This is due to the fact that sedimentary rocks have low magnetic susceptibilities compared to igneous and metamorphic rocks. Areas with high magnetic susceptibilities in the Karoo basins denote Jurassic volcanic intrusives (Letaba and Jozini Formations). Most neighbouring geological bodies have high magnetic susceptibilities (e.g. Beit-Bridge Complex and Soutpansberg Group).

7.6.2 Lithologic units identification

The combination of gravimetric, magnetic and radiometric maps is useful for detecting major lithological and structural variations. In a lithological sense the most persistent low values are observed in association with the Karoo rocks, a trend distinguishable at all frequencies. High apparent resistivities are seen over a range of lithologies but are especially perceptible for the granitic rocks of the Beit-Bridge Complex and the metasedimentary rocks of the Soutpansberg Group.

Overlying the Cambrian Beit-Bridge Complex and the Proterozoic Soutpansberg Group is the late Carboniferous and early Permian Karoo succession comprising: (i) an early Pennsylvanian fluvio-glacial Tshidzi Formation comprising of diamictite and minor sandstone; (ii) a late Pennsylvanian to Middle Permian fluvial deposit with sandstone units and coal measures (Madzaringwe and Mikambeni Formations) ; and (iii) an early Triassic to late Triassic fluvial deposits composed of sandstone and shale units (Fripp, Solitude, Klopperfontein, Bosbokpoort and Clarens Formations); (iv) and lastly the Letaba and Lebombo Jurassic basalts (Please refer to Chapter 10, Figures 10.5, 10.6, 10.8, 10.10 and 10.11).

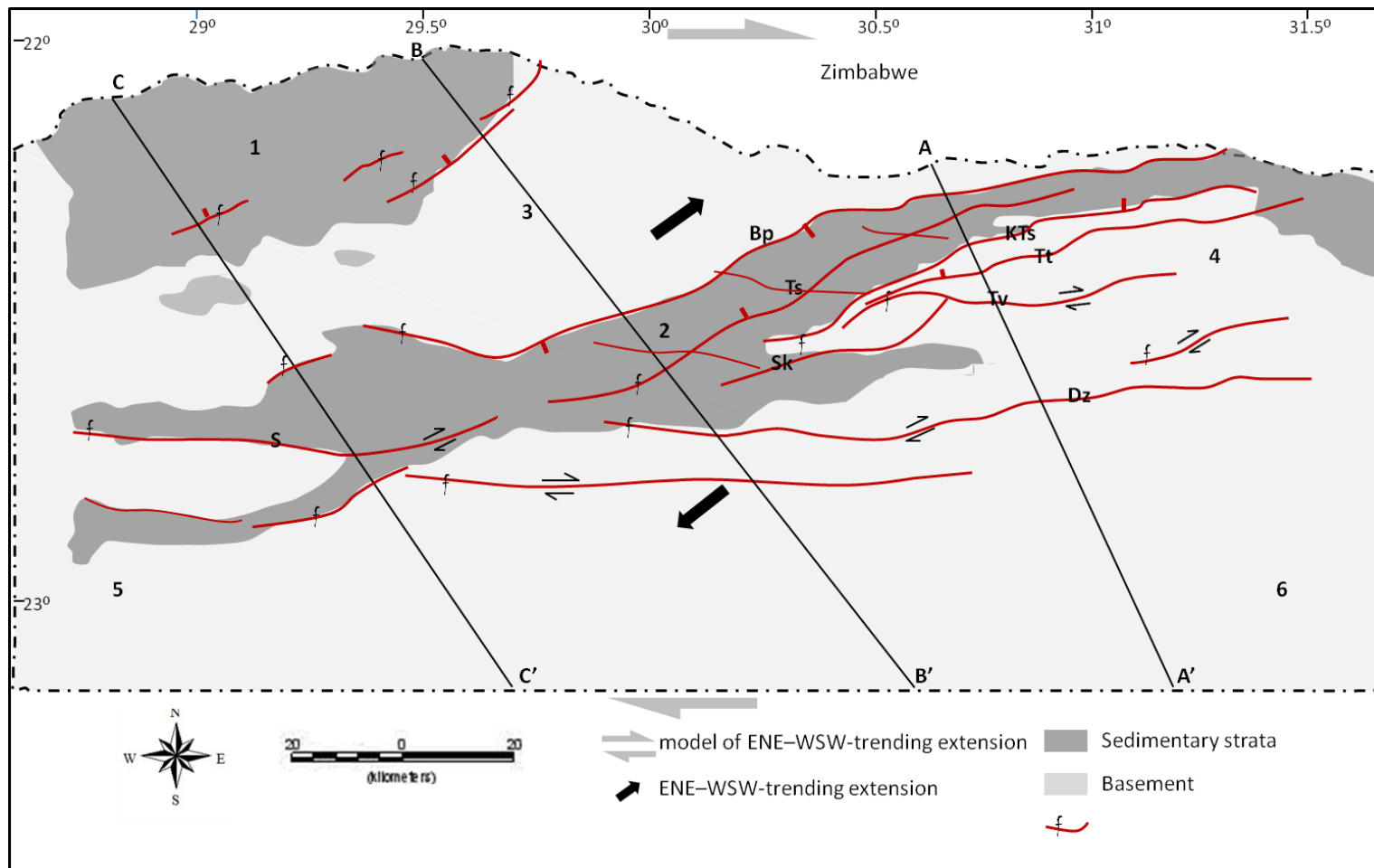


Figure 7.15: Tectonic setting of the Tuli and Soutpansberg Basins. (1) Tuli Basin; (2) Soutpansberg Basin; (3) Beit-Bridge Complex; (4) Soutpansberg Group; (5) Blouberg Group; (6) Archaean granite and gneiss; (Bp) Bosbokpoort Fault; (Ts) Tshipise Fault; (KTs) Klein Tshipise Fault; (S) Siloam Fault; (Tt) Tshamatsha Fault; (Tv) Tshamavhudzi Fault; (Dz) Dzundwini Fault; (Sk) Shakadza Fault.

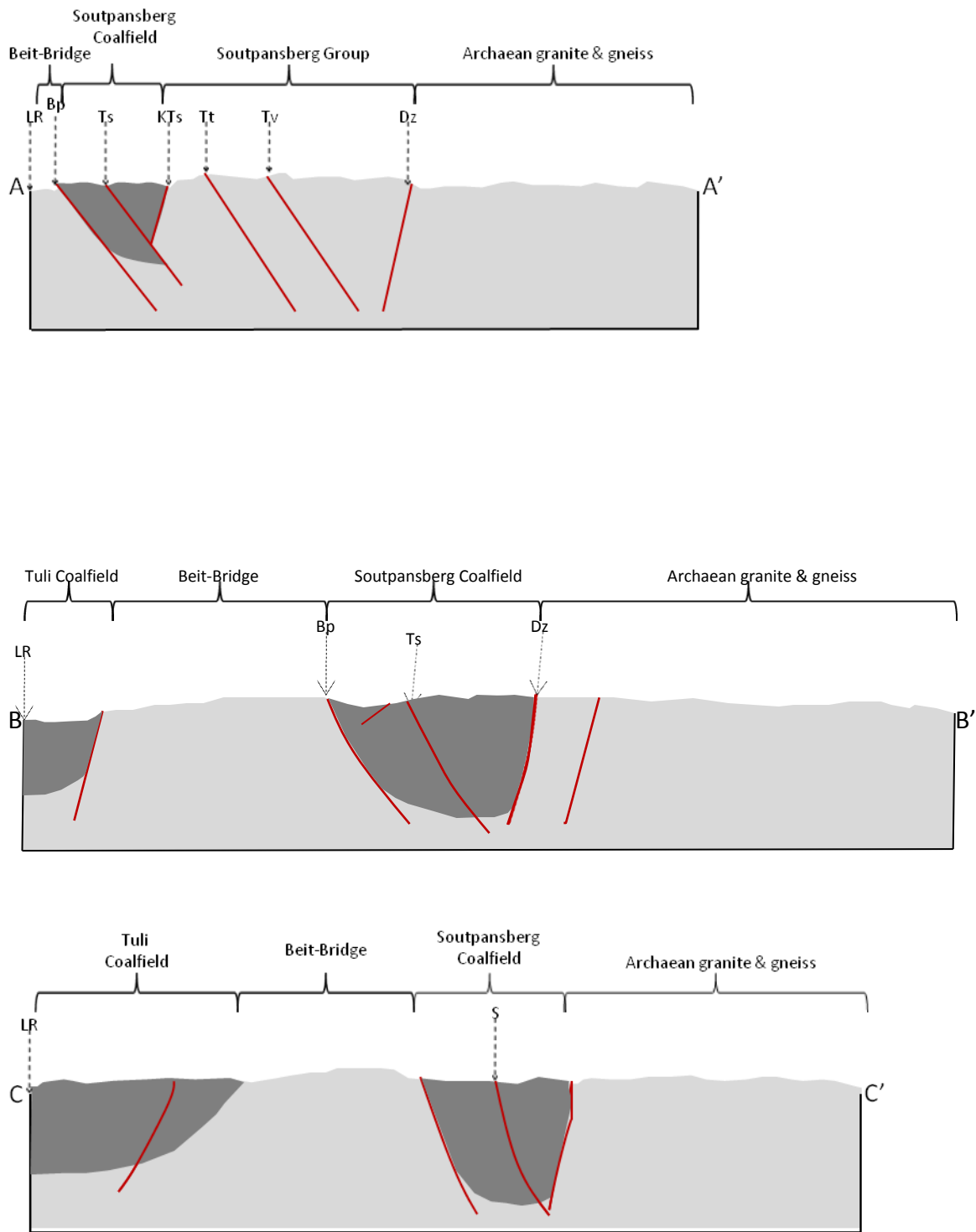


Figure 7.16: Cross-sections of the Tuli and Soutpansberg Basins showing major structures (See Figure 7.15). (LR) Limpopo River; Bp) Bosbokpoort Fault; (Ts) Tshipise Fault; (KTs) Klein Tshipise Fault; (S) Siloam Fault; (Tt) Tshamatsha Fault; (Tv) Tshamavhudzi Fault; (Dz) Dzundwini Fault.

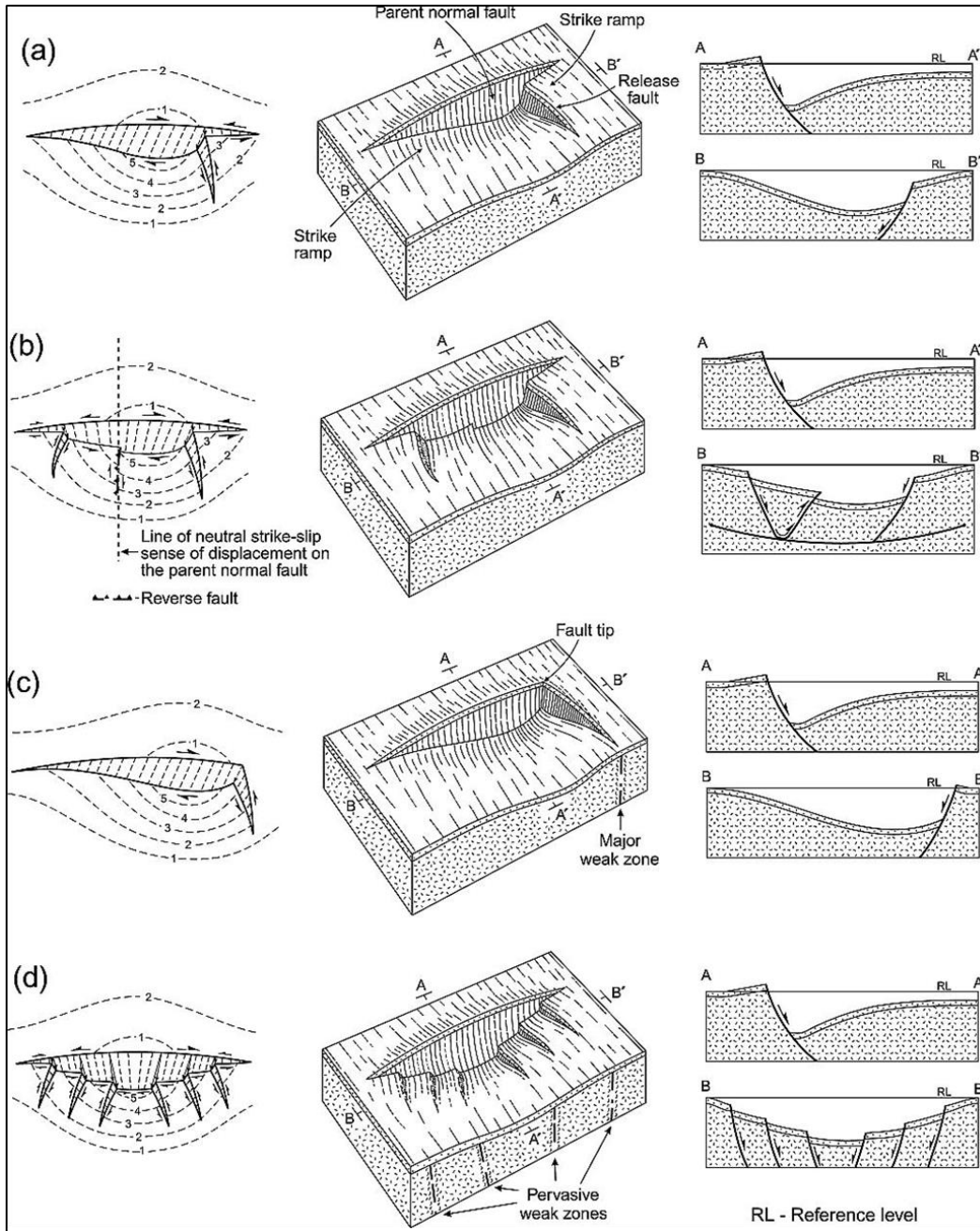


Figure 7.17: Idealized formation of some basic types of release faults. They may form in the strike ramps (a and b) or at the normal fault tips (c). The cross-sections B-B' show that release faults do not present footwall uplift. Structural contours indicated by numbers 1 (highest) to 5 (lowest). Arrows in maps represent the apparent lateral movements originated by the release faults. Release fault: a variety of cross fault in linked extensional fault systems (Destro, 1995).

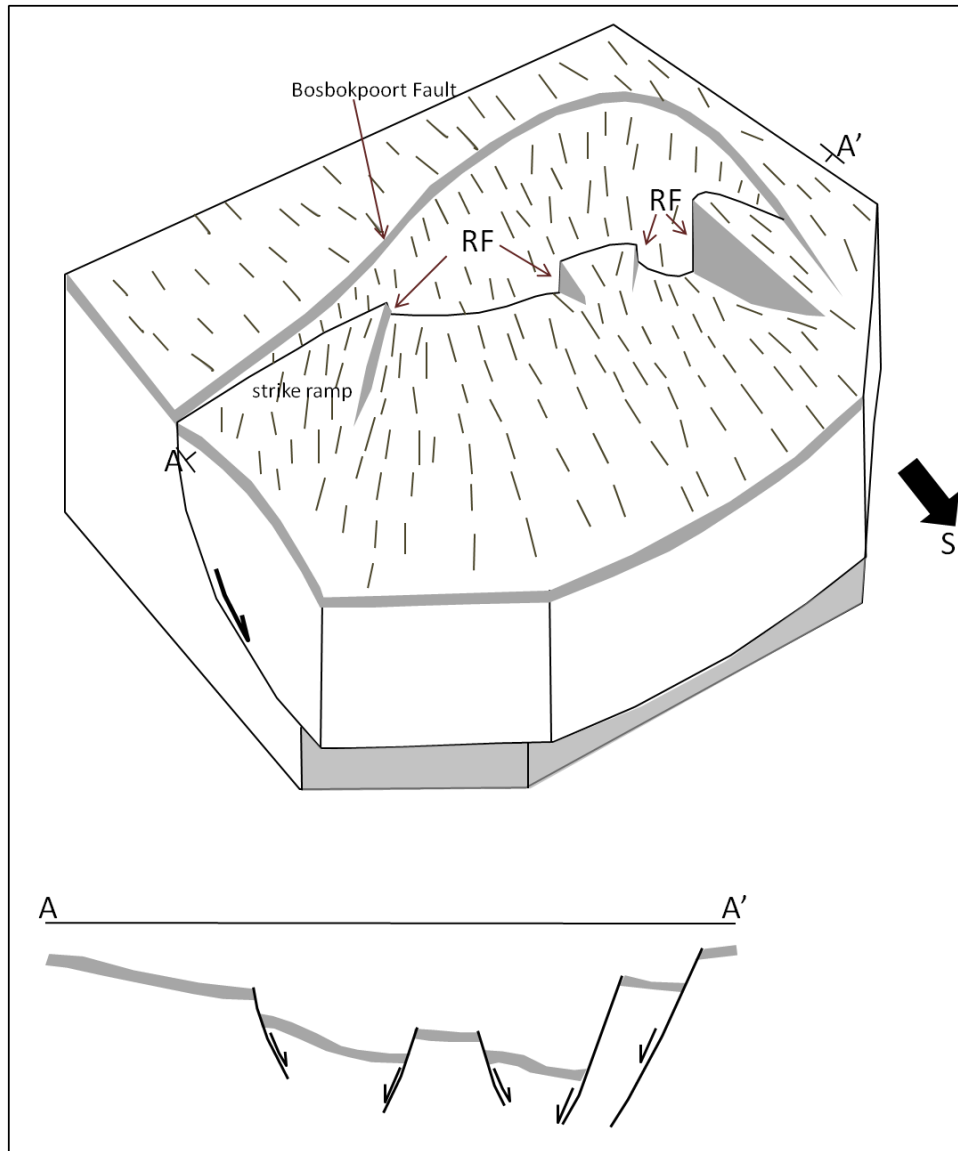


Figure 7.18: Model block diagram and cross-section showing the internal geometry of the Soutpansberg Basin. Release faults control the structural framework of the basin in response to varying throws along the strike of the Bosbokpoort fault. The beds dip between 50° and 70°.

7.7. Conclusions

The major structural systems are well defined on the gravity and magnetics. The more outstanding features are:

- The East-North-East fault system has a notable signature, defining two magnetic domains on both southern and northern sides of the Soutpansberg Basin. The West-North-West is also outlined, with its recognized control on the contact between the Mopane Coalfield and the Beitbridge Complex
- Intrusive emplacements are mainly fault controlled. They trend in the same direction as the two fault systems.
- Jurassic volcanics (Letaba and Jozini Formations) follow a SW-NE trend, outcropping in the east (Soutpansberg Basin), producing a strong magnetic response in this area, and partly buried in the west, where magnetic intensity tends to be reduced.
- The two major fault systems in the Soutpansberg Basin were recognised by the gravity and magnetic techniques and they trend in the same direction as the Palala and Tshipise Streightening Shear Zones.

With the magnetic features it was possible to define the major lithologic units and to extend them under covered areas. The more outstanding signatures are:

- The area has a vast incidence of volcanic units, of Jurassic and Cretaceous age. The more magnetic and extensive are the Mesozoic Letaba and Jozini Formations of the Lebombo Group. It was possible to extend their coverage from east to west under the sedimentary cover. Generally volcanic units have a signature of high frequency and widespread distributed anomalies, with amplitude depending on the lithology of the unit. The area is mainly composed of basalts and rhyolites.
- Sedimentary units were outlined according to weak, amorphous magnetic signatures and low gravity densities. Most of these areas are fault controlled and are related to basins delimited by vertical-movement faults. The unit is composed of sandstone, siltstone, shale and coal which are Late Carboniferous to Late Permian in age.
- Metamorphic units have little occurrence in the area.

The radiometric interpretation was focused on outlining structures and contacts and on the delineation of radiometric signatures in areas defined as anomalous in terms of:

- the occurrence of radiometric anomalies defined from the Th, U and K radiometric images.

- coincidence of the above with intrusives mapped from magnetics, and/or the presence of faults controlling the intrusions.

The structural mapping based on the radiometric data correlates well with the magnetic structural interpretation. It maps the major faults and defines shallow contacts between some units. The radiometric responses are a good guide to the provenance of the sedimentary cover, which is useful for interpreting geochemical data.

CHAPTER 8

COAL ANALYSIS OF THE SOUTPANSBERG AND TULI COALFIELDS

Abstract

Over 2000 widely distributed borehole data with proximate coal analysis were used to analyse the coal qualities of the Soutpansberg and Tuli Coalfields in order to establish the rank of coal; to show the ratio of combustible to incombustible constituents and to provide basis for exploration. Major elements (in wt%) of coal samples were analysed by X-ray Fluorescence Spectrometry (XRF) for ash content. The most abundant major components in both coal and ash samples are Si followed by Al, Fe and Ca. The main trend in the major oxides indicates that the coal used in the present study is a higher-ash coking bituminous coal which is enriched in elements associated with probable detrital minerals. The Soutpansberg Coalfield samples were both sialic and ferrocalsialic in chemical composition (i.e. essentially Fe, Ca, Al and Si). The Tuli Coalfield samples plotted in the sialic group (i.e. Si and Al).

8.1. Introduction

Coal is formed in three stages, i.e., microbial, biochemical and geochemical (Swaine, 1990). The microbial stage involves the initial formation of peat and requires wet and acidic conditions. It also requires proximity to an area such as a rising sea or subsiding land to cover the decomposition of plant material quickly. The biochemical stage begins when sediments suddenly cover the peat. Finally, the start of the geochemical stage occurs as the plant structure becomes compacted and plant material begins to alter (Swaine, 1990). The rock that we refer to as coal is derived principally from decomposed organic matter (plants) consisting primarily of the element carbon (C). When coal is burned, it produces energy in the form of heat, which is used to power machines such as steam engines or to drive turbines that produce electricity. "Coal quality" is the term used to refer to the properties and characteristics of coal that influence its behavior and use. Among the coal-quality characteristics that will be important for future coal use are the concentrations, distribution, and forms of the many elements contained in the coal that we intend to burn. Knowledge of these quality characteristics in the South African coal deposits may allow us to use this essential energy resource more efficiently and effectively and with less undesirable environmental impact.

There are two methods of coal analysis, namely: the ultimate and proximate analysis. The ultimate analysis determine all coal component elements, solids or gaseous while the proximate determines the fixed carbon, volatile matter, moisture and ash percentages. Both

analyses are used to establish the rank of coal; to show the ratio of combustible to incombustible constituents; or to provide basis for exploration, buying and selling and otherwise evaluating coal for various purposes. The proximate analysis is the most often used analysis for characterizing coals in connection with their utilization because of its simplicity (Huggins, 2002). The American Society for Testing Materials (ASTM)* and the International Organisation of Standardisation (ISO)* are applied in all the analysis of coal. In this project coal was analysed using the proximate method.

In terms of the South African Code for reporting of Mineral Resources & Reserves [*SAMREC Code (2007)] and the “Guide to the systematic evaluation of coal resources and coal reserves” (South African National Standard 10320:2004, as amended), both the Soutpansberg and the Tuli coal deposits are classified as a ‘thick interbedded coal seam’-type deposits. The objective of this study was to analyse the coal quality of the Soutpansberg and Tuli Coalfields and to determine which coal is suited the best and for which kind of industry, (for example, combustion, liquefaction, gasification) and determining the rank of the coal along with its intrinsic characteristics. The analysis will also help in the development of geologic and geochemical models for the interpretation and prediction of coal quality and for relating these factors to the stratigraphic and sedimentological framework. The standard classification by rank is shown in Table 8.1 below.

Table 8.1: Standard Classification of Coals by Rank (ASTM D388-05)*.

<i>Type</i>	<i>Fixed Carbon (wt %)</i>	<i>Volatile Matter (wt %)</i>	<i>Ash (wt %)</i>	<i>Moisture (wt %)</i>
Anthracite	75-85	2-12	4-15	3-6
Bituminous	50-70	15-45	4-15	2-15
Sub-Bituminous	30-57	28-45	3-10	10-25
Lignite	25-30	24-32	3-15	25-45

*SAMREC, (South African Mineral Resource Committee). 2007. SAMREC, Marshalltown, South Africa.

*ASTM, 1999. ASTM D388-05: Standard Classification of Coals by Rank, ASTM International, West Conshohocken, PA. < <http://www.astm.org/Standards/D388.htm> >

8.2. Methodologies

Over 2000 widely distributed borehole data with proximate coal analysis were used to analyse the coal qualities of the Soutpansberg and Tuli Coalfields. All these sets of borehole data resulted from the extensive coal exploration activities in the study area by different companies over the past 50 years. All borehole data and coal analysis used in this study is kept in the Council for Geoscience (CGS) archives. Since the borehole data and coal analysis were from different companies with different descriptive standards, it was necessary to convert the descriptions to a common format before the data could be used for coal analysis. Coal sample positions were verified against coal seam occurrences, and raw coal analyses were compared to lithological descriptions. The coal zones (group of seams) are in the lower, middle and upper parts of the Karoo strata; however, they are separated by shale and minor sandstone dominated intervals. Thus they were grouped into three, namely the upper, middle and basal seams (De Jagger, 1986; Ortlepp, 1986). In all the data from the CGS, the analysis of floatation at air dry basis was used.

Major elements (wt%) of coal samples were analysed by X-ray fluorescence spectrometry (XRF) for ash content in coals. The most abundant major components in both coal and ash samples are Si followed by Al, Fe and Ca. The ash content of coal was determined by measuring the X-ray fluorescence of Si, Al, Ca and Fe using a diffraction spectrometer at the CGS.

*ISO., 2005. International Standard 11760: 2005 (E) Classification of Coals, 9 pp.

Coal comes in four main types or ranks: lignite or brown coal, sub-bituminous, bituminous or black coal and anthracite (Speight, 2005). Each type of coal has a certain set of physical parameters which are mostly controlled by moisture, volatile content (in terms of aliphatic or aromatic hydrocarbons) and carbon content (Hower and Eble, 1996).

Moisture is an important property of coal, as all coals are mined wet. Groundwater and other source of moisture are known as adventitious moisture and readily evaporates. Moisture held within the coal itself is known as inherent moisture and is analysed quantitatively. Moisture may occur in four possible forms within coal:

- Surface moisture: water held on the surface of coal particles or macerals.
- Hygroscopic moisture: water held by capillary action within the microfractures of the coal.
- Decomposition moisture: water held within the coal's decomposed organic compounds.
- Mineral moisture: water which comprises part of the crystal structure of hydrous silicates such as clays.

Total moisture is analysed by loss of mass between an untreated sample and the sample once analysed. This is achieved by any of the following methods;

- Heating the coal with toluene.
- Drying in a minimum free-space oven at 150°C within a nitrogen atmosphere.
- Drying in air at 100°C to 105°C and relative loss of mass determined.

Volatile matter in coal refers to the components of coal, except for moisture, which is liberated at high temperatures in the absence of air. This is usually a mixture of short and long chain hydrocarbons, aromatic hydrocarbons and some sulphur. Any coal which has a high volatile matter content: can ignite easily burns with long smoky yellow flame, has low calorific value, needs large furnace volume for combustion and has a high tendency of catching fire.

Ash content of coal is the non-combustible residue left after coal is burnt. It represents the bulk mineral matter after carbon, oxygen, sulphur and water (including from clays) has been driven off during combustion. There are two types of mineral matter namely: inherent and extraneous. Inherent comes from inorganic constituent of plant materials, but the amount is less whereas extraneous comes from the amount that gets associated with substances

during its conversion process. Relation between mineral matter (MM) and ash is given as: $MM = 1.08Ash + 0.555$. Coal containing high ash is harder and stronger, low calorific value and will produce slag.

The fixed carbon content of the coal is the carbon found in the material which is left after volatile materials are driven off. This differs from the ultimate carbon content of the coal because some carbon is lost in hydrocarbons with the volatiles. Fixed carbon is used as an estimate of the amount of coke that will be yielded from a sample of coal. Fixed carbon is determined by removing the mass of volatiles determined by the volatility test from the original mass of the coal sample.

8.3. Results of Proximate Analysis

As defined by the *ASTM D121, proximate analysis separates the products into four parameters: (1) moisture (M), (2) volatile matter (VM), (3) ash (A) and (4) fixed carbon (C), (Table 8.1). The first three parameters are determined by experimentation in the laboratory and then the fixed carbon is calculated gravimetrically using the following formula (Speight, 2005):

$$C=100-(M+VM+A)$$

Where: C: Fixed Carbon, M: Moisture, VM: Volatile Matter and A: Ash

The parameters are measured in weight percent (wt. %) and are calculated in several different bases. AR (as-received) basis is the most widely used basis in industrial applications. AR basis puts all variables into consideration and uses the total weight as the basis of measurement. AD (air-dried) basis neglect the presence of moistures other than inherent moisture while DB (dry-basis) leaves out all moistures, including surface moisture, inherent moisture, and other moistures. DAF (dry, ash free) basis neglect all moisture and ash constituent in coal. A general evaluation of the quality of coal can be made on the basis of data furnished by the proximate analysis.

*ASTM, 1999. ASTM D121: Standard Terminology of Coal and Coke, ASTM International, West Conshohocken, PA. <<http://www.astm.org/Standards/D12>>

8.3.1. Tshipise-Pafuri Coal Analysis (Central and Eastern Soutpansberg)

The percentages of moisture (M), volatile matter (VM) ash content (A) and fixed carbon (C) of all the seams have been shown in Figures 8.1, 8.2 and 8.3, the total averages are shown in Table 8.2 and Figure 8.4. The fixed carbon ranges from 60% to 70% with an average of 65.45% in the upper seams; 62.99% in the middle seams and 65.53% in the basal seams. The ash yields are low ranging from 15% to 25%, the moisture content is generally low with an average of 0.48% for the upper seam; 0.47% for the middle seams and 0.44% for the basal seams, (Table 8.2 and Figures 8.1 to 8.4). The coals of the Tshipise-Pafuri Basin are bituminous coking coal in rank and they can be utilized for steel generation.

Table 8.2: Averages of proximate analysis of all seams in the Tuli Coalfield.

Seams	Moisture content (%)	Ash content (%)	Volatile matter (%)	Fixed carbon (%)
Upper	0.48	21.77	12.30	65.45
Middle	0.47	22.17	14.36	62.99
Basal	0.44	20.66	13.38	65.53

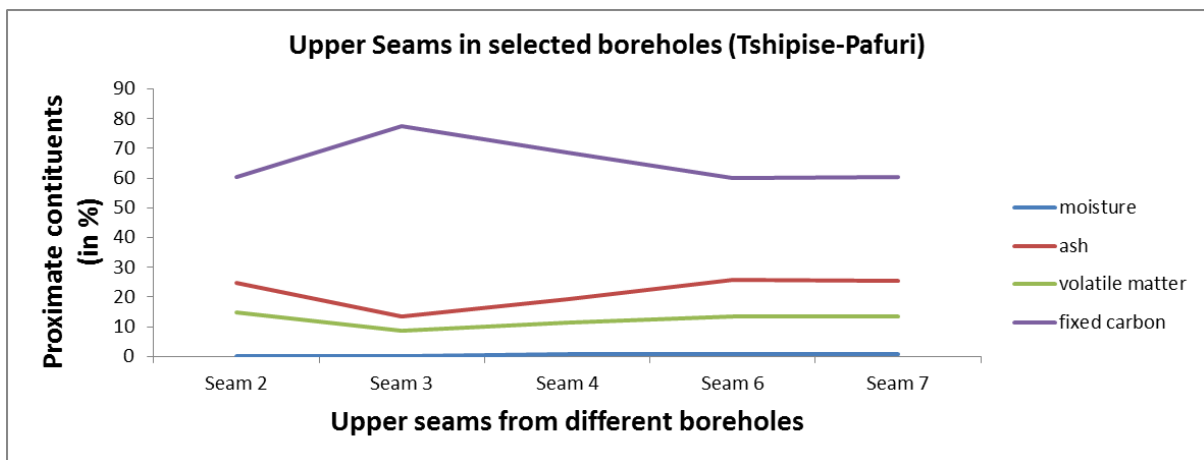


Figure 8.1: Proximate analysis of coal samples in the upper seams (Tshipise-Pafuri Coalfield).

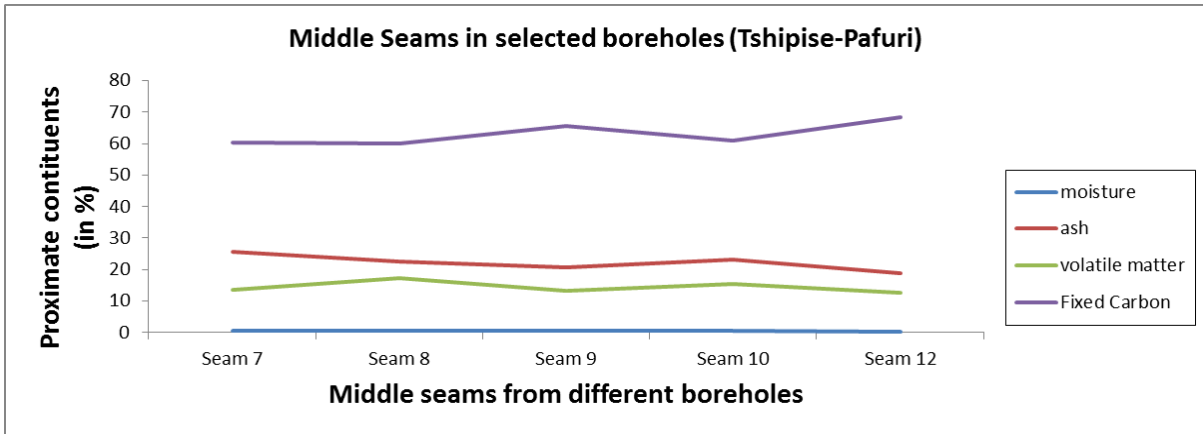


Figure 8.2: Proximate analysis of coal samples in the middle seams (Tshipise-Pafuri Coalfield).

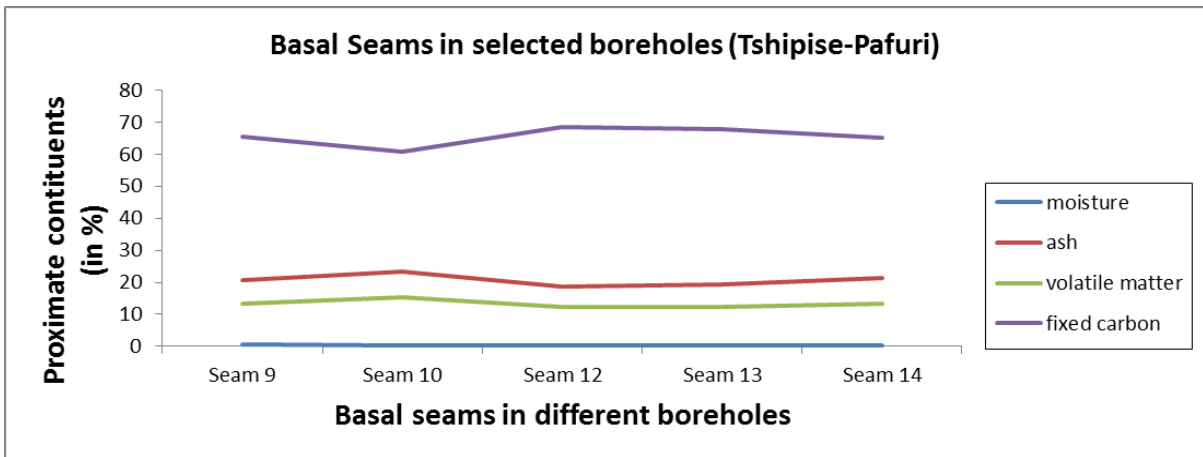


Figure 8.3: Proximate analysis of coal samples in the basal seams (Tshipise-Pafuri Coalfield).

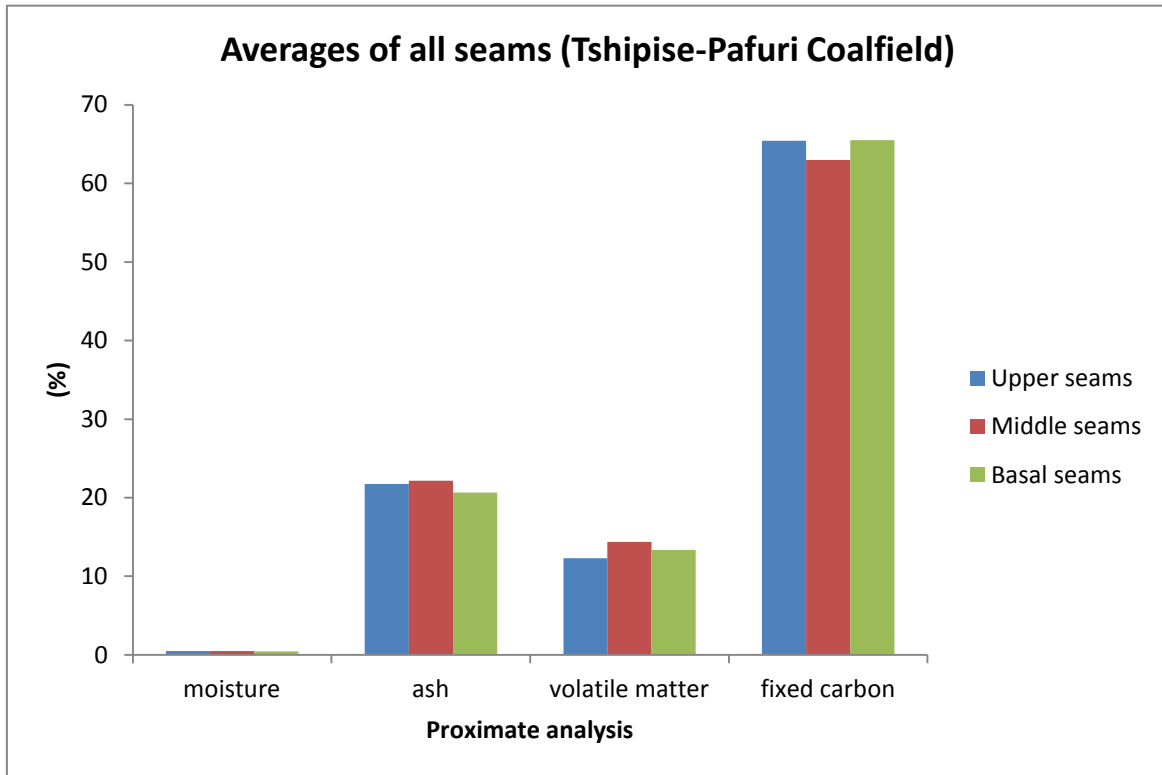


Figure 8.4: Averages of all seams in the Tshipise-Pafuri Coalfield.

8.3.2. Mopane Coal Analysis (Western Soutpansberg)

The proximate parameters of the Mopane Coalfield are given in Table 8.3. The ash averages are 21.61% in the upper seams; 21.32% in the middle seams and 16.98% in the basal seams. The fixed carbon averages are 49.81% in the upper seams; 48.92% in the middle seams and 52.28% in the basal seams. It may be observed from Table 8.3 and Figures 8.5, 8.6, 8.7 and 8.8 that the upper seams of the farms of the Mopane Coalfield has the highest moisture content (average, 1.13%). In general coals from the coalfield contain lower amounts of moisture, have volatile matter contents of 20 to 32 percent i.e., the low and medium volatile bituminous ranks (Table 8.3). Coals of the Mopane Basin are generally sub-bituminous coking coal in rank. These coals could be utilized in steel making and for industrial purposes (i.e. ethanol, gases, and liquid fuels).

Table 8.3: Averages of proximate analysis of all seams in the Mopane Coalfield.

<i>Seams</i>	<i>Moisture Content (%)</i>	<i>Ash content (%)</i>	<i>Volatile matter (%)</i>	<i>Fixed Carbon (%)</i>
Upper	1.13	21.61	28.22	49.81
Middle	0.99	21.32	28.67	48.92
Basal	0.99	16.98	29.72	52.28

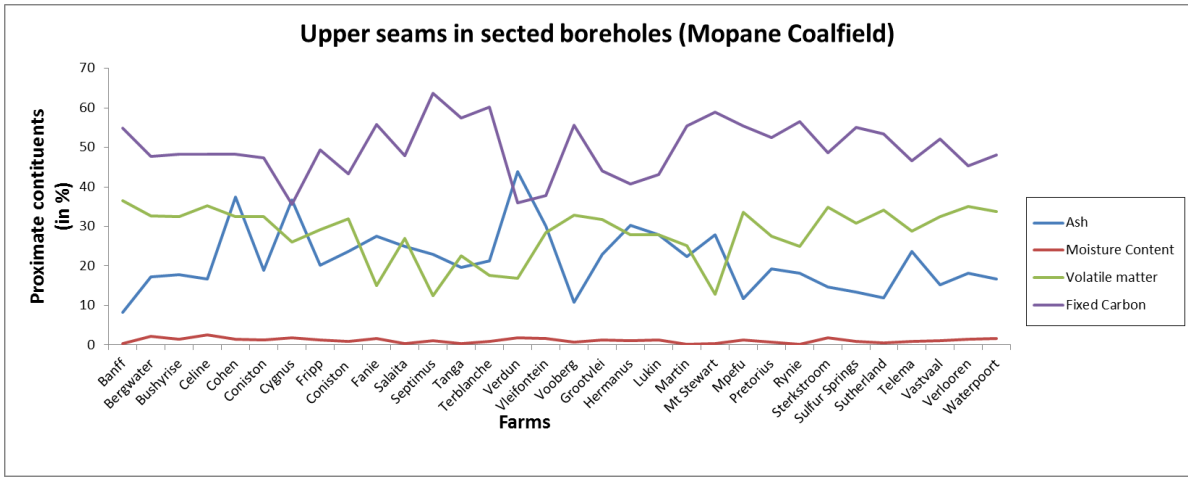


Figure 8.5: Proximate analysis of coal samples in the upper seams (Mopane Coalfield).

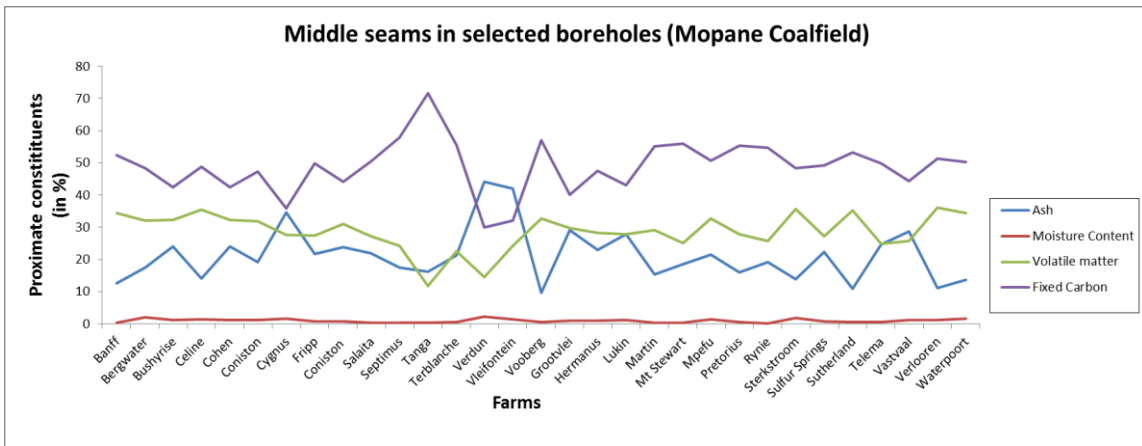


Figure 8.6: Proximate analysis of coal samples in the middle seams (Mopane Coalfield).

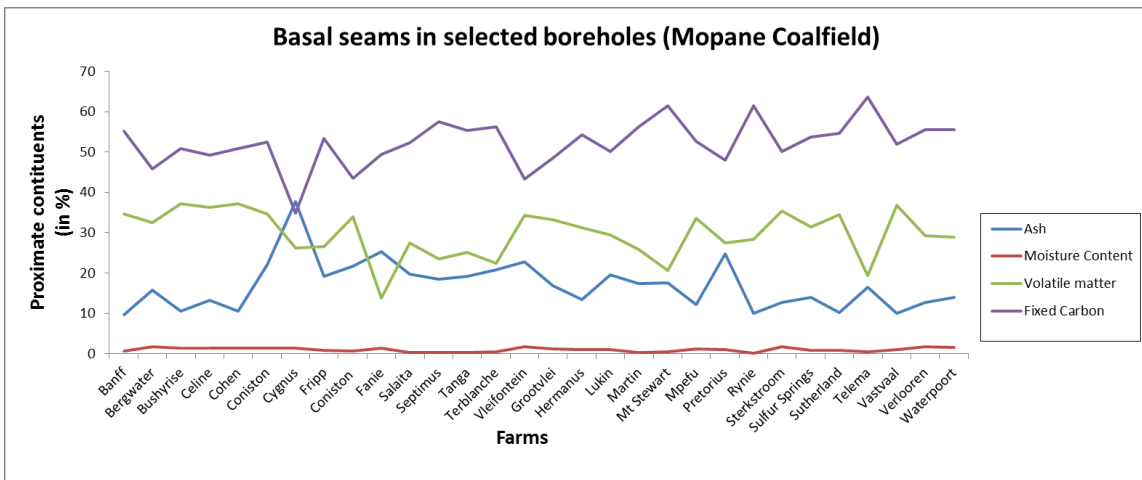


Figure 8.7: Proximate analysis of coal samples in the basal seams (Mopane Coalfield).

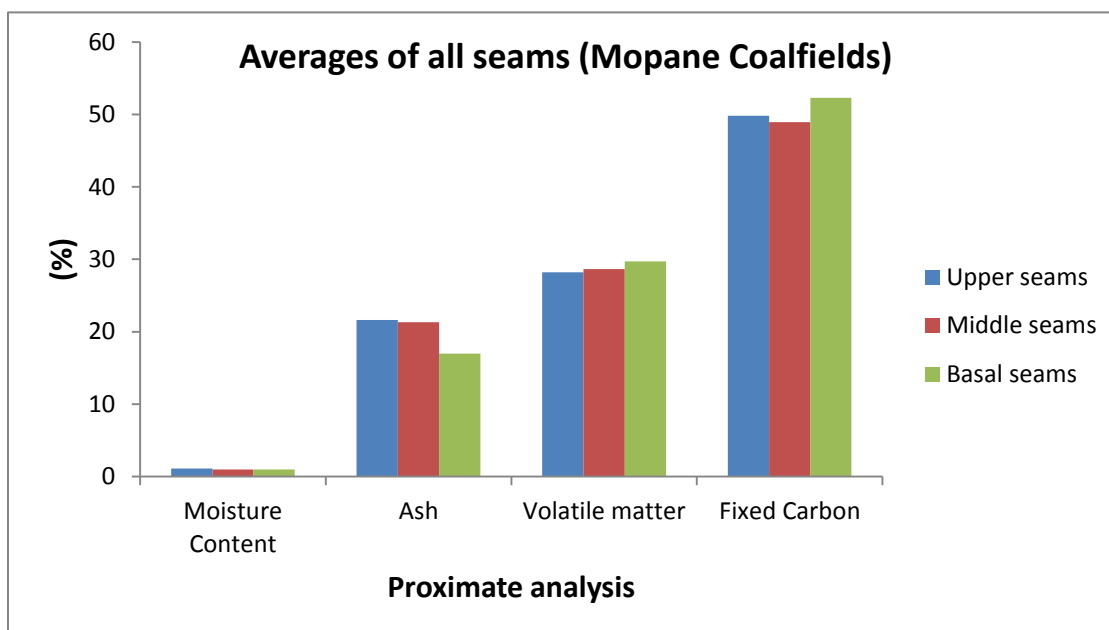


Figure 8.8: Averages of all seams in the Mopane Coalfield.

8.3.3. Tuli Coal Analysis

The percentages of moisture (M), volatile matter (VM) ash content (A) and fixed carbon (C) of all the seams are shown in Figures 8.9, 8.10 and 8.11, the total averages are shown in Table 8.4 and Figure 8.12. In the Tuli Coalfield, the ash content of coals are 36.61% in the upper seams; 37.45% in the middle seams and 34.34% in the basal seams. The fixed carbon averages are 39.48% in the upper seams; 31.56% in the middle seams and 39.49% in the basal seams. It may be observed from Table 8.4 and Figure 8.12 shows that the middle seams have the highest moisture content with an average of 2.14% and the basal seam has the lowest (1.44%). Generally the moisture values varied from 1% to 2.8%. From this we can conclude that coal from the middle seams will take more time for heating and will have lower calorific value.

The upper seams have the highest volatile matter content, with an average of 25.24% and 24.73% respectively, whereas the middle seams has the lowest volatile matter content (20.65%), (Table 8.4 and Figure 8.12). Coals with high volatile-matter content ignite easily and are highly reactive in combustion applications. With an increase in the volatile matter content of coal, there is a decrease in the calorific value of coal. The upper and basal seams could be utilized for combustion applications very conveniently.

The fixed carbon content which has a direct relation with the calorific value varied between 39.48% (upper seams), 39.77% (middle seams) and 39.49% (basal seams). It could be observed from Table 8.4 and Figures 8.9, 8.10, 8.11 and 8.12 that the fixed carbon content

of the samples are below 40% and it is expected that their calorific value will be low. The coals of the Tuli Coalfield are lignitic to sub-bituminous coking coal in rank and they can be utilized in steel generation and other small industries for combustion processes.

Table 8.4: Averages of proximate analysis of all seams in the Tuli Coalfield.

<i>Seams</i>	<i>Moisture content (%)</i>	<i>Ash content (%)</i>	<i>Volatile matter (%)</i>	<i>Fixed carbon (%)</i>
Upper	1.67	33.61	25.24	39.48
Middle	2.14	37.45	20.65	39.77
Basal	1.44	34.34	24.73	39.49

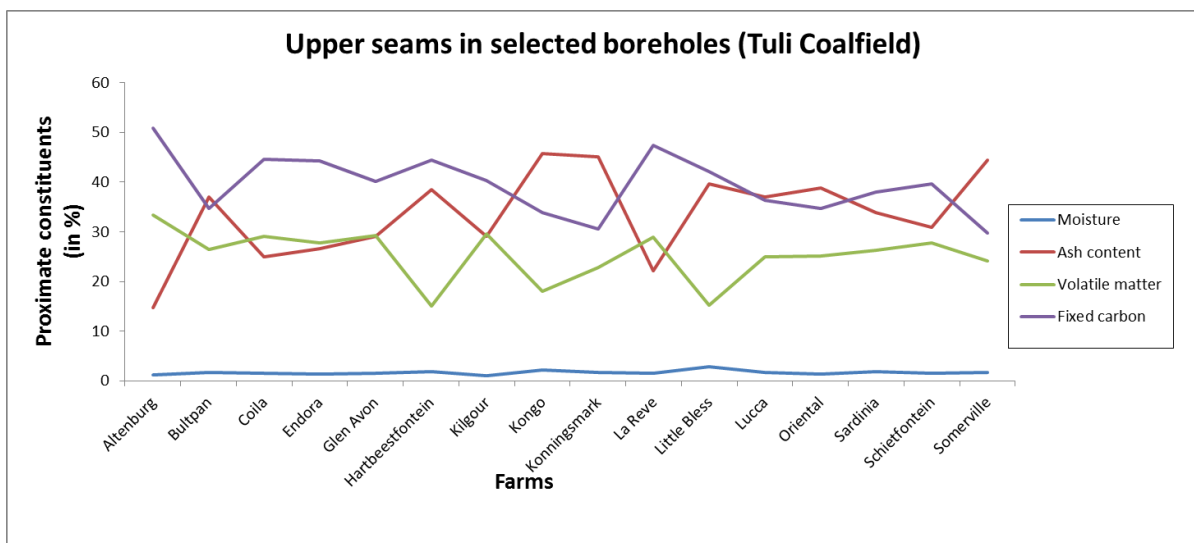


Figure 8.9: Proximate analysis of coal samples in the upper seams (Tuli Coalfield).

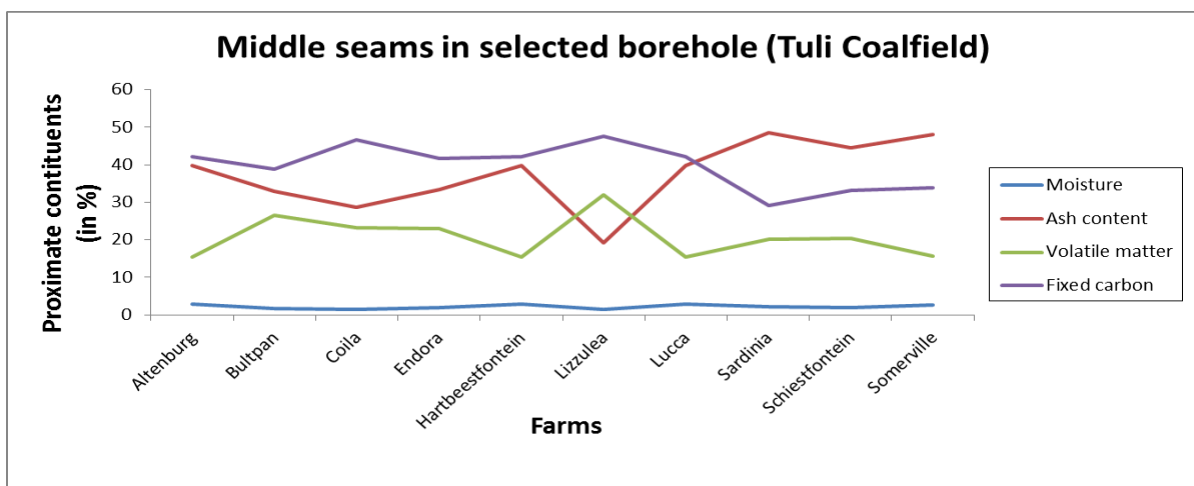


Figure 8.10: Proximate analysis of coal samples in the middle seams (Tuli Coalfield).

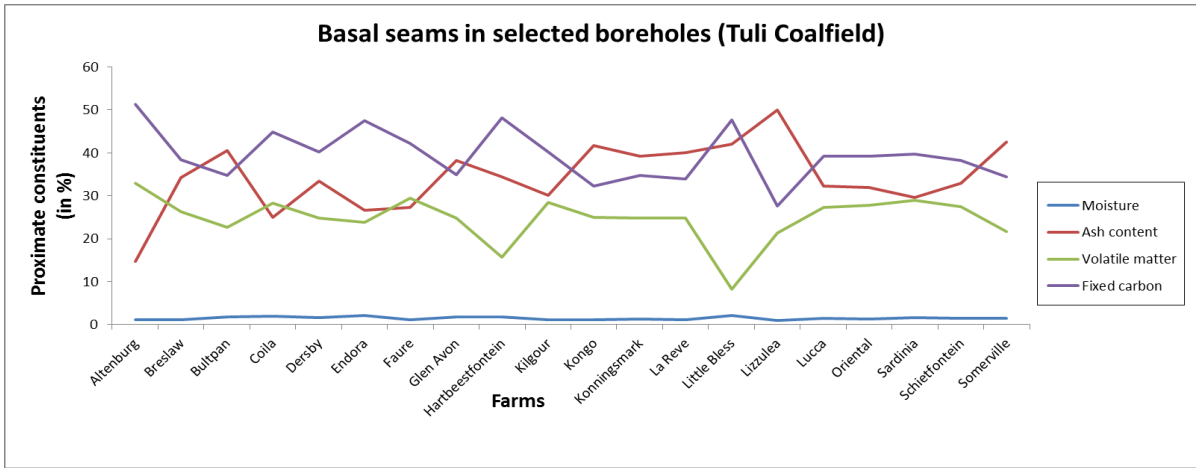


Figure 8.11: Proximate analysis of coal samples in the basal seams (Tuli Coalfield).

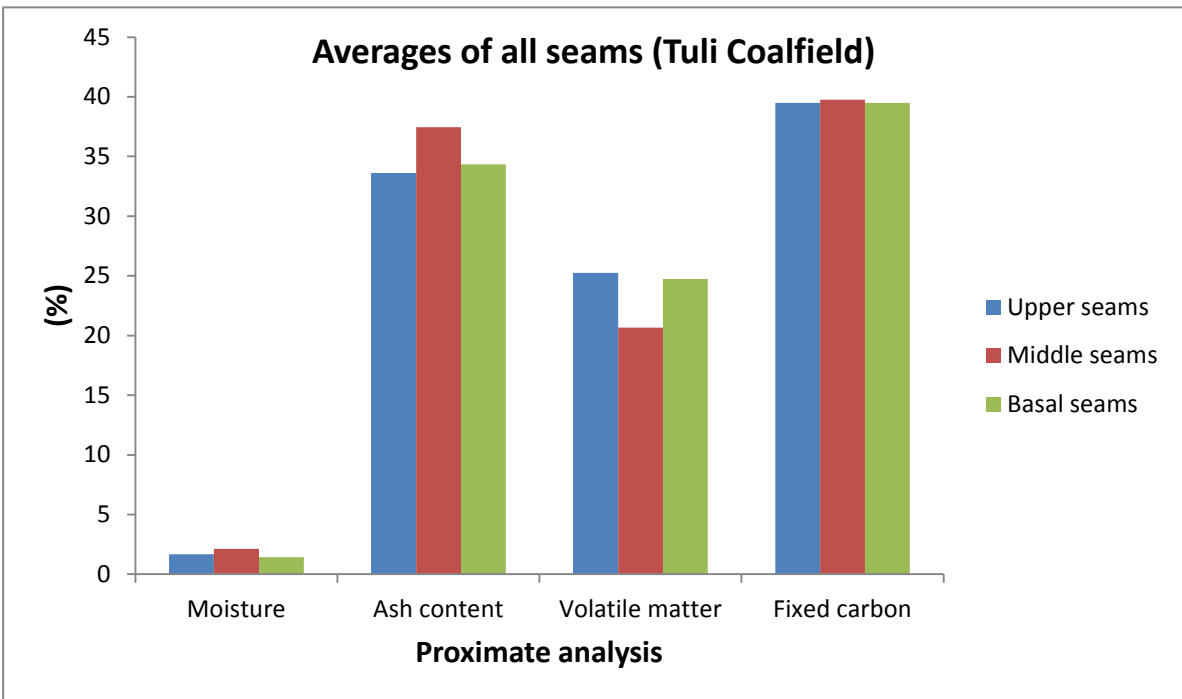


Figure 8.12: Averages of all seams in the Tuli Coalfield.

8.4. Coal Ash Analysis

Coal ash is comprised of compounds of Silicon, Aluminum, Iron and Calcium with smaller amounts of compounds of Magnesium, Titanium, Sodium and Potassium. Although these constituents are reported as oxides by the analyst, they occur in ash as a mixture of silicates, oxides and sulphates with small quantities of phosphates and other compounds. The composition of ash from different coals varies widely, depending on the quantities of clay, shale, pyrite, calcite and other minerals present in the coals. The source of iron oxide shown in ash analysis is pyrite, one of the most commonly occurring mineral impurities in coal. Sulphur, combined with iron in the form of marcasite, is known as pyritic sulphur.

Two classes of ash-forming mineral matter generally recognised as occurring in coal are: (1) inherent mineral matter and (2) extraneous mineral matter. The inherent mineral matter is the portion which is organically combined with coal. It contains chemical elements, such as iron, phosphorous, sulphur, calcium, potassium and magnesium. They are considered essential to the proper growth of plants. Other elements, such as silicon, sodium, manganese and aluminum are found in many plants although they are not generally considered essential to normal plant growth. Extraneous mineral matter in coal is defined as the part of the mineral matter that is foreign to the plant material and contributing to the formation of the coal. It is considered to consist of minerals deposited with the peat or those deposited in cleavage and fracture cracks after the peat had been consolidated. The inorganic constituents in coal are tabulated in Table 8.5.

Table 8.5: Inorganic constituents in coal (Marson and Cobb, 1925).

Inorganic constituent	Forms of coal
Silicon	Silicates and sand
Aluminium	Aluminium in combination with silica
Iron	Pyrite and marcasite (sulphide)
	Ferrous oxide
	Ferrous carbonate
	Ferrous sulphate
	Ferric oxide
	Ferric sulphate
	'Organic' iron
	Iron silicates
	} In small quantities
Calcium	Lime, Carbonate, sulphate, silicates
Magnesium	Carbonates, Silicates
Sodium and Potassium	Silicates, Carbonates, Chlorides
Manganese	Carbonates, Silicates
Sulphur (inorganic)	Pyrite, Marcasite
	Ferrous sulphate
	Ferric sulphate
	Calcium sulphate
	} In small quantities
Phosphorous	Phosphates

Major elements (wt%) of coal samples were analysed by X-ray fluorescence spectrometry (XRF) for ash content in coals at the Council for Geoscience. Table 8.6 shows the major element analysis of coal ash in the Soutpansberg and Tuli Coalfields. These elements may occur in both organic and inorganic constituents of coal and each element has dominant associations and affinities with different phases in the coal. The most abundant major components in both coal and ash samples are Si followed by Al, Fe and Ca. The least abundant components in the pulverised coal and ash are Ti, Mg, Na, K, P, Cr and Mn. The bulk chemical composition and classification systems of coal ash always include data for the Loss on ignition (LOI). The LOI and volatile (H₂O) components are relatively enriched in the pulverised coal sample.

Table 8.6: XRF Analysis of coal ash in the Soutpansberg and Tuli Coalfields.

Ash	Tshipise -Pafuri1	Tshipise -Pafuri2	Tshipise -Pafuri3	Tshipise -Pafuri4	Mopane1	Mopane2	Mopane3	Tuli1	Tuli2	Tuli3
SiO ₂	18.58	6.81	17.79	7.32	4.52	3.08	3.87	3.53	5.77	4.47
TiO ₂	0.28	0.09	0.65	0.29	0.11	0.08	0.14	0.13	0.17	0.14
Al ₂ O ₃	7.52	2.05	10.04	4.88	2.59	1.80	2.75	2.64	3.91	2.82
Fe ₂ O ₃ (t)	0.29	0.82	0.30	0.21	4.92	2.25	1.19	1.15	0.19	0.16
MnO	0.00	0.02	0.01	0.01	0.01	0.03	0.01	0.01	0.01	0.01
MgO	0.28	0.46	0.88	0.52	1.81	3.47	0.51	0.64	0.45	0.41
CaO	0.48	0.87	3.55	1.14	4.85	8.57	1.51	1.75	0.90	0.94
Na ₂ O	0.01	0.02	0.20	0.15	0.01	0.12	0.01	0.02	0.02	0.02
K ₂ O	0.33	0.13	0.56	0.08	0.04	0.03	0.03	0.03	0.05	0.04
P ₂ O ₅	0.02	0.03	0.43	0.04	0.01	0.01	0.01	0.01	0.01	0.01
Cr ₂ O ₃	0.00	0.00	0.00	0.00	0.001	0.001	0.00	0.00	0.00	0.00
L.O.I.	72.08	88.06	64.82	85.03	79.14	78.38	89.21	88.52	88.11	90.57
Total	99.80	99.35	99.24	99.67	98.00	97.82	99.25	98.46	99.59	99.59
H ₂ O	0.82	0.58	4.71	5.14	4.01	3.96	4.68	4.12	4.38	4.74

8.4.1. Results

Bulk chemical composition as determined by XRF analysis of all the coal fly ash samples revealed major presence of SiO₂, Al₂O₃, Fe₂O₃ and CaO and minor presence of TiO₂, Na₂O, K₂O, P₂O₅ and Cr₂O₃ (Figure 8.13). Fe₂O₃ (Ferric Oxide) and SiO₂ (quartz) were the major species identified, quartz being the only original unaltered coal mineral phase present. During the decomposition of clay minerals (Kaolinite, Al₂Si₂O₅(OH)₄) entrapped in the parent coal, Mullite (3Al₂O₃2SiO₂) is formed. The high concentration of MgO in fly ash in the Mopane Coalfield could suggest possible formation of enstatite (Mg₂Si₂O₆) upon accompanying depletion of quartz.

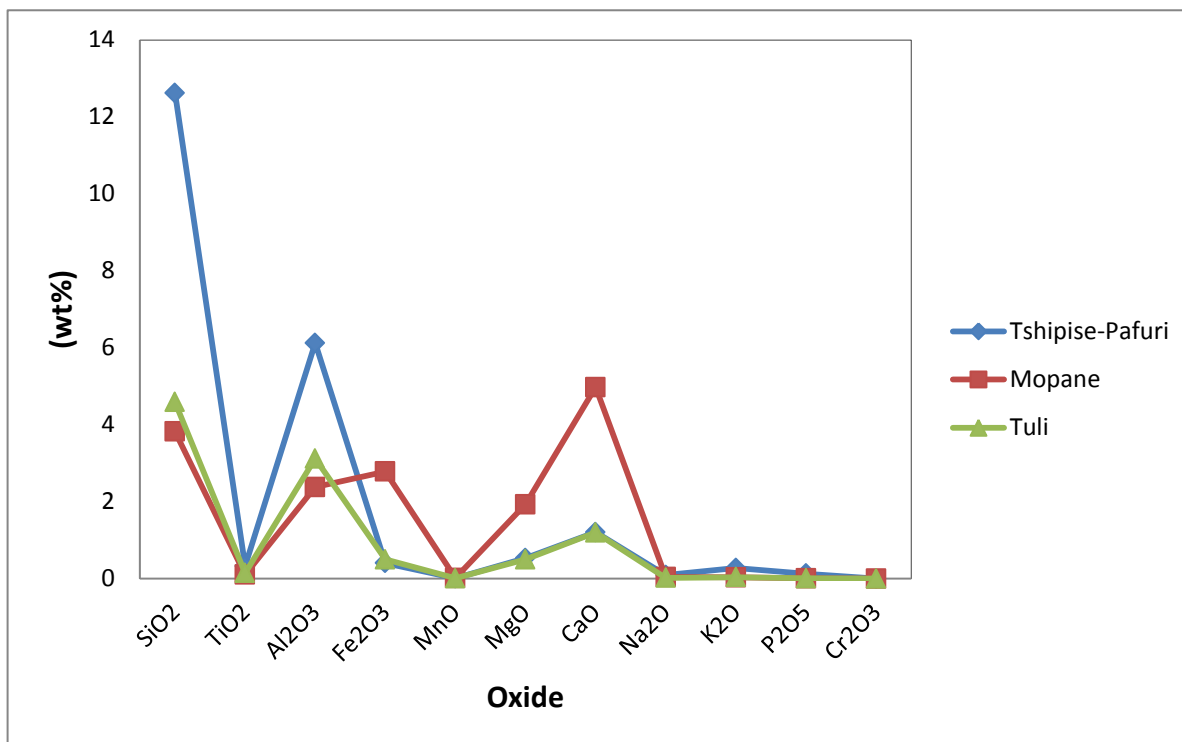


Figure 8.13: Average weight percentages of the ashes in the Soutpansberg (Tshipise-Pafuri and Mopane) and Tuli Coalfields.

Classified fly ash based on the intersection of the sum of their major oxides: sialic: $\text{SiO}_2 + \text{Al}_2\text{O}_3 + \text{TiO}_2$; calcic: $\text{CaO} + \text{MgO} + \text{Na}_2\text{O} + \text{K}_2\text{O}$; and ferric: $\text{Fe}_2\text{O}_3 + \text{MnO} + \text{P}_2\text{O}_5$ were plotted in a ternary diagram (Figure 8.14). Based on the chemical composition of coal ash, about seven intermediate fly ash subgroups exist, such as sialic, ferrosialic, calsialic, ferrocalsialic, ferric, calcic and ferrocalsialic fly ash (Vassilev and Vassileva, 2007). The Mopane Coalfield coal samples were both sialic and ferrocalsialic in chemical composition (i.e. essentially Fe, Ca, Al and Si). Most of the Tuli Coalfield samples plotted in the sialic group (i.e. Si and Al). The Tshipise-Pafuri Coalfield coal samples plotted in the ferrocalsialic and ferrosialic groups (i.e. Fe, Ca and Al).

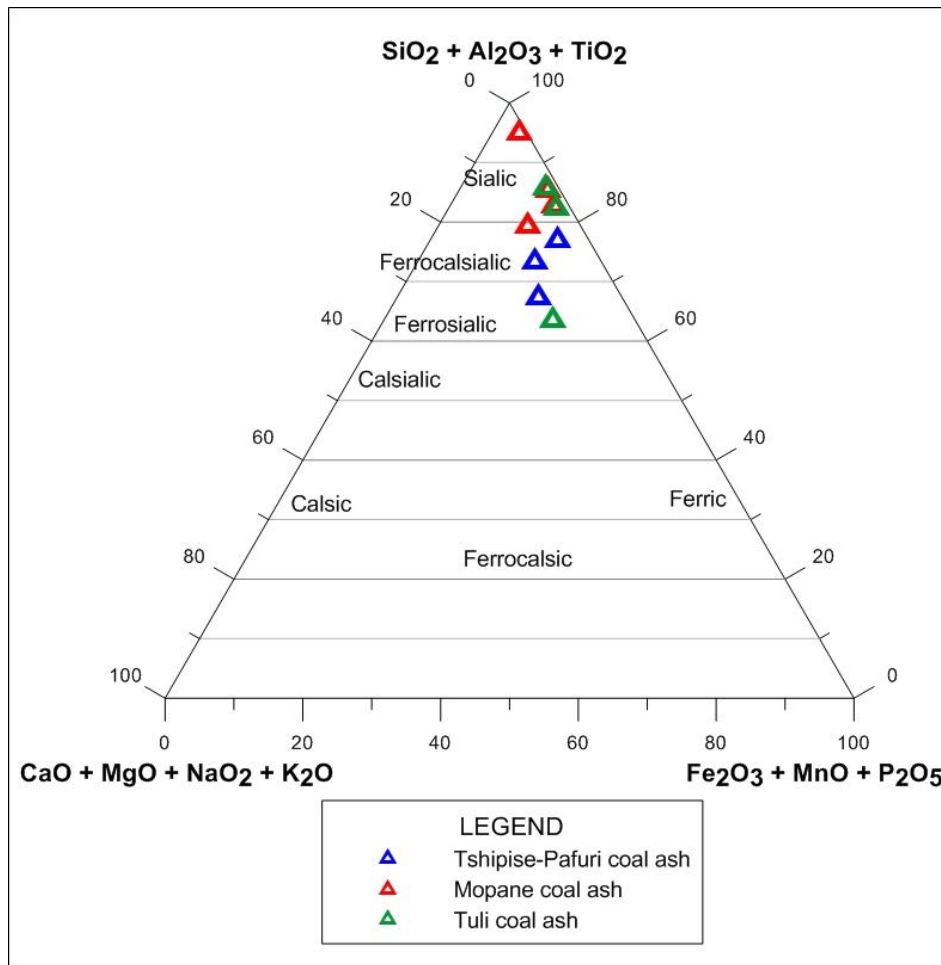


Figure 8.14: Ternary oxide plots for classification of the coal ash analysis in the Soutpansberg and Tuli Coalfields.

The main trend in the major oxides indicates that the coal used in the present study is a higher-ash coal which is enriched in elements associated with probable detrital minerals. The Soutpansberg Coalfield samples were both sialic and ferrocalsialic in chemical composition (i.e. essentially Fe, Ca, Al and Si). The Tuli Coalfield samples plotted in the sialic group (i.e. Si and Al).

8.5. Discussions

The coal deposits of the Tuli and the Soutpansberg (Mopane and Tshipise-Pafuri Coalfield), are contained within a coal zones (group of seams), consisting of layers of average to good quality bituminous coking coal, intercalated with non-coal material (shales and minor sandstones). The coal portion of these zones is generally of good coking quality but often comprises only a relative small portion of the total thickness. It could be observed from the study that the coal seams contain low quantity of moisture, medium to high volatile matter, medium to high amount of ash in general. The fixed Carbon ranges from 30% to 60%. Based on this study the coals may be ranked lignitic to bituminous coking coals.

Three coal zones (group of seams) are present in the Soutpansberg and the Tuli Coalfields. The lowermost of these zones (basal seams) contains the highest proportions of coal to shale. The principal coal development of economic importance is contained in the Basal seams. There is no much significant difference in the middle and upper seams.

Coals of the Mopane Coalfield are generally sub-bituminous in rank. These coals could be utilized in steel manufacturing and for industrial purposes. The coals of the Tuli Coalfield are lignitic to sub-bituminous in rank and they can be utilized in steel generation and other small industries for combustion processes. The coals of the Tshipise-Pafuri Coalfield are bituminous in rank and they can be utilized for steel generation and in other small scale industries for combustion purposes. The coal requires proper pollution controls, because they give rise to huge amounts of harmful, poisonous, or very unpleasant fumes during burning, because the ash contents are very high.

The results show that in both the coalfields the deeper coals have a high rank compared to shallow coals. The coal rank in the Soutpansberg (Tshipise-Pafuri) Coalfield is higher than both the Soutpansberg (Mopane) and Tuli Coalfields. There is no much significant difference between the Mopane and Tuli Coalfields. Currently, the data used represents a generalized view of the Soutpansberg and Tuli Coalfields coal quality, based on old data from different exploration companies. The majority of the data is more than 30 years old.

Based on the study of coal ash analysis, the Mopane Coalfield coal samples were both sialic and ferrocalsialic in chemical composition. Most of the Tuli Coalfield samples plotted in the sialic group. The Tshipise-Pafuri Coalfield coal samples plotted in the ferrocalsialic and ferrosialic groups.

In the Soutpansberg Coalfield (Tshipise-Pafuri), the thickest coal zone in this region is to be found some distance to the east of Waterpoort, comprising up to nine composite seams separated by carbonaceous mudstone, over a stratigraphic interval of about 40 m. Over the entire region, particularly in the Waterpoort sector, the coal bearing sequences are severely affected by faulting. In the western shallow sector and in the near-western deep sector of the Soutpansberg coalfield, coal occurrences are poorly to inconsistently developed and thus have limited exploitation potential. In the Central Sector of the coalfield, as well as parts of the eastern sector, the “coal measures” occur at depth below a relatively full sequence of Karoo strata and in many places the coal zone is located at more than 300 m below surface in these localities. The lower most composite ‘seam’ is up to 4m thick in places. The vitrinite of the coal in the area is 88%.

The coal in the Mopane Coalfield to a depth of approximately 15 m below surface is weathered and leached and this coal zone would not be mined. The individual coal seams are extremely difficult to correlate and the seams increase and decrease in thickness throughout the whole horizon. The coal zone thickness varies between 14 and 85 m and the cumulative coal thickness within the zone varies between 6 m and 33 m. Thick coal deposits are known to develop in areas where the climate is humid, vegetation is abundant, the water table is at a high level relative to the topography and within high accommodation system tracts where the rates of creation of accommodation was high relative to the sediment input (Reineck and Singh, 1973; Miall, 1982; Catuneanu, 2004). Such areas included delta plains, floodplains with backswamps and swamps in the subaerial environments (Reineck and Singh, 1973). Where vegetation is less abundant or where the rates of sediment input is high, thick peat accumulation is less important and complex lakes and swamps result (Reading, 1996).

A distinct coal zone, up to 20 m thick is developed in the shales. The zone contains six independent continuous seams. There are two exploitable seams which are 1.2 m and 1.6 m thick. They occur in a 10 m coal zone. The seams consists of thinly banded bright and dull coal with numerous thin mudstone partings, vitrinite (70%) making up most of the coal. Based on the results of proximate analysis and coal ash analysis, the Soutpansberg Coalfield is likely to present better opportunities for identification of potentially exploitable coal deposits as compared to the Tuli Coalfield.

8.6. Conclusions

It could be observed from this study that the:

- Coal samples analysed contain low to medium quantity of moisture, medium volatile matter and high amount of ash in general.
- The main trend in the major oxides indicates that the coal used in the present study is a higher-ash coking bituminous coal which is enriched in elements associated with probable detrital minerals. Thus all these coals could be used for iron and steel making and in other small scale industries for combustion purposes. However, proper pollution control arrangements are required to be made since these coals are expected to give rise to huge amount of noxious pollutants during burning, because the ash content of the coals are very high.
- The study has revealed that the eastern Soutpansberg Coalfield is likely to present better opportunities for identification of potentially exploitable coal deposits as compared to the Tuli Coalfield.

CHAPTER 9

DIAGENESIS OF THE SANDSTONES IN THE SOUTPANSBERG AND TULI COALFIELDS

Abstract

This chapter aims to provide a general account of the diagenesis of sandstones in the Mikambeni and Madzaringwe Formations of the Soutpansberg and Tuli Coalfields. The diagenesis of the Tuli and Soutpansberg sandstones can be divided broadly into early, middle and late diagenetic stages. The main diagenetic processes that have affected the sandstones in the study area include mechanical compaction, cementation and the dissolution of framework grains and cements. Sandstone diagenesis in the coalfields is largely controlled by pre-burial factors such as depositional environment and sediment composition. Compaction and cementation were the major early diagenetic processes for sandstone. Quartz cement as pore filling and overgrowths is one of the most abundant cements in both the Soutpansberg and the Tuli sandstones. Iron oxide cementation is also noticeable during early diagenesis of the sandstones. Calcite cementation was also observed as pore-filling material and as well as a replacement mineral of detrital grains. Pore-lining and pore-filling illite-smectite and kaolinite are more abundant in the sandstones with a higher percentage of matrix content. The late diagenesis stage includes quartz and feldspar overgrowths, seritisation, chlorite alteration, grain deformation, pressure-solution and fracturing and albitisation. During the late diagenesis stage, seritisation and chloritisation of smectite clays were developed. Chlorite is notable in sandstones having large quantities of volcanic rock fragment and detrital micas, indicating detrital grain composition controls on its diagenetic minerals. Albitization of feldspar grains in the coalfields occurred during the middle and later stages of diagenesis. As the sediments were progressively buried, albitization began when they reached the minimum burial temperature of about 80^oc required for the replacement.

9.1. Introduction

Diagenesis is the term used for all of the changes that a sediment undergoes after deposition and before the transition to metamorphism. They include compaction, deformation, dissolution, cementation, authigenesis, replacement, recrystallisation, hydration, bacterial action, and development of concretions. Diagenesis begins at the moment after sediments are deposited, and it continues to a point in history when (1) either deep burial or orogenic buckling cause the initiation of metamorphism; or (2) when excavation initiates

weathering and erosion. Two diagenetic phases will be discussed in this chapter namely, the early and late diagenesis.

9.2. Methodologies

This study is based on samples representing different depths and lithological types collected from the Mikambeni and Madzaringwe Formations of the Soutpansberg and Tuli Coalfields. The description of primary and authigenic mineralogy of the sandstones is based on study of microscope thin sections, including point counting and SEM and X-ray diffraction (XRD) analyses. Natural thin-sections were coated with carbon or gold using a Leica Emitech K950 Evaporator and gold using an Anatech Hummer VI Gold Coater respectively. Scanning Electron Microscopy (SEM) was done by using Jeol JSM 6400, equipped with a link system Energy Dispersive X-ray microanalyser (EDX). The samples were examined in Secondary Electron Imaging (SEI) and backscattered electron (BSE) modes of imaging. Both SEM and petrographic microscopy were done at the University of Fort Hare and Rhodes University.

9.3. Diagenesis Processes

Diagenetic features of Mikambeni and Madzaringwe sandstones are subdivided into early, middle and late stages. Time is relative with the earliest diagenetic event occurring shortly after deposition and the latest occurring up until present time. The main diagenetic processes that have affected the sandstones include mechanical compaction, cementation and the dissolution of framework grains and cements. Early diagenetic processes include mechanical compaction, silica and calcite cementation, clay mineral (pore lining and pore-filling kaolinite and smectite), feldspar authigenesis and the formation of hematite coatings. Late diagenesis includes albitization of K-feldspar, chloritisation and seritisation of smectite and kaolinite. Late diagenetic minerals occur mostly as replacement minerals of detrital grains and early-formed diagenetic minerals, over-compaction. The diagenetic constituents are described in order of their abundance. Diagenetic processes can cause significant changes in initial sandstone composition (Wilkinson *et al.*, 2001). The most common diagenetic alterations are complete or partial dissolution or replacement of unstable detrital grains and precipitation of pore-filling cements. The factors affecting sandstone diagenesis are: the depositional environment; composition of the original grains; texture of the sediments; pore-

fluid migrations and the burial history. These factors are discussed in the diagenetic processes below.

9.3.1. Early Diagenetic processes

Early diagenesis covers everything that may happen after the sediment is laid down (deposited) until it first becomes rock consolidated hard rock. Processes in this stage are mechanical (bioturbation, compaction and porosity reduction), chemical (dissolution/precipitation, cementation), organic (micrite-envelope, bioturbation, bacterial action) and lastly lithification. Early diagenetic processes include mechanical compaction, silica and calcite cementation, clay mineral (pore lining and pore-filling kaolinite and smectite) and feldspar authigenesis and the formation of hematite coatings.

In the initial stages, the compaction of the grains involved dewatering and a closer packing of grains. Silica cementation may be in the form of quartz overgrowths and quartz cements. Quartz overgrowths are the most common type of silica cement. Silica cement is precipitated around the quartz grain and in optical continuity, so that the grain and cement extinguish together under crossed polarized microscope. The result of overgrowths commonly gives the grain euhedral crystal faces..

Calcite is frequently an early to middle diagenetic cement. Calcite precipitation, takes place when the solubility product is exceeded, often occurs through an increase in the activity of the carbonate ion. In shallow subsurface, this may happen through evaporation of vadose or near-surface phreatic ground water. At depth carbonate precipitation can be brought about by an increase in pH and temperature (Aref, 2011).

Although in many sandstone samples, feldspars were altered to kaolinite and illite, feldspar overgrowths do occur on detrital grains. They are most common on K-feldspars. For authigenic feldspar, alkaline pore waters rich in Na, K, Al and Si are necessary. These elements are derived from hydrolysis and dissolution of less stable grains within the sediment (Aref, 2011). Illite, kaolinite and smectite are the most common clays in the sandstones. They occur as pore-filling and pore-lining cements and clay rims around grains. Alkaline pore fluids with sufficient K, Si and Al are required for illite authigenetic environmental conditions; while kaolinite requires more acid pore waters. The ions for kaolinite and illite precipitation are largely derived from the alteration of detrital minerals, in particular clay minerals and feldspars.

The hematite occurs as a very thin coating around grains, but also stains red clay minerals and authigenic quartz and feldspar. The source and origin of hematite pigments

might have been that the amorphous iron compounds formed through moist tropical laterite weathering in upland areas, are transported and deposited along the sediments and then converted to hematite (Aref, 2011). Another possibility is whereby the iron is supplied by intrastratal solution of detrital silicates such as magnetite, hornblende, olivine, biotite and augite. In oxidizing diagenetic environment, the iron reprecipitated as hematite. The hematite is coloured red and develops above the water table if the groundwater is acidic and oxidized (Aref, 2011).

9.3.2. Late Diagenetic processes

Late diagenesis covers everything that may happen to sedimentary rocks between consolidation and the lowest temperature and low pressure of metamorphism. It involves processes affecting the sediments at deeper levels, and also during and after uplift. During deeper burial, pore waters are modified further by reactions with clay minerals, dissolution of unstable grains, precipitation of authigenic minerals and mixing with waters from other sources. Processes in this stage are albitisation of feldspar, sericitisation, chloritisation, pressure-solution, grain-deformation and fracturing.

During the middle and later stage, sericitisation and chloritisation of smectite clays were developed. Sericitisation involved the replacement of feldspar or feldspathoids by fine micas, while chloritisation refers to the replacement of any mafic mineral by chlorite.

Albitisation of feldspar is a process of total or partial replacement of plagioclase feldspar or alkali feldspar with albite. It is a common process during which hydrothermal fluids convert plagioclase and/or K-feldspar into albite in deep burial environments. Albitisation of feldspar probably occurred during fracturing of the detrital feldspar grains.

9.4. Results of diagenetic features

9.4.1. Compaction

The sandstones of the Mikambeni and Madzaringwe Formations were subjected to moderate to intense mechanical and chemical compaction during its continuous burial as evident from the change of grain contacts, with long and concavo-convex types and sutured contacts (Figures 9.1, 9.2, 9.3 and 9.4) of neighbouring framework grains, dominate in these sandstones.

Long and embayed contacts are very abundant in the samples examined (Figures 9.1A and B). This suggests a moderate degree of compaction. Sutured grain contacts and fractured

grains are also common. In moderately to deeper burial zones, mechanical compaction in the sandstones is evidenced by the fracturing of quartz and feldspars (Figure 9.4). Progressive burial resulted in increasing compaction and porosity loss initially by grain rotation or slippage leading to eventual fracture of more resistant minerals. This results in pressure dissolution, which is a deformation mechanism that involves the dissolution of minerals at grain to grain contacts into an aqueous pore fluid in areas of relatively high stress (Figure 9.3). Grain fracturing is also evidence of significant compaction (Figure 9.4). These observations in thin section suggest that the rocks are tightly compacted.

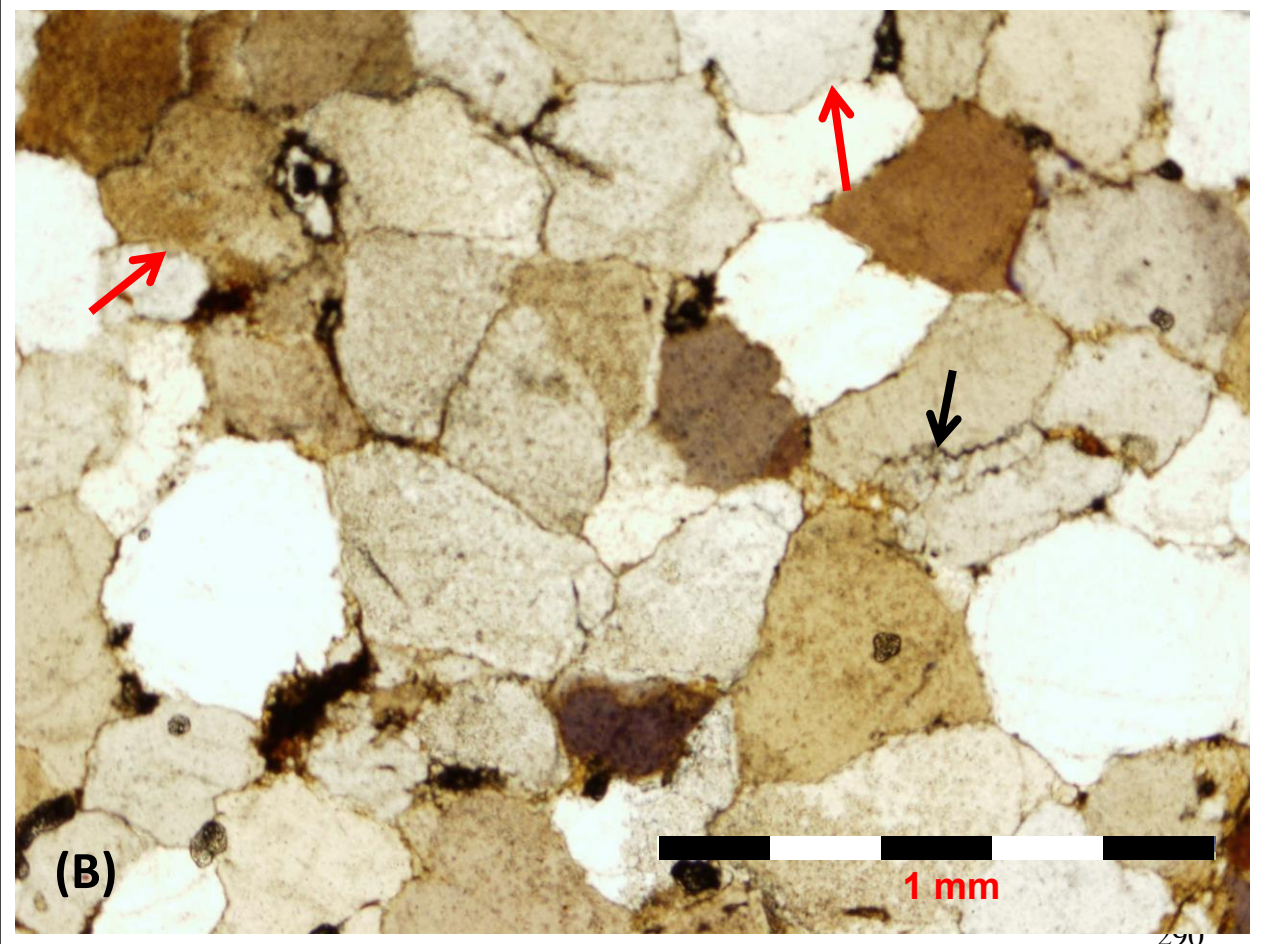
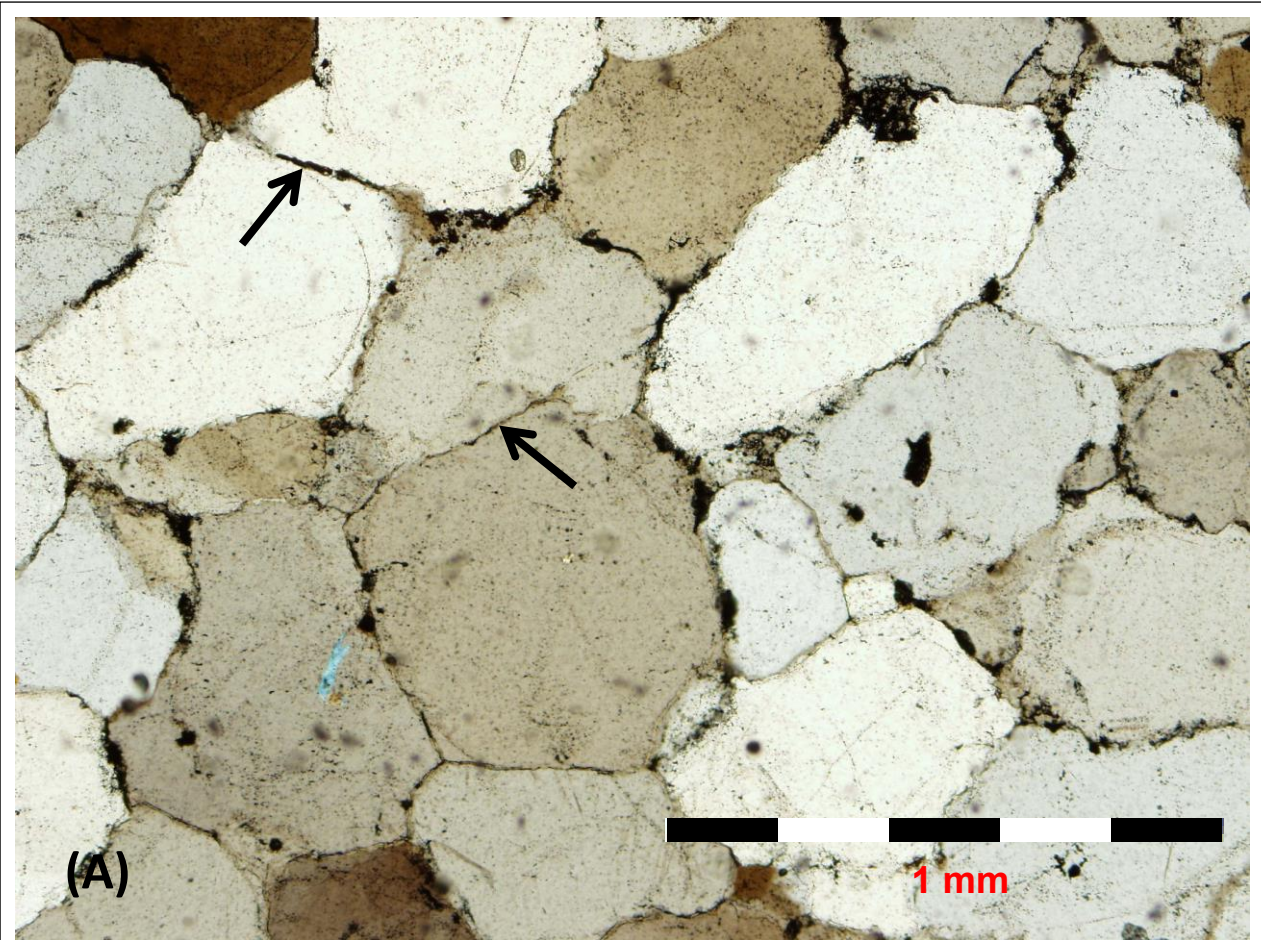


Figure 9.1: (A) Photomicrographs of tightly mosaic grain-texture, showing also straight contacts (arrows) between neighbouring framework grains; (B) Photomicrographs of concavo-convex contact (red arrows) and intergranular contacts (black arrow) between neighbouring framework grains in the Soutpansberg Coalfield.

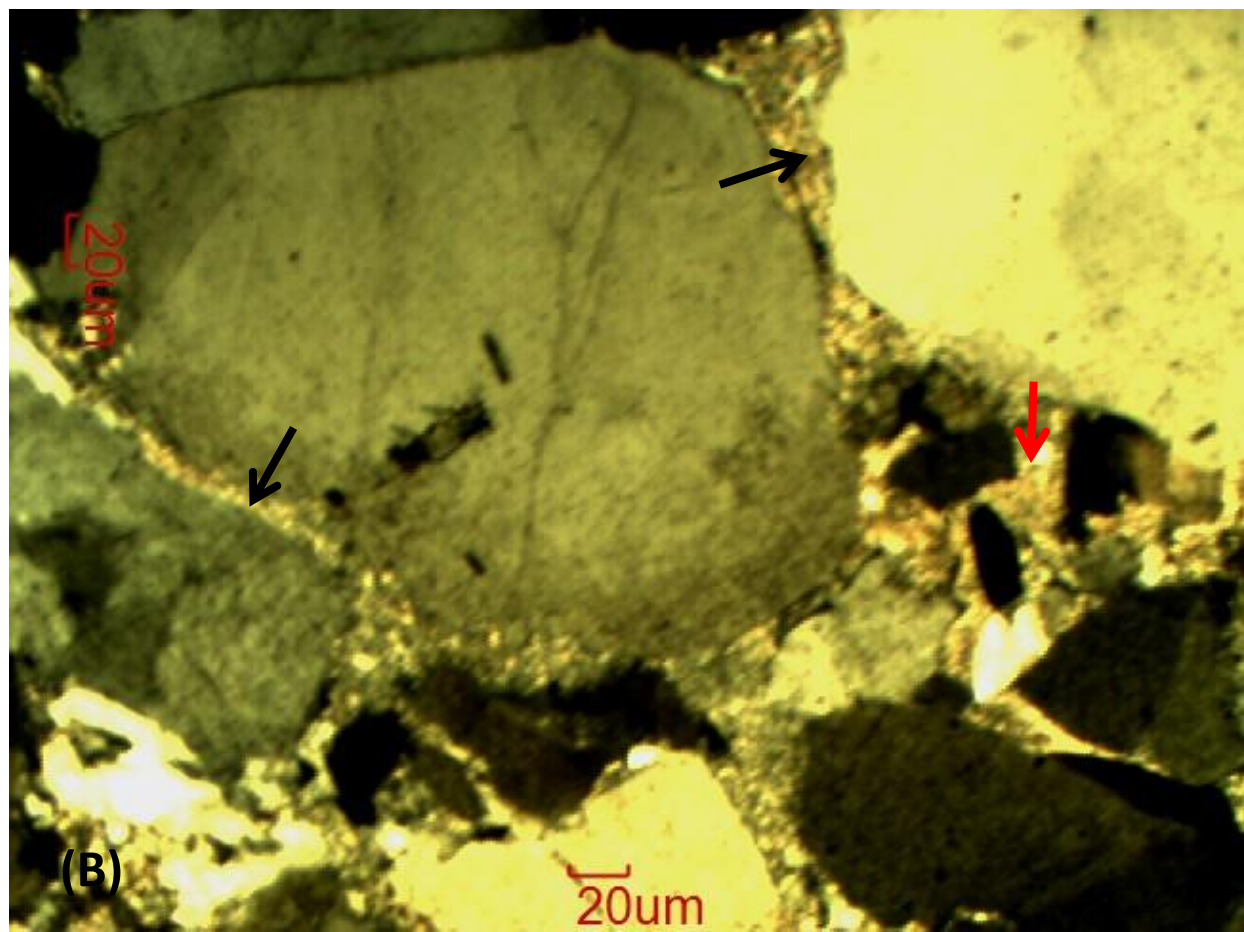
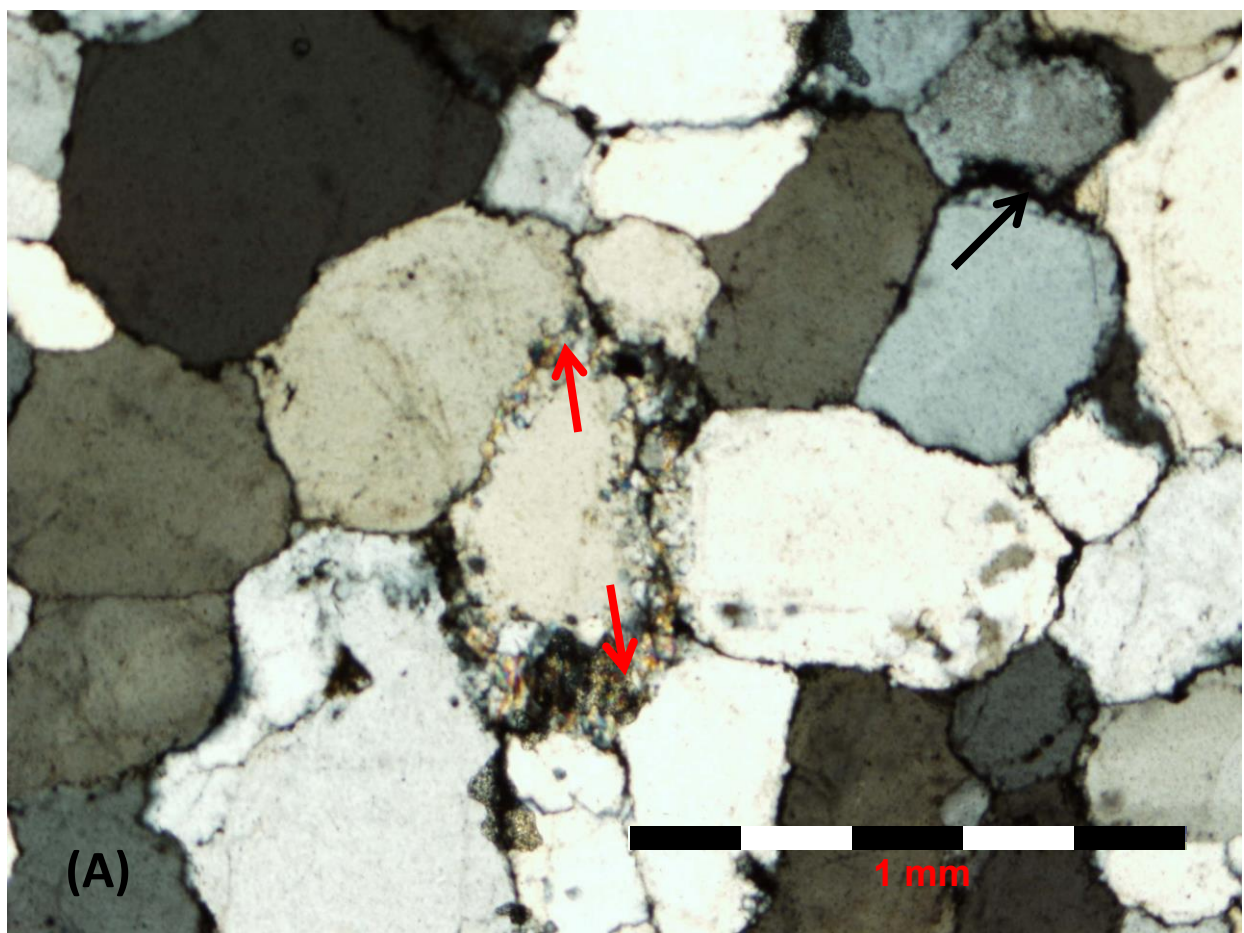


Figure 9.2: (A) Photomicrographs of quartz grains and grain-coating hematite (black arrow), the red arrows shows pressure shadow texture due to clays developing in low pressure areas; (B) Photomicrographs of pore-lining clays (black arrow) and pore filling (red arrow) between neighbouring grains in the Soutpansberg Coalfield.

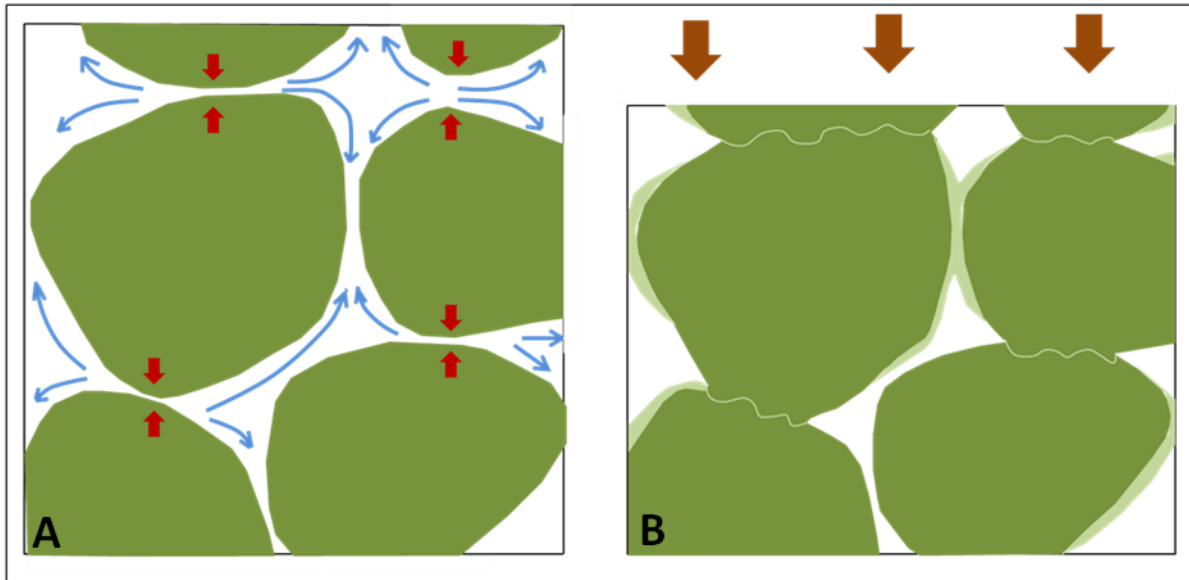
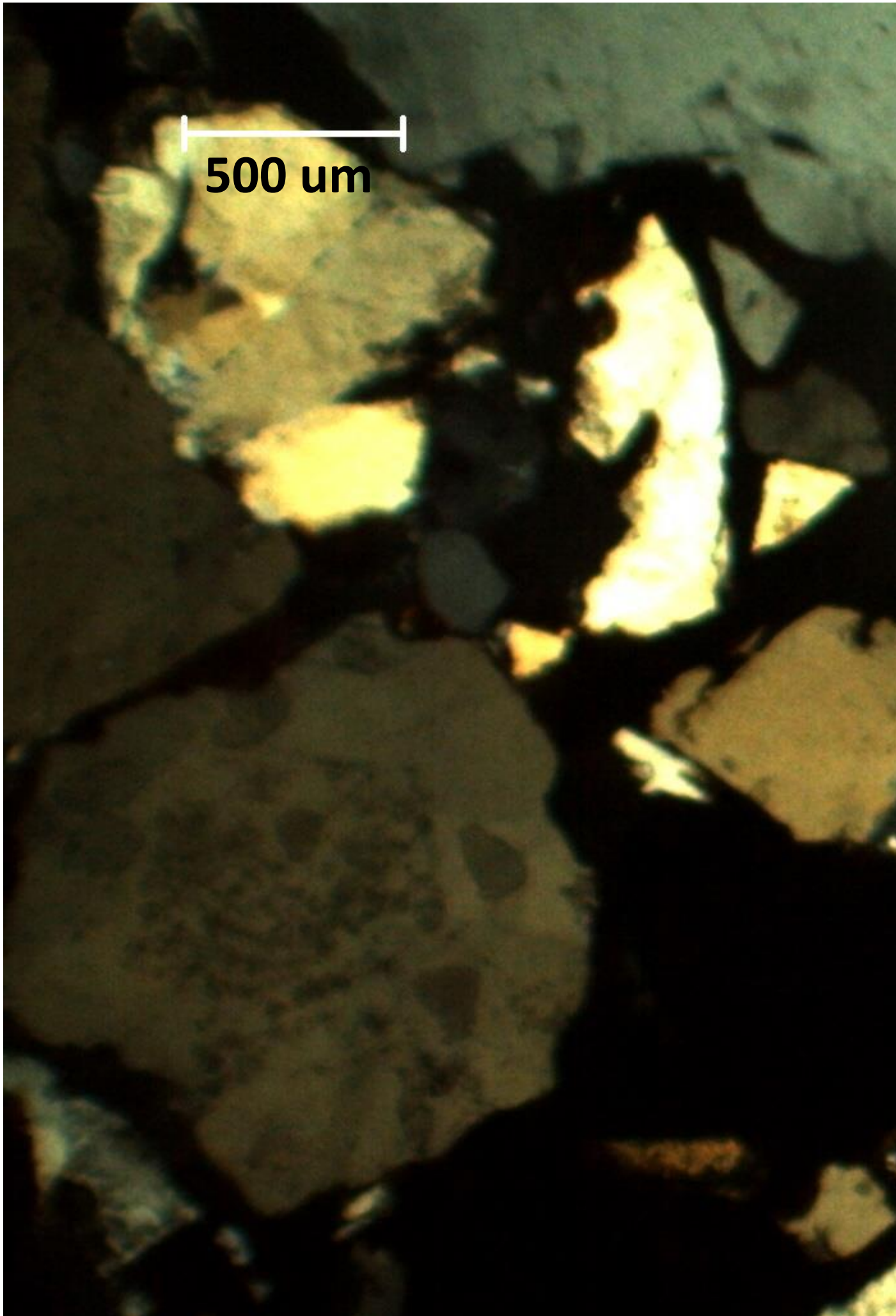


Figure 9.3: Schematic diagram of pressure solution accommodating compression/compaction in a clastic rock. A: shows the situation before compaction. Blue arrows indicate the movement of particles and pore-fluids. Red arrows indicate areas of maximum stress (= grain contacts). B: shows the situation after compaction. In light coloured areas new mineral growth has reduced pore space (pore-linings).



500 um

Figure 9.4: Fracturing of grains (red arrow) in the Mikambeni Formation of the Soutpansberg Coalfield.

9.4.2. Pore lining and pore filling clays

Authigenic clays present in the sandstone samples of the formations consist mostly of kaolinite, illite, and illite/smectite. Authigenic clays originate from a variety of sources. Deformation and alteration of labile grains due to compaction create clays in pseudomatrix. Dissolution of feldspar grains and albitization of plagioclase liberates aluminum that may precipitate as kaolinite. Illite-smectite sometimes forms as alteration products of volcanic grains and biotite.

Illite, illite-smectite, and chlorite formed as pore-lining and pore-filing clays. These clays formed early in the diagenetic history as indicated by the occurrence of clay rims on detrital grains, sometimes separating the grains from overgrowths (Figure 9.5). Earlier clays crystallized within intergranular pore space created during an earlier stage of dissolution. Illite-smectite occurs as a grain coating (pore-lining) (Figures 9.6, 9.7, 9.8 and 9.9), and also as a replacement of grain-coating clays. Pore-filling and pore-bridging illite-smectite (Figures 9.6 and 9.7) also occurs. Illite-smectite is often represented by lath, or hair-like crystals oriented perpendicular to the detrital grain surfaces. Under the SEM, Illite/Smectite clays show corn flake morphology.

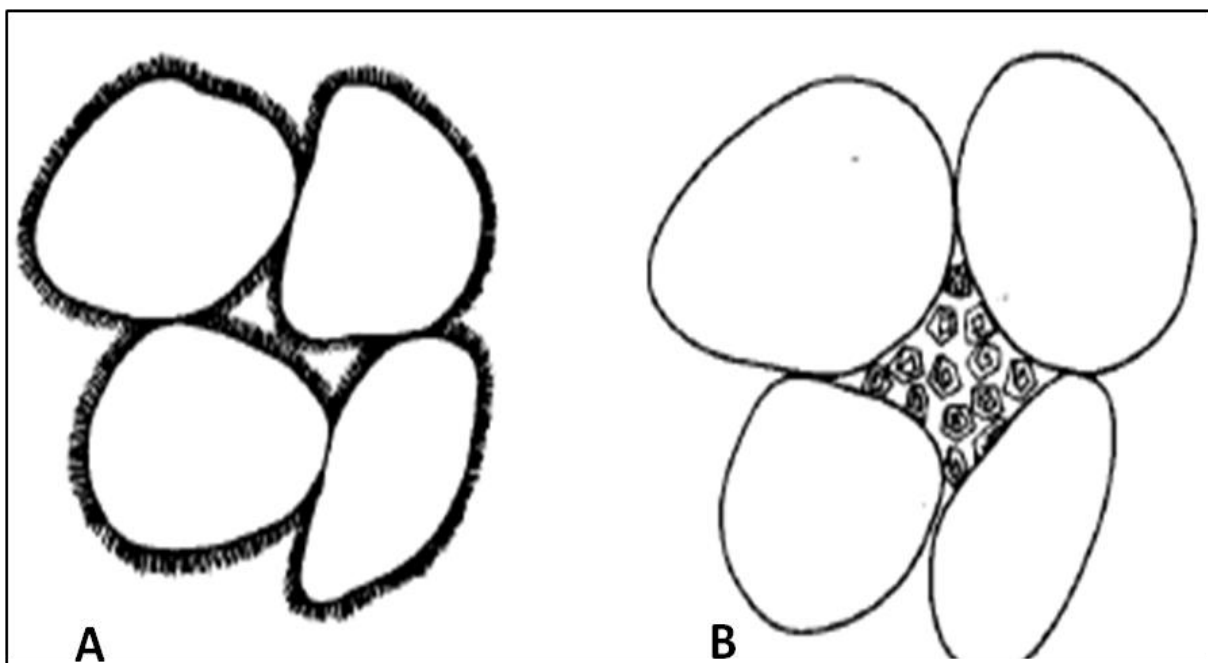


Figure 9.5: A: Pore lining clays, B: Pore filling clays (Bjorlykke, 1989).

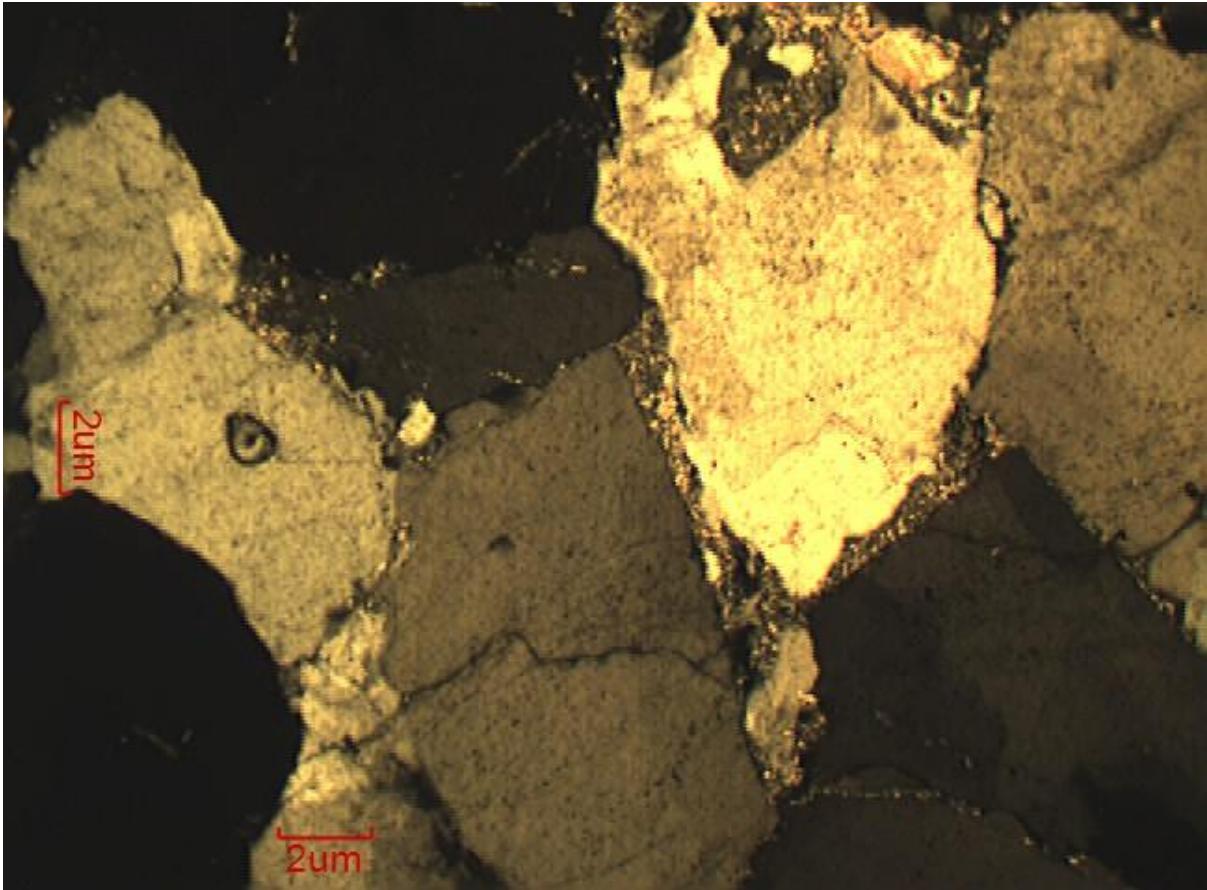


Figure 9.6: Photomicrographs of pore filling clays around quartz grains in the Mikambeni Formation of the Soutpansberg Coalfield.

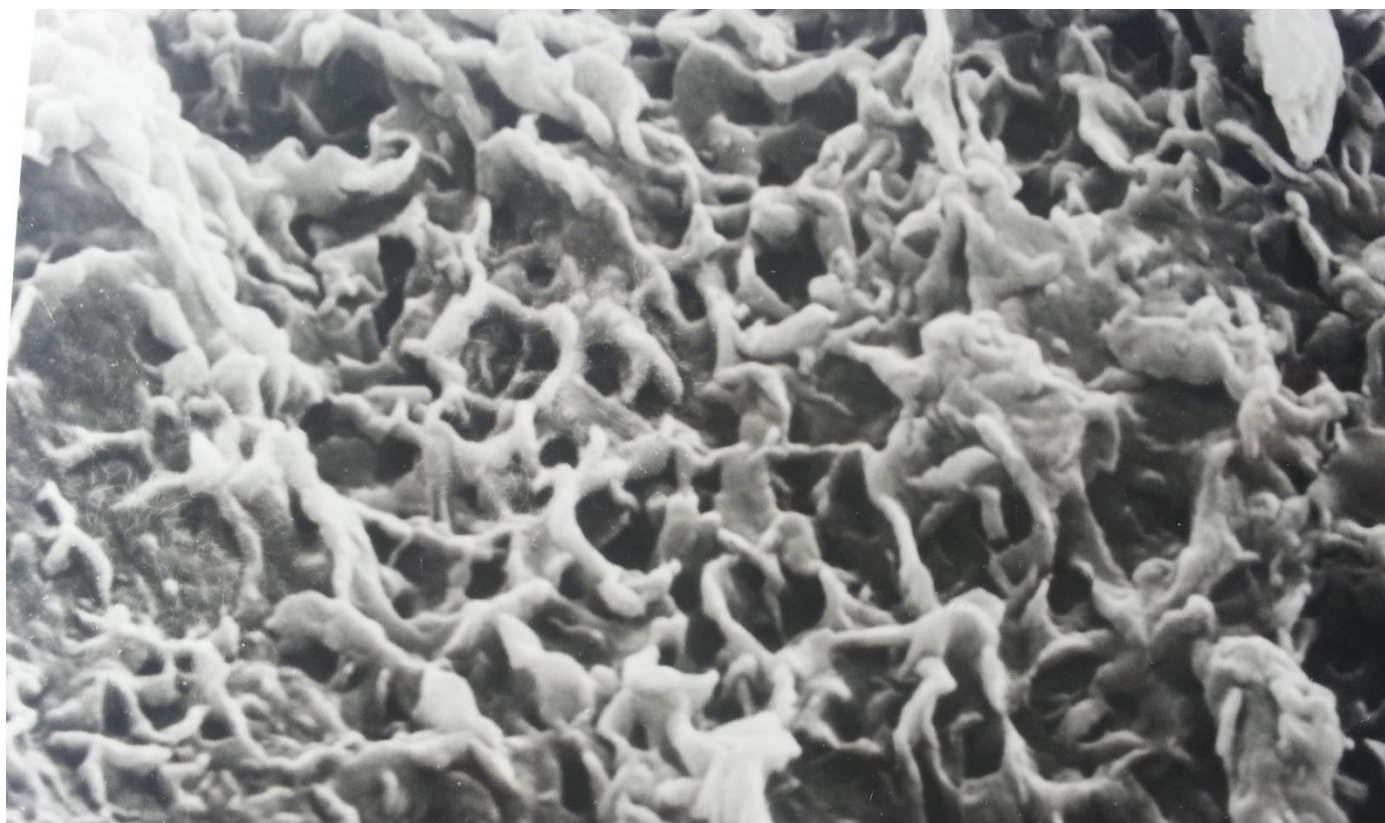
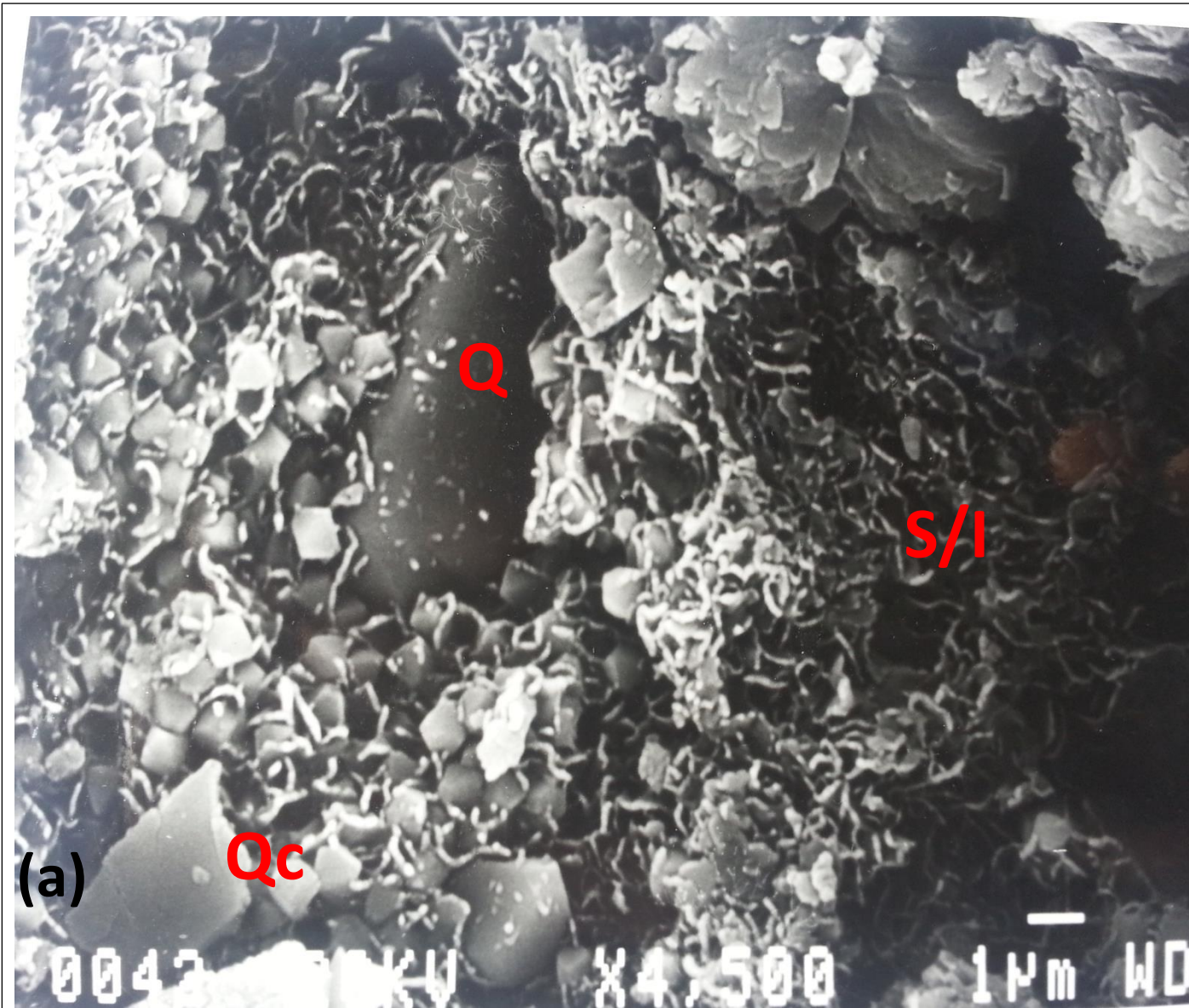


Figure 9.7: (a) SEM photomicrographs of clay cements in sandstones showing smectite (S) and illite (I) filling pores between quartz (Q) grains, also showing are quartz cements (Qc); (b) Smectite to illite recrystallisation.

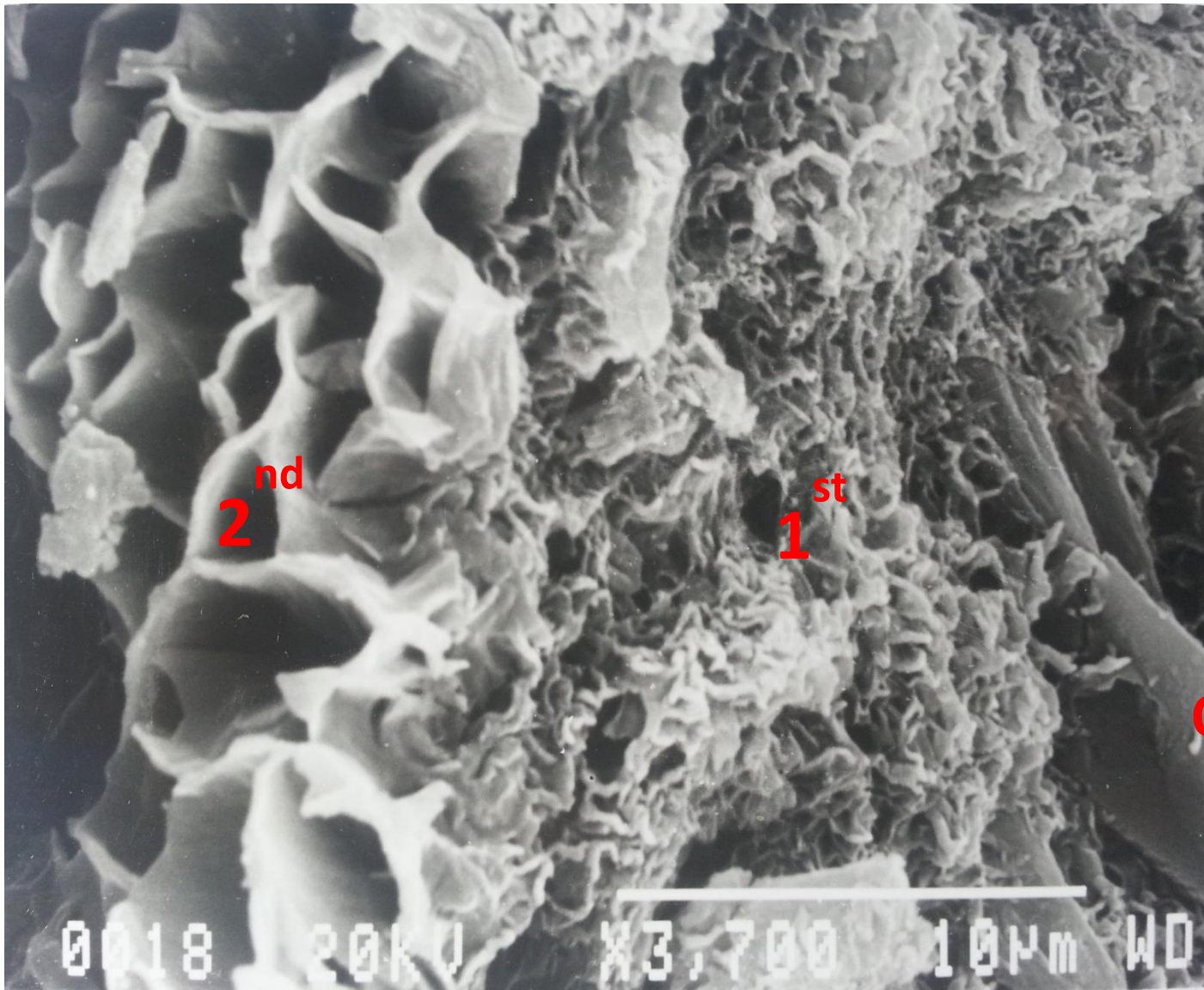


Figure 9.8: SEM photomicrographs showing two stages of smectite/illite cement between quartz (Q) grains. The middle is the first stage (1st) of fine smectite/illite cement, and left is the second stage (2nd) of coarse smectite/illite cement.

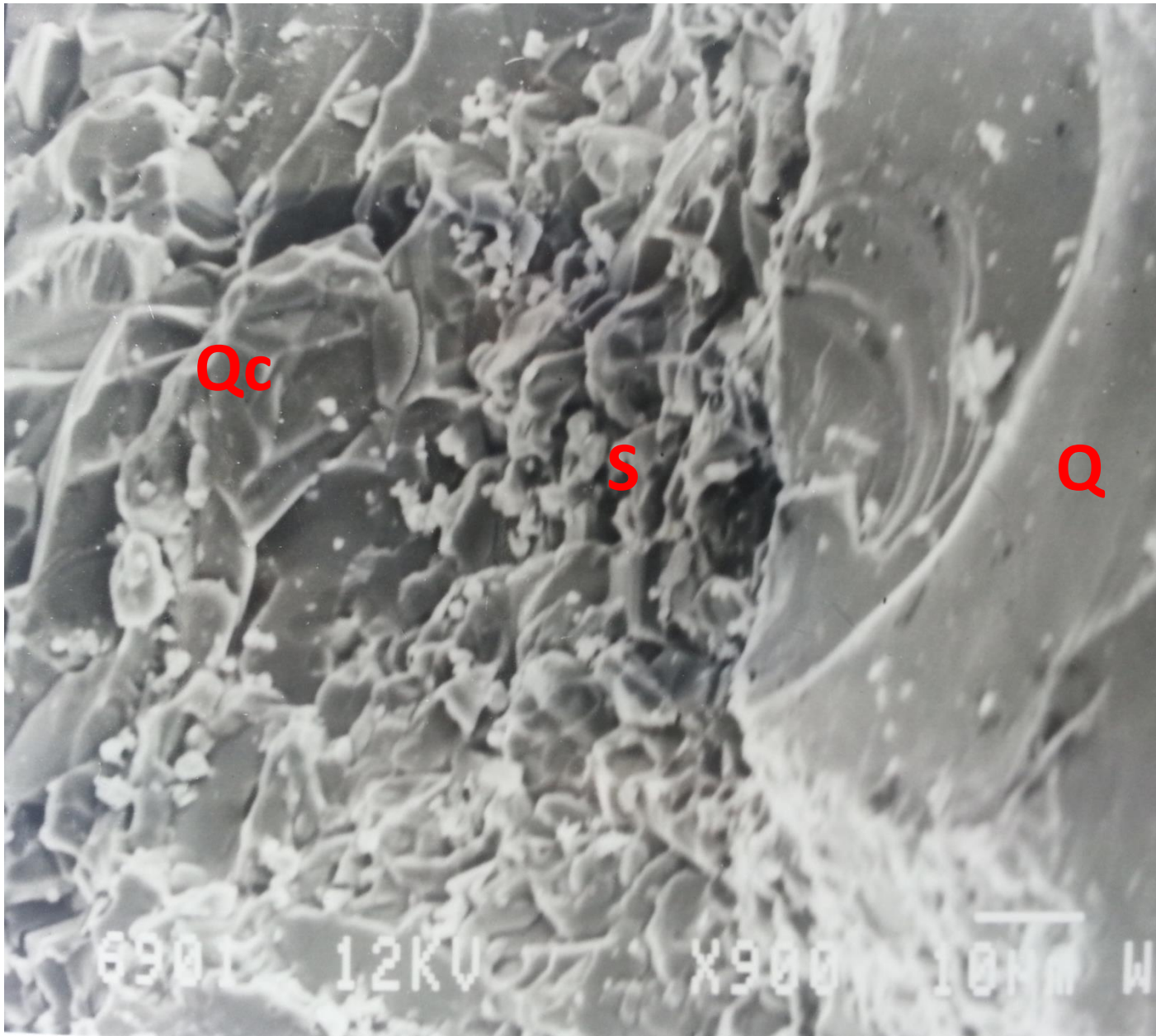


Figure 9.9: SEM photomicrograph showing a detrital quartz grain (Q), first stage cement of smectite (S) and second stage cement of quartz cement (Qc).

9.4.3. Quartz Cementation

Quartz cement occurs as both pore-filling and overgrowths in the samples. It appears that most of the pore-filling quartz cement is derived from the sands themselves (authigenic) or quartz sands worn away from other rocks (detrital) (Figures 9.12 and 9.13). Quartz overgrowths are abundant in the matrix-poor sandstones. These overgrowths in crystallographic (and optical) continuity with the original quartz grains (Figure 9.10). The overgrowth cement grows outward from the original grains (Figure 9.10). Some grain dust-

line (dirt forming an irregular coating on the surface of the grain) is developed (Figure 9.12A). Small/incomplete pyramidal quartz overgrowths (Figure 9.12B and 9.13A) are also developed. Quartz overgrowths are common near sites of intergranular crystals and the pores are often engulfed by large overgrowths (Figure 9.13B). In some cases, the boundaries between the detrital quartz and the quartz overgrowths are marked by clay coatings, dust lines and fluid inclusions (Figure 9.13A). Complete euhedral quartz overgrowths are common in the sandstones where the chlorite cements are rare or present in minor amounts. Feldspar overgrowths have been found as trace in some sandstone. The abundance volume of quartz cement in the samples is interpreted to be caused largely by their mineralogical maturity.

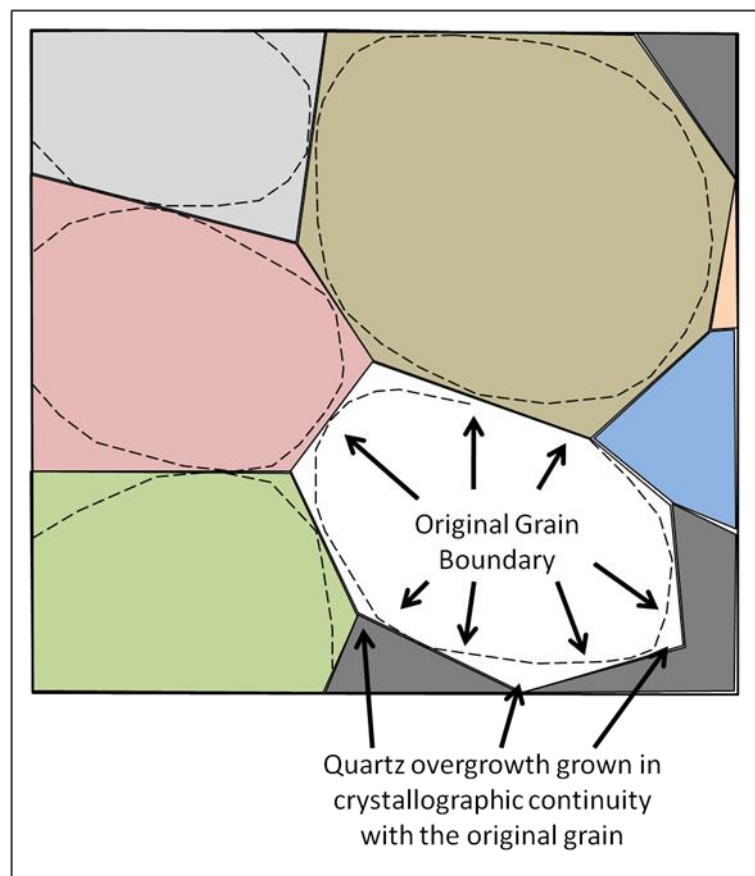


Figure 9.10: Sketch showing formation of quartz overgrowths (Redrawn after Nelson, 2013).

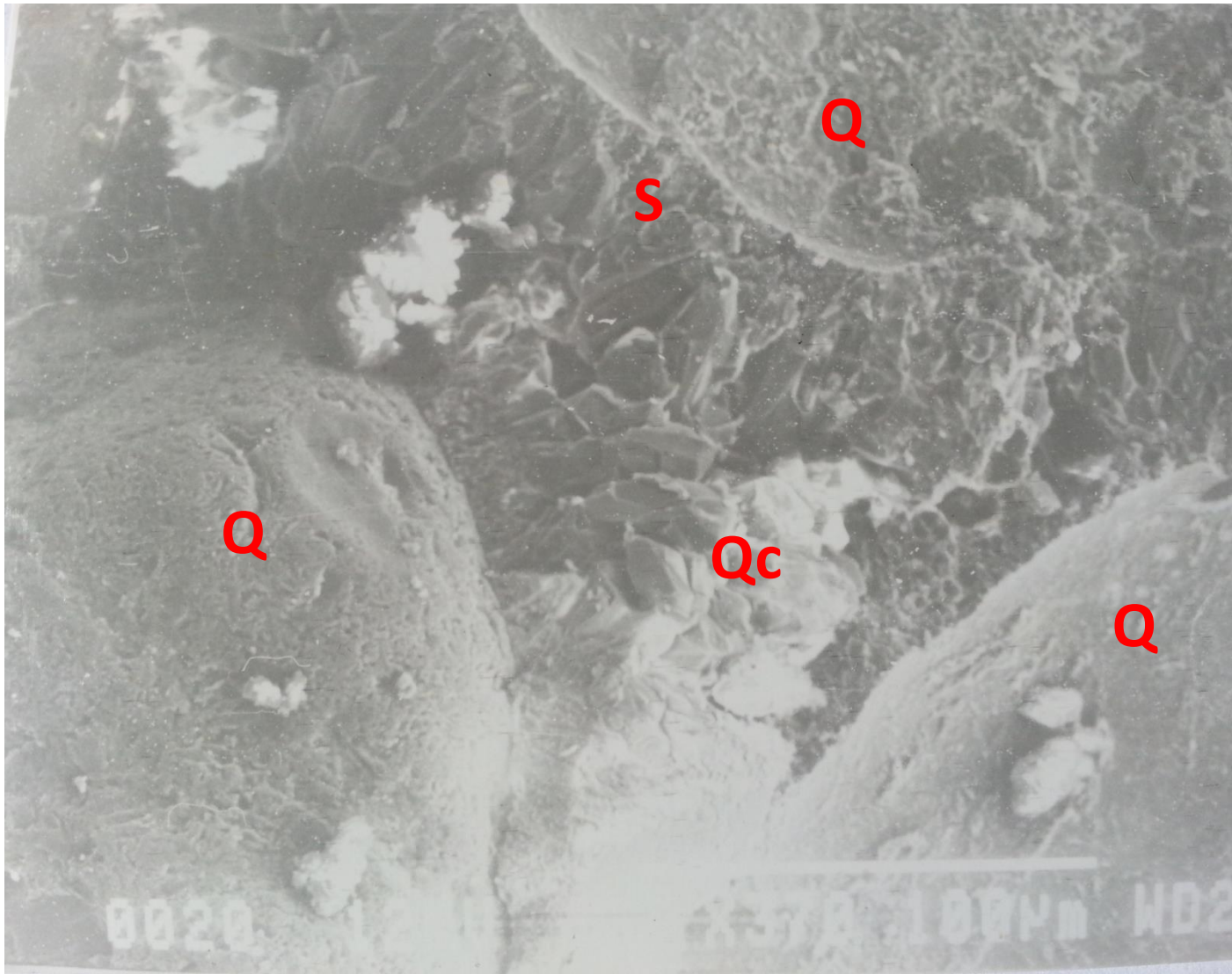


Figure 9.11: SEM photomicrographs of sandstone, showing quartz grains (Q), first stage cement of smectite (S) and second stage cement of quartz (Qc).

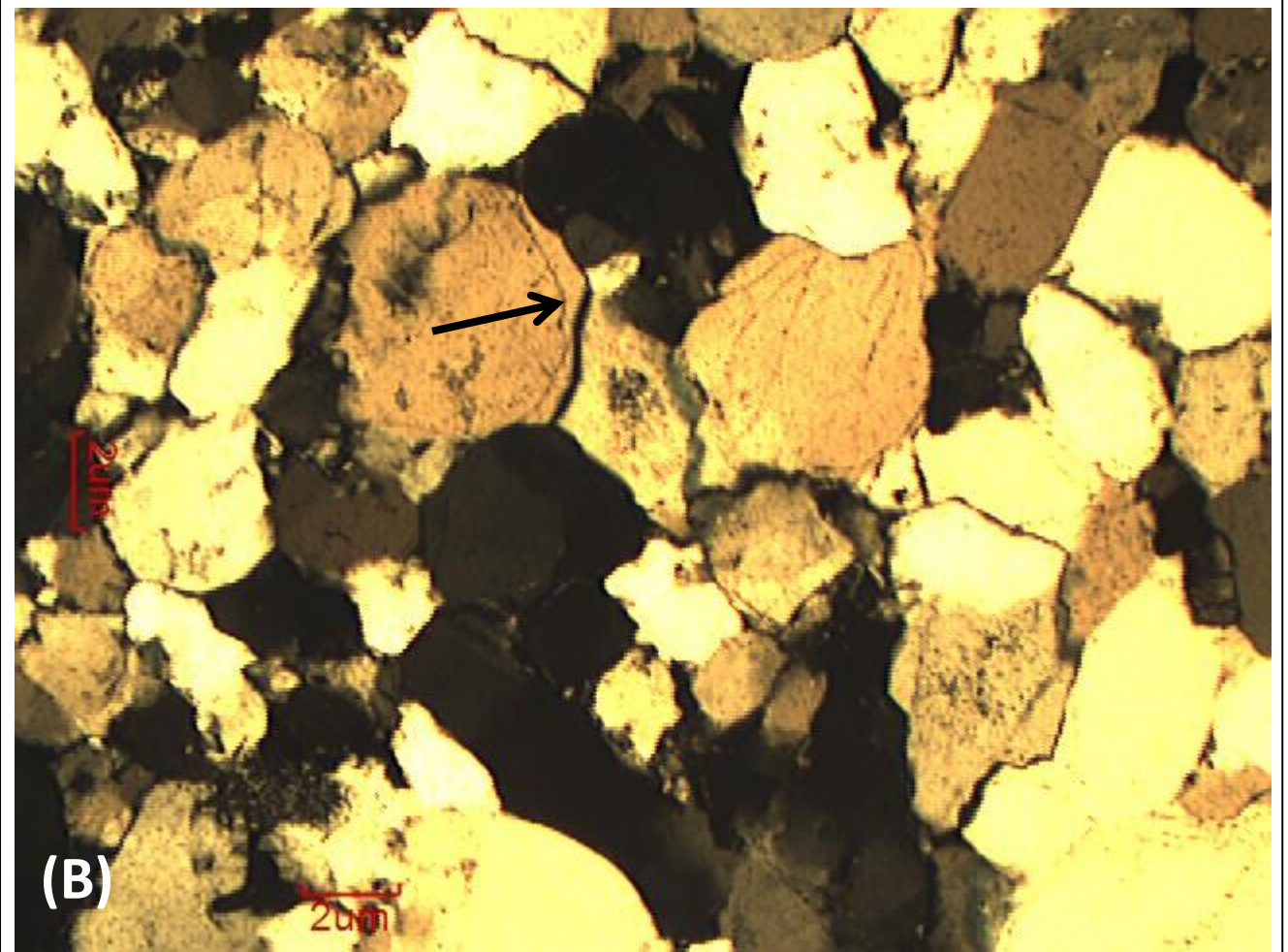
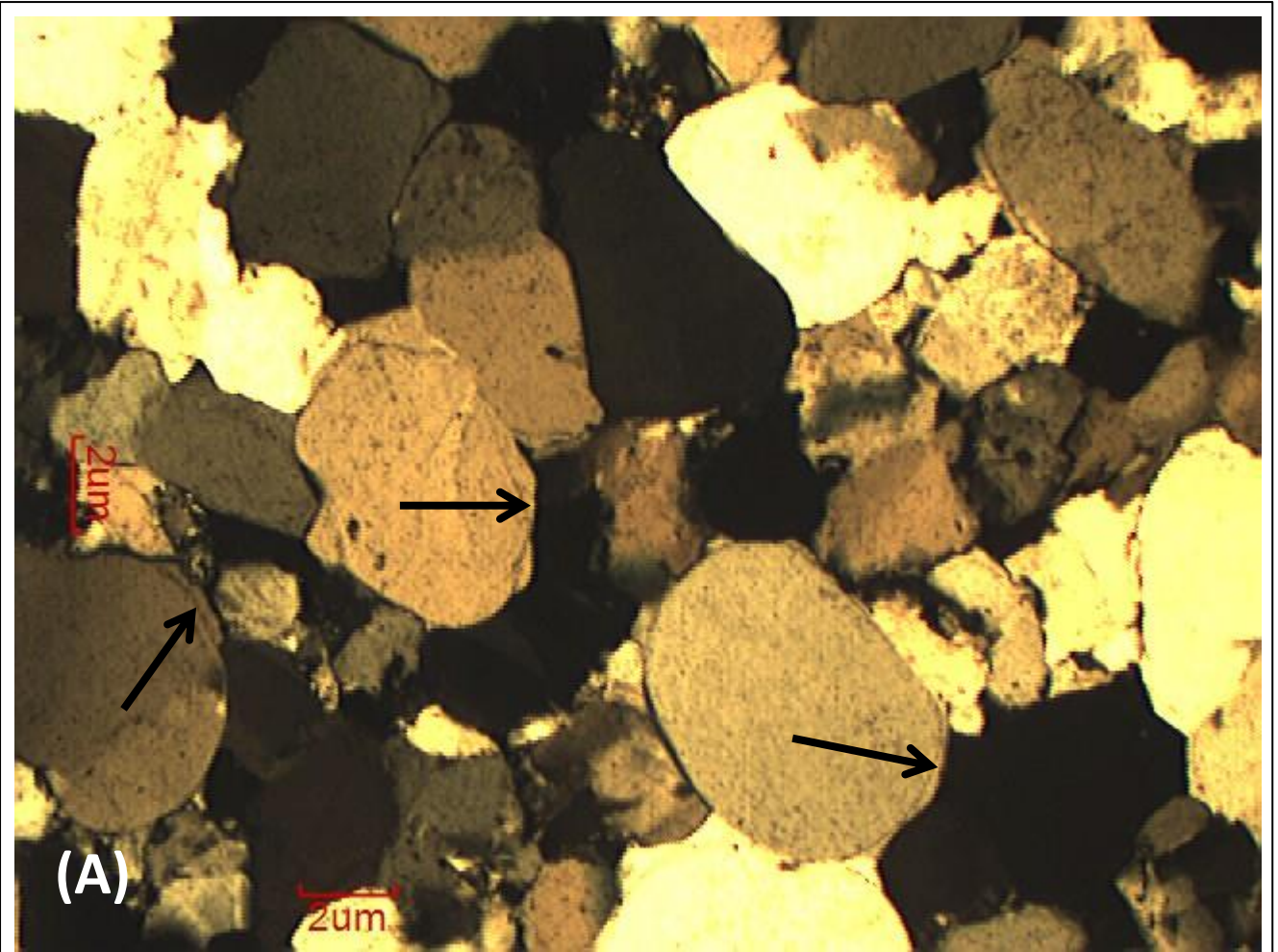


Figure 9.12: Photomicrographs of sandstone, showing quartz overgrowth (arrows) cementing quartz grains in (A) Mikambeni Formation of the Tuli Coalfield; B: Mikambeni Formation in the Soutpansberg Coalfield.

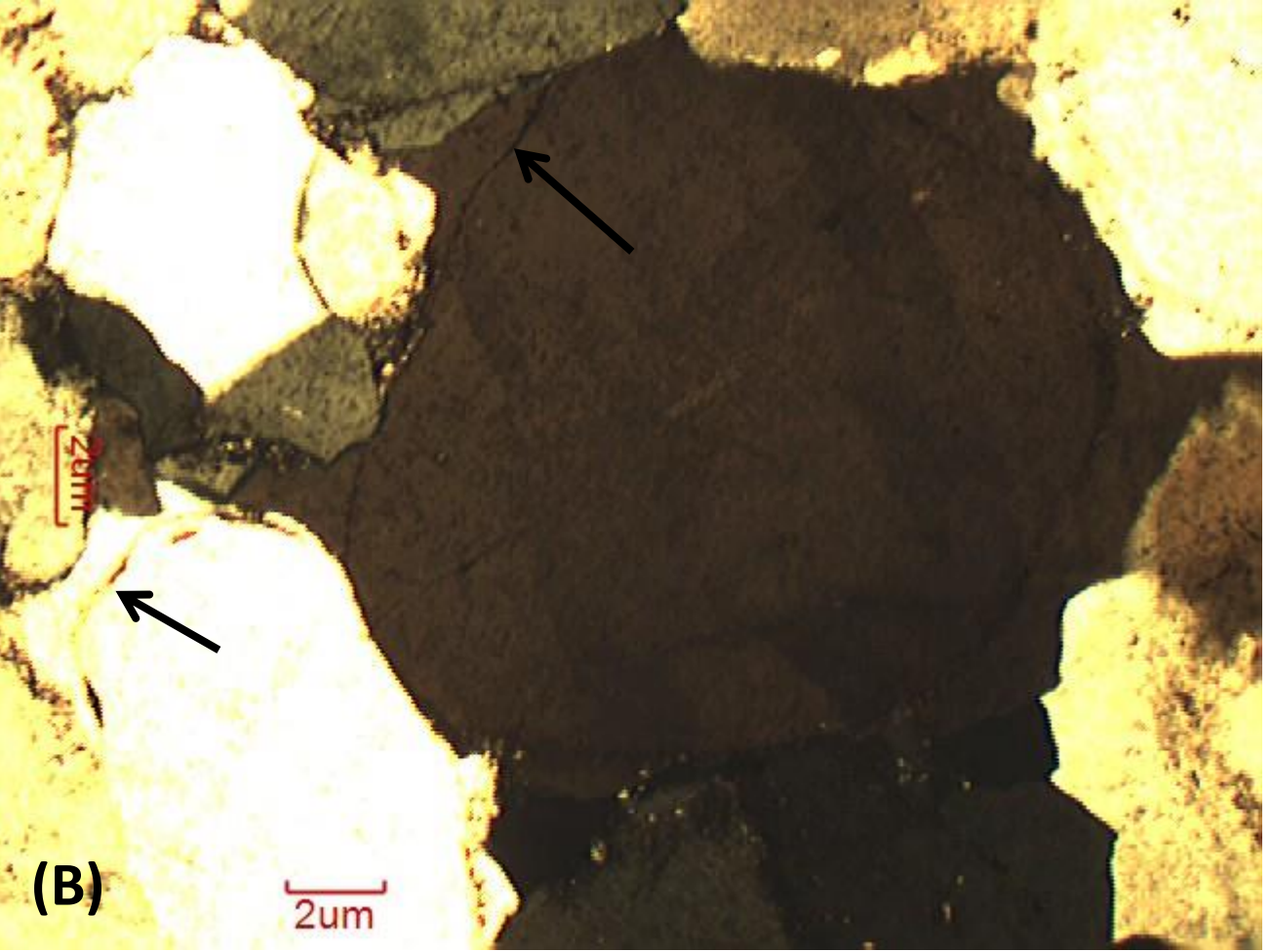
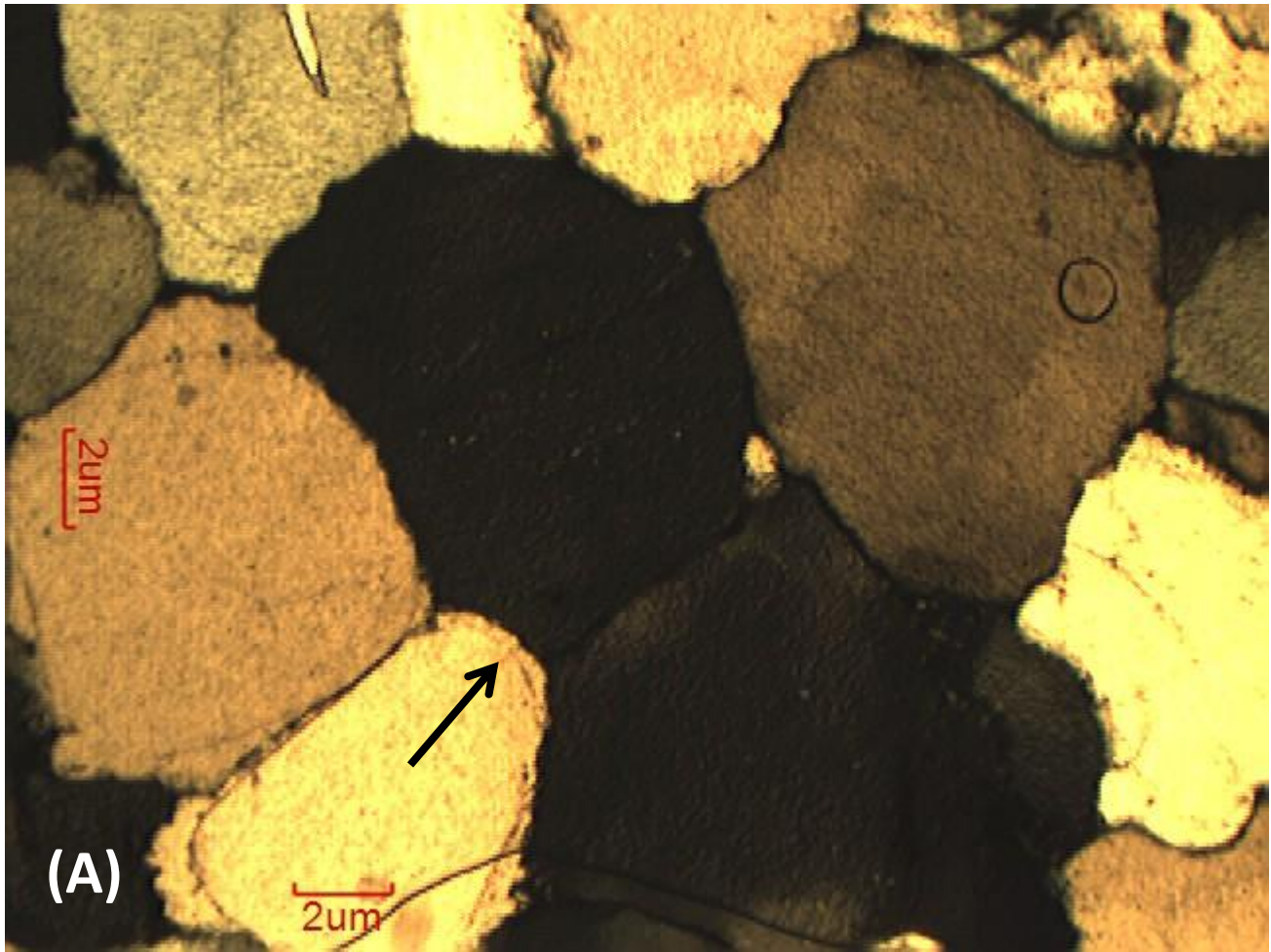


Figure 9.13: Photomicrographs of sandstone, showing quartz overgrowth (arrows) cementing quartz grains in (A and B) Mikambeni Formation of the Soutpansberg Coalfield.

9.4.4. Chlorite cementation

Authigenic chlorite occurs in the coalfields in two forms: grain coating (pore-lining) and pore-filling. Well crystallised chlorite is observed in most sandstone samples of the coalfields. In other samples the chlorite replaced many detrital grains, including quartz, feldspar and rock fragments. Most chlorite occurring in the coalfields post-dated other diagenetic minerals. Early pore-filling and secondary chlorite is interpreted to have been formed largely by dissolution of volcanic rock fragments followed by in situ precipitation.

9.4.5. Calcite cementation

Calcite cementation occurs mostly as a pore-filling and as well as a replacement mineral of detrital grains (Figure 9.14). Calcite replaced feldspar and quartz grains partly or completely, mostly at their margins. Locally these grains were severely attacked and replaced by calcite, and replacement even penetrated into the cores of grains (Figure 9.14). The calcite cementation seems to post-dates quartz overgrowth.

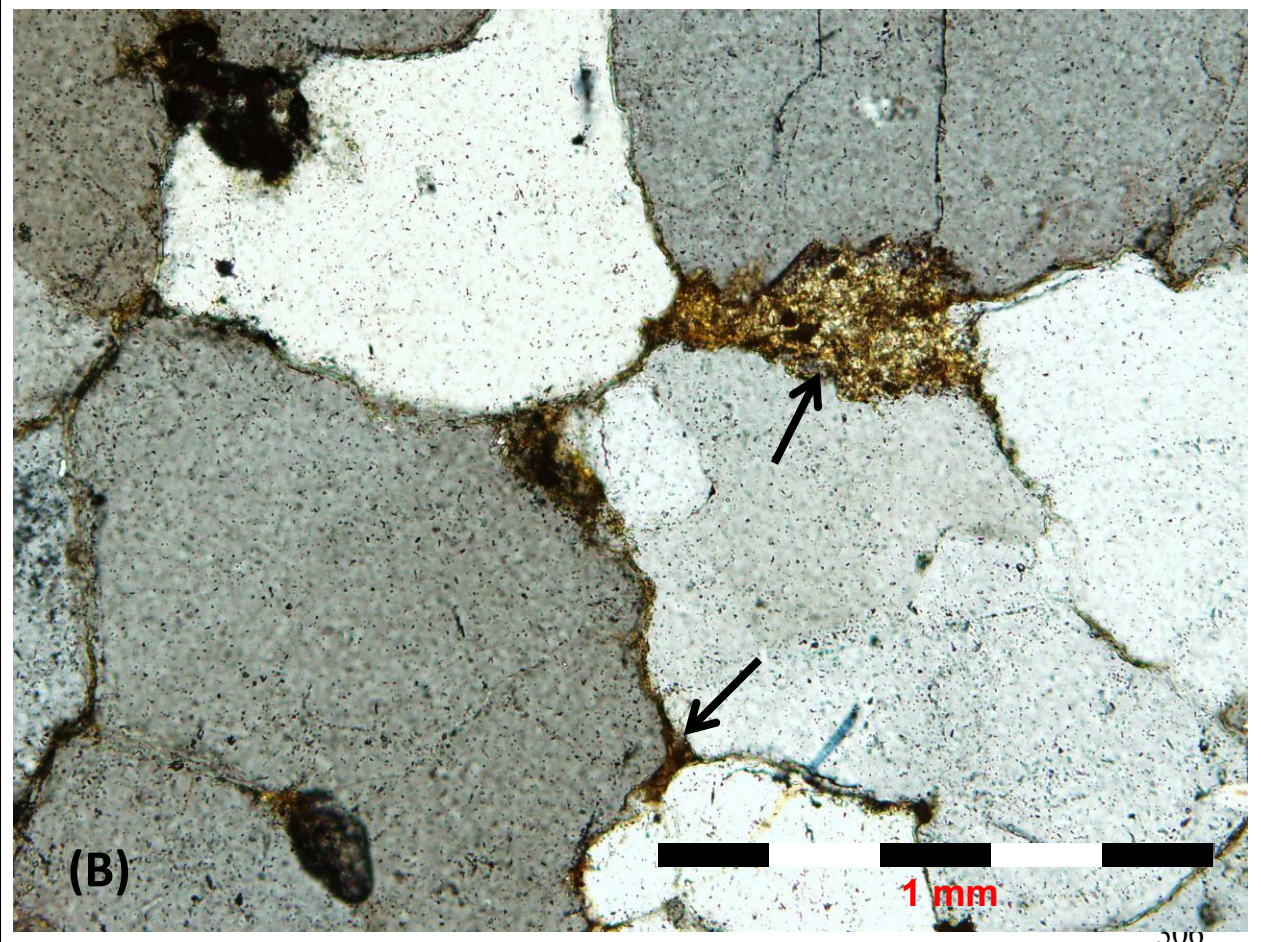
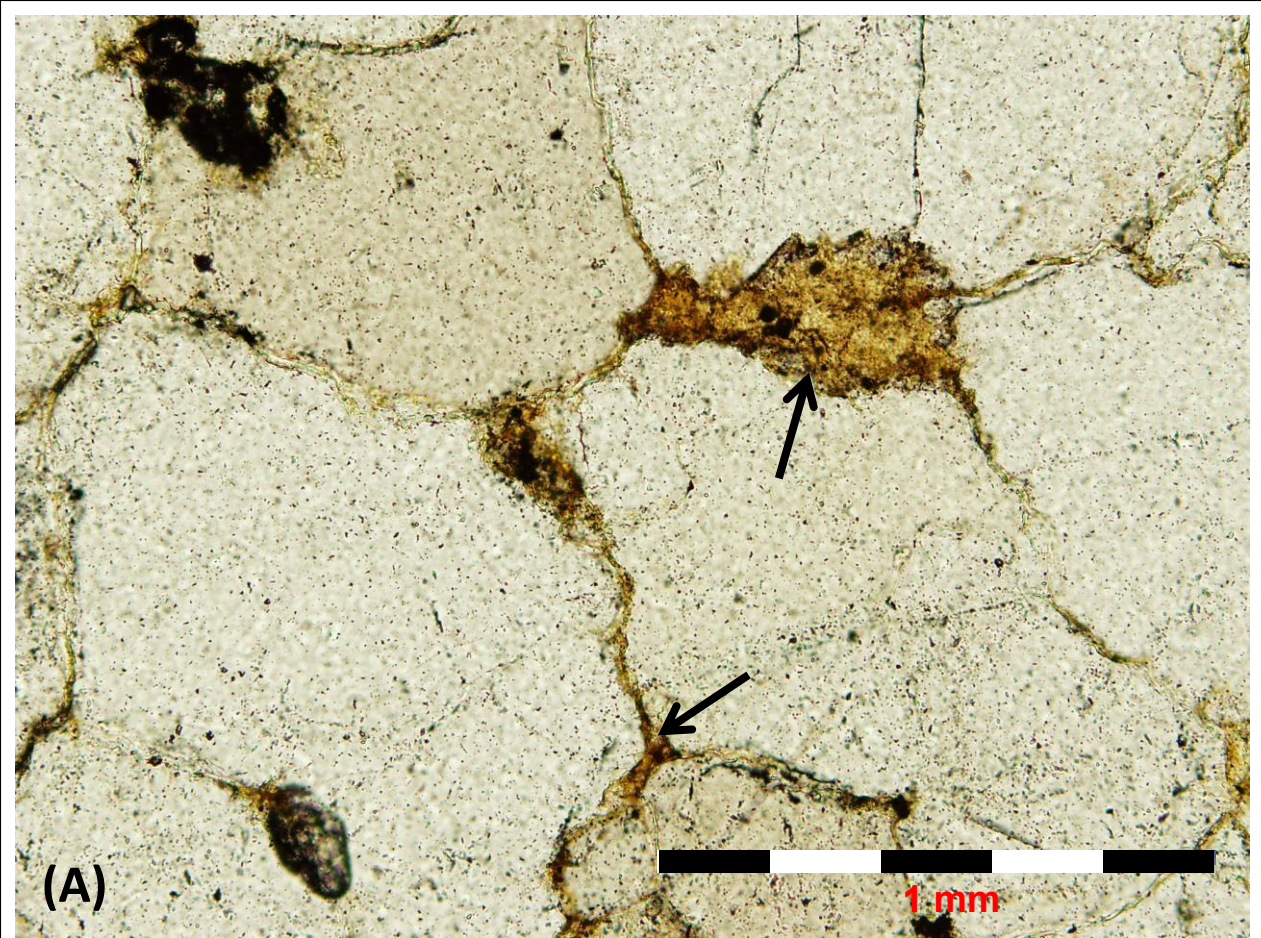


Figure 9.14: Calcite cementation in the Mikambeni Formation of the Soutpansberg Coalfield (A: plane polarized, B: cross polarized).

9.4.6. Albitisation of feldspar

Albitisation of feldspar is one of the major diagenetic changes during late-stage diagenesis in the coalfields. Detrital plagioclases, which are partially to almost completely albitised, are recognized throughout the sequence. K-feldspar is less extensively albitised than plagioclase in sandstones (Figures 9.15 and 9.16). Feldspar albitisation is most extensive in the Soutpansberg. Albitisation occurred preferentially along microfractures, cleavages and grain contact margins. In these sandstones, Na^+ might have been supplied by dissolution and alteration of igneous sediments, and by well circulated fluids passing through faults. On contrary feldspars occurring in some Tuli sandstones show no or weak albitisation or alteration, probably because feldspars in these sandstones were isolated from the reactive fluids during diagenesis.

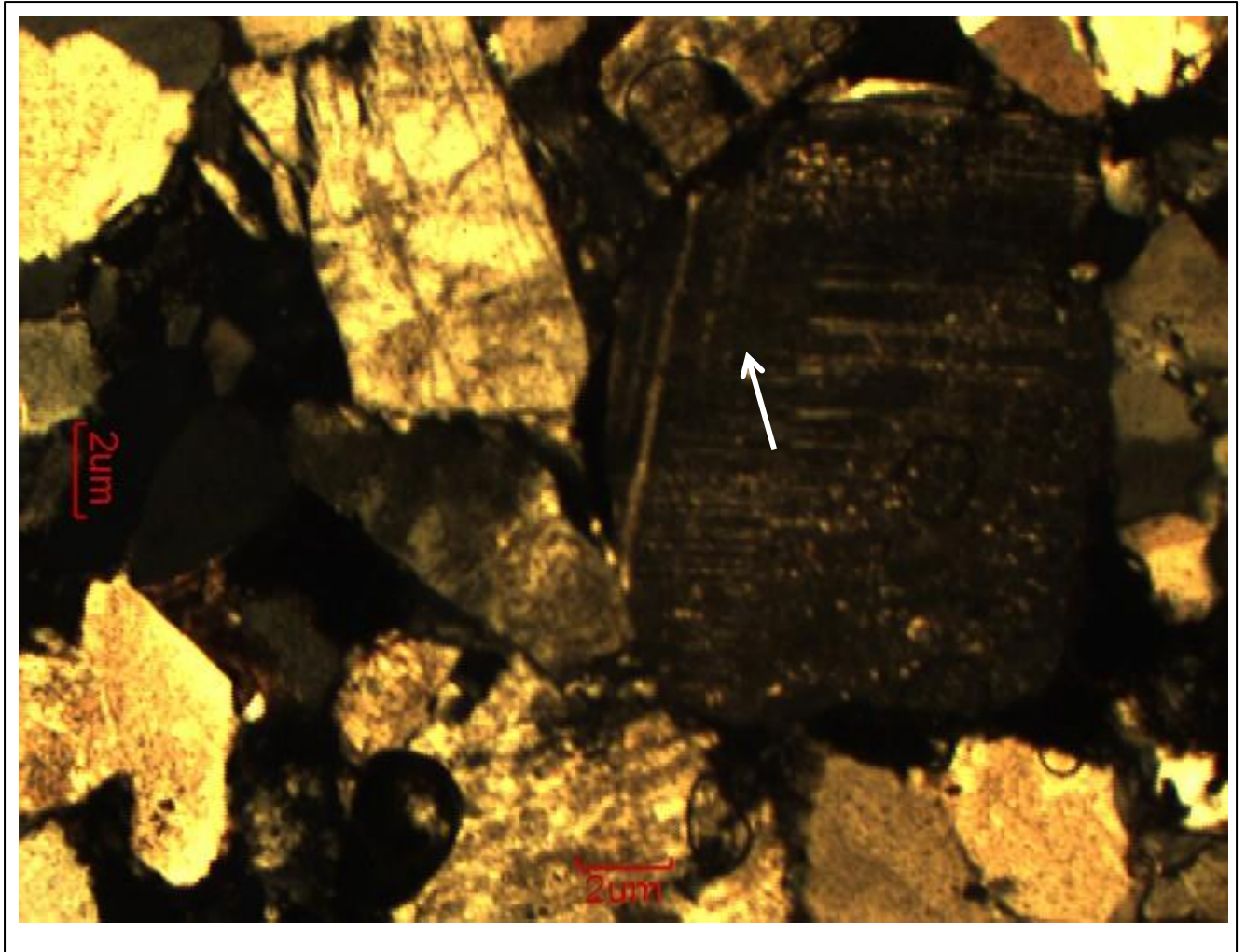


Figure 9.15: Partially albitised plagioclase (arrow) in the Mikambeni Formation of the Soutpansberg Coalfield. The albitised part within a plagioclase grain shows absence of twinning and cloudy appearance.

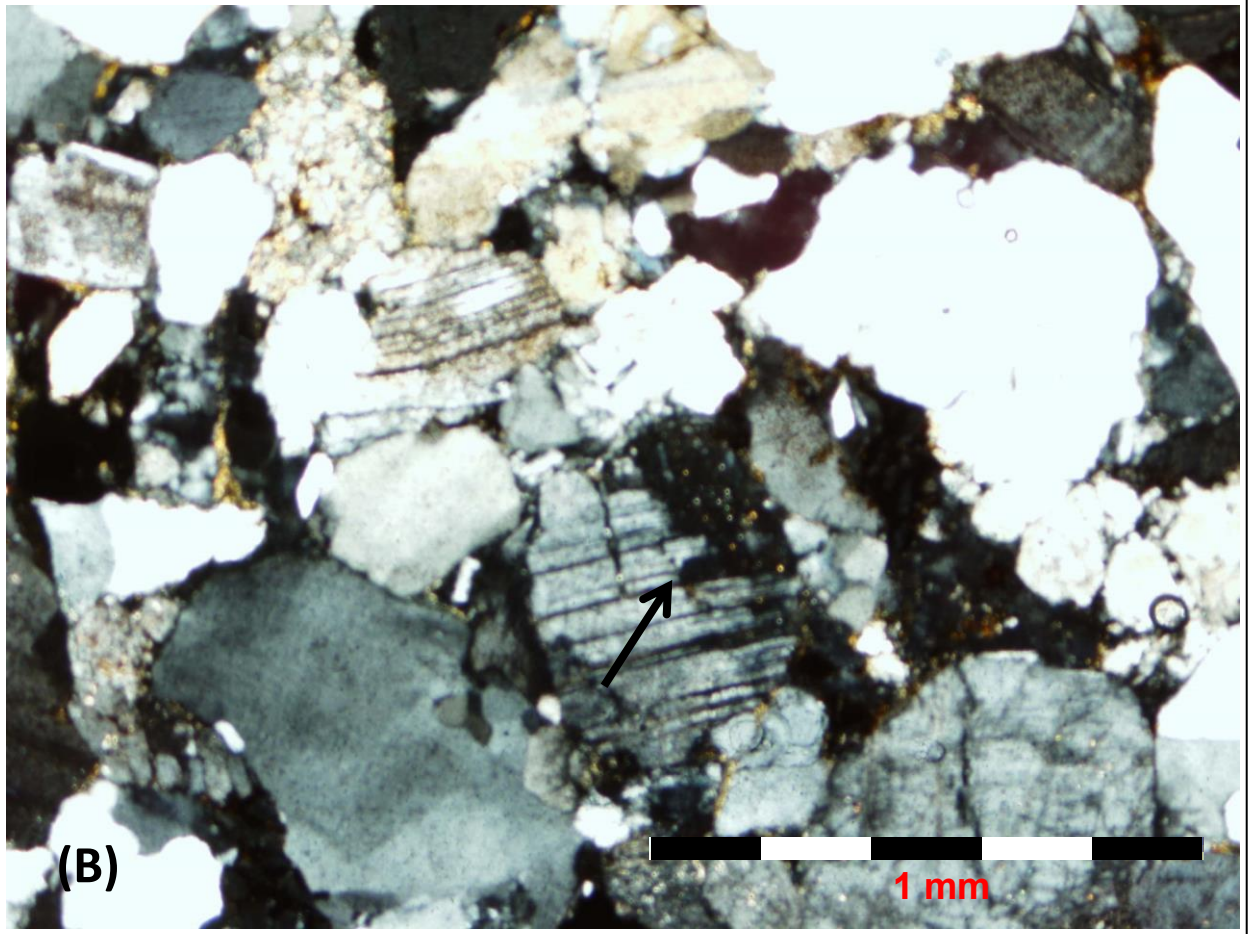
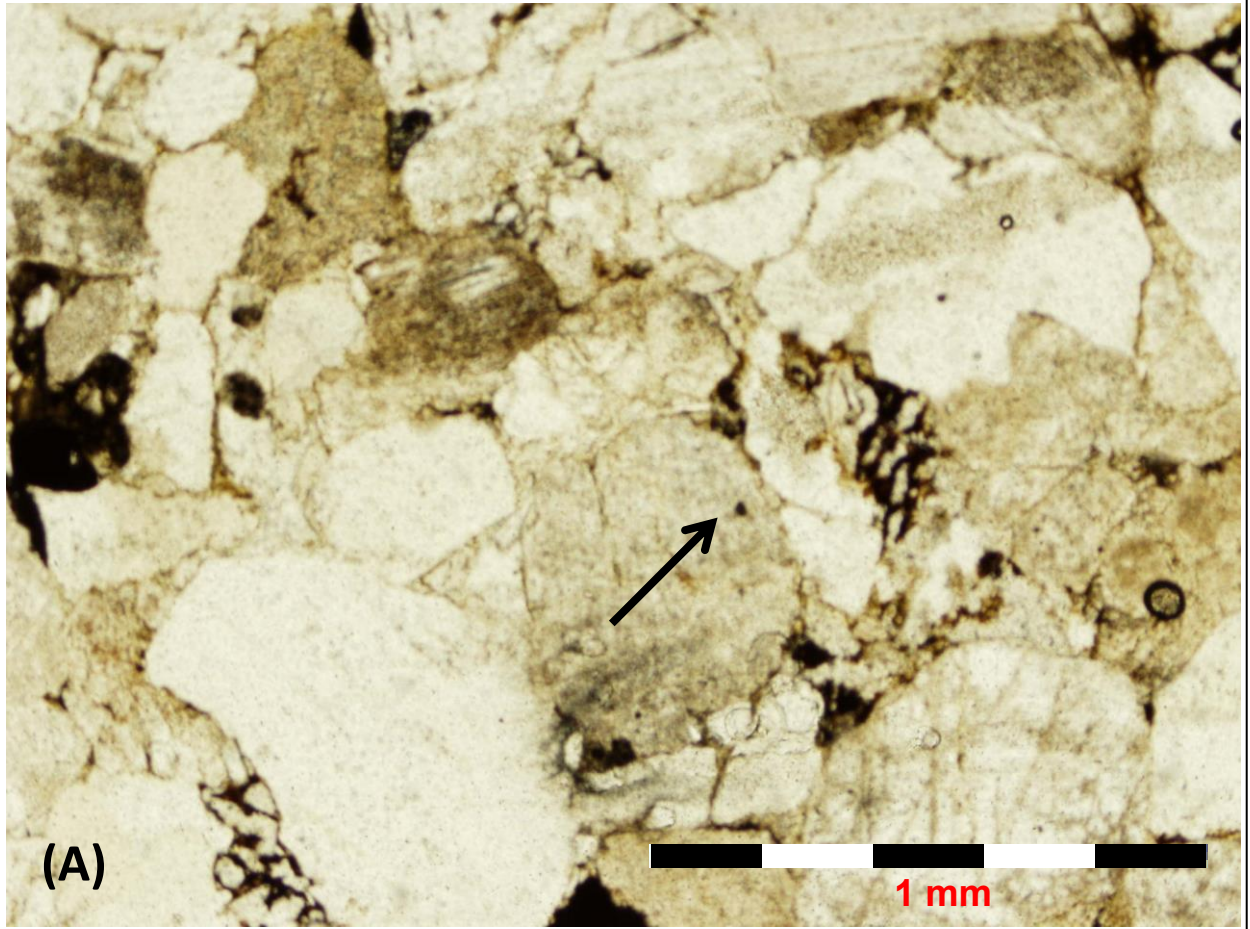


Figure 9.16: Photomicrographs of albitised plagioclase; A and B shows a plane and cross polarized partially albitised plagioclase (arrows) from the Tuli Coalfield.

9.5. Discussions

Diagenesis of both the Mikambeni and Madzaringwe Formations of the Tuli and Soutpansberg sandstones can be divided broadly into early and late diagenetic stages. Early diagenetic processes include mechanical compaction, silica and calcite cementation, clay mineral (pore lining and pore-filling kaolinite and smectite), feldspar authigenesis and the formation of hematite coatings. Late diagenesis includes albitization of feldspar, seritisation, chloritisation pressure-solution, deformation and fracturing.

Diagenetic processes that affect sandstones include compaction, grain alteration, precipitation of pore-filling cement, and dissolution of grain material or cement. Factors that influence burial diagenesis include depositional environment, detrital mineralogy, pore-water chemistry, hydrology, temperature, and pressure (Hayes and Boles, 1992).

Quartz cement as pore filling and overgrowths is the most abundant cements in both the Tuli and the Soutpansberg sandstones. The main factors that control the amount of quartz cement in sandstones are: framework composition; residence time in the “silica mobility window”; and fluid composition, flow volume and pathways (McBride, 1989). Thus, the type of sedimentary basin in which sand was deposited strongly controls the cementation process. The most likely important sources of silica for quartz cements within unmetamorphosed sandstones include pressure solution of detrital quartz grains at grain contacts and at stylolites, albitisation and dissolution of K-feldspar grains.

The compositions and abundance of authigenic clays differs between the two coalfields. Authigenetic clays in the Soutpansberg sandstones are more abundant compared to the Tuli sandstones. Earlier illite-smectite and chlorite clays precipitated and crystallized within intragranular pore space created during an earlier stage of diagenesis. Smectite and kaolinite are more abundant in rocks with higher matrix content. Calcite is notable in the sandstones with its poikilotopic nature filling pores between grains. Chlorite is notable in sandstones having large quantities of volcanic rock fragment and detrital micas.

Late diagenesis of the sandstones was largely controlled by their burial diagenetic environment. First, albitisation of feldspar occurred preferentially along the microfractures, cleavages and grain contact margins in deep burial environment. Albitisation of feldspars is a common and very significant reaction that takes place during burial diagenesis of arkosic sandstones. The albitisation reaction occurs locally at stressed grain contacts, presumably due

to the resultant high sodium content (Boles and Ramseyer, 1988). In the same time other controlling factors of albitisation could be pore-water composition, which could bring Na-source to the system.. Thus, authigenic albite provides information about the composition of the formation pore-fluids from which the albite precipitated. Albitisation depends on the stability of the detrital grains and on the degree of pore-water saturation with respect to sodium and silicate contents (Kastner and Siever, 1979). Albitisation of feldspar grains in the coalfields occurred during the middle and later stages of diagenesis. As the sediments were progressively buried, albitisation began when they reached the minimum temperature of 80°C required for the reaction. The albitisation textures observed in thin section and SEM provide further understanding about the occurrence of diagenetic albite.

The main diagenetic differences of the Mikambeni and Madzaringwe Formations in the Soutpansberg and Tuli Coalfields are tabulated in Table 9.1.

Table 9.1: Main differences in diagenesis between the two formations (Mikambeni and Madzaringwe) in the Soutpansberg and Tuli Coalfields.

	<i>Tuli</i>		<i>Soutpansberg</i>	
	Mikambeni	Madzaringwe	Mikambeni	Madzaringwe
Sandstone Classification	Quartz-arenites	Quartz-arenites to feldspathic litharenites	Quartz-arenites to lithic arkose	Quartz-arenites and litharenites to feldspathic litharenites
Compaction	Moderate to intense	Moderate to intense	Moderate to intense	Moderate to intense
Quartz cementation	Pore filling and minor overgrowths	Pore filling and minor overgrowths	Pore filling and abundant overgrowths	Pore filling and abundant overgrowths
Calcite cementation	Pore –filling and replacement grains	Pore –filling and replacement grains	Pore –filling and replacement grains	Pore –filling and replacement grains
Clay content	Pore-lining and pore-filling, Minor	Pore-lining and pore-filling, Abundant	Pore-lining and pore-filling, Minor	Pore-lining and pore-filling, Abundant
Feldspar authigenesis	Quartz overgrowths	Quartz overgrowths	Quartz overgrowths	Quartz overgrowths
Occurrence of chlorite	Grain coating	Grain coating	Grain coating	Grain coating
Albitisation	None	Chemical reaction, Minor	Chemical reaction Abundant	Chemical reaction Abundant
Hematite cementation	Coating and pore filling	Coating and pore filling	Coating and pore filling	Coating and pore filling

During early diagenesis in the Mikambeni and Madzaringwe Formations of the Soutpansberg Coalfield, large amounts of pore-filling and quartz overgrowths occurred. Early diagenetic processes include mechanical compaction, silica and calcite cementation, clay mineral (pore lining and pore-filling kaolinite, illite and smectite), feldspar authigenesis and the formation of hematite coatings. During burial mechanical and chemical compaction started to reduce pore spaces and some clays (smectite) matrices altered to form illite and also kaolinite was formed. During the middle and later stage, sericitisation and chloritisation of smectite clays and later albitisation of feldspar, suture contact and fracturing of grains were developed (Figure 9.17).

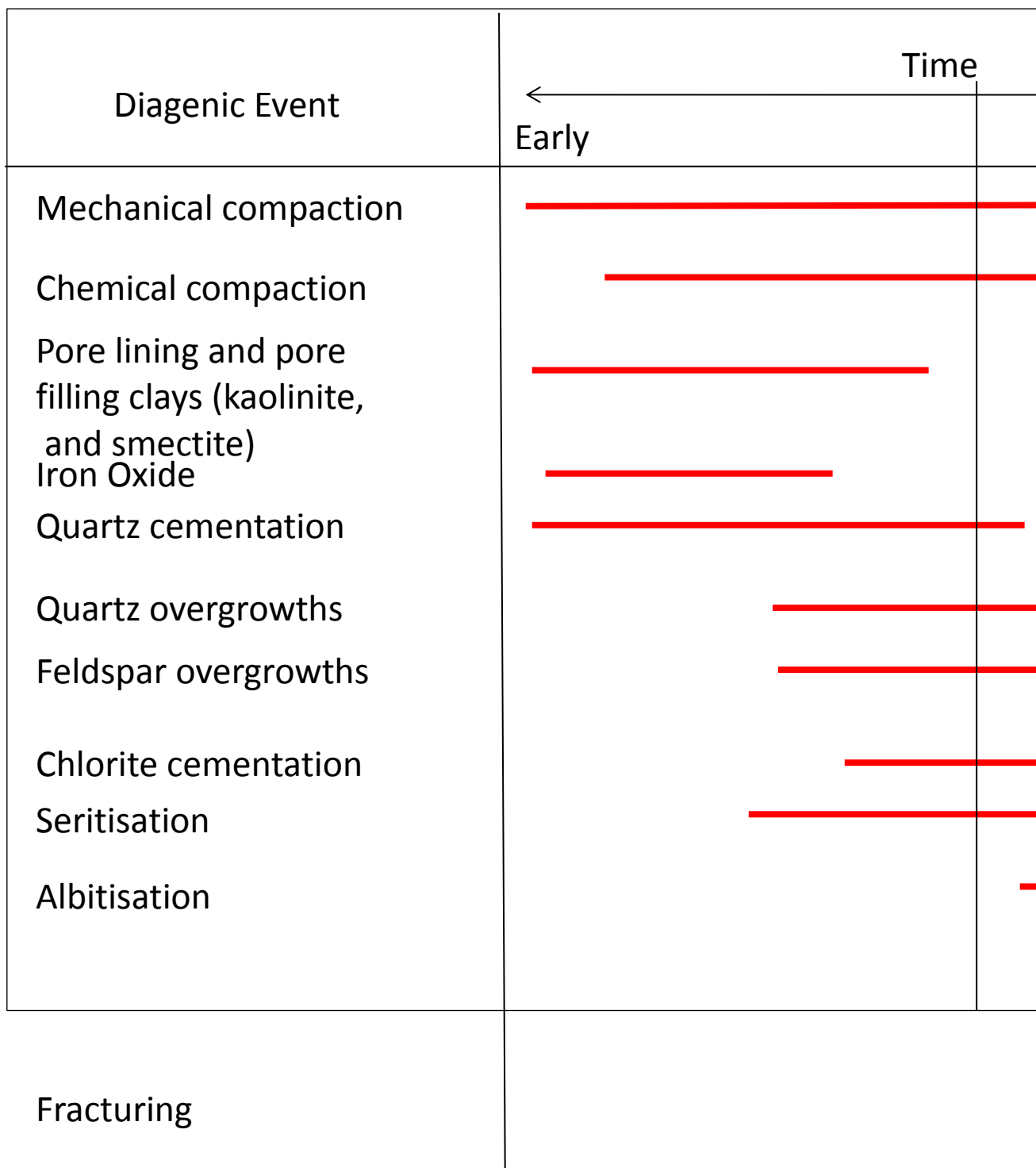


Figure 9.17: Mineral paragenesis sequence of the Madzaringwe and Mikambeni Formations in the Soutpansberg Coalfield.

During early diagenesis in the Mikambeni and Madzaringwe Formations of the Tuli Coalfield, mechanical compaction and chemical dissolution, pore filling and pore lining clays (illite, smectite and kaolinite) occurred. With burial, illite and seritisation of smectite clays that originated from matrix and the alteration of volcanic rock fragments took place. At the middle to later stage of diagenesis, chlorite is interpreted to have been formed largely by dissolution of volcanic rock fragments followed by in situ precipitation. During later diagenesis, albitisation of feldspar, suture grain contact, stylolite and grain fracturing began to form (Figure 9.18).

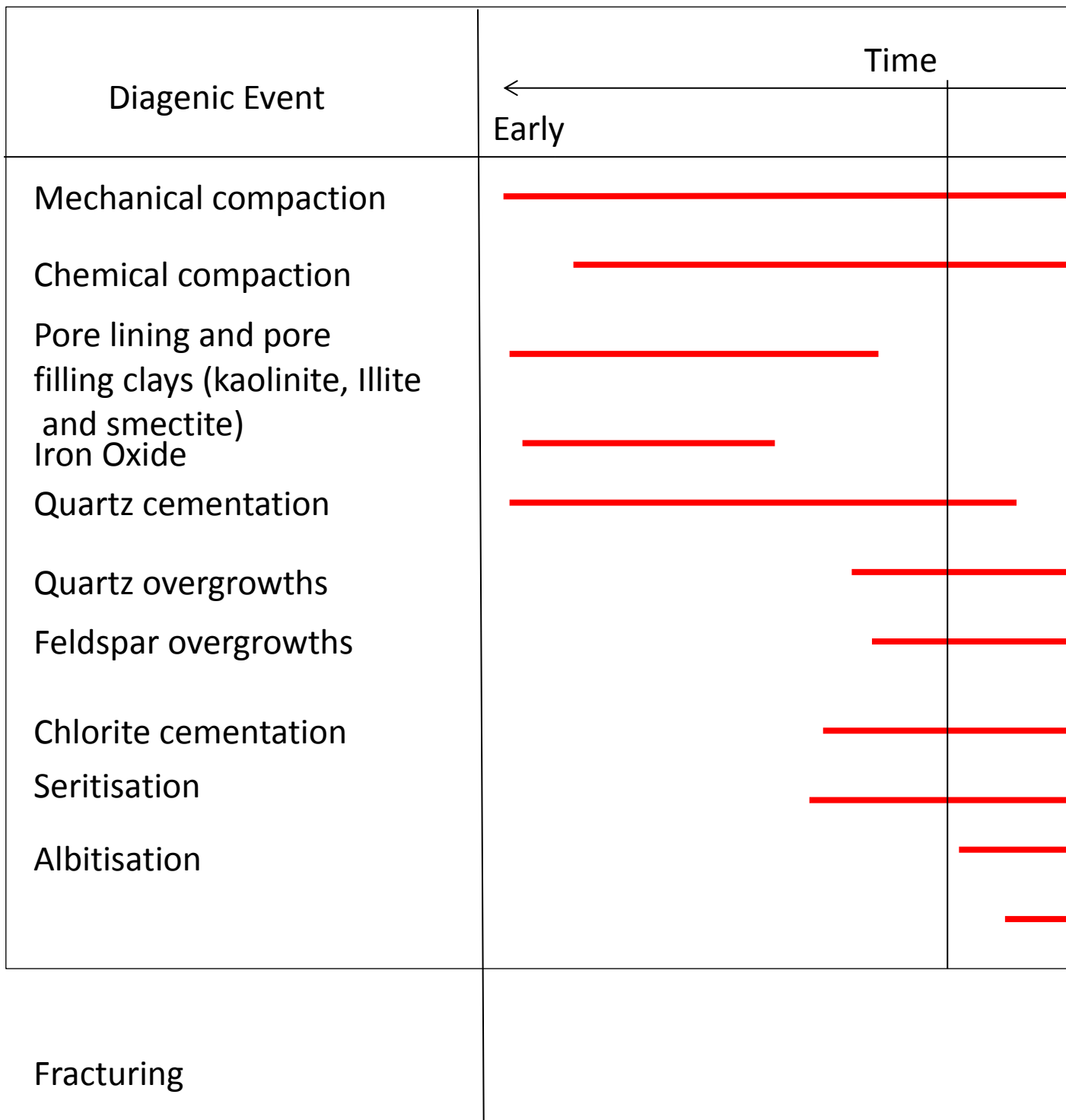


Figure 9.18: Mineral paragenesis sequence of the Madzaringwe and Mikambeni Formations in the Tuli Coalfield.

9.6. Conclusions

Diagenetic features of Mikambeni and Madzaringwe sandstones are subdivided into early and late stages. Time is relative with the earliest diagenetic event occurring shortly after deposition and the latest occurring up until present time. The main diagenetic processes that have affected the sandstones include mechanical compaction, cementation and the dissolution of framework grains and cements. Early diagenetic processes include mechanical compaction, silica and calcite cementation, clay mineral (pore lining and pore-filling kaolinite and smectite), feldspar authigenesis and the formation of hematite coatings. Late diagenesis includes albitization of K-feldspar, chloritisation and seritisation of smectite and minor fracturing. Late diagenetic minerals occur mostly as replacement minerals of detrital grains and early-formed diagenetic minerals, over-compaction (grain suture contact, and pressure-solution) are well present in the study areas.

The two formations in the coalfields show no significant differences in general diagenetic features and sequence of mineral growth. Authigenic clays present in the sandstone samples of the formations consist mostly of kaolinite, illite, and illite/smectite. Authigenic clays originated from a variety of sources. Deformation and alteration of labile grains due to compaction create clays in pseudomatrix. Dissolution of feldspar grains and albitization of plagioclase liberates aluminum that may precipitate as kaolinite. Illite-smectite sometimes forms as alteration products of volcanic grains and biotite.

Quartz cement occurs as both pore-filling and overgrowths in the samples. It appears that most of the pore-filling quartz cement is derived from the sands themselves (authigenic) or quartz sands worn away from other rocks (detrital). Quartz overgrowths are abundant in the matrix-poor sandstones. Authigenic chlorite occurs in the coalfields in two forms: grain coating (pore-lining) and pore-filling. Calcite cementation occurs mostly as a pore-filling and as well as a replacement mineral of detrital grains. Calcite replaced feldspar and quartz grains partly or completely, mostly at their margins. Albitisation of feldspar is one of the major diagenetic changes during late-stage diagenesis in the areas of all the coalfields.

CHAPTER 10

SUBSIDENCE ANALYSIS OF THE SOUTPANSBERG AND TULI COALFIELDS

Abstract

This chapter aims to understand the basin subsidence analysis of the Tuli and Soutpansberg Basins. The subsidence history of the Tuli and Soutpansberg Basins was reconstructed by a tectonic subsidence analysis by the method of Backstripping technique. Furthermore, PetroMod 1D Software was used to construct burial, depth and time plots in order to investigate the timing of hydrocarbon generation, migration and accumulation as well as the subsidence and uplift processes of the basins. The subsidence within the basins supports the primary graben system which must have been centered within the present basins, and later became a region of major faulting. This gave way to the Late Carboniferous rapid subsidence, with areas of greater extension subsiding more rapidly. The Early Permian (last phase) is characterised by a slow subsidence representing the post-rift thermal subsidence. The rift flanks were gradually uplifted and, and then generally subsided as a results of thermal contraction after the extension terminated. Further, the originally uplifted rift flanks were subsequently eroded and the Late Triassic beds (i.e. Clarens) were deposited in a basin caused by the Karoo thermal subsidence stage in a mainly fluvial environment. Based on these observations on the subsidence curves, it is possible to infer that the first stage of positive inflexion (~ 290 Ma) is therefore recognised as the first stage of Tuli and Soutpansberg Basin formation. No significant hydrocarbon (oil and gas) has ever been found in the exploration history of the Soutpansberg and Tuli Basins.

10.1. Introduction

Backstripping is a technique used to quantitatively estimate the depth that the basement would be in the absence of sediment and water loading (Watts and Ryan, 1976). This depth provides a measure of the unknown tectonic driving forces that are responsible for basin formation (tectonic subsidence or uplift). By comparing backstripped curves to theoretical curves for basin subsidence and uplift it is possible to deduce information on the basin forming mechanisms. The main aim of this study was to determine the subsidence history of the Tuli and Soutpansberg Basins. This is best achieved by conducting a tectonic subsidence analysis. The subsidence analysis technique has been described by many authors including: Sleep (1971); Watts and Ryan (1976); Watts (1978); Van Hinte (1978). The subsidence of a sedimentary basin can be mainly attributed to three processes, namely:

tectonic subsidence, water and sediment loading and lastly sedimentary compaction. Tectonic subsidence is the sinking of the basement in the absence of water and sediments and is controlled by tectonic forces associated with the basin formation and evolution. Water and sediment loading refers to the effect of the weight of the water and sediments in the basin. Sediment compaction refers to the decrease in sediment volume as they are buried and compacted. The shape and magnitude of these three components of subsidence can be estimated from well logs, borehole and outcrop section using the “backstripping” technique (Allen and Allen, 2004; Watts, 2001). The technique removes from each layer the effects of sediment compaction, water and sediment loading, thereby producing a tectonic subsidence curve on the time versus sediment thickness graph.

Stratigraphic and palaeobathymetric data are used to quantitatively estimate the depth that the basement would be in the absence of sediments and water loading. This depth provides a measure of the unknown 'tectonic driving forces' that are responsible for basin formation and, for this reason, have been termed the tectonic subsidence or uplift of the basin. By comparing backstripping curves to theoretical curves for basin subsidence and uplift it has been possible to deduce information on the basin forming processes and mechanisms.

10.2. Methodology

The subsidence history of the Tuli and Soutpansberg Basins was reconstructed by a tectonic subsidence analysis involving the Backstripping technique. The tectonic subsidence computation was done with the OSXBackstrip program which was developed by Cardozo (2012) (University of Stavanger, Norway). The program performs a “1D Airy Backstripping” based on the approach by Watts (2001) and Allen and Allen (2004). It is used for predicting the tectonic subsidence of sedimentary basins. Furthermore, PetroMod 1D Software by Schlumberger was used to construct burial, depth and time plots. The plots included burial history, temperature, porosity, pressure, vitrinite reflectance (R_o) and thermal conductivity of the basins. These plots were useful in modelling the passive margin setting and the source rock maturation and hydrocarbon generation of the Soutpansberg and Tuli basins. The methods used in the backstripping technique are discussed below:

10.2.1. Age assessment

The accuracy of geohistory plots heavily depends on the density of biostratigraphic check points, on the resolution of the available biotas and, when transforming relative ages into numerical ages, on the choice of the reference timescale (Sciunnach and Garzanti, 1996).

However, differences in numerical ages between recent timescales are relatively small, and the choice among them does not significantly affect the shape of the tectonic subsidence curve (Loup, 1992). In the present analysis, standard timescales by SACS (1980); Brandl (1981); Brandl (2002); Bordy and Catuneanu (2001); Bordy and Catuneanu (2002a, b and c); Johnson *et al.* (2006) were adopted. The age ranges used in this study for the Tuli and Soutpansberg Basins shown in Table 10.1 represent the best synthesis presently available and used nationally.

Table 10.1: The lithostratigraphic units deposited in the Tuli and Soutpansberg Basins. *the ages and thicknesses of the units are from SACS (1980); Brandl (1981); Brandl (2002); Bordy and Catuneanu (2001); Bordy and Catuneanu (2002a, b and c); Johnson *et al.* (1996).

<i>Unit</i>	<i>Thickness*(m)</i>	<i>Depth(km)</i>	<i>Age*(Ma)</i>	<i>Lithologies</i>
Surface deposits	60	0.06	Recent	Sand, gravel, scree
Clarens Formation	150	0.21	198	Sandstone
Bosbokpoort Formation	100	0.31	215	Sandstone + shale
Kloppersfontein Formation	20	0.33	240	Sandstone
Solitude Formation	170	0.5	250	Sandstone
Fripp Formation	110	0.61	252	Sandstone
Mikambeni Formation	150	0.76	256	Shale + coal
Madzaringwe Formation	200	0.96	260	Shale + coal
Tshidzi Formation	20	0.98	300	Glacial diamictite

10.2.2. Decompaction

The first step towards a correct subsidence interpretation is the decompaction of the observed sediment thicknesses. Undeformed curves lead to underestimate initial subsidence, and generally do not allow the correct identification of concave-upward curve tracts (i.e., the typical pattern of thermal subsidence curves). Decompaction is the running of a unit's compaction history in reverse, and this is achieved by considering sedimentary rock as a mixture of sedimentary grains and interstitial pores. The volume of sediment grains remains constant while the water is squeezed out during compaction from the overlying sediment load. Two main approaches to decompaction can be adopted:

- decompaction can be accounted for by moving the considered layer back up empirical curves of porosity loss with burial (Hamilton, 1959; Bond and Kominz, 1984; Watts and Ryan, 1976; Corfield *et al.*, 2005);

- an analytical approach to decompaction is based on the widely accepted expression for porosity loss with burial (Allen and Allen, 2004):

Initially, the subsidence history diagram is simply a graphical representation of the burial history, but the total subsidence is equal to the sum of all vertical movement, including tectonic and sediment load subsidence (Sediment load is derived from unit composition and porosity).

$$\rho_{\text{rock}} = \Phi(\rho_{\text{pore H}_2\text{O}}) + (1 - \Phi) (\rho_{\text{grains}}) \quad [1]$$

$$\rho_{\text{sed}} = \sum_{i=1}^n \frac{(\rho_{\text{rock}i})(\text{THI}_i)}{S} \quad [2]$$

$$\text{Sed. load subsidence} = Z_t \left[\frac{\rho_{\text{sed}} - \rho_w}{\rho_m - \rho_w} \right] \quad [3]$$

Where: Φ = porosity

Z_t = column thickness,

ρ = density

S = total decompacted thickness = $\sum (\text{THI})$

THI = decompacted thickness of interval

$$= [(1 - \Phi) / (1 - \Phi_{\text{init}})] * Z_i$$

With: Φ_{init} for: Sandstone = 0.5, Shale = 0.6, and Limestone = 0.7

Density

ρ_{sed} = density of sediment column (weighted average)

ρ_w = density of pore water = 1 g/cm³

ρ_m = density of mantle = 3.33 to 5.7 g/cm³

Grain densities

ρ_{grains} for Sandstone = 2.2 to 2.8 g/cm³,

ρ_{grains} for Limestone = 2.3 to 2.7 g/cm³ and

ρ_{grains} for Shale = 2.4 to 2.8 g/cm³

The parameters (initial porosity and solid density) of the different lithologies have been taken from Sclater and Christie (1980), as they suppose an exponential decrease in porosity with depth depending on the lithology of the rock in question. An analytical

approach to decompaction is based on the widely accepted expression for porosity loss with burial (Allen and Allen, 2004):

$$\Phi = \Phi_0 e^{-cy} \quad [4]$$

Where Φ = porosity at any depth z ; Φ_0 = porosity at the surface; c = lithological compaction coefficient; and y = depth in kilometres.

The equation used for the decompaction approximation method after Van Hinte (1978) is given as:

$$Td = [Tp (1 - \Phi) / (1 - \Phi_0)] \quad [5]$$

Where Td is the decompacted thickness, Tp is the present thickness of the vertical section; Φ is the final/present porosity and Φ_0 is the unconsolidated/initial porosity. The decrease of porosity with depth is illustrated for a number of different lithologies in Figure 10.1. The Figure shows that porosity decreases rapidly with depth. Figure 10.2 shows the decompaction scheme developed by Allen and Allen (2004).

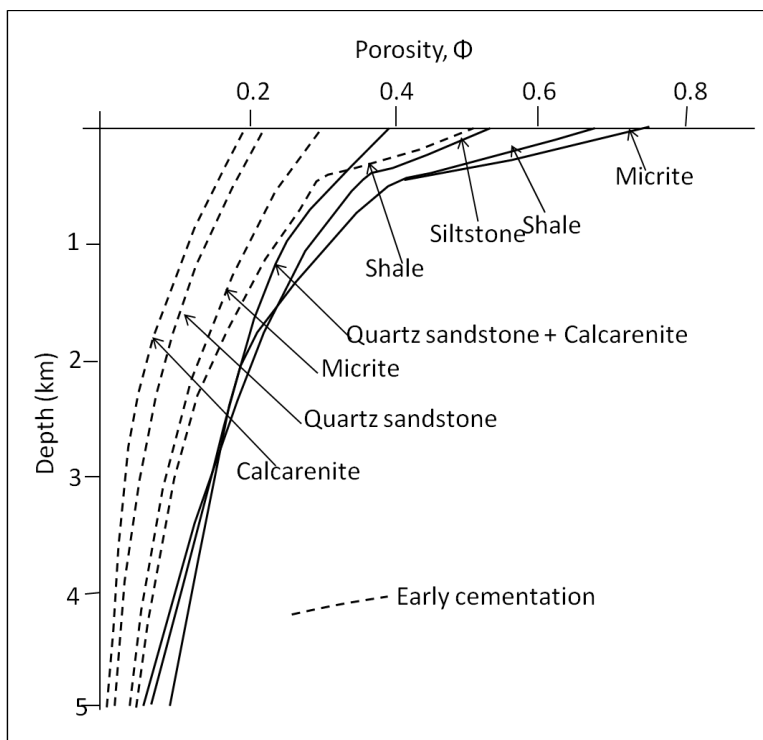


Figure 10.1: Summary of porosity vs depth curves for different lithologies. After Bond & Kominz (1984).

Following Eq. (4), the measured stratigraphic thicknesses can be decompacted by expressing the total volume V_t of the sedimentary column as $V_t = V_s + V_w$. V_s is the volume of sediment grains, which remains constant during compaction, and V_w is pore volume, which

equals the volume of interstitial water in the assumption of a water saturated sediment. Loss of V_t during compaction is assumed to be due only to a decrease of V_w . Total pore volume of sediment between two generic depths y_1 and y_2 is obtained by integration from y_1 and y_2 of Eq. (4), which gives:

$$V = \Phi_o (e^{-cy_1} - e^{-cy_2})/c \quad [6]$$

As we decompact the sedimentary column (Figure 10.2), the top and bottom of a given sedimentary package are brought to the new depths y^*_1 and y^*_2 ($y_1 > y^*_1$, $y_2 > y^*_2$, $y^*_2 - y^*_1 > y_2 - y_1$). A new pore volume $V^*_w > V_w$ can thus be calculated. The decompact thickness equals V_s plus V^*_w , as follows:

$$y_2 - y_1 = y^*_2 - y^*_1 + \Phi_o [(e^{-cy^*_1} - e^{-cy^*_2})(e^{-cy_1} - e^{-cy_2})]/c \quad [7]$$

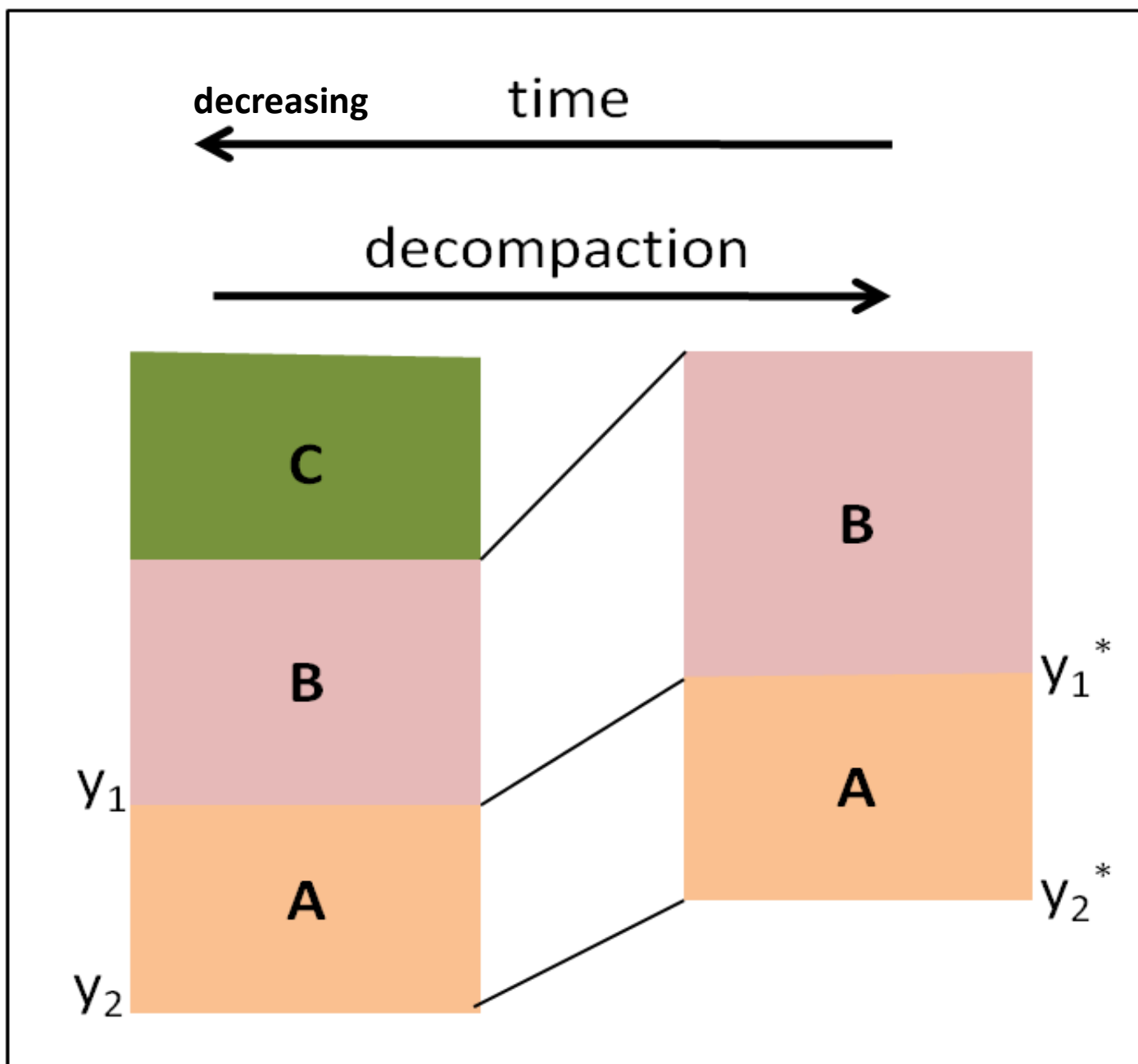


Figure 10.2: Decompanction scheme. Units A and B are restored to different depths and thicknesses after removal of the superposed unit C (after Allen and Allen, 2004).

To calculate the decompacted thicknesses for each unit, average lithological compaction coefficients for five main lithologies (i.e. sandstone, shale, limestone, dolomite and shaly sand) from Frostick and Steel (1993) given in Table 10.2 were used for the lithostratigraphic units in Tuli and Soutpansberg strata. The percentage of decompaction for all the lithostratigraphic units is determined as the total decompacted thickness divided by the total compacted thickness of the section. The reason for this is to determine which section decompacted more and which one less.

Table 10.2: Compaction coefficients and parameters for main lithological types (Sclater and Christie, 1980).

<i>Lithology</i>	<i>Surface porosity (Φ_0)</i>	<i>Compaction coefficient $c(km^{-1})$</i>	<i>Sediment grain density $\rho_{sg}(kgm^{-3})$</i>
Shale	0.63	0.51	2720
Sandstone	0.49	0.27	2650
Shaly sandstone	0.56	0.39	2680
Dolomite	0.31	0.22	2850
Limestone	0.51	0.52	2710

10.2.3. Backstripping

To backstrip multiple layers there is need to "restore" all the stratigraphic units in a sequence for each time step, decompacting the younger units and compacting the older ones. The tectonic subsidence is calculated from the sediment thickness and the average density of the entire sedimentary sequence at a particular time. In the local loading model, the "backstripped" thickness Z of a given unit (assuming that water load is ineffective in compacting sediment) is obtained from the simple equation (Watts and Ryan, 1976):

$$Z=S (\rho_m-\rho_s)/(\rho_m-\rho_w) \quad [8]$$

Where:

S is the total thickness of the sedimentary column corrected for compaction.

ρ_m , ρ_s , and ρ_w are the densities of the lithospheric mantle, sediments, and seawater, respectively.

Standard values of 3.33 for ρ_m and 1.035 for ρ_w can be assumed as constants.

ρ_s must be determined step by step because it changes progressively as the sedimentary units pile up.

The total thickness S is easily obtained by summing all the individual thicknesses. The formula adopted to calculate the bulk density of the sedimentary column (Allen and Allen, 2004) is:

$$\rho_s = \sum_{i=1}^n \{ [\Phi_{ipw} + (1 - \Phi_i)\rho_{sg_i}] / S \} y_i \quad [9]$$

Where:

Φ_i is the average porosity, ρ_{sg_i} the sediment grain density, and y_i the thickness of the i -th layer.

10.2.4. Palaeobathymetric and eustatic corrections

A depth plot for the chosen basement after backstripping must be corrected based on palaeobathymetry data. Failure to include paleobathymetric and eustatic corrections in the subsidence plot results in strong deformation of the curves. Bathymetric estimations are mainly made from palaeontological and palaeoecological data, petrographical composition and sedimentary structures of rocks (Frostick and Steel, 1993). In order to calculate the amount of tectonic subsidence or uplift purified from eustatic effects, sea-level changes must be quantified through the stratigraphic column, and subtracted from the backstripped subsidence figures. Not much study has been done on the water-level fluctuations in the northern Karoo sub-basins. Therefore, data from the literature are sparse or of insufficient reliability to provide good estimates of the bathymetry for the Tuli and Soutpansberg basins. Thus, in this study the effects of palaeobathymetry and water-level fluctuations on the tectonic subsidence calculations are ignored.

10.2.5. The 1D Airy Backstripping

As mentioned earlier, the 1D Airy backstripping was done using a computer program based on the approach described by Allen and Allen (1990); Allen and Allen (2004); Watts (2001). It predicts the subsidence of a basin (a combination of basement and sediment load-driven subsidence with an exponential reduction of porosity). The OSXBackstrip program works with three components for data input namely:

- Lithology: This comprises lithology-dependent values, including parameters for the decompaction exponential function, such as the initial porosity Φ and the porosity reduction coefficient C .
- Strata: These are the general properties of the stratigraphic units, which are independent of the actual well (borehole outcrop) location, such as sedimentation depth, age, sea level, name of a stratigraphic unit, well or outcrop data, such as local thickness of strata and lithological composition.

- A backstrip plot where the progressive decompaction of the sediments can be observed and a tectonic subsidence plot where the total thickness curve, the total subsidence (decompacted) curve, the decompacted curve corrected for sediment.

10.2.6. Sources of error

The combined impact of approximations in the input values for Φ_0 and c was assessed not to exceed $\pm 16\%$ of the calculated value for the decompacted thickness (Gallagher, 1989). The layer thickness is derived from well data or outcrops (e.g. stratigraphic sections). Uncertainties are derived from the unknown amount of erosion or from an erroneous stratigraphic classification. This leads to inaccuracy in age, which is based on either biostratigraphy, or chronostratigraphic correlations or geochronology. Quantification of lithological parameters (e.g. lithology, porosity) is often derived from geochemical and sedimentological analyses or from geophysical well logs. Thus, these factors are dependent on the quality of the analysis or measurements. Nevertheless, the results, although presented quantitatively in Section 10.2 below, are believed to be reliable only in a semi quantitative sense, because of the many sources of uncertainty associated with several basic assumptions (e.g., time frame, palaeowater depth, eustasy, choice of a physical model for lithospheric stretching and isostasy vs. flexure).

10.3. Results and Interpretations

The calculated compaction and decompaction estimates obtained using Van Hinte's (1978) equation [4] for porosity at any depth are presented in Table 10.3. The percent compaction and porosity at depth was calculated to demonstrate an average porosity reduction with depth in the sandstones and shales of basins. These graphs were plotted to show the difference in thicknesses between the compacted and decompacted sections of the eight lithostratigraphic units (formations).

Table 10.3: Calculated results for porosity at specific depths, decompacted thickness, Percentage compaction and decompaction and thickness difference for lithostratigraphic units in the Tuli and Soutpansberg Basins. * Φ_0 values are from Table 10.2

Formation	Compacted thickness (m)	Lithology	Porosity at surface (% Φ_s)	Porosity at any depth (Φ)	Decompacted thickness (m)	% Compaction	% Decom paction	Thickness difference (m)
Clarens	150	Sandstone	0.49	0.463	157.5	95.2	105	7.5
Bosbokpoort	100	Sandstone + shale	0.56	0.451	124.8	80.1	124.8	24.8
Klopperfontein	20	Sandstone	0.49	0.448	21.6	92.6	108	1.6
Solitude	170	Sandstone	0.49	0.428	190.7	89.1	112.2	20.7
Fripp	110	Sandstone	0.49	0.416	126	87.3	114.5	16
Mikambeni	150	Shale + coal	0.63	0.427	232.3	64.6	154.9	82.3
Madzaringwe	200	Shale + coal	0.63	0.386	331.9	60.3	166	131.9
Tshidzi	20	Glacial diamictite	0.56	0.382	28.1	71.2	140.5	8.1

Figure 10.3 shows thicknesses of compacted segments compared to decompacting segments. A percentage compaction ranging from 95.2 to 87.3% is calculated for the Clarens to Fripp Formations sandstones, and the porosity is ranging from 0.463 to 0.416. The percentage compaction ranging from 64.6 to 60.3% is calculated for the shale+coal units (Mikambeni and Madzaringwe Formations) and the porosity is ranging from 0.427 to 0.386. The percentage compaction of the glacial diamictite Tshidzi Formation is calculated to be 71.2% and the porosity is 0.382. In all the different units the porosity is observed to decrease with increasing depth of burial.

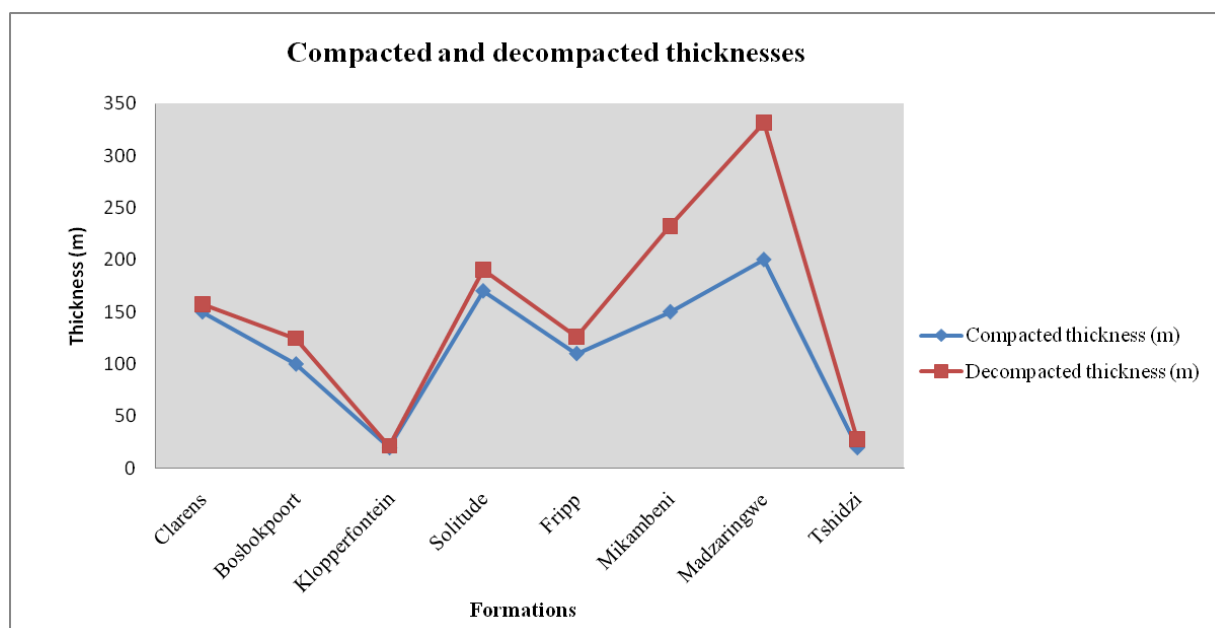


Figure 10.3: The thicknesses of compacted segments compared to decompacting segments.

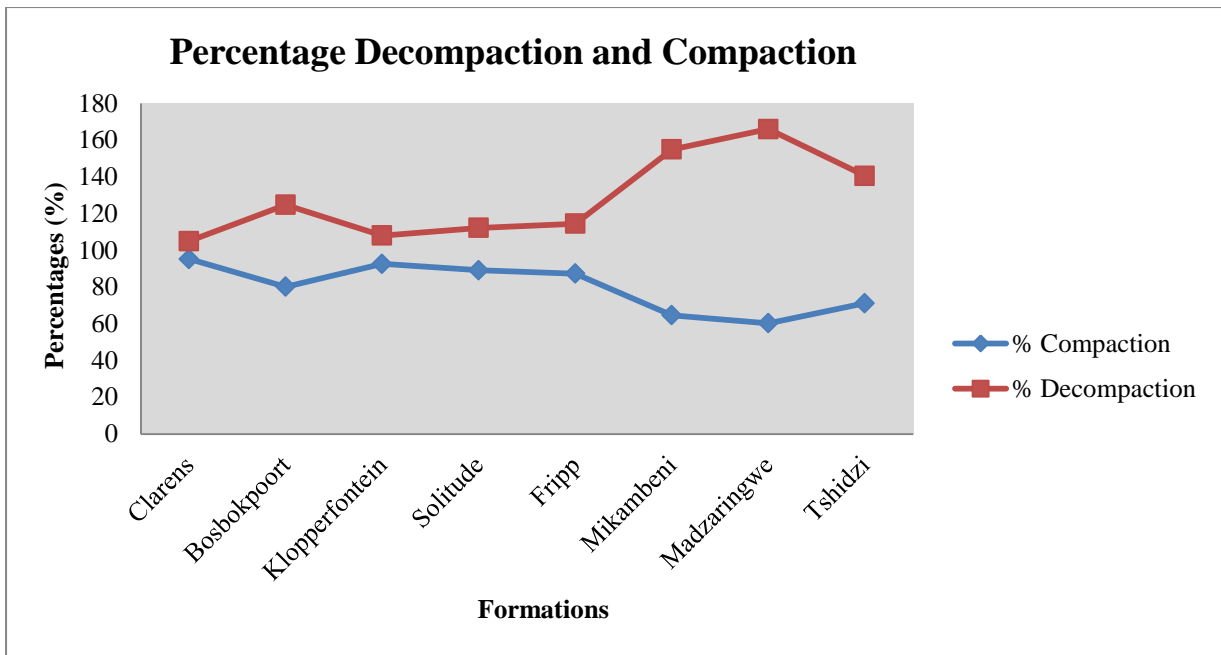


Figure 10.4: The percentage decompaction compared to percentage compaction per formation in basins.

10.3.1. The 1D Airy subsidence model

Backstripped and subsidence curves for the eight lithostratigraphic units in the Tuli and Soutpansberg Basins (Table 10.3) during the Permo-Carboniferous time are shown in Figures 10.5 and 10.6. In this study the Airy model is adopted, and changes in sediment-supply and water-loading in the basins are simply accounted for by assuming a homogeneous local, airy-type isostatic adjustment for the lithosphere. After decompaction, the total load of sediments must be estimated and removed from the basin, in which case the basement will rebound isostatically to give the “tectonic subsidence”. For the purpose of this work it is assumed that the water depth (W_d) throughout the basin’s development is zero. This is because, lithologically, both the basins are suggested to be of mainly alluvial to fluvial origin (Brandl, 1981 and Brandl, 2002). The subsidence curves are the results from an inverse model and not direct observation, and should be interpreted accordingly with more emphasis on relative rather than absolute values. Interpretations of the curves are based on the shape and timing of representative subsidence curves.

The decompacted curves (Figures 10.5 and 10.6) suggest a three-phase rifting during the Karoo time:

- A linear subsidence curve during the interval of 300-259 Ma with a subsidence rate of 2.86 mMa^{-1} (Figure 10.6, arrow 1). This was during the Late Carboniferous and Early Permian resulted in the deposition of the diamictite Tshidzi Formation. This subsidence phase corresponds to deposition of the Madzaringwe and Mikambeni Formations during the interval of 290-260 Ma and 260-256 Ma respectively, with a decreasing subsidence rate of 27.2 and 4.3 Ma^{-1} . This phase is characterised by the concave-up profile. The phase is related to the initial extensional fault controlled subsidence of the basins. This subsidence phase for the Late Carboniferous-Early Permian correlates directly with the study of the basins by Brandl (2002) (i.e. the Karoo sedimentation appears to have been fault-controlled from the onset).
- This was followed by a rapid subsidence in the Late Permian (Figure 10.6, arrow 2). This phase was very short lived and is expressed on the subsidence curves by a two-fold change in subsidence pattern: (1) a convex-upward profile denoting a short and rapid subsidence phase at a subsidence rate of 4.3 mMa^{-1} (Figure 10.7) corresponding to deposition of the Mikambeni Formation at the time interval of 260-256 Ma; and (2) another convex-upward profile is noticed on the subsidence curve during the interval of 256-252 Ma expressing a short phase of rapid subsidence with subsidence rate that increases through time at 3.1 mMa^{-1} corresponding to deposition of the Fripp Formation. The phase is also related to the fault controlled subsidence of the basins.
- The last phase (Figure 10.6, arrow 3) characterised by a slow subsidence represents the post-rift thermal subsidence. During the Late Permian-Early Triassic another convex-upward profile is expressed on the subsidence curve during the interval of 252-198 Ma, and interpreted as slow flexural subsidence with slow subsidence rates of 14.3 mMa^{-1} , 3.57 mMa^{-1} , 21.45 mMa^{-1} and 8.58 mMa^{-1} corresponding to deposition of the Solitude (250 Ma), Klopperfontein (240 Ma), Bosbokpoort (215 Ma) and Clarens Formations (198 Ma) respectively.

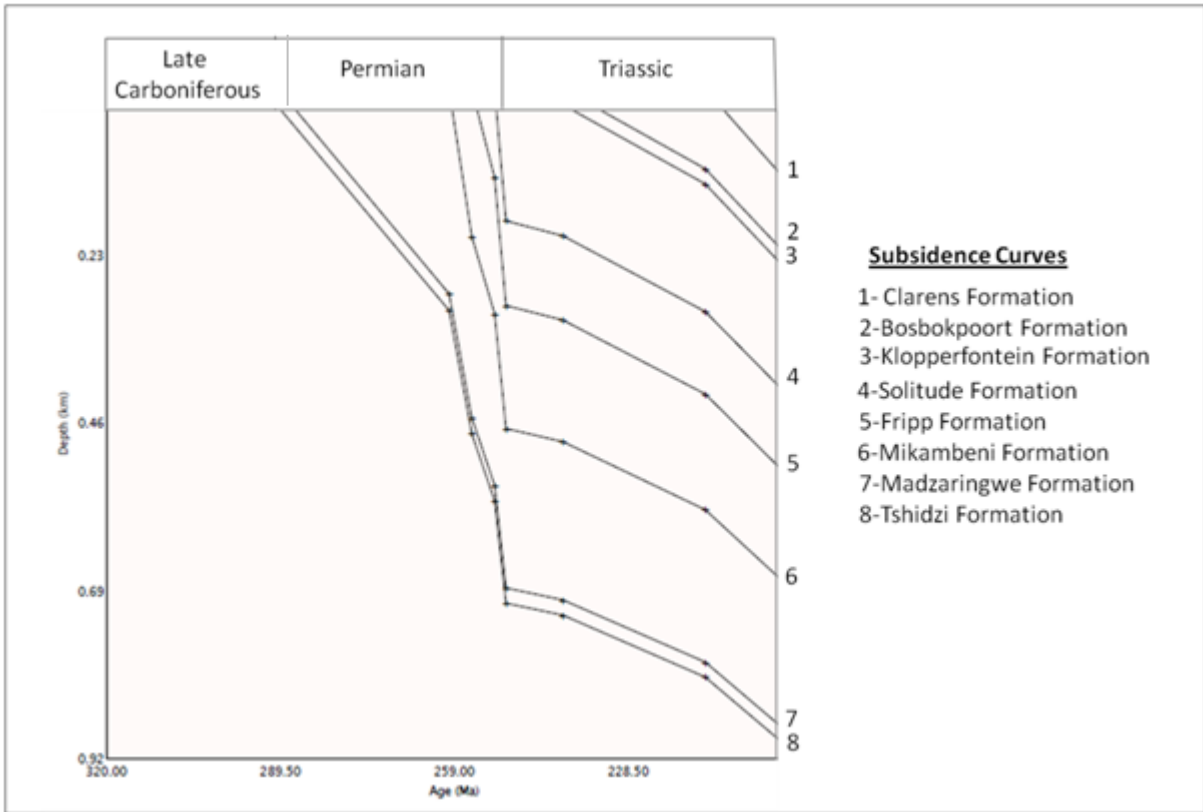


Figure 10.5: Backstripping plots of the Tuli and Soutpansberg Basins. Boundaries of the eight selected horizons are recognized on the subsidence curves with ages corresponding to the age of the top surface of each horizon.

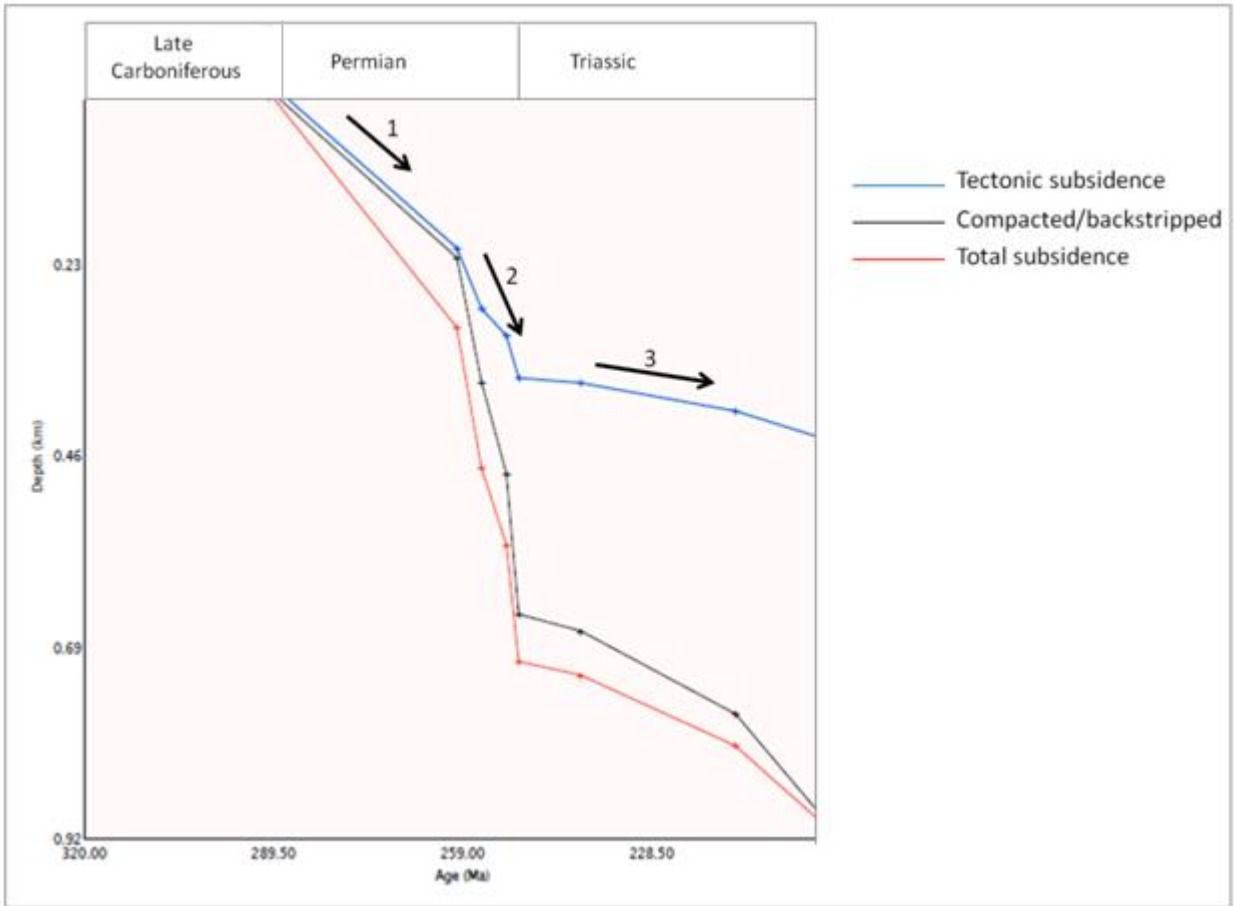


Figure 10.6: Tectonic subsidence curves of the Tuli and Soutpansberg Basins. Note the three phases indicated by black arrows.

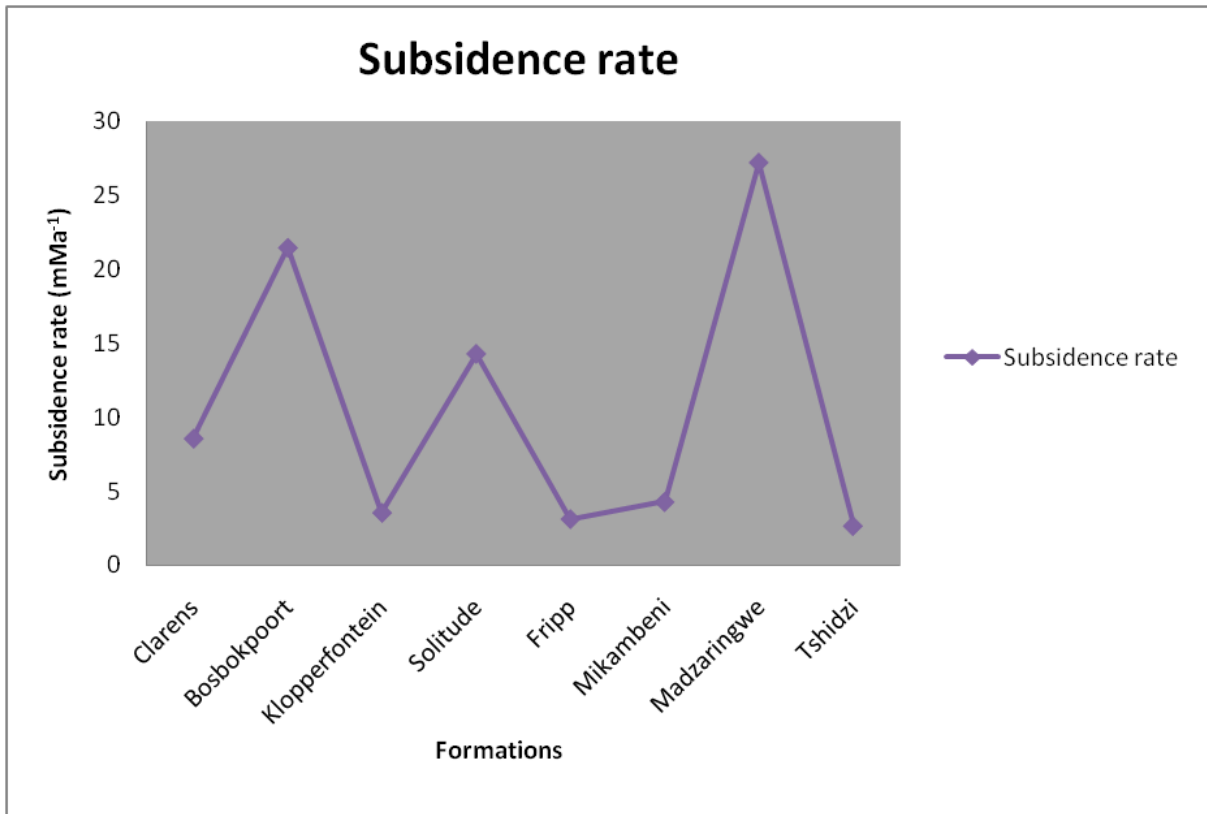


Figure 10.7: Subsidence rates over time and corresponding to lithostratigraphic units in basins.

10.3.2. The 1D PetroMod modelling

Sedimentary basins contain thick sediment packages that represent the depositional history since basin formation e.g. the rifting, drifting and subsequently subsidence phases. Many of these basins are important repositories for hydrocarbon accumulation and are areas of high economic interest. PetroMod 1D Software (Version 10) by Schlumberger was used for a preliminary modelling and investigation of the timing of hydrocarbon generation, migration and accumulation. In this study it is additionally used to understand the burial depth (subsidence and uplift) of the Soutpansberg and Tuli Basins.

10.3.2.1. Source rock maturation and hydrocarbon generation

The present preliminary study has outlined the overall source potential of the Late Carboniferous and the Permian sequences in the Soutpansberg and Tuli Basins in relation to stratigraphic evolution of the successions. The evaluation and stratigraphic relations suggest that potentials of the basins are restricted to discrete intervals, which in both the basins include the oil and gas prone Late Pennsylvanian to Middle Permian bituminous to sub-bituminous coals of the Madzaringwe and Mikambeni Formations. The evolution of vitrinite reflectance (i.e. maturity) of the entire source rocks (Figure 10.12A) was extracted from the

model shown in Figure 10.8. Based on the study by Peters and Cassa (1994), rocks with a vitrinite reflectance less than 0.6% are classified immature (Table 10.4). The vitrinite reflectance (R_o) of the source rocks at these stratigraphically separated intervals are classified immature, thus limiting any hydrocarbon accumulations in the basins. The R_o of the basins ranges from 0.2 to 0.45% (Figure 10.12A). The R_o values are low due to the sampling area was shallow buried and the inorganic matter was immature.

Table 10.4: Level of thermal maturity for oil (Peters and Cassa, 1994).

Level of Thermal Maturity						
Stage of Thermal Maturity for oil	Maturation			Generation		
	R_o	T_{max}	Thermal Alteration	Bitumen/TOC	Bitumen	Production Index
	(%)	°C	Index (TAI)		(mg/g rock)	[S1/(S1+S2)]
Immature	0.2-0.6	<435	1.5-2.6	<0.05	<50	<0.10
Mature						
Early	0.6-0.65	435-445	2.6-2.7	0.05-0.010	50-100	0.10-0.15
Peak	0.65-0.9	445-450	2.7-2.9	0.15-0.25	150-250	0.25-0.40
Late	0.9-1.35	450-470	2.9-3.3	_____	_____	>0.40
Post mature	>1.35	>470	>3.3	_____	_____	_____

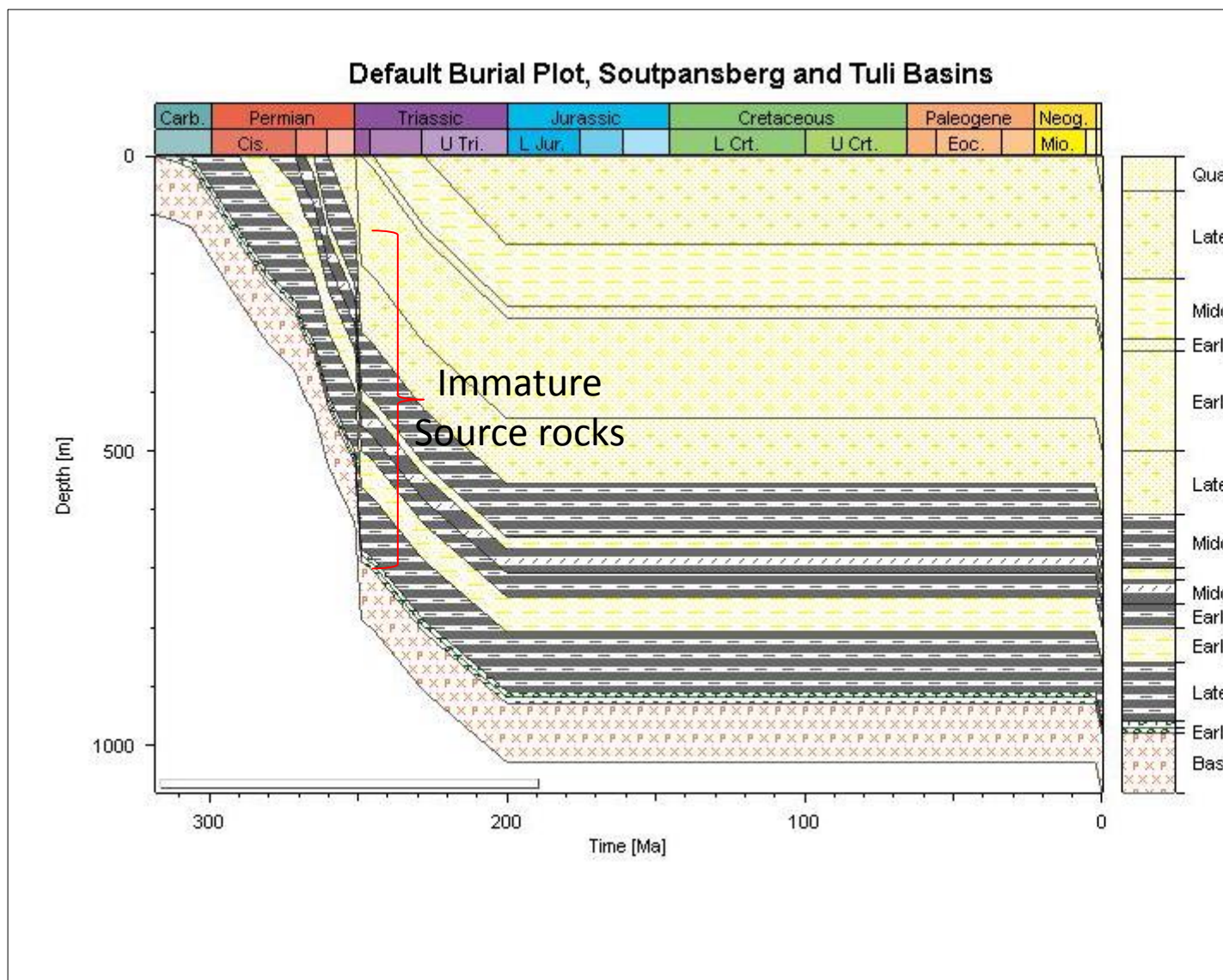


Figure 10.8: Burial history plots of the Soutpansberg and Tuli Basins.

Generally, the higher the temperature and the deeper the burial depth, the more the hydrocarbon component formed. Though temperature is the critical factor, the amount of time that the organic material is exposed to heat and pressure is also an important factor in the production of hydrocarbons. These factors determine the relative amounts of natural gas versus oil that is found in a particular reservoir. Figure 10.9 below shows the relationship between depth, temperature, and probable petroleum production. Figures 10.10 and 10.12C shows the burial history and temperature evolution of the Soutpansberg and Tuli Basins.

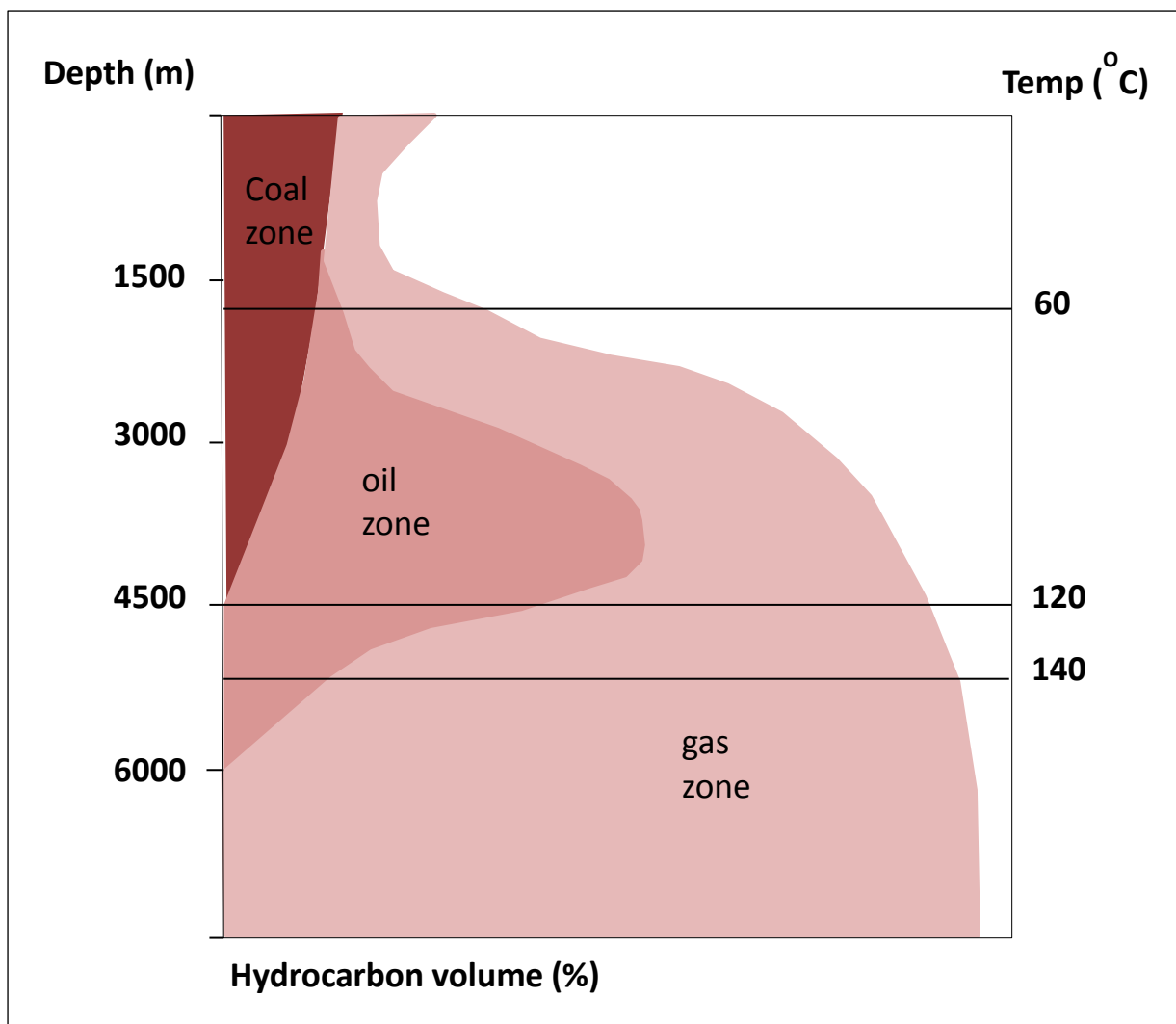


Figure 10.9: Relationship between depth, temperature, and petroleum production (from © www.natgas.info*).

*Natural gas formation 2013, accessed 20 April 2013, < [http:// www.natgas.info/html/gasformation.html](http://www.natgas.info/html/gasformation.html) >.

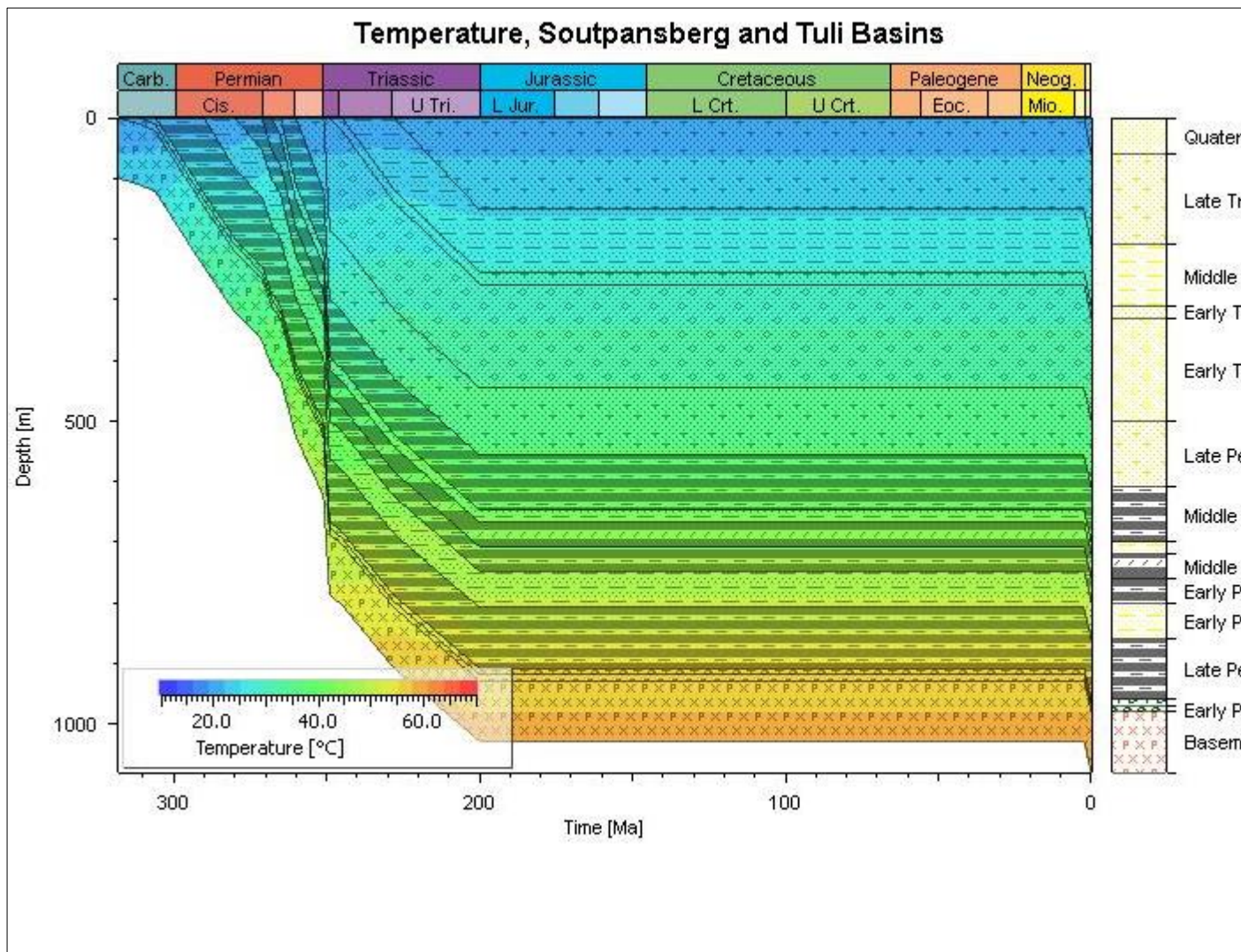


Figure 10.10: Burial History and temperature evolution of the Soutpansberg and Tuli Basins.

Compaction of sandstones is driven by the net stress (eqn 10) induced by the overburden load.

$$S_e = \rho g h - p \quad (10)$$

S_e is the net stress, ρ the average density of overlying sediment column, g the acceleration due to gravity, h the overburden thickness and p the pore-pressure. In hydrostatically pressured sandstones, the net stress increases with burial depth. In some cases, however, the net stress within the reservoir is strongly reduced by high formation pressures, and this may influence the rate of compaction. Figure 10.12 shows the pore, hydrostatic and lithostatic pressure of the Soutpansberg and Tuli Basins.

An overall trend of decreasing porosity with increasing pore-pressure is apparent (Figure 10.12B and C). Deeply buried sandstones are generally less porous than the shallow sandstones, thus limiting any hydrocarbon accumulation.

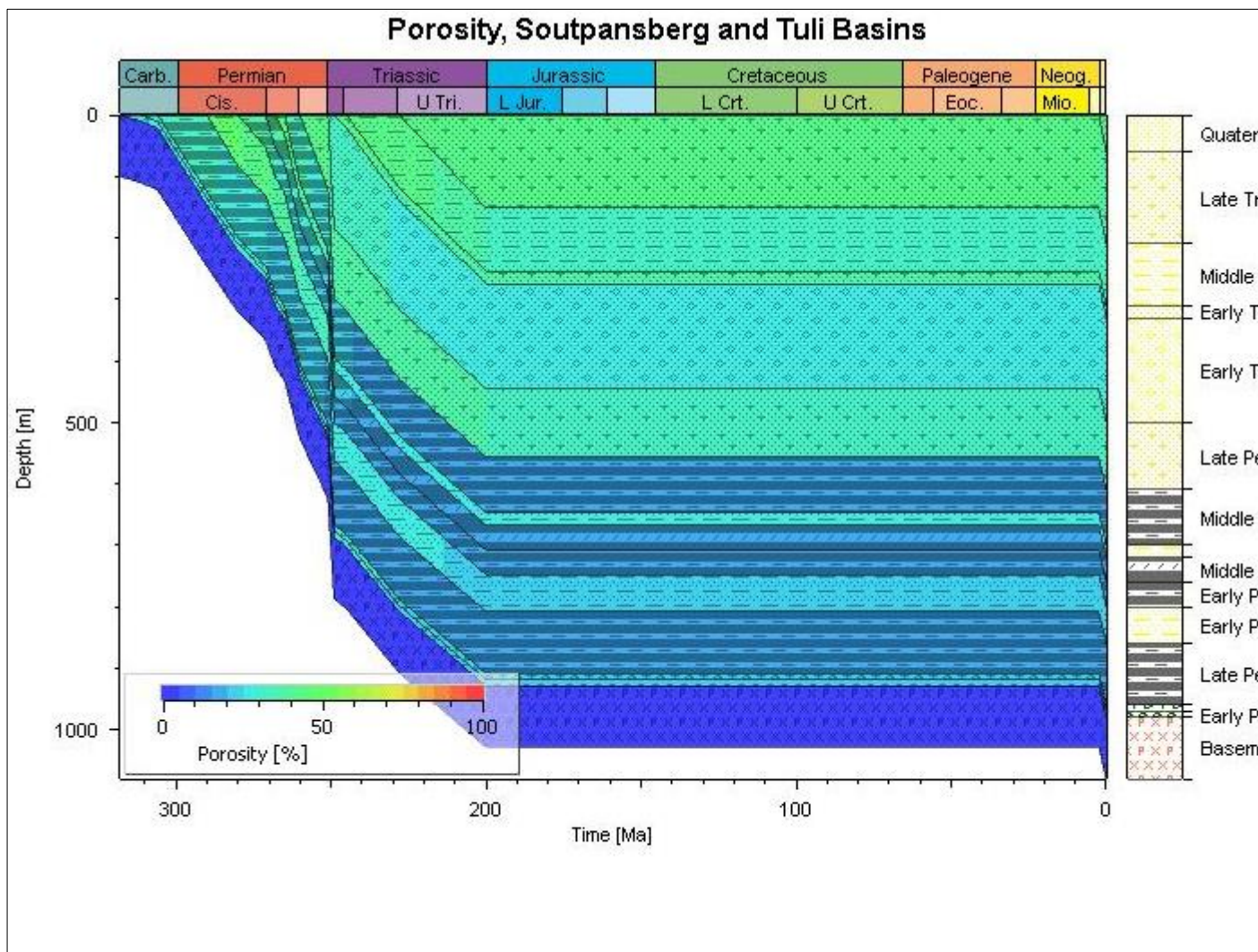
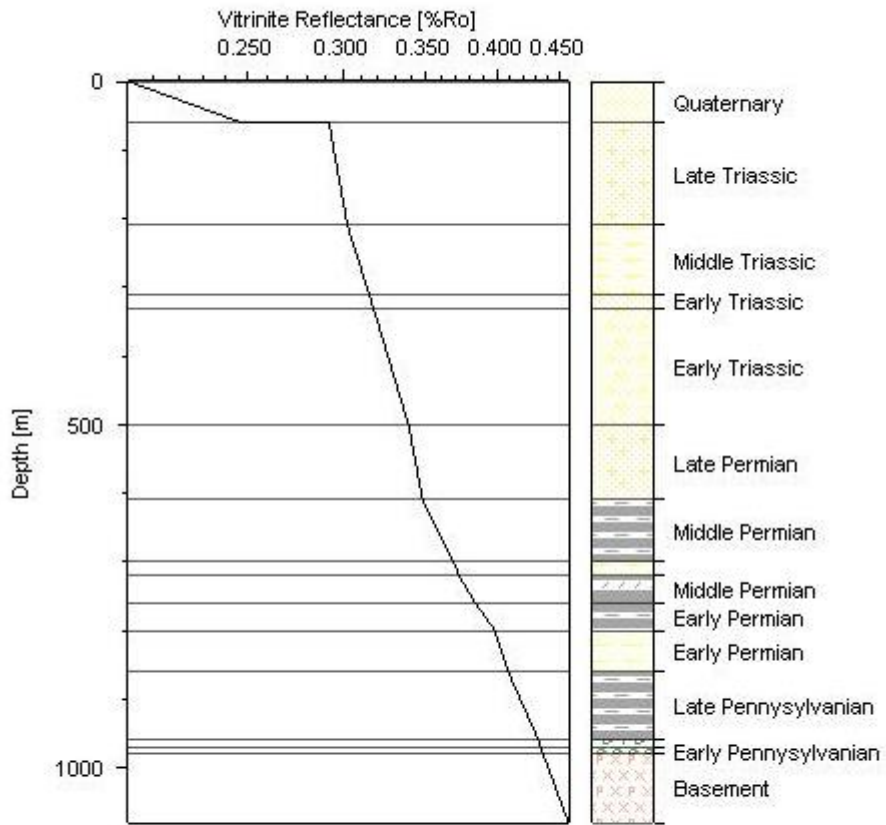


Figure 10.11: Burial History and porosity of the Soutpansberg and Tuli Basins.

Vitrinite Reflectance, Soutpansberg and Tuli Basins

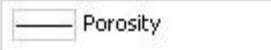


(A)

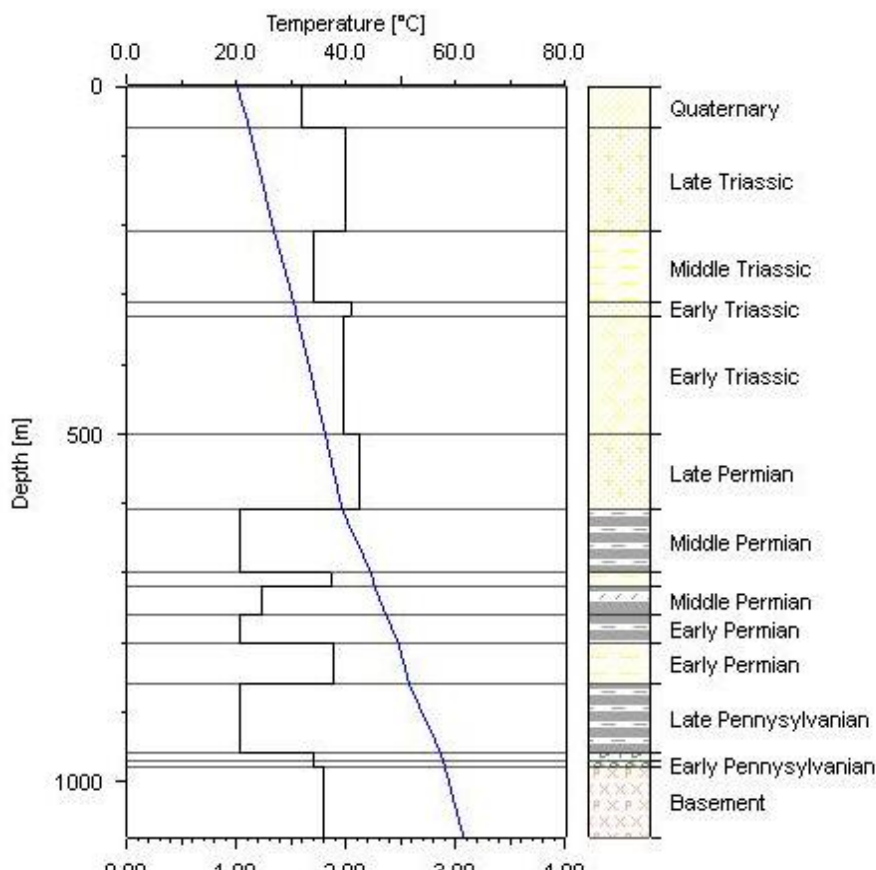


PM PetroMod

(B)



Thermal Conductivity: Vertical, Soutpansberg and Tuli Basins



Pressure, Soutpansberg and Tuli Basins

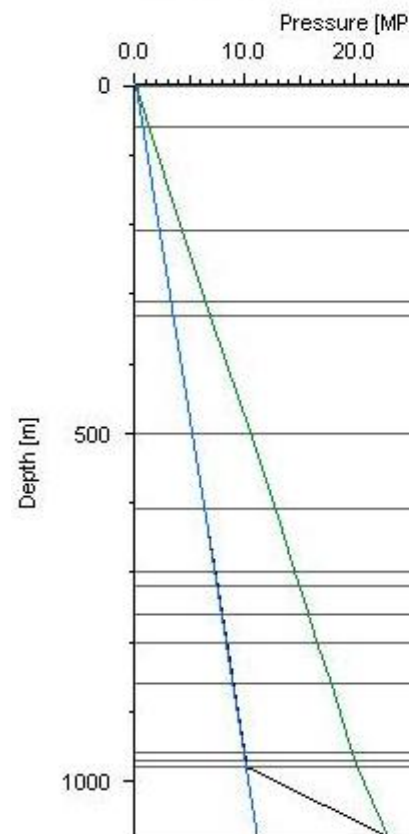


Figure 10.12: Depth plots (Vitrinite reflectance, Porosity, thermal conductivity and pressure) of the Soutpansberg and Tuli Basins.

10.4. Discussions

The subsidence plot in Figure 10.6 displays concave and convex-upward curves. According to McKenzie (1978), the concave-upwards subsidence curves are characteristic of tectonic and thermal stages of lithospheric extension involving mechanical stretching. Relating this theory to the Gondwana, subduction of the Palaeo-Pacific oceanic plate under the Gondwana plate possibly during the Mid-Carboniferous, which formed a magmatic arc may have caused stretching and then slow thermal subsidence of the lithosphere. These caused passive continental margins (mechanically extended and thermally subsided lithosphere). The subsidence of the basins is believed to be initiated and thermally controlled by tectonic (i.e. faults of basements blocks) rather than thermal events (i.e. sediment burial).

Based on the preliminary study of source rock maturation and hydrocarbon generation, no significant hydrocarbon accumulations that can merit oil and gas exploration were found in the Soutpansberg and Tuli Basins. This may be due to the sediments being immature and the basin being shallow (maximum-1000 m).

Jurassic basalts cap the Karoo stratigraphic sequence in the basins (Reid *et al.*, 1997). The Karoo mafic igneous province, formed at 183 Ma, and is characterised by the presence of voluminous basaltic intrusive complexes within the Karoo Basin, extrusive lava sequences and hydrothermal vent complexes (Svensen *et al.*, 2006). It is not known whether the magma injected, during the Jurassic, destroyed all hydrocarbons.

The sedimentary basins are fault-bounded and form half grabens. The half-graben geometry is directly controlled by the deformation (displacement) field surrounding the boundary fault system (Figures 10.6). The subsidence plots in (Figures 10.5 and 10.6) displayed linear and convex-upward curves with the subsidence rates de-accelerating early on and then accelerating through the Permo-Carboniferous period. The tectonic subsidence curves show a phase resembling that of a passive continental margin characterised by slow to

medium subsidence rate, and a phase of rapid subsidence with the onset of foreland basin evolution (Einsele, 2000). The development of a passive margin along the southern margin of the Kalahari Craton resulted from the occurrence of extensional tectonics in the Early Palaeozoic.

In this context, the internal part of the Karoo basin was superimposed on a passive continental margin, i.e. on lithosphere which was already mechanically extended and had thermally subsided. Relating this theory to the SW Gondwana, subduction of the Palaeo-Pacific oceanic plate under the Gondwana plate possibly during the mid-Carboniferous, which formed a magmatic arc may have caused stretching and then slow thermal subsidence of the lithosphere. In agreement to this theory, Visser and Praekelt (1996) proposed thermal subsidence associated with release of Gondwana heat as the main process responsible for the formation and location of the basin. In addition, Catuneanu *et al.* (1998) proposed that interplay of these tectonic mechanisms, combined with the influence exerted by the inherent structures of the underlying Precambrian basement, resulted in the formation of discrete depozones that follow regional tectonic trends (Figure 10.13).

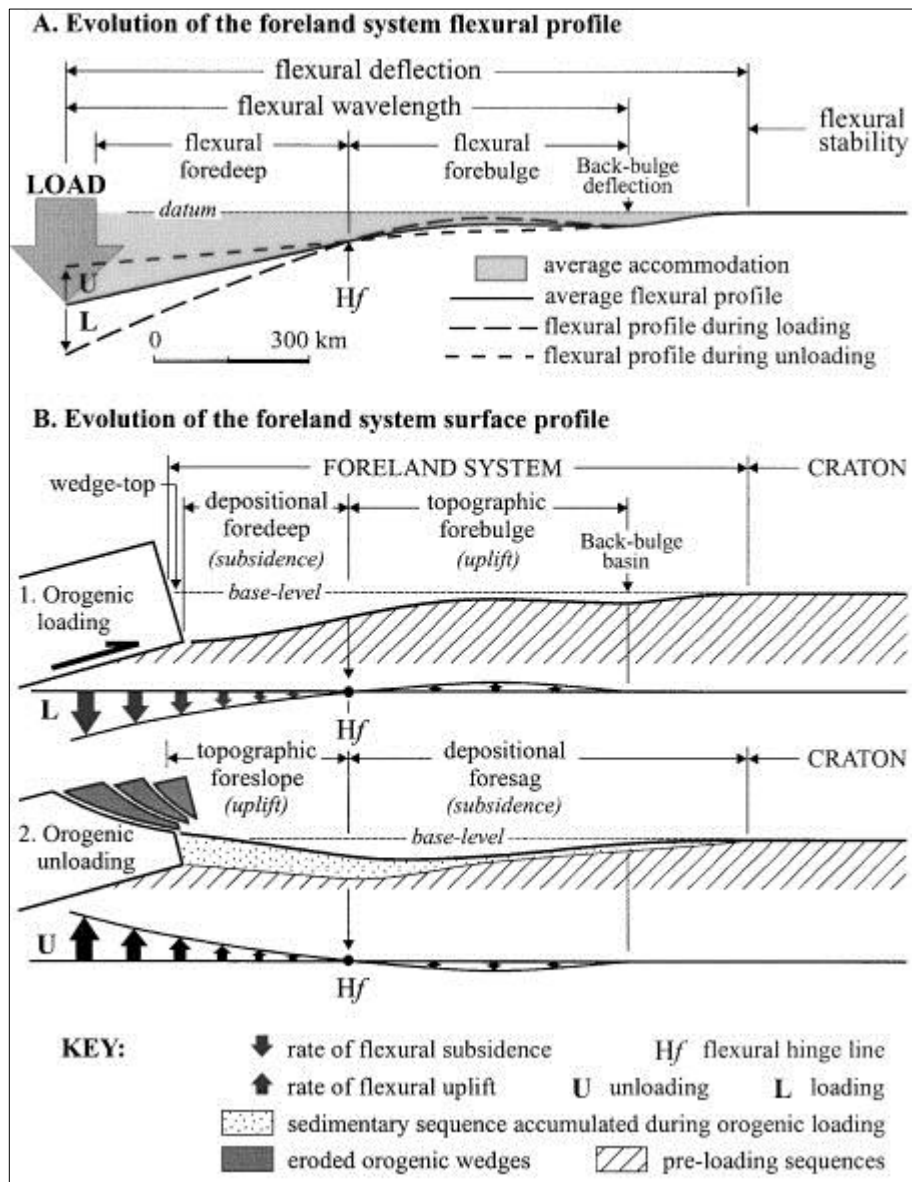


Figure 10.13: Flexural and surface profiles illustrating the evolution of the foreland system during stages of orogenic loading and unloading (after Catuneanu *et al.*, 1998). Not to vertical scale.

The initial occurrence of extensional tectonics and the development of a passive margin implies that the subsidence was initiated and mainly controlled by mechanical (i.e. detachment faults of basement blocks that occurred during rifting), as it has been discussed in structural and geophysical analysis, rather than thermal geologic events (i.e. sediment burial). In addition, variations in the flexural rigidity along the strike of the basin possibly led to unpredictable lateral changes in the subsidence history (Figure 10.5). The suggested model showed a good agreement with the lithostratigraphic data, in particular, it explains the

thickness of sediments in the coalfields, their formation and rapid subsidence. A proposed basinal fill model of the Soutpansberg and Tuli Basins is illustrated in Figure 10.14.

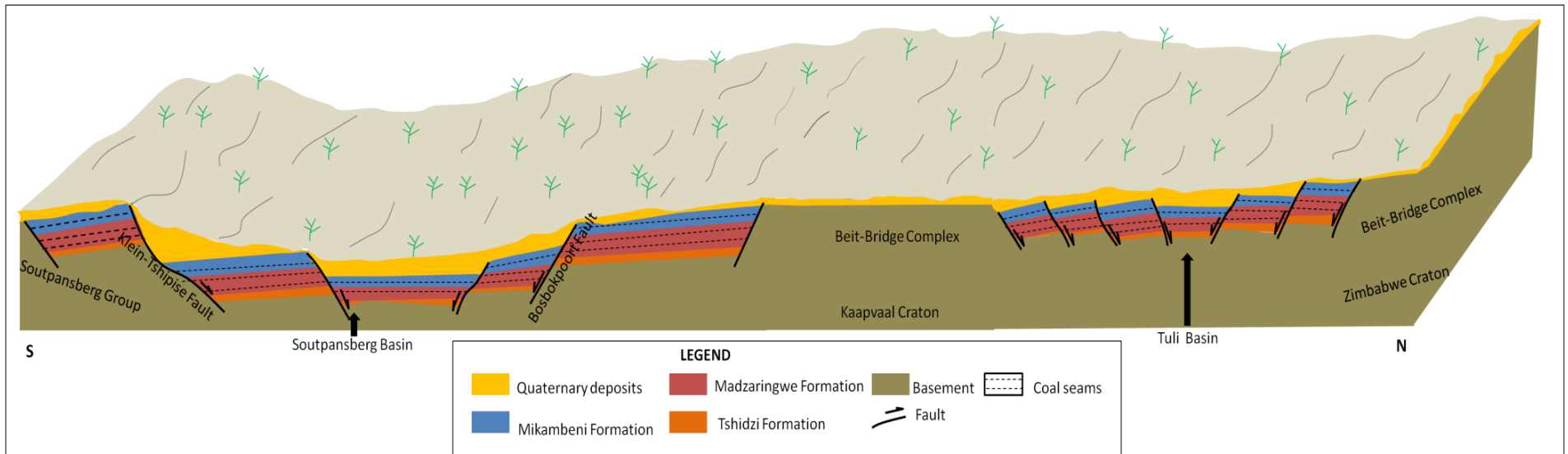


Figure 10.14: Proposed basinal fill model of the Soutpansberg and Tuli Coalfields with major faulting. Figure not to scale.

10.5. Conclusions

The analysis of stratigraphic sequences and subsidence of the Soutpansberg and Tuli Basins has enabled the following scheme to be proposed.

- The primary graben system was initiated during the Late Carboniferous at the beginning of the Karoo tectonic events. Previous workers (Brandl (2002); Bordy and Catuneanu (2001); Bordy and Catuneanu (2002a, b and c)) suggest that general uplift was initiated at about 300 Ma.
- Structural geology study by Brandl (1981); Bumby *et al.* (2001) suggest a two intersecting fault system which controlled sedimentation, one which trends north-east-north and another trending west-north-west to north-west.
- Subsidence within the basin system argues for the primary graben which must have been centered within the present basins, and later became a region of major faulting. This gave way to the Late Carboniferous to Early Permian rapid subsidence with areas of greater extension subsiding more rapidly (Flores, 1970; Forster, 1975). The rift flanks were gradually uplifted and when extension terminated, a general subsidence took over as a result of thermal contraction. The originally uplifted rift flanks were subsequently eroded. This suggests that the Late Triassic beds (i.e. Clarens) were deposited in basin caused by the Karoo thermal subsidence stage in a mainly fluvial-playa environment.
- Conclusively, the Soutpansberg and Tuli Basins subsided rapidly as orogenic loading increased, leading to the conclusion that periods of thrusting in the Soutpansberg Group, Waterberg Group and the Beit-Bridge Complex and periods of subsidence of both the Soutpansberg and Tuli Karoo basins are simultaneous. The tectonic subsidence is consistent with tectonic models that propose a Permo-Carboniferous basin formation.

CHAPTER 11

SUMMARY

Since the establishment of a basic correlative framework of the Karoo Supergroup rocks in the Soutpansberg and Tuli Coalfields, theories of basin development in the Main Karoo Basin in South Africa (the reference basin of all Karoo-aged basins in southern Africa) have been reviewed. Whilst the published data gives an overview of the geology of the basins and the coalfields, there is lack of integrated basinal analysis of the research areas. This research project is aimed at new insight in the stratigraphy, sedimentology, mineralogy, petrology, geophysics, geochemistry, diagenesis of sandstone, coal analysis and basin subsidence history of the Soutpansberg and Tuli Coal-Basins. In addition, the collected geometrical data in this study compared to inferred depositional environments in order to make a cohesive contribution to concepts of the evolutionary history of the coalfields.

This study, using over 2000 borehole logs and field work has shown that it is possible to correlate sedimentary facies and facies associations and of the Karoo Supergroup across the Tuli and Soutpansberg Coalfields. The Tshidzi, Madzaringwe and Mikambeni Formations make up the Soutpansberg and Tuli Coalfields' stratigraphy and they are both hosted in the Soutpansberg and Tuli Basins respectively. The Tshidzi Formation is developed at the base of the Karoo Sequence and consists of diamictite. The Madzaringwe Formation is divided into three members: the Basal Member, a laminated, grey and black carbonaceous shale and coal; the Middle Member, alternating beds of shale and fine-coarse grained sandstone to siltstone; Upper Member, a laminated, grey and black carbonaceous shale and coal. Succeeding the Madzaringwe Formation is the Mikambeni Formation. This formation can be subdivided into two members (Lower and Upper Members). The Lower Member is characterised by laminated, grey and black carbonaceous shale and coal and sandy shale/mudstone. The Middle Member is characterised by alternating beds of shale and fine-coarse grained siltstone.

The study of both the structural and geophysical analysis have revealed the structural and tectonic settings of the two coalfields. Paleostress inversion techniques were performed using an improved Right-Dihedral method, followed by rotational optimization. The main stress field in the Soutpansberg Basin is characterized by W-E to ENE-WSW extension and N-S to NNW-SSE compression. The main stress field in the Tuli Basin is characterized by N-S to NNW-SSE compression and W-E to ENE-WSW extension. The orientation of the principal stress axes (σ_1 , σ_2 , and σ_3) and the ratio of the principal stress differences (R) show

that σ_1 and σ_3 are generally sub-vertical and σ_2 is sub-horizontal in most of the paleostress tensors, which are belonging to a major normal fault system with σ_1 swinging around NNE direction.

Gravity, magnetic and radiometric surveys of various scales was used to outline the distribution of rocks and mineral types, structural trends, basement trends and hence gave information on the overall structure and distribution of the coal-bearing sequence. The shapes and trends of the basins with respect to the faults clearly indicate that the origin of the basins is the result of overstepped divergent directional faults. The fault traces step left, forming areas of tension, where the basins were nucleated following the major E-W trending crustal discontinuity. The whole study area consists of two easterly tilted basins with half-graben geometry separated by uplifted Archaean (Beit-Bridge Complex) and Proterozoic (Soutpansberg Group) blocks. Sedimentary units were outlined according to weak amorphous magnetic signatures and low gravity densities. Most of these areas are fault controlled and are related to basins delimited by vertical-movement faults. The unit is composed of sandstone, siltstone, shale and coal which are Late Carboniferous to Late Permian in age. Jurassic volcanics (Letaba and Jozini Formations) follow a SW-NE trend, outcropping in the east (Soutpansberg Basin), producing a strong magnetic response in this area, and partly buried in the west, where magnetic intensity tends to be reduced. The geological evolution of the Karoo strata, at least since the Upper Carboniferous, essentially follows the type model for passive continental margin terrain which related to persistent oceanic crust subduction. Sedimentation is restricted to associated fore-arc basins. Both the basins are characterised by normal faults trending north-northeast in the Soutpansberg and east-northeast in the Tuli Coalfield.

A total of sixteen major lithofacies were identified in the coalfields. Internal and external geometry strata in the coalfields have been subdivided into seven distinct facies associations (FA), which are: Glacial diamictite and sandstone (FA 1), Clast supported conglomerate and sandstone (FA 2), Tabular cross-bedded sandstone (FA 3), Trough and planar cross-bedded sandstone (FA 4), Fine calcareous and micaceous siltstone and mudstone (FA 5), Sandy shale/mudstone (FA 6), Laminated or thin-bedded Carbonaceous shale/mudstone (FA 7). Detailed analysis of lithofacies types and facies assemblages in the Soutpansberg and Tuli Basin suggests a fluvial depositional and fluvioglacial environment. The paleocurrent analysis shows that the source was from north-east direction and the paleoflow was towards the south-west direction in both coalfields.

The identified facies associations indicate the following depositional environments: fluvio-glacial depositional environment (FA1, Tshidzi Formation); meandering and braided fluvial channels (FA 6 and FA 7, Madzaringwe Lower Member); fluvial channels, crevasse splays, levees and crevasse channels (FA 2, FA 3, FA 4 and FA 5, Madzaringwe, Middle Member); fluvial channels, crevasse splays (FA 6 and FA 7, Madzaringwe Upper Member); meandering and braided fluvial channels, crevasse splays (FA 6, Mikambeni, Lower Member) and lastly meandering fluvial channels and crevasse splays (FA 2, FA 3, FA 4 and FA 5, Mikambeni, Upper Member).

Petrographic and geochemical studies of sandstones, their provenances and relationships to the tectonic settings in the Soutpansberg and Tuli Coalfields have not been investigated previously. The combination of sandstone petrography and geochemistry studies has been used to identify provenance and ancient tectonic environment characteristics of the sedimentary basins. Sandstone petrography and detrital modes on discrimination diagrams indicate that the Late Carboniferous and Early Permian succession was derived from craton interior and recycled orogen provenances. The geochemical data of major elements show that sandstone and shales have the same source. The results of the study suggest uplifted basement source areas dominated by sedimentary rocks and/or granite-gneiss rocks. A passive continental margin source is therefore suggested for both basins.

The subsidence of the basins is believed to be initiated and thermally controlled by tectonics (i.e. faults of basements blocks) rather than sedimentary burial. The subsidence within the basins supports the primary graben system which must have been centered within the present basins, and later became a region of major faulting. The first subsidence phase (Late Carboniferous) resulted in the deposition of the diamictite Tshidzi, Formation. This subsidence phase corresponds to the interval of 290-260 Ma. This phase is characterised by the concave-up profile. The phase is related to the initial extensional fault controlled subsidence of the basins. The second phase was very short lived and is expressed on the subsidence curves by a two-fold change in subsidence pattern: (1) a convex-upward profile denoting a short and rapid subsidence phase at a subsidence rate corresponding to deposition of the Mikambeni and Madzaringwe Formations. This was during the interval of 260-256 Ma; and (2) another convex-upward profile is noticed on the subsidence curve during the interval of 256-252 Ma, corresponding to deposition of the Fripp Formation. The last phase is characterised by a slow subsidence represents the post-rift thermal subsidence. The

subsidence corresponds to the deposition of the Solitude (250 Ma), Klopperfontein (240 Ma), Bosbokpoort (215 Ma) and Clarens Formations (198 Ma) respectively.

The diagenesis of the Tuli and Soutpansberg sandstones can be divided broadly into early and late diagenetic stages. The main diagenetic processes that have affected the sandstones in the study area include mechanical compaction, cementation and the dissolution of framework grains and cements. Sandstone diagenesis in the coalfields is largely controlled by pre-burial factors such as depositional environment and sediment composition. Compaction, cementation, were the major early diagenetic processes for sandstone. The sandstones show signs of being well compacted mechanically and chemically based on the abundance of long and interpenetrating mosaic grain contacts, deformed ductile grains, fractured and broken framework grains, sutured quartz grains. Quartz cement as pore filling and overgrowths is one of the most abundant cements in both the Tuli and the Soutpansberg sandstones. Calcite cementation was also observed as pore-filling and as well as a replacement mineral of matrix and detrital grains. Pore-lining and pore-filling Illite-smectite and kaolinite are more abundant in the sandstones with a higher percentage of matrix content. During the middle and later stage, seritisation and chloritisation of smectite clays was developed. Chlorite is notable in sandstones having large quantities of volcanic rock fragment and detrital micas, indicating detrital grain composition controls on its diagenetic minerals. Albitization of feldspar grains in the coalfields occurred during the middle and later stages of diagenesis. The Soutpansberg and Tuli Coalfield sandstones are typically medium to coarse-grained moderately sorted arenites to feldspathic litharenites interbedded with minor shales. The sandstone contains abundant quartz, plagioclase and potassium feldspars, and rock fragments.

Textural relationships between authigenic minerals and cements suggest the following paragenetic sequence for the Soutpansberg and Tuli sandstone: (1) pore lining and pore filling clays, (2) mechanical compaction, (3) chemical compaction, (4) quartz and iron oxide cementation, (5) quartz and feldspar overgrowths, (6) seritisation (7) chlorite alteration, (8) grain deformation, pressure-solution and fracturing, (9) albitisation.

It can be concluded that, based on the coal analysis and data currently available, the Soutpansberg Coalfield (especially the eastern part) is likely to present better opportunities for potentially exploitable coal deposits as compared to the Tuli Coalfield. The Tshikondeni Colliery is actively exploiting high quality coking coals, under complex geological conditions, in the Tshipise-Pafuri Coalfield. However it is suggested that further exploration of the areas is needed.

REFERENCES

Allen, P.A. and Allen, J.R., 1990. Basin Analysis: Principles and Applications. 1st edition, Blackwell Scientific Publications, Oxford, 449 pp.

Allen, P.A. and Allen, J.R., 2004. Basin Analysis: Principles and Applications. 2nd edition, Blackwell, Scientific Publications, Oxford, 560 pp.

Arem, M.A.M., 2011. Clastic Sedimentary Rocks, Sandstone diagenesis. King Abdulaziz University, Jeddah, Saudi Arabia, 35 pp.

Bahnemann, K.P., 1972. A review of the structure, stratigraphy and metamorphism of the basement rocks of the Messina District, Northern Transvaal. DSc thesis, University of Pretoria, South Africa, unpublished, 416 pp.

Barker, O.B., 1983. A proposed geotectonic model for the Soutpansberg Group within the Limpopo Mobile Belt, South Africa. In: Van Biljon, W.J. and Legg, J.H. (Editors), The Limpopo Belt. Special Publication. Geological Society of South Africa, 8, 181-190.

Barton, J.M., Jr. and Key, R.M., 1981. The tectonic development of the Limpopo Mobile Belt, and the evolution of the Archean cratons of Southern Africa, In: A. Kroner (Editor), Precambrian Plate Tectonics. Elsevier, Amsterdam, 185-212.

Barton, J.M., Jr., Barnett, W. and Barton, E.S., 2003. The geology of the area surrounding the Venetia kimberlite pipes, Limpopo Belt, South Africa: a complex assembly of terranes and granitoid magmatism. South African Journal of Geology, 106, 109-128.

Bauluz, B., Mayayo, M.J., Fernandez-Nieto, C. and Gonzalez-Lopez, J.M., 2000. Geochemistry of Precambrian and Paleozoic siliciclastic rocks from the Iberian Range (NE Spain): implications for source-area weathering, sorting, provenance, and tectonic setting. Chemical Geology, 168, 135-150.

Bauluz, B., Nieto, F., Mata, P., Giorgetti, G., Arkai, P. and Peacor, D., 2005. Retrograde diagenesis: a widespread process on a regional scale. Clay Minerals, 1, 93-104.

Bhatia, M.R., 1983. Plate tectonics and geochemical composition of sandstones. *Journal of Geology*, 91, 611-627.

Bhatia, M.R., 1985. Plate tectonics and geochemical composition of sandstones: a reply. *Journal of Geology*, 93, 85-87.

Bhatia, M.R. and Crook, K.A.W., 1986. Trace element characteristics of greywacke and tectonic setting discrimination of sedimentary basins. *Contributions to Mineralogy and Petrology*, 92, 181-193.

Bjorlykke, K., 1989. *Sedimentology and Petroleum Geology*. Springer-Verlag, New York, 263 pp.

Boles, J.R., 1982. Active albitisation of Plagioclase, Gulf Coast Tertiary. *American Journal of Science*, 282, 165-180.

Boles, J.R. and Ramseyer, L., 1988. Albitisation of plagioclase and vitrinite reflectance as paleothermal indicators, San Joaquin basin. In: S.A. Graham (Editor), *Studies of the Geology of the San Joaquin basin, Pacific Section*. Society of Economic, Paleontology and Mineralogy, 60, 129-139.

Boggs, S. 2001. *Principles of sedimentology and stratigraphy*. 3rd edition, New Jersey, Prentice-Hall. 726 pp.

Bond, G.C. and Kominz, M.A., 1984. Construction of tectonic subsidence curves for the early Paleozoic miogeocline, Southern Canadian Rocky Mountains: Implications for subsidence mechanisms, age of breakup and crustal thinning. *Geological Society of America Bulletin*, 95, 155-173.

Bordy, E.M., 2000. *Sedimentology of the Karoo Supergroup in the Tuli Basin (Limpopo River area, South Africa)*. Ph.D. Thesis, Rhodes University, South Africa, unpublished, 266 pp.

Bordy, E.M. and Catuneanu, O., 2001. Sedimentology of the Upper Karoo fluvial strata in the Tuli Basin, South Africa. *Journal of African Earth Sciences*, 33, 605-629.

Bordy, E.M. and Catuneanu, O., 2002a. Sedimentology of the Beaufort - Molteno Karoo fluvial strata in the Tuli Basin, South Africa. *South African Journal of Geology*, 105, 51-66.

Bordy, E.M. and Catuneanu, O., 2002b. Sedimentology and palaeontology of upper Karoo aeolian strata (Early Jurassic) in the Tuli Basin, South Africa. *Journal of African Earth Sciences*, 35, 301-314.

Bordy, E.M. and Catuneanu, O., 2002c. Sedimentology of the lower Karoo Supergroup fluvial strata in the Tuli Basin, South Africa. *Journal of African Earth Sciences*, 35, 503-521.

Bott, M.H.P., 1959. The mechanisms of oblique slip faulting. *Geological Magazine*, 96, 109-117.

Bracciali, L., Marroni, M., Pandolfi, L. and Rocchi, S., 2007. Geochemistry and petrography of Western Tethys Cretaceous sedimentary covers (Corsica and Northern Apennines): from source areas to configuration of margins. In: J. Arribas, S. Critelli., M.J. Johnsson, (Editors), *Sedimentary Provenance and Petrogenesis: Perspectives from Petrography and Geochemistry*. Geological Society of American Special Paper, 420, 73-93.

Brandl, G., 1981. The geology of the Messina area. Explanation, sheet 2230, Messina, Geological Survey of South Africa, 35 pp.

Brandl, G., 2002. The geology of the Alldays area. Explanation sheet 2228, Alldays, Geological Survey South Africa, 71 pp.

Brandl, G. and McCourt, S., 1980. A lithostratigraphic subdivision of the Karoo Sequence in the north-eastern Transvaal. *Annals Geological Survey of South Africa*, 14, 51-56.

Bumby, A.J., Eriksson, P.G., van der Merwe, R. and Steyn G.L., 2001. A half-graben setting for the Proterozoic Soutpansberg Group (South Africa): evidence from the Blouberg area. *Sedimentary Geology*, 147, 37-56.

Bumby, A.J. and van der Merve, R., 2004. The Limpopo Belt of Southern Africa: a Neoproterozoic to Palaeoproterozoic orogen. In: P.G. Eriksson., W., Altermann, D.R., Nelson,

W.U., Mueller. and O. Catuneanu (Editors), The Precambrian Earth: Tempos and Events. Elsevier, Amsterdam, 217-233.

Cairncross B., 2001. An overview of the Permian (Karoo) coal deposits of Southern Africa. *Journal of African Earth Science*, 33, 529-562.

Catuneanu, O., Hancox, P.J. and Rubidge, B.S., 1998. Reciprocal flexural behaviour and contrasting stratigraphies: a new basin development model for the Karoo retroarc foreland system, South Africa. *Basin Research*, 10, 417-439.

Catuneanu, O., Hancox, P.J., Cairncross, B. and Rubidge, B.S., 2002. Foredeep submarine fans and forebulge deltas: orogenic off-loading in the underfilled Karoo Basin. *Journal of African Earth Sciences*, 35, 489-502.

Catuneanu, O., 2004. Retroarc foreland systems-evolution through time. *Journal of African Earth Sciences*, 38, 225-242.

Chidley, C.M., 1985. The geology of the country around Evangelina and Pontdrift (1:50,000 sheets 2228BD and 2229A). Unpublished South African Geological Survey Report. Pietersburg, South Africa, 22 pp.

Corfield, R.I., Watts, A.B. and Searle, M.P., 2005. Subsidence of the North Indian Continental Margin, Zaskar Himalaya, NW India. *Journal of the Geological Society of London*, 162, 135-146.

Crook, K.A.W., 1974. Lithogenesis and geotectonics: the significance of compositional variation in flysch arenites (greywackes). *Society of Economic, Paleontology and Mineralogy Special Publication*, 19, 304-310.

DAFF, (Department of Agriculture, Forestry and Fisheries), 2012. Protected trees 1, Tree species protected in terms of Section 12 (d) of the National Forest Act No. 84 of 1988, South Africa.

.

Daszinnies, M.C., Jacobs, J., Wartho, J.A. and Gantham, G.H., 2009. Post Pan-African thermo-tectonic evolution of the north Mozambican basement and its implication for the Gondwana rifting. Inferences from $^{40}\text{Ar}/^{39}\text{Ar}$ hornblende, biotite and titanite fission-track dating. The Geological Society of London, Special Publication 342. 261-287.

De Jager, F.S.J., 1976. Coal. In: C.B. Coetzee (Editor), Mineral resources of the Republic of South Africa, Department of Mines, Geological Survey, 289-330 pp.

De Jager, F.S.J., 1986. Coal occurrences of the central, north-western, northern and eastern Transvaal. In: C.R. Anhaeusser and S. Maske (Editors), Mineral Deposits of Southern Africa vols. I and II, Geological Society of South Africa, Johannesburg, 2047-2055.

Delvaux, D., 2012. WINTENSOR, VERSION 4.0.3, Royal Museum for Central Africa, Tervuren, Belgium Dept. Geology-Mineralogy.

Delvaux, D. Moeys, R., Stapel., G., Petit, C., Levi, K., Miroshnichenko, A., Ruzhich, V. and San'kov, V., 1997. Paleostress reconstructions and geodynamics of the Baikal region, Central Asia, Part 2. Cenozoic rifting. Tectonophysics, 282, 1-38.

Delvaux, D. and Sperner, B., 2003. New aspects of tectonic stress inversion with reference to the Tensor Program. Royal Museum for Central Africa, Tervuren, Belgium Dept. Geology-Mineralogy.

Destro, N., 1995. Release fault: a variety of cross fault in linked extensional fault systems in the Sergipe-Alagoas Basin, NE Brazil. Journal of Structural Geology, 17, 615-629.

De Wit, M.J., van Reenen, D.D. and Roering, C., 1992. Geologic Observation across a Tectono-Metamorphic Boundary in the Babangu Area, Giyani Greenstone Belt, South Africa. Precambrian Research, 55, 111-122.

Dickinson, W.R., 1985. Interpreting provenance relation from detrital modes of sandstones. In: G.G. Zuffa, (Editor), Provenance of Arenites. D. Reidel Publishing Company, 333-363.

Dickinson, W.R. and Suczek., C.A. 1979. Plate tectonics and sandstone compositions. *American Association of Petroleum Geologist Bulletin*, 63, 2164-2182.

Dickinson, W.R., Beard, L.S., Brakenridge, G.R., Evjavec, J.L., Ferguson, R.C., Inman, K.F., Knepp, R.A., Lindberg, F.A. and Ryberg, P.T., 1983, Provenance of North American Phanerozoic sandstones in relation to tectonic setting. *Geological Society of America Bulletin*, 94, 222-235.

Diessel, C.F.K., 2007. Utility of coal petrology for sequence-stratigraphic analysis. *International Journal of Coal Geology*, 70, 3-34.

Diessel, C.F.K., 1992. *Coal-Bearing Depositional System*. Springer-Verlag, Berlin, 721 pp.

Einsele, G., 2000. *Sedimentary Basins. Evolution, Facies, and Sediment Budget*. 2nd edition, Springer-Verlag, Berlin, 792 pp.

Falcon R.M.S., 1986. A brief review of the origin, formation and distribution of coal in southern Africa. In: C.R. Anhaeusser and S. Maske (Editors), *Mineral Deposits of Southern Africa*, Geological Society of South Africa, 1879-1898 pp.

Fedo, C. M., Young, G. M. and Nesbitt, H. W., 1997. Paleoclimate control on the composition of the Paleoproterozoic Serpent formation, Huronian Supergroup, Canada, a greenhouse to icehouse transition, *Precambrian Res*, 86, 201-223.

Fisher, W. L., Brown, L. F., Jr., Scott, A. J. and McGowen, J. H., 1969. Delta systems in the exploration for oil and gas: A research colloquium: Bureau of Economic Geology, The University of Texas at Austin, Austin, Texas, August 27-29, 1969.

Flores, G., 1970. Suggested Origin of the Mozambique Channel: Transvaal. *Geological Society of South Africa*, 73, 1-16.

Flores, R., 1981. Coal deposition in fluvial paleoenvironments of the Paleocene Tongue River Member of the Fort Union Formation, Powder River basin, Wyoming and Montana. In: F.

Etheridge and R. Flores (Editors), Models for Exploration. Special Publication of the Society of Economic, Recent and Ancient Non-marine Depositional Environments. *Palaeontologists and Mineralogists*, 31, 169-90.

Floyd, P.A. and Leveridge, B.E. 1987. Tectonic environment of the Devonian Gramscatho basin, south Cornwall: framework mode and geochemical evidence from turbiditic sandstones. *Journal of the Geological Society London*, 144, 531-542.

Floyd, P.A., Winchester, J.A. and Park, R.G. 1989. Geochemistry and tectonic setting of Lewisian clastic metasediments from the Early Proterozoic Loch Maree Group of Gairloch, N.W. Scotland. *Precambrian Research*, 45 (1-3), 203-214.

Folk, R.L., 1980. *Petrology of Sedimentary Rocks*. Hemphill Publishing, Austin, TX, 184 pp.

Forster, R., 1975. The geological history of the sedimentary basin of southern Mozambique, and some aspects of the origin of the Mozambique Channel. *Palaeogeography, Palaeoclimate and Palaeoecology*, 17, 276-287.

Fripp, R.E.P., 1981. The ancient river gneisses, Limpopo Belt, South Africa. *Geological Society of Australia Special Publication*, 7, 329-335.

Frostick, L.E. and Steel, R.J., 1993. Tectonic controls and signatures in sedimentary successions. Special publication of the International Association of Sedimentologists, Blackwell Scientific Publications, 20, 139-142.

Gallagher, K., 1989. An examination of some uncertainties associated with estimates of sedimentation rates and tectonic subsidence. *Basin Research*, 2, 97-114.

Galloway, W.E., 1975. Process framework for describing the morphologic and stratigraphic evolution of deltaic depositional systems. In: M.L. Broussard (Editor), *Deltas, Models for Exploration*. Houston Geological Society, Houston, TX. 87-98.

Gawthorpe, R.L. and Colella, A., 1990. Tectonic controls on coarse grained delta depositional systems in rift basins. In: A. Colella and D.B. Prior (Editors), Coarse-grained Deltas. International Association of Sedimentologist Special Publication, 10, 113-127.

Groenewald, P.B., Grantham, G.H. and Watkeys, M.K., 1991. Geological evidence for a Proterozoic to Mesozoic link between southeastern Africa and Dronning Maud Land, Antarctica. Journal of the Geological Society of London, 148, 1115-1123.

Geological Map, Alldays., 2000. Scale 1:250,000, Sheet 2228-Geological Series. Council for Geosciences, Republic of South Africa.

Halbich, I.W., Fitch, F.J. and Miller, J.A., 1983. Dating the Cape orogeny. In: A.P.G. Sohng and I.W. Halbich (Editors), Geodynamics of the Cape Fold Belt, Special Publication, Geological Society of South Africa, 12, 149-164.

Hamilton, E.L., 1959. Thickness and consolidation of deep-sea sediments. Bulletin of the Geological Society of America, 70, 1399-1424.

Hayes, M. J., and Boles, J. R., 1992, Volumetric relations between dissolved plagioclase and kaolinite in sandstones: implications for aluminum mass transfer in the San Joaquin basin, California. In: D.W. Houseknecht and E.D. Pittman (Editors), Origin, diagenesis and petrophysics of clay minerals in sandstones. Society of Economic, Paleontology and Mineralogy Special Publication, 47, 111-123.

Heinz, P., Kitazato, H., Schmiedl, G. and Hemleben, C., 2001. Response of deep-sea benthic foraminifera to simulated phytoplankton pulses under laboratory conditions. Journal of Foraminiferal Research, 31, 210-227.

Herron, M.M., 1988. Geochemical classification of terrigenous sands and shales from core or log data. Journal of Sedimentary Petrology, 58, 820-829.

Holz, M., Kalkreuth, W. and Banerjee, I., 2002. Sequence stratigraphy of paralic coal-bearing strata: an overview. International Journal of Coal Geology, 48, 147-179.

Hower, J.C. and Eble, C.F., 1996. Coal Quality and Utilisation, Energy Minerals Division Hourglass, 30, 1-8.

Huggins, F.E., 2002. Overview of analytical methods for inorganic constituents in coal. International. Journal of Coal Geol, 50, 169-214.

Ingersoll, R.V., Bulard, T.F., Ford, R.L., Grimm, J.P., Pickle, J.P. and Sares, S.W., 1984. The effect of grain size on detrital modes: a text of the Gazzi-Dickinson Point Counting method. Journal of Sedimentary Petrology, 54, 103-116.

Ingersoll, R.V., 1988. Tectonics of sedimentary basins. Geological Society of America Bulletin 100, 1704-1719.

Ingersoll, R.V. and Suczek, C.A., 1979. Petrology and provenance of Neogene sand from Nicobar and Bengal fans. DSDP sites 211 and 218. Journal of Sedimentary Petrology, 49, 1217-1228.

Johnson, M. R., Van Vuuren C. J., Hegenberger W. F., Key R. and Show U., 1996. Stratigraphy of the Karoo Supergroup in Southern Africa: an overview. Journal of African Earth Sciences, 23, 3-15.

Johnson, M. R., Visser, J.N.J., Cole, D.I., Wickens, H.D., Christie, A.D.M., Roberts, D.L., and Brandl, G., 2006. Sedimentary rocks of the Karoo Supergroup. In: M. R. Johnson, C.R., Anhaeusser and R.J. Thomas (Editors), The geology of South Africa. Geological Society of South Africa and the Council for Geoscience, 461-499.

Kastner, M. and Siever, R., 1979. Low temperature feldspars in sedimentary rocks. American Journal of Science, 279, 435-479.

Larsen, G. and Chilingar, G.V., 1983. Diagenesis in sediments and sedimentary rocks, 2: New York, Elsevier Scientific Publishing Company, 572 pp.

Loup, B., 1992. Evolution de la partie septentrionale du domaine helvétique en Suisse occidentale au Trias et au Lias: contrôle par subsidence thermique et variations du niveau marin. Ph.D. Thesis, Université de Genève, unpublished, 298 pp.

Madhavaraju, J. and Lee, Y.I., 2010. Influence of Deccan volcanism in the sedimentary rocks of Late Maastrichtian-Danian age of Cauvery basin South-eastern India: constraints from geochemistry. *Current Science*, 98, 528-537.

Marson, C. B. and Cobb, J. W., 1925. Influence of the Ash Constituents in the Carbonisation and Gasification of Coal, With Special Reference to Nitrogen and Sulphur. Part 1, Preparation and Preliminary Examination of Special Cokes. *Gas Journal of London*, 171, 39-46.

Maslov, A.V., Krupenin, M.T. and Gareev, E.Z., 2003. Lithological, lithochemical and geochemical indicators of Paleoclimate: Evidence from Riphean of the Southern Urals. *Lithology and Mineral Resources*, 38, 427-446.

Maslov, A.V., Gareev, E.Z. and Podkovyrov, V.N., 2010. Upper Riphean and Vendian sandstones of the Bashkirian anticlinorium. *Lithology and Mineral Resources*, 45, 285-301.

McBride, E. F., 1989. Quartz cement in sandstones: a review. *Earth Science Reviews*, 26, 69-112.

McCann, T., 1991. Petrological and geochemical determination of provenance in the southern Welsh Basin. In: A. C. Morton, S. P., Todd and P. D. W. Haughton (Editors), *Developments in Sedimentary Provenance*. Geological Society Special Publication, 57, 215-230.

McCourt, S. and Vearncombe, J.R., 1987. Shear Zones Bounding the Central Zone of the Limpopo Mobile Belt, Southern Africa. *Journal of Structural Geology*, 9, 127-137.

McCourt, S. and Vearncombe, J.R., 1992. Structure of the Limpopo Belt and adjacent granitoid-greenstone terranes: Implication for late Archean Crustal Evolution in Southern Africa, *Precambrian Research*, 55, 553-570.

McKenzie, D., 1978. Some remarks on the development of sedimentary basins. *Earth planet science letters*, *Earth planetary Science Letters*, 40, 25-32.

McLennan, S.M. and Taylor, S.R., 1991. *Sedimentary rocks and crustal evolution: tectonic*

setting and secular trends. *Journal of Geology*, 99, 1-21.

McLennan, S.M., Hemming, S., McDaniel, D.K. and Hanson, G.N. 1993. Geochemical approaches to sedimentation, provenance and tectonics. In: M.J. Johnsson and A. Basu, (Editors), *Processes Controlling the Composition of Clastic Sediments*. Geological Society of American Special Paper, 21-40.

Miall, A.D. 1978. Lithofacies types and vertical profile models in braided river deposits: a summary. In: A.D. Miall (Editor), *Fluvial Sedimentology*. Canadian Society of Petroleum Geologists Memoir, 5, 597-604.

Miall, A.D., 1981. Late Cretaceous and Paleogene sedimentation and tectonics in the Canadian Arctic Islands. In: A.D. Miall (Editor), *Sedimentation and Tectonics in Alluvial Basins*. Special Paper, Geological Association of Canada, 27, 221-272.

Miall, A.D., 1982. Tertiary sedimentation and tectonics in the Judge Daly Basin, northeast Ellesmere Island, Arctic Canada. *Energy, Mines, and Resources Canada*, 17 pp.

Miall, A.D., 1988. Facies architecture in clastic sedimentary basins. In: *New Perspectives*. In: K. L. Kleinspehn and C. Paola (Editors), *Basin Analysis*. Springer-Verlag, New York, 67-81.

Miall, A. D., 1990. *Principles of Sedimentary Basin Analysis*. 2nd edition, Springer-Verlag, New York Inc, 668 pp.

Miall, A.D., 2000. *Principles of Sedimentary Basin Analysis*. 3rd edition, Springer-Verlag, New York Inc, 616 pp.

Milsom, J., 2003. *Field Geophysics*. 3rd edition, John Wiley & Sons Ltd England, 249 pp.

Murali, AV., Parthasarathy, R., Mahadevan, TM. and Sankar Das, M., 1983. Trace element characteristics, REE patterns and partition coefficients of zircons from different geological environments-A case study on Indian zircons. *Geochimica et Cosmochimica Acta*, 47, 2047-2052.

Mussett, A.E. and Khan, M.A., 2000. Looking into the Earth: An Introduction to Geological Geophysics, Cambridge University Press, Cambridge, 470 pp.

Nelson, S. A., 2013. Sandstone and Conglomerates. Petrology Notes, Tulane University, 12 pp.

Nesbitt, H.W. and Young, G.M., 1982. Early Proterozoic climates and plate motions inferred from major element chemistry of lutites. *Nature*, 299, 715-717.

Nesbitt, H.W. and Young, G.M., 1984. Prediction of some weathering trends of plutonic and volcanic rocks based upon thermodynamic and kinetic consideration. *Geochimica et Cosmochimica Acta*, 48, 1523-1534.

Nesbitt, H.W. and Young, G.M., 1996. Petrogenesis of sediments in the absence of chemical weathering: effects of abrasion and sorting on bulk composition and mineralogy. *Sedimentology*, 43, 341-358.

Nesbitt, H.W., Fedo, C.M. and Young, G.M., 1997. Quartz and feldspar stability, steady and non-steady state weathering and petrogenesis of siliciclastic sands and muds. *Journal of Geology*, 105, 173-191.

Ortlepp G.J., 1986. Limpopo Coalfield. In: C.R. Anhaeusser and S. Maske (Editors), *Mineral Deposits of Southern Africa*, Geological Society of South Africa, Johannesburg, 2057-2062.

Orton, G.J. and Reading, H.G., 1993. Variability of deltaic processes in terms of sediment supply, with particular emphasis on grain size. *Sedimentology*, 40, 475-512.

Peters, K.E. and Cassa, M.R., 1994. Applied Source Rock Geochemistry. In: L.B. Magoon and W.G. Dow (Editors), *The Petroleum System-From Source to Trap*. American Association of Petroleum Geologists Memoir, 60, 93-120.

Pettijohn, F.J., 1957. *Sedimentary Rocks*. 2nd edition, Harper and Brothers, New York, 718 pp.

- Pettijohn, F.J., 1975. *Sedimentary Rocks*. 3rd edition, Harper & Tow, New York, 628 pp.
- Pettijohn, F.J., Potter, P.E. and Siever, R., 1987. *Sand and sandstone*, 2nd edition. Springer-Verlag, 533 pp.
- Pienaar, J.C., 1985. *Die Lithologie van Alldays omgewing in Noord Transvaal*. MSc. Thesis, Rand Afrikaans University, Johannesburg, unpublished, 158 pp.
- Potter, P.E. and Pettijohn, F.J., 1963. *Paleocurrents and Basin Analysis*, Academic Press, New York, 296 pp..
- Pretorius, S. J., 1992. *Die litologie, struktuur en metamorfose van die kompleks Beitbrug wes van Messina en oos van Swartwater*. Bulletin, Geological Survey of South Africa, 105, 40 pp.
- Reading, H. G., 1996. *Sedimentary Environments Processes, Facies and Stratigraphy*. 3rd edition, Blackwell Scientific Publications, 688 pp.
- Reineck, H.E. and Singh, I.B., 1973. *Depositional Sedimentary Environments*. Springer-Verlag, Berlin, 439 pp.
- Reynolds, J.M., 1997. *An Introduction to Applied and Environmental Geophysics*. John Wiley and Sons Ltd, Chichester, 796 pp.
- Riva, R.M., Gunter, B.C., Urban, T.J., Vermeersen, B.L.A., Lindenbergh, R.C., Helsen, M.M., Bamber, J. L., van de Wal, R. S.W., van den Broeke, M.R. and Schutz, B.E., 2009. *Glacial Isostatic Adjustment over Antarctica from combined ICES at and GRACE satellite data*. *Earth and Planetary Science Letters*, 516-523.
- Reid, D.L., Rex, D.C. and Brandl, G., 1997. *Karoo basalts in the Ellisras sub-basin, Northern Province*. *South African Journal of Geology*, 100, 151-156.
- Roberts, D.L., 1992. *The Springbok Flats basin-a preliminary report*, Geological Survey of South Africa Report, 1992-0197.
- Roering, C., van Reenen, D.D., Smit, C.A., Barton, J.M., de Beer, J.H., de Wit, M.J., Stetler, E.H., van Schalkwyk, J.F., Stevens, G. and Pretorius, S., 1992. *Tectonic Model of the Evolution of the Limpopo Belt*. *Precambrian Research*, 55, 539-552.

Rollinson, H.R., 1993. Using geochemical data: evaluation, presentation, interpretation, Essex, Longman Scientific Technical, 344 p.

Roser, B.P. and Korsch, R.J., 1986. Determination of tectonic setting of sandstone-mudstone suites using SiO₂ content and K₂O/Na₂O ratio. *Journal of Geology*, 94, 635-650.

Roser, B.P. and Korsch, R.J., 1988. Provenance signatures of sandstone-mudstone suites determined using discriminant function analysis of major-element data. *Chemical Geology*, 67, 119-139.

Rust, B.R., 1972. Structure and process in a braided river. *Sedimentology*, 18, 221-245.

Rust, I.C., 1975. Tectonic and sedimentary framework of Gondwana basins in southern Africa. In: K.S.W. Campbell (Editor), *Gondwana Geology*, Australian National University Press, Canberra, 537-564.

SACS, (South African Committee of Stratigraphy). 1980. Department of Mineral and Energy Affairs, Geological Survey: Obtainable from the Government Printer, 1980.

SAWS, (South African Weather Services). 2011. *Climate of South Africa*, WB42. Climate statistics, 1961-2010, Pretoria.

Schaller M., Steiner O., Studer I., Holzer L., Herwegh M. and Kramers J. D., 1999. Exhumation of Limpopo Central Zone granulites and dextral continent-scale transcurrent movement at 2.0 Ga along the Palala Shear Zone, Northern Province, South Africa. *Precambrian Research*, 96, 263-288.

Schlische, R.W., 1991. Half-graben filling models: New constraints on continental extensional basin development. *Basin Research*, 3, 123-141.

Schlische, R. W. and Anders, M. H., 1996. Stratigraphic effects and tectonic implications of the growth of normal faults and extensional basins. In: K.K. Beratan (Editor), *Reconstructing the Structural History of Basin and Range Extension Using Sedimentology and Stratigraphy*. GSA Special Paper, 303, 183-203.

- Sciunnach, D. Garzanti, E., 1996. Sedimentary record of Late Paleozoic rift and breakup in Northern Gondwana (Thini Chu Group and Tamba-Kurkur Fm.; Dolpo Tethys Himalaya, Nepal). *Geodinamica Acta*, 9, 41-56.
- Sclater, J.G. and Christie, P.A.F., 1980. Continental stretching: an explanation of the post Mid-Cretaceous subsidence of the central North Sea basin. *Journal of Geophysical Research*, 85, 3711-3739.
- Sleep, N.H., 1971. Thermal effects of the formation of Atlantic continental margins by continental break-up. *Geophysical Journal of the Royal Astronomical Society*, 24, 325-350.
- Snyman, J.P., 1998. Coal. In: M.G.C. Wilson and C.R. Anhaeusser (Editors), *The mineral resources of South Africa*. Council for Geoscience, 16, 136-161.
- Sohnge, P.G., Le Roex, H. D. and Nel, H. J., 1948. The geology of the country around Messina. An explanation of Sheet No. 46 (Messina). *South African Geological Survey*, 82 pp.
- Speight, J.G., 2005. *Handbook of Coal Analysis*. Wiley and Sons, 240 pp.
- Sperner, B., Muller, B., Heidbach, O., Delvaux, D., Reinecker, J. and Fuchs, K., 2003. Tectonic stress in the Earth's crust: advances in the World Stress Map project. In: D.A. Nieuwland (Editor), *New Insights into Structural Interpretation and Modelling*, Geological Society of London Special Publications, 212. 101-116.
- Sullivan, J.H., 1995. The geology of the coal-bearing rocks of the Karoo Sequence in the Tshikondeni mine area, northern Transvaal. M.Sc. Thesis, University of Pretoria, unpublished, 159 pp.
- Sullivan J.H., Brink V.D.S. and Sullivan D., 1994. Against all odds: the profitable exploitation of coal at Tshikondeni mine. In: C.R. Anhaeusser (Editor), *Proceedings of the XVth CMMI Congress, Symposium Series S14*, South African Institute of Mining and Metallurgy, Johannesburg, 165-170.

Svensen, H., Jamtveit, B., Planke, S. and Chevallier, L., 2006. Structure and evolution of hydrothermal vent complexes in the Karoo Basin, South Africa. *Journal of the Geological Society*. London, 163, 671-682.

Swaine, D.J., 1990. *Trace Elements in Coal*. London, Butterworths, 278 pp.

Taylor, S.R. and McLennan, S.M., 1985. *The Continental Crust: Its Composition and Evolution*. Blackwell Scientific Publications, 312 pp.

Thabo F.E. and Sullivan J.H., 2000. The geotechnical aspects of Tshikondeni Coal Mine. *Journal of African Earth Sciences*, 31, 78-79.

Toulkeridis, T., Clauer, N., Kröner, A., Reimer, T. and Todt, W., 1999. Characterization, provenance, and tectonic setting of Fig Tree greywackes from the Archaen Barberton Greenstone Belt, South Africa. *Sedimentary Geology*, 124, 113-129.

Tucker, M.E., 2001. *Sedimentary Petrology: An Introduction to the Origin of Sedimentary Rocks*. 3rd edition, Blackwell Science Ltd, USA, 262 pp.

Van der Berg, H.J., 1980. Die sedimentologie van die Soutpansberg-steenkoolveld met spesiale verwysing na steenkoolvorming. M.Sc. thesis, University of Orange Free State, Bloemfontein, unpublished, 127 pp.

Van Hinte, J.E., 1978. Geohistory analysis - application of micropaleontology in exploration geology. *American Association of Petroleum Geologists Bulletin*, 62, 201-222.

Van Reenen, D.D., Roering, C., Ashwal, L.D. and de Wit, M.J., 1987. Regional Geological Setting of the Limpopo Belt, *Precambrian Research*, 55, 1-5.

Van Reenen, D.D., Barton, J.M. and Roering, C., 1987. Deep crustal response to continental collision: the Limpopo Belt of Southern Africa. *Geology*, 15: 11-14.

Van Reenen, D.D., Roering, C., Ashwal, L.D. and de Wit, M.J., 1992. Regional Geological Setting of the Limpopo Belt, *Precambrian Research*, 55, 1-5.

Van Wagoner, J.C., Posamentier, H.W., Mitchum, R.M., Jr, Vail P.R. And Sarg J.F., 1988. An overview of the fundamentals of sequence stratigraphy and key definitions. *Sea-Level Changes: An Integrated Approach*. Society of Economic Paleontology and Mineralogy Special Publications. 39-45.

Vassilev S.V. and Vassileva, C. G., 2007. A new approach for the classification of coal fly ashes based on their origin, composition, properties and behaviour. *Fuel*, 86, 1490-1512.

Visser, D.J.L., 1984. Geological map of the Republic of South Africa, Transkei, Bophuthatswana, Venda and Ciskei and the Kingdoms of Lesotho and Swaziland, Department of Minerals and Energy Affairs, Pretoria, Republic of South Africa.

Visser, J.N.J. and Praekelt, H.E., 1996. Subduction, mega-shear systems and Late Paleozoic basin development of Gondwana. *Geologische Rundschau*, 86, 632-646.

Walker, R.G. and Cant, D.J., 1984, *Sandy Fluvial Systems*. In: R.G. Walker (Editor), *Facies Models*, 2nd edition, Geoscience, Canada, Reprint Series 1, 71-89.

Wallace, R.E., 1951. Geometry of shearing stress and relation to faulting. *Journal of Geology*, 59, 118-130.

Wani, H. and Mondal, M.E.A., 2010. Petrological and geochemical evidence of the Paleoproterozoic and the Meso-Neoproterozoic sedimentary rocks of the Bastar craton, Indian Peninsula: implications on paleoweathering and Proterozoic crustal evolution. *Journal of Asian Earth Sciences*, 38, 220-232.

Ward, C.R., 1984. *Coal Geology and Coal Technology*, Blackwell Scientific Publications, Melbourne, 345 pp.

Watkeys, M.K., 1984. The Precambrian Geology of the Limpopo Mobile Belt north and west of Messina. Ph.D. Thesis, University of the Witwatersrand, Johannesburg, unpublished, 391 pp.

Watkeys, M.K. and Sweeney, R.J., 1988. Tuli-Lebombo volcanism and Gondwana rifting. Extended abstracts, *Geocongress 88*, Durban: University of Natal, 38. 725-728.

Watts, A.B., 1978. An analysis of isostasy in the world's oceans: 1. Hawaiian-Emperor Seamount Chain. *Journal of Geophysics Research*, 83, 5989-6004.

Watts, A.B., 2001. *Isostasy and flexure of the lithosphere*. Cambridge Univ. Press. 458 pp.

Watts, A.B. and Ryan, W.B.F., 1976. Flexure of the lithosphere and continental margin basins. *Tectonophysics*, 36, 25-44.

Weaver, C.E., 1989. *Clays, Muds, and Shales*. Elsevier, New York. 819 pp.

Wilkinson, M., Milliken, K.L., and Haszeldine, R.S., 2001, Systematic destruction of K-feldspar in deeply buried rift and passive margin sandstones. *Journal of the Geological Society, London*, 158, 675-683.

Yerino, L.N. and Maynard, J.B., 1984. Petrography of modern marine sands from the Peru-Chile Trench and adjacent areas. *Sedimentology*, 31, 83-89.

Zuffa, G.G., 1985. Optical analyses of arenites: Influence of methodology on compositional results. In G.G. Zuffa (Editor), *Provenance of Arenites*, NATO ASI Series, Series C. Mathematical and Physical Sciences, 148, 165-189.

APPENDICES

Appendix A: Facies Classification

Table A1: Facies classification of fluvial deposits (Miall, 1978).

Facies code	Facies	Sedimentary structures	Interpretation
Gmm	Matrix - supported, massive gravel	Weak grading	Plastic debris flow (high - strength, viscous)
Gmg	Matrix - supported gravel	Inverse to normal grading	Pseudoplastic debris flow (low strength, viscous)
Gci	Clast - supported gravel	Inverse grading	Clastic rich debris flow (high strength), or pseudoplastic debris flow (low strength)
Gcm	Clastic-supported, massive gravel	-	Pseudoplastic debris flow (inertial bedload, turbulent flow)
Gh	Clastic-supported, crudely bedded gravel	Horizontal bedding, imbrication	Longitudinal bedforms, lag deposits, sieve deposits
Gt	Gravel, stratified	Trough crossbeds	Minor channel fills
Gp	Gravel, stratified	Planar crossbeds	Transverse bedforms, deltaic growths from older bar remnants
St	Sand, fine to v. Coarse, may be pebbly	Solitary or grouped trough crossbeds	Simously crested and linguoid (3-D) dunes
Sp	Sand, fine to v. Coarse, may be pebbly	Solitary or grouped planar crossbeds	Transverse and linguoid bedforms (2-D dunes)
Sr	Sand very fine to coarse	Ripple crosslamination	Ripples (lower flow regime)
Sh	Sand, v. Fine to coarse, may be pebbly	Horizontal lamination, parting or streaming lineation	Plane-bed flow (critical flow)
Sl	Sand, v. Fine to coarse, may be pebbly	Low-angle (< 150) croaabeeds	Scour fills, humpback or washed-out dunes, antidunes
Ss	Sand, fine to v. Coarse, may be pebbly	Broad, shallow scours	Scour fill
Sm	Sand, fine to coarse	Massive, or faint lamination	Sediment-gravity flow deposits
Fl	Sand, silt, mud	Fine lamination, v. Small ripples	Overbank, abandoned channel, or waning flood deposits
Fsm	Silt, mud	Massive	Back swamp or abandoned channel deposits
Fm	Mud, silt	Massive, desiccation cracks	Overbank, abandoned channel, or drape deposits
Fr	Mud, silt	Massive, roots, bioturbation	Root bed, incipient soil
C	Coal, carbonaceous mud	Plants, mud films	Vegetated swamp deposits
P	Paleosol carbonate (calcite, siderite)	Pedogenic features	Soil with chemical precipitation

V., Very; *D.*, dimensional

Appendix B: Paleostress Analysis using the WINTENSOR Program developed by Delvaux, 2012

Win-Tensor is the Windows version of the Tensor program (Win-Tensor) developed originally in DOS. The program has been developed in order to meet the needs of field geologists active in brittle fault analysis and paleostress reconstructions, an emerging standard method in structural geology. The program uses the Right-Dihedral method, followed by the Rotational Optimization. The following figures illustrate the procedure.

The data and digitising sheets

WinTensor Version : 1.3.46

Image Data Window

Fault-slip data Worksheet - [CBARKNEW.txt]

Unlock File Validation Properties Comments Formulas Stereonets Processing

Site properties: Project Code, Outcrop Code, Stereonets - Id: 001, Data Row 1 (Id= 001) / Definition Id, Data Value, Data Value, 001

Digitize orientation data from Stereonet

Image commands: [L] [P] [C] [A] [M] [Point: 45.81 / 347.91]

Properties definition: Colors: Graticule, Net border, Net Bg, Data; Symbol Size: Automatic, 3, Data format

Step 1: Definition of Net Center and Radius:

- Mode 1: First point on center, second on border
- Mode 2: First point on border, second on center
- Mode 3: First point on border, second on opposite border relative to center

Step 2: Digitize data:

- Plane as Great Circle (Type of Plane / Joint)
 - alone: two successive points on the fault trace
 - with lineation/slip direction: one additional point on the line
 - with slip line: one additional point on the line and one for the definition of the slip sense
- Tangent-lineation: pole of plane & movement plane, slip sense
- Plane as pole
- Line-Axis (Type of Axis / Line)
- Focal mechanism as beachball with indication of extensional dielder

Buttons: Start, Reset, Valider, Delete, Change Image, Re-Initialise, Invert Slip Sense, Stop, Restart, Redefine net, Transfer

N°	Id	Data	Plane	Line	Slip	Comments		
		Type	Dip	Dip-Ds	Plunge	Azim.	Sense	
11	02	XX-006	1	80	115	35	033	XX
12	02	XX-005	1	43	298	42	283	NS
13	02	XX-004	1	65	179	44	114	NS
14	02	XX-003	1	65	126	53	177	ND
14	02	XX-002	1	59	332	54	005	ND
14	02	XX-001	1	77	348	70	298	NS

Slip line	Slip	Subsets	Fracture plan			
ng	Azim.	Sense	Temp	Final	Dip	Dig
34	135	ND	0,1	0,1	56	3
36	155	ND	0,2	0,1	54	3
37	114	NS	0,2	0,1	39	2
35	164	ND	0,1	0,1	35	3
38	308	NS	0,1	0,1	32	1
39	338	ND	0,2	0,1	31	1
36	322	ND	0,2	0,1	54	1
31	288	NS	0,1	0,1	29	1
34	121	ND	0,2	0,1	56	3
33	109	ND	0,1	0,1	57	2
31	337	ND	0,3	0,1	59	1
39	136	ND	0,2	0,1	51	3
40	136	ND	0,2	0,1	50	3
39	137	ND	0,2	0,1	51	3

The processing sheets

WinTensor Version : 1.3.46

Processing Worksheet - [CBARKNEW.txt]

Subset Manager: 0, 0.0, 0.1, 0.2, 0.3, 0.4, 0.5, 0.6, 0.7, 0.8, 0.9, 1, 2, 3, 4, 5, 6, 7, 8, 9

Data Worksheet Stereonet Base diag. Statistics P B T Analysis Right Dihedron Rot. Optimization Mohr diag.

Right Dihedron: Selected Data 48, Valid data 48, Cone angle 16.7, Weighting

Results:

Axis	Raw	Orthog	Nbr.	C.V.	C.A.
a1	85/223	85/223	43	0	19.8
a2	05/030	05/030	70	97	
a3	02/120	02/120	24	100	25.7

R: 0.29, Mean Counting Dev. 22.7 ± 5.3
 R': 0.29, Pure EXTENSIONAL
 Reg. NF, SHmax 030, Shmin 120

Data separation: Counting Deviation (C.D.) Threshold: Do, C.D. = Mean C.D. + 1, Auto

Data Compatible: 38, Data not compatible: 10
 Subset indexes: 0.0, 0.9
 Initial subset: 48, Used data: 100%, Final subset: 48

Display Control: Grid, Stress Symbol, Stress axes, Stress arrows, Stress axis legend, Counting scale, Histogram

Count.Dev.(%) histogram: frequency x weight 78

Data Id	Compiled fault-slip data	Subsets	Results	Comments										
N°	Id	Type	Plane	Line	Slip	CL	WR	Ac	St	I	T	S	C.D.(%)	
1	True	001-a	7	42/094	34/135	ND	X	6	1	1	0,1	0,1	19.68	19611028 22h45 53.60
2	True	001-b	7	56/315	48/274	NS	X	6	1	1	0,1	0,1	19.68	19611028 22h45 53.60
3	True	003-a	7	41/122	36/155	ND	X	6	1	1	0,1	0,2	18.53	19620813 20h11 53.70
4	True	003-b	7	54/335	49/302	NS	X	6	1	1	0,1	0,1	18.53	19620813 20h11 53.70
5	True	005-a	7	52/123	51/114	NS	X	5	1	1	0,1	0,2	21.86	19621028 08h29 55.60
6	True	005-b	7	39/294	38/303	ND	X	5	1	1	0,1	0,1	21.86	19621028 08h29 55.60
7	True	007-a	7	66/113	55/164	ND	X	4	1	1	0,1	0,1	28.95	19630131 18h30 53.11
8	True	007-b	7	35/344	24/293	NS	X	4	1	1	0,1	0,2	28.95	19630131 18h30 53.11

Table B1: Compiled Data Set of the Tshipise-Pafuri Basin.

Fault Plane		Slip Line		Slip Sense
Dip	Dip direction	Plunge	Azimuth	
15	75	8	17	NS
29	71	20	23	NS
32	81	16	19	NS
16	35	16	55	ND
26	57	24	31	NS
21	56	20	34	NS
36	57	34	34	NS
45	50	44	39	NS
36	36	35	54	ND
23	27	19	63	ND
27	11	0	100	ND
29	57	29	63	ND
45	32	42	57	ND
29	28	25	61	ND
59	35	58	54	ND
68	25	64	59	ND
73	65	70	30	NS
68	55	67	36	NS
59	50	59	40	NS
59	35	58	54	ND
45	36	44	54	ND
51	35	49	54	ND
63	40	63	50	ND
59	70	52	30	NS
55	75	40	21	NS
45	32	42	57	ND
29	38	29	52	ND
76	40	76	50	ND
Maximum	76	81	76	100
Minimum	15	11	0	17
Average	43.5	46.57143	39.39286	46.10714

Where: NS-Normal strike slip; ND-Normal dip slip.

Table B2: Compiled Data Set of the Mopane Basin.

Fault Plane		Slip Line		Slip Sense
Dip	Dip direction	Plunge	Azimuth	
40	60	36	32	NS
63	77	56	36	NS
63	60	60	33	NS
63	42	63	48	ND
51	42	50	58	ND
34	80	19	20	NS
34	40	34	50	ND
51	80	37	28	NS
55	60	52	32	NS
59	70	52	30	NS
63	60	60	33	NS
51	63	46	31	NS
68	66	64	31	NS
81	60	80	33	NS
84	66	83	32	NS
84	75	82	34	NS
81	72	78	33	NS
75	65	72	32	NS
42	40	42	50	ND
48	68	39	26	NS
Maximum	84	80	83	58
Minimum	34	40	19	20
Average	59.5	62.3	55.25	35.1

Where: NS-Normal strike slip; ND-Normal dip slip.

Table B3: Compiled Data Set of the Tuli Coalfield

Fault Plane		Slip Line		Slip Sense
Dip	Dip direction	Plunge	Azimuth	
44	30	40	58	ND
55	15	45	61	ND
73	32	72	53	ND
78	35	78	55	ND
78	43	78	47	ND
73	38	73	52	ND
72	35	72	45	ND
68	35	68	45	ND
55	42	55	48	ND
25	30	22	59	ND
84	26	83	58	ND
87	38	87	55	ND
88	35	88	45	ND
88	33	88	47	ND
88	38	88	52	ND
87	37	87	53	ND
86	33	86	57	ND
81	38	81	55	ND
82	37	82	53	ND
80	39	80	51	ND
78	52	78	38	NS
Maximum	88	52	88	61
Minimum	25	15	22	38
Average	73.80952	35.28571	72.90476	51.7619

Where: NS-Normal strike slip; ND-Normal dip slip.

Appendix C: Geochemical and Mineralogical Results

Table C1: Results of major elements (wt%) analysed by X-ray fluorescence spectrometry.

Sample	TMKS1 Tuli	PC1	PC2	PCLM1 T-P	PCLS1 T-P	PMZM1 T-P	PMKM2 T-P	TPMZS2 T-P	PSLM1 T-P	TBSS1 Tuli	TKLS1 Tuli shale	TKL S2 Tuli	TLTS1 Tuli	MMKS1 Mopane	TMKS2 Tuli	TPMKS4 Mopane
SiO ₂	93.06	18.58	6.81	77.84	85.72	50.08	58.42	90.66	79.20	89.06	84.29	95.5 2	96.91	86.15	93.45	98.33
TiO ₂	0.76	0.28	0.09	0.52	0.14	0.47	1.17	0.07	0.64	0.19	0.21	0.08	0.06	0.27	0.10	0.07
Al ₂ O ₃	4.45	7.52	2.05	7.53	8.59	11.08	27.27	6.19	10.12	5.54	5.99	2.42	1.55	6.94	3.09	0.76
Fe ₂ O ₃ (t)	0.59	0.29	0.82	1.28	0.93	23.84	2.62	0.54	3.13	0.95	1.28	0.55	0.45	1.78	2.63	1.04
MnO	0.005	0.003	0.020	0.265	0.034	0.325	0.022	0.007	0.029	0.011	0.021	0.00 6	0.006	0.021	0.011	0.006
MgO	0.02	0.28	0.46	0.90	0.13	1.50	1.02	0.16	0.88	0.46	0.68	0.11	0.15	0.85	0.02	0.00
CaO	0.05	0.48	0.87	4.93	0.27	1.86	0.20	0.43	0.24	0.24	2.14	0.03	0.04	0.19	0.03	0.01
Na ₂ O	<0.01	<0.01	0.02	1.91	3.86	<0.01	0.04	<0.01	1.28	0.79	0.77	0.03	<0.01	0.86	<0.01	<0.01
K ₂ O	0.32	0.33	0.13	0.29	0.10	2.44	2.64	1.16	2.54	1.92	2.04	1.13	0.90	2.47	0.07	0.02
P ₂ O ₅	0.036	0.020	0.028	0.014	0.013	0.509	0.080	0.017	0.015	0.015	0.013	0.00 6	0.006	0.015	0.037	0.012
Cr ₂ O ₃	0.006	0.002	0.001	0.004	0.003	0.010	0.018	<0.001	0.006	<0.001	0.001	<0.0 01	<0.001	0.002	0.001	<0.001
L.O.I.	1.27	72.08	88.06	4.97	0.44	8.22	6.69	1.42	1.91	0.82	2.39	0.44	0.16	1.07	1.28	0.23
Total	100.39	99.80	99.35	100.45	100.24	100.25	100.19	100.59	99.98	100.00	99.83	100. 32	100.21	100.62	100.55	100.32
H ₂ O ^c	0.26	0.82	0.58	0.57	0.19	1.29	3.15	0.32	1.06	0.49	0.52	0.20	0.11	0.52	0.14	0.06

Table C2: Results of major elements (wt%) analysed by X-ray fluorescence spectrometry.

Sample	TPBSM1 Mopane	TPMKM 1 Mopane	TPMK S1 T-P	TPMKS2 Mopane	TPMKS3 Mopane	TPMKS4 Mopane	TPMZ S1 T-P	TSLs1 Tuli shale	TPMKM 2 T-P	MMKM1 Mopane	MFRS1 Mopane	PFRS1 T-P	12/76	
													Certified	Result
SiO ₂	50.17	50.84	94.72	92.84	78.14	98.33	93.32	80.98	57.42	90.43	82.57	97.09	45.42	46.27
TiO ₂	3.74	1.08	0.10	0.12	0.56	0.07	0.35	0.15	0.77	0.35	0.57	0.13	1.54	1.53
Al ₂ O ₃	12.19	20.54	3.04	3.60	15.48	0.76	4.38	11.55	18.60	5.00	2.40	1.81	16.62	16.41
Fe ₂ O ₃ (t)	12.19	19.71	1.16	0.86	0.85	1.04	0.95	1.04	10.85	0.91	12.26	0.84	9.73	9.94
MnO	0.120	0.023	0.008	0.006	0.004	0.006	0.007	0.028	0.052	0.015	0.020	0.006	0.180	0.178
MgO	5.56	0.10	0.14	0.27	0.00	0.00	0.02	0.12	2.46	0.37	0.03	0.05	8.15	8.00
CaO	7.99	0.12	0.04	0.21	0.01	0.01	0.03	0.62	0.35	0.45	0.05	0.02	10.93	10.83
Na ₂ O	1.90	<0.01	<0.01	<0.01	<0.01	<0.01	<0.01	4.96	0.17	1.26	<0.01	<0.01	3.65	3.23
K ₂ O	2.74	0.36	0.67	1.50	0.00	0.02	0.17	0.30	6.62	0.18	0.06	0.39	0.70	0.68
P ₂ O ₅	0.583	0.046	0.014	0.010	0.018	0.012	0.029	0.048	0.153	0.006	0.171	0.007	0.259	0.264
Cr ₂ O ₃	0.020	0.023	<0.001	<0.001	0.010	<0.001	0.007	0.001	0.014	<0.001	0.008	<0.001	0.074	0.064
L.O.I.	2.50	7.57	0.75	1.01	5.73	0.23	1.46	0.36	2.75	1.30	2.45	0.41	2.50	2.40
Total	99.71	100.12	100.52	100.31	100.56	100.32	100.54	100.15	100.22	100.28	100.43	100.62	99.75	99.80
H ₂ O ⁻	1.15	0.59	0.10	0.80	0.17	0.06	0.10	0.13	0.41	0.27	0.30	0.17	0.18	0.08

NB* 12/76 is a secondary amphibolite reference material

T-P: Tshipise-Pafuri

Table C3: Results of X-ray Diffraction (XRD).

Sample	Calcite	Dolomite	Hematite	Goethite	Clinopyroxene	K-feldspar	Plagioclase	Quartz	Mica	Chlorite/ Kaolinite	Kaolinite	Chlorite	Amphibole	Palygorskite	Pyrophyllite	Ilmenite	Spinel?	Smectite	I/S Interstratification	Amorphous material
MFRS1	-	-	2	-	-	-	-	90	-	-	7	-	-	-	-	-	-	-	-	*
MMKM1	-	-	-	-	-	-	9	82	-	-	7	-	-	-	-	-	-	-	2	-
MMKS1	-	-	-	-	-	-	-	85	-	-	12	-	-	-	-	-	-	-	2	-
PC1	-	5	-	-	-	-	-	37	-	-	58	-	-	-	-	-	-	-	-	-
PC2	-	18	-	-	-	-	-	38	-	-	44	-	-	-	-	-	-	-	-	-
PCLM1	-	11	1	-	-	-	18	65	2	-	2	-	-	-	-	-	-	-	-	-
PCLS1	-	-	-	-	-	-	29	71	-	-	-	-	-	-	-	-	-	-	-	-
PFRS1	-	-	-	-	-	1	-	97	-	-	-	-	-	-	-	-	-	-	2	-
PMKM1	-	-	16	-	-	9	3	32	35	5	-	-	-	-	-	-	-	-	-	-
PMKM2	-	-	-	-	-	-	-	34	25	7	-	-	-	-	29	-	-	5	-	-
PMZM1	-	6	-	10	-	-	-	72	6	-	-	-	-	6	-	-	-	-	-	-
PMZS2	1	-	-	-	-	-	1	92	-	-	-	-	-	6	-	-	-	-	-	-
PSLM1	-	-	2	-	-	4	13	76	3	-	-	-	-	3	-	-	-	-	-	-
TBSS1	-	-	-	-	-	5	6	82	2	2	-	-	-	1	-	-	-	3	-	-
TKLS1	5	-	-	-	-	3	6	80	2	1	-	-	-	2	-	-	-	-	-	-
TKLS2	-	-	-	-	-	3	1	94	-	-	-	-	-	-	-	-	-	-	1	-
TLTS1	-	-	-	-	-	2	1	95	-	-	-	-	-	-	-	-	-	-	2	-
TMKS1	-	-	-	-	-	5	6	84	2	-	-	-	-	-	-	-	-	3	-	-
TMKS2	-	-	-	-	-	-	-	87	-	-	11	-	-	-	-	-	-	-	2	-
TMKS3	-	-	-	-	-	6	10	77	5	-	-	3	-	-	-	-	-	-	-	-
TPBSM1	-	-	-	-	32	-	43	6	-	-	-	8	-	-	-	3	-	8	-	-
TPMKM1	-	-	25	-	-	-	-	38	-	-	37	-	-	-	-	-	-	-	-	-
TPMKS1	-	-	trace	-	-	1	1	94	2	-	2	-	-	-	-	-	-	-	-	-
TPMKS2	-	-	-	-	-	3	-	91	-	-	-	-	-	-	-	-	-	5	-	-
TPMKS3	-	-	1	-	-	-	-	95	-	-	3	-	-	-	-	-	-	-	2	-
TPMKS4	-	-	-	-	-	1	-	56	-	-	42	-	-	-	-	-	-	-	1	-

TPMZS1	-	-	-	-	-	-	-	48	1	-	51	-	-	-	-	-	-	1	-
TSLS1	-	-	-	-	-	-	39	57	2	-	-	-	1	-	-	-	2	-	-

Samples scanned from 2 to 70° 2θ Cu_{Kα} radiation at a speed of 0.02° 2θ steps size/0.5 sec, LYNXEYE detector and generator settings of 40 kV and 40mA. Phase concentrations are determined as semiquantitative estimates, using relative peak heights/areas proportions (Brime, 1985).

Table C4: Results of trace elements (ppm) analysed by X-ray fluorescence spectrometry.

Sampl e	TSLS 1 (Tuli)	TMKS 3 (Tuli)	TSLS 3 (Tuli)	TKLS 1 (Tuli)	TBSS 1 (Tuli)	TKLS 2 (Tuli)	TPMKM 2 (T-P)	TPMZS 3 (T-P)	TPBSM 1 (T-P)	TPMKS 1 (T-P)	TPMKS 2 (T-P)	TPSLS 3 (T-P)	TPMKS 4 (T-P)	TPMKS 3 (T-P)	TPMKS 5 (T-P)	TPMKS 6 (Mopane)	TPMKS 7 (Mopane)	MMKM 1 (Mopane)
As	<4	<4	<4	<4	<4	<4	<4	<4	<4	<4	<4	<4	<4	<4	<4	<4	<4	<4
Ba	151	397	201	255	419	357	79	103	1 078	171	1 705	109	11	21	16	312	324	49
Bi	<3	<3	<3	<3	<3	<3	<3	<3	<3	<3	<3	<3	<3	<3	<3	<3	<3	<3
Br	<2	<2	<2	<2	<2	<2	<2	<2	<2	<2	<2	<2	<2	<2	<2	<2	<2	<2
Ce	17	31	<10	14	29	28	75	16	99	59	<10	<10	20	20	<10	<10	14	27
Co	5.6	5.4	1.9	3	3.9	4.5	3	3.1	41	3.6	5.6	3.3	3.6	3.7	2.2	3.3	3.1	6.9
Cr	24	32	31	20	21	26	116	37	129	34	33	12	12	101	33	23	47	24
Cs	<5	<5	<5	<5	<5	<5	<5	<5	<5	<5	<5	<5	<5	<5	<5	<5	<5	<5
Cu	4.2	9.5	5	3.6	5.3	6.3	75	2.8	87	6.4	5.5	4.9	<2	9.1	<2	6.2	3.2	5.1
Ga	10	8.4	1.5	2.1	6.2	7.3	28	3.7	22	3	6.2	3.7	<1	21	<1	3.2	8.4	4.4
Ge	<1	<1	<1	<1	<1	<1	<1	<1	<1	<1	<1	<1	<1	<1	<1	<1	<1	<1
Hf	3.6	6.1	5.1	4.9	6.1	7.9	5.2	3.9	8.3	3.5	<3	6.2	<3	7	<3	6.1	4.2	11
La	12	18	<10	<10	13	14	43	<10	55	35	<10	<10	<10	<10	<10	<10	<10	<10
Mo	<2	<2	<2	<2	<2	<2	<2	<2	<2	<2	<2	2.7	<2	<2	<2	<2	<2	<2
Nb	1.3	6.2	1.3	1.6	4.3	4.4	5	2.1	19	<1	<1	<1	1.1	6.7	<1	2.3	1.2	6.5
Nd	11	17	<10	12	17	15	47	<10	56	45	<10	<10	<10	<10	<10	<10	<10	11
Ni	9.7	10	2.5	7.1	7	7.4	29	6	119	6.5	18	5.4	5	11	2.4	6.5	6.4	6.4

Pb	9.5	14	4.3	7.5	10	14	14	4.1	5.3	6.9	3.9	4	2.4	5.9	2.5	7.5	7	6
Rb	10	83	20	27	55	64	22	24	41	18	4.9	10	<2	<2	2.7	42	7.9	8.8
Sc	<3	3.1	<3	<3	<3	3.3	32	<3	19	<3	<3	<3	<3	11	<3	<3	<3	<3
Se	<1	<1	<1	<1	<1	<1	1.2	<1	<1	<1	<1	<1	<1	<1	<1	<1	<1	<1
Sm	<10	<10	<10	<10	<10	<10	<10	<10	13	<10	<10	<10	<10	<10	<10	<10	<10	<10
Sr	299	69	28	27	70	71	57	4.9	497	6.9	139	3	8.2	13	6.5	39	210	52
Ta	<2	<2	<2	<2	<2	<2	<2	<2	2.5	<2	<2	<2	<2	<2	<2	<2	<2	<2
Th	3.1	6.7	3.6	3.4	4.1	<3	8	6.9	7.5	3.8	3.2	3.9	6	17	4.4	3.3	3.6	5
Tl	<3	<3	<3	<3	<3	<3	<3	<3	<3	<3	<3	<3	<3	<3	<3	<3	<3	<3
U	<2	2.2	<2	<2	<2	<2	<2	<2	<2	<2	2	<2	<2	<2	<2	<2	<2	2.2
V	22	29	11	4.7	13	20	1 062	6.3	262	23	66	20	4.5	177	3.7	15	16	19
W	<3	<3	<3	<3	<3	<3	3	<3	<3	<3	<3	<3	<3	<3	<3	<3	<3	<3
Y	9.8	11	3.6	5.9	8.5	9.7	9.5	9.7	36	16	2.7	5.2	5.4	5.8	1.9	4.6	4.7	13
Yb	<3	<3	<3	<3	<3	<3	<3	<3	<3	<3	<3	<3	<3	<3	<3	<3	<3	<3
Zn	4	17	<3	5.8	6.4	11	16	<3	103	<3	3.1	3.7	<3	9	<3	<3	<3	10
Zr	95	276	60	106	238	226	134	84	383	50	44	48	38	183	21	227	75	437

Table C5: Results of trace elements (ppm) analysed by X-ray fluorescence spectrometry.

Sample	(Mopane)	MMKM2 (Mopane)	PC1 (T-P)	PFRS1 (T-P)	PCLM1 (T-P)	PM2M1 (T-P)	PMKM1 (Mopane)	PM2S2 (T-P)	PMKM2 (Mopane)	GSS-1	
										Certified	Result
As	10	<4	<4	<4	<4	13	<4	<4	7.9	33.5	36
Ba	437	143	183	67	124	281	1 178	631	588	590	602
Bi	<3	<3	<3	<3	<3	<3	<3	<3	<3	1.17	<3
Br	<2	3.5	<2	<2	<2	<2	<2	<2	5.9	2.9	<2
Ce	58	170	24	31	48	132	91	107	128	70	74
Co	11	6.8	9.7	3.1	9.7	45	27	68	12	14.2	18
Cr	94	161	14	24	40	46	102	775	125	62	65
Cs	<5	<5	<5	<5	<5	<5	<5	<5	<5	9.0	<5
Cu	15	19	3.7	2.4	11	17	2.3	49	48	21	18
Ga	12	41	15	1.6	7.2	16	24	11	35	19.3	19
Ge	<1	1.6	2	<1	<1	1.5	<1	<1	<1	1.3	<1
Hf	11	8.2	4.5	4.3	12	4.9	<3	9.1	7.3	6.8	6
La	29	58	15	<10	16	62	50	55	65	34	36
Mo	<2	<2	2.3	<2	<2	3.8	<2	<2	2.9	1.4	3
Nb	11	20	2.6	2.3	9.1	11	13	17	24	16.6	16
Nd	25	48	<10	14	22	57	37	58	58	28	26
Ni	22	78	23	4.2	16	119	68	787	57	20.4	23
Pb	18	18	6.9	4.4	11	13	26	3.4	37	98	102
Rb	102	22	7.5	12	18	114	269	30	118	140	148
Sc	6.4	18	4.5	<3	3.8	25	24	11	21	11.2	12
Se	<1	<1	<1	<1	<1	1.6	<1	<1	<1	0.14	<1
Sm	<10	11	<10	<10	<10	12	<10	10	11	5.2	<10
Sr	82	16	122	7.1	139	158	39	674	128	155	165
Ta	<2	<2	<2	<2	<2	<2	2.3	2.6	2.1	3.2	2
Th	11	35	4.9	5	9	13	20	5.6	29	11	12

Tl	<3	<3	<3	<3	<3	<3	<3	<3	<3	<3	<3
U	3.1	3.5	<2	<2	<2	8.5	3.7	5.4	9.2	4.4	4
V	44	110	19	33	20	70	78	147	141	77	86
W	<3	<3	5.9	<3	<3	4.4	3.6	<3	4.1	4.7	4
Y	26	29	10	8	27	84	34	18	50	26	27
Yb	<3	3.8	<3	<3	3.2	<3	<3	3.5	4.2	<3	<3
Zn	25	17	13	<3	28	241	52	96	78	666	710
Zr	449	255	41	126	492	139	157	335	257	258	264

APPENDIX D: Subsidence Analysis

Data input

Bases should be deeper than tops, and the depth, age, sea level and water depths at the base of a given unit are equal to the depth, age, sea level and water depth at the top of the unit immediately below (see table below).

- Unit base (base) and top (top) as depths (km) from the ground surface.
- The age of unit base (Age b) and the unit top (Age t) in Ma
- Sea-level at the time of deposition of the unit base (SLb) and top (SLt) in km sediment load.
- The sea-level is reported relative to present sea-level, positive numbers indicate above present sea-level, while negative numbers below sea
- Water depth at the time of deposition of the unit base (WDb) and top (WDt) in Km, WD should be positive numbers
- Porosity coefficient (C) in Km^{-1} is between 0-1.
- Grain density (ρ_c) in Kg/m. The dry density is a positive number.
- Surface porosity (Φ) as percentage %, between 0-100.

Table D1: Data input table for the Backstripping and plotting of the subsidence curve on OSXBackstrip programme.

Name	Base	AgeB	SLb	WDb	Top	Aget	SLt	WDt	Pc	C	Φ	Type
Tshidzi	0.98	320	0	0	0.96	290	0	0	2650	0.27	49	1
Madzaringwe	0.96	290	0	0	0.76	260	0	0	2720	0.51	63	1
Mikambeni	0.76	260	0	0	0.61	256	0	0	2720	0.51	63	1
Fripp	0.61	256	0	0	0.5	252	0	0	2650	0.27	49	1
Solitude	0.5	252	0	0	0.33	250	0	0	2650	0.27	49	1
Klopperfontein	0.33	250	0	0	0.31	240	0	0	2650	0.27	49	1
Bosbokpoort	0.31	240	0	0	0.21	215	0	0	2680	0.56	56	1
Clarens	0.21	215	0	0	0.06	198	0	0	2650	0.27	49	1

The subsidence of a sedimentary basin can be attributed to three processes: tectonic subsidence, water and sediment loading, and sediment compaction. These three components of subsidence can be estimated from a stratigraphic section using a procedure called "backstripping" (Allen and Allen, 1990). Backstripping removes from each sedimentary layer

the effects of sediment compaction, water and sediment loading; thus extracting from the section tectonic subsidence curve. OSXBackstrip is a program to perform "1D Airy backstripping with exponential reduction of porosity". Stratigraphic units can be easily input in a table, and backstripping and tectonic subsidence plots and tables can be rapidly produced.